Chapter 1

Parameterization of Stillinger-Weber Potential for Two-Dimensional Atomic Crystals

Jin-Wu Jiang and Yu-Ping Zhou

Additional information is available at the end of the chapter

http://dx.doi.org/10.5772/intechopen.71929

Abstract

We parametrize the Stillinger-Weber potential for 156 two-dimensional atomic crystals (TDACs). Parameters for the Stillinger-Weber potential are obtained from the valence force field (VFF) model following the analytic approach (Nanotechnology. 2015;**26**:315706), in which the valence force constants are determined by the phonon spectrum. The Stillinger-Weber potential is an efficient nonlinear interaction and is applicable for numerical simulations of nonlinear physical or mechanical processes. The supplemental resources for all simulations in the present work are available online in http://jiangjinwu.org/sw, including a Fortran code to generate crystals' structures, files for molecular dynamics simulations using LAMMPS, files for phonon calculations with the Stillinger-Weber potential using GULP, and files for phonon calculations with the valence force field model using GULP.

Keywords: layered crystal, Stillinger-Weber potential, molecular dynamics simulation, empirical potential

PACS: 78.20.Bh, 63.22.-m, 62.25.-g

1. Introduction

The atomic interaction is of essential importance in the numerical investigation of most physical or mechanical processes [1]. The present work provides parameters for the Stillinger-Weber (SW) empirical potential for 156 two-dimensional atomic crystals (TDACs). In practical applications, these layered materials are usually played as Lego on atomic scale to construct the van der Waals heterostructures with comprehensive properties [2]. The computational cost of *ab initio* for the heterostructure will be substantially increased as compared with one individual atomic layer, because the unit cell for the heterostructure is typically very large resulting from the mismatch of the lattice constants of different layered components. The empirical potential will be a competitive alternative to help out this difficult situation, considering their high efficiency.

In the early stage before 1980s, the computation ability of the scientific community was quite limited. At that time, the valence force field (VFF) model was one popular empirical potential for the description of the atomic interaction, since the VFF model is linear and can be applied in the analytic derivation of most elastic quantities [3]. In this model, each VFF term corresponds to a particular motion style in the crystal. Hence, each parameter in the VFF model usually has clear physical essence, which is beneficial for the parameterization of this model. For instance, the bond stretching term in the VFF model is directly related to the frequency of the longitudinal optical phonon modes, so the force constant of the bond stretching term can be determined from the frequencies of the longitudinal optical phonon modes. The VFF model can thus serve as the starting point for developing atomic empirical potentials for different crystals.

While the VFF model is beneficial for the fastest numerical simulation, its strong limitation is the absence of nonlinear effect. Due to this limitation, the VFF model is not applicable to nonlinear phenomena, for which other potential models with nonlinear components are required. Some representative potential models are (in the order of their simulation costs) SW potential [4], Tersoff potential [5], Brenner potential [6], *ab initio* approaches, etc. The SW potential is one of the simplest potential forms with nonlinear effects included. An advanced feature for the SW potential is that it includes the nonlinear effect, and keeps the numerical simulation at a very fast level.

Considering its distinct advantages, the present article aims at providing the SW potential for 156 TDACs. We will determine parameters for the SW potential from the VFF model, following the analytic approach proposed by one of the present authors (JWJ) [7]. The VFF constants are fitted to the phonon spectrum or the elastic properties in the TDACs.

In this paper, we parametrize the SW potential for 156 TDACs. All structures discussed in the present work are listed in **Tables 1–9**. The supplemental materials are freely available online

1H-ScO_2	1H-ScS_2	1H-$ScSe_2$	1H-$ScTe_2$	1H-$TiTe_2$	1H-VO_2	1H-VS_2	1H-VSe_2	1H-VTe_2
1H-CrO_2	1H-CrS_2	1H-$CrSe_2$	1H-$CrTe_2$	1H-MnO_2	1H-FeO_2	1H-FeS_2	1H-$FeSe_2$	1H-$FeTe_2$
1H-$CoTe_2$	1H-NiS_2	1H-$NiSe_2$	1H-$NiTe_2$	1H-NbS_2	1H-$NbSe_2$	1H-MoO_2	1H-MoS_2	1H-$MoSe_2$
1H-$MoTe_2$	1H-TaS_2	1H-$TaSe_2$	1H-WO_2	1H-WS_2	1H-WSe_2	1H-WTe_2		

The structure is shown in **Figure 1**.

Table 1. 1H-MX_2, with M as the transition metal and X as oxygen or dichalcogenide.

1T-ScO_2	1T-ScS_2	1T-$ScSe_2$	1T-$ScTe_2$	1T-TiS_2	1T-$TiSe_2$	1T-$TiTe_2$	1T-VS_2	1T-VSe_2
1T-VTe_2	1T-MnO_2	1T-MnS_2	1T-$MnSe_2$	1T-$MnTe_2$	1T-$CoTe_2$	1T-NiO_2	1T-NiS_2	1T-$NiSe_2$
1T-$NiTe_2$	1T-ZrS_2	1T-$ZrSe_2$	1T-$ZrTe_2$	1T-NbS_2	1T-$NbSe_2$	1T-$NbTe_2$	1T-MoS_2	1T-$MoSe_2$
1T-$MoTe_2$	1T-TcS_2	1T-$TcSe_2$	1T-$TcTe_2$	1T-$RhTe_2$	1T-PdS_2	1T-$PdSe_2$	1T-$PdTe_2$	1T-SnS_2
1T-$SnSe_2$	1T-HfS_2	1T-$HfSe_2$	1T-$HfTe_2$	1T-TaS_2	1T-$TaSe_2$	1T-$TaTe_2$	1T-WS_2	1T-WSe_2
1T-WTe_2	1T-ReS_2	1T-$ReSe_2$	1T-$ReTe_2$	1T-$IrTe_2$	1T-PtS_2	1T-$PtSe_2$	1T-$PtTe_2$	

The structure is shown in **Figure 71**.

Table 2. 1T-MX_2, with M as the transition metal and X as oxygen or dichalcogenide.

Black phosphorus	p-Arsenene	p-Antimonene	p-Bismuthene
The structure is shown in **Figures 178** or **183**.			

Table 3. Puckered (p-) M, with M from group V.

	p-SiO	p-GeO	p-SnO
p-CS	p-SiS	p-GeS	p-SnS
p-CSe	p-SiSe	p-GeSe	p-SnSe
p-CTe	p-SiTe	p-GeTe	p-SnTe
The structure is shown in **Figure 189**, and particularly **Figure 191** for p-MX with X = O.			

Table 4. Puckered MX, with M from group IV and X from group VI.

Silicene	**Germanene**	**Stanene**	**Indiene**
Blue phosphorus	b-Arsenene	b-Antimonene	b-Bismuthene
The structure is shown in **Figure 222**.			

Table 5. Buckled (b-) M, with M from group IV or V.

b-CO	b-SiO	b-GeO	b-SnO
b-CS	b-SiS	b-GeS	b-SnS
b-CSe	b-SiSe	b-GeSe	b-SnSe
b-CTe	b-SiTe	b-GeTe	b-SnTe
The structure is shown in **Figure 239**.			

Table 6. Buckled MX, with M from group IV and X from group VI.

b-SnGe	b-SiGe	b-SnSi	b-InP	b-InAs	b-InSb	b-GaAs	b-GaP	b-AlSb
The structure is shown in **Figure 239**.								

Table 7. Buckled MX, with both M and X from group IV or M from group III and X from group V.

BO	AlO	GaO	InO
BS	AlS	GaS	InS
BSe	AlSe	GaSe	InSe
BTe	AlTe	GaTe	InTe
The structure is shown in **Figure 290**.			

Table 8. Bi-buckled MX, with M from group III and X from group VI.

Borophene

Table 9. The structure is shown in **Figure 323**.

in [1], including a Fortran code to generate crystals' structures, files for molecular dynamics simulations using LAMMPS, files for phonon calculations with the SW potential using GULP, and files for phonon calculations with the valence force field model using GULP.

2. VFF model and SW potential

2.1. VFF model

The VFF model is one of the most widely used linear models for the description of atomic interactions [3]. The bond stretching and the angle bending are two typical motion styles for most covalent bonding materials. The bond stretching describes the energy variation for a bond due to a bond variation $\Delta r = r - r_0$, with r_0 as the initial bond length. The angle bending gives the energy increment for an angle resulting from an angle variation $\Delta\theta = \theta - \theta_0$, with θ_0 as the initial angle. In the VFF model, the energy variations for the bond stretching and the angle bending are described by the following quadratic forms,

$$V_r = \frac{1}{2}K_r(\Delta r)^2, \tag{1}$$

$$V_\theta = \frac{1}{2}K_\theta(\Delta\theta)^2, \tag{2}$$

where K_r and K_θ are two force constant parameters. These two potential expressions in Eqs. (1) and (2) are directly related to the optical phonon modes in the crystal. Hence, their force constant parameters K_r and K_θ are usually determined by fitting to the phonon dispersion.

2.2. SW potential

In the SW potential, energy increments for the bond stretching and angle bending are described by the following two-body and three-body forms,

$$V_2(r_{ij}) = A(B/r_{ij} - 1)e^{[\rho/(r_{ij} - r_{max})]}, \tag{3}$$

$$V_3(\theta_{ijk}) = Ke^{[\rho_1/(r_{ij} - r_{max12}) + \rho_2/(r_{ik} - r_{max13})]} (\cos\theta_{ijk} - cos\theta_0)^2 \tag{4}$$

where V_2 corresponds to the bond stretching and V_3 associates with the angle bending. The cut-offs r_{max}, r_{max12}, and r_{max13} are geometrically determined by the material's structure. There are five unknown geometrical parameters, i.e., ρ and B in the two-body V_2 term and ρ_1, ρ_2, and θ_0 in the three-body V_3 term, and two energy parameters A and K. There is a constraint among these parameters due to the equilibrium condition [7],

$$\rho = \frac{-4B(d - r_{max})^2}{(Bd - d^5)}, \tag{5}$$

where d is the equilibrium bond length from experiments. Eq. (5) ensures that the bond has an equilibrium length d and the V_2 interaction for this bond is at the energy minimum state at the equilibrium configuration.

The energy parameters A and K in the SW potential can be analytically derived from the VFF model as follows,

$$A = \frac{K_r}{\alpha e^{[\rho/(d - r_{max})]}}, \tag{6}$$

$$K = \frac{K_\theta}{2\sin^2\theta_0 e^{[\rho_1/(d_1 - r_{max12}) + \rho_2/(d_2 - r_{max13})]}}, \tag{7}$$

where the coefficient α in Eq. (6) is,

$$\begin{aligned} \alpha = & \left[\frac{\rho}{(d - r_{max})^2}\right]^2 (B/d^4 - 1) \\ & + \left[\frac{2\rho}{(d - r_{max})^3}\right](B/d^4 - 1) \\ & + \left[\frac{\rho}{(d - r_{max})^2}\right]\left(\frac{8B}{d^5}\right) + \left(\frac{20B}{d^6}\right). \end{aligned} \tag{8}$$

In some situations, the SW potential is also written into the following form,

$$V_2(r_{ij}) = \epsilon A_L(B_L\sigma^p r_{ij}^{-p} - \sigma^q r_{ij}^{-q})e^{[\sigma/(r_{ij} - a\sigma)]}, \tag{9}$$

$$\begin{aligned} V_3(\theta_{ijk}) = & \epsilon\lambda e^{[\gamma\sigma/(r_{ij} - a\sigma) + \gamma\sigma/(r_{jk} - a\sigma)]} \\ & (\cos\theta_{ijk} - \cos\theta_0)^2. \end{aligned} \tag{10}$$

The parameters here can be determined by comparing the SW potential forms in Eqs. (9) and (10) with Eqs. (3) and (4). It is obvious that $p = 4$ and $q = 0$. Eqs. (9) and (10) have two more parameters than Eqs. (3) and (4), so we can set $\epsilon = 1.0$ eV and $\gamma = 1.0$. The other parameters in Eqs. (9) and (10) are related to these parameters in Eqs. (3) and (4) by the following equations

$$A_L = A, \tag{11}$$

$$\sigma = \rho, \tag{12}$$

$$B_L = B/\rho^4, \tag{13}$$

$$a = r_{max}/\rho, \tag{14}$$

$$\lambda = K. \tag{15}$$

The SW potential is implemented in GULP using Eqs. (3) and (4). The SW potential is implemented in LAMMPS using Eqs. (9) and (10).

In the rest of this article, we will develop the VFF model and the SW potential for layered crystals. The VFF model will be developed by fitting to the phonon dispersion from experiments or first-principles calculations. The SW potential will be developed following the above analytic parameterization approach. In this work, GULP [8] is used for the calculation of phonon dispersion and the fitting process, while LAMMPS [9] is used for molecular dynamics simulations. The OVITO [10] and XCRYSDEN [11] packages are used for visualization. All simulation scripts for GULP and LAMMPS are available online in [1].

3. 1H-SCO_2

Most existing theoretical studies on the single-layer 1H-ScO_2 are based on the first-principles calculations. In this section, we will develop the SW potential for the single-layer 1H-ScO_2.

The structure for the single-layer 1H-ScO_2 is shown in **Figure 1** (with M = Sc and X = O). Each Sc atom is surrounded by six O atoms. These O atoms are categorized into the top group (e.g.,

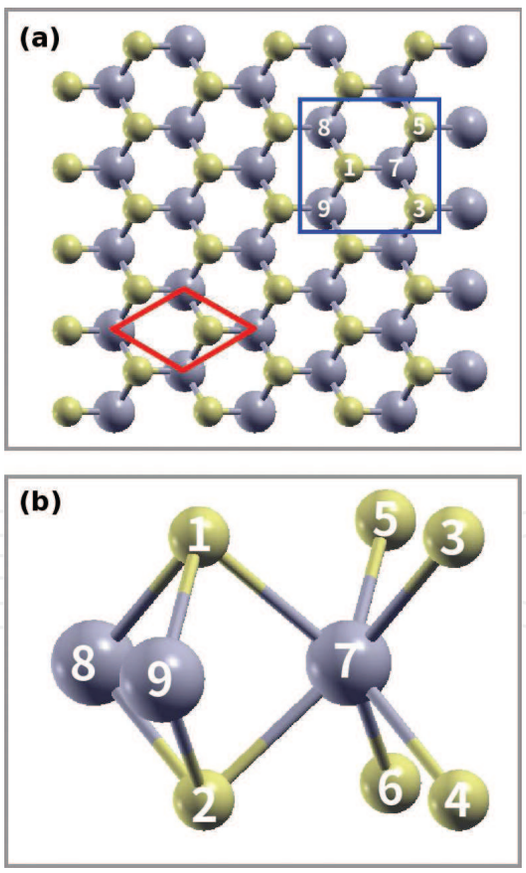

Figure 1. Configuration of the 1H-MX_2 in the 1H phase. (a) Top view. The unit cell is highlighted by a red parallelogram. (b) Enlarged view of atoms in the blue box in (a). Each M atom is surrounded by six X atoms, which are categorized into the top and bottom groups. Atoms X 1, 3, and 5 are from the top group, while atoms X 2, 4, and 6 are from the bottom group. M atoms are represented by larger gray balls. X atoms are represented by smaller yellow balls.

atoms 1, 3, and 5) and bottom group (e.g., atoms 2, 4, and 6). Each O atom is connected to three Sc atoms. The structural parameters are from the first-principles calculations [12], including the lattice constant a = 3.16 Å and the bond length $d_{Sc-O} = 2.09$ Å. The resultant angles are $\theta_{ScOO} = \theta_{OScSc} = 98.222^\circ$ and $\theta_{ScOO'} = 58.398^\circ$, in which atoms O and O′ are from different (top or bottom) groups.

Table 10 shows four VFF terms for the single-layer 1H-ScO_2; one of which is the bond stretching interaction shown by Eq. (1), while the other three terms are the angle bending interaction shown by Eq. (2). These force constant parameters are determined by fitting to the acoustic branches in the phonon dispersion along ΓM as shown in **Figure 2(a)**. The *ab initio* calculations for the phonon dispersion are from [12]. **Figure 2(b)** shows that the VFF model and the SW potential give exactly the same phonon dispersion, as the SW potential is derived from the VFF model.

The parameters for the two-body SW potential used by GULP are shown in **Table 11**. The parameters for the three-body SW potential used by GULP are shown in **Table 12**. Some representative parameters for the SW potential used by LAMMPS are listed in **Table 13**. We note that 12 atom types have been introduced for the simulation of the single-layer 1H-ScO_2 using LAMMPS, because the angles around atom Sc in **Figure 1** (with M = Sc and X = O) are not distinguishable in LAMMPS. We have suggested two options to differentiate these angles by implementing some additional constraints in LAMMPS, which can be accomplished by modifying the source file of LAMMPS [13, 14]. According to our experience, it is not so convenient for some users to implement these constraints and recompile the LAMMPS package. Hence, in the present work, we differentiate the angles by introducing more atom types, so it is not necessary to modify the LAMMPS package. **Figure 3** (with M = Sc and X = O) shows that, for 1H-ScO_2, we can differentiate these angles around the Sc atom by assigning these six neighboring O atoms with different atom types. It can be found that twelve atom types are necessary for the purpose of differentiating all six neighbors around one Sc atom.

We use LAMMPS to perform MD simulations for the mechanical behavior of the single-layer 1H-ScO_2 under uniaxial tension at 1 and 300 K. **Figure 4** shows the stress-strain curve for the tension of a single-layer 1H-ScO_2 of dimension 100 × 100 Å. Periodic boundary conditions are applied in both armchair and zigzag directions. The single-layer 1H-ScO_2 is stretched uniaxially along the armchair or zigzag direction. The stress is calculated without involving the actual thickness of the quasi-two-dimensional structure of the single-layer 1H-ScO_2. The

VFF type	**Bond stretching**		**Angle bending**	
Expression	$\frac{1}{2}K_{Sc-O}(\Delta r)^2$	$\frac{1}{2}K_{Sc-O-O}(\Delta\theta)^2$	$\frac{1}{2}K_{Sc-O-O'}(\Delta\theta)^2$	$\frac{1}{2}K_{O-Sc-Sc}(\Delta\theta)^2$
Parameter	9.417	4.825	4.825	4.825
r_0 or θ_0	2.090	98.222	58.398	98.222

The second line gives an explicit expression for each VFF term. The third line is the force constant parameters. Parameters are in the unit of ev/Å^2 for the bond stretching interaction and in the unit of eV for the angle bending interaction. The fourth line gives the initial bond length (in the unit of Å) for the bond stretching interaction and the initial angle (in the unit of degrees) for the angle bending interaction. The angle θ_{ijk} has atom i as the apex.

Table 10. The VFF model for single-layer 1H-ScO_2.

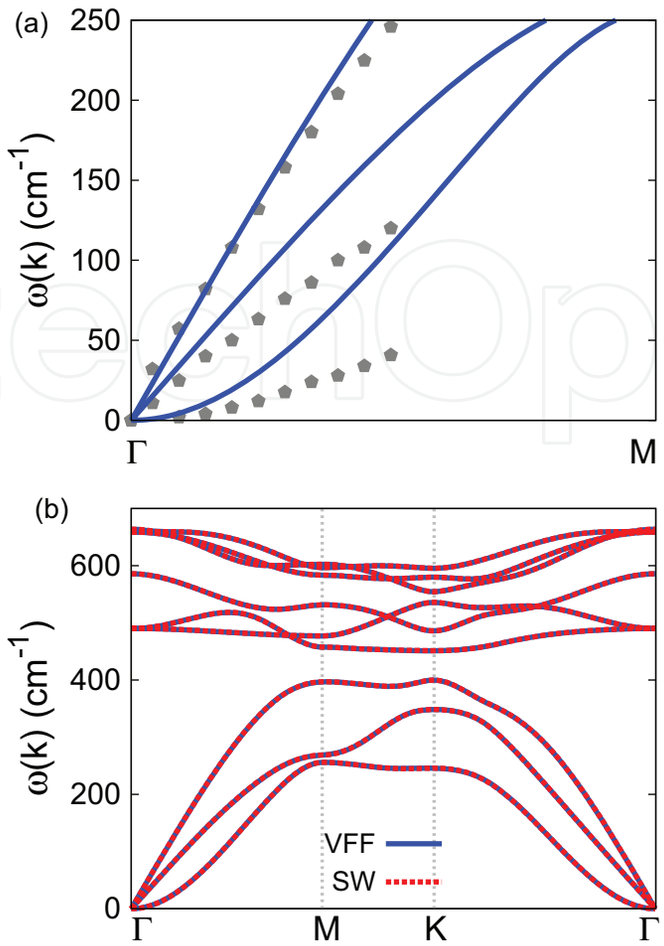

Figure 2. Phonon spectrum for single-layer 1H-ScO_2. (a) Phonon dispersion along the direction ΓM in the Brillouin zone. The results from the VFF model (lines) are comparable with the *ab initio* results (pentagons) from [12]. (b) The phonon dispersion from the SW potential is exactly the same as that from the VFF model.

	A (eV)	ρ (Å)	B (Å^4)	r_{min} (Å)	r_{max}(Å)
Sc-O	7.506	1.380	9.540	0.0	2.939

Table 11. Two-body SW potential parameters for single-layer 1H-ScO_2 used by GULP [8] as expressed in Eq. (3).

	K (eV)	θ_0 (°)	ρ_1 (Å)	ρ_2 (Å)	$r_{min\ 12}$ (Å)	$r_{max\ 12}$ (Å)	$r_{min\ 13}$ (Å)	$r_{max\ 13}$ (Å)	$r_{min\ 23}$ (Å)	$r_{max\ 23}$ (Å)
θ_{Sc-O-O}	63.576	98.222	1.380	1.380	0.0	2.939	0.0	2.939	0.0	3.460
$\theta_{Sc-O-O'}$	85.850	58.398	1.380	1.380	0.0	2.939	0.0	2.939	0.0	3.460
$\theta_{O-Sc-Sc}$	63.576	98.222	1.380	1.380	0.0	2.939	0.0	2.939	0.0	3.460

The angle θ_{ijk} in the first line indicates the bending energy for the angle with atom i as the apex.

Table 12. Three-body SW potential parameters for single-layer 1H-ScO_2 used by GULP [8] as expressed in Eq. (4).

	ϵ (eV)	σ (Å)	a	λ	γ	cos θ_0	A_L	B_L	p	q	Tol
Sc_1—O_1—O_1	1.000	1.380	2.129	0.000	1.000	0.000	7.506	2.627	4	0	0.0
Sc_1—O_1—O_3	1.000	0.000	0.000	63.576	1.000	−0.143	0.000	0.000	4	0	0.0
Sc_1—O_1—O_2	1.000	0.000	0.000	85.850	1.000	0.524	0.000	0.000	4	0	0.0
O_1—Sc_1—Sc_3	1.000	0.000	0.000	63.576	1.000	−0.143	0.000	0.000	4	0	0.0

Table 13. SW potential parameters for single-layer 1H-ScO_2 used by LAMMPS [9] as expressed in Eqs. (9) and (10).

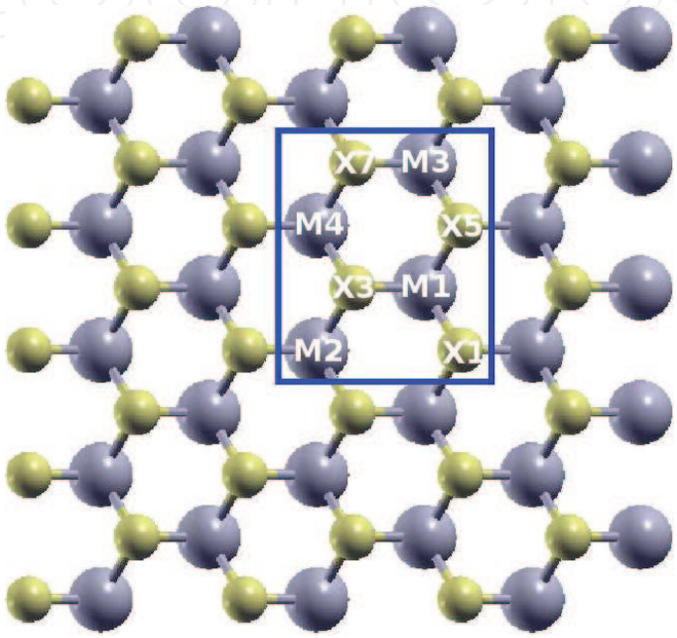

Figure 3. Twelve atom types are introduced to distinguish angles around each M atom for the single-layer 1H-MX_2. Atoms X_1, X_3, X_5, and X_7 are from the top layer. The other four atoms X_2, X_4, X_6, and X_8 are from the bottom layer, which are not displayed in the figure.

Young's modulus can be obtained by a linear fitting of the stress-strain relation in the small strain range of [0, 0.01]. The Young's modulus is 126.3 and 125.4 N/m along the armchair and zigzag directions, respectively. The Young's modulus is essentially isotropic in the armchair and zigzag directions. The Poisson's ratio from the VFF model and the SW potential is $\nu_{xy} = \nu_{yx} = 0.16$.

There is no available value for nonlinear quantities in the single-layer 1H-ScO_2. We have thus used the nonlinear parameter $B = 0.5d^4$ in Eq. (5), which is close to the value of B in most materials. The value of the third-order nonlinear elasticity D can be extracted by fitting the stress-strain relation to the function $\sigma = E\epsilon + \frac{1}{2}D\epsilon^2$ with E as the Young's modulus. The values of D from the present SW potential are −652.8 and −683.3 N/m along the armchair and zigzag directions, respectively. The ultimate stress is about 12.2 N/m at the ultimate strain of 0.19 in the armchair direction at the low temperature of 1 K. The ultimate stress is about 11.7 N/m at the ultimate strain of 0.23 in the zigzag direction at the low temperature of 1 K.

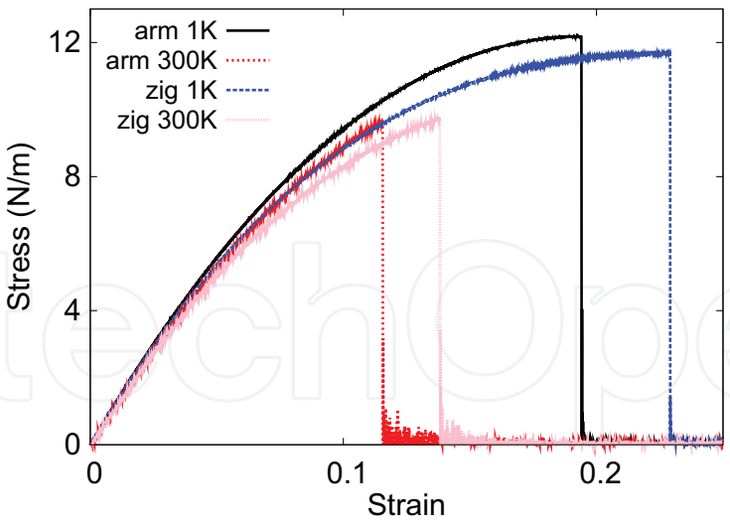

Figure 4. Stress-strain for single-layer 1H-ScO_2 of dimension 100 × 100 Å along the armchair and zigzag directions.

4. 1H-SCS_2

Most existing theoretical studies on the single-layer 1H-ScS_2 are based on the first-principles calculations. In this section, we will develop the SW potential for the single-layer 1H-ScS_2.

The structure for the single-layer 1H-ScS_2 is shown in **Figure 1** (with M = Sc and X = S). Each Sc atom is surrounded by six S atoms. These S atoms are categorized into the top group (e.g., atoms 1, 3, and 5) and bottom group (e.g., atoms 2, 4, and 6). Each S atom is connected to three Sc atoms. The structural parameters are from the first-principles calculations [12], including the lattice constant a = 3.70 Å and the bond length $d_{Sc-S} = 2.52$ Å. The resultant angles are $\theta_{ScSS} = \theta_{SScSc} = 94.467^\circ$ and $\theta_{ScSS'} = 64.076^\circ$, in which atoms S and S′ are from different (top or bottom) groups.

Table 14 shows four VFF terms for the single-layer 1H-ScS_2; one of which is the bond stretching interaction shown by Eq. (1), while the other three terms are the angle bending interaction shown by Eq. (2). These force constant parameters are determined by fitting to the acoustic branches in the phonon dispersion along the ΓM as shown in **Figure 5(a)**. The *ab initio* calculations for the phonon dispersion are from [12]. **Figure 5(b)** shows that the VFF model

VFF type	**Bond stretching**	**Angle bending**		
Expression	$\frac{1}{2}K_{Sc-S}(\Delta r)^2$	$\frac{1}{2}K_{Sc-S-S}(\Delta\theta)^2$	$\frac{1}{2}K_{Sc-S-S'}(\Delta\theta)^2$	$\frac{1}{2}K_{S-Sc-Sc}(\Delta\theta)^2$
Parameter	5.192	2.027	2.027	2.027
r_0 or θ_0	2.520	94.467	64.076	94.467

The second line gives an explicit expression for each VFF term. The third line is the force constant parameters. Parameters are in the unit of ev/Å^2 for the bond stretching interaction and in the unit of eV for the angle bending interaction. The fourth line gives the initial bond length (in the unit of Å) for the bond stretching interaction and the initial angle (in the unit of degrees) for the angle bending interaction. The angle θ_{ijk} has atom i as the apex.

Table 14. The VFF model for single-layer 1H-ScS_2.

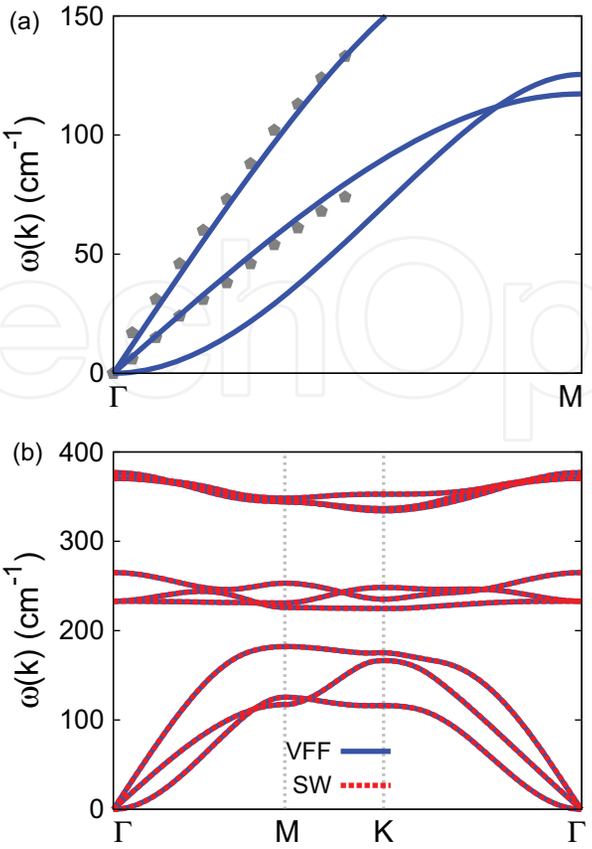

Figure 5. Phonon spectrum for single-layer 1H-ScS_2. (a) Phonon dispersion along the ΓM direction in the Brillouin zone. The results from the VFF model (lines) are comparable with the *ab initio* results (pentagons) from [12]. (b) The phonon dispersion from the SW potential is exactly the same as that from the VFF model.

and the SW potential give exactly the same phonon dispersion, as the SW potential is derived from the VFF model.

The parameters for the two-body SW potential used by GULP are shown in **Table 15**. The parameters for the three-body SW potential used by GULP are shown in **Table 16**. Some representative parameters for the SW potential used by LAMMPS are listed in **Table 17**. We note that 12 atom types have been introduced for the simulation of the single-layer 1H-ScS_2 using LAMMPS, because the angles around atom Sc in **Figure 1** (with M = Sc and X = S) are not distinguishable in LAMMPS. We have suggested two options to differentiate these angles by implementing some additional constraints in LAMMPS, which can be accomplished by modifying the source file of LAMMPS [13, 14]. According to our experience, it is not so convenient for some users to implement these constraints and recompile the LAMMPS package. Hence, in the present work, we differentiate the angles by introducing more atom types, so it is not necessary to modify the LAMMPS package. **Figure 2** (with M = Sc and X = S) shows that, for

	A (eV)	ρ (Å)	B (Å^4)	r_{min} (Å)	r_{max}(Å)
Sc—S	5.505	1.519	20.164	0.0	3.498

Table 15. Two-body SW potential parameters for single-layer 1H-ScS_2 used by GULP [8] as expressed in Eq. (3).

	K (eV)	θ_0 (°)	ρ_1 (Å)	ρ_2 (Å)	$r_{\min 12}$ (Å)	$r_{\max 12}$ (Å)	$r_{\min 13}$ (Å)	$r_{\max 13}$ (Å)	$r_{\min 23}$ (Å)	$r_{\max 23}$ (Å)
$\theta_{\mathrm{Sc-S-S}}$	22.768	94.467	1.519	1.519	0.0	3.498	0.0	3.498	0.0	4.132
$\theta_{\mathrm{Sc-S-S'}}$	27.977	64.076	1.519	1.519	0.0	3.498	0.0	3.498	0.0	4.132
$\theta_{\mathrm{S-Sc-Sc}}$	22.768	94.467	1.519	1.519	0.0	3.498	0.0	3.498	0.0	4.132

The angle θ_{ijk} in the first line indicates the bending energy for the angle with atom i as the apex.

Table 16. Three-body SW potential parameters for single-layer 1H-ScS_2 used by GULP [8] as expressed in Eq. (4).

	ϵ (eV)	σ (Å)	a	λ	γ	$\cos\theta_0$	A_L	B_L	p	q	Tol
Sc_1—S_1—S_1	1.000	1.519	2.303	0.000	1.000	0.000	5.505	3.784	4	0	0.0
Sc_1—S_1—S_3	1.000	0.000	0.000	22.768	1.000	−0.078	0.000	0.000	4	0	0.0
Sc_1—S_1—S_2	1.000	0.000	0.000	27.977	1.000	0.437	0.000	0.000	4	0	0.0
S_1—Sc_1—Sc_3	1.000	0.000	0.000	22.768	1.000	−0.078	0.000	0.000	4	0	0.0

Table 17. SW potential parameters for single-layer 1H-ScS_2 used by LAMMPS [9] as expressed in Eqs. (9) and (10).

1H-ScS_2, we can differentiate these angles around the Sc atom by assigning these six neighboring S atoms with different atom types. It can be found that twelve atom types are necessary for the purpose of differentiating all six neighbors around one Sc atom.

We use LAMMPS to perform MD simulations for the mechanical behavior of the single-layer 1H-ScS_2 under uniaxial tension at 1 and 300 K. **Figure 6** shows the stress-strain curve for the tension of a single-layer 1H-ScS_2 of dimension 100 × 100 Å. Periodic boundary conditions are applied in both armchair and zigzag directions. The single-layer 1H-ScS_2 is stretched uniaxially along the armchair or zigzag direction. The stress is calculated without involving the actual thickness of the quasi-two-dimensional structure of the single-layer 1H-ScS_2. The Young's modulus can be obtained by a linear fitting of the stress-strain relation in the small strain range of [0, 0.01]. The

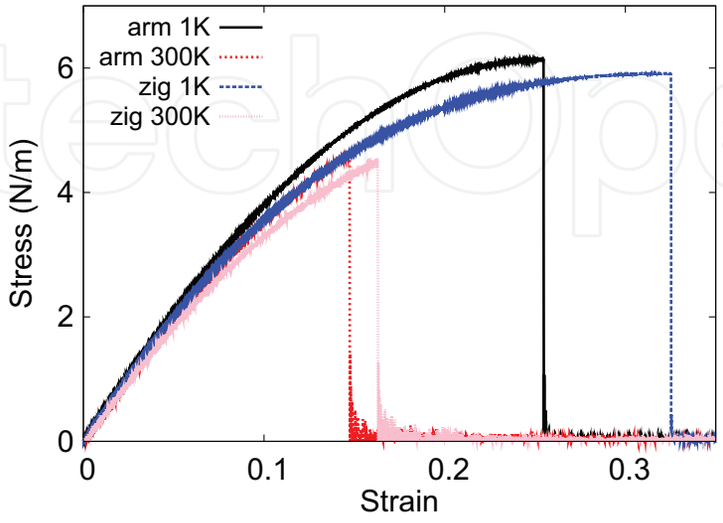

Figure 6. Stress-strain for single-layer 1H-ScS_2 of dimension 100 × 100 Å along the armchair and zigzag directions.

Young's modulus is 43.8 and 43.2 N/m along the armchair and zigzag directions, respectively. The Young's modulus is essentially isotropic in the armchair and zigzag directions. The Poisson's ratio from the VFF model and the SW potential is $\nu_{xy} = \nu_{yx} = 0.30$.

There is no available value for nonlinear quantities in the single-layer 1H-ScS_2. We have thus used the nonlinear parameter $B = 0.5d^4$ in Eq. (5), which is close to the value of B in most materials. The value of the third-order nonlinear elasticity D can be extracted by fitting the stress-strain relation to the function $\sigma = E\epsilon + \frac{1}{2}D\epsilon^2$ with E as the Young's modulus. The values of D from the present SW potential are -146.9 and -159.1 N/m along the armchair and zigzag directions, respectively. The ultimate stress is about 6.1 N/m at the ultimate strain of 0.25 in the armchair direction at the low temperature of 1 K. The ultimate stress is about 5.9 N/m at the ultimate strain of 0.32 in the zigzag direction at the low temperature of 1 K.

5. 1H-$SCSE_2$

Most existing theoretical studies on the single-layer 1H-$ScSe_2$ are based on the first-principles calculations. In this section, we will develop the SW potential for the single-layer 1H-$ScSe_2$.

The structure for the single-layer 1H-$ScSe_2$ is shown in **Figure 1** (with M = Sc and X = Se). Each Sc atom is surrounded by six Se atoms. These Se atoms are categorized into the top group (e.g., atoms 1, 3, and 5) and bottom group (e.g., atoms 2, 4, and 6). Each Se atom is connected to three Sc atoms. The structural parameters are from the first-principles calculations [12], including the lattice constant a = 3.38 Å and the bond length $d_{Sc-Se} = 2.65$ Å. The resultant angles are $\theta_{\mathrm{ScSeSe}} = \theta_{\mathrm{SeScSc}} = 92.859^\circ$ and $\theta_{\mathrm{ScSeSe'}} = 66.432^\circ$, in which atoms Se and Se′ are from different (top or bottom) groups.

Table 18 shows four VFF terms for the single-layer 1H-$ScSe_2$; one of which is the bond stretching interaction shown by Eq. (1), while the other three terms are the angle bending interaction shown by Eq. (2). These force constant parameters are determined by fitting to the acoustic branches in the phonon dispersion along the ΓM as shown in **Figure 7(a)**. The *ab initio* calculations for the phonon dispersion are from [12]. **Figure 7(b)** shows that the VFF model and the SW potential give exactly the same phonon dispersion, as the SW potential is derived from the VFF model.

VFF type	Bond stretching	Angle bending		
Expression	$\frac{1}{2}K_{\mathrm{Sc-Se}}(\Delta r)^2$	$\frac{1}{2}K_{\mathrm{Sc-Se-Se}}(\Delta\theta)^2$	$\frac{1}{2}K_{\mathrm{Sc-Se-Se'}}(\Delta\theta)^2$	$\frac{1}{2}K_{\mathrm{Se-Sc-Sc}}(\Delta\theta)^2$
Parameter	5.192	2.027	2.027	2.027
r_0 or θ_0	2.650	92.859	66.432	92.859

The second line gives an explicit expression for each VFF term. The third line is the force constant parameters. Parameters are in the unit of eV/Å^2 for the bond stretching interaction and in the unit of eV for the angle bending interaction. The fourth line gives the initial bond length (in the unit of Å) for the bond stretching interaction and the initial angle (in the unit of degrees) for the angle bending interaction. The angle θ_{ijk}has atom i as the apex.

Table 18. The VFF model for single-layer 1H-$ScSe_2$.

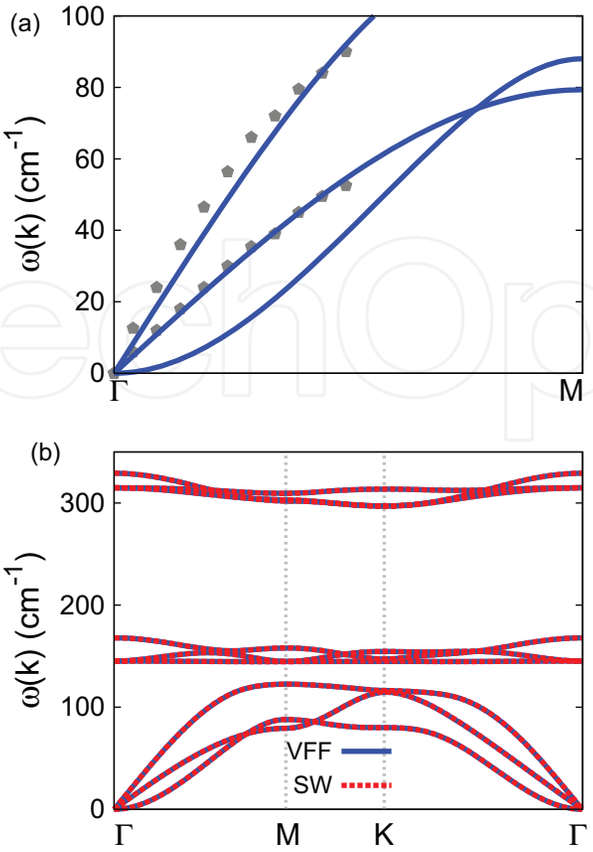

Figure 7. Phonon spectrum for single-layer 1H-$ScSe_2$. (a) Phonon dispersion along the ΓM direction in the Brillouin zone. The results from the VFF model (lines) are comparable with the *ab initio* results (pentagons) from [12]. (b) The phonon dispersion from the SW potential is exactly the same as that from the VFF model.

The parameters for the two-body SW potential used by GULP are shown in **Table 19**. The parameters for the three-body SW potential used by GULP are shown in **Table 20**. Some representative parameters for the SW potential used by LAMMPS are listed in **Table 21**. We note that 12 atom types have been introduced for the simulation of the single-layer 1H-$ScSe_2$

	A (eV)	ρ (Å)	B (Å^4)	r_{min} (Å)	r_{max}(Å)
Sc-Se	5.853	1.533	24.658	0.0	3.658

Table 19. Two-body SW potential parameters for single-layer 1H-$ScSe_2$ used by GULP [8] as expressed in Eq. (3).

	K (eV)	θ_0 (°)	ρ_1 (Å)	ρ_2 (Å)	$r_{min\ 12}$ (Å)	$r_{max\ 12}$ (Å)	$r_{min\ 13}$ (Å)	$r_{max\ 13}$ (Å)	$r_{min\ 23}$ (Å)	$r_{max\ 23}$ (Å)
$\theta_{Sc-Se-Se}$	21.292	92.859	1.533	1.533	0.0	3.658	0.0	3.658	0.0	4.327
$\theta_{Sc-Se-Se'}$	25.280	66.432	1.533	1.533	0.0	3.658	0.0	3.658	0.0	4.327
$\theta_{Se-Sc-Sc}$	21.292	92.859	1.533	1.533	0.0	3.658	0.0	3.658	0.0	4.327

The angle θ_{ijk} in the first line indicates the bending energy for the angle with atom i as the apex.

Table 20. Three-body SW potential parameters for single-layer 1H-$ScSe_2$ used by GULP [8] as expressed in Eq. (4).

using LAMMPS, because the angles around atom Sc in **Figure 1** (with M = Sc and X = Se) are not distinguishable in LAMMPS. We have suggested two options to differentiate these angles by implementing some additional constraints in LAMMPS, which can be accomplished by modifying the source file of LAMMPS [13, 14]. According to our experience, it is not so convenient for some users to implement these constraints and recompile the LAMMPS package. Hence, in the present work, we differentiate the angles by introducing more atom types, so it is not necessary to modify the LAMMPS package. **Figure 2** (with M = Sc and X = Se) shows that, for 1H-$ScSe_2$, we can differentiate these angles around the Sc atom by assigning these six neighboring Se atoms with different atom types. It can be found that twelve atom types are necessary for the purpose of differentiating all six neighbors around one Sc atom.

We use LAMMPS to perform MD simulations for the mechanical behavior of the single-layer 1H-$ScSe_2$ under uniaxial tension at 1 and 300 K. **Figure 8** shows the stress-strain curve for the tension of a single-layer 1H-$ScSe_2$ of dimension 100 × 100 Å. Periodic boundary conditions are applied in both armchair and zigzag directions. The single-layer 1H-$ScSe_2$ is stretched uniaxially along the armchair or zigzag direction. The stress is calculated without involving the actual thickness of the quasi-two-dimensional structure of the single-layer 1H-$ScSe_2$. The Young's modulus can be obtained by a linear fitting of the stress-strain relation in the small strain range of [0, 0.01]. The Young's modulus is 39.4 and 39.9 N/m along the armchair and zigzag directions, respectively.

	ϵ (eV)	σ (Å)	a	λ	γ	cos θ_0	A_L	B_L	p	q	Tol
Sc_1—Se_1-Se_1	1.000	1.533	2.386	0.000	1.000	0.000	5.853	4.464	4	0	0.0
Sc_1—Se_1—Se_3	1.000	0.000	0.000	21.292	1.000	−0.050	0.000	0.000	4	0	0.0
Sc_1—Se_1—Se_2	1.000	0.000	0.000	25.280	1.000	0.400	0.000	0.000	4	0	0.0
Se_1—Sc_1—Sc_3	1.000	0.000	0.000	21.292	1.000	−0.050	0.000	0.000	4	0	0.0

Table 21. SW potential parameters for single-layer 1H-$ScSe_2$ used by LAMMPS [9] as expressed in Eqs. (9) and (10).

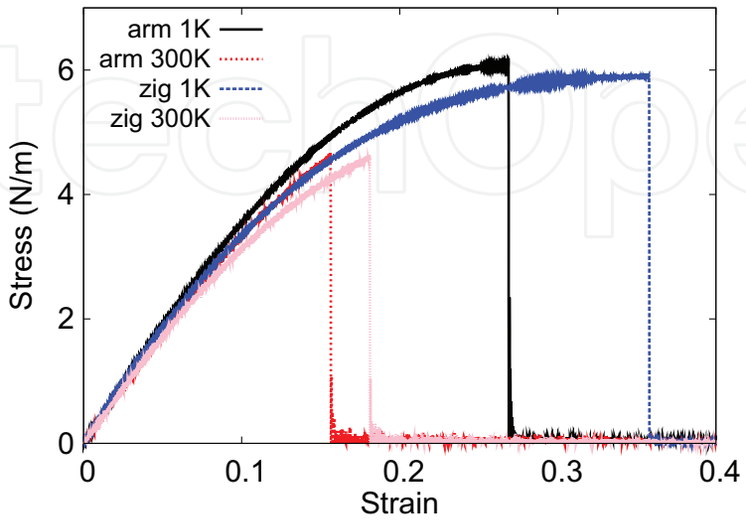

Figure 8. Stress-strain for single-layer 1H-$ScSe_2$ of dimension 100 × 100 Å along the armchair and zigzag directions.

The Young's modulus is essentially isotropic in the armchair and zigzag directions. The Poisson's ratio from the VFF model and the SW potential is $\nu_{xy} = \nu_{yx} = 0.32$.

There is no available value for nonlinear quantities in the single-layer 1H-$ScSe_2$. We have thus used the nonlinear parameter $B = 0.5d^4$ in Eq. (5), which is close to the value of B in most materials. The value of the third-order nonlinear elasticity D can be extracted by fitting the stress-strain relation to the function $\sigma = E\epsilon + \frac{1}{2}D\epsilon^2$ with E as the Young's modulus. The values of D from the present SW potential are -115.7 and -135.7 N/m along the armchair and zigzag directions, respectively. The ultimate stress is about 6.1 N/m at the ultimate strain of 0.27 in the armchair direction at the low temperature of 1 K. The ultimate stress is about 5.9 N/m at the ultimate strain of 0.35 in the zigzag direction at the low temperature of 1 K.

6. 1H-$SCTE_2$

Most existing theoretical studies on the single-layer 1H-$ScTe_2$ are based on the first-principles calculations. In this section, we will develop the SW potential for the single-layer 1H-$ScTe_2$.

The structure for the single-layer 1H-$ScTe_2$ is shown in **Figure 1** (with M = Sc and X = Te). Each Sc atom is surrounded by six Te atoms. These Te atoms are categorized into the top group (e.g., atoms 1, 3, and 5) and bottom group (e.g., atoms 2, 4, and 6). Each Te atom is connected to three Sc atoms. The structural parameters are from the first-principles calculations [12], including the lattice constant a = 3.62 Å and the bond length $d_{\mathrm{Sc-Te}} = 2.89$ Å. The resultant angles are $\theta_{\mathrm{ScTeTe}} = \theta_{\mathrm{TeScSc}} = 77.555^\circ$ and $\theta_{\mathrm{ScTeTe'}} = 87.364^\circ$, in which atoms Te and Te′ are from different (top or bottom) groups.

Table 22 shows four VFF terms for the single-layer 1H-$ScTe_2$; one of which is the bond stretching interaction shown by Eq. (1), while the other three terms are the angle bending interaction shown by Eq. (2). These force constant parameters are determined by fitting to the acoustic branches in the phonon dispersion along the ΓM as shown in **Figure 9(a)**. The *ab initio* calculations for the phonon dispersion are from [12]. There is only one (longitudinal) acoustic branch available. We find that the VFF parameters can be chosen to be the same as that of the 1H-$ScSe_2$, from which the longitudinal acoustic branch agrees with the *ab initio* results as shown in **Figure 9(a)**. It has also been shown that the VFF parameters can be the same for $TaSe_2$ and $NbSe_2$ of similar

VFF type	**Bond stretching**	**Angle bending**		
Expression	$\frac{1}{2}K_{\mathrm{Sc-Te}}(\Delta r)^2$	$\frac{1}{2}K_{\mathrm{Sc-Te-Te}}(\Delta\theta)^2$	$\frac{1}{2}K_{\mathrm{Sc-Te-Te'}}(\Delta\theta)^2$	$\frac{1}{2}K_{\mathrm{Te-Sc-Sc}}(\Delta\theta)^2$
Parameter	5.192	2.027	2.027	2.027
r_0 or θ_0	2.890	77.555	87.364	87.364

The second line gives an explicit expression for each VFF term. The third line is the force constant parameters. Parameters are in the unit of eV/Å^2 for the bond stretching interaction and in the unit of eV for the angle bending interaction. The fourth line gives the initial bond length (in the unit of Å) for the bond stretching interaction and the initial angle (in the unit of degrees) for the angle bending interaction. The angle θ_{ijk} has atom i as the apex.

Table 22. The VFF model for single-layer 1H-$ScTe_2$.

http://dx.doi.org/10.5772/intechopen.71929

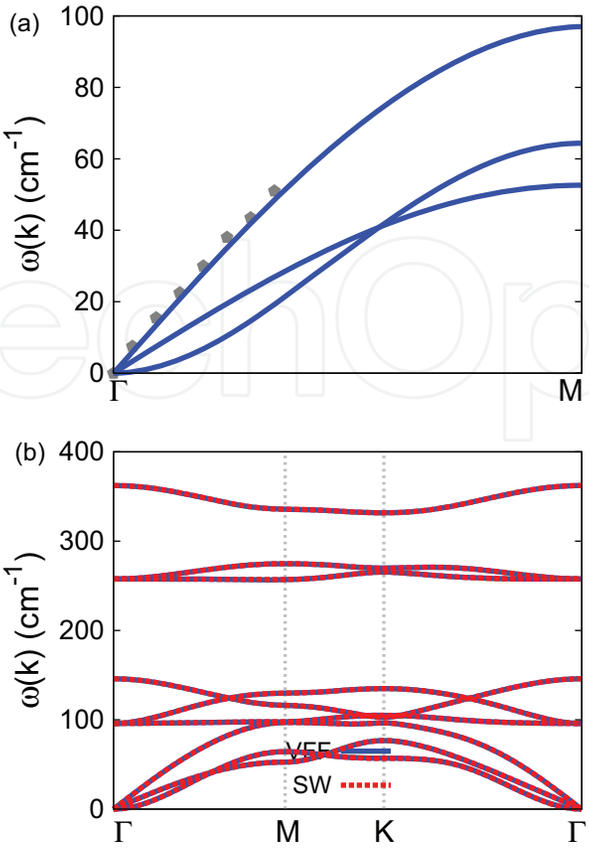

Figure 9. Phonon spectrum for single-layer 1H-$ScTe_2$. (a) Phonon dispersion along the ΓM direction in the Brillouin zone. The results from the VFF model (lines) are comparable with the *ab initio* results (pentagons) from [12]. (b) The phonon dispersion from the SW potential is exactly the same as that from the VFF model.

structure [15]. **Figure 9(b)** shows that the VFF model and the SW potential give exactly the same phonon dispersion, as the SW potential is derived from the VFF model.

The parameters for the two-body SW potential used by GULP are shown in **Table 23**. The parameters for the three-body SW potential used by GULP are shown in **Table 24**. Some representative parameters for the SW potential used by LAMMPS are listed in **Table 25**. We note that 12 atom types have been introduced for the simulation of the single-layer 1H-$ScTe_2$ using LAMMPS, because the angles around atom Sc in **Figure 1** (with M = Sc and X = Te) are not distinguishable in LAMMPS. We have suggested two options to differentiate these angles by implementing some additional constraints in LAMMPS, which can be accomplished by modifying the source file of LAMMPS [13, 14]. According to our experience, it is not so convenient for some users to implement these constraints and recompile the LAMMPS package. Hence, in the present work, we differentiate the angles by introducing more atom types, so it is not necessary to modify the LAMMPS package. **Figure 2** (with M = Sc and X = Te) shows

	A (eV)	ρ (Å)	B (Å^4)	$r_{\min}$ (Å)	$r_{\max}$ (Å)
Sc-Te	4.630	1.050	34.879	0.0	3.761

Table 23. Two-body SW potential parameters for single-layer 1H-$ScTe_2$ used by GULP [8] as expressed in Eq. (3).

	K (eV)	θ_0 (°)	ρ_1 (Å)	ρ_2 (Å)	$r_{\min 12}$ (Å)	$r_{\max 12}$ (Å)	$r_{\min 13}$ (Å)	$r_{\max 13}$ (Å)	$r_{\min 23}$ (Å)	$r_{\max 23}$ (Å)
$\theta_{\mathrm{Sc-Te-Te}}$	11.848	77.555	1.050	1.050	0.0	3.761	0.0	3.761	0.0	4.504
$\theta_{\mathrm{Sc-Te-Te'}}$	11.322	87.364	1.050	1.050	0.0	3.761	0.0	3.761	0.0	4.504
$\theta_{\mathrm{Te-Sc-Sc}}$	11.848	77.555	1.050	1.050	0.0	3.761	0.0	3.761	0.0	4.504

The angle θ_{ijk} in the first line indicates the bending energy for the angle with atom i as the apex.

Table 24. Three-body SW potential parameters for single-layer 1H-$ScTe_2$ used by GULP [8] as expressed in Eq. (4).

	ϵ (eV)	σ (Å)	a	λ	γ	$\cos\theta_0$	A_L	B_L	p	q	Tol
Sc_1—Te_1—Te_1	1.000	1.050	3.581	0.000	1.000	0.000	4.630	28.679	4	0	0.0
Sc_1—Te_1—Te_3	1.000	0.000	0.000	11.848	1.000	0.216	0.000	0.000	4	0	0.0
Sc_1—Te_1—Te_2	1.000	0.000	0.000	11.322	1.000	0.046	0.000	0.000	4	0	0.0
Te_1—Sc_1—Sc_3	1.000	0.000	0.000	11.848	1.000	0.216	0.000	0.000	4	0	0.0

Table 25. SW potential parameters for single-layer 1H-$ScTe_2$ used by LAMMPS [9] as expressed in Eqs. (9) and (10).

that, for 1H-$ScTe_2$, we can differentiate these angles around the Sc atom by assigning these six neighboring Te atoms with different atom types. It can be found that twelve atom types are necessary for the purpose of differentiating all six neighbors around one Sc atom.

We use LAMMPS to perform MD simulations for the mechanical behavior of the single-layer 1H-$ScTe_2$ under uniaxial tension at 1 and 300 K. **Figure 10** shows the stress-strain curve for the tension of a single-layer 1H-$ScTe_2$ of dimension 100 × 100 Å. Periodic boundary conditions are applied in both armchair and zigzag directions. The single-layer 1H-$ScTe_2$ is stretched uniaxially along the armchair or zigzag direction. The stress is calculated without involving the actual thickness of the quasi-two-dimensional structure of the single-layer 1H-$ScTe_2$. The Young's modulus can be obtained by a linear fitting of the stress-strain relation in the small

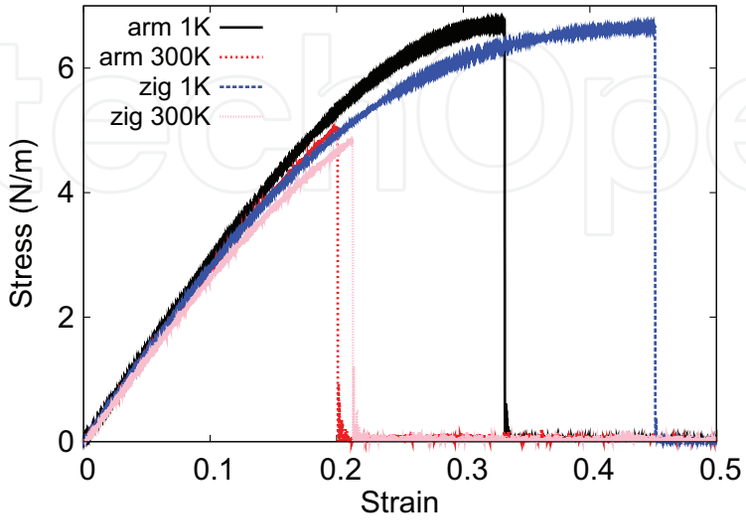

Figure 10. Stress-strain for single-layer 1H-$ScTe_2$ of dimension 100 × 100 Å along the armchair and zigzag directions.

strain range of [0, 0.01]. The Young's modulus is 29.3 and 28.8 N/m along the armchair and zigzag directions, respectively. The Young's modulus is essentially isotropic in the armchair and zigzag directions. The Poisson's ratio from the VFF model and the SW potential is $\nu_{xy} = \nu_{yx} = 0.38$.

There is no available value for nonlinear quantities in the single-layer 1H-$ScTe_2$. We have thus used the nonlinear parameter $B = 0.5d^4$ in Eq. (5), which is close to the value of B in most materials. The value of the third-order nonlinear elasticity D can be extracted by fitting the stress-strain relation to the function $\sigma = E\epsilon + \frac{1}{2}D\epsilon^2$ with E as the Young's modulus. The values of D from the present SW potential are -43.2 and -59.3 N/m along the armchair and zigzag directions, respectively. The ultimate stress is about 6.7 N/m at the ultimate strain of 0.33 in the armchair direction at the low temperature of 1 K. The ultimate stress is about 6.7 N/m at the ultimate strain of 0.45 in the zigzag direction at the low temperature of 1 K.

7. 1H-$TITE_2$

Most existing theoretical studies on the single-layer 1H-$TiTe_2$ are based on the first-principles calculations. In this section, we will develop both VFF model and the SW potential for the single-layer 1H-$TiTe_2$.

The structure for the single-layer 1H-$TiTe_2$ is shown in **Figure 1** (with M = Ti and X = Se). Each Ti atom is surrounded by six Te atoms. These Te atoms are categorized into the top group (e.g., atoms 1, 3, and 5) and bottom group (e.g., atoms 2, 4, and 6). Each Te atom is connected to three Ti atoms. The structural parameters are from [12], including the lattice constant $a = 3.62$ Å and the bond length $d_{\mathrm{Ti-Te}} = 2.75$ Å. The resultant angles are $\theta_{\mathrm{TiTeTe}} = \theta_{\mathrm{TeTiTi}} = 82.323^\circ$ and $\theta_{\mathrm{TiTeTe'}} = 81.071^\circ$, in which atoms Te and Te′ are from different (top or bottom) groups.

Table 26 shows the VFF terms for the 1H-$TiTe_2$; one of which is the bond stretching interaction shown by Eq. (1), while the other terms are the angle bending interaction shown by Eq. (2). These force constant parameters are determined by fitting to the three acoustic branches in the phonon dispersion along the ΓM as shown in **Figure 11(a)**. The *ab initio* calculations for the

VFF type	**Bond stretching**	**Angle bending**		
Expression	$\frac{1}{2}K_{\mathrm{Ti-Te}}(\Delta r)^2$	$\frac{1}{2}K_{\mathrm{Ti-Te-Te}}(\Delta\theta)^2$	$\frac{1}{2}K_{\mathrm{Ti-Te-Te'}}(\Delta\theta)^2$	$\frac{1}{2}K_{\mathrm{Te-Ti-Ti}}(\Delta\theta)^2$
Parameter	4.782	3.216	3.216	3.216
r_0 or θ_0	2.750	82.323	81.071	82.323

The second line gives an explicit expression for each VFF term. The third line is the force constant parameters. Parameters are in the unit of eV/Å^2 for the bond stretching interaction and in the unit of eV for the angle bending interaction. The fourth line gives the initial bond length (in the unit of Å) for the bond stretching interaction and the initial angle (in the unit of degrees) for the angle bending interaction. The angle θ_{ijk} has atom i as the apex.

Table 26. The VFF model for single-layer 1H-$TiTe_2$.

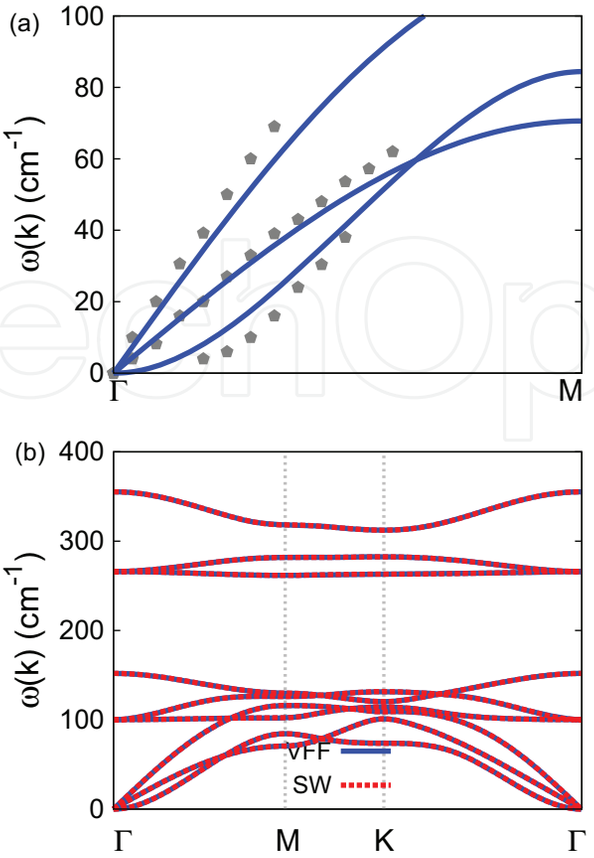

Figure 11. Phonon dispersion for single-layer 1H-$TiTe_2$. (a) The VFF model is fitted to the three acoustic branches in the long wave limit along the *Γ*M direction. The *ab initio* results (gray pentagons) are from Ref. [12]. (b) The VFF model (blue lines) and the SW potential (red lines) give the same phonon dispersion for single-layer 1H-$TiTe_2$ along ΓMKΓ.

phonon dispersion are from [12]. **Figure 11(b)** shows that the VFF model and the SW potential give exactly the same phonon dispersion, as the SW potential is derived from the VFF model.

The parameters for the two-body SW potential used by GULP are shown in **Table 27**. The parameters for the three-body SW potential used by GULP are shown in **Table 28**. Parameters for the SW potential used by LAMMPS are listed in **Table 29**. We note that 12 atom types have been introduced for the simulation of the single-layer 1H-$TiTe_2$ using LAMMPS, because the angles around atom Ti in **Figure 1** (with M = Ti and X = Te) are not distinguishable in LAMMPS. We have suggested two options to differentiate these angles by implementing some additional constraints in LAMMPS, which can be accomplished by modifying the source file of LAMMPS [13, 14]. According to our experience, it is not so convenient for some users to implement these constraints and recompile the LAMMPS package. Hence, in the present work, we differentiate the angles by introducing more atom types, so it is not necessary to modify the LAMMPS package. **Figure 2** (with M = Ti and X = Te) shows that, for 1H-$TiTe_2$, we

	A (eV)	ρ (Å)	B (Å^4)	r_{min} (Å)	r_{max} (Å)
Ti-Te	4.414	1.173	28.596	0.0	3.648

Table 27. Two-body SW potential parameters for single-layer 1H-$TiTe_2$ used by GULP [8] as expressed in Eq. (3).

	K (eV)	θ_0 (°)	ρ_1 (Å)	ρ_2 (Å)	$r_{\min 12}$ (Å)	$r_{\max 12}$ (Å)	$r_{\min 13}$ (Å)	$r_{\max 13}$ (Å)	$r_{\min 23}$ (Å)	$r_{\max 23}$ (Å)
$\theta_{\text{Ti–Te–Te}}$	22.321	82.323	1.173	1.173	0.0	3.648	0.0	3.648	0.0	4.354
$\theta_{\text{Ti–Te–Te}'}$	22.463	81.071	1.173	1.173	0.0	3.648	0.0	3.648	0.0	4.354
$\theta_{\text{Te–Ti–Ti}}$	11.321	82.323	1.173	1.173	0.0	3.648	0.0	3.648	0.0	4.354

The angle θ_{ijk} in the first line indicates the bending energy for the angle with atom i as the apex.

Table 28. Three-body SW potential parameters for single-layer 1H-$TiTe_2$ used by GULP [8] as expressed in Eq. (4).

	ϵ (eV)	σ (Å)	a	λ	γ	$\cos\theta_0$	A_L	B_L	p	q	Tol
Ti_1-Te_1-Te_1	1.000	1.173	3.110	0.000	1.000	0.000	4.414	15.100	4	0	0.0
Ti_1-Te_1-Te_3	1.000	0.000	0.000	22.321	1.000	0.134	0.000	0.000	4	0	0.0
Ti_1-Te_1-Te_2	1.000	0.000	0.000	22.463	1.000	0.155	0.000	0.000	4	0	0.0
Te_1-Ti_1-Ti_3	1.000	0.000	0.000	22.321	1.000	0.134	0.000	0.000	4	0	0.0

Atom types in the first column are displayed in **Figure 2** (with M = Ti and X = Te).

Table 29. SW potential parameters for single-layer 1H-$TiTe_2$ used by LAMMPS [9] as expressed in Eqs. (9) and (10).

can differentiate these angles around the Ti atom by assigning these six neighboring Te atoms with different atom types. It can be found that twelve atom types are necessary for the purpose of differentiating all six neighbors around one Ti atom.

We use LAMMPS to perform MD simulations for the mechanical behavior of the single-layer 1H-$TiTe_2$ under uniaxial tension at 1 and 300 K. **Figure 12** shows the stress-strain curve for the tension of a single-layer 1H-$TiTe_2$ of dimension 100 × 100 Å. Periodic boundary conditions are applied in both armchair and zigzag directions. The single-layer 1H-$TiTe_2$ is stretched uniaxially along the armchair or zigzag direction. The stress is calculated without involving the actual

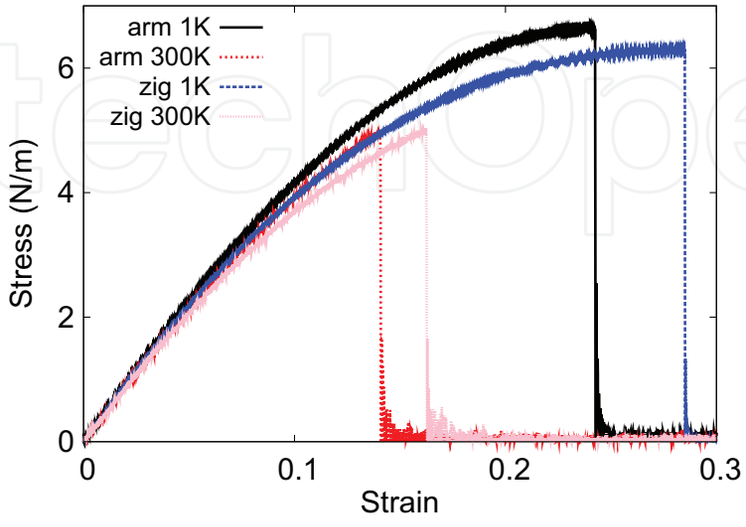

Figure 12. Stress-strain for single-layer 1H-$TiTe_2$ of dimension 100 × 100 Å along the armchair and zigzag directions.

thickness of the quasi-two-dimensional structure of the single-layer 1H-$TiTe_2$. The Young's modulus can be obtained by a linear fitting of the stress-strain relation in the small strain range of [0, 0.01]. The Young's modulus is 47.9 and 47.1 N/m along the armchair and zigzag directions, respectively. The Young's modulus is essentially isotropic in the armchair and zigzag directions. The Poisson's ratio from the VFF model and the SW potential is $\nu_{xy} = \nu_{yx} = 0.29$.

There is no available value for the nonlinear quantities in the single-layer 1H-$TiTe_2$. We have thus used the nonlinear parameter $B = 0.5d^4$ in Eq. (5), which is close to the value of B in most materials. The value of the third-order nonlinear elasticity D can be extracted by fitting the stress-strain relation to the function $\sigma = E\epsilon + \frac{1}{2}D\epsilon^2$ with E as the Young's modulus. The values of D from the present SW potential are -158.6 and -176.3 N/m along the armchair and zigzag directions, respectively. The ultimate stress is about 6.6 N/m at the ultimate strain of 0.24 in the armchair direction at the low temperature of 1 K. The ultimate stress is about 6.3 N/m at the ultimate strain of 0.28 in the zigzag direction at the low temperature of 1 K.

8. 1H-VO_2

Most existing theoretical studies on the single-layer 1H-VO_2 are based on the first-principles calculations. In this section, we will develop the SW potential for the single-layer 1H-VO_2.

The structure for the single-layer 1H-VO_2 is shown in **Figure 1** (with M = V and X = O). Each V atom is surrounded by six O atoms. These O atoms are categorized into the top group (e.g., atoms 1, 3, and 5) and bottom group (e.g., atoms 2, 4, and 6). Each O atom is connected to three V atoms. The structural parameters are from the first-principles calculations [12], including the lattice constant $a = 2.70$ Å and the bond length $d_{\mathrm{V-O}} = 1.92$ Å. The resultant angles are $\theta_{\mathrm{VOO}} = \theta_{\mathrm{OVV}} = 89.356^\circ$ and $\theta_{\mathrm{VOO'}} = 71.436^\circ$, in which atoms O and O′ are from different (top or bottom) groups.

Table 30 shows four VFF terms for the single-layer 1H-VO_2; one of which is the bond stretching interaction shown by Eq. (1), while the other three terms are the angle bending interaction shown by Eq. (2). These force constant parameters are determined by fitting to the acoustic branches in the phonon dispersion along the ΓM as shown in **Figure 13(a)**. The *ab initio* calculations for the phonon dispersion are from [12]. **Figure 13(b)** shows that the VFF

VFF type	Bond stretching	Angle bending		
Expression	$\frac{1}{2}K_{\mathrm{V-O}}(\Delta r)^2$	$\frac{1}{2}K_{\mathrm{V-O-O}}(\Delta\theta)^2$	$\frac{1}{2}K_{\mathrm{V-O-O'}}(\Delta\theta)^2$	$\frac{1}{2}K_{\mathrm{O-V-V}}(\Delta\theta)^2$
Parameter	9.417	4.825	4.825	4.825
r_0 or θ_0	1.920	89.356	71.436	89.356

The second line gives an explicit expression for each VFF term. The third line is the force constant parameters. Parameters are in the unit of $\mathrm{eV/\AA^2}$ for the bond stretching interaction and in the unit of eV for the angle bending interaction. The fourth line gives the initial bond length (in the unit of Å) for the bond stretching interaction and the initial angle (in the unit of degrees) for the angle bending interaction. The angle θ_{ijk} has atom i as the apex.

Table 30. The VFF model for single-layer 1H-VO_2.

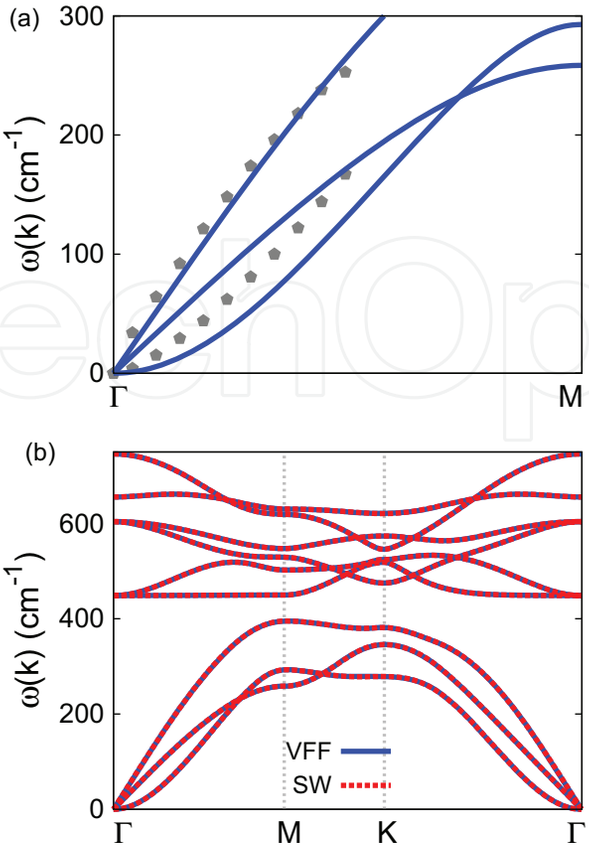

Figure 13. Phonon spectrum for single-layer 1H-VO_2. (a) Phonon dispersion along the ΓM direction in the Brillouin zone. The results from the VFF model (lines) are comparable with the *ab initio* results (pentagons) from [12]. (b) The phonon dispersion from the SW potential is exactly the same as that from the VFF model.

model and the SW potential give exactly the same phonon dispersion, as the SW potential is derived from the VFF model.

The parameters for the two-body SW potential used by GULP are shown in **Table 31**. The parameters for the three-body SW potential used by GULP are shown in **Table 32**. Some representative

	A (eV)	ρ (Å)	B (Å^4)	r_{min} (Å)	r_{max} (Å)
V-O	5.105	1.011	6.795	0.0	2.617

Table 31. Two-body SW potential parameters for single-layer 1H-VO_2 used by GULP [8] as expressed in Eq. (3).

	K (eV)	θ_0 (°)	ρ_1 (Å)	ρ_2 (Å)	$r_{min\,12}$ (Å)	$r_{max\,12}$ (Å)	$r_{min\,13}$ (Å)	$r_{max\,13}$ (Å)	$r_{min\,23}$ (Å)	$r_{max\,23}$ (Å)
θ_{V-O-O}	43.951	89.356	1.011	1.011	0.0	2.617	0.0	2.617	0.0	3.105
$\theta_{V-O-O'}$	48.902	71.436	1.011	1.011	0.0	2.617	0.0	2.617	0.0	3.105
θ_{O-V-V}	43.951	89.356	1.011	1.011	0.0	2.617	0.0	2.617	0.0	3.105

The angle θ_{ijk} in the first line indicates the bending energy for the angle with atom i as the apex.

Table 32. Three-body SW potential parameters for single-layer 1H-VO_2 used by GULP [8] as expressed in Eq. (4).

	ϵ (eV)	σ (Å)	a	λ	γ	cos θ_0	A_L	B_L	p	q	Tol
V_1-O_1-O_1	1.000	1.011	2.589	0.000	1.000	0.000	5.105	6.509	4	0	0.0
V_1-O_1-O_3	1.000	0.000	0.000	43.951	1.000	0.011	0.000	0.000	4	0	0.0
V_1-O_1-O_2	1.000	0.000	0.000	48.902	1.000	0.318	0.000	0.000	4	0	0.0
O_1-V_1-V_3	1.000	0.000	0.000	43.951	1.000	0.011	0.000	0.000	4	0	0.0

Table 33. SW potential parameters for single-layer 1H-VO_2 used by LAMMPS [9] as expressed in Eqs. (9) and (10).

parameters for the SW potential used by LAMMPS are listed in **Table 33**. We note that 12 atom types have been introduced for the simulation of the single-layer 1H-VO_2 using LAMMPS, because the angles around atom V in **Figure 1** (with M = V and X = O) are not distinguishable in LAMMPS. We have suggested two options to differentiate these angles by implementing some additional constraints in LAMMPS, which can be accomplished by modifying the source file of LAMMPS [13, 14]. According to our experience, it is not so convenient for some users to implement these constraints and recompile the LAMMPS package. Hence, in the present work, we differentiate the angles by introducing more atom types, so it is not necessary to modify the LAMMPS package. **Figure 2** (with M = V and X = O) shows that, for 1H-VO_2, we can differentiate these angles around the V atom by assigning these six neighboring O atoms with different atom types. It can be found that twelve atom types are necessary for the purpose of differentiating all six neighbors around one V atom.

We use LAMMPS to perform MD simulations for the mechanical behavior of the single-layer 1H-VO_2 under uniaxial tension at 1 and 300 K. **Figure 14** shows the stress-strain curve for the tension of a single-layer 1H-VO_2 of dimension 100 × 100 Å. Periodic boundary conditions are applied in both armchair and zigzag directions. The single-layer 1H-VO_2 is stretched uniaxially along the armchair or zigzag direction. The stress is calculated without involving the actual thickness of the quasi-two-dimensional structure of the single-layer 1H-VO_2. The Young's modulus can be obtained by a linear fitting of the stress-strain relation in the

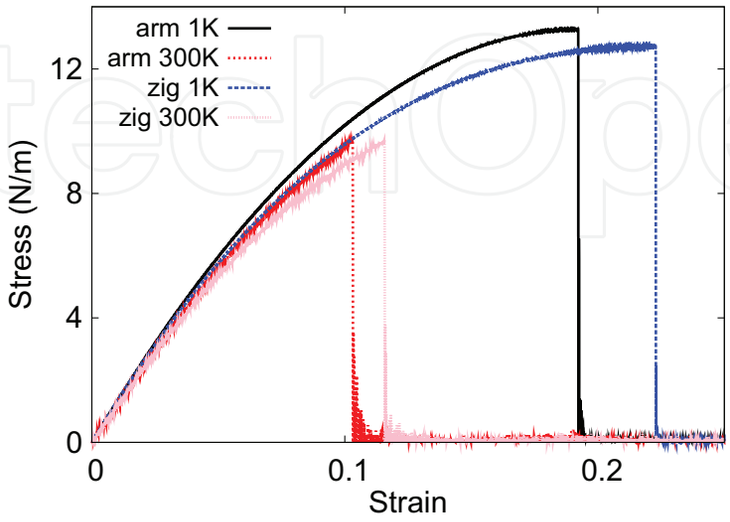

Figure 14. Stress-strain for single-layer 1H-VO_2 of dimension 100 × 100 Å along the armchair and zigzag directions.

small strain range of [0, 0.01]. The Young's modulus is 133.0 and 132.9 N/m along the armchair and zigzag directions, respectively. The Young's modulus is essentially isotropic in the armchair and zigzag directions. The Poisson's ratio from the VFF model and the SW potential is $\nu_{xy} = \nu_{yx} = 0.17$.

There is no available value for nonlinear quantities in the single-layer 1H-VO_2. We have thus used the nonlinear parameter $B = 0.5d^4$ in Eq. (5), which is close to the value of B in most materials. The value of the third-order nonlinear elasticity D can be extracted by fitting the stress-strain relation to the function $\sigma = E\epsilon + \frac{1}{2}D\epsilon^2$ with E as the Young's modulus. The values of D from the present SW potential are -652.3 and -705.8 N/m along the armchair and zigzag directions, respectively. The ultimate stress is about 13.3 N/m at the ultimate strain of 0.19 in the armchair direction at the low temperature of 1 K. The ultimate stress is about 12.7 N/m at the ultimate strain of 0.22 in the zigzag direction at the low temperature of 1 K.

9. 1H-VS_2

Most existing theoretical studies on the single-layer 1H-VS_2 are based on the first-principles calculations. In this section, we will develop both VFF model and the SW potential for the single-layer 1H-VS_2.

The structure for the single-layer 1H-VS_2 is shown in **Figure 1** (with M = V and X = S). Each V atom is surrounded by six S atoms. These S atoms are categorized into the top group (e.g., atoms 1, 3, and 5) and bottom group (e.g., atoms 2, 4, and 6). Each S atom is connected to three V atoms. The structural parameters are from [12], including the lattice constant $a = 3.09$ Å and the bond length $d_{\mathrm{V-S}} = 2.31$ Å. The resultant angles are $\theta_{\mathrm{VSS}} = \theta_{\mathrm{SVV}} = 83.954^\circ$ and $\theta_{\mathrm{VSS'}} = 78.878^\circ$, in which atoms S and S′ are from different (top or bottom) groups.

Table 34 shows the VFF terms for the 1H-VS_2; one of which is the bond stretching interaction shown by Eq. (1), while the other terms are the angle bending interaction shown by Eq. (2). These force constant parameters are determined by fitting to the three acoustic branches in the phonon dispersion along the ΓM as shown in **Figure 15(a)**. The *ab initio* calculations for the phonon dispersion are from [16]. The phonon dispersion can also be found in other *ab initio*

VFF type	Bond stretching	Angle bending		
Expression	$\frac{1}{2}K_{\mathrm{V-S}}(\Delta r)^2$	$\frac{1}{2}K_{\mathrm{V-S-S}}(\Delta\theta)^2$	$\frac{1}{2}K_{\mathrm{V-S-S'}}(\Delta\theta)^2$	$\frac{1}{2}K_{\mathrm{S-V-V}}(\Delta\theta)^2$
Parameter	8.392	4.074	4.074	4.074
r_0 or θ_0	2.310	83.954	78.878	83.954

The second line gives an explicit expression for each VFF term. The third line is the force constant parameters. Parameters are in the unit of eV/Å^2 for the bond stretching interaction and in the unit of eV for the angle bending interaction. The fourth line gives the initial bond length (in the unit of Å) for the bond stretching interaction and the initial angle (in the unit of degrees) for the angle bending interaction. The angle θ_{ijk} has atom i as the apex.

Table 34. The VFF model for single-layer 1H-VS_2.

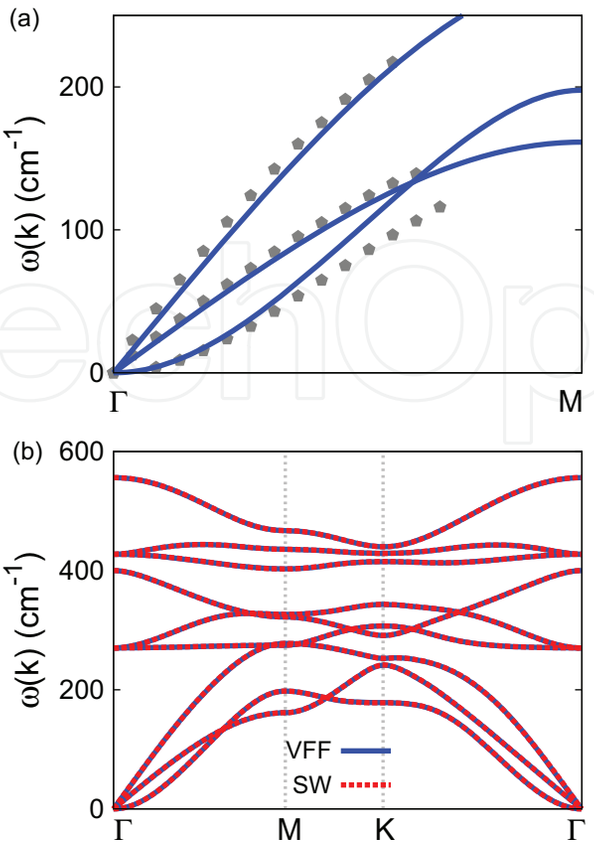

Figure 15. Phonon dispersion for single-layer 1H-VS_2. (a) The VFF model is fitted to the three acoustic branches in the long wave limit along the ΓM direction. The *ab initio* results (gray pentagons) are from [16]. (b) The VFF model (blue lines) and the SW potential (red lines) give the same phonon dispersion for single-layer 1H-VS_2 along ΓMKΓ.

calculations [12]. **Figure 15(b)** shows that the VFF model and the SW potential give exactly the same phonon dispersion, as the SW potential is derived from the VFF model.

The parameters for the two-body SW potential used by GULP are shown in **Table 35**. The parameters for the three-body SW potential used by GULP are shown in **Table 36**. Parameters

	A (eV)	ρ (Å)	B (Å^4)	r_{min} (Å)	r_{max}(Å)
V—S	5.714	1.037	14.237	0.0	3.084

Table 35. Two-body SW potential parameters for single-layer 1H-VS_2 used by GULP [8] as expressed in Eq. (3).

	K (eV)	θ_0 (°)	ρ_1 (Å)	ρ_2 (Å)	$r_{min\ 12}$ (Å)	$r_{max\ 12}$ (Å)	$r_{min\ 13}$ (Å)	$r_{max\ 13}$ (Å)	$r_{min\ 23}$ (Å)	$r_{max\ 23}$ (Å)
θ_{V-S-S}	30.059	83.954	1.037	1.037	0.0	3.084	0.0	3.084	0.0	3.676
$\theta_{V-S-S'}$	30.874	78.878	1.037	1.037	0.0	3.084	0.0	3.084	0.0	3.676
θ_{S-V-V}	30.059	83.954	1.037	1.037	0.0	3.084	0.0	3.084	0.0	3.676

The angle θ_{ijk} in the first line indicates the bending energy for the angle with atom i as the apex.

Table 36. Three-body SW potential parameters for single-layer 1H-VS_2 used by GULP [8] as expressed in Eq. (4).

	ϵ (eV)	σ (Å)	a	λ	γ	cos θ_0	A_L	B_L	p	q	Tol
V_1—S_1—S_1	1.000	1.037	2.973	0.000	1.000	0.000	5.714	12.294	4	0	0.0
V_1—S_1—S_3	1.000	0.000	0.000	30.059	1.000	0.105	0.000	0.000	4	0	0.0
V_1—S_1—S_2	1.000	0.000	0.000	30.874	1.000	0.193	0.000	0.000	4	0	0.0
S_1—V_1—V_3	1.000	0.000	0.000	30.059	1.000	0.105	0.000	0.000	4	0	0.0

Atom types in the first column are displayed in **Figure 2** (with M = V and X = S).

Table 37. SW potential parameters for single-layer 1H-VS_2 used by LAMMPS [9] as expressed in Eqs. (9) and (10).

for the SW potential used by LAMMPS are listed in **Table 37**. We note that 12 atom types have been introduced for the simulation of the single-layer 1H-VS_2 using LAMMPS, because the angles around atom V in **Figure 1** (with M = V and X = S) are not distinguishable in LAMMPS. We have suggested two options to differentiate these angles by implementing some additional constraints in LAMMPS, which can be accomplished by modifying the source file of LAMMPS [13, 14]. According to our experience, it is not so convenient for some users to implement these constraints and recompile the LAMMPS package. Hence, in the present work, we differentiate the angles by introducing more atom types, so it is not necessary to modify the LAMMPS package. **Figure 2** (with M = V and X = S) shows that, for 1H-VS_2, we can differentiate these angles around the V atom by assigning these six neighboring S atoms with different atom types. It can be found that twelve atom types are necessary for the purpose of differentiating all six neighbors around one V atom.

We use LAMMPS to perform MD simulations for the mechanical behavior of the single-layer 1H-VS_2 under uniaxial tension at 1 and 300 K. **Figure 16** shows the stress-strain curve for the tension of a single-layer 1H-VS_2 of dimension 100 × 100 Å. Periodic boundary conditions are applied in both armchair and zigzag directions. The single-layer 1H-VS_2 is stretched uniaxially along the armchair or zigzag direction. The stress is calculated without involving the actual

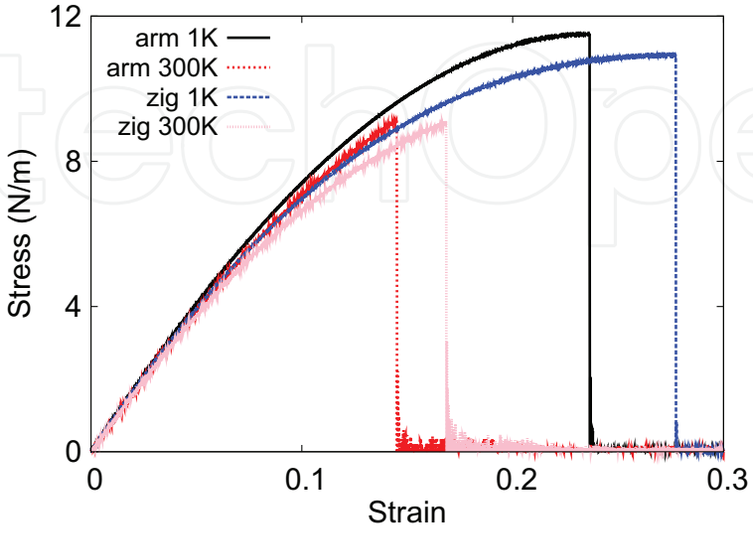

Figure 16. Stress-strain for single-layer 1H-VS_2 of dimension 100 × 100 Å along the armchair and zigzag directions.

thickness of the quasi-two-dimensional structure of the single-layer 1H-VS_2. The Young's modulus can be obtained by a linear fitting of the stress-strain relation in the small strain range of [0, 0.01]. The Young's modulus is 86.5 and 85.3 N/m along the armchair and zigzag directions, respectively. The Young's modulus is essentially isotropic in the armchair and zigzag directions. The Poisson's ratio from the VFF model and the SW potential is $\nu_{xy} = \nu_{yx} = 0.28$.

There is no available value for the nonlinear quantities in the single-layer 1H-VS_2. We have thus used the nonlinear parameter $B = 0.5d^4$ in Eq. (5), which is close to the value of B in most materials. The value of the third-order nonlinear elasticity D can be extracted by fitting the stress-strain relation to the function $\sigma = E\epsilon + \frac{1}{2}D\epsilon^2$ with E as the Young's modulus. The values of D from the present SW potential are -302.0 and -334.7 N/m along the armchair and zigzag directions, respectively. The ultimate stress is about 11.5 N/m at the ultimate strain of 0.23 in the armchair direction at the low temperature of 1 K. The ultimate stress is about 10.9 N/m at the ultimate strain of 0.27 in the zigzag direction at the low temperature of 1 K.

10. 1H-VSe_2

Most existing theoretical studies on the single-layer 1H-VSe_2 are based on the first-principles calculations. In this section, we will develop both VFF model and the SW potential for the single-layer 1H-VSe_2.

The structure for the single-layer 1H-VSe_2 is shown in **Figure 1** (with M = V and X = Se). Each V atom is surrounded by six Se atoms. These Se atoms are categorized into the top group (e.g., atoms 1, 3, and 5) and bottom group (e.g., atoms 2, 4, and 6). Each Se atom is connected to three V atoms. The structural parameters are from [12], including the lattice constant $a = 3.24$ Å and the bond length $d_{\mathrm{V—Se}} = 2.45$ Å. The resultant angles are $\theta_{\mathrm{VSeSe}} = \theta_{\mathrm{SeVV}} = 82.787^\circ$ and $\theta_{\mathrm{VSeSe'}} = 80.450^\circ$, in which atoms Se and Se′ are from different (top or bottom) groups.

Table 38 shows the VFF terms for the 1H-VSe_2; one of which is the bond stretching interaction shown by Eq. (1), while the other terms are the angle bending interaction shown by Eq. (2). These force constant parameters are determined by fitting to the three acoustic branches in the phonon dispersion along the ΓM as shown in **Figure 17(a)**. The *ab initio* calculations for the

VFF type	Bond stretching	Angle bending		
Expression	$\frac{1}{2}K_{\mathrm{V—Se}}(\Delta r)^2$	$\frac{1}{2}K_{\mathrm{V—Se—Se}}(\Delta\theta)^2$	$\frac{1}{2}K_{\mathrm{V—Se—Se'}}(\Delta\theta)^2$	$\frac{1}{2}K_{\mathrm{Se—V—V}}(\Delta\theta)^2$
Parameter	6.492	4.716	4.716	4.716
r_0 or θ_0	2.450	82.787	80.450	82.787

The second line gives an explicit expression for each VFF term. The third line is the force constant parameters. Parameters are in the unit of eV/Å^2 for the bond stretching interaction and in the unit of eV for the angle bending interaction. The fourth line gives the initial bond length (in the unit of Å) for the bond stretching interaction and the initial angle (in the unit of degrees) for the angle bending interaction. The angle θ_{ijk} has atom i as the apex.

Table 38. The VFF model for single-layer 1H-VSe_2.

http://dx.doi.org/10.5772/intechopen.71929

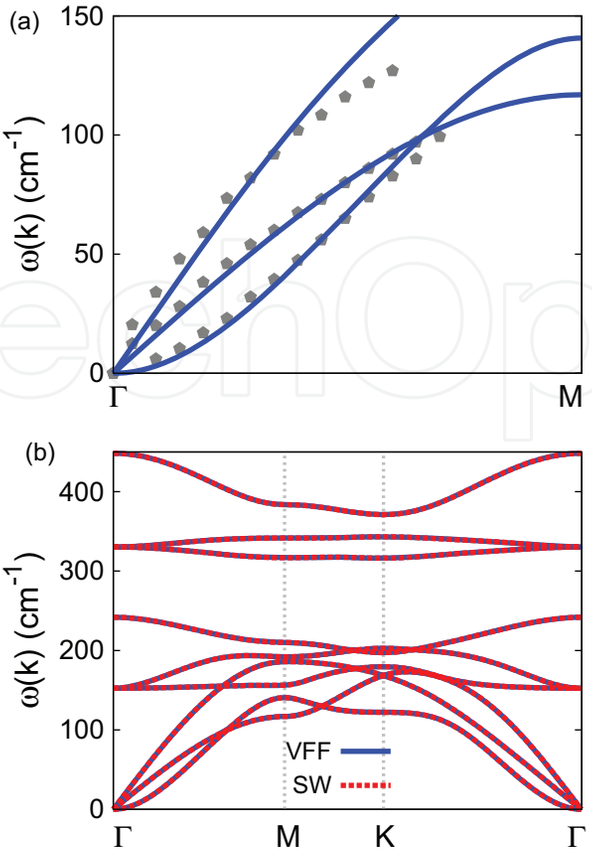

Figure 17. Phonon dispersion for single-layer 1H-VSe_2. (a) The VFF model is fitted to the three acoustic branches in the long wave limit along the ΓM direction. The *ab initio* results (gray pentagons) are from [12]. (b) The VFF model (blue lines) and the SW potential (red lines) give the same phonon dispersion for single-layer 1H-VSe_2 along ΓMKT.

phonon dispersion are from [12]. **Figure 17(b)** shows that the VFF model and the SW potential give exactly the same phonon dispersion, as the SW potential is derived from the VFF model.

The parameters for the two-body SW potential used by GULP are shown in **Table 39**. The parameters for the three-body SW potential used by GULP are shown in **Table 40**. Parameters

	A(eV)	ρ(Å)	B(Å^4)	r_{min}(Å)	r_{max}(Å)
V—Se	4.817	1.061	18.015	0.0	3.256

Table 39. Two-body SW potential parameters for single-layer 1H-VSe_2 used by GULP [8] as expressed in Eq. (3).

	K (eV)	θ_0 (°)	ρ_1 (Å)	ρ_2 (Å)	r_{min12} (Å)	r_{max12} (Å)	r_{min13} (Å)	r_{max13} (Å)	r_{min23} (Å)	r_{max23} (Å)
$\theta_{V—Se—Se}$	33.299	82.787	1.061	1.061	0.0	3.256	0.0	3.256	0.0	3.884
$\theta_{V—Se—Se'}$	33.702	80.450	1.061	1.061	0.0	3.256	0.0	3.256	0.0	3.884
$\theta_{Se—V—V}$	33.299	82.787	1.061	1.061	0.0	3.256	0.0	3.256	0.0	3.884

The angle θ_{ijk} in the first line indicates the bending energy for the angle with atom i as the apex.

Table 40. Three-body SW potential parameters for single-layer 1H-VSe_2 used by GULP [8] as expressed in Eq. (4).

for the SW potential used by LAMMPS are listed in **Table 41**. We note that 12 atom types have been introduced for the simulation of the single-layer 1H-VSe_2 using LAMMPS, because the angles around atom V in **Figure 1** (with M = V and X = Se) are not distinguishable in LAMMPS. We have suggested two options to differentiate these angles by implementing some additional constraints in LAMMPS, which can be accomplished by modifying the source file of LAMMPS [13, 14]. According to our experience, it is not so convenient for some users to implement these constraints and recompile the LAMMPS package. Hence, in the present work, we differentiate the angles by introducing more atom types, so it is not necessary to modify the LAMMPS package. **Figure 2** (with M = V and X = Se) shows that, for 1H-Vse_2, we can differentiate these angles around the V atom by assigning these six neighboring Se atoms with different atom types. It can be found that 12 atom types are necessary for the purpose of differentiating all 6 neighbors around 1 V atom.

We use LAMMPS to perform MD simulations for the mechanical behavior of the single-layer 1H-VSe_2 under uniaxial tension at 1 and 300 K. **Figure 18** shows the stress-strain curve for the tension of a single-layer 1H-VSe_2 of dimension 100×100 Å. Periodic boundary conditions are applied in both armchair and zigzag directions. The single-layer 1H-VSe_2 is stretched uniaxially along the armchair or zigzag direction. The stress is calculated without involving

	ϵ (eV)	σ (Å)	α	λ	γ	cos θ_0	A_L	B_L	p	q	Tol
V_1—Se_1—Se_1	1.000	1.061	3.070	0.000	1.000	0.000	4.817	14.236	4	0	0.0
V_1—Se_1—Se_3	1.000	0.000	0.000	33.299	1.000	0.126	0.000	0.000	4	0	0.0
V_1—Se_1—Se_2	1.000	0.000	0.000	33.702	1.000	0.166	0.000	0.000	4	0	0.0
Se_1—V_1—V_3	1.000	0.000	0.000	33.299	1.000	0.126	0.000	0.000	4	0	0.0

Atom types in the first column are displayed in **Figure 2** (with M = V and X = Se).

Table 41. SW potential parameters for single-layer 1H-VSe_2 used by LAMMPS [9] as expressed in Eqs. (9) and (10).

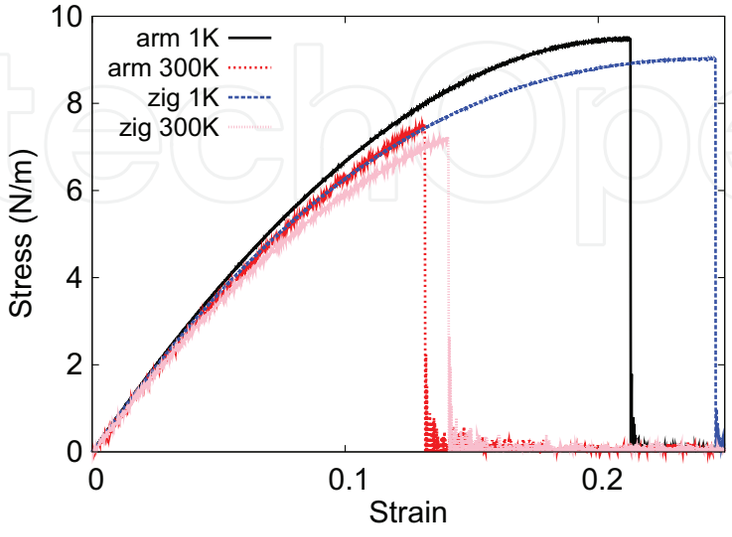

Figure 18. Stress-strain for single-layer 1H-VSe_2 of dimension 100×100 Å along the armchair and zigzag directions.

the actual thickness of the quasi-two-dimensional structure of the single-layer 1H-VSe_2. The Young's modulus can be obtained by a linear fitting of the stress-strain relation in the small strain range of [0, 0.01]. The Young's modulus is 81.7 and 80.6 N/m along the armchair and zigzag directions, respectively. The Young's modulus is essentially isotropic in the armchair and zigzag directions. The Poisson's ratio from the VFF model and the SW potential is $\nu_{xy} = \nu_{yx} = 0.23$.

There is no available value for the nonlinear quantities in the single-layer 1H-VSe_2. We have thus used the nonlinear parameter $B = 0.5d^4$ in Eq. (5), which is close to the value of B in most materials. The value of the third-order nonlinear elasticity D can be extracted by fitting the stress-strain relation to the function $\sigma = E\epsilon + \frac{1}{2}D\epsilon^2$ with E as the Young's modulus. The values of D from the present SW potential are -335.2 and -363.3 N/m along the armchair and zigzag directions, respectively. The ultimate stress is about 9.5 N/m at the ultimate strain of 0.21 in the armchair direction at the low temperature of 1 K. The ultimate stress is about 9.0 N/m at the ultimate strain of 0.24 in the zigzag direction at the low temperature of 1 K.

11. 1H-VTe_2

Most existing theoretical studies on the single-layer 1H-VTe_2 are based on the first-principles calculations. In this section, we will develop both VFF model and the SW potential for the single-layer 1H-VTe_2.

The structure for the single-layer 1H-VTe_2 is shown in **Figure 1** (with M = V and X = Te). Each V atom is surrounded by six Te atoms. These Te atoms are categorized into the top group (e.g., atoms 1, 3, and 5) and bottom group (e.g., atoms 2, 4, and 6). Each Te atom is connected to three V atoms. The structural parameters are from [12], including the lattice constant $a = 3.48$ Å and the bond length $d_{\mathrm{V—Te}} = 2.66$ Å. The resultant angles are $\theta_{\mathrm{VTeTe}} = \theta_{\mathrm{TeVV}} = 81.708^\circ$ and $\theta_{\mathrm{VTeTe'}} = 81.891^\circ$, in which atoms Te and Te' are from different (top or bottom) groups.

Table 42 shows the VFF terms for the 1H-VTe_2; one of which is the bond stretching interaction shown by Eq. (1), while the other terms are the angle bending interaction shown by Eq. (2). These force constant parameters are determined by fitting to the three acoustic branches in the phonon dispersion along the ΓM as shown in **Figure 19(a)**. The *ab initio* calculations for the

VFF type	Bond stretching	Angle bending		
Expression	$\frac{1}{2}K_{\mathrm{V—Te}}(\Delta r)^2$	$\frac{1}{2}K_{\mathrm{V—Te—Te}}(\Delta\theta)^2$	$\frac{1}{2}K_{\mathrm{V—Te—Te'}}(\Delta\theta)^2$	$\frac{1}{2}K_{\mathrm{Te—V—V}}(\Delta\theta)^2$
Parameter	6.371	4.384	4.384	4.384
r_0 or θ_0	2.660	81.708	81.891	81.708

The second line gives an explicit expression for each VFF term. The third line is the force constant parameters. Parameters are in the unit of eV/Å^2 for the bond stretching interaction and in the unit of eV for the angle bending interaction. The fourth line gives the initial bond length (in the unit of Å) for the bond stretching interaction and the initial angle (in the unit of degrees) for the angle bending interaction. The angle θ_{ijk} has atom i as the apex.

Table 42. The VFF model for single-layer 1H-VTe_2.

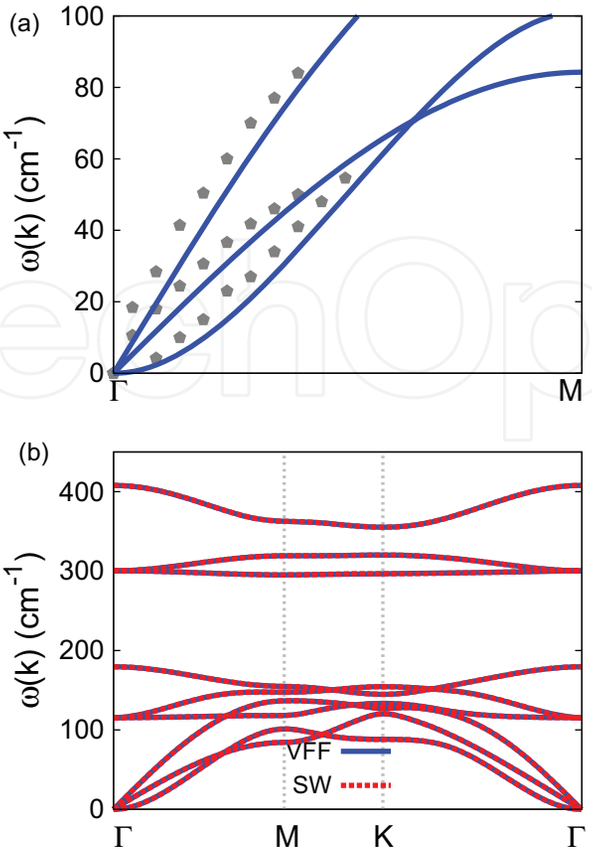

Figure 19. Phonon dispersion for single-layer 1H-VTe_2. (a) The VFF model is fitted to the three acoustic branches in the long wave limit along the ΓM direction. The *ab initio* results (gray pentagons) are from [12]. (b) The VFF model (blue lines) and the SW potential (red lines) give the same phonon dispersion for single-layer 1H-VTe_2 along ΓMKΓ.

phonon dispersion are from [12]. **Figure 19(b)** shows that the VFF model and the SW potential give exactly the same phonon dispersion, as the SW potential is derived from the VFF model.

The parameters for the two-body SW potential used by GULP are shown in **Table 43**. The parameters for the three-body SW potential used by GULP are shown in **Table 44**. Parameters

	A (eV)	ρ (Å)	B (Å^4)	r_{min} (Å)	r_{max} (Å)
V—Te	5.410	1.112	25.032	0.0	3.520

Table 43. Two-body SW potential parameters for single-layer 1H-VTe_2 used by GULP [8] as expressed in Eq. (3).

	K (eV)	θ_0 (°)	ρ_1 (Å)	ρ_2 (Å)	$r_{min\,12}$ (Å)	$r_{max\,12}$ (Å)	$r_{min\,13}$ (Å)	$r_{max\,13}$ (Å)	$r_{min\,23}$ (Å)	$r_{max\,23}$ (Å)
$\theta_{V—Te—Te}$	29.743	81.708	1.112	1.112	0.0	3.520	0.0	3.520	0.0	4.203
$\theta_{V—Te—Te'}$	29.716	81.891	1.112	1.112	0.0	3.520	0.0	3.520	0.0	4.203
$\theta_{Te—V—V}$	29.743	81.708	1.112	1.112	0.0	3.520	0.0	3.520	0.0	4.203

The angle θ_{ijk} in the first line indicates the bending energy for the angle with atom i as the apex.

Table 44. Three-body SW potential parameters for single-layer 1H-VTe_2 used by GULP [8] as expressed in Eq. (4).

	ϵ (eV)	σ (Å)	a	λ	γ	$\cos\theta_0$	A_L	B_L	p	q	Tol
V_1—Te_1—Te_1	1.000	1.112	3.164	0.000	1.000	0.000	5.410	16.345	4	0	0.0
V_1—Te_1—Te_3	1.000	0.000	0.000	29.743	1.000	0.144	0.000	0.000	4	0	0.0
V_1—Te_1—Te_2	1.000	0.000	0.000	29.716	1.000	0.141	0.000	0.000	4	0	0.0
Te_1—V_1—V_3	1.000	0.000	0.000	29.743	1.000	0.144	0.000	0.000	4	0	0.0

Atom types in the first column are displayed in **Figure 2** (with M = V and X = Te).

Table 45. SW potential parameters for single-layer 1H-VTe_2 used by LAMMPS [9] as expressed in Eqs. (9) and (10).

for the SW potential used by LAMMPS are listed in **Table 45**. We note that 12 atom types have been introduced for the simulation of the single-layer 1H-VTe_2 using LAMMPS, because the angles around atom V in **Figure 1** (with M = V and X = Te) are not distinguishable in LAMMPS. We have suggested two options to differentiate these angles by implementing some additional constraints in LAMMPS, which can be accomplished by modifying the source file of LAMMPS [13, 14]. According to our experience, it is not so convenient for some users to implement these constraints and recompile the LAMMPS package. Hence, in the present work, we differentiate the angles by introducing more atom types, so it is not necessary to modify the LAMMPS package. **Figure 2** (with M = V and X = Te) shows that, for 1H-VTe_2, we can differentiate these angles around the V atom by assigning these six neighboring Te atoms with different atom types. It can be found that 12 atom types are necessary for the purpose of differentiating all 6 neighbors around 1 V atom.

We use LAMMPS to perform MD simulations for the mechanical behavior of the single-layer 1H-VTe_2 under uniaxial tension at 1 and 300 K. **Figure 20** shows the stress-strain curve for the tension of a single-layer 1H-VTe_2 of dimension 100 $\times$ 100 Å. Periodic boundary conditions are applied in both armchair and zigzag directions. The single-layer 1H-VTe_2 is stretched uniaxially along the armchair or zigzag direction. The stress is calculated without involving the actual thickness of the quasi-two-dimensional structure of the single-layer 1H-VTe_2. The

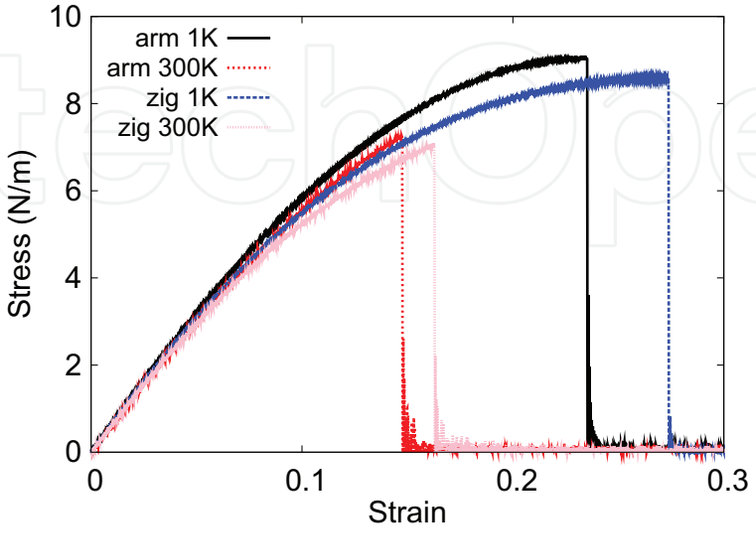

Figure 20. Stress-strain for single-layer 1H-VTe_2 of dimension 100×100 Å along the armchair and zigzag directions.

Young's modulus can be obtained by a linear fitting of the stress-strain relation in the small strain range of [0, 0.01]. The Young's modulus is 68.1 and 66.8 N/m along the armchair and zigzag directions, respectively. The Young's modulus is essentially isotropic in the armchair and zigzag directions. The Poisson's ratio from the VFF model and the SW potential is $\nu_{xy} = \nu_{yx} = 0.28$.

There is no available value for the nonlinear quantities in the single-layer 1H-VTe_2. We have thus used the nonlinear parameter $B = 0.5d^4$ in Eq. (5), which is close to the value of B in most materials. The value of the third-order nonlinear elasticity D can be extracted by fitting the stress-strain relation to the function $\sigma = E\epsilon + \frac{1}{2}D\epsilon^2$ with E as the Young's modulus. The values of D from the present SW potential are -237.4 and -260.4 N/m along the armchair and zigzag directions, respectively. The ultimate stress is about 9.0 N/m at the ultimate strain of 0.23 in the armchair direction at the low temperature of 1 K. The ultimate stress is about 8.6 N/m at the ultimate strain of 0.27 in the zigzag direction at the low temperature of 1 K.

12. 1H-CrO_2

Most existing theoretical studies on the single-layer 1H-CrO_2 are based on the first-principles calculations. In this section, we will develop the SW potential for the single-layer 1H-CrO_2.

The structure for the single-layer 1H-CrO_2 is shown in **Figure 1** (with M = Cr and X = O). Each Cr atom is surrounded by six O atoms. These O atoms are categorized into the top group (e.g., atoms 1, 3, and 5) and bottom group (e.g., atoms 2, 4, and 6). Each O atom is connected to three Cr atoms. The structural parameters are from the first-principles calculations [12], including the lattice constant $a = 2.58$ Å and the bond length $d_{\mathrm{Cr—O}} = 1.88$ Å. The resultant angles are $\theta_{\mathrm{CrOO}} = \theta_{\mathrm{OCrCr}} = 86.655^\circ$ and $\theta_{\mathrm{CrOO'}} = 75.194^\circ$, in which atoms O and O′ are from different (top or bottom) groups.

Table 46 shows four VFF terms for the single-layer 1H-CrO_2; one of which is the bond stretching interaction shown by Eq. (1), while the other three terms are the angle bending interaction shown by Eq. (2). These force constant parameters are determined by fitting to the acoustic branches in the phonon dispersion along the ΓM as shown in **Figure 21(a)**. The *ab initio* calculations for the phonon dispersion are from [12]. **Figure 21(b)** shows that the VFF

VFF type	**Bond stretching**	**Angle bending**		
Expression	$\frac{1}{2}K_{\mathrm{Cr—O}}(\Delta r)^2$	$\frac{1}{2}K_{\mathrm{Cr—O—O}}(\Delta\theta)^2$	$\frac{1}{2}K_{\mathrm{Cr—O—O'}}(\Delta\theta)^2$	$\frac{1}{2}K_{\mathrm{O—Cr—Cr}}(\Delta\theta)^2$
Parameter	12.881	8.039	8.039	8.039
r_0 or θ_0	1.880	86.655	75.194	86.655

The second line gives an explicit expression for each VFF term. The third line is the force constant parameters. Parameters are in the unit of eV/Å^2 for the bond stretching interaction and in the unit of eV for the angle bending interaction. The fourth line gives the initial bond length (in the unit of Å) for the bond stretching interaction and the initial angle (in the unit of degrees) for the angle bending interaction. The angle θ_{ijk} has atom i as the apex.

Table 46. The VFF model for single-layer 1H-CrO_2.

http://dx.doi.org/10.5772/intechopen.71929

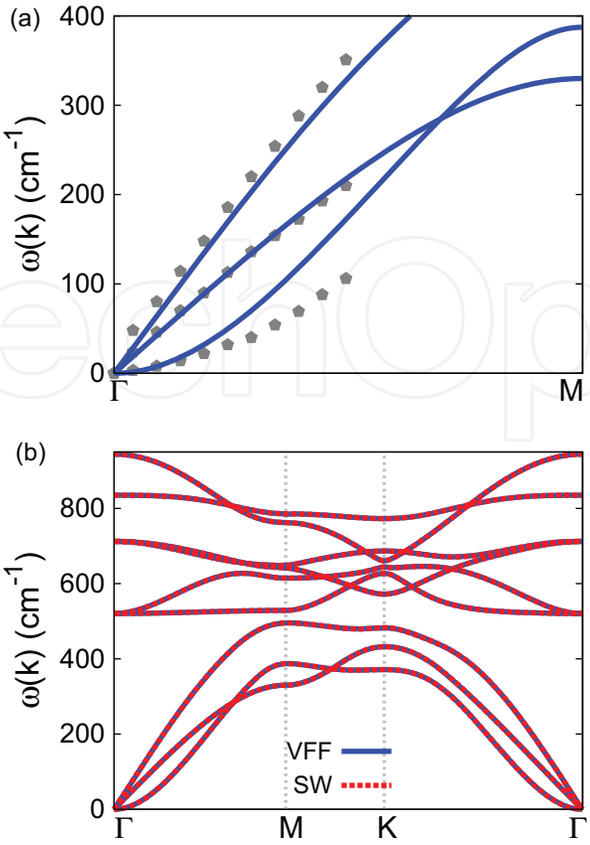

Figure 21. Phonon spectrum for single-layer 1H-CrO_2. (a) Phonon dispersion along the ΓM direction in the Brillouin zone. The results from the VFF model (lines) are comparable with the *ab initio* results (pentagons) from [12]. (b) The phonon dispersion from the SW potential is exactly the same as that from the VFF model.

model and the SW potential give exactly the same phonon dispersion, as the SW potential is derived from the VFF model.

The parameters for the two-body SW potential used by GULP are shown in **Table 47**. The parameters for the three-body SW potential used by GULP are shown in **Table 48**. Some representative parameters for the SW potential used by LAMMPS are listed in **Table 49**. We

	A (eV)	ρ (Å)	B (Å^4)	r_{min} (Å)	r_{max} (Å)
Cr—O	6.343	0.916	6.246	0.0	2.536

Table 47. Two-body SW potential parameters for single-layer 1H-CrO_2 used by GULP [8] as expressed in Eq. (3).

	K (eV)	θ_0 (°)	ρ_1 (Å)	ρ_2 (Å)	$r_{min\,12}$ (Å)	$r_{max\,12}$ (Å)	$r_{min\,13}$ (Å)	$r_{max\,13}$ (Å)	$r_{min\,23}$ (Å)	$r_{max\,23}$ (Å)
$\theta_{Cr—O—O}$	65.805	86.655	0.916	0.916	0.0	2.536	0.0	2.536	0.0	3.016
$\theta_{Cr—O—O'}$	70.163	75.194	0.916	0.916	0.0	2.536	0.0	2.536	0.0	3.016
$\theta_{O—Cr—Cr}$	65.805	86.655	0.916	0.916	0.0	2.536	0.0	2.536	0.0	3.016

The angle θ_{ijk} in the first line indicates the bending energy for the angle with atom i as the apex.

Table 48. Three-body SW potential parameters for single-layer 1H-CrO_2 used by GULP [8] as expressed in Eq. (4).

	ϵ (eV)	σ (Å)	a	λ	γ	$\cos\theta_0$	A_L	B_L	p	q	Tol
Cr_1—O_1—O_1	1.000	0.916	2.769	0.000	1.000	0.000	6.242	8.871	4	0	0.0
Cr_1—O_1—O_3	1.000	0.000	0.000	65.805	1.000	0.058	0.000	0.000	4	0	0.0
Cr_1—O_1—O_2	1.000	0.000	0.000	70.163	1.000	0.256	0.000	0.000	4	0	0.0
O_1—Cr_1—Cr_3	1.000	0.000	0.000	65.805	1.000	0.058	0.000	0.000	4	0	0.0

Table 49. SW potential parameters for single-layer 1H-CrO_2 used by LAMMPS [9] as expressed in Eqs. (9) and (10).

note that 12 atom types have been introduced for the simulation of the single-layer 1H-CrO_2 using LAMMPS, because the angles around atom Cr in **Figure 1** (with M = Cr and X = O) are not distinguishable in LAMMPS. We have suggested two options to differentiate these angles by implementing some additional constraints in LAMMPS, which can be accomplished by modifying the source file of LAMMPS [13, 14]. According to our experience, it is not so convenient for some users to implement these constraints and recompile the LAMMPS package. Hence, in the present work, we differentiate the angles by introducing more atom types, so it is not necessary to modify the LAMMPS package. **Figure 2** (with M = Cr and X = O) shows that, for 1H-CrO_2, we can differentiate these angles around the Cr atom by assigning these six neighboring O atoms with different atom types. It can be found that 12 atom types are necessary for the purpose of differentiating all 6 neighbors around 1 Cr atom.

We use LAMMPS to perform MD simulations for the mechanical behavior of the single-layer 1H-CrO_2 under uniaxial tension at 1 and 300 K. **Figure 22** shows the stress-strain curve for the tension of a single-layer 1H-CrO_2 of dimension 100 × 100 Å. Periodic boundary conditions are applied in both armchair and zigzag directions. The single-layer 1H-CrO_2 is stretched uniaxially along the armchair or zigzag direction. The stress is calculated without involving the actual thickness of the quasi-two-dimensional structure of the single-layer 1H-CrO_2. The Young's modulus can be obtained by a linear fitting of the stress-strain relation in the small strain range of [0, 0.01]. The Young's modulus is 210.6 and 209.0 N/m along the armchair and

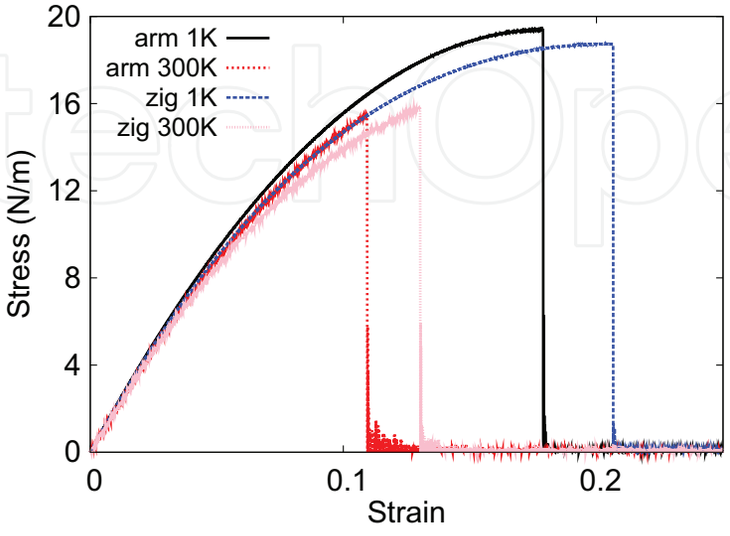

Figure 22. Stress-strain for single-layer 1H-CrO_2 of dimension 100×100 Å along the armchair and zigzag directions.

zigzag directions, respectively. The Young's modulus is essentially isotropic in the armchair and zigzag directions. The Poisson's ratio from the VFF model and the SW potential is $\nu_{xy} = \nu_{yx} = 0.13$.

There is no available value for nonlinear quantities in the single-layer 1H-CrO_2. We have thus used the nonlinear parameter $B = 0.5d^4$ in Eq. (5), which is close to the value of B in most materials. The value of the third-order nonlinear elasticity D can be extracted by fitting the stress-strain relation to the function $\sigma = E\epsilon + \frac{1}{2}D\epsilon^2$ with E as the Young's modulus. The values of D from the present SW potential are -1127.7 and -1185.8 N/m along the armchair and zigzag directions, respectively. The ultimate stress is about 19.4 N/m at the ultimate strain of 0.18 in the armchair direction at the low temperature of 1 K. The ultimate stress is about 18.7 N/m at the ultimate strain of 0.20 in the zigzag direction at the low temperature of 1 K.

13. 1H-CrS_2

Most existing theoretical studies on the single-layer 1H-CrS_2 are based on the first-principles calculations. In this section, we will develop both VFF model and the SW potential for the single-layer 1H-CrS_2.

The structure for the single-layer 1H-CrS_2 is shown in **Figure 1** (with M = Cr and X = S). Each Cr atom is surrounded by six S atoms. These S atoms are categorized into the top group (e.g., atoms 1, 3, and 5) and bottom group (e.g., atoms 2, 4, and 6). Each S atom is connected to three Cr atoms. The structural parameters are from [17], including the lattice constant $a = 2.99$ Å and the bond length $d_{\mathrm{Cr—S}} = 2.254$ Å. The resultant angles are $\theta_{\mathrm{CrSS}} = \theta_{\mathrm{SCrCr}} = 83.099^\circ$ and $\theta_{\mathrm{CrSS'}} = 80.031^\circ$, in which atoms S and S′ are from different (top or bottom) groups.

Table 50 shows four VFF terms for the 1H-CrS_2; one of which is the bond stretching interaction shown by Eq. (1), while the other three terms are the angle bending interaction shown by Eq. (2). These force constant parameters are determined by fitting to the three acoustic branches in the phonon dispersion along the ΓM as shown in **Figure 23(a)**. The *ab initio* calculations for the phonon dispersion are from [17]. Similar phonon dispersion can also be found in other *ab initio*

VFF type	Bond stretching	Angle bending		
Expression	$\frac{1}{2}K_{\mathrm{Cr—S}}(\Delta r)^2$	$\frac{1}{2}K_{\mathrm{Cr—S—S}}(\Delta\theta)^2$	$\frac{1}{2}K_{\mathrm{Cr—S—S'}}(\Delta\theta)^2$	$\frac{1}{2}K_{\mathrm{S—Cr—Cr}}(\Delta\theta)^2$
Parameter	8.752	4.614	4.614	4.614
r_0 or θ_0	2.254	83.099	80.031	83.099

The second line gives an explicit expression for each VFF term. The third line is the force constant parameters. Parameters are in the unit of eV/Å^2 for the bond stretching interaction and in the unit of eV for the angle bending interaction. The fourth line gives the initial bond length (in the unit of Å) for the bond stretching interaction and the initial angle (in the unit of degrees) for the angle bending interaction. The angle θ_{ijk} has atom i as the apex.

Table 50. The VFF model for single-layer 1H-CrS_2.

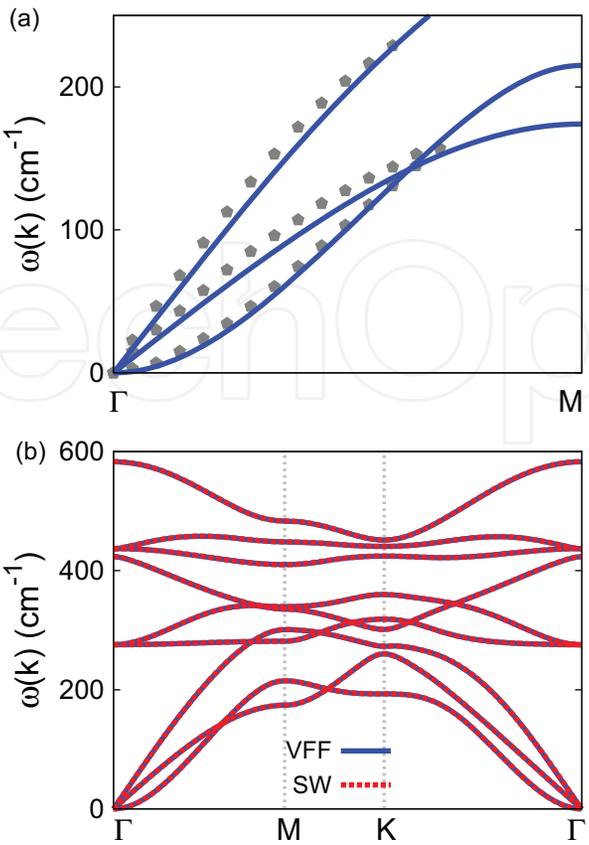

Figure 23. Phonon dispersion for single-layer 1H-CrS_2. (a) The VFF model is fitted to the three acoustic branches in the long wave limit along the ΓM direction. The *ab initio* results (gray pentagons) are from [17]. (b) The VFF model (blue lines) and the SW potential (red lines) give the same phonon dispersion for single-layer 1H-CrS_2 along ΓMKΓ.

calculations [12]. **Figure 23(b)** shows that the VFF model and the SW potential give exactly the same phonon dispersion, as the SW potential is derived from the VFF model.

The parameters for the two-body SW potential used by GULP are shown in **Table 51**. The parameters for the three-body SW potential used by GULP are shown in **Table 52**. Parameters

	A (eV)	ρ (Å)	B (Å^4)	r_{min} (Å)	r_{max} (Å)
Cr—S	5.544	0.985	12.906	0.0	2.999

Table 51. Two-body SW potential parameters for single-layer 1HCrS$_2$ used by GULP [8] as expressed in Eq. (3).

	K (eV)	θ_0 (°)	ρ_1 (Å)	ρ_2 (Å)	$r_{min\,12}$ (Å)	$r_{max\,12}$ (Å)	$r_{min\,13}$ (Å)	$r_{max\,13}$ (Å)	$r_{min\,23}$ (Å)	$r_{max\,23}$ (Å)
$\theta_{Cr—S—S}$	32.963	83.099	0.985	0.985	0.0	2.999	0.0	2.999	0.0	3.577
$\theta_{Cr—S—S'}$	33.491	80.031	0.985	0.985	0.0	2.999	0.0	2.999	0.0	3.577
$\theta_{S—Cr—Cr}$	32.963	83.099	0.985	0.985	0.0	2.999	0.0	2.999	0.0	3.577

The angle θ_{ijk} in the first line indicates the bending energy for the angle with atom i as the apex.

Table 52. Three-body SW potential parameters for single-layer 1H-CrS_2 used by GULP [8] as expressed in Eq. (4).

	ϵ (eV)	σ (Å)	a	λ	γ	$\cos\theta_0$	A_L	B_L	p	q	Tol
Cr_1—S_1—S_1	1.000	0.985	3.043	0.000	1.000	0.000	5.544	13.683	4	0	0.0
Cr_1—S_1—S_3	1.000	0.000	0.000	32.963	1.000	0.120	0.000	0.000	4	0	0.0
Cr_1—S_1—S_2	1.000	0.000	0.000	33.491	1.000	0.173	0.000	0.000	4	0	0.0
S_1—Cr_1—Cr_3	1.000	0.000	0.000	32.963	1.000	0.120	0.000	0.000	4	0	0.0

Atom types in the first column are displayed in **Figure 2** (with M = Cr and X = S).

Table 53. SW potential parameters for single-layer 1H-CrS_2 used by LAMMPS [9] as expressed in Eqs. (9) and (10).

for the SW potential used by LAMMPS are listed in **Table 53**. We note that 12 atom types have been introduced for the simulation of the single-layer 1H-CrS_2 using LAMMPS, because the angles around atom Cr in **Figure 1** (with M = Cr and X = S) are not distinguishable in LAMMPS. We have suggested two options to differentiate these angles by implementing some additional constraints in LAMMPS, which can be accomplished by modifying the source file of LAMMPS [13, 14] According to our experience, it is not so convenient for some users to implement these constraints and recompile the LAMMPS package. Hence, in the present work, we differentiate the angles by introducing more atom types, so it is not necessary to modify the LAMMPS package. **Figure 2** (with M = Cr and X = S) shows that, for 1H-CrS_2, we can differentiate these angles around the Cr atom by assigning these six neighboring S atoms with different atom types. It can be found that 12 atom types are necessary for the purpose of differentiating all 6 neighbors around 1 Cr atom.

We use LAMMPS to perform MD simulations for the mechanical behavior of the single-layer 1H-CrS_2 under uniaxial tension at 1 and 300 K. **Figure 24** shows the stress-strain curve for the tension of a single-layer 1H-CrS_2 of dimension 100 × 100 Å. Periodic boundary conditions are applied in both armchair and zigzag directions. The single-layer 1H-CrS_2 is stretched uniaxially along the armchair or zigzag direction. The stress is calculated without involving the actual thickness of the quasi-two-dimensional structure of the single-layer 1H-CrS_2. The

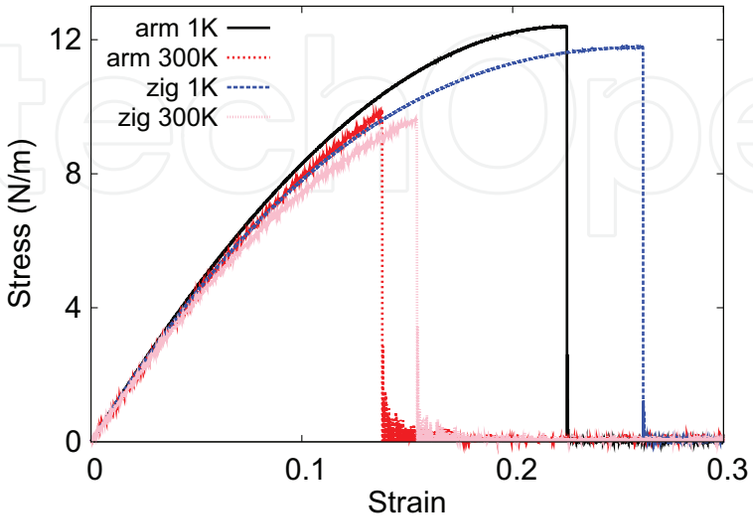

Figure 24. Stress-strain for single-layer 1H-CrS_2 of dimension 100 × 100 Å along the armchair and zigzag directions.

Young's modulus can be obtained by a linear fitting of the stress-strain relation in the small strain range of [0, 0.01]. The Young's modulus is 98.4 and 97.8 N/m along the armchair and zigzag directions, respectively. The Young's modulus is essentially isotropic in the armchair and zigzag directions. These values are in reasonably agreement with the *ab initio* results, e.g., 112.0 N/m from [18], or 111.9 N/m from [19]. The Poisson's ratio from the VFF model and the SW potential is $\nu_{xy} = \nu_{yx} = 0.26$, which agrees with the *ab initio* value of 0.27 [18, 19].

There is no available value for the nonlinear quantities in the single-layer 1H-CrS_2. We have thus used the nonlinear parameter $B = 0.5d^4$ in Eq. (5), which is close to the value of B in most materials. The value of the third-order nonlinear elasticity D can be extracted by fitting the stress-strain relation to the function $\sigma = E\epsilon + \frac{1}{2}D\epsilon^2$ with E as the Young's modulus. The values of D from the present SW potential are -364.8 and -409.3 N/m along the armchair and zigzag directions, respectively. The ultimate stress is about 12.4 N/m at the ultimate strain of 0.22 in the armchair direction at the low temperature of 1 K. The ultimate stress is about 11.8 N/m at the ultimate strain of 0.26 in the zigzag direction at the low temperature of 1 K.

14. 1H-$CrSe_2$

Most existing theoretical studies on the single-layer 1H-$CrSe_2$ are based on the first-principles calculations. In this section, we will develop both VFF model and the SW potential for the single-layer 1H-$CrSe_2$.

The structure for the single-layer 1H-$CrSe_2$ is shown in **Figure 1** (with M = Cr and X = Se). Each Cr atom is surrounded by six Se atoms. These Se atoms are categorized into the top group (e.g., atoms 1, 3, and 5) and bottom group (e.g., atoms 2, 4, and 6). Each Se atom is connected to three Cr atoms. The structural parameters are from [12], including the lattice constant $a = 3.13$ Å and the bond length $d_{\text{Cr—Se}} = 2.38$ Å. The resultant angles are $\theta_{\text{CrSeSe}} = \theta_{\text{SeCrCr}} = 82.229^\circ$ and $\theta_{\text{CrSeSe}'} = 81.197^\circ$, in which atoms Se and Se' are from different (top or bottom) groups.

Table 54 shows four VFF terms for the 1H-$CrSe_2$; one of which is the bond stretching interaction shown by Eq. (1), while the other three terms are the angle bending interaction shown by Eq. (2). These force constant parameters are determined by fitting to the three acoustic

VFF type	Bond stretching	Angle bending		
Expression	$\frac{1}{2}K_{\text{Cr—Se}}(\Delta r)^2$	$\frac{1}{2}K_{\text{Cr—Se—Se}}(\Delta\theta)^2$	$\frac{1}{2}K_{\text{Cr—Se—Se}'}(\Delta\theta)^2$	$\frac{1}{2}K_{\text{Se—Cr—Cr}}(\Delta\theta)^2$
Parameter	9.542	4.465	4.465	4.465
r_0 or θ_0	2.380	82.229	81.197	82.229

The second line gives an explicit expression for each VFF term. The third line is the force constant parameters. Parameters are in the unit of $\text{eV}/\text{Å}^2$ for the bond stretching interaction and in the unit of eV for the angle bending interaction. The fourth line gives the initial bond length (in the unit of Å) for the bond stretching interaction and the initial angle (in the unit of degrees) for the angle bending interaction. The angle θ_{ijk} has atom i as the apex.

Table 54. The VFF model for single-layer 1H-$CrSe_2$.

branches in the phonon dispersion along the ΓM as shown in **Figure 25(a)**. The *ab initio* calculations for the phonon dispersion are from [12]. **Figure 25(b)** shows that the VFF model and the SW potential give exactly the same phonon dispersion, as the SW potential is derived from the VFF model.

The parameters for the two-body SW potential used by GULP are shown in **Table 55**. The parameters for the three-body SW potential used by GULP are shown in **Table 56**. Parameters for the SW potential used by LAMMPS are listed in **Table 57**. We note that 12 atom types have been introduced for the simulation of the single-layer 1H-$CrSe_2$ using LAMMPS, because the angles around atom Cr in **Figure 1** (with M = Cr and X = Se) are not distinguishable in LAMMPS. We have suggested two options to differentiate these angles by implementing some additional constraints in LAMMPS, which can be accomplished by modifying the source file of LAMMPS [13, 14]. According to our experience, it is not so convenient for some users to

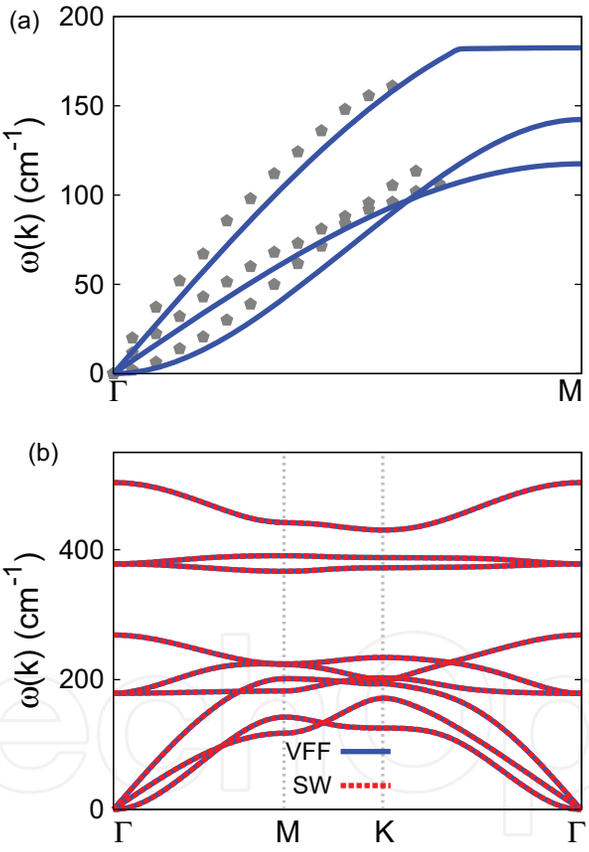

Figure 25. Phonon dispersion for single-layer 1H-$CrSe_2$. (a) The VFF model is fitted to the three acoustic branches in the long wave limit along the ΓM direction. The *ab initio* results (gray pentagons) are from [21]. (b) The VFF model (blue lines) and the SW potential (red lines) give the same phonon dispersion for single-layer 1H-$CrSe_2$ along ΓMKΓ.

	A (eV)	ρ (Å)	B (Å^4)	r_{min} (Å)	r_{max} (Å)
Cr—Se	6.581	1.012	16.043	0.0	3.156

Table 55. Two-body SW potential parameters for single-layer 1H-$CrSe_2$ used by GULP [8] as expressed in Eq. (3).

	K (eV)	θ_0 (°)	ρ_1 (Å)	ρ_2 (Å)	$r_{\min 12}$ (Å)	$r_{\max 12}$ (Å)	$r_{\min 13}$ (Å)	$r_{\max 13}$ (Å)	$r_{\min 23}$ (Å)	$r_{\max 23}$ (Å)
$\theta_{\mathrm{Cr—Se—Se}}$	30.881	82.229	1.012	1.012	0.0	3.156	0.0	3.156	0.0	3.767
$\theta_{\mathrm{Cr—Se—Se'}}$	31.044	81.197	1.012	1.012	0.0	3.156	0.0	3.156	0.0	3.767
$\theta_{\mathrm{Se—Cr—Cr}}$	30.881	82.229	1.012	1.012	0.0	3.156	0.0	3.156	0.0	3.767

The angle θ_{ijk} in the first line indicates the bending energy for the angle with atom i as the apex.

Table 56. Three-body SW potential parameters for single-layer 1H-$CrSe_2$ used by GULP [8] as expressed in Eq. (4).

	ϵ (eV)	σ (Å)	a	λ	γ	$\cos\theta_0$	A_L	B_L	p	q	Tol
$\mathrm{Cr_1—Se_1—Se_1}$	1.000	1.012	3.118	0.000	1.000	0.000	6.581	15.284	4	0	0.0
$\mathrm{Cr_1—Se_1—Se_3}$	1.000	0.000	0.000	30.881	1.000	0.135	0.000	0.000	4	0	0.0
$\mathrm{Cr_1—Se_1—Se_2}$	1.000	0.000	0.000	31.044	1.000	0.153	0.000	0.000	4	0	0.0
$\mathrm{Se_1—Cr_1—Cr_3}$	1.000	0.000	0.000	30.881	1.000	0.135	0.000	0.000	4	0	0.0

Atom types in the first column are displayed in **Figure 2** (with M = Cr and X = Se).

Table 57. SW potential parameters for single-layer 1H-$CrSe_2$ used by LAMMPS [9] as expressed in Eqs. (9) and (10).

implement these constraints and recompile the LAMMPS package. Hence, in the present work, we differentiate the angles by introducing more atom types, so it is not necessary to modify the LAMMPS package. **Figure 2** (with M = Cr and X = Se) shows that, for 1H-$CrSe_2$, we can differentiate these angles around the Cr atom by assigning these six neighboring Se atoms with different atom types. It can be found that 12 atom types are necessary for the purpose of differentiating all 6 neighbors around 1 Cr atom.

We use LAMMPS to perform MD simulations for the mechanical behavior of the single-layer 1H-$CrSe_2$ under uniaxial tension at 1 and 300 K. **Figure 26** shows the stress-strain curve for the

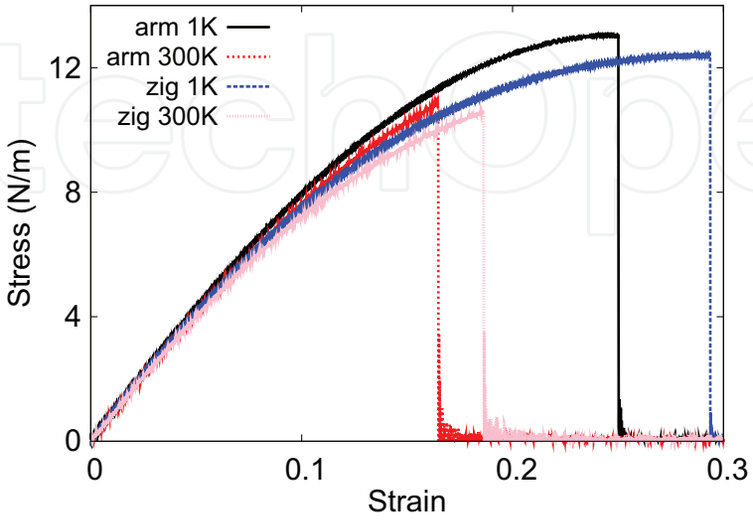

Figure 26. Stress-strain for single-layer 1H-$CrSe_2$ of dimension 100 × 100 Å along the armchair and zigzag directions.

tension of a single-layer 1H-$CrSe_2$ of dimension 100×100 Å. Periodic boundary conditions are applied in both armchair and zigzag directions. The single-layer 1H-$CrSe_2$ is stretched uniaxially along the armchair or zigzag direction. The stress is calculated without involving the actual thickness of the quasi-two-dimensional structure of the single-layer 1H-$CrSe_2$. The Young's modulus can be obtained by a linear fitting of the stress-strain relation in the small strain range of [0, 0.01]. The Young's modulus is 90.0 and 89.0 N/m along the armchair and zigzag directions, respectively. The Young's modulus is essentially isotropic in the armchair and zigzag directions. These values are in reasonably agreement with the *ab initio* results, e.g., 88.0 N/m from [18], or 87.9 N/m from [19]. The Poisson's ratio from the VFF model and the SW potential is $\nu_{xy} = \nu_{yx} = 0.30$, which agrees with the *ab initio* value of 0.30 [18, 19].

There is no available value for the nonlinear quantities in the single-layer 1H-$CrSe_2$. We have thus used the nonlinear parameter $B = 0.5d^4$ in Eq. (5), which is close to the value of B in most two-dimensional atomic layered materials. The value of the third-order nonlinear elasticity D can be extracted by fitting the stress-strain relation to the function $\sigma = E\epsilon + \frac{1}{2}D\epsilon^2$ with E as the Young's modulus. The values of D from the present SW potential are -279.6 and -318.8 N/m along the armchair and zigzag directions, respectively. The ultimate stress is about 13.0 N/m at the ultimate strain of 0.25 in the armchair direction at the low temperature of 1 K. The ultimate stress is about 12.4 N/m at the ultimate strain of 0.29 in the zigzag direction at the low temperature of 1 K.

15. 1H-$CrTe_2$

Most existing theoretical studies on the single-layer 1H-$CrTe_2$ are based on the first-principles calculations. In this section, we will develop both VFF model and the SW potential for the single-layer 1H-$CrTe_2$.

The structure for the single-layer 1H-$CrTe_2$ is shown in **Figure 1** (with M = Cr and X = Te). Each Cr atom is surrounded by six Te atoms. These Te atoms are categorized into the top group (e.g., atoms 1, 3, and 5) and bottom group (e.g., atoms 2, 4, and 6). Each Te atom is connected to three Cr atoms. The structural parameters are from [12], including the lattice constant $a = 3.39$ Å and the bond length $d_{\text{Cr—Te}} = 2.58$ Å. The resultant angles are $\theta_{\text{CrTeTe}} = \theta_{\text{TeCrCr}} = 82.139^\circ$ and $\theta_{\text{CrTeTe}'} = 81.316^\circ$, in which atoms Te and Te' are from different (top or bottom) groups.

Table 58 shows three VFF terms for the 1H-$CrTe_2$; one of which is the bond stretching interaction shown by Eq. (1), while the other two terms are the angle bending interaction shown by Eq. (2). These force constant parameters are determined by fitting to the three acoustic branches in the phonon dispersion along the ΓM as shown in **Figure 27(a)**. The *ab initio* calculations for the phonon dispersion are from [12]. **Figure 27(b)** shows that the VFF model and the SW potential give exactly the same phonon dispersion, as the SW potential is derived from the VFF model.

The parameters for the two-body SW potential used by GULP are shown in **Table 59**. The parameters for the three-body SW potential used by GULP are shown in **Table 60**. Parameters for the SW potential used by LAMMPS are listed in **Table 61**. We note that 12 atom types have

VFF type	Bond stretching	Angle bending		
Expression	$\frac{1}{2}K_{\mathrm{Cr—Te}}(\Delta r)^2$	$\frac{1}{2}K_{\mathrm{Cr—Te—Te}}(\Delta\theta)^2$	$\frac{1}{2}K_{\mathrm{Cr—Te—Te'}}(\Delta\theta)^2$	$\frac{1}{2}K_{\mathrm{Te—Cr—Cr}}(\Delta\theta)^2$
Parameter	8.197	4.543	4.543	4.543
r_0 or θ_0	2.580	82.139	81.316	82.139

The second line gives an explicit expression for each VFF term. The third line is the force constant parameters. Parameters are in the unit of eV/Å^2 for the bond stretching interaction and in the unit of eV for the angle bending interaction. The fourth line gives the initial bond length (in the unit of Å) for the bond stretching interaction and the initial angle (in the unit of degrees) for the angle bending interaction. The angle θ_{ijk} has atom i as the apex.

Table 58. The VFF model for single-layer 1H-$CrTe_2$.

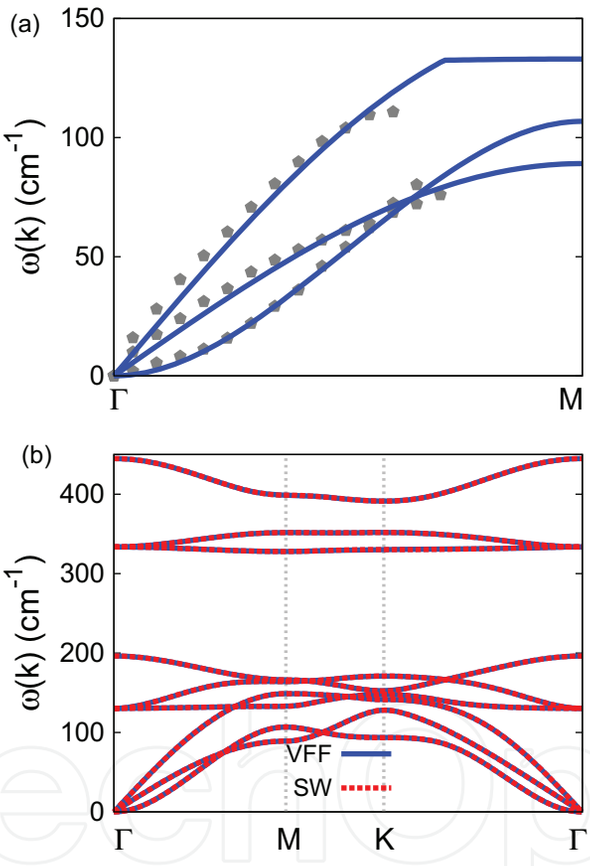

Figure 27. Phonon dispersion for single-layer 1H-$CrTe_2$. (a) The VFF model is fitted to the three acoustic branches in the long wave limit along the ΓM direction. The *ab initio* results (gray pentagons) are from [12]. (b) The VFF model (blue lines) and the SW potential (red lines) give the same phonon dispersion for single-layer 1H-$CrTe_2$ along ΓMKΓ.

	A (eV)	ρ (Å)	B (Å^4)	r_{min} (Å)	r_{max} (Å)
Cr—Te	6.627	1.094	22.154	0.0	3.420

Table 59. Two-body SW potential parameters for single-layer 1H-$CrTe_2$ used by GULP [8] as expressed in Eq. (3).

	K (eV)	θ_0 (°)	ρ_1 (Å)	ρ_2 (Å)	$r_{\min 12}$ (Å)	$r_{\max 12}$ (Å)	$r_{\min 13}$ (Å)	$r_{\max 13}$ (Å)	$r_{\min 23}$ (Å)	$r_{\max 23}$ (Å)
$\theta_{\text{Cr—Te—Te}}$	31.316	82.139	1.094	1.094	0.0	3.420	0.0	3.420	0.0	4.082
$\theta_{\text{Cr—Te—Te}'}$	31.447	81.316	1.094	1.094	0.0	3.420	0.0	3.420	0.0	4.082
$\theta_{\text{Te—Cr—Cr}}$	31.316	82.139	1.094	1.094	0.0	3.420	0.0	3.420	0.0	4.082

The angle θ_{ijk} in the first line indicates the bending energy for the angle with atom i as the apex.

Table 60. Three-body SW potential parameters for single-layer 1H-$CrTe_2$ used by GULP [8] as expressed in Eq. (4).

	ϵ (eV)	σ (Å)	a	λ	γ	$\cos\theta_0$	A_L	B_L	p	q	Tol
Cr_1—Te_1—Te_1	1.000	1.094	3.126	0.000	1.000	0.000	6.627	15.461	4	0	0.0
Cr_1—Te_1—Te_3	1.000	0.000	0.000	31.316	1.000	0.137	0.000	0.000	4	0	0.0
Cr_1—Te_1—Te_2	1.000	0.000	0.000	31.447	1.000	0.151	0.000	0.000	4	0	0.0
Te_1—Cr_1—Cr_3	1.000	0.000	0.000	31.316	1.000	0.137	0.000	0.000	4	0	0.0

Atom types in the first column are displayed in **Figure 2** (with M = Cr and X = Te).

Table 61. SW potential parameters for single-layer 1H-$CrTe_2$ used by LAMMPS [9] as expressed in Eqs. (9) and (10).

been introduced for the simulation of the single-layer 1H-$CrTe_2$ using LAMMPS, because the angles around atom Cr in **Figure 1** (with M = Cr and X = Te) are not distinguishable in LAMMPS. We have suggested two options to differentiate these angles by implementing some additional constraints in LAMMPS, which can be accomplished by modifying the source file of LAMMPS [13, 14]. According to our experience, it is not so convenient for some users to implement these constraints and recompile the LAMMPS package. Hence, in the present work, we differentiate the angles by introducing more atom types, so it is not necessary to modify the LAMMPS package. **Figure 2** (with M = Cr and X = Te) shows that, for 1H-$CrTe_2$, we can differentiate these angles around the Cr atom by assigning these six neighboring Te atoms with different atom types. It can be found that 12 atom types are necessary for the purpose of differentiating all 6 neighbors around 1 Cr atom.

We use LAMMPS to perform MD simulations for the mechanical behavior of the single-layer 1H-$CrTe_2$ under uniaxial tension at 1 and 300 K. **Figure 28** shows the stress-strain curve for the tension of a single-layer 1H-$CrTe_2$ of dimension 100 × 100 Å. Periodic boundary conditions are applied in both armchair and zigzag directions. The single-layer 1H-$CrTe_2$ is stretched uniaxially along the armchair or zigzag direction. The stress is calculated without involving the actual thickness of the quasi-two-dimensional structure of the single-layer 1H-$CrTe_2$. The Young's modulus can be obtained by a linear fitting of the stress-strain relation in the small strain range of [0, 0.01]. The Young's modulus is 77.2 and 76.4 N/m along the armchair and zigzag directions, respectively. The Young's modulus is essentially isotropic in the armchair and zigzag directions. These values are in reasonably agreement with the *ab initio* results, e.g., 63.9 N/m from [18, 19]. The Poisson's ratio from the VFF model and the SW potential is $\nu_{xy} = \nu_{yx} = 0.30$, which agrees with the *ab initio* value of 0.30 [18, 19].

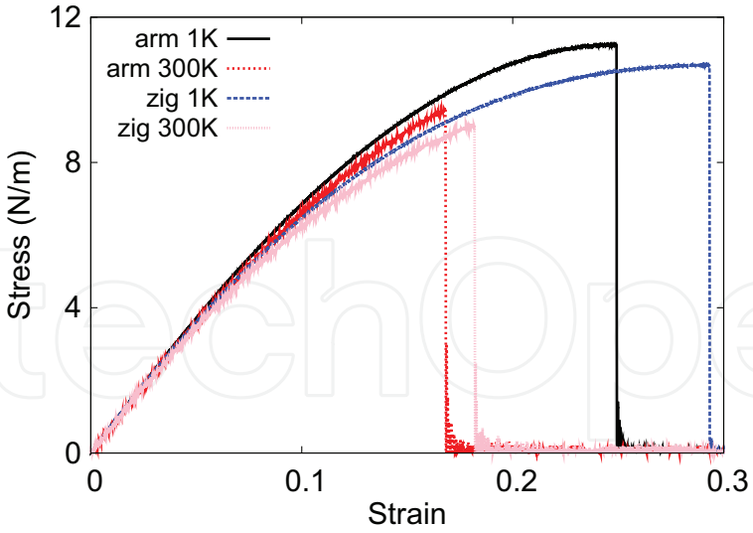

Figure 28. Stress-strain for single-layer 1H-$CrTe_2$ of dimension 100 × 100 Å along the armchair and zigzag directions.

There is no available value for the nonlinear quantities in the single-layer 1H-$CrTe_2$. We have thus used the nonlinear parameter $B = 0.5d^4$ in Eq. (5), which is close to the value of B in most two-dimensional atomic layered materials. The value of the third-order nonlinear elasticity D can be extracted by fitting the stress-strain relation to the function $\sigma = E\epsilon + \frac{1}{2}D\epsilon^2$ with E as the Young's modulus. The values of D from the present SW potential are -237.1 and -280.8 N/m along the armchair and zigzag directions, respectively. The ultimate stress is about 11.2 N/m at the ultimate strain of 0.25 in the armchair direction at the low temperature of 1 K. The ultimate stress is about 10.7 N/m at the ultimate strain of 0.29 in the zigzag direction at the low temperature of 1 K.

16. 1H-MnO_2

Most existing theoretical studies on the single-layer 1H-MnO_2 are based on the first-principles calculations. In this section, we will develop the SW potential for the single-layer 1H-MnO_2.

The structure for the single-layer 1H-MnO_2 is shown in **Figure 1** (with M = Mn and X = O). Each Mn atom is surrounded by six O atoms. These O atoms are categorized into the top group (e.g., atoms 1, 3, and 5) and bottom group (e.g., atoms 2, 4, and 6). Each O atom is connected to three Mn atoms. The structural parameters are from the first-principles calculations [12], including the lattice constant $a = 2.61$ Å and the bond length $d_{\mathrm{Mn—O}} = 1.87$ Å. The resultant angles are $\theta_{\mathrm{MnOO}} = \theta_{\mathrm{OMnMn}} = 88.511^\circ$ and $\theta_{\mathrm{MnOO'}} = 72.621^\circ$, in which atoms O and O′ are from different (top or bottom) groups.

Table 62 shows four VFF terms for the single-layer 1H-MnO_2; one of which is the bond stretching interaction shown by Eq. (1), while the other three terms are the angle bending interaction shown by Eq. (2). These force constant parameters are determined by fitting to the acoustic branches in the phonon dispersion along the ΓM as shown in **Figure 29(a)**. The *ab*

initio calculations for the phonon dispersion are from [12]. Typically, the transverse acoustic branch has a linear dispersion, so is higher than the flexural branch. However, it can be seen that the transverse acoustic branch is close to the flexural branch, which should be due to the underestimation from the *ab initio* calculations. **Figure 29(b)** shows that the VFF model and the SW potential give exactly the same phonon dispersion, as the SW potential is derived from the VFF model.

VFF type	**Bond stretching**	**Angle bending**		
Expression	$\frac{1}{2}K_{\mathrm{Mn-O}}(\Delta r)^2$	$\frac{1}{2}K_{\mathrm{Mn-O-O}}(\Delta\theta)^2$	$\frac{1}{2}K_{\mathrm{Mn-O-O'}}(\Delta\theta)^2$	$\frac{1}{2}K_{\mathrm{O-Mn-Mn}}(\Delta\theta)^2$
Parameter	9.382	6.253	6.253	6.253
r_0 or θ_0	1.870	88.511	72.621	88.511

The second line gives an explicit expression for each VFF term. The third line is the force constant parameters. Parameters are in the unit of $\mathrm{eV/\AA^2}$ for the bond stretching interaction and in the unit of eV for the angle bending interaction. The fourth line gives the initial bond length (in the unit of Å) for the bond stretching interaction and the initial angle (in the unit of degrees) for the angle bending interaction. The angle θ_{ijk} has atom i as the apex.

Table 62. The VFF model for single-layer 1H-MnO_2.

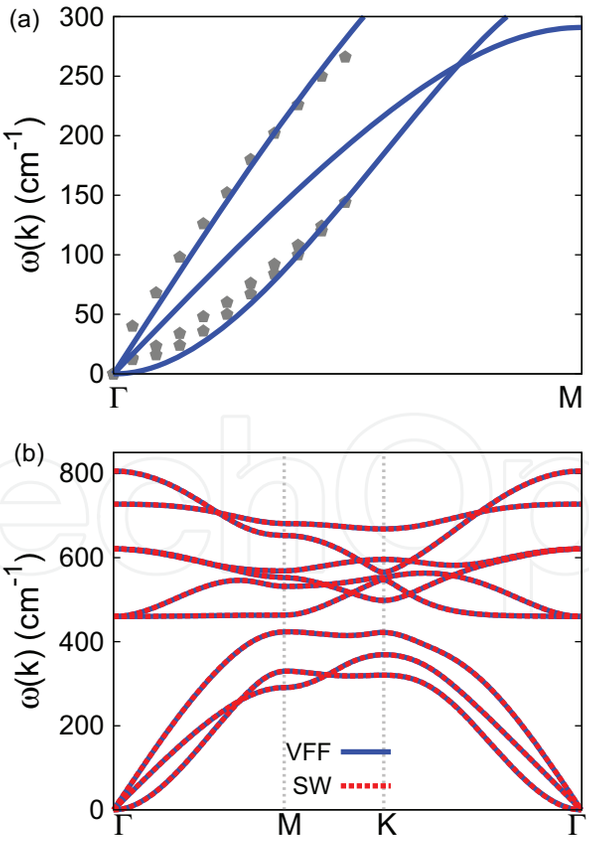

Figure 29. Phonon spectrum for single-layer 1H-MnO_2. (a) Phonon dispersion along the ΓM direction in the Brillouin zone. The results from the VFF model (lines) are comparable with the *ab initio* results (pentagons) from [12]. (b) The phonon dispersion from the SW potential is exactly the same as that from the VFF model.

The parameters for the two-body SW potential used by GULP are shown in **Table 63**. The parameters for the three-body SW potential used by GULP are shown in **Table 64**. Some representative parameters for the SW potential used by LAMMPS are listed in **Table 65**. We note that 12 atom types have been introduced for the simulation of the single-layer 1H-MnO_2 using LAMMPS, because the angles around atom Mn in **Figure 1** (with M = Mn and X = O) are not distinguishable in LAMMPS. We have suggested two options to differentiate these angles by implementing some additional constraints in LAMMPS, which can be accomplished by modifying the source file of LAMMPS [13, 14]. According to our experience, it is not so convenient for some users to implement these constraints and recompile the LAMMPS package. Hence, in the present work, we differentiate the angles by introducing more atom types, so it is not necessary to modify the LAMMPS package. **Figure 2** (with M = Mn and X = O) shows that, for 1H-MnO_2, we can differentiate these angles around the Mn atom by assigning these six neighboring O atoms with different atom types. It can be found that 12 atom types are necessary for the purpose of differentiating all 6 neighbors around 1 Mn atom.

We use LAMMPS to perform MD simulations for the mechanical behavior of the single-layer 1H-MnO_2 under uniaxial tension at 1 and 300 K. **Figure 30** shows the stress-strain curve for the tension of a single-layer 1H-MnO_2 of dimension 100 × 100 Å. Periodic boundary conditions are applied in both armchair and zigzag directions. The single-layer 1H-MnO_2 is stretched uniaxially

	A (eV)	ρ (Å)	B (Å^4)	r_{min} (Å)	r_{max} (Å)
Mn—O	4.721	0.961	6.114	0.0	2.540

Table 63. Two-body SW potential parameters for single-layer 1H-MnO_2 used by GULP [8] as expressed in Eq. (3).

	K (eV)	θ_0 (°)	ρ_1 (Å)	ρ_2 (Å)	r_{min12} (Å)	r_{max12} (Å)	r_{min13} (Å)	r_{max13} (Å)	r_{min23} (Å)	r_{max23} (Å)
$\theta_{Mn—O—O}$	55.070	88.511	0.961	0.961	0.0	2.540	0.0	2.540	0.0	3.016
$\theta_{Mn—O—O'}$	60.424	72.621	0.961	0.961	0.0	2.540	0.0	2.540	0.0	3.016
$\theta_{O—Mn—Mn}$	55.070	88.511	0.961	0.961	0.0	2.540	0.0	2.540	0.0	3.016

The angle θ_{ijk} in the first line indicates the bending energy for the angle with atom i as the apex.

Table 64. Three-body SW potential parameters for single-layer 1H-MnO_2 used by GULP [8] as expressed in Eq. (4).

	ϵ (eV)	σ (Å)	a	λ	γ	cos θ_0	A_L	B_L	p	q	Tol
$Mn_1—O_1—O_1$	1.000	0.961	2.643	0.000	1.000	0.000	4.721	7.158	4	0	0.0
$Mn_1—O_1—O_3$	1.000	0.000	0.000	55.070	1.000	0.026	0.000	0.000	4	0	0.0
$Mn_1—O_1—O_2$	1.000	0.000	0.000	60.424	1.000	0.299	0.000	0.000	4	0	0.0
$O_1—Mn_1—Mn_3$	1.000	0.000	0.000	55.070	1.000	0.026	0.000	0.000	4	0	0.0

Table 65. SW potential parameters for single-layer 1H-MnO_2 used by LAMMPS [9] as expressed in Eqs. (9) and (10).

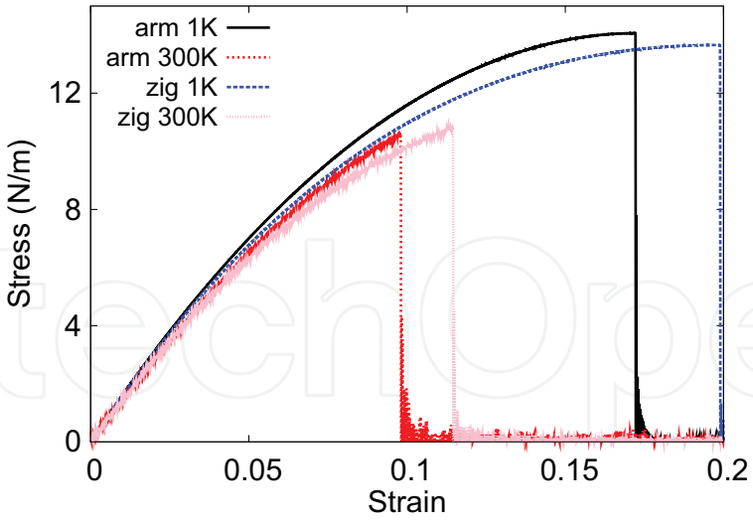

Figure 30. Stress-strain for single-layer 1H-MnO_2 of dimension 100 × 100 Å along the armchair and zigzag directions.

along the armchair or zigzag direction. The stress is calculated without involving the actual thickness of the quasi-two-dimensional structure of the single-layer 1H-MnO_2. The Young's modulus can be obtained by a linear fitting of the stress-strain relation in the small strain range of [0, 0.01]. The Young's modulus is 161.1 and 160.2 N/m along the armchair and zigzag directions, respectively. The Young's modulus is essentially isotropic in the armchair and zigzag directions. The Poisson's ratio from the VFF model and the SW potential is $\nu_{xy} = \nu_{yx} = 0.10$.

There is no available value for nonlinear quantities in the single-layer 1H-MnO_2. We have thus used the nonlinear parameter $B = 0.5d^4$ in Eq. (5), which is close to the value of B in most materials. The value of the third-order nonlinear elasticity D can be extracted by fitting the stress-strain relation to the function $\sigma = E\epsilon + \frac{1}{2}D\epsilon^2$ with E as the Young's modulus. The values of D from the present SW potential are −915.9 and −957.1 N/m along the armchair and zigzag directions, respectively. The ultimate stress is about 14.1 N/m at the ultimate strain of 0.17 in the armchair direction at the low temperature of 1 K. The ultimate stress is about 13.7 N/m at the ultimate strain of 0.20 in the zigzag direction at the low temperature of 1 K.

17. 1H-FeO_2

Most existing theoretical studies on the single-layer 1H-FeO_2 are based on the first-principles calculations. In this section, we will develop the SW potential for the single-layer 1H-FeO_2.

The structure for the single-layer 1H-FeO_2 is shown in **Figure 1** (with M = Fe and X = O). Each Fe atom is surrounded by six O atoms. These O atoms are categorized into the top group (e.g., atoms 1, 3, and 5) and bottom group (e.g., atoms 2, 4, and 6). Each O atom is connected to three Fe atoms. The structural parameters are from the first-principles calculations [12], including the lattice constant $a = 2.62$ Å and the bond length $d_{\text{Fe—O}} = 1.88$ Å. The resultant angles are $\theta_{\text{FeOO}} = \theta_{\text{OFeFe}} = 88.343^\circ$ and $\theta_{\text{FeOO}'} = 72.856^\circ$, in which atoms O and O′ are from different (top or bottom) groups.

Table 66 shows four VFF terms for the single-layer 1H-FeO_2; one of which is the bond stretching interaction shown by Eq. (1), while the other three terms are the angle bending interaction shown by Eq. (2). These force constant parameters are determined by fitting to the three acoustic branches in the phonon dispersion along the ΓM as shown in **Figure 31(a)**. The *ab initio* calculations for the phonon dispersion are from [12]. **Figure 31(b)** shows that the VFF

VFF type	**Bond stretching**	**Angle bending**		
Expression	$\frac{1}{2}K_{\mathrm{Fe—O}}(\Delta r)^2$	$\frac{1}{2}K_{\mathrm{Fe—O—O}}(\Delta\theta)^2$	$\frac{1}{2}K_{\mathrm{Fe—O—O'}}(\Delta\theta)^2$	$\frac{1}{2}K_{\mathrm{O—Fe—Fe}}(\Delta\theta)^2$
Parameter	8.377	3.213	3.213	3.213
r_0 or θ_0	1.880	88.343	72.856	88.343

The second line gives an explicit expression for each VFF term. The third line is the force constant parameters. Parameters are in the unit of $\mathrm{eV/\AA^2}$ for the bond stretching interaction and in the unit of eV for the angle bending interaction. The fourth line gives the initial bond length (in the unit of Å) for the bond stretching interaction and the initial angle (in the unit of degrees) for the angle bending interaction. The angle θ_{ijk} has atom i as the apex.

Table 66. The VFF model for single-layer 1H-FeO_2.

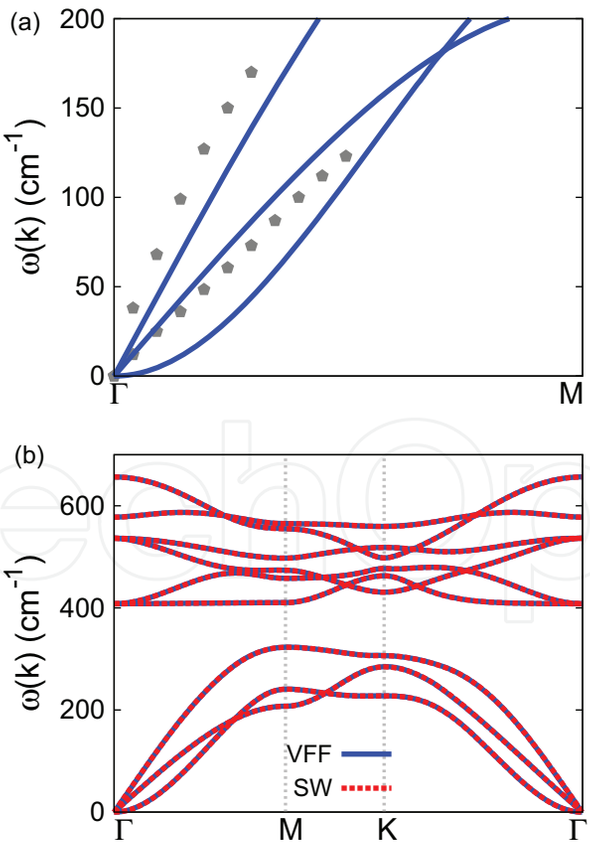

Figure 31. Phonon spectrum for single-layer 1H-FeO_2. (a) Phonon dispersion along the ΓM direction in the Brillouin zone. The results from the VFF model (lines) are comparable with the *ab initio* results (pentagons) from [12]. (b) The phonon dispersion from the SW potential is exactly the same as that from the VFF model.

model and the SW potential give exactly the same phonon dispersion, as the SW potential is derived from the VFF model.

The parameters for the two-body SW potential used by GULP are shown in **Table 67**. The parameters for the three-body SW potential used by GULP are shown in **Table 68**. Some representative parameters for the SW potential used by LAMMPS are listed in **Table 69**. We note that 12 atom types have been introduced for the simulation of the single-layer 1H-FeO_2 using LAMMPS, because the angles around atom Fe in **Figure 1** (with M = Fe and X = O) are not distinguishable in LAMMPS. We have suggested two options to differentiate these angles by implementing some additional constraints in LAMMPS, which can be accomplished by modifying the source file of LAMMPS [13, 14]. According to our experience, it is not so convenient for some users to implement these constraints and recompile the LAMMPS package. Hence, in the present work, we differentiate the angles by introducing more atom types, so it is not necessary to modify the LAMMPS package. **Figure 2** (with M = Fe and X = O) shows that, for 1H-FeO_2, we can differentiate these angles around the Fe atom by assigning these six neighboring O atoms with different atom types. It can be found that 12 atom types are necessary for the purpose of differentiating all 6 neighbors around 1 Fe atom.

We use LAMMPS to perform MD simulations for the mechanical behavior of the single-layer 1H-FeO_2 under uniaxial tension at 1 and 300 K. **Figure 32** shows the stress-strain curve for the tension of a single-layer 1H-FeO_2 of dimension 100×100 Å. Periodic boundary conditions are applied in both armchair and zigzag directions. The single-layer 1H-FeO_2 is stretched

	A (eV)	ρ (Å)	B (Å^4)	r_{min} (Å)	r_{max} (Å)
Fe—O	4.242	0.962	6.246	0.0	2.552

Table 67. Two-body SW potential parameters for single-layer 1H-FeO_2 used by GULP [8] as expressed in Eq. (3).

	K (eV)	θ_0 (°)	ρ_1 (Å)	ρ_2 (Å)	r_{min12} (Å)	r_{max12} (Å)	r_{min13} (Å)	r_{max13} (Å)	r_{min23} (Å)	r_{max23} (Å)
$\theta_{Fe—O—O}$	28.105	88.343	0.962	0.962	0.0	2.552	0.0	2.552	0.0	3.031
$\theta_{Fe—O—O'}$	30.754	72.856	0.962	0.962	0.0	2.552	0.0	2.552	0.0	3.031
$\theta_{O—Fe—Fe}$	28.105	88.343	0.962	0.962	0.0	2.552	0.0	2.552	0.0	3.031

The angle θ_{ijk} in the first line indicates the bending energy for the angle with atom i as the apex.

Table 68. Three-body SW potential parameters for single-layer 1H-FeO_2 used by GULP [8] as expressed in Eq. (4).

	ϵ (eV)	σ (Å)	a	λ	γ	$\cos\theta_0$	A_L	B_L	p	q	Tol
$Fe_1—O_1—O_1$	1.000	0.962	2.654	0.000	1.000	0.000	4.242	7.298	4	0	0.0
$Fe_1—O_1—O_3$	1.000	0.000	0.000	28.105	1.000	0.029	0.000	0.000	4	0	0.0
$Fe_1—O_1—O_2$	1.000	0.000	0.000	30.754	1.000	0.295	0.000	0.000	4	0	0.0
$O_1—Fe_1—Fe_3$	1.000	0.000	0.000	28.105	1.000	0.029	0.000	0.000	4	0	0.0

Table 69. SW potential parameters for single-layer 1H-FeO_2 used by LAMMPS [9] as expressed in Eqs. (9) and (10).

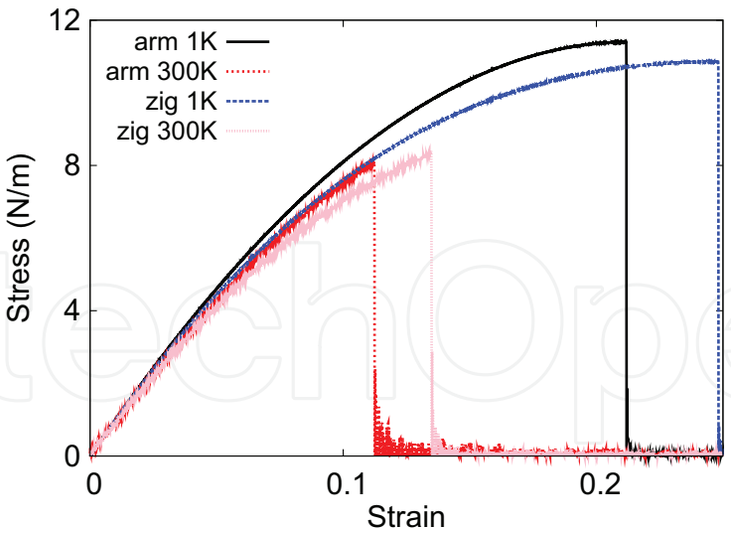

Figure 32. Stress-strain for single-layer 1H-FeO_2 of dimension 100 × 100 Å along the armchair and zigzag directions.

uniaxially along the armchair or zigzag direction. The stress is calculated without involving the actual thickness of the quasi-two-dimensional structure of the single-layer 1H-FeO_2. The Young's modulus can be obtained by a linear fitting of the stress-strain relation in the small strain range of [0, 0.01]. The Young's modulus is 100.2 and 99.3 N/m along the armchair and zigzag directions, respectively. The Young's modulus is essentially isotropic in the armchair and zigzag directions. The Poisson's ratio from the VFF model and the SW potential is $\nu_{xy} = \nu_{yx} = 0.23$.

There is no available value for nonlinear quantities in the single-layer 1H-FeO_2. We have thus used the nonlinear parameter $B = 0.5d^4$ in Eq. (5), which is close to the value of B in most materials. The value of the third-order nonlinear elasticity D can be extracted by fitting the stress-strain relation to the function $\sigma = E\epsilon + \frac{1}{2}D\epsilon^2$ with E as the Young's modulus. The values of D from the present SW potential are −423.4 and −460.2 N/m along the armchair and zigzag directions, respectively. The ultimate stress is about 11.4 N/m at the ultimate strain of 0.21 in the armchair direction at the low temperature of 1 K. The ultimate stress is about 10.9 N/m at the ultimate strain of 0.25 in the zigzag direction at the low temperature of 1 K.

18 1H-FES_2

Most existing theoretical studies on the single-layer 1H-FeS_2 are based on the first-principles calculations. In this section, we will develop the SW potential for the single-layer 1H-FeS_2.

The structure for the single-layer 1H-FeS_2 is shown in **Figure 1** (with M=Fe and X=S). Each Fe atom is surrounded by six S atoms. These S atoms are categorized into the top group (e.g., atoms 1, 3, and 5) and bottom group (e.g., atoms 2, 4, and 6). Each S atom is connected to three Fe atoms. The structural parameters are from the first-principles calculations [12], including the lattice constant $a = 3.06$ Å and the bond length $d_{\text{Fe–S}} = 2.22$ Å. The resultant angles are

$\theta_{\mathrm{FeSS}} = \theta_{\mathrm{SFeFe}} = 87.132^\circ$ and $\theta_{\mathrm{FeSS'}} = 74.537^\circ$, in which atoms S and S′ are from different (top or bottom) groups.

Table 70 shows four VFF terms for the single-layer 1H-FeS_2; one of which is the bond stretching interaction shown by Eq. (1), while the other three terms are the angle bending interaction shown by Eq. (2). These force constant parameters are determined by fitting to the three acoustic branches in the phonon dispersion along the ΓM as shown in **Figure 33(a)**. The *ab initio* calculations for the phonon dispersion are from Ref. [12]. **Figure 33(b)** shows that the

VFF type	**Bond stretching**	**Angle bending**		
Expression	$\frac{1}{2}K_{\mathrm{Fe-S}}(\Delta r)^2$	$\frac{1}{2}K_{\mathrm{Fe-S-S}}(\Delta\theta)^2$	$\frac{1}{2}K_{\mathrm{Fe-S-S'}}(\Delta\theta)^2$	$\frac{1}{2}K_{\mathrm{S-Fe-Fe}}(\Delta\theta)^2$
Parameter	6.338	3.964	3.964	3.964
r_0 or θ_0	2.220	87.132	74.537	87.132

The second line gives an explicit expression for each VFF term. The third line is the force constant parameters. Parameters are in the unit of eV/Å^2 for the bond stretching interaction and in the unit of eV for the angle bending interaction. The fourth line gives the initial bond length (in the unit of Å) for the bond stretching interaction and the initial angle (in the unit of degrees) for the angle bending interaction. The angle θ_{ijk} has atom i as the apex.

Table 70. The VFF model for single-layer 1H-FeS_2.

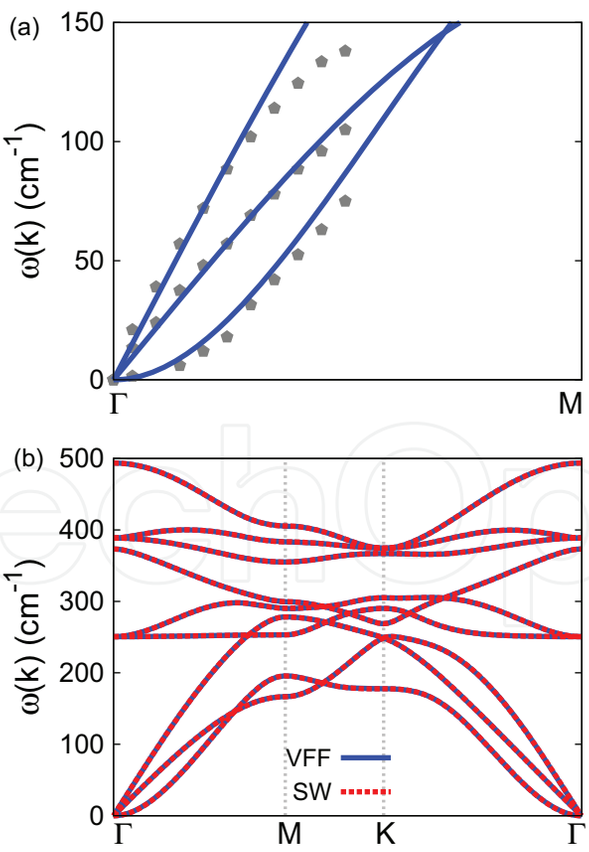

Figure 33. Phonon spectrum for single-layer 1H-FeS_2. (a) Phonon dispersion along the ΓM direction in the Brillouin zone. The results from the VFF model (lines) are comparable with the *ab initio* results (pentagons) from Ref. [12]. (b) The phonon dispersion from the SW potential is exactly the same as that from the VFF model.

VFF model and the SW potential give exactly the same phonon dispersion, as the SW potential is derived from the VFF model.

The parameters for the two-body SW potential used by GULP are shown in **Table 71**. The parameters for the three-body SW potential used by GULP are shown in **Table 72**. Some representative parameters for the SW potential used by LAMMPS are listed in **Table 73**. We note that 12 atom types have been introduced for the simulation of the single-layer 1H-FeS_2 using LAMMPS, because the angles around atom Fe in **Figure 1** (with M=Fe and X=S) are not distinguishable in LAMMPS. We have suggested two options to differentiate these angles by implementing some additional constraints in LAMMPS, which can be accomplished by modifying the source file of LAMMPS [13, 14]. According to our experience, it is not so convenient for some users to implement these constraints and recompile the LAMMPS package. Hence, in the present work, we differentiate the angles by introducing more atom types, so it is not necessary to modify the LAMMPS package. **Figure 2** (with M=Fe and X=S) shows that, for 1H-FeS_2, we can differentiate these angles around the Fe atom by assigning these six neighboring S atoms with different atom types. It can be found that 12 atom types are necessary for the purpose of differentiating all 6 neighbors around 1 Fe atom.

We use LAMMPS to perform MD simulations for the mechanical behavior of the single-layer 1H-FeS_2 under uniaxial tension at 1 and 300 K. **Figure 34** shows the stress-strain curve for the tension of a single-layer 1H-FeS_2 of dimension 100 × 100 Å. Periodic boundary conditions are applied in both armchair and zigzag directions. The single-layer 1H-FeS_2 is stretched

	A (eV)	ρ (Å)	B (Å^4)	r_{min} (Å)	r_{max} (Å)
Fe—S	4.337	1.097	12.145	0.0	3.000

Table 71. Two-body SW potential parameters for single-layer 1H-FeS_2 used by GULP [8] as expressed in Eq. (3).

	K (eV)	θ_0 (°)	ρ_1 (Å)	ρ_2 (Å)	r_{min12} (Å)	r_{max12} (Å)	r_{min13} (Å)	r_{max13} (Å)	r_{min23} (Å)	r_{max23} (Å)
θ_{Fe-S-S}	33.060	87.132	1.097	1.097	0.0	3.000	0.0	3.000	0.0	3.567
$\theta_{Fe-S-S'}$	35.501	74.537	1.097	1.097	0.0	3.000	0.0	3.000	0.0	3.567
$\theta_{S-Fe-Fe}$	33.060	87.132	1.097	1.097	0.0	3.000	0.0	3.000	0.0	3.567

The angle θ_{ijk} in the first line indicates the bending energy for the angle with atom i as the apex.

Table 72. Three-body SW potential parameters for single-layer 1H-FeS_2 used by GULP [8] as expressed in Eq. (4).

	ϵ (eV)	σ (Å)	a	λ	γ	$\cos\theta_0$	A_L	B_L	p	q	Tol
Fe_1—S_1—S_1	1.000	1.097	2.735	0.000	1.000	0.000	4.337	8.338	4	0	0.0
Fe_1—S_1—S_3	1.000	0.000	0.000	33.060	1.000	0.050	0.000	0.000	4	0	0.0
Fe_1—S_1—S_2	1.000	0.000	0.000	35.501	1.000	0.267	0.000	0.000	4	0	0.0
S_1—Fe_1—Fe_3	1.000	0.000	0.000	33.060	1.000	0.050	0.000	0.000	4	0	0.0

Table 73. SW potential parameters for single-layer 1H-FeS_2 used by LAMMPS [9] as expressed in Eqs. (9) and (10).

http://dx.doi.org/10.5772/intechopen.71929

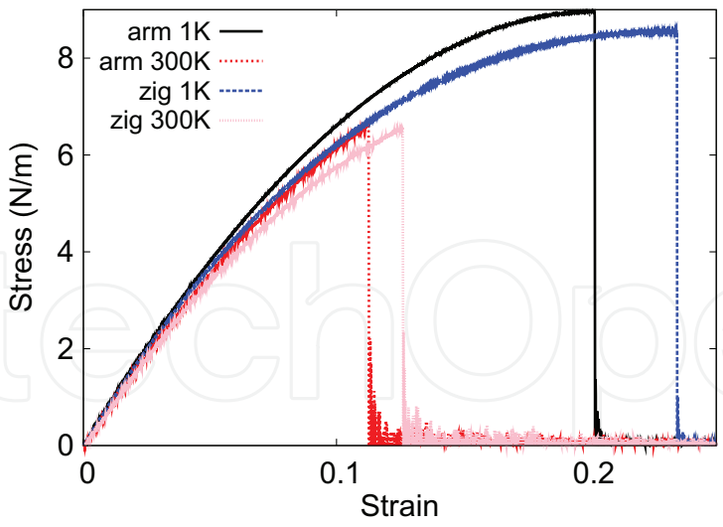

Figure 34. Stress-strain for single-layer 1H-FeS_2 of dimension 100 × 100 Å along the armchair and zigzag directions.

uniaxially along the armchair or zigzag direction. The stress is calculated without involving the actual thickness of the quasi-two-dimensional structure of the single-layer 1H-FeS_2. The Young's modulus can be obtained by a linear fitting of the stress-strain relation in the small strain range of [0, 0.01]. The Young's modulus is 83.6 and 83.4 N/m along the armchair and zigzag directions, respectively. The Young's modulus is essentially isotropic in the armchair and zigzag directions. The Poisson's ratio from the VFF model and the SW potential is $\nu_{xy} = \nu_{yx} = 0.20$.

There is no available value for nonlinear quantities in the single-layer 1H-FeS_2. We have thus used the nonlinear parameter $B = 0.5d^4$ in Eq. (5), which is close to the value of B in most materials. The value of the third-order nonlinear elasticity D can be extracted by fitting the stress-strain relation to the function $\sigma = E\epsilon + \frac{1}{2}D\epsilon^2$ with E as the Young's modulus. The values of D from the present SW potential are -377.5 and -412.7 N/m along the armchair and zigzag directions, respectively. The ultimate stress is about 9.0 N/m at the ultimate strain of 0.20 in the armchair direction at the low temperature of 1 K. The ultimate stress is about 8.6 N/m at the ultimate strain of 0.23 in the zigzag direction at the low temperature of 1 K.

19. 1H-$FESE_2$

Most existing theoretical studies on the single-layer 1H-$FeSe_2$ are based on the first-principles calculations. In this section, we will develop the SW potential for the single-layer 1H-$FeSe_2$.

The structure for the single-layer 1H-$FeSe_2$ is shown in **Figure 1** (with M=Fe and X=Se). Each Fe atom is surrounded by six Se atoms. These Se atoms are categorized into the top group (e.g., atoms 1, 3, and 5) and bottom group (e.g., atoms 2, 4, and 6). Each Se atom is connected to three Fe atoms. The structural parameters are from the first-principles calculations [12], including the lattice constant $a = 3.22$ Å and the bond length $d_{\mathrm{Fe-Se}} = 2.35$ Å. The resultant angles are

$\theta_{\mathrm{FeSeSe}} = \theta_{\mathrm{SeFeFe}} = 86.488^\circ$ and $\theta_{\mathrm{FeSeSe'}} = 75.424^\circ$, in which atoms Se and Se′ are from different (top or bottom) groups.

Table 74 shows four VFF terms for the single-layer 1H-$FeSe_2$; one of which is the bond stretching interaction shown by Eq. (1), while the other three terms are the angle bending interaction shown by Eq. (2). These force constant parameters are determined by fitting to the three acoustic branches in the phonon dispersion along the ΓM as shown in **Figure 35(a)**. The

VFF type	Bond stretching	Angle bending		
Expression	$\frac{1}{2}K_{\mathrm{Fe-Se}}(\Delta r)^2$	$\frac{1}{2}K_{\mathrm{Fe-Se-Se}}(\Delta\theta)^2$	$\frac{1}{2}K_{\mathrm{Fe-Se-Se'}}(\Delta\theta)^2$	$\frac{1}{2}K_{\mathrm{Se-Fe-Fe}}(\Delta\theta)^2$
Parameter	6.338	3.964	3.964	3.964
r_0 or θ_0	2.350	86.488	75.424	86.488

The second line gives an explicit expression for each VFF term. The third line is the force constant parameters. Parameters are in the unit of eV/Å^2 for the bond stretching interaction and in the unit of eV for the angle bending interaction. The fourth line gives the initial bond length (in the unit of Å) for the bond stretching interaction and the initial angle (in the unit of degrees) for the angle bending interaction. The angle θ_{ijk} has atom i as the apex.

Table 74. The VFF model for single-layer 1H-$FeSe_2$.

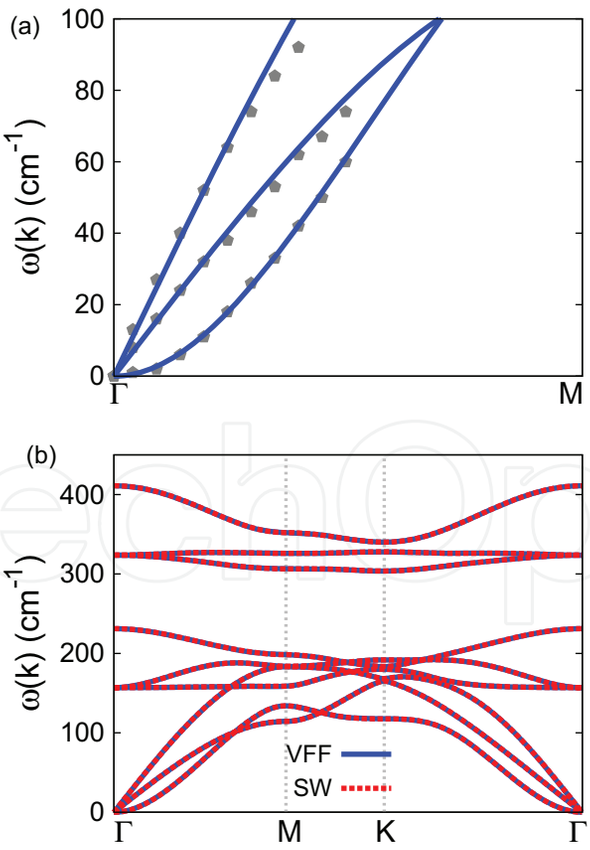

Figure 35. Phonon spectrum for single-layer 1H-$FeSe_2$. (a) Phonon dispersion along the ΓM direction in the Brillouin zone. The results from the VFF model (lines) are comparable with the *ab initio* results (pentagons) from Ref. [12]. (b) The phonon dispersion from the SW potential is exactly the same as that from the VFF model.

ab initio calculations for the phonon dispersion are from Ref. [12]. **Figure 35(b)** shows that the VFF model and the SW potential give exactly the same phonon dispersion, as the SW potential is derived from the VFF model.

The parameters for the two-body SW potential used by GULP are shown in **Table 75**. The parameters for the three-body SW potential used by GULP are shown in **Table 76**. Some representative parameters for the SW potential used by LAMMPS are listed in **Table 77**. We note that 12 atom types have been introduced for the simulation of the single-layer 1H-$FeSe_2$ using LAMMPS, because the angles around atom Fe in **Figure 1** (with M=Fe and X=Se) are not distinguishable in LAMMPS. We have suggested two options to differentiate these angles by implementing some additional constraints in LAMMPS, which can be accomplished by modifying the source file of LAMMPS [13, 14]. According to our experience, it is not so convenient for some users to implement these constraints and recompile the LAMMPS package. Hence, in the present work, we differentiate the angles by introducing more atom types, so it is not necessary to modify the LAMMPS package. **Figure 2** (with M=Fe and X=Se) shows that, for 1H-$FeSe_2$, we can differentiate these angles around the Fe atom by assigning these six neighboring Se atoms with different atom types. It can be found that 12 atom types are necessary for the purpose of differentiating all 6 neighbors around 1 Fe atom.

We use LAMMPS to perform MD simulations for the mechanical behavior of the single-layer 1H-$FeSe_2$ under uniaxial tension at 1 and 300 K. **Figure 36** shows the stress-strain curve for the tension of a single-layer 1H-$FeSe_2$ of dimension 100 × 100 Å. Periodic boundary conditions are

	A (eV)	ρ (Å)	B (Å^4)	$r_{\min}$ (Å)	$r_{\max}$ (Å)
Fe-Se	4.778	1.139	15.249	0.0	3.168

Table 75. Two-body SW potential parameters for single-layer 1H-$FeSe_2$ used by GULP [8] as expressed in Eq. (3).

	K (eV)	θ_0 (°)	ρ_1 (Å)	ρ_2 (Å)	$r_{\min 12}$ (Å)	$r_{\max 12}$ (Å)	$r_{\min 13}$ (Å)	$r_{\max 13}$ (Å)	$r_{\min 23}$ (Å)	$r_{\max 23}$ (Å)
$\theta_{\mathrm{Fe-Se-Se}}$	32.235	86.488	1.139	1.139	0.0	3.168	0.0	3.168	0.0	3.768
$\theta_{\mathrm{Fe-Se-Se'}}$	34.286	75.424	1.139	1.139	0.0	3.168	0.0	3.168	0.0	3.768
$\theta_{\mathrm{Se-Fe-Fe}}$	32.235	86.488	1.139	1.139	0.0	3.168	0.0	3.168	0.0	3.768

The angle θ_{ijk} in the first line indicates the bending energy for the angle with atom i as the apex.

Table 76. Three-body SW potential parameters for single-layer 1H-$FeSe_2$ used by GULP [8] as expressed in Eq. (4).

	ϵ (eV)	σ (Å)	a	λ	γ	$\cos\theta_0$	A_L	B_L	p	q	Tol
Fe_1—Se_1—Se_1	1.000	1.139	2.781	0.000	1.000	0.000	4.778	9.049	4	0	0.0
Fe_1—Se_1—Se_3	1.000	0.000	0.000	32.235	1.000	0.061	0.000	0.000	4	0	0.0
Fe_1—Se_1—Se_2	1.000	0.000	0.000	34.286	1.000	0.252	0.000	0.000	4	0	0.0
Se_1—Fe_1—Fe_3	1.000	0.000	0.000	32.235	1.000	0.061	0.000	0.000	4	0	0.0

Table 77. SW potential parameters for single-layer 1H-$FeSe_2$ used by LAMMPS [9] as expressed in Eqs. (9) and (10).

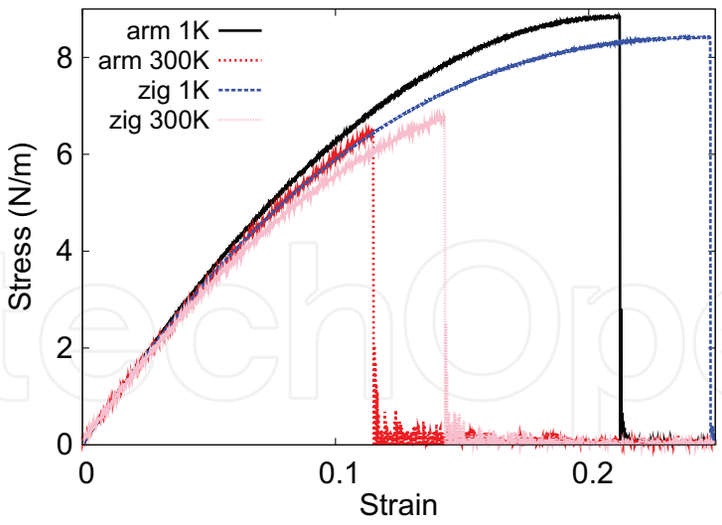

Figure 36. Stress-strain for single-layer 1H-$FeSe_2$ of dimension 100 × 100 Å along the armchair and zigzag directions.

applied in both armchair and zigzag directions. The single-layer 1H-$FeSe_2$ is stretched uniaxially along the armchair or zigzag direction. The stress is calculated without involving the actual thickness of the quasi-two-dimensional structure of the single-layer 1H-$FeSe_2$. The Young's modulus can be obtained by a linear fitting of the stress-strain relation in the small strain range of [0, 0.01]. The Young's modulus is 77.3 and 77.4 N/m along the armchair and zigzag directions, respectively. The Young's modulus is essentially isotropic in the armchair and zigzag directions. The Poisson's ratio from the VFF model and the SW potential is $\nu_{xy} = \nu_{yx} = 0.23$.

There is no available value for nonlinear quantities in the single-layer 1H-$FeSe_2$. We have thus used the nonlinear parameter $B = 0.5d^4$ in Eq. (5), which is close to the value of B in most materials. The value of the third-order nonlinear elasticity D can be extracted by fitting the stress-strain relation to the function $\sigma = E\epsilon + \frac{1}{2}D\epsilon^2$ with E as the Young's modulus. The values of D from the present SW potential are −323.8 and −360.8 N/m along the armchair and zigzag directions, respectively. The ultimate stress is about 8.8 N/m at the ultimate strain of 0.21 in the armchair direction at the low temperature of 1 K. The ultimate stress is about 8.4 N/m at the ultimate strain of 0.25 in the zigzag direction at the low temperature of 1 K.

20. 1H-$FETE_2$

Most existing theoretical studies on the single-layer 1H-$FeTe_2$ are based on the first-principles calculations. In this section, we will develop the SW potential for the single-layer 1H-$FeTe_2$.

The structure for the single-layer 1H-$FeTe_2$ is shown in **Figure 1** (with M=Fe and X=Te). Each Fe atom is surrounded by six Te atoms. These Te atoms are categorized into the top group (e.g., atoms 1, 3, and 5) and bottom group (e.g., atoms 2, 4, and 6). Each Te atom is connected to three Fe atoms. The structural parameters are from the first-principles calculations [12],

including the lattice constant $a = 3.48$ Å and the bond length $d_{\mathrm{Fe-Te}} = 2.53$ Å. The resultant angles are $\theta_{\mathrm{FeTeTe}} = \theta_{\mathrm{TeFeFe}} = 86.904^{\circ}$ and $\theta_{\mathrm{FeTeTe'}} = 74.851^{\circ}$, in which atoms Te and Te' are from different (top or bottom) groups.

Table 78 shows four VFF terms for the single-layer 1H-$FeTe_2$; one of which is the bond stretching interaction shown by Eq. (1), while the other three terms are the angle bending interaction shown by Eq. (2). These force constant parameters are determined by fitting to the two in-plane acoustic branches in the phonon dispersion along the ΓM as shown in **Figure 37(a)**. The *ab initio* calculations for the phonon dispersion are from Ref. [12]. **Figure 37(b)** shows that the VFF model and the SW potential give exactly the same phonon dispersion, as the SW potential is derived from the VFF model.

The parameters for the two-body SW potential used by GULP are shown in **Table 79**. The parameters for the three-body SW potential used by GULP are shown in **Table 80**. Some representative parameters for the SW potential used by LAMMPS are listed in **Table 81**. We note that 12 atom types have been introduced for the simulation of the single-layer 1H-$FeTe_2$ using LAMMPS, because the angles around atom Fe in **Figure 1** (with M=Fe and X=Te) are not distinguishable in LAMMPS. We have suggested two options to differentiate these angles by implementing some additional constraints in LAMMPS, which can be accomplished by modifying the source file of LAMMPS [13, 14]. According to our experience, it is not so convenient for some users to implement these constraints and recompile the LAMMPS package. Hence, in the present work, we differentiate the angles by introducing more atom types, so it is not necessary to modify the LAMMPS package. **Figure 2** (with M=Fe and X=Te) shows that, for 1H-$FeTe_2$, we can differentiate these angles around the Fe atom by assigning these six neighboring Te atoms with different atom types. It can be found that 12 atom types are necessary for the purpose of differentiating all 6 neighbors around 1 Fe atom.

We use LAMMPS to perform MD simulations for the mechanical behavior of the single-layer 1H-$FeTe_2$ under uniaxial tension at 1 and 300 K. **Figure 38** shows the stress-strain curve for the tension of a single-layer 1H-$FeTe_2$ of dimension 100×100 Å. Periodic boundary conditions are applied in both armchair and zigzag directions. The single-layer 1H-$FeTe_2$ is stretched uniaxially along the armchair or zigzag direction. The stress is calculated without involving the actual thickness of the quasi-two-dimensional structure of the single-layer 1H-$FeTe_2$. The Young's modulus can be obtained by a linear fitting of the stress-strain relation in the small

VFF type	**Bond stretching**	**Angle bending**		
Expression	$\frac{1}{2}K_{\mathrm{Fe-Te}}(\Delta r)^2$	$\frac{1}{2}K_{\mathrm{Fe-Te-Te}}(\Delta\theta)^2$	$\frac{1}{2}K_{\mathrm{Fe-Te-Te'}}(\Delta\theta)^2$	$\frac{1}{2}K_{\mathrm{Te-Fe-Fe}}(\Delta\theta)^2$
Parameter	6.338	3.964	3.964	3.964
r_0 or θ_0	2.530	86.904	74.851	86.904

The second line gives an explicit expression for each VFF term. The third line is the force constant parameters. Parameters are in the unit of eV/Å^2 for the bond stretching interaction and in the unit of eV for the angle bending interaction. The fourth line gives the initial bond length (in the unit of Å) for the bond stretching interaction and the initial angle (in the unit of degrees) for the angle bending interaction. The angle θ_{ijk} has atom i as the apex.

Table 78. The VFF model for single-layer 1H-$FeTe_2$.

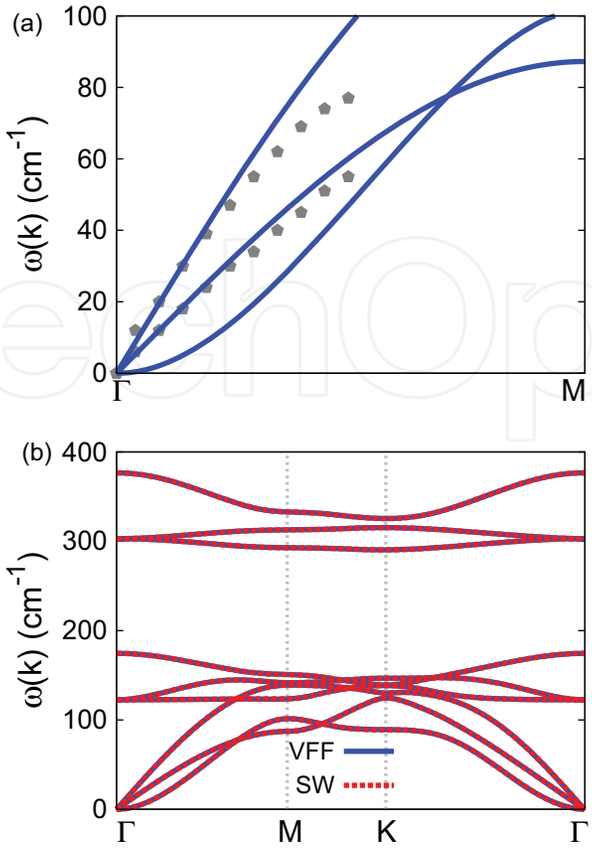

Figure 37. Phonon spectrum for single-layer 1H-$FeTe_2$. (a) Phonon dispersion along the ΓM direction in the Brillouin zone. The results from the VFF model (lines) are comparable with the *ab initio* results (pentagons) from Ref. [12]. (b) The phonon dispersion from the SW potential is exactly the same as that from the VFF model.

	A (eV)	ρ (Å)	B (Å^4)	r_{min} (Å)	r_{max} (Å)
Fe—Te	5.599	1.242	20.486	0.0	3.416

Table 79. Two-body SW potential parameters for single-layer 1H-$FeTe_2$ used by GULP [8] as expressed in Eq. (3).

	K (eV)	θ_0 (°)	ρ_1 (Å)	ρ_2 (Å)	$r_{min\,12}$ (Å)	$r_{max\,12}$ (Å)	$r_{min\,13}$ (Å)	$r_{max\,13}$ (Å)	$r_{min\,23}$ (Å)	$r_{max\,23}$ (Å)
$\theta_{Fe-Te-Te}$	32.766	86.904	1.242	1.242	0.0	3.416	0.0	3.416	0.0	4.062
$\theta_{Fe-Te-Te'}$	35.065	74.851	1.242	1.242	0.0	3.416	0.0	3.416	0.0	4.062
$\theta_{Te-Fe-Fe}$	32.766	86.904	1.242	1.242	0.0	3.416	0.0	3.416	0.0	4.062

The angle θ_{ijk} in the first line indicates the bending energy for the angle with atom i as the apex.

Table 80. Three-body SW potential parameters for single-layer 1H-$FeTe_2$ used by GULP [8] as expressed in Eq. (4).

strain range of [0, 0.01]. The Young's modulus is 69.6 and 69.8 N/m along the armchair and zigzag directions, respectively. The Young's modulus is essentially isotropic in the armchair and zigzag directions. The Poisson's ratio from the VFF model and the SW potential is $\nu_{xy} = \nu_{yx} = 0.25$.

http://dx.doi.org/10.5772/intechopen.71929

	ϵ (eV)	σ (Å)	a	λ	γ	$\cos\theta_0$	A_L	B_L	p	q	Tol
Fe_1—Te_1—Te_1	1.000	1.242	2.751	0.000	1.000	0.000	5.599	8.615	4	0	0.0
Fe_1—Te_1—Te_3	1.000	0.000	0.000	32.766	1.000	0.054	0.000	0.000	4	0	0.0
Fe_1—Te_1—Te_2	1.000	0.000	0.000	35.065	1.000	0.261	0.000	0.000	4	0	0.0
Te_1—Fe_1—Fe_3	1.000	0.000	0.000	32.766	1.000	0.054	0.000	0.000	4	0	0.0

Table 81. SW potential parameters for single-layer 1H-$FeTe_2$ used by LAMMPS [9] as expressed in Eqs. (9) and (10).

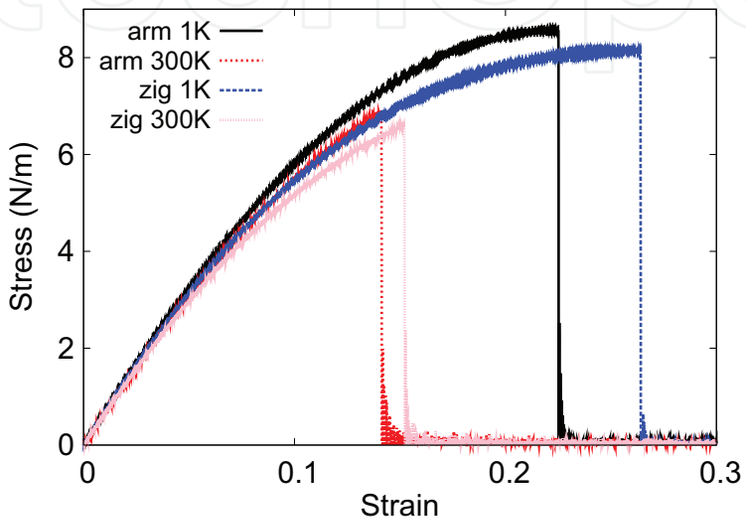

Figure 38. Stress-strain for single-layer 1H-$FeTe_2$ of dimension 100 × 100 Å along the armchair and zigzag directions.

There is no available value for nonlinear quantities in the single-layer 1H-$FeTe_2$. We have thus used the nonlinear parameter $B = 0.5d^4$ in Eq. (5), which is close to the value of B in most materials. The value of the third-order nonlinear elasticity D can be extracted by fitting the stress-strain relation to the function $\sigma = E\epsilon + \frac{1}{2}D\epsilon^2$ with E as the Young's modulus. The values of D from the present SW potential are −267.5 and −302.8 N/m along the armchair and zigzag directions, respectively. The ultimate stress is about 8.6 N/m at the ultimate strain of 0.22 in the armchair direction at the low temperature of 1 K. The ultimate stress is about 8.1 N/m at the ultimate strain of 0.26 in the zigzag direction at the low temperature of 1 K.

21. 1H-$COTE_2$

Most existing theoretical studies on the single-layer 1H-$CoTe_2$ are based on the first-principles calculations. In this section, we will develop the SW potential for the single-layer 1H-$CoTe_2$.

The structure for the single-layer 1H-$CoTe_2$ is shown in **Figure 1** (with M=Co and X=Te). Each Co atom is surrounded by six Te atoms. These Te atoms are categorized into the top group (e.g., atoms 1, 3, and 5) and bottom group (e.g., atoms 2, 4, and 6). Each Te atom is connected to

three Co atoms. The structural parameters are from the first-principles calculations [12], including the lattice constant $a = 3.52$ Å and the bond length $d_{\mathrm{Co-Te}} = 2.51$ Å. The resultant angles are $\theta_{\mathrm{CoTeTe}} = \theta_{\mathrm{TeCoCo}} = 89.046^{\circ}$ and $\theta_{\mathrm{CoTeTe'}} = 71.873^{\circ}$, in which atoms Te and Te′ are from different (top or bottom) groups.

Table 82 shows four VFF terms for the single-layer 1H-$CoTe_2$; one of which is the bond stretching interaction shown by Eq. (1), while the other three terms are the angle bending interaction shown by Eq. (2). These force constant parameters are determined by fitting to the acoustic branches in the phonon dispersion along the ΓM as shown in **Figure 39(a)**. The *ab initio* calculations for the phonon dispersion are from Ref. [12]. **Figure 39(b)** shows that the VFF model and the SW potential give exactly the same phonon dispersion, as the SW potential is derived from the VFF model.

The parameters for the two-body SW potential used by GULP are shown in **Table 83**. The parameters for the three-body SW potential used by GULP are shown in **Table 84**. Some representative parameters for the SW potential used by LAMMPS are listed in **Table 85**. We note that 12 atom types have been introduced for the simulation of the single-layer 1H-$CoTe_2$ using LAMMPS, because the angles around atom Co in **Figure 1** (with M=Co and X=Te) are not distinguishable in LAMMPS. We have suggested two options to differentiate these angles by implementing some additional constraints in LAMMPS, which can be accomplished by modifying the source file of LAMMPS [13, 14]. According to our experience, it is not so convenient for some users to implement these constraints and recompile the LAMMPS package. Hence, in the present work, we differentiate the angles by introducing more atom types, so it is not necessary to modify the LAMMPS package. **Figure 2** (with M=Co and X=Te) shows that, for 1H-$CoTe_2$, we can differentiate these angles around the Co atom by assigning these six neighboring Te atoms with different atom types. It can be found that 12 atom types are necessary for the purpose of differentiating all 6 neighbors around 1 Co atom.

We use LAMMPS to perform MD simulations for the mechanical behavior of the single-layer 1H-$CoTe_2$ under uniaxial tension at 1 and 300 K. **Figure 40** shows the stress-strain curve for the tension of a single-layer 1H-$CoTe_2$ of dimension 100×100 Å. Periodic boundary conditions are applied in both armchair and zigzag directions. The single-layer 1H-$CoTe_2$ is stretched uniaxially along the armchair or zigzag direction. The stress is calculated without involving

VFF type	**Bond stretching**	**Angle bending**		
Expression	$\frac{1}{2}K_{\mathrm{Co-Te}}(\Delta r)^2$	$\frac{1}{2}K_{\mathrm{Co-Te-Te}}(\Delta\theta)^2$	$\frac{1}{2}K_{\mathrm{Co-Te-Te'}}(\Delta\theta)^2$	$\frac{1}{2}K_{\mathrm{Te-Co-Co}}(\Delta\theta)^2$
Parameter	6.712	2.656	2.656	2.656
r_0 or θ_0	2.510	89.046	71.873	89.046

The second line gives an explicit expression for each VFF term. The third line is the force constant parameters. Parameters are in the unit of eV/Å^2 for the bond stretching interaction and in the unit of eV for the angle bending interaction. The fourth line gives the initial bond length (in the unit of Å^2) for the bond stretching interaction and the initial angle (in the unit of degrees) for the angle bending interaction. The angle θ_{ijk} has atom i as the apex.

Table 82. The VFF model for single-layer 1H-$CoTe_2$.

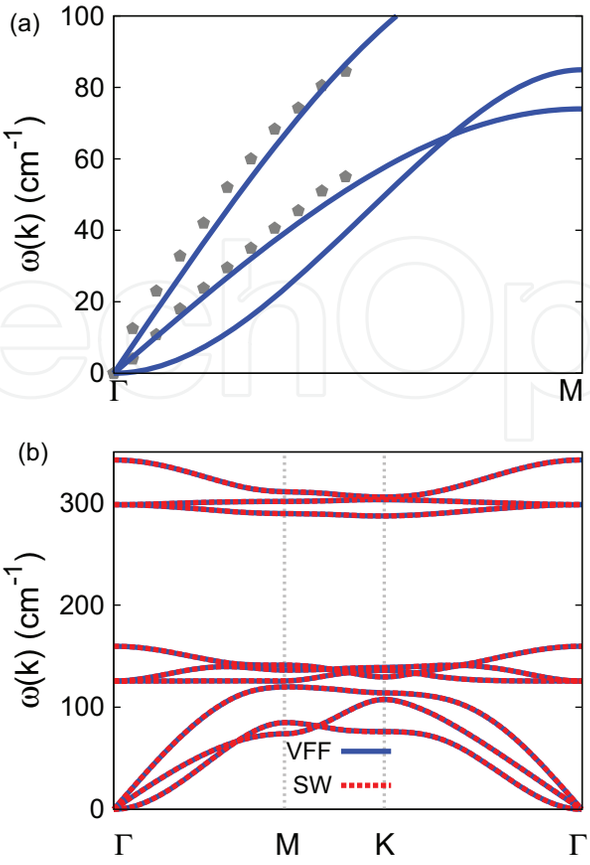

Figure 39. Phonon spectrum for single-layer 1H-$CoTe_2$. (a) Phonon dispersion along the ΓM direction in the Brillouin zone. The results from the VFF model (lines) are comparable with the *ab initio* results (pentagons) from Ref. [12]. (b) The phonon dispersion from the SW potential is exactly the same as that from the VFF model.

	A (eV)	ρ (Å)	B (Å^4)	r_{min} (Å)	r_{max} (Å)
Co—Te	6.169	1.310	19.846	0.0	3.417

Table 83. Two-body SW potential parameters for single-layer 1H-$CoTe_2$ used by GULP [8] as expressed in Eq. (3).

	K (eV)	θ_0 (°)	ρ_1 (Å)	ρ_2 (Å)	r_{min12} (Å)	r_{max12} (Å)	r_{min13} (Å)	r_{max13} (Å)	r_{min23} (Å)	r_{max23} (Å)
$\theta_{Co-Te-Te}$	23.895	89.046	1.310	1.310	0.0	3.417	0.0	3.417	0.0	4.055
$\theta_{Co-Te-Te'}$	26.449	71.873	1.310	1.310	0.0	3.417	0.0	3.417	0.0	4.055
$\theta_{Te-Co-Co}$	23.895	89.046	1.310	1.310	0.0	3.417	0.0	3.417	0.0	4.055

The angle θ_{ijk} in the first line indicates the bending energy for the angle with atom i as the apex.

Table 84. Three-body SW potential parameters for single-layer 1H-$CoTe_2$ used by GULP [8] as expressed in Eq. (4).

the actual thickness of the quasi-two-dimensional structure of the single-layer 1H-$CoTe_2$. The Young's modulus can be obtained by a linear fitting of the stress-strain relation in the small strain range of [0, 0.01]. The Young's modulus is 53.7 and 54.3 N/m along the armchair and

	ϵ (eV)	σ (Å)	a	λ	γ	$\cos\theta_0$	A_L	B_L	p	q	Tol
Co_1—Te_1—Te_1	1.000	1.310	2.608	0.000	1.000	0.000	6.169	6.739	4	0	0.0
Co_1—Te_1—Te_3	1.000	0.000	0.000	23.895	1.000	0.017	0.000	0.000	4	0	0.0
Co_1—Te_1—Te_2	1.000	0.000	0.000	26.449	1.000	0.311	0.000	0.000	4	0	0.0
Te_1—Co_1—Co_3	1.000	0.000	0.000	23.895	1.000	0.017	0.000	0.000	4	0	0.0

Table 85. SW potential parameters for single-layer 1H-$CoTe_2$ used by LAMMPS [9] as expressed in Eqs. (9) and (10).

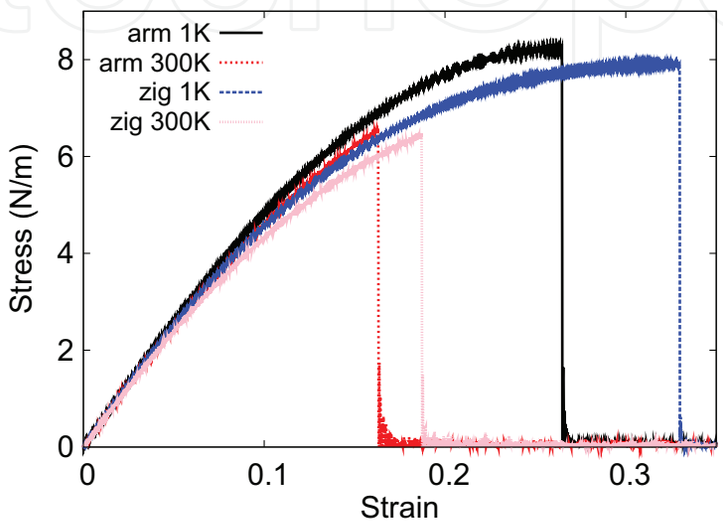

Figure 40. Stress-strain for single-layer 1H-$CoTe_2$ of dimension 100 × 100 Å along the armchair and zigzag directions.

zigzag directions, respectively. The Young's modulus is essentially isotropic in the armchair and zigzag directions. The Poisson's ratio from the VFF model and the SW potential is $\nu_{xy} = \nu_{yx} = 0.32$.

There is no available value for nonlinear quantities in the single-layer 1H-$CoTe_2$. We have thus used the nonlinear parameter $B = 0.5d^4$ in Eq. (5), which is close to the value of B in most materials. The value of the third-order nonlinear elasticity D can be extracted by fitting the stress-strain relation to the function $\sigma = E\epsilon + \frac{1}{2}D\epsilon^2$ with E as the Young's modulus. The values of D from the present SW potential are −157.2 and −187.9 N/m along the armchair and zigzag directions, respectively. The ultimate stress is about 8.2 N/m at the ultimate strain of 0.26 in the armchair direction at the low temperature of 1 K. The ultimate stress is about 7.9 N/m at the ultimate strain of 0.33 in the zigzag direction at the low temperature of 1 K.

22. 1H-NIS_2

Most existing theoretical studies on the single-layer 1H-NiS_2 are based on the first-principles calculations. In this section, we will develop the SW potential for the single-layer 1H-NiS_2.

The structure for the single-layer 1H-NiS_2 is shown in **Figure 1** (with M=Ni and X=S). Each Ni atom is surrounded by six S atoms. These S atoms are categorized into the top group (e.g., atoms 1, 3, and 5) and bottom group (e.g., atoms 2, 4, and 6). Each S atom is connected to three Ni atoms. The structural parameters are from the first-principles calculations [12], including the lattice constant $a = 3.40$ Å and the bond length $d_{\mathrm{Ni-S}} = 2.24$ Å. The resultant angles are $\theta_{\mathrm{NiSS}} = \theta_{\mathrm{SNiNi}} = 98.740^\circ$ and $\theta_{\mathrm{NiSS'}} = 57.593^\circ$, in which atoms S and S′ are from different (top or bottom) groups.

Table 86 shows four VFF terms for the single-layer 1H-NiS_2; one of which is the bond stretching interaction shown by Eq. (1), while the other three terms are the angle bending interaction shown by Eq. (2). These force constant parameters are determined by fitting to the acoustic branches in the phonon dispersion along the ΓM as shown in **Figure 41(a)**. The *ab initio* calculations for the phonon dispersion are from Ref. [12]. **Figure 41(b)** shows that the VFF model and the SW potential give exactly the same phonon dispersion, as the SW potential is derived from the VFF model.

The parameters for the two-body SW potential used by GULP are shown in **Table 87**. The parameters for the three-body SW potential used by GULP are shown in **Table 88**. Some representative parameters for the SW potential used by LAMMPS are listed in **Table 89**. We note that 12 atom types have been introduced for the simulation of the single-layer 1H-NiS_2 using LAMMPS, because the angles around atom Ni in **Figure 1** (with M=Ni and X=S) are not distinguishable in LAMMPS. We have suggested two options to differentiate these angles by implementing some additional constraints in LAMMPS, which can be accomplished by modifying the source file of LAMMPS [13, 14]. According to our experience, it is not so convenient for some users to implement these constraints and recompile the LAMMPS package. Hence, in the present work, we differentiate the angles by introducing more atom types, so it is not necessary to modify the LAMMPS package. **Figure 2** (with M=Ni and X=S) shows that, for 1H-NiS_2, we can differentiate these angles around the Ni atom by assigning these six neighboring S atoms with different atom types. It can be found that 12 atom types are necessary for the purpose of differentiating all 6 neighbors around 1 Ni atom.

We use LAMMPS to perform MD simulations for the mechanical behavior of the single-layer 1H-NiS_2 under uniaxial tension at 1 and 300 K. **Figure 42** shows the stress-strain curve for the tension of a single-layer 1H-NiS_2 of dimension 100×100 Å. Periodic boundary conditions are

VFF type	**Bond stretching**	**Angle bending**		
Expression	$\frac{1}{2}K_{\mathrm{Ni-S}}(\Delta r)^2$	$\frac{1}{2}K_{\mathrm{Ni-S-S}}(\Delta\theta)^2$	$\frac{1}{2}K_{\mathrm{Ni-S-S'}}(\Delta\theta)^2$	$\frac{1}{2}K_{\mathrm{S-Ni-Ni}}(\Delta\theta)^2$
Parameter	6.933	3.418	3.418	3.418
r_0 or θ_0	2.240	98.740	57.593	98.740

The second line gives an explicit expression for each VFF term. The third line is the force constant parameters. Parameters are in the unit of eV/Å^2 for the bond stretching interaction and in the unit of eV for the angle bending interaction. The fourth line gives the initial bond length (in the unit of Å) for the bond stretching interaction and the initial angle (in the unit of degrees) for the angle bending interaction. The angle θ_{ijk} has atom i as the apex.

Table 86. The VFF model for single-layer 1H-NiS_2.

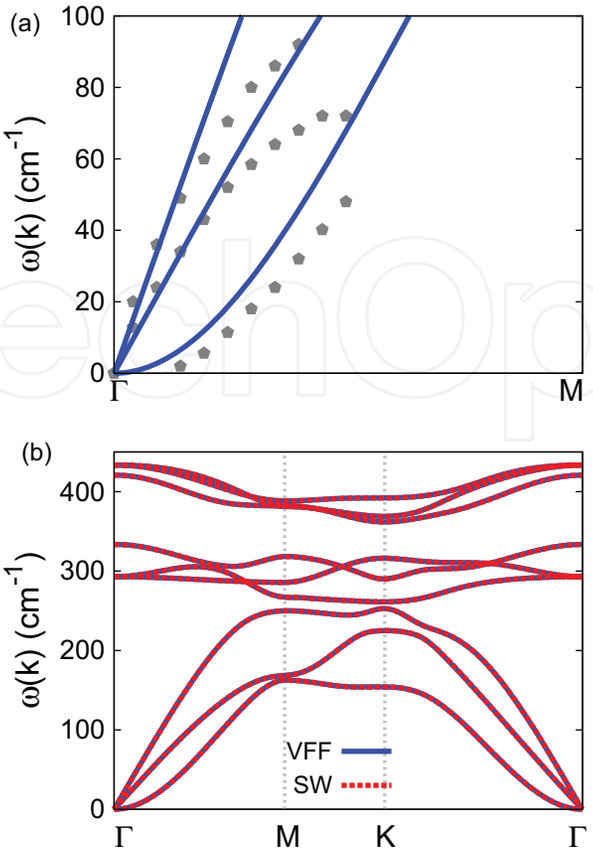

Figure 41. Phonon spectrum for single-layer 1H-NiS_2. (a) Phonon dispersion along the ΓM direction in the Brillouin zone. The results from the VFF model (lines) are comparable with the *ab initio* results (pentagons) from Ref. [12]. (b) The phonon dispersion from the SW potential is exactly the same as that from the VFF model.

	A (eV)	ρ (Å)	B (Å^4)	r_{min} (Å)	r_{max} (Å)
Ni-S	6.425	1.498	12.588	0.0	3.156

Table 87. Two-body SW potential parameters for single-layer 1H-NiS_2 used by GULP [8] as expressed in Eq. (3).

	K (eV)	θ_0 (°)	ρ_1 (Å)	ρ_2 (Å)	r_{min12} (Å)	r_{max12} (Å)	r_{min13} (Å)	r_{max13} (Å)	r_{min23} (Å)	r_{max23} (Å)
θ_{Ni-S-S}	46.062	98.740	1.498	1.498	0.0	3.156	0.0	3.156	0.0	3.713
$\theta_{Ni-S-S'}$	63.130	57.593	1.498	1.498	0.0	3.156	0.0	3.156	0.0	3.713
$\theta_{S-Ni-Ni}$	46.062	98.740	1.498	1.498	0.0	3.156	0.0	3.156	0.0	3.713

The angle θ_{ijk} in the first line indicates the bending energy for the angle with atom i as the apex.

Table 88. Three-body SW potential parameters for single-layer 1H-NiS_2 used by GULP [8] as expressed in Eq. (4).

applied in both armchair and zigzag directions. The single-layer 1H-NiS_2 is stretched uniaxially along the armchair or zigzag direction. The stress is calculated without involving the actual thickness of the quasi-two-dimensional structure of the single-layer 1H-NiS_2. The Young's modulus can be obtained by a linear fitting of the stress-strain relation in the small

	ϵ (eV)	σ (Å)	a	λ	γ	$\cos\theta_0$	A_L	B_L	p	q	Tol
Ni_1—S_1—S_1	1.000	1.498	2.107	0.000	1.000	0.000	6.425	2.502	4	0	0.0
Ni_1—S_1—S_3	1.000	0.000	0.000	46.062	1.000	−0.152	0.000	0.000	4	0	0.0
Ni_1—S_1—S_2	1.000	0.000	0.000	63.130	1.000	0.536	0.000	0.000	4	0	0.0
S_1—Ni_1—Ni_3	1.000	0.000	0.000	46.062	1.000	−0.152	0.000	0.000	4	0	0.0

Table 89. SW potential parameters for single-layer 1H-NiS_2 used by LAMMPS [9] as expressed in Eqs. (9) and (10).

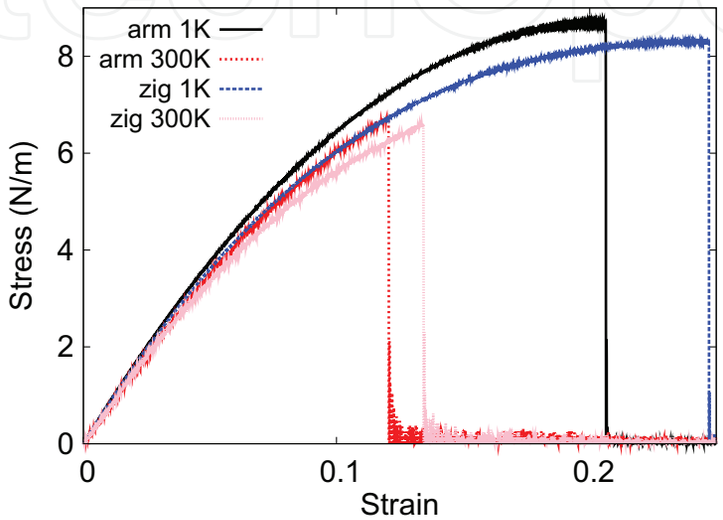

Figure 42. Stress-strain for single-layer 1H-NiS_2 of dimension 100 × 100 Å along the armchair and zigzag directions.

strain range of [0, 0.01]. The Young's modulus is 84.0 and 82.5 N/m along the armchair and zigzag directions, respectively. The Young's modulus is essentially isotropic in the armchair and zigzag directions. The Poisson's ratio from the VFF model and the SW potential is $\nu_{xy} = \nu_{yx} = 0.19$.

There is no available value for nonlinear quantities in the single-layer 1H-NiS_2. We have thus used the nonlinear parameter $B = 0.5d^4$ in Eq. (5), which is close to the value of B in most materials. The value of the third-order nonlinear elasticity D can be extracted by fitting the stress-strain relation to the function $\sigma = E\epsilon + \frac{1}{2}D\epsilon^2$ with E as the Young's modulus. The values of D from the present SW potential are −403.2 and −414.8 N/m along the armchair and zigzag directions, respectively. The ultimate stress is about 8.7 N/m at the ultimate strain of 0.20 in the armchair direction at the low temperature of 1 K. The ultimate stress is about 8.3 N/m at the ultimate strain of 0.24 in the zigzag direction at the low temperature of 1 K.

23. 1H-$NISE_2$

Most existing theoretical studies on the single-layer 1H-$NiSe_2$ are based on the first-principles calculations. In this section, we will develop the SW potential for the single-layer 1H-$NiSe_2$.

The structure for the single-layer 1H-$NiSe_2$ is shown in **Figure 1** (with M=Ni and X=Se). Each Ni atom is surrounded by six Se atoms. These Se atoms are categorized into the top group (e.g., atoms 1, 3, and 5) and bottom group (e.g., atoms 2, 4, and 6). Each Se atom is connected to three Ni atoms. The structural parameters are from the first-principles calculations [12], including the lattice constant $a = 3.33$ Å and the bond length $d_{\mathrm{Ni-Se}} = 2.35$ Å. The resultant angles are $\theta_{\mathrm{NiSeSe}} = \theta_{\mathrm{SeNiNi}} = 90.228^\circ$ and $\theta_{\mathrm{NiSeSe'}} = 70.206^\circ$, in which atoms Se and Se′ are from different (top or bottom) groups.

Table 90 shows four VFF terms for the single-layer 1H-$NiSe_2$; one of which is the bond stretching interaction shown by Eq. (1), while the other three terms are the angle bending interaction shown by Eq. (2). These force constant parameters are determined by fitting to the acoustic branches in the phonon dispersion along the ΓM as shown in **Figure 43(a)**. The *ab initio* calculations for the phonon dispersion are from Ref. [12]. The lowest acoustic branch (flexural mode) is almost linear in the *ab initio* calculations, which may be due to the violation of the rigid rotational invariance [20]. **Figure 43(b)** shows that the VFF model and the SW potential give exactly the same phonon dispersion, as the SW potential is derived from the VFF model.

The parameters for the two-body SW potential used by GULP are shown in **Table 91**. The parameters for the three-body SW potential used by GULP are shown in **Table 92**. Some representative parameters for the SW potential used by LAMMPS are listed in **Table 93**. We note that 12 atom types have been introduced for the simulation of the single-layer 1H-$NiSe_2$ using LAMMPS, because the angles around atom Ni in **Figure 1** (with M=Ni and X=Se) are not distinguishable in LAMMPS. We have suggested two options to differentiate these angles by implementing some additional constraints in LAMMPS, which can be accomplished by modifying the source file of LAMMPS [13, 14]. According to our experience, it is not so convenient for some users to implement these constraints and recompile the LAMMPS package. Hence, in the present work, we differentiate the angles by introducing more atom types, so it is not necessary to modify the LAMMPS package. **Figure 2** (with M=Ni and X=Se) shows that, for 1H-$NiSe_2$, we can differentiate these angles around the Ni atom by assigning these six neighboring Se atoms with different atom types. It can be found that 12 atom types are necessary for the purpose of differentiating all 6 neighbors around 1 Ni atom.

We use LAMMPS to perform MD simulations for the mechanical behavior of the single-layer 1H-$NiSe_2$ under uniaxial tension at 1 and 300 K. **Figure 44** shows the stress-strain curve for the

VFF type	**Bond stretching**	**Angle bending**		
Expression	$\frac{1}{2}K_{\mathrm{Ni-Se}}(\Delta r)^2$	$\frac{1}{2}K_{\mathrm{Ni-Se-Se}}(\Delta\theta)^2$	$\frac{1}{2}K_{\mathrm{Ni-Se-Se'}}(\Delta\theta)^2$	$\frac{1}{2}K_{\mathrm{Se-Ni-Ni}}(\Delta\theta)^2$
Parameter	4.823	2.171	2.171	2.171
r_0 or θ_0	2.350	90.228	70.206	90.228

The second line gives an explicit expression for each VFF term. The third line is the force constant parameters. Parameters are in the unit of eV/c^2 for the bond stretching interaction and in the unit of eV for the angle bending interaction. The fourth line gives the initial bond length (in the unit of eV/Å^2) for the bond stretching interaction and the initial angle (in the unit of degrees) for the angle bending interaction. The angle θ_{ijk} has atom i as the apex.

Table 90. The VFF model for single-layer 1H-$NiSe_2$.

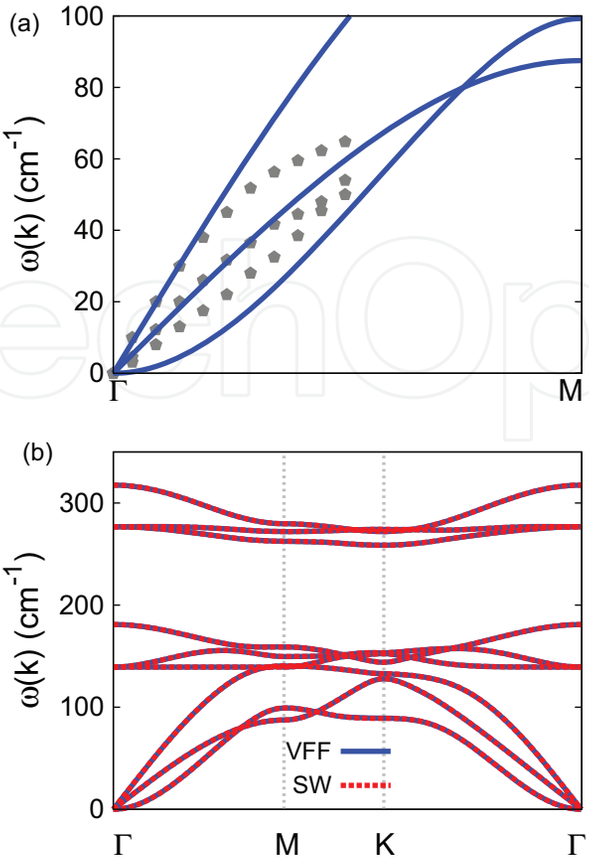

Figure 43. Phonon spectrum for single-layer 1H-$NiSe_2$. (a) Phonon dispersion along the ΓM direction in the Brillouin zone. The results from the VFF model (lines) are comparable with the *ab initio* results (pentagons) from Ref. [12]. (b) The phonon dispersion from the SW potential is exactly the same as that from the VFF model.

	A (eV)	ρ (Å)	B (Å^4)	r_{min} (Å)	r_{max} (Å)
Ni—Se	4.004	1.267	15.249	0.0	3.213

Table 91. Two-body SW potential parameters for single-layer 1H-$NiSe_2$ used by GULP [8] as expressed in Eq. (3).

	K (eV)	θ_0 (°)	ρ_1 (Å)	ρ_2 (Å)	$r_{min\,12}$ (Å)	$r_{max\,12}$ (Å)	$r_{min\,13}$ (Å)	$r_{max\,13}$ (Å)	$r_{min\,23}$ (Å)	$r_{max\,23}$ (Å)
$\theta_{Ni-Se-Se}$	20.479	90.228	1.267	1.267	0.0	3.213	0.0	3.213	0.0	3.809
$\theta_{Ni-Se-Se'}$	23.132	70.206	1.267	1.267	0.0	3.213	0.0	3.213	0.0	3.809
$\theta_{Se-Ni-Ni}$	20.479	90.228	1.267	1.267	0.0	3.213	0.0	3.213	0.0	3.809

The angle θ_{ijk} in the first line indicates the bending energy for the angle with atom i as the apex.

Table 92. Three-body SW potential parameters for single-layer 1H-$NiSe_2$ used by GULP [8] as expressed in Eq. (4).

tension of a single-layer 1H-$NiSe_2$ of dimension 100 × 100 Å. Periodic boundary conditions are applied in both armchair and zigzag directions. The single-layer 1H-$NiSe_2$ is stretched uniaxially along the armchair or zigzag direction. The stress is calculated without involving the actual thickness of the quasi-two-dimensional structure of the single-layer 1H-$NiSe_2$. The

	ϵ (eV)	σ (Å)	a	λ	γ	$\cos\theta_0$	A_L	B_L	p	q	Tol
Ni_1—Se_1—Se_1	1.000	1.267	2.535	0.000	1.000	0.000	4.004	5.913	4	0	0.0
Ni_1—Se_1—Se_3	1.000	0.000	0.000	20.479	1.000	−0.004	0.000	0.000	4	0	0.0
Ni_1—Se_1—Se_2	1.000	0.000	0.000	23.132	1.000	0.339	0.000	0.000	4	0	0.0
Se_1—Ni_1—Ni_3	1.000	0.000	0.000	20.479	1.000	−0.004	0.000	0.000	4	0	0.0

Table 93. SW potential parameters for single-layer 1H-$NiSe_2$ used by LAMMPS [9] as expressed in Eqs. (9) and (10).

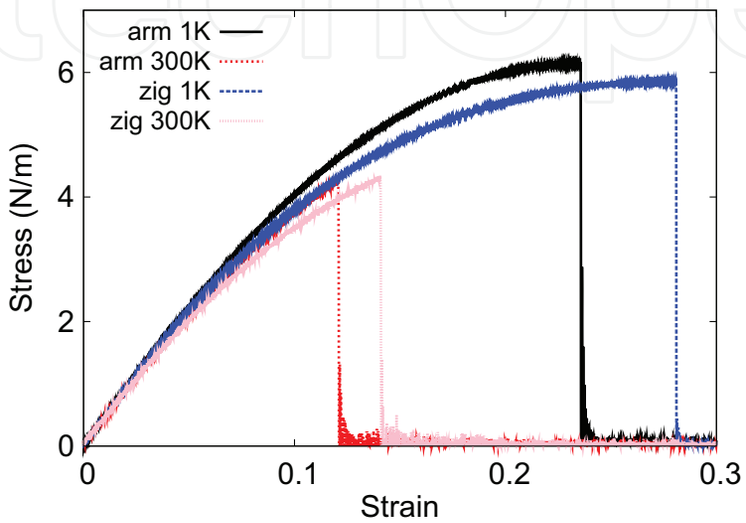

Figure 44. Stress-strain for single-layer 1H-$NiSe_2$ of dimension 100 × 100 Å along the armchair and zigzag directions

Young's modulus can be obtained by a linear fitting of the stress-strain relation in the small strain range of [0, 0.01]. The Young's modulus is 47.6 and 47.8 N/m along the armchair and zigzag directions, respectively. The Young's modulus is essentially isotropic in the armchair and zigzag directions. The Poisson's ratio from the VFF model and the SW potential is $\nu_{xy} = \nu_{yx} = 0.27$.

There is no available value for nonlinear quantities in the single-layer 1H-$NiSe_2$. We have thus used the nonlinear parameter $B = 0.5d^4$ in Eq. (5), which is close to the value of B in most materials. The value of the third-order nonlinear elasticity D can be extracted by fitting the stress-strain relation to the function $\sigma = E\epsilon + \frac{1}{2}D\epsilon^2$ with E as the Young's modulus. The values of D from the present SW potential are −173.9 and −197.6 N/m along the armchair and zigzag directions, respectively. The ultimate stress is about 6.1 N/m at the ultimate strain of 0.23 in the armchair direction at the low temperature of 1 K. The ultimate stress is about 5.9 N/m at the ultimate strain of 0.28 in the zigzag direction at the low temperature of 1 K.

24. 1H-$NITE_2$

Most existing theoretical studies on the single-layer 1H-$NiTe_2$ are based on the first-principles calculations. In this section, we will develop the SW potential for the single-layer 1H-$NiTe_2$.

The structure for the single-layer 1H-$NiTe_2$ is shown in **Figure 1** (with M=Ni and X=Te). Each Ni atom is surrounded by six Te atoms. These Te atoms are categorized into the top group (e.g., atoms 1, 3, and 5) and bottom group (e.g., atoms 2, 4, and 6). Each Te atom is connected to three Ni atoms. The structural parameters are from the first-principles calculations [12], including the lattice constant $a = 3.59$ Å and the bond length $d_{\mathrm{Ni-Te}} = 2.54$ Å. The resultant angles are $\theta_{\mathrm{NiTeTe}} = \theta_{\mathrm{TeNiNi}} = 89.933^\circ$ and $\theta_{\mathrm{NiTeTe'}} = 70.624^\circ$, in which atoms Te and Te' are from different (top or bottom) groups.

Table 94 shows four VFF terms for the single-layer 1H-$NiTe_2$; one of which is the bond stretching interaction shown by Eq. (1), while the other three terms are the angle bending interaction shown by Eq. (2). These force constant parameters are determined by fitting to the acoustic branches in the phonon dispersion along the ΓM as shown in **Figure 45(a)**. The *ab initio* calculations for the phonon dispersion are from Ref. [12]. The lowest acoustic branch (flexural mode) is almost linear in the *ab initio* calculations, which may be due to the violation of the rigid rotational invariance [20]. The transverse acoustic branch is very close to the longitudinal acoustic branch in the *ab initio* calculations. **Figure 45(b)** shows that the VFF model and the SW potential give exactly the same phonon dispersion, as the SW potential is derived from the VFF model.

The parameters for the two-body SW potential used by GULP are shown in **Table 95**. The parameters for the three-body SW potential used by GULP are shown in **Table 96**. Some representative parameters for the SW potential used by LAMMPS are listed in **Table 97**. We note that 12 atom types have been introduced for the simulation of the single-layer 1H-$NiTe_2$ using LAMMPS, because the angles around atom Ni in **Figure 1** (with M=Ni and X=Te) are not distinguishable in LAMMPS. We have suggested two options to differentiate these angles by implementing some additional constraints in LAMMPS, which can be accomplished by modifying the source file of LAMMPS [13, 14]. According to our experience, it is not so convenient for some users to implement these constraints and recompile the LAMMPS package. Hence, in the present work, we differentiate the angles by introducing more atom types, so it is not necessary to modify the LAMMPS package. **Figure 2** (with M=Ni and X=Te) shows that, for 1H-$NiTe_2$, we can differentiate these angles around the Ni atom by assigning these six neighboring Te atoms with different atom types. It can be found that 12 atom types are necessary for the purpose of differentiating all 6 neighbors around 1 Ni atom.

VFF type	**Bond stretching**	**Angle bending**		
Expression	$\frac{1}{2}K_{\mathrm{Ni-Te}}(\Delta r)^2$	$\frac{1}{2}K_{\mathrm{Ni-Te-Te}}(\Delta\theta)^2$	$\frac{1}{2}K_{\mathrm{Ni-Te-Te'}}(\Delta\theta)^2$	$\frac{1}{2}K_{\mathrm{Te-Ni-Ni}}(\Delta\theta)^2$
Parameter	6.712	2.656	2.656	2.656
r_0 or θ_0	2.540	89.933	70.624	89.933

The second line gives an explicit expression for each VFF term. The third line is the force constant parameters. Parameters are in the unit of eV/Å^2 for the bond stretching interaction and in the unit of eV for the angle bending interaction. The fourth line gives the initial bond length (in the unit of Å) for the bond stretching interaction and the initial angle (in the unit of degrees) for the angle bending interaction. The angle θ_{ijk} has atom i as the apex.

Table 94. The VFF model for single-layer 1H-$NiTe_2$.

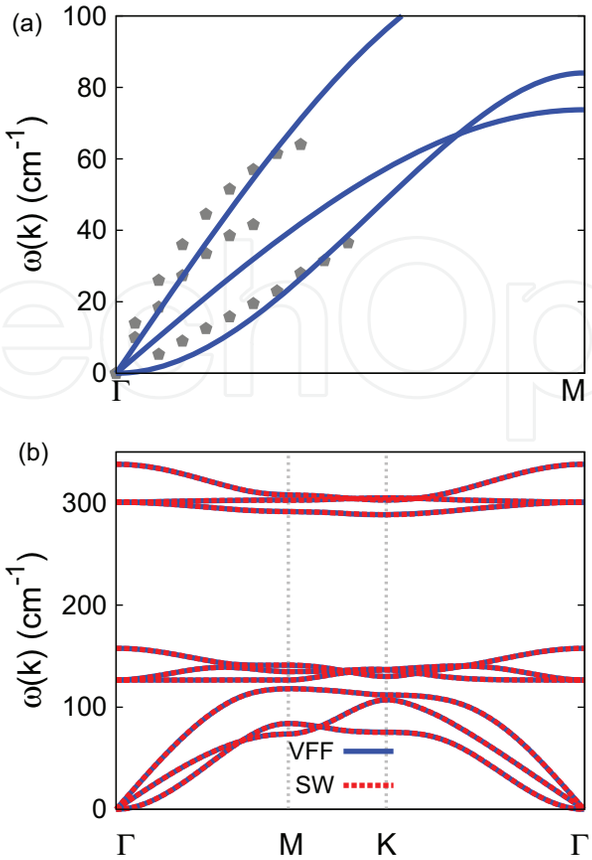

Figure 45. Phonon spectrum for single-layer 1H-$NiTe_2$. (a) Phonon dispersion along the ΓM direction in the Brillouin zone. The results from the VFF model (lines) are comparable with the *ab initio* results (pentagons) from Ref. [12]. (b) The phonon dispersion from the SW potential is exactly the same as that from the VFF model.

	A (eV)	ρ (Å)	B (Å^4)	r_{min} (Å)	r_{max} (Å)
Ni—Te	6.461	1.359	20.812	0.0	3.469

Table 95. Two-body SW potential parameters for single-layer 1H-$NiTe_2$ used by GULP [8] as expressed in Eq. (3).

	K (eV)	θ_0 (°)	ρ_1 (Å)	ρ_2 (Å)	$r_{min\,12}$ (Å)	$r_{max\,12}$ (Å)	$r_{min\,13}$ (Å)	$r_{max\,13}$ (Å)	$r_{min\,23}$ (Å)	$r_{max\,23}$ (Å)
$\theta_{Ni-Te-Te}$	24.759	89.933	1.359	1.359	0.0	3.469	0.0	3.469	0.0	4.114
$\theta_{Ni-Te-Te'}$	27.821	70.624	1.359	1.359	0.0	3.469	0.0	3.469	0.0	4.114
$\theta_{Te-Ni-Ni}$	24.759	89.933	1.359	1.359	0.0	3.469	0.0	3.469	0.0	4.114

The angle θ_{ijk} in the first line indicates the bending energy for the angle with atom i as the apex.

Table 96. Three-body SW potential parameters for single-layer 1H-$NiTe_2$ used by GULP [8] as expressed in Eq. (4).

We use LAMMPS to perform MD simulations for the mechanical behavior of the single-layer 1H-$NiTe_2$ under uniaxial tension at 1 and 300 K. **Figure 46** shows the stress-strain curve for the tension of a single-layer 1H-$NiTe_2$ of dimension 100 × 100 Å. Periodic boundary conditions are

	ϵ (eV)	σ (Å)	a	λ	γ	$\cos\theta_0$	A_L	B_L	p	q	Tol
Ni_1—Te_1—Te_1	1.000	1.359	2.553	0.000	1.000	0.000	6.461	6.107	4	0	0.0
Ni_1—Te_1—Te_3	1.000	0.000	0.000	24.759	1.000	0.001	0.000	0.000	4	0	0.0
Ni_1—Te_1—Te_2	1.000	0.000	0.000	27.821	1.000	0.332	0.000	0.000	4	0	0.0
Te_1—Ni_1—Ni_3	1.000	0.000	0.000	24.759	1.000	0.001	0.000	0.000	4	0	0.0

Table 97. SW potential parameters for single-layer 1H-$NiTe_2$ used by LAMMPS [9] as expressed in Eqs. (9) and (10).

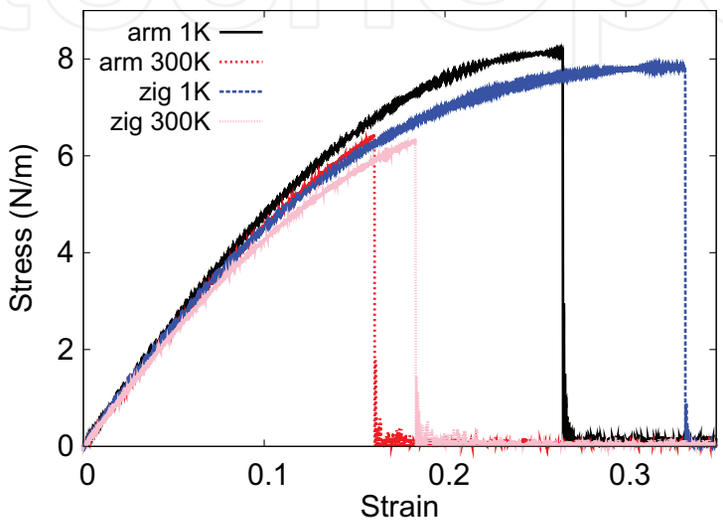

Figure 46. Stress-strain for single-layer 1H-$NiTe_2$ of dimension 100 × 100 Å along the armchair and zigzag directions.

applied in both armchair and zigzag directions. The single-layer 1H-$NiTe_2$ is stretched uniaxially along the armchair or zigzag direction. The stress is calculated without involving the actual thickness of the quasi-two-dimensional structure of the single-layer 1H-$NiTe_2$. The Young's modulus can be obtained by a linear fitting of the stress-strain relation in the small strain range of [0, 0.01]. The Young's modulus is 53.2 and 53.6 N/m along the armchair and zigzag directions, respectively. The Young's modulus is essentially isotropic in the armchair and zigzag directions. The Poisson's ratio from the VFF model and the SW potential is $\nu_{xy} = \nu_{yx} = 0.32$.

There is no available value for nonlinear quantities in the single-layer 1H-$NiTe_2$. We have thus used the nonlinear parameter $B = 0.5d^4$ in Eq. (5), which is close to the value of B in most materials. The value of the third-order nonlinear elasticity D can be extracted by fitting the stress-strain relation to the function $\sigma = E\epsilon + \frac{1}{2}D\epsilon^2$ with E as the Young's modulus. The values of D from the present SW potential are −156.6 and −184.8 N/m along the armchair and zigzag directions, respectively. The ultimate stress is about 8.1 N/m at the ultimate strain of 0.26 in the armchair direction at the low temperature of 1 K. The ultimate stress is about 7.8 N/m at the ultimate strain of 0.33 in the zigzag direction at the low temperature of 1 K.

25. 1H-NBS_2

In 1983, the VFF model was developed to investigate the lattice dynamical properties in the bulk 2H-NbS_2 [21]. In this section, we will develop the SW potential for the single-layer 1H-NbS_2.

The structure for the single-layer 1H-NbS_2 is shown in **Figure 1** (with M=Nb and X=S). Each Nb atom is surrounded by six S atoms. These S atoms are categorized into the top group (e.g., atoms 1, 3, and 5) and bottom group (e.g., atoms 2, 4, and 6). Each S atom is connected to three Nb atoms. The structural parameters are from Ref. [21], including the lattice constant $a = 3.31$ Å and the bond length $d_{\mathrm{Nb-S}} = 2.47$ Å. The resultant angles are $\theta_{\mathrm{NbSS}} = \theta_{\mathrm{SNbNb}} = 84.140^\circ$ and $\theta_{\mathrm{NbSS'}} = 78.626^\circ$, in which atoms S and S′ are from different (top or bottom) groups.

Table 98 shows four VFF terms for the 1H-NbS_2; one of which is the bond stretching interaction shown by Eq. (1), while the other three terms are the angle bending interaction shown by Eq. (2). These force constant parameters are determined by fitting to the three acoustic branches in the phonon dispersion along the ΓM as shown in **Figure 47(a)**. The theoretical phonon frequencies (gray pentagons) are from Ref. [21], which are the phonon dispersion of bulk 2H-NbS_2. We have used these phonon frequencies as the phonon dispersion of the single-layer 1H-NbS_2, as the interlayer interaction in the bulk 2H-NbS_2 only induces weak effects on the two in-plane acoustic branches. The interlayer coupling will strengthen the out-of-plane acoustic branch (flexural branch), so the flexural branch from the present VFF model (blue line) is lower than the theoretical results for bulk 2H-NbS_2 (gray pentagons). **Figure 47(b)** shows that the VFF model and the SW potential give exactly the same phonon dispersion, as the SW potential is derived from the VFF model.

The parameters for the two-body SW potential used by GULP are shown in **Table 99**. The parameters for the three-body SW potential used by GULP are shown in **Table 100**. Parameters for the SW potential used by LAMMPS are listed in **Table 101**. We note that 12 atom types have been introduced for the simulation of the single-layer 1H-NbS_2 using LAMMPS, because the angles around atom Nb in **Figure 1** (with M=Nb and X=S) are not distinguishable in LAMMPS. We have suggested two options to differentiate these angles by implementing some additional constraints in LAMMPS, which can be accomplished by modifying the source file of LAMMPS [13, 14]. According to our experience, it is not so convenient for some users to implement these constraints and recompile the LAMMPS package. Hence, in the present work,

VFF type	**Bond stretching**	**Angle bending**		
Expression	$\frac{1}{2}K_{Nb-S}(\Delta r)^2$	$\frac{1}{2}K_{Nb-S-S}(\Delta\theta)^2$	$\frac{1}{2}K_{Nb-S-S'}(\Delta\theta)^2$	$\frac{1}{2}K_{S-Nb-Nb}(\Delta\theta)^2$
Parameter	8.230	4.811	4.811	4.811
r_0 or θ_0	2.470	84.140	78.626	84.140

The second line gives an explicit expression for each VFF term. The third line is the force constant parameters. Parameters are in the unit of eV/Å^2 for the bond stretching interaction and in the unit of eV for the angle bending interaction. The fourth line gives the initial bond length (in the unit of Å) for the bond stretching interaction and the initial angle (in the unit of degrees) for the angle bending interaction. The angle θ_{ijk} has atom i as the apex.

Table 98. The VFF model for single-layer 1H-NbS_2.

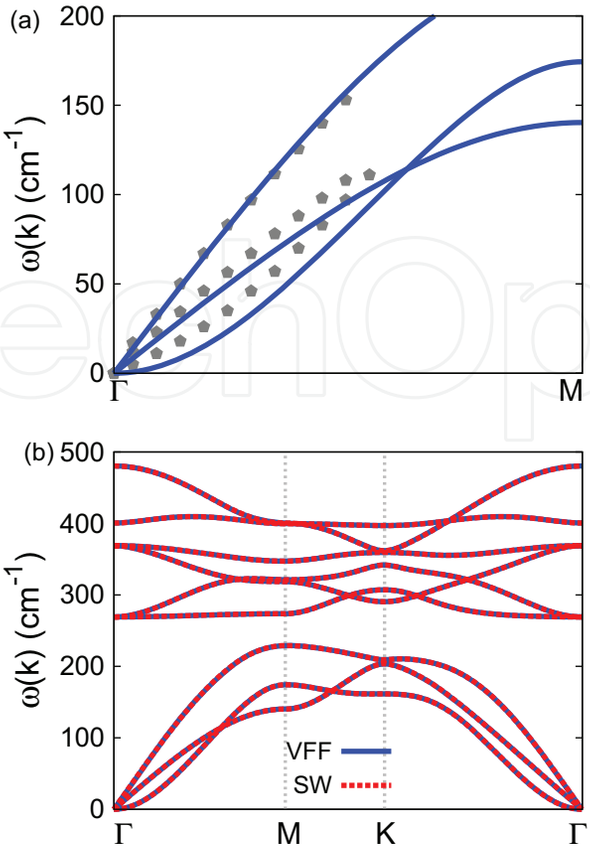

Figure 47. Phonon dispersion for single-layer 1H-NbS_2. (a) The VFF model is fitted to the three acoustic branches in the long wave limit along the ΓM direction. The theoretical results (gray pentagons) are from Ref. [21]. The blue lines are from the present VFF model. (b) The VFF model (blue lines) and the SW potential (red lines) give the same phonon dispersion for single-layer 1H-NbS_2 along ΓMKΓ.

	A (eV)	ρ (Å)	B (Å^4)	r_{min} (Å)	r_{max} (Å)
Nb—S	6.439	1.116	18.610	0.0	3.300

Table 99. Two-body SW potential parameters for single-layer 1H-NbS_2 used by GULP [8] as expressed in Eq. (3).

	K (eV)	θ_0 (°)	ρ_1 (Å)	ρ_2 (Å)	$r_{min\,12}$ (Å)	$r_{max\,12}$ (Å)	$r_{min\,13}$ (Å)	$r_{max\,13}$ (Å)	$r_{min\,23}$ (Å)	$r_{max\,23}$ (Å)
θ_{Nb-S-S}	35.748	84.140	1.116	1.116	0.0	3.300	0.0	3.300	0.0	3.933
$\theta_{Nb-S-S'}$	36.807	78.626	1.116	1.116	0.0	3.300	0.0	3.300	0.0	3.933
$\theta_{S-Nb-Nb}$	35.748	84.140	1.116	1.116	0.0	3.300	0.0	3.300	0.0	3.933

The angle θ_{ijk} in the first line indicates the bending energy for the angle with atom i as the apex.

Table 100. Three-body SW potential parameters for single-layer 1H-NbS_2 used by GULP [8] as expressed in Eq. (4).

we differentiate the angles by introducing more atom types, so it is not necessary to modify the LAMMPS package. **Figure 2** (with M=Nb and X=S) shows that, for 1H-NbS_2, we can differentiate these angles around the Nb atom by assigning these six neighboring S atoms with

	ϵ (eV)	σ (Å)	a	λ	γ	$\cos\theta_0$	A_L	B_L	p	q	Tol
Nb_1—S_1—S_1	1.000	1.116	2.958	0.000	1.000	0.000	6.439	12.014	4	0	0.0
Nb_1—S_1—S_3	1.000	0.000	0.000	35.748	1.000	0.102	0.000	0.000	4	0	0.0
Nb_1—S_1—S_2	1.000	0.000	0.000	36.807	1.000	0.197	0.000	0.000	4	0	0.0
S_1—Nb_1—Nb_3	1.000	0.000	0.000	35.748	1.000	0.102	0.000	0.000	4	0	0.0

Atom types in the first column are displayed in **Figure 2** (with M=Nb and X=S).

Table 101. SW potential parameters for single-layer 1H-NbS_2 used by LAMMPS [9] as expressed in Eqs. (9) and (10).

different atom types. It can be found that 12 atom types are necessary for the purpose of differentiating all 6 neighbors around 1 Nb atom.

We use LAMMPS to perform MD simulations for the mechanical behavior of the single-layer 1H-NbS_2 under uniaxial tension at 1 and 300 K. **Figure 48** shows the stress-strain curve for the tension of a single-layer 1H-NbS_2 of dimension 100 × 100 Å. Periodic boundary conditions are applied in both armchair and zigzag directions. The single-layer 1H-NbS_2 is stretched uniaxially along the armchair or zigzag direction. The stress is calculated without involving the actual thickness of the quasi-two-dimensional structure of the single-layer 1H-NbS_2. The Young's modulus can be obtained by a linear fitting of the stress-strain relation in the small strain range of [0, 0.01]. The Young's modulus is 87.7 and 87.2 N/m along the armchair and zigzag directions, respectively. The Young's modulus is essentially isotropic in the armchair and zigzag directions. The Poisson's ratio from the VFF model and the SW potential is $\nu_{xy} = \nu_{yx} = 0.27$.

There is no available value for the nonlinear quantities in the single-layer 1H-NbS_2. We have thus used the nonlinear parameter $B = 0.5d^4$ in Eq. (5), which is close to the value of B in most materials. The value of the third-order nonlinear elasticity D can be extracted by fitting the

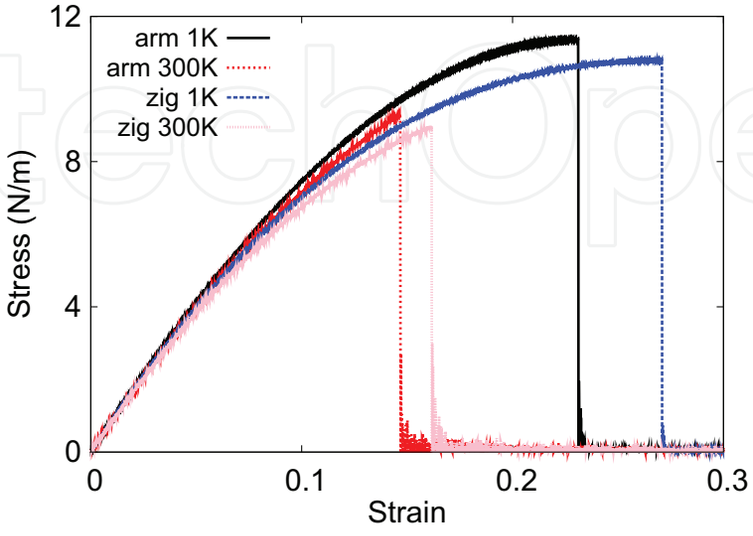

Figure 48. Stress-strain for single-layer 1H-NbS_2 of dimension 100 × 100 Å along the armchair and zigzag directions.

stress-strain relation to the function $\sigma = E\epsilon + \frac{1}{2}D\epsilon^2$ with E as the Young's modulus. The values of D from the present SW potential are -315.3 and -355.1 N/m along the armchair and zigzag directions, respectively. The ultimate stress is about 11.4 N/m at the ultimate strain of 0.23 in the armchair direction at the low temperature of 1 K. The ultimate stress is about 10.8 N/m at the ultimate strain of 0.27 in the zigzag direction at the low temperature of 1 K.

26. 1H-$NBSE_2$

In 1983, the VFF model was developed to investigate the lattice dynamical properties in the bulk 2H-$NbSe_2$ [15, 21]. In this section, we will develop the SW potential for the single-layer 1H-$NbSe_2$.

The structure for the single-layer 1H-$NbSe_2$ is shown in **Figure 1** (with M=Nb and X=Se). Each Nb atom is surrounded by six Se atoms. These Se atoms are categorized into the top group (e.g., atoms 1, 3, and 5) and bottom group (e.g., atoms 2, 4, and 6). Each Se atom is connected to three Nb atoms. The structural parameters are from Ref. [21], including the lattice constant $a = 3.45$ Å and the bond length $d_{\mathrm{Nb-Se}} = 2.60$ Å. The resultant angles are $\theta_{\mathrm{NbSeSe}} = \theta_{\mathrm{SNbNb}} = 83.129^\circ$ and $\theta_{\mathrm{NbSeSe'}} = 79.990^\circ$, in which atoms Se and Se' are from different (top or bottom) groups.

Table 102 shows four VFF terms for the 1H-$NbSe_2$; one of which is the bond stretching interaction shown by Eq. (1), while the other three terms are the angle bending interaction shown by Eq. (2). These force constant parameters are determined by fitting to the three acoustic branches in the phonon dispersion along the ΓM as shown in **Figure 49(a)**. The theoretical phonon frequencies (gray pentagons) are from Ref. [21], which are the phonon dispersion of bulk 2H-$NbSe_2$. We have used these phonon frequencies as the phonon dispersion of the single-layer 1H-$NbSe_2$, as the interlayer interaction in the bulk 2H-$NbSe_2$ only induces weak effects on the two in-plane acoustic branches. The interlayer coupling will strengthen the out-of-plane acoustic branch (flexural branch), so the flexural branch from the present VFF model (blue line) is lower than the theoretical results for bulk 2H-$NbSe_2$ (gray pentagons). It turns out that the VFF parameters for the single-layer 1H-$NbSe_2$ are the same as the single-layer NbS_2. The phonon dispersion for single-layer 1H-$NbSe_2$ was also shown in

VFF type	**Bond stretching**	**Angle bending**		
Expression	$\frac{1}{2}K_{\mathrm{Nb-Se}}(\Delta r)^2$	$\frac{1}{2}K_{\mathrm{Nb-Se-Se}}(\Delta\theta)^2$	$\frac{1}{2}K_{\mathrm{Nb-Se-Se'}}(\Delta\theta)^2$	$\frac{1}{2}K_{\mathrm{Se-Nb-Nb}}(\Delta\theta)^2$
Parameter	8.230	4.811	4.811	4.811
r_0 or θ_0	2.600	83.129	79.990	83.129

The second line gives an explicit expression for each VFF term. The third line is the force constant parameters. Parameters are in the unit of eV/Å^2 for the bond stretching interaction and in the unit of eV for the angle bending interaction. The fourth line gives the initial bond length (in the unit of Å) for the bond stretching interaction and the initial angle (in the unit of degrees) for the angle bending interaction. The angle θ_{ijk} has atom i as the apex.

Table 102. The VFF model for single-layer 1H-$NbSe_2$.

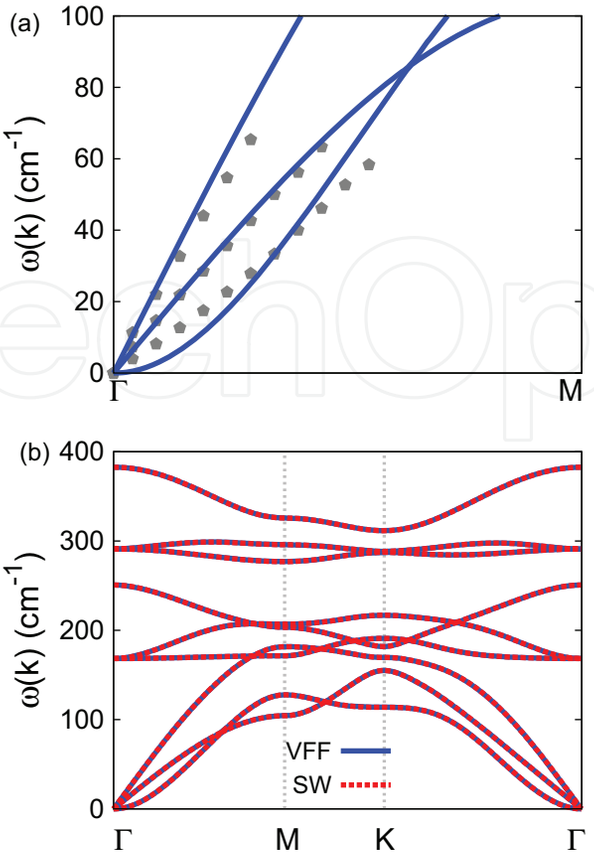

Figure 49. Phonon dispersion for single-layer 1H-$NbSe_2$. (a) The VFF model is fitted to the three acoustic branches in the long wave limit along the ΓM direction. The theoretical results (gray pentagons) are from Ref. [15]. The blue lines are from the present VFF model. (b) The VFF model (blue lines) and the SW potential (red lines) give the same phonon dispersion for single-layer 1H-$NbSe_2$ along ΓMKΓ.

Ref. [12]. **Figure 49(b)** shows that the VFF model and the SW potential give exactly the same phonon dispersion, as the SW potential is derived from the VFF model.

The parameters for the two-body SW potential used by GULP are shown in **Table 103**. The parameters for the three-body SW potential used by GULP are shown in **Table 104**. Parameters for the SW potential used by LAMMPS are listed in **Table 105**. We note that 12 atom types have been introduced for the simulation of the single-layer 1H-$NbSe_2$ using LAMMPS, because the angles around atom Nb in **Figure 1** (with M=Nb and X=Se) are not distinguishable in LAMMPS. We have suggested two options to differentiate these angles by implementing some additional constraints in LAMMPS, which can be accomplished by modifying the source file of LAMMPS [13, 14]. According to our experience, it is not so convenient for some users to implement these constraints and recompile the LAMMPS package. Hence, in the present work,

	A (eV)	ρ (Å)	B (Å^4)	r_{min} (Å)	r_{max} (Å)
Nb-Se	6.942	1.138	22.849	0.0	3.460

Table 103. Two-body SW potential parameters for single-layer 1H-$NbSe_2$ used by GULP [8] as expressed in Eq. (3).

http://dx.doi.org/10.5772/intechopen.71929

	K (eV)	θ_0 (°)	ρ_1 (Å)	ρ_2 (Å)	r_{min12} (Å)	r_{max12} (Å)	r_{min13} (Å)	r_{max13} (Å)	r_{min23} (Å)	r_{max23} (Å)
$\theta_{Nb-Se-Se}$	34.409	83.129	1.138	1.138	0.0	3.460	0.0	3.460	0.0	4.127
$\theta_{Nb-Se-Se'}$	34.973	79.990	1.138	1.138	0.0	3.460	0.0	3.460	0.0	4.127
$\theta_{Se-Nb-Nb}$	34.409	83.129	1.138	1.138	0.0	3.460	0.0	3.460	0.0	4.127

The angle θ_{ijk} in the first line indicates the bending energy for the angle with atom i as the apex.

Table 104. Three-body SW potential parameters for single-layer 1H-$NbSe_2$ used by GULP [8] as expressed in Eq. (4).

	ϵ (eV)	σ (Å)	a	λ	γ	$\cos\theta_0$	A_L	B_L	p	q	Tol
Nb_1—Se_1—Se_1	1.000	1.138	3.041	0.000	1.000	0.000	6.942	13.631	4	0	0.0
Nb_1—Se_1—Se_3	1.000	0.000	0.000	34.409	1.000	0.120	0.000	0.000	4	0	0.0
Nb_1—Se_1—Se_2	1.000	0.000	0.000	34.973	1.000	0.174	0.000	0.000	4	0	0.0
Se_1—Nb_1—Nb_3	1.000	0.000	0.000	34.409	1.000	0.120	0.000	0.000	4	0	0.0

Atom types in the first column are displayed in **Figure 2** (with M=Nb and X=Se).

Table 105. SW potential parameters for single-layer 1H-$NbSe_2$ used by LAMMPS [9] as expressed in Eqs. (9) and (10).

we differentiate the angles by introducing more atom types, so it is not necessary to modify the LAMMPS package. **Figure 2** (with M=Nb and X=Se) shows that, for 1H-$NbSe_2$, we can differentiate these angles around the Nb atom by assigning these six neighboring Se atoms with different atom types. It can be found that 12 atom types are necessary for the purpose of differentiating all 6 neighbors around 1 Nb atom.

We use LAMMPS to perform MD simulations for the mechanical behavior of the single-layer 1H-$NbSe_2$ under uniaxial tension at 1 and 300 K. **Figure 50** shows the stress-strain curve for the tension of a single-layer 1H-$NbSe_2$ of dimension 100 × 100 Å. Periodic boundary conditions

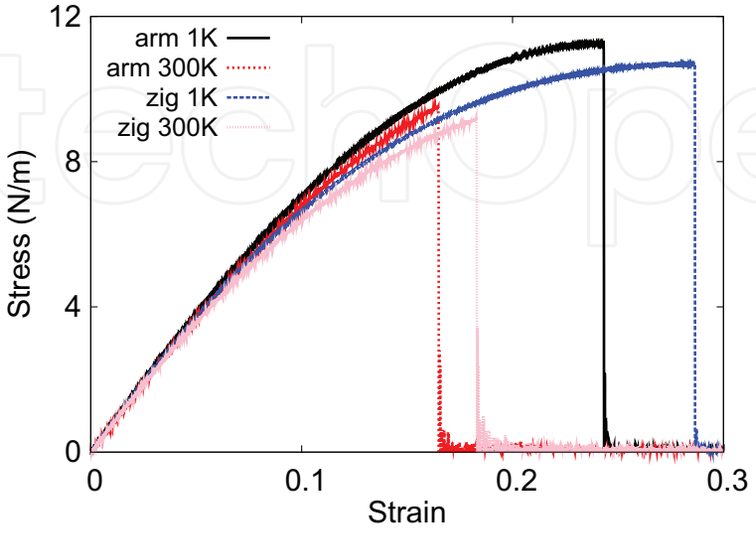

Figure 50. Stress-strain for single-layer 1H-$NbSe_2$ of dimension 100 × 100 Å along the armchair and zigzag directions.

are applied in both armchair and zigzag directions. The single-layer 1H-$NbSe_2$ is stretched uniaxially along the armchair or zigzag direction. The stress is calculated without involving the actual thickness of the quasi-two-dimensional structure of the single-layer 1H-$NbSe_2$. The Young's modulus can be obtained by a linear fitting of the stress-strain relation in the small strain range of [0, 0.01]. The Young's modulus is 80.2 and 80.7 N/m along the armchair and zigzag directions, respectively. The Young's modulus is essentially isotropic in the armchair and zigzag directions. The Poisson's ratio from the VFF model and the SW potential is $\nu_{xy} = \nu_{yx} = 0.29$.

There is no available value for the nonlinear quantities in the single-layer 1H-$NbSe_2$. We have thus used the nonlinear parameter $B = 0.5d^4$ in Eq. (5), which is close to the value of B in most materials. The value of the third-order nonlinear elasticity D can be extracted by fitting the stress-strain relation to the function $\sigma = E\epsilon + \frac{1}{2}D\epsilon^2$ with E as the Young's modulus. The values of D from the present SW potential are -258.8 and -306.1 N/m along the armchair and zigzag directions, respectively. The ultimate stress is about 11.2 N/m at the ultimate strain of 0.24 in the armchair direction at the low temperature of 1 K. The ultimate stress is about 10.7 N/m at the ultimate strain of 0.28 in the zigzag direction at the low temperature of 1 K.

27. 1H-MoO_2

Most existing theoretical studies on the single-layer 1H-MoO_2 are based on the first-principles calculations. In this section, we will develop the SW potential for the single-layer 1H-MoO_2.

The structure for the single-layer 1H-MoO_2 is shown in **Figure 1** (with M = Mo and X = O). Each Mo atom is surrounded by six O atoms. These O atoms are categorized into the top group (e.g., atoms 1, 3, and 5) and bottom group (e.g., atoms 2, 4, and 6). Each O atom is connected to three Mo atoms. The structural parameters are from the first-principles calculations [12], including the lattice constant $a = 2.78$ Å and the bond length $d_{\mathrm{Mo-O}} = 2.00$ Å. The resultant angles are $\theta_{\mathrm{MoOO}} = \theta_{\mathrm{OMoMo}} = 88.054^\circ$ and $\theta_{\mathrm{MoOO'}} = 73.258^\circ$, in which atoms O and O′ are from different (top or bottom) groups.

Table 106 shows four VFF terms for the single-layer 1H-MoO_2; one of which is the bond stretching interaction shown by Eq. (1), while the other three terms are the angle bending

VFF type	Bond stretching	Angle bending		
Expression	$\frac{1}{2}K_{\mathrm{Mo-O}}(\Delta r)^2$	$\frac{1}{2}K_{\mathrm{Mo-O-O}}(\Delta\theta)^2$	$\frac{1}{2}K_{\mathrm{Mo-O-O'}}(\Delta\theta)^2$	$\frac{1}{2}K_{\mathrm{O-Mo-Mo}}(\Delta\theta)^2$
Parameter	14.622	8.410	8.410	8.410
r_0 or θ_0	2.000	88.054	73.258	88.054

The second line gives an explicit expression for each VFF term. The third line is the force constant parameters. Parameters are in the unit of eV/Å^2 for the bond stretching interaction and in the unit of eV for the angle bending interaction. The fourth line gives the initial bond length (in the unit of Å) for the bond stretching interaction and the initial angle (in the unit of degrees) for the angle bending interaction. The angle θ_{ijk} has atom i as the apex.

Table 106. The VFF model for single-layer 1H-MoO_2.

http://dx.doi.org/10.5772/intechopen.71929

interaction shown by Eq. (2). These force constant parameters are determined by fitting to the acoustic branches in the phonon dispersion along the ΓM as shown in **Figure 51(a)**. The *ab initio* calculations for the phonon dispersion are from Ref. [12]. **Figure 51(b)** shows that the VFF model and the SW potential give exactly the same phonon dispersion, as the SW potential is derived from the VFF model.

The parameters for the two-body SW potential used by GULP are shown in **Table 107**. The parameters for the three-body SW potential used by GULP are shown in **Table 108**. Some representative parameters for the SW potential used by LAMMPS are listed in **Table 109**. We note that 12 atom types have been introduced for the simulation of the single-layer 1H-MoO_2 using LAMMPS, because the angles around atom Mo in **Figure 1** (with M = Mo and X = O) are not distinguishable in LAMMPS. We have suggested two options to differentiate these angles by implementing some additional constraints in LAMMPS, which can be accomplished by modifying the source file of LAMMPS [13, 14]. According to our experience, it is not so

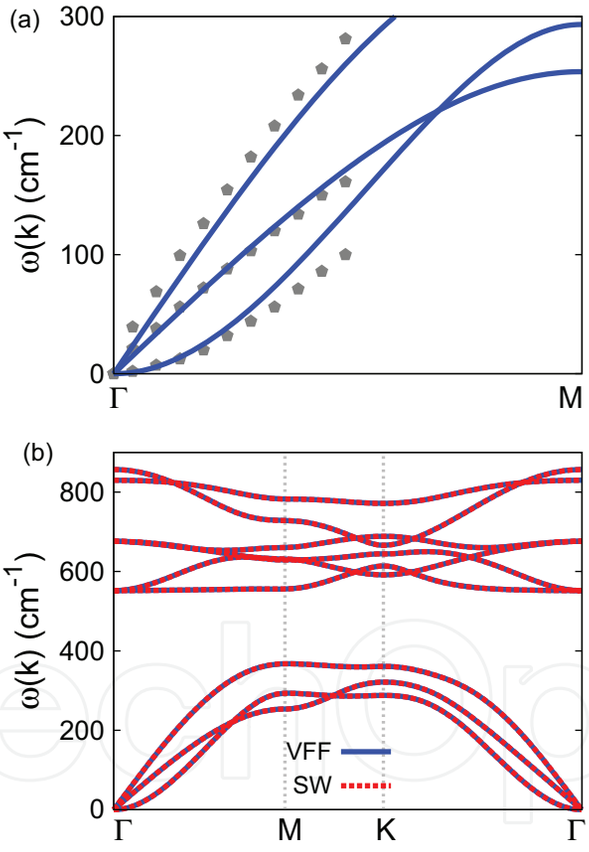

Figure 51. Phonon spectrum for single-layer 1H-MoO_2. (a) Phonon dispersion along the ΓM direction in the Brillouin zone. The results from the VFF model (lines) are comparable with the *ab initio* results (pentagons) from Ref. [12]. (b) The phonon dispersion from the SW potential is exactly the same as that from the VFF model.

	A (eV)	ρ (Å)	B (Å^4)	r_{min}(Å)	r_{max}(Å)
Mo-O	8.317	1.015	8.000	0.0	2.712

Table 107. Two-body SW potential parameters for single-layer 1H-MoO_2 used by GULP [8] as expressed in Eq. (3).

	K (eV)	θ_0(°)	ρ_1(Å)	ρ_2(Å)	$r_{\min 12}$(Å)	$r_{\max 12}$(Å)	$r_{\min 13}$(Å)	$r_{\max 13}$(Å)	$r_{\min 23}$(Å)	$r_{\max 23}$(Å)
$\theta_{\text{Mo–O–O}}$	72.735	88.054	1.015	1.015	0.0	2.712	0.0	2.712	0.0	3.222
$\theta_{\text{Mo–O–O}'}$	79.226	73.258	1.015	1.015	0.0	2.712	0.0	2.712	0.0	3.222
$\theta_{\text{O–Mo–Mo}}$	72.735	88.054	1.015	1.015	0.0	2.712	0.0	2.712	0.0	3.222

The angle θ_{ijk} in the first line indicates the bending energy for the angle with atom i as the apex.

Table 108. Three-body SW potential parameters for single-layer 1H-MoO_2 used by GULP [8] as expressed in Eq. (4).

	ϵ (eV)	σ(Å)	a	λ	γ	$\cos\theta_0$	A_L	B_L	p	q	Tol
Mo_1—O_1—O_1	1.000	1.015	2.673	0.000	1.000	0.000	8.317	7.541	4	0	0.0
Mo_1—O_1—O_3	1.000	0.000	0.000	72.735	1.000	0.034	0.000	0.000	4	0	0.0
Mo_1—O_1—O_2	1.000	0.000	0.000	79.226	1.000	0.288	0.000	0.000	4	0	0.0
O_1—Mo_1—Mo_3	1.000	0.000	0.000	72.735	1.000	0.034	0.000	0.000	4	0	0.0

Table 109. SW potential parameters for single-layer 1H-MoO_2 used by LAMMPS [9] as expressed in Eqs. (9) and (10).

convenient for some users to implement these constraints and recompile the LAMMPS package. Hence, in the present work, we differentiate the angles by introducing more atom types, so it is not necessary to modify the LAMMPS package. **Figure 2** (with M = Mo and X = O) shows that, for 1H-MoO_2, we can differentiate these angles around the Mo atom by assigning these six neighboring O atoms with different atom types. It can be found that 12 atom types are necessary for the purpose of differentiating all 6 neighbors around 1 Mo atom.

We use LAMMPS to perform MD simulations for the mechanical behavior of the single-layer 1H-MoO_2 under uniaxial tension at 1 and 300 K. **Figure 52** shows the stress-strain curve for the tension of a single-layer 1H-MoO_2 of dimension 100 × 100 Å. Periodic boundary conditions are

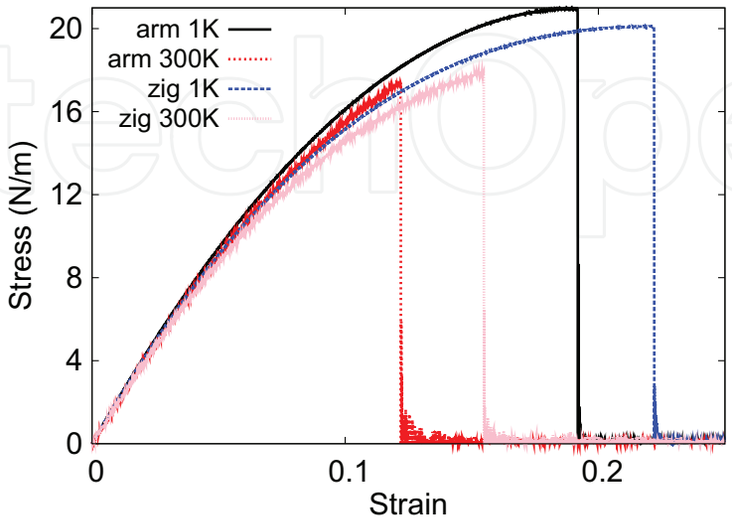

Figure 52. Stress-strain for single-layer 1H-MoO_2 of dimension 100 × 100 Å along the armchair and zigzag directions.

applied in both armchair and zigzag directions. The single-layer 1H-MoO_2 is stretched uniaxially along the armchair or zigzag direction. The stress is calculated without involving the actual thickness of the quasi-two-dimensional structure of the single-layer 1H-MoO_2. The Young's modulus can be obtained by a linear fitting of the stress-strain relation in the small strain range of [0, 0.01]. The Young's modulus is 210.0 and 209.3 N/m along the armchair and zigzag directions, respectively. The Young's modulus is essentially isotropic in the armchair and zigzag directions. The Poisson's ratio from the VFF model and the SW potential is $\nu_{xy} = \nu_{yx} = 0.17$.

There is no available value for nonlinear quantities in the single-layer 1H-MoO_2. We have thus used the nonlinear parameter $B = 0.5d^4$ in Eq. (5), which is close to the value of B in most materials. The value of the third-order nonlinear elasticity D can be extracted by fitting the stress-strain relation to the function $\sigma = E\epsilon + \frac{1}{2}D\epsilon^2$ with E as the Young's modulus. The values of D from the present SW potential are -1027.8 and -1106.8 N/m along the armchair and zigzag directions, respectively. The ultimate stress is about 21.0 N/m at the ultimate strain of 0.19 in the armchair direction at the low temperature of 1 K. The ultimate stress is about 20.1 N/m at the ultimate strain of 0.22 in the zigzag direction at the low temperature of 1 K.

28. 1H-MoS_2

Several potentials have been proposed to describe the interaction for the single-layer 1H-MoS_2. In 1975, Wakabayashi et al. developed a VFF model to calculate the phonon spectrum of the bulk 2H-MoS_2 [22]. In 2009, Liang et al. parameterized a bond-order potential for 1H-MoS_2 [23], which is based on the bond order concept underlying the Brenner potential [6]. A separate force field model was parameterized in 2010 for MD simulations of bulk 2H-MoS_2 [24]. The present author (J.W.J.) and his collaborators parameterized the SW potential for 1H-MoS_2 in 2013 [13], which was improved by one of the present authors (J.W.J.) in 2015 [7]. Recently, another set of parameters for the SW potential were proposed for the single-layer 1H-MoS_2 [25].

We show the VFF model and the SW potential for single-layer 1H-MoS_2 in this section. These potentials have been developed in previous works. The VFF model presented here is from Ref. [22], while the SW potential presented in this section is from Ref. [7].

The structural parameters for the single-layer 1H-MoS_2 are from the first-principles calculations as shown in **Figure 1** (with M = Mo and X = S) [26]. The Mo atom layer in the single-layer 1H-MoS_2 is sandwiched by two S atom layers. Accordingly, each Mo atom is surrounded by six S atoms, while each S atom is connected to three Mo atoms. The bond length between neighboring Mo and S atoms is $d = 2.382$ Å, and the angles are $\theta_{\mathrm{MoSS}} = 80.581^\circ$ and $\theta_{\mathrm{SMoMo}} = 80.581^\circ$.

The VFF model for single-layer 1H-MoS_2 is from Ref. [22], which is able to describe the phonon spectrum and the sound velocity accurately. We have listed the first three leading force constants for single-layer 1H-MoS_2 in **Table 110**, neglecting other weak interaction terms. The SW potential parameters for single-layer 1H-MoS_2 used by GULP are listed in **Tables 111** and **112**.

VFF type	Bond stretching	Angle bending	
Expression	$\frac{1}{2}K_{Mo-S}(\Delta r_{Mo-S})^2$	$\frac{1}{2}K_{MoSS}(\Delta\theta_{MoSS})^2$	$\frac{1}{2}K_{SMoMo}(\Delta\theta_{SMoMo})^2$
Parameter	8.640	5.316	4.891
r_0 or θ_0	2.382	80.581	80.581

The second line gives the expression for each VFF term. Parameters are in the unit of eV/Å^2 for the bond stretching interaction and in the unit of eV for the angle bending interaction. The fourth line gives the initial bond length (in the unit of Å) for the bond stretching interaction and the initial angle (in the unit of degrees) for the angle bending interaction. The angle θ_{ijk} has atom i as the apex.

Table 110. The VFF model parameters for single-layer 1H-MoS_2 from Ref. [22].

	A (eV)	ρ (Å)	B (Å^4)	$r_{\min}$ (Å)	$r_{\max}$ (Å)
r_{Mo-S}	6.918	1.252	17.771	0.0	3.16

Table 111. Two-body SW potential parameters for single-layer 1H-MoS_2 used by GULP [8] as expressed in Eq. (3).

	K (eV)	θ_0 (°)	ρ_1 (Å)	ρ_2(Å)	$r_{\min 12}$ (Å)	$r_{\max 12}$(Å)	$r_{\min 13}$ (Å)	$r_{\max 13}$ (Å)	$r_{\min 23}$ (Å)	$r_{\max 23}$ (Å)
θ_{MoSS}	67.883	81.788	1.252	1.252	0.0	3.16	0.0	3.16	0.0	3.78
θ_{SMoMo}	62.449	81.788	1.252	1.252	0.0	3.16	0.0	3.16	0.0	4.27

The angle θ_{ijk} in the first line indicates the bending energy for the angle with atom i as the apex.

Table 112. Three-body SW potential parameters for single-layer 1H-MoS_2 used by GULP [8] as expressed in Eq. (4).

The SW potential parameters for single-layer 1H-MoS_2 used by LAMMPS [9] are listed in **Table 113**. We note that 12 atom types have been introduced for the simulation of the single-layer 1H-MoS_2 using LAMMPS, because the angles around atom Mo in **Figure 1** (with M = Mo and X = S) are not distinguishable in LAMMPS. We have suggested two options to differentiate these angles by implementing some additional constraints in LAMMPS, which can be accomplished by modifying the source file of LAMMPS [13, 14]. According to our experience, it is not so convenient for some users to implement these constraints and recompile the LAMMPS package. Hence, in the present work, we differentiate the angles by introducing more atom types, so it is not necessary to modify the LAMMPS package. **Figure 2** (with M = Mo and X = S)

	ϵ (eV)	σ(Å)	a	λ	γ	$\cos\theta_0$	A_L	B_L	p	q	Tol
Mo_1—S_1—S_1	1.000	1.252	2.523	0.000	1.000	0.000	6.918	7.223	4	0	0.0
Mo_1—S_1—S_3	1.000	0.000	0.000	67.883	1.000	0.143	0.000	0.000	4	0	0.0
S_1—Mo_1—Mo_3	1.000	0.000	0.000	62.449	1.000	0.143	0.000	0.000	4	0	0.0

Atom types in the first column are displayed in **Figure 2** (with M = Mo and X = S).

Table 113. SW potential parameters for single-layer 1H-MoS2 used by LAMMPS 9 as expressed in Eqs. (9) and 10.

shows that, for 1H-MoS_2, we can differentiate these angles around the Mo atom by assigning these six neighboring S atoms with different atom types. It can be found that 12 atom types are necessary for the purpose of differentiating all 6 neighbors around 1 Mo atom.

We use GULP to compute the phonon dispersion for the single-layer 1H-MoS_2 as shown in **Figure 53**. The results from the VFF model are quite comparable with the experiment data. The phonon dispersion from the SW potential is the same as that from the VFF model, which indicates that the SW potential has fully inherited the linear portion of the interaction from the VFF model.

We use LAMMPS to perform MD simulations for the mechanical behavior of the single-layer 1H-MoS_2 under uniaxial tension at 1 and 300 K. **Figure 54** shows the stress-strain curve during

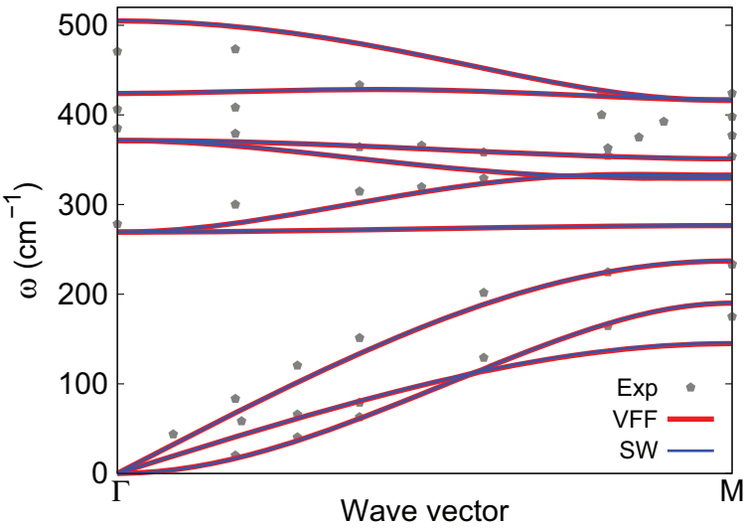

Figure 53. Phonon spectrum for single-layer 1H-MoS_2. Phonon dispersion along the ΓM direction in the Brillouin zone. The results from the VFF model (lines) are comparable with the experiment data (pentagons) from Ref. [22]. The phonon dispersion from the SW potential is exactly the same as that from the VFF model.

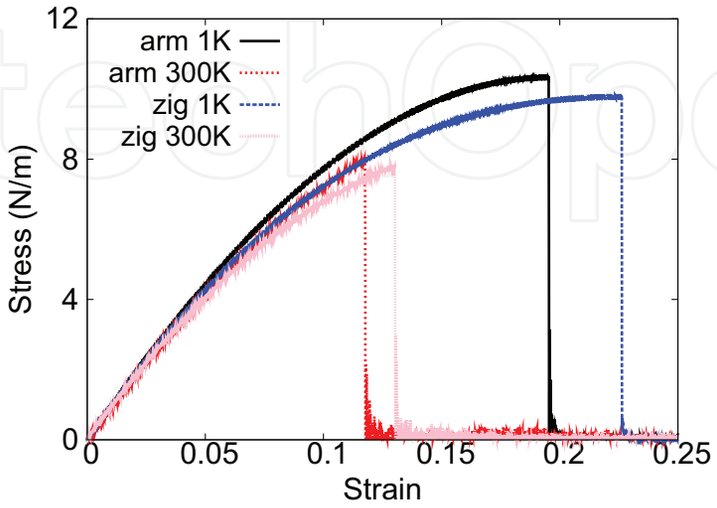

Figure 54. Stress-strain for single-layer 1H-MoS_2 of dimension 100 × 100 Å along the armchair and zigzag directions.

the tension of a single-layer 1H-MoS_2 of dimension 100 × 100 Å. Periodic boundary conditions are applied in both armchair and zigzag directions. The single-layer 1H-MoS_2 is stretched uniaxially along the armchair or zigzag direction. The stress is calculated without involving the actual thickness of the quasi-two-dimensional structure of the single-layer 1H-MoS_2. The Young's modulus can be obtained by a linear fitting of the stress-strain relation in the small strain range of [0, 0.01]. The Young's modulus is 97 and 96 N/m along the armchair and zigzag directions, respectively. The Young's modulus is isotropic in the armchair and zigzag directions. These values are in considerable agreement with the experimental results, e.g., 120 ± 30 N/m from Refs [27, 28], or 180 ± 60 N/m from Ref. [29]. The third-order nonlinear elastic constant D can be obtained by fitting the stress-strain relation to $\sigma = E\epsilon + \frac{1}{2}D\epsilon^2$ with E as the Young's modulus. The values of D are −418 and −461 N/m along the armchair and zigzag directions, respectively. The Poisson's ratio from the VFF model and the SW potential is $\nu_{xy} = \nu_{yx} = 0.27$.

29. 1H-$MoSe_2$

There is a recent parameter set for the SW potential in the single-layer 1H-$MoSe_2$ [25]. In this section, we will develop both VFF model and the SW potential for the single-layer 1H-$MoSe_2$.

The structure for the single-layer 1H-$MoSe_2$ is shown in **Figure 1** (with M = Mo and X = Se). Each Mo atom is surrounded by six Se atoms. These Se atoms are categorized into the top group (e.g., atoms 1, 3, and 5) and bottom group (e.g., atoms 2, 4, and 6). Each Se atom is connected to three Mo atoms. The structural parameters are from Ref. [30], including the lattice constant $a = 3.321$ Å and the bond length $d_{\mathrm{Mo-Se}} = 2.528$ Å. The resultant angles are $\theta_{\mathrm{MoSeSe}} = \theta_{\mathrm{SeMoMo}} = 82.119^\circ$ and $\theta_{\mathrm{MoSeSe'}} = 81.343^\circ$, in which atoms Se and Se′ are from different (top or bottom) groups.

Table 114 shows four VFF terms for the 1H-$MoSe_2$; one of which is the bond stretching interaction shown by Eq. (1), while the other three terms are the angle bending interaction shown by Eq. (2). These force constant parameters are determined by fitting to the three acoustic branches in the phonon dispersion along the ΓM as shown in **Figure 55(a)**. The *ab initio* calculations for the phonon dispersion are from Ref. [30]. Similar phonon dispersion can

VFF type	Bond stretching	Angle bending		
Expression	$\frac{1}{2}K_{Mo-Se}(\Delta r)^2$	$\frac{1}{2}K_{Mo-Se-Se}(\Delta\theta)^2$	$\frac{1}{2}K_{Mo-Se-Se'}(\Delta\theta)^2$	$\frac{1}{2}K_{Se-Mo-Mo}(\Delta\theta)^2$
Parameter	7.928	6.945	6.945	5.782
r_0 or θ_0	2.528	82.119	81.343	82.119

The second line gives an explicit expression for each VFF term. The third line is the force constant parameters. Parameters are in the unit of eV/Å^2 for the bond stretching interaction and in the unit of eV for the angle bending interaction. The fourth line gives the initial bond length (in the unit of Å) for the bond stretching interaction and the initial angle (in the unit of degrees) for the angle bending interaction. The angle θ_{ijk} has atom i as the apex.

Table 114. The VFF model for single-layer 1H-$MoSe_2$.

http://dx.doi.org/10.5772/intechopen.71929

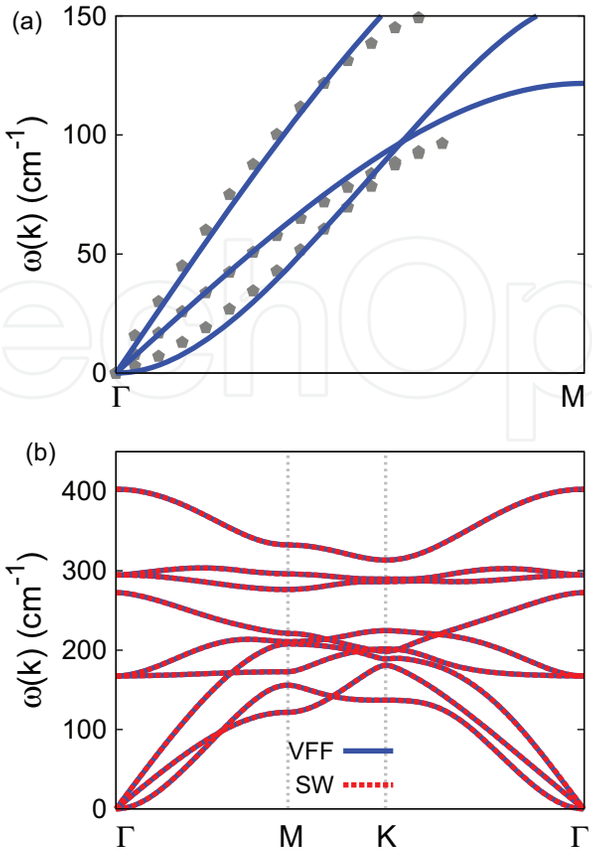

Figure 55. Phonon dispersion for single-layer 1H-$MoSe_2$. (a) The VFF model is fitted to the three acoustic branches in the long wave limit along the ΓM direction. The *ab initio* results (gray pentagons) are from Ref. [30]. (b) The VFF model (blue lines) and the SW potential (red lines) give the same phonon dispersion for single-layer 1H-$MoSe_2$ along ΓMKΓ.

also be found in other *ab initio* calculations [12, 31–34]. **Figure 55(b)** shows that the VFF model and the SW potential give exactly the same phonon dispersion, as the SW potential is derived from the VFF model.

The parameters for the two-body SW potential used by GULP are shown in **Table 115**. The parameters for the three-body SW potential used by GULP are shown in **Table 116**. Parameters for the SW potential used by LAMMPS are listed in **Table 117**. We note that 12 atom types have been introduced for the simulation of the single-layer 1H-$MoSe_2$ using LAMMPS, because the angles around atom Mo in **Figure 1** (with M = Mo and X = Se) are not distinguishable in LAMMPS. We have suggested two options to differentiate these angles by implementing some additional constraints in LAMMPS, which can be accomplished by modifying the source file of LAMMPS [13, 14]. According to our experience, it is not so convenient for some users to implement these constraints and recompile the LAMMPS package. Hence, in the present work,

	A (eV)	ρ (Å)	B (Å^4)	r_{min} (Å)	r_{max} (Å)
Mo-Se	5.737	0.913	18.787	0.0	3.351

Table 115. Two-body SW potential parameters for single-layer 1H-$MoSe_2$ used by GULP [8] as expressed in Eq. (3).

	K (eV)	θ_0(°)	ρ_1(Å)	ρ_2(Å)	$r_{\min 12}$(Å)	$r_{\max 12}$(Å)	$r_{\min 13}$(Å)	$r_{\max 13}$(Å)	$r_{\min 23}$(Å)	$r_{\max 23}$(Å)
$\theta_{\text{Mo–Se–Se}}$	32.526	82.119	0.913	0.913	0.0	3.351	0.0	3.351	0.0	4.000
$\theta_{\text{Mo–Se–Se}'}$	32.654	81.343	0.913	0.913	0.0	3.351	0.0	3.351	0.0	4.000
$\theta_{\text{Se–Mo–Mo}}$	27.079	82.119	0.913	0.913	0.0	3.351	0.0	3.351	0.0	4.000

The angle θ_{ijk} in the first line indicates the bending energy for the angle with atom i as the apex.

Table 116. Three-body SW potential parameters for single-layer 1H-$MoSe_2$ used by GULP [8] as expressed in Eq. (4).

	σ(eV)	a(Å)	λ	γ	$\cos\theta_0$	A_L	B_L	p	q	100 × 100	Tol
Mo_1—Se_1—Se_1	1.000	0.913	3.672	0.000	1.000	0.000	5.737	27.084	4	0	0.0
Mo_1—Se_1—Se_3	1.000	0.000	0.000	32.526	1.000	0.137	0.000	0.000	4	0	0.0
Mo_1—Se_1—Se_2	1.000	0.000	0.000	32.654	1.000	0.151	0.000	0.000	4	0	0.0
Se_1—Mo_1—Mo_3	1.000	0.000	0.000	27.079	1.000	0.137	0.000	0.000	4	0	0.0

Atom types in the first column are displayed in **Figure 2** (with M = Mo and X = Se).

Table 117. SW potential parameters for single-layer 1H-$MoSe_2$ used by LAMMPS [9] as expressed in Eqs. (9) and (10).

we differentiate the angles by introducing more atom types, so it is not necessary to modify the LAMMPS package. **Figure 2** (with M = Mo and X = Se) shows that, for 1H-$MoSe_2$, we can differentiate these angles around the Mo atom by assigning these six neighboring Se atoms with different atom types. It can be found that 12 atom types are necessary for the purpose of differentiating all 6 neighbors around 1 Mo atom.

We use LAMMPS to perform MD simulations for the mechanical behavior of the single-layer 1H-$MoSe_2$ under uniaxial tension at 1 and 300 K. **Figure 56** shows the stress-strain curve during the tension of a single-layer 1H-$MoSe_2$ of dimension 100 × 100Å. Periodic boundary

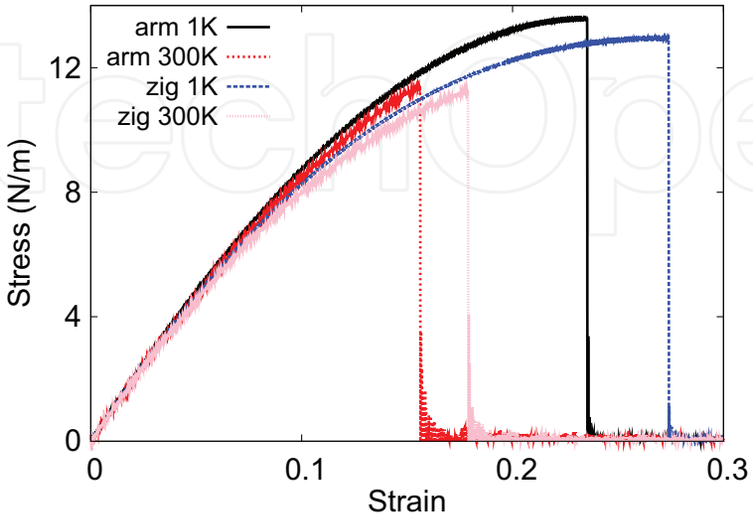

Figure 56. Stress-strain for single-layer 1H-$MoSe_2$ of dimension 100 × 100 Å along the armchair and zigzag directions.

conditions are applied in both armchair and zigzag directions. The single-layer 1H-$MoSe_2$ is stretched uniaxially along the armchair or zigzag direction. The stress is calculated without involving the actual thickness of the quasi-two-dimensional structure of the single-layer 1H-$MoSe_2$. The Young's modulus can be obtained by a linear fitting of the stress-strain relation in the small strain range of [0, 0.01]. The Young's modulus is 103.0 and 101.8 N/m along the armchair and zigzag directions, respectively. The Young's modulus is essentially isotropic in the armchair and zigzag directions. These values are in considerable agreement with the experimental results, e.g., 103.9 N/m from Ref. [18], or 113.9 N/m from Ref. [35]. The Poisson's ratio from the VFF model and the SW potential is $\nu_{xy} = \nu_{yx} = 0.24$, which agrees quite well with the *ab initio* value of 0.23 [18].

We have determined the nonlinear parameter to be $B = 0.46d^4$ in Eq. (5) by fitting to the third-order nonlinear elastic constant D from the *ab initio* calculations [35]. We have extracted the value of $D = -383.7$ N/m by fitting the stress-strain relation along the armchair direction in the *ab initio* calculations to the function $\sigma = E\epsilon + \frac{1}{2}D\epsilon^2$ with E as the Young's modulus. The values of D from the present SW potential are -365.4 and -402.4 N/m along the armchair and zigzag directions, respectively. The ultimate stress is about 13.6 N/m at the ultimate strain of 0.23 in the armchair direction at the low temperature of 1 K. The ultimate stress is about 13.0 N/m at the ultimate strain of 0.27 in the zigzag direction at the low temperature of 1 K.

30. 1H-$MoTe_2$

Most existing theoretical studies on the single-layer 1H-$MoTe_2$ are based on the first-principles calculations. In this section, we will develop both VFF model and the SW potential for the single-layer 1H-$MoTe_2$.

The structure for the single-layer 1H-$MoTe_2$ is shown in **Figure 1** (with M = Mo and X = Te). Each Mo atom is surrounded by six Te atoms. These Te atoms are categorized into the top group (e.g., atoms 1, 3, and 5) and bottom group (e.g., atoms 2, 4, and 6). Each Te atom is connected to three Mo atoms. The structural parameters are from Ref. [36], including the lattice constant $a = 3.55$Å and the bond length $d_{\mathrm{Mo-Te}} = 2.73$Å. The resultant angles are $\theta_{\mathrm{MoTeTe}} = \theta_{\mathrm{TeMoMo}} = 81.111^\circ$ and $\theta_{\mathrm{MoTeTe'}} = 82.686^\circ$, in which atoms Te and Te′ are from different (top or bottom) groups.

Table 118 shows four VFF terms for the 1H-$MoTe_2$; one of which is the bond stretching interaction shown by Eq. (1), while the other three terms are the angle bending interaction shown by Eq. (2). These force constant parameters are determined by fitting to the three acoustic branches in the phonon dispersion along the ΓM as shown in **Figure 57(a)**. The *ab initio* calculations for the phonon dispersion are from Ref. [36]. Similar phonon dispersion can also be found in other *ab initio* calculations [12, 34, 37]. **Figure 57(b)** shows that the VFF model and the SW potential give exactly the same phonon dispersion, as the SW potential is derived from the VFF model.

The parameters for the two-body SW potential used by GULP are shown in **Table 119**. The parameters for the three-body SW potential used by GULP are shown in **Table 120**. Parameters

VFF type	Bond stretching	Angle bending		
Expression	$\frac{1}{2}K_{\mathrm{Mo-Te}}(\Delta r)^2$	$\frac{1}{2}K_{\mathrm{Mo-Te-Te}}(\Delta\theta)^2$	$\frac{1}{2}K_{\mathrm{Mo-Te-Te'}}(\Delta\theta)^2$	$\frac{1}{2}K_{\mathrm{Te-Mo-Mo}}(\Delta\theta)^2$
Parameter	6.317	6.184	6.184	5.225
r_0 or θ_0	2.730	81.111	82.686	81.111

The second line gives an explicit expression for each VFF term. The third line is the force constant parameters. Parameters are in the unit of eV/Å^2 for the bond stretching interaction and in the unit of eV for the angle bending interaction. The fourth line gives the initial bond length (in the unit of Å) for the bond stretching interaction and the initial angle (in the unit of degrees) for the angle bending interaction. The angle θ_{ijk} has atom i as the apex.

Table 118. The VFF model for single-layer 1H-$MoTe_2$.

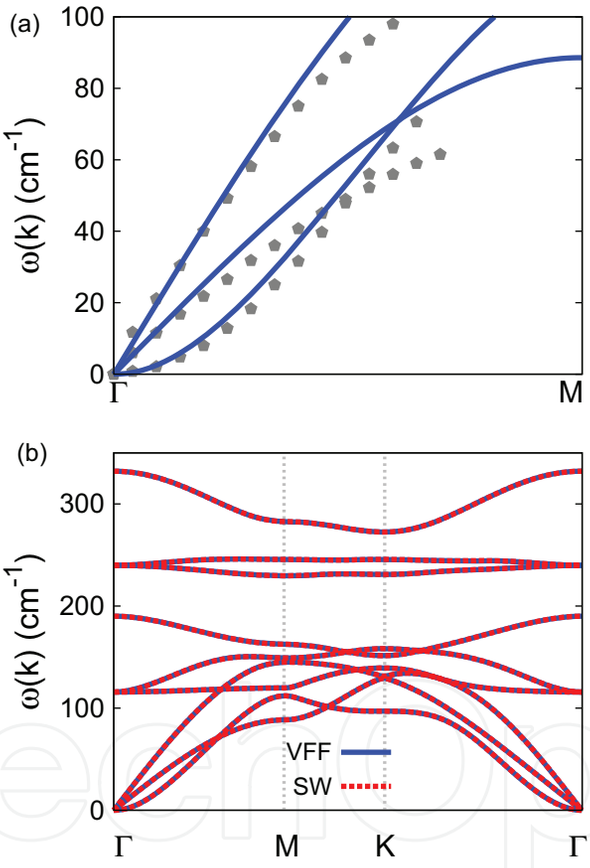

Figure 57. Phonon dispersion for single-layer 1H-$MoTe_2$. (a) The VFF model is fitted to the three acoustic branches in the long wave limit along the ΓM direction. The *ab initio* results (gray pentagons) are from Ref. [36]. (b) The VFF model (blue lines) and the SW potential (red lines) give the same phonon dispersion for single-layer 1H-$MoTe_2$ along ΓMKΓ.

	A (eV)	ρ (Å)	B (Å^4)	r_{min} (Å)	r_{max} (Å)
Mo-Te	5.086	0.880	24.440	0.0	3.604

Table 119. Two-body SW potential parameters for single-layer 1H-$MoTe_2$ used by GULP [8] as expressed in Eq. (3).

	K (eV)	θ_0 (°)	ρ_1 (Å)	ρ_2 (Å)	$r_{\min 12}$ (Å)	$r_{\max 12}$ (Å)	$r_{\min 13}$ (Å)	$r_{\max 13}$ (Å)	$r_{\min 23}$ (Å)	$r_{\max 23}$ (Å)
$\theta_{\text{Mo–Te–Te}}$	23.705	81.111	0.880	0.880	0.0	3.604	0.0	3.604	0.0	4.305
$\theta_{\text{Mo–Te–Te}'}$	23.520	82.686	0.880	0.880	0.0	3.604	0.0	3.604	0.0	4.305
$\theta_{\text{Te–Mo–Mo}}$	20.029	81.111	0.880	0.880	0.0	3.604	0.0	3.604	0.0	4.305

The angle θ_{ijk} in the first line indicates the bending energy for the angle with atom i as the apex.

Table 120. Three-body SW potential parameters for single-layer 1H-$MoTe_2$ used by GULP [8] as expressed in Eq. (4).

for the SW potential used by LAMMPS are listed in **Table 121**. We note that 12 atom types have been introduced for the simulation of the single-layer 1H-$MoTe_2$ using LAMMPS, because the angles around atom Mo in **Figure 1** (with M = Mo and X = Te) are not distinguishable in LAMMPS. We have suggested two options to differentiate these angles by implementing some additional constraints in LAMMPS, which can be accomplished by modifying the source file of LAMMPS [13, 14]. According to our experience, it is not so convenient for some users to implement these constraints and recompile the LAMMPS package. Hence, in the present work, we differentiate the angles by introducing more atom types, so it is not necessary to modify the LAMMPS package. **Figure 2** (with M = Mo and X = Te) shows that, for 1H-$MoTe_2$, we can differentiate these angles around the Mo atom by assigning these six neighboring Te atoms with different atom types. It can be found that 12 atom types are necessary for the purpose of differentiating all 6 neighbors around 1 Mo atom.

We use LAMMPS to perform MD simulations for the mechanical behavior of the single-layer 1H-$MoTe_2$ under uniaxial tension at 1 and 300 K. **Figure 58** shows the stress-strain curve for the tension of a single-layer 1H-$MoTe_2$ of dimension 100×100Å. Periodic boundary conditions are applied in both armchair and zigzag directions. The single-layer 1H-$MoTe_2$ is stretched uniaxially along the armchair or zigzag direction. The stress is calculated without involving the actual thickness of the quasi-two-dimensional structure of the single-layer 1H-$MoTe_2$. The Young's modulus can be obtained by a linear fitting of the stress-strain relation in the small strain range of [0, 0.01]. The Young's modulus is 79.8 and 78.5 N/m along the armchair and zigzag directions, respectively. The Young's modulus is essentially isotropic in the armchair and zigzag directions. These values are in considerable agreement with the experimental results, e.g., 79.4 N/m from Ref. [18], or 87.0 N/m from Ref. [35]. The Poisson's ratio from the VFF model and the SW potential is $\nu_{xy} = \nu_{yx} = 0.25$, which agrees with the *ab initio* value of 0.24 [18].

	ϵ (eV)	σ (Å)	a	λ	γ	$\cos\theta_0$	A_L	B_L	p	q	Tol
Mo_1—Te_1—Te_1	1.000	0.900	4.016	0.000	1.000	0.000	5.169	37.250	4	0	0.0
Mo_1—Te_1—Te_3	1.000	0.000	0.000	24.163	1.000	0.143	0.000	0.000	4	0	0.0
Te_1—Mo_1—Mo_3	1.000	0.000	0.000	20.416	1.000	0.143	0.000	0.000	4	0	0.0

Atom types in the first column are displayed in **Figure 2** (with M = Mo and X = Te).

Table 121. SW potential parameters for single-layer 1H-$MoTe_2$ used by LAMMPS [9] as expressed in Eqs. (9) and (10).

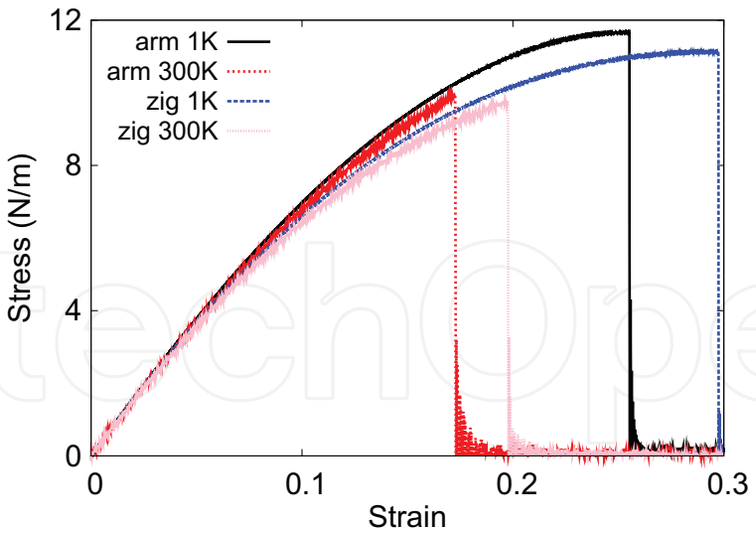

Figure 58. Stress-strain for single-layer 1H-$MoTe_2$ of dimension θ_0 Å along the armchair and zigzag directions.

We have determined the nonlinear parameter to be $B = 0.44d^4$ in Eq. (5) by fitting to the third-order nonlinear elastic constant D from the *ab initio* calculations [35]. We have extracted the value of $D = -278.2$ N/m by fitting the stress-strain relation along the armchair direction in the *ab initio* calculations to the function $\sigma = E\epsilon + \frac{1}{2}D\epsilon^2$ with E as the Young's modulus. The values of D from the present SW potential are -250.5 and -276.6 N/m along the armchair and zigzag directions, respectively. The ultimate stress is about 11.7 N/m at the ultimate strain of 0.25 in the armchair direction at the low temperature of 1 K. The ultimate stress is about 11.1 N/m at the ultimate strain of 0.29 in the zigzag direction at the low temperature of 1 K.

31. 1H-TaS_2

In 1983, the VFF model was developed to investigate the lattice dynamical properties in the bulk 2H-TaS_2 [21]. In this section, we will develop the SW potential for the single-layer 1H-TaS_2.

The structure for the single-layer 1H-TaS_2 is shown in **Figure 1** (with M = Ta and X = S). Each Ta atom is surrounded by six S atoms. These S atoms are categorized into the top group (e.g., atoms 1, 3, and 5) and bottom group (e.g., atoms 2, 4, and 6). Each S atom is connected to three Ta atoms. The structural parameters are from Ref. [21], including the lattice constant $a = 3.315$Å and the bond length $d_{\mathrm{Ta-S}} = 2.48$Å. The resultant angles are $\theta_{\mathrm{TaSS}} = \theta_{\mathrm{STaTa}} = 83.879^\circ$ and $\theta_{\mathrm{TaSS'}} = 78.979^\circ$, in which atoms S and S′ are from different (top or bottom) groups.

Table 122 shows the VFF terms for the 1H-TaS_2; one of which is the bond stretching interaction shown by Eq. (1), while the others are the angle bending interaction shown by Eq. (2). These force constant parameters are determined by fitting to the three acoustic branches in the phonon dispersion along the ϵ as shown in **Figure 59(a)**. The theoretical phonon frequencies (gray pentagons) are from Ref. [21], which are the phonon dispersion of bulk 2H-TaS_2. We

VFF type	Bond stretching	Angle bending		
Expression	$\frac{1}{2}K_{\mathrm{Ta-S}}(\Delta r)^2$	$\frac{1}{2}K_{\mathrm{Ta-S-S}}(\Delta\theta)^2$	$\frac{1}{2}K_{\mathrm{Ta-S-S'}}(\Delta\theta)^2$	$\frac{1}{2}K_{\mathrm{S-Ta-Ta}}(\Delta\theta)^2$
Parameter	8.230	4.811	4.811	4.811
r_0 or θ_0	2.480	83.879	78.979	83.879

The second line gives an explicit expression for each VFF term. The third line is the force constant parameters. Parameters are in the unit of eV/Å^2 for the bond stretching interaction and in the unit of eV for the angle bending interaction. The fourth line gives the initial bond length (in the unit of Å) for the bond stretching interaction and the initial angle (in the unit of degrees) for the angle bending interaction. The angle θ_{ijk} has atom i as the apex.

Table 122. The VFF model for single-layer 1H-TaS_2.

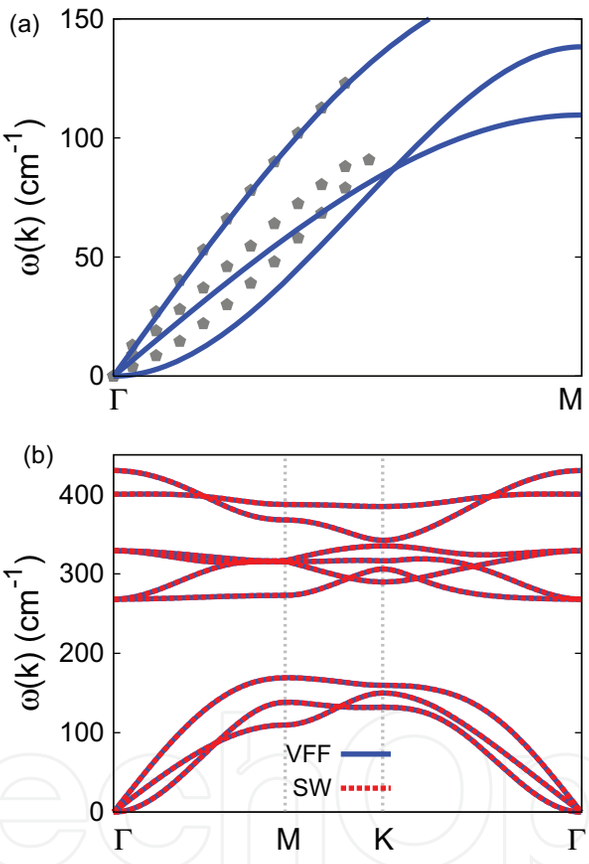

Figure 59. Phonon dispersion for single-layer 1H-TaS_2. (a) The VFF model is fitted to the three acoustic branches in the long wave limit along the ΓM direction. The theoretical results (gray pentagons) are from Ref. [21]. The blue lines are from the present VFF model. (b) The VFF model (blue lines) and the SW potential (red lines) give the same phonon dispersion for single-layer 1H-TaS_2 along ΓMKΓ.

have used these phonon frequencies as the phonon dispersion of the single-layer 1H-TaS_2, as the interlayer interaction in the bulk 2H-TaS_2 only induces weak effects on the two in-plane acoustic branches. The interlayer coupling will strengthen the out-of-plane acoustic (flexural) branch, so the flexural branch from the present VFF model (blue line) is lower than the theoretical results for bulk 2H-TaS_2 (gray pentagons). **Figure 59(b)** shows that the VFF model

and the SW potential give exactly the same phonon dispersion, as the SW potential is derived from the VFF model.

The parameters for the two-body SW potential used by GULP are shown in **Table 123**. The parameters for the three-body SW potential used by GULP are shown in **Table 124**. Parameters for the SW potential used by LAMMPS are listed in **Table 125**. We note that 12 atom types have been introduced for the simulation of the single-layer 1H-TaS_2 using LAMMPS, because the angles around atom Ta in **Figure 1** (with M = Ta and X = S) are not distinguishable in LAMMPS. We have suggested two options to differentiate these angles by implementing some additional constraints in LAMMPS, which can be accomplished by modifying the source file of LAMMPS [13, 14]. According to our experience, it is not so convenient for some users to implement these constraints and recompile the LAMMPS package. Hence, in the present work, we differentiate the angles by introducing more atom types, so it is not necessary to modify the LAMMPS package. **Figure 2** (with M = Ta and X = S) shows that, for 1H-TaS_2, we can differentiate these angles around the Ta atom by assigning these six neighboring S atoms with different atom types. It can be found that 12 atom types are necessary for the purpose of differentiating all 6 neighbors around 1 Ta atom.

We use LAMMPS to perform MD simulations for the mechanical behavior of the single-layer 1H-TaS_2 under uniaxial tension at 1 and 300 K. **Figure 60** shows the stress-strain curve for the

	A (eV)	ρ (Å)	B (Å^4)	$r_{\min}$ (Å)	$r_{\max}$ (Å)
Ta-S	6.446	1.111	18.914	0.0	3.310

Table 123. Two-body SW potential parameters for single-layer 1H-TaS_2 used by GULP [8] as expressed in Eq. (3).

	K (eV)	θ_0 (°)	ρ_1 (Å)	ρ_2 (Å)	$r_{\min\ 12}$ (Å)	$r_{\max\ 12}$ (Å)	$r_{\min\ 13}$ (Å)	$r_{\max\ 13}$ (Å)	$r_{\min\ 23}$ (Å)	$r_{\max\ 23}$ (Å)
$\theta_{\mathrm{Ta-S-S}}$	35.396	83.879	1.111	1.111	0.0	3.310	0.0	3.310	0.0	3.945
$\theta_{\mathrm{Ta-S-S'}}$	36.321	78.979	1.111	1.111	0.0	3.310	0.0	3.310	0.0	3.945
$\theta_{\mathrm{S-Ta-Ta}}$	35.396	83.879	1.111	1.111	0.0	3.310	0.0	3.310	0.0	3.945

The angle θ_{ijk} in the first line indicates the bending energy for the angle with atom i as the apex.

Table 124. Three-body SW potential parameters for single-layer 1H-TaS_2 used by GULP [8] as expressed in Eq. (4).

	ϵ (eV)	σ (Å)	a	λ	γ	$\cos\theta_0$	A_L	B_L	p	q	Tol
Ta_1—S_1—S_1	1.000	1.111	2.979	0.000	1.000	0.000	6.446	12.408	4	0	0.0
Ta_1—S_1—S_3	1.000	0.000	0.000	35.396	1.000	0.107	0.000	0.000	4	0	0.0
Ta_1—S_1—S_2	1.000	0.000	0.000	36.321	1.000	0.191	0.000	0.000	4	0	0.0
S_1—Ta_1—Ta_3	1.000	0.000	0.000	35.396	1.000	0.107	0.000	0.000	4	0	0.0

Atom types in the first column are displayed in **Figure 2** (with M = Ta and X = S).

Table 125. SW potential parameters for single-layer 1H-TaS_2 used by LAMMPS [9] as expressed in Eqs. (9) and (10).

http://dx.doi.org/10.5772/intechopen.71929

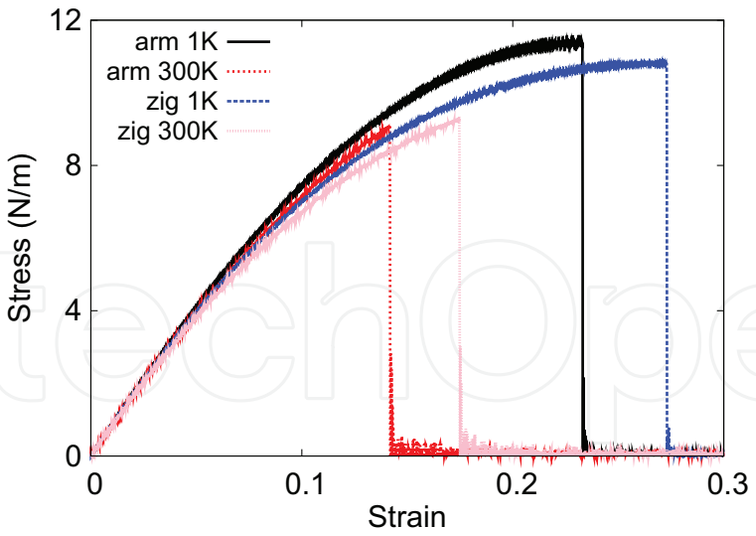

Figure 60. Stress-strain for single-layer 1H-TaS_2 of dimension 100 × 100Å along the armchair and zigzag directions.

tension of a single-layer 1H-TaS_2 of dimension 100 × 100Å. Periodic boundary conditions are applied in both armchair and zigzag directions. The single-layer 1H-TaS_2 is stretched uniaxially along the armchair or zigzag direction. The stress is calculated without involving the actual thickness of the quasi-two-dimensional structure of the single-layer 1H-TaS_2. The Young's modulus can be obtained by a linear fitting of the stress-strain relation in the small strain range of [0, 0.01]. The Young's modulus is 87.4 and 86.6 N/m along the armchair and zigzag directions, respectively. The Poisson's ratio from the VFF model and the SW potential is $\nu_{xy} = \nu_{yx} = 0.27$.

There is no available value for the nonlinear quantities in the single-layer 1H-TaS_2. We have thus used the nonlinear parameter $B = 0.5d^4$ in Eq. (5), which is close to the value of B in most materials. The value of the third-order nonlinear elasticity D can be extracted by fitting the stress-strain relation to the function $\sigma = E\epsilon + \frac{1}{2}D\epsilon^2$ with E as the Young's modulus. The values of D from the present SW potential are −313.0 and −349.3 N/m along the armchair and zigzag directions, respectively. The ultimate stress is about 11.4 N/m at the ultimate strain of 0.23 in the armchair direction at the low temperature of 1 K. The ultimate stress is about 10.8 N/m at the ultimate strain of 0.27 in the zigzag direction at the low temperature of 1 K.

32. 1H-$TaSe_2$

The VFF model was developed to investigate the lattice dynamical properties in the bulk 2H-$TaSe_2$ [15, 21]. In this section, we will develop the SW potential for the single-layer 1H-$TaSe_2$.

The structure for the single-layer 1H-$TaSe_2$ is shown in **Figure 1** (with M = Ta and X = Se). Each Ta atom is surrounded by six Se atoms. These Se atoms are categorized into the top group (e.g., atoms 1, 3, and 5) and bottom group (e.g., atoms 2, 4, and 6). Each Se atom is connected to

three Ta atoms. The structural parameters are from Ref. [21], including the lattice constant $a = 3.436$Å and the bond length $d_{\mathrm{Ta-Se}} = 2.59$Å. The resultant angles are $\theta_{\mathrm{TaSeSe}} = \theta_{\mathrm{SeTaTa}} = 83.107^\circ$ and $\theta_{\mathrm{TaSeSe'}} = 80.019^\circ$, in which atoms Se and Se′ are from different (top or bottom) groups.

Table 126 shows the VFF terms for the 1H-$TaSe_2$; one of which is the bond stretching interaction shown by Eq. (1), while the others are the angle bending interaction shown by Eq. (2). These force constant parameters are determined by fitting to the three acoustic branches in the phonon dispersion along the ΓM as shown in **Figure 61(a)**. The theoretical phonon frequencies (gray pentagons) are from Ref. [21], which are the phonon dispersion of bulk 2H-$TaSe_2$. We have used these phonon frequencies as the phonon dispersion of the single-layer 1H-$TaSe_2$, as the interlayer interaction in the bulk 2H-$TaSe_2$ only induces weak effects on the two in-plane acoustic branches. The interlayer coupling will strengthen the out-of-plane acoustic branch (flexural branch), so the flexural branch from the present VFF model (blue line) is lower than the theoretical results for bulk 2H-$TaSe_2$ (gray pentagons). **Figure 61(b)** shows that the VFF model and the SW potential give exactly the same phonon dispersion, as the SW potential is derived from the VFF model.

The parameters for the two-body SW potential used by GULP are shown in **Table 127**. The parameters for the three-body SW potential used by GULP are shown in **Table 128**. Parameters for the SW potential used by LAMMPS are listed in **Table 129**. We note that 12 atom types have been introduced for the simulation of the single-layer 1H-$TaSe_2$ using LAMMPS, because the angles around atom Ta in **Figure 1** (with M = Ta and X = Se) are not distinguishable in LAMMPS. We have suggested two options to differentiate these angles by implementing some additional constraints in LAMMPS, which can be accomplished by modifying the source file of LAMMPS [13, 14]. According to our experience, it is not so convenient for some users to implement these constraints and recompile the LAMMPS package. Hence, in the present work, we differentiate the angles by introducing more atom types, so it is not necessary to modify the LAMMPS package. **Figure 2** (with M = Ta and X = Se) shows that, for 1H-$TaSe_2$, we can differentiate these angles around the Ta atom by assigning these six neighboring Se atoms with different atom types. It can be found that 12 atom types are necessary for the purpose of differentiating all 6 neighbors around 1 Ta atom.

VFF type	**Bond stretching**	**Angle bending**		
Expression	$\frac{1}{2}K_{\mathrm{Ta-Se}}(\Delta r)^2$	$\frac{1}{2}K_{\mathrm{Ta-Se-Se}}(\Delta\theta)^2$	$\frac{1}{2}K_{\mathrm{Ta-Se-Se'}}(\Delta\theta)^2$	$\frac{1}{2}K_{\mathrm{Se-Ta-Ta}}(\Delta\theta)^2$
Parameter	8.230	4.811	4.811	4.811
r_0 or θ_0	2.590	83.107	80.019	83.107

The second line gives an explicit expression for each VFF term. The third line is the force constant parameters. Parameters are in the unit of eV/Å^2 for the bond stretching interaction and in the unit of eV for the angle bending interaction. The fourth line gives the initial bond length (in the unit of Å) for the bond stretching interaction and the initial angle (in the unit of degrees) for the angle bending interaction. The angle θ_{ijk} has atom i as the apex.

Table 126. The VFF model for single-layer 1H-$TaSe_2$.

http://dx.doi.org/10.5772/intechopen.71929

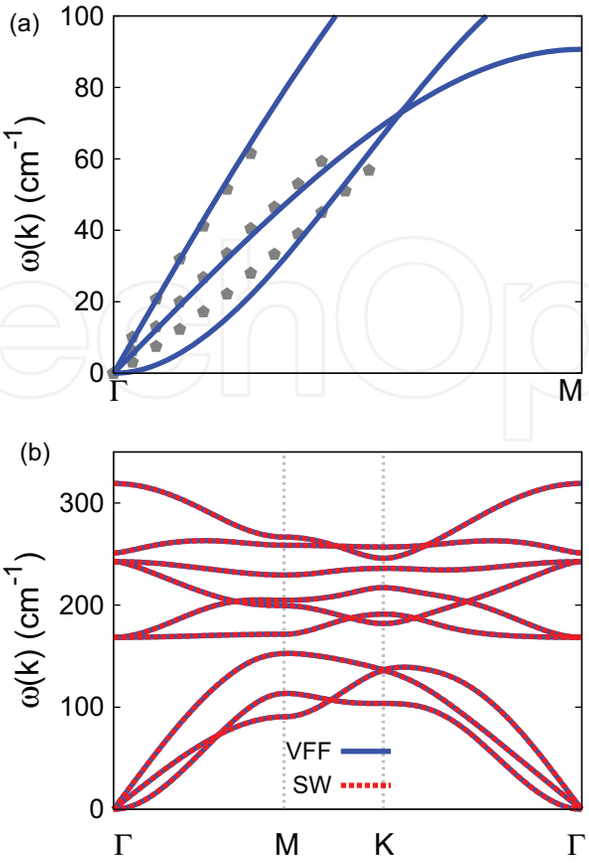

Figure 61. Phonon dispersion for single-layer 1H-$TaSe_2$. (a) The VFF model is fitted to the three acoustic branches in the long wave limit along the ΓM direction. The theoretical results (gray pentagons) are from Ref. [15]. The blue lines are from the present VFF model. (b) The VFF model (blue lines) and the SW potential (red lines) give the same phonon dispersion for single-layer 1H-$TaSe_2$ along ΓMKΓ.

	A (eV)	ρ (Å)	B (Å^4)	$r_{\min}$ (Å)	$r_{\max}$ (Å)
Ta—Se	6.885	1.133	22.499	0.0	3.446

Table 127. Two-body SW potential parameters for single-layer 1H-$TaSe_2$ used by GULP [8] as expressed in Eq. (3).

	K (eV)	θ_0 (°)	ρ_1 (Å)	ρ_2 (Å)	$r_{\min\ 12}$ (Å)	$r_{\max\ 12}$ (Å)	$r_{\min\ 13}$ (Å)	$r_{\max\ 13}$ (Å)	$r_{\min\ 23}$ (Å)	$r_{\max\ 23}$ (Å)
$\theta_{\mathrm{Ta-Se-Se}}$	34.381	83.107	1.133	1.133	0.0	3.446	0.0	3.446	0.0	4.111
$\theta_{\mathrm{Ta-Se-Se'}}$	34.936	80.019	1.133	1.133	0.0	3.446	0.0	3.446	0.0	4.111
$\theta_{\mathrm{Se-Ta-Ta}}$	34.381	83.107	1.133	1.133	0.0	3.446	0.0	3.446	0.0	4.111

The angle θ_{ijk} in the first line indicates the bending energy for the angle with atom i as the apex.

Table 128. Three-body SW potential parameters for single-layer 1H-$TaSe_2$ used by GULP [8] as expressed in Eq. (4).

We use LAMMPS to perform MD simulations for the mechanical behavior of the single-layer 1H-$TaSe_2$ under uniaxial tension at 1 and 300 K. **Figure 62** shows the stress-strain curve for the tension of a single-layer 1H-$TaSe_2$ of dimension 100 × 100Å. Periodic boundary conditions are

	ϵ (eV)	σ (Å)	a	λ	γ	$\cos\theta_0$	A_L	B_L	p	q	Tol
Ta_1—Se_1—Se_1	1.000	1.133	3.043	0.000	1.000	0.000	6.885	13.668	4	0	0.0
Ta_1—Se_1—Se_3	1.000	0.000	0.000	34.381	1.000	0.120	0.000	0.000	4	0	0.0
Ta_1—Se_1—Se_2	1.000	0.000	0.000	34.936	1.000	0.173	0.000	0.000	4	0	0.0
Se_1—Ta_1—Ta_3	1.000	0.000	0.000	34.381	1.000	0.120	0.000	0.000	4	0	0.0

Atom types in the first column are displayed in **Figure 2** (with M = Ta and X = Se).

Table 129. SW potential parameters for single-layer 1H-$TaSe_2$ used by LAMMPS [16] as expressed in Eqs. (9) and (10).

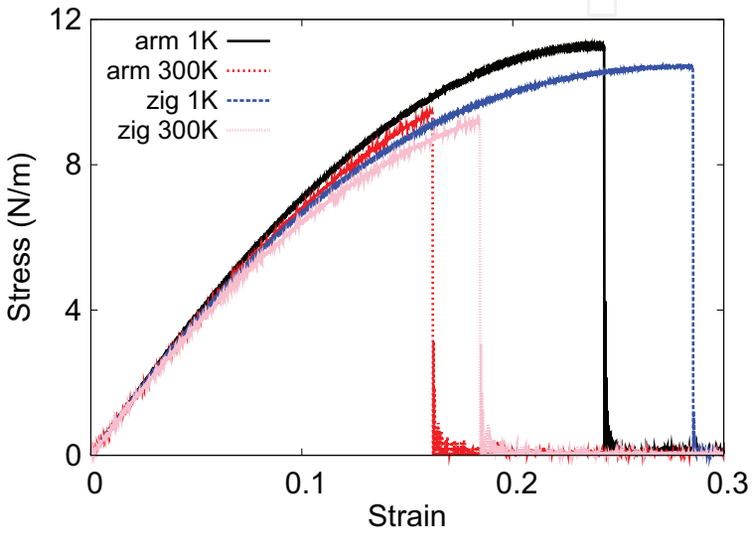

Figure 62. Stress-strain for single-layer 1H-$TaSe_2$ of dimension 100 × 100Å along the armchair and zigzag directions.

applied in both armchair and zigzag directions. The single-layer 1H-$TaSe_2$ is stretched uniaxially along the armchair or zigzag direction. The stress is calculated without involving the actual thickness of the quasi-two-dimensional structure of the single-layer 1H-$TaSe_2$. The Young's modulus can be obtained by a linear fitting of the stress-strain relation in the small strain range of [0, 0.01]. The Young's modulus is 80.8 and 81.1 N/m along the armchair and zigzag directions, respectively. The Young's modulus is essentially isotropic in the armchair and zigzag directions. The Poisson's ratio from the VFF model and the SW potential is $\nu_{xy} = \nu_{yx} = 0.29$.

There is no available value for the nonlinear quantities in the single-layer 1H-$TaSe_2$. We have thus used the nonlinear parameter $B = 0.5d^4$ in Eq. (5), which is close to the value of B in most materials. The value of the third-order nonlinear elasticity D can be extracted by fitting the stress-strain relation to the function $\sigma = E\epsilon + \frac{1}{2}D\epsilon^2$ with E as the Young's modulus. The values of D from the present SW potential are −263.3 and −308.6 N/m along the armchair and zigzag directions, respectively. The ultimate stress is about 11.3 N/m at the ultimate strain of 0.24 in the armchair direction at the low temperature of 1 K. The ultimate stress is about 10.7 N/m at the ultimate strain of 0.28 in the zigzag direction at the low temperature of 1 K.

33. 1H-WO_2

Most existing theoretical studies on the single-layer 1H-WO_2 are based on the first-principles calculations. In this section, we will develop the SW potential for the single-layer 1H-WO_2.

The structure for the single-layer 1H-WO_2 is shown in **Figure 1** (with M = W and X = O). Each W atom is surrounded by six O atoms. These O atoms are categorized into the top group (e.g., atoms 1, 3, and 5) and bottom group (e.g., atoms 2, 4, and 6). Each O atom is connected to three W atoms. The structural parameters are from the first-principles calculations [12], including the lattice constant $a = 2.80$Å and the bond length $d_{\mathrm{W-O}} = 2.03$Å. The resultant angles are $\theta_{\mathrm{WOO}} = \theta_{\mathrm{OWW}} = 87.206^{\circ}$ and $\theta_{\mathrm{WOO'}} = 74.435^{\circ}$, in which atoms O and O′ are from different (top or bottom) groups.

Table 130 shows four VFF terms for the single-layer 1H-WO_2; one of which is the bond stretching interaction shown by Eq. (1), while the other three terms are the angle bending interaction shown by Eq. (2). These force constant parameters are determined by fitting to the acoustic branches in the phonon dispersion along the ΓM as shown in **Figure 63(a)**. The *ab initio* calculations for the phonon dispersion are from Ref. [12]. **Figure 63(b)** shows that the VFF model and the SW potential give exactly the same phonon dispersion, as the SW potential is derived from the VFF model.

The parameters for the two-body SW potential used by GULP are shown in **Table 131**. The parameters for the three-body SW potential used by GULP are shown in **Table 132**. Some representative parameters for the SW potential used by LAMMPS are listed in **Table 133**. We note that 12 atom types have been introduced for the simulation of the single-layer 1H-WO_2 using LAMMPS, because the angles around atom W in **Figure 1** (with M = W and X = O) are not distinguishable in LAMMPS. We have suggested two options to differentiate these angles by implementing some additional constraints in LAMMPS, which can be accomplished by modifying the source file of LAMMPS [13, 14]. According to our experience, it is not so convenient for some users to implement these constraints and recompile the LAMMPS package. Hence, in the present work, we differentiate the angles by introducing more atom types, so it is not necessary to modify the LAMMPS package. **Figure 2** (with M = W and X = O) shows that, for 1H-WO_2, we can differentiate these angles around the W atom by assigning these six

VFF type	**Bond stretching**	**Angle bending**		
Expression	$\frac{1}{2}K_{\mathrm{W-O}}(\Delta r)^2$	$\frac{1}{2}K_{\mathrm{W-O-O}}(\Delta\theta)^2$	$\frac{1}{2}K_{\mathrm{W-O-O'}}(\Delta\theta)^2$	$\frac{1}{2}K_{\mathrm{O-W-W}}(\Delta\theta)^2$
Parameter	15.318	10.276	10.276	10.276
r_0 or θ_0	2.030	87.206	74.435	87.206

The second line gives an explicit expression for each VFF term. The third line is the force constant parameters. Parameters are in the unit of eV/Å^2 for the bond stretching interaction and in the unit of eV for the angle bending interaction. The fourth line gives the initial bond length (in the unit of Å) for the bond stretching interaction and the initial angle (in the unit of degrees) for the angle bending interaction. The angle θ_{ijk} has atom i as the apex.

Table 130. The VFF model for single-layer 1H-WO_2.

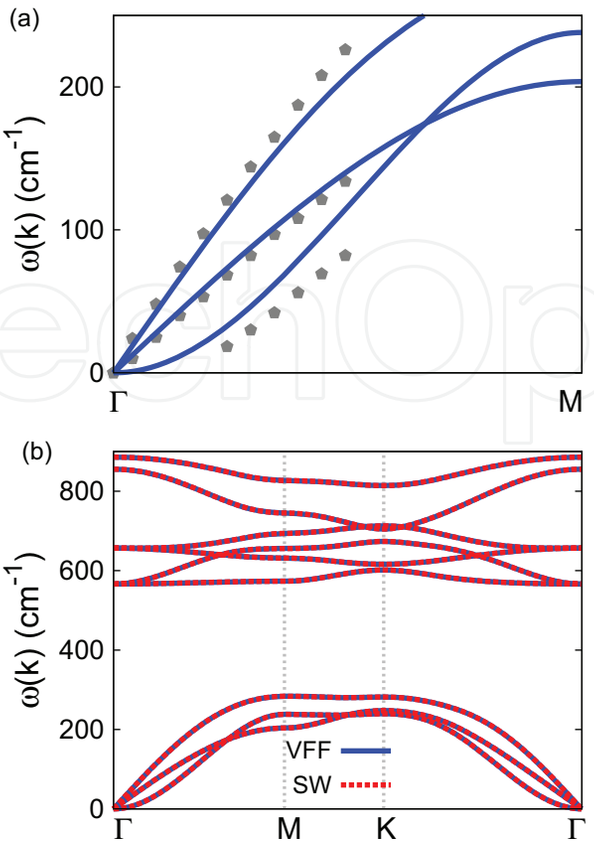

Figure 63. Phonon spectrum for single-layer 1H-WO_2. (a) Phonon dispersion along the $a = 2.80$ direction in the Brillouin zone. The results from the VFF model (lines) are comparable with the *ab initio* results (pentagons) from Ref. [12]. (b) The phonon dispersion from the SW potential is exactly the same as that from the VFF model.

	A (eV)	ρ (Å)	B (Å^4)	r_{min} (Å)	r_{max} (Å)
W—O	8.781	1.005	8.491	0.0	2.744

Table 131. Two-body SW potential parameters for single-layer 1H-WO_2 used by GULP [8] as expressed in Eq. (3).

	K (eV)	θ_0 (°)	ρ_1 (Å)	ρ_2 (Å)	$r_{\text{min 12}}$ (Å)	$r_{\text{max 12}}$ (Å)	$r_{\text{min 13}}$ (Å)	$r_{\text{max 13}}$ (Å)	$r_{\text{min 23}}$ (Å)	$r_{\text{max 23}}$ (Å)
$\theta_{\text{W–O–O}}$	85.955	87.206	1.005	1.005	0.0	2.744	0.0	2.744	0.0	3.262
$\theta_{\text{W–O–O}'}$	92.404	74.435	1.005	1.005	0.0	2.744	0.0	2.744	0.0	3.262
$\theta_{\text{O–W–W}}$	85.955	87.206	1.005	1.005	0.0	2.744	0.0	2.744	0.0	3.262

The angle θ_{ijk} in the first line indicates the bending energy for the angle with atom i as the apex.

Table 132. Three-body SW potential parameters for single-layer 1H-WO_2 used by GULP [8] as expressed in Eq. (4).

neighboring O atoms with different atom types. It can be found that 12 atom types are necessary for the purpose of differentiating all 6 neighbors around 1 W atom.

We use LAMMPS to perform MD simulations for the mechanical behavior of the single-layer 1H-WO_2 under uniaxial tension at 1 and 300 K. **Figure 64** shows the stress-strain curve for the

http://dx.doi.org/10.5772/intechopen.71929

	ϵ (eV)	σ (Å)	a	λ	γ	$\cos\theta_0$	A_L	B_L	p	q	Tol
W_1—O_1—O_1	1.000	1.005	2.730	0.000	1.000	0.000	8.781	8.316	4	0	0.0
W_1—O_1—O_3	1.000	0.000	0.000	85.955	1.000	0.049	0.000	0.000	4	0	0.0
W_1—O_1—O_2	1.000	0.000	0.000	92.404	1.000	0.268	0.000	0.000	4	0	0.0
O_1—W_1—W_3	1.000	0.000	0.000	85.955	1.000	0.049	0.000	0.000	4	0	0.0

Table 133. SW potential parameters for single-layer 1H-WO_2 used by LAMMPS [9] as expressed in Eqs. (9) and (10).

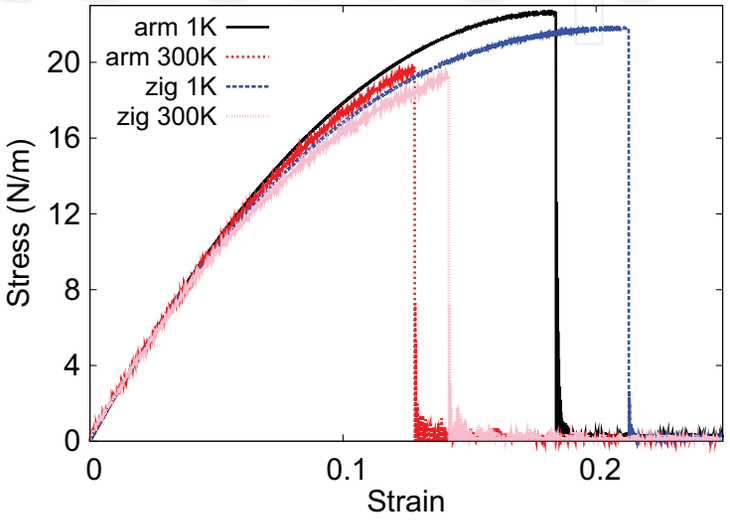

Figure 64. Stress-strain for single-layer 1H-WO_2 of dimension 100 × 100Å along the armchair and zigzag directions.

tension of a single-layer 1H-WO_2 of dimension 100 × 100Å. Periodic boundary conditions are applied in both armchair and zigzag directions. The single-layer 1H-WO_2 is stretched uniaxially along the armchair or zigzag direction. The stress is calculated without involving the actual thickness of the quasi-two-dimensional structure of the single-layer 1H-WO_2. The Young's modulus can be obtained by a linear fitting of the stress-strain relation in the small strain range of [0, 0.01]. The Young's modulus is 237.1 and 237.2 N/m along the armchair and zigzag directions, respectively. The Young's modulus is essentially isotropic in the armchair and zigzag directions. The Poisson's ratio from the VFF model and the SW potential is $\nu_{xy} = \nu_{yx} = 0.15$.

There is no available value for nonlinear quantities in the single-layer 1H-WO_2. We have thus used the nonlinear parameter $B = 0.5d^4$ in Eq. (5), which is close to the value of B in most materials. The value of the third-order nonlinear elasticity D can be extracted by fitting the stress-strain relation to the function $\sigma = E\epsilon + \frac{1}{2}D\epsilon^2$ with E as the Young's modulus. The values of D from the present SW potential are −1218.0 and −1312.9 N/m along the armchair and zigzag directions, respectively. The ultimate stress is about 22.6 N/m at the ultimate strain of 0.18 in the armchair direction at the low temperature of 1 K. The ultimate stress is about 21.8 N/m at the ultimate strain of 0.21 in the zigzag direction at the low temperature of 1 K

34. 1H-WS_2

Most existing theoretical studies on the single-layer 1H-WS_2 are based on the first-principles calculations. In this section, we will develop both VFF model and the SW potential for the single-layer 1H-WS_2.

Table 134 shows the VFF terms for the 1H-WS_2; one of which is the bond stretching interaction shown by Eq. (1), while the other terms are the angle bending interaction shown by Eq. (2). These force constant parameters are determined by fitting to the three acoustic branches in the phonon dispersion along the ΓM as shown in **Figure 65(a)**. The *ab initio* calculations for the phonon dispersion are from Ref. [31]. Similar phonon dispersion can also be found in other *ab initio* calculations [12, 26, 34, 38, 39]. **Figure 65(b)** shows that the VFF model and the SW potential give exactly the same phonon dispersion, as the SW potential is derived from the VFF model.

The parameters for the two-body SW potential used by GULP are shown in **Table 135**. The parameters for the three-body SW potential used by GULP are shown in **Table 136**. Parameters for the SW potential used by LAMMPS are listed in **Table 137**. We note that 12 atom types have been introduced for the simulation of the single-layer 1H-WS_2 using LAMMPS, because the angles around atom W in **Figure 1** (with M = W and X = S) are not distinguishable in LAMMPS. We have suggested two options to differentiate these angles by implementing some additional constraints in LAMMPS, which can be accomplished by modifying the source file of LAMMPS [13, 14]. According to our experience, it is not so convenient for some users to implement these constraints and recompile the LAMMPS package. Hence, in the present work, we differentiate the angles by introducing more atom types, so it is not necessary to modify the LAMMPS package. **Figure 2** (with M = W and X = S) shows that, for 1H-WS_2, we can differentiate these angles around the W atom by assigning these six neighboring S atoms with different atom types. It can be found that 12 atom types are necessary for the purpose of differentiating all 6 neighbors around 1 W atom.

The parameters for the two-body SW potential used by GULP are shown in **Table 131**. The parameters for the three-body SW potential used by GULP are shown in **Table 132**. Some representative parameters for the SW potential used by LAMMPS are listed in **Table 133**. We note that 12 atom types have been introduced for the simulation of the single-layer 1H-WO_2

VFF type	Bond stretching	Angle bending		
Expression	$\frac{1}{2}K_{W-S}(\Delta r)^2$	$\frac{1}{2}K_{W-S-S}(\Delta\theta)^2$	$\frac{1}{2}K_{W-S-S'}(\Delta\theta)^2$	$\frac{1}{2}K_{S-W-W}(\Delta\theta)^2$
Parameter	8.701	7.421	7.421	6.607
r_0 or θ_0	2.390	81.811	81.755	81.811

The second line gives an explicit expression for each VFF term. The third line is the force constant parameters. Parameters are in the unit of $eV/Å^2$ for the bond stretching interaction and in the unit of eV for the angle bending interaction. The fourth line gives the initial bond length (in the unit of Å) for the bond stretching interaction and the initial angle (in the unit of degrees) for the angle bending interaction. The angle θ_{ijk} has atom i as the apex.

Table 134. The VFF model for single-layer 1H-WS_2.

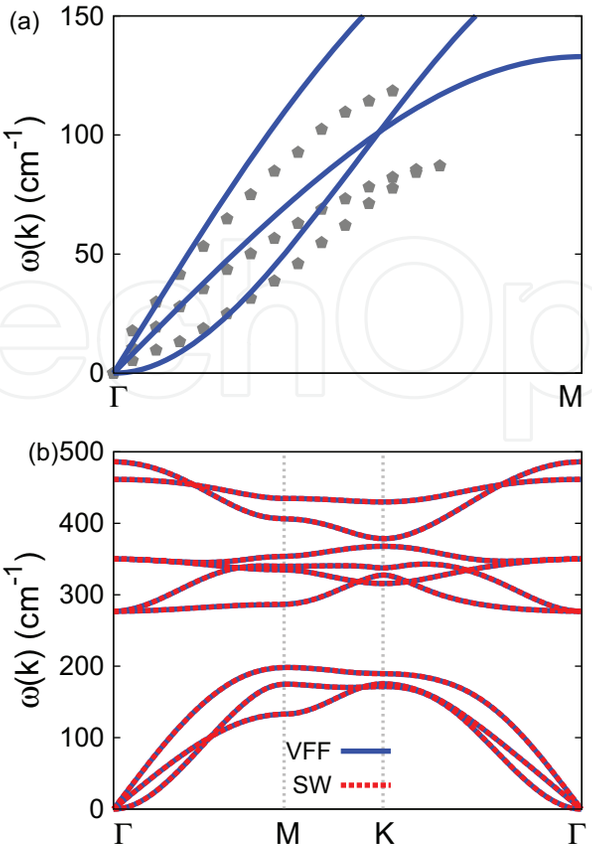

Figure 65. Phonon dispersion for single-layer 1H-WS_2. (a) The VFF model is fitted to three acoustic branches in the long wave limit along the ΓMKΓ direction. The *ab initio* results (gray pentagons) are from Ref. [31]. (b) The VFF model (blue lines) and the SW potential (red lines) give the same phonon dispersion for single-layer 1H-WS_2 along $B = 0.5d^4$.

	A (eV)	ρ (Å)	B (Å^4)	$r_{\min}$ (Å)	$r_{\max}$ (Å)
W—S	5.664	0.889	15.335	0.0	3.164

Table 135. Two-body SW potential parameters for single-layer 1H-WS_2 used by GULP [8] as expressed in Eq. (3).

	K (eV)	θ_0 (°)	ρ_1 (Å)	ρ_2 (Å)	$r_{\min\,12}$ (Å)	$r_{\max\,12}$ (Å)	$r_{\min\,13}$ (Å)	$r_{\max 13}$ (Å)	$r_{\min\,23}$ (Å)	$r_{\max 23}$ (Å)
θ_{W-S-S}	37.687	81.811	0.889	0.889	0.0	3.164	0.0	3.164	0.0	3.778
$\theta_{W-S-S'}$	37.697	81.755	0.889	0.889	0.0	3.164	0.0	3.164	0.0	3.778
θ_{S-W-W}	33.553	81.811	0.889	0.889	0.0	3.164	0.0	3.164	0.0	3.778

The angle θ_{ijk} in the first line indicates the bending energy for the angle with atom i as the apex.

Table 136. Three-body SW potential parameters for single-layer 1H-WS_2 used by GULP [8] as expressed in Eq. (4).

using LAMMPS, because the angles around atom W in **Figure 1** (with M = W and X = O) are not distinguishable in LAMMPS. We have suggested two options to differentiate these angles by implementing some additional constraints in LAMMPS, which can be accomplished by

	ϵ (eV)	σ(Å)	a	λ	γ	$\cos\theta_0$	A_L	B_L	p	q	Tol
W_1—S_1—S_1	1.000	0.889	3.558	0.000	1.000	0.000	5.664	24.525	4	0	0.0
W_1—S_1—S_3	1.000	0.000	0.000	37.687	1.000	0.142	0.000	0.000	4	0	0.0
W_1—S_1—S_2	1.000	0.000	0.000	37.697	1.000	0.143	0.000	0.000	4	0	0.0
S_1—W_1—W_3	1.000	0.000	0.000	33.553	1.000	0.142	0.000	0.000	4	0	0.0

Atom types in the first column are displayed in **Figure 2** (with M = W and X = S).

Table 137. SW potential parameters for single-layer 1H-WS_2 used by LAMMPS [9] as expressed in Eqs. (9) and (10).

modifying the source file of LAMMPS [13, 14]. According to our experience, it is not so convenient for some users to implement these constraints and recompile the LAMMPS package. Hence, in the present work, we differentiate the angles by introducing more atom types, so it is not necessary to modify the LAMMPS package. **Figure 2** (with M = W and X = O) shows that, for 1H-WO_2, we can differentiate these angles around the W atom by assigning these six neighboring O atoms with different atom types. It can be found that 12 atom types are necessary for the purpose of differentiating all 6 neighbors around 1 W atom.

We use LAMMPS to perform MD simulations for the mechanical behavior of the single-layer 1H-WS_2 under uniaxial tension at 1 and 300 K. **Figure 66** shows the stress-strain curve for the tension of a single-layer 1H-WS_2 of dimension 100 × 100 Å. Periodic boundary conditions are applied in both armchair and zigzag directions. The single-layer 1H-WS_2 is stretched uniaxially along the armchair or zigzag direction. The stress is calculated without involving the actual thickness of the quasi-two-dimensional structure of the single-layer 1H-WS_2. The Young's modulus can be obtained by a linear fitting of the stress-strain relation in the small strain range of [0, 0.01]. The Young's modulus is 121.5 N/m along both armchair and zigzag directions. These values are in reasonable agreement with the *ab initio* results, e.g., 139.6 N/m

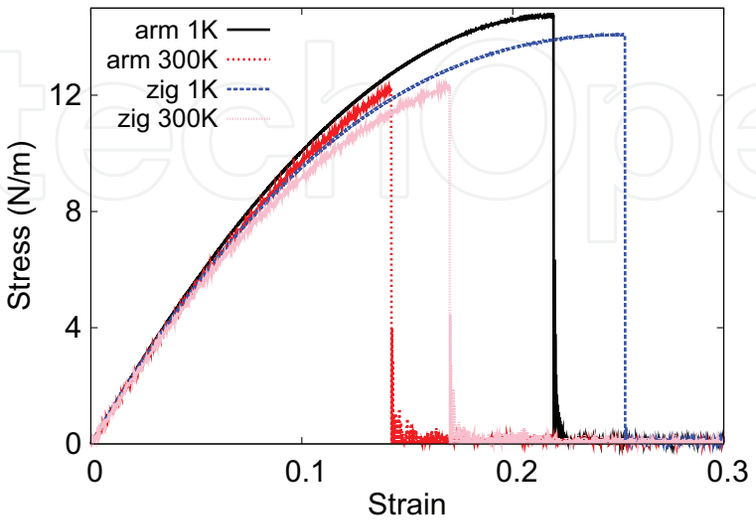

Figure 66. Stress-strain for single-layer 1H-WS_2 of dimension $\frac{1}{2}K_{W-S}(\Delta r)^2$ Å along the armchair and zigzag directions.

from Ref. [18], or 148.5 N/m from Ref. [35]. The Poisson's ratio from the VFF model and the SW potential is $\nu_{xy} = \nu_{yx} = 0.21$, which agrees with the *ab initio* value of 0.22 [18].

We have determined the nonlinear parameter to be $B = 0.47d^4$ in Eq. (5) by fitting to the third-order nonlinear elastic constant D from the *ab initio* calculations [35]. We have extracted the value of $D = -502.9$ N/m by fitting the stress-strain relation along the armchair direction in the *ab initio* calculations to the function $\sigma = E\epsilon + \frac{1}{2}D\epsilon^2$ with E as the Young's modulus. The values of D from the present SW potential are -472.8 and -529.6 N/m along the armchair and zigzag directions, respectively. The ultimate stress is about 14.7 N/m at the ultimate strain of 0.22 in the armchair direction at the low temperature of 1 K. The ultimate stress is about 14.1 N/m at the ultimate strain of 0.25 in the zigzag direction at the low temperature of 1 K.

35. 1H-WSe_2

Most existing theoretical studies on the single-layer 1H-WSe_2 are based on the first-principles calculations. Norouzzadeh and Singh provided one set of parameters for the SW potential for the single-layer 1H-WSe_2 [40]. In this section, we will develop both VFF model and the SW potential for the single-layer 1H-WSe_2.

The structure for the single-layer 1H-WSe_2 is shown in **Figure 1** (with M = W and X = Se). Each W atom is surrounded by six Se atoms. These Se atoms are categorized into the top group (e.g., atoms 1, 3, and 5) and bottom group (e.g., atoms 2, 4, and 6). Each Se atom is connected to three W atoms. The structural parameters are from [12], including the lattice constant $a = 3.25$ Å and the bond length $d_{\mathrm{W-Se}} = 2.51$ Å. The resultant angles are $\theta_{\mathrm{WSeSe}} = \theta_{\mathrm{SeWW}} = 80.693^\circ$ and $\theta_{\mathrm{WSeSe'}} = 83.240^\circ$, in which atoms Se and Se′ are from different (top or bottom) groups.

Table 138 shows three VFF terms for the 1H-WSe_2; one of which is the bond stretching interaction shown by Eq. (1), while the other two terms are the angle bending interaction shown by Eq. (2). These force constant parameters are determined by fitting to the three acoustic branches in the phonon dispersion along the ΓM as shown in **Figure 67(a)**. The *ab initio* calculations for the phonon dispersion are from [31]. Similar phonon dispersion can also be found in other *ab initio* calculations [12, 33, 34, 39, 41]. **Figure 67(b)** shows that the VFF

VFF type	Bond stretching	Angle bending		
Expression	$\frac{1}{2}K_{\mathrm{W-Se}}(\Delta r)^2$	$\frac{1}{2}K_{\mathrm{W-Se-Se}}(\Delta\theta)^2$	$\frac{1}{2}K_{\mathrm{W-Se-Se'}}(\Delta\theta)^2$	$\frac{1}{2}K_{\mathrm{Se-W-W}}(\Delta\theta)^2$
Parameter	8.286	8.513	8.513	7.719
r_0 or θ_0	2.510	80.693	83.140	80.693

The second line gives an explicit expression for each VFF term. The third line is the force constant parameters. Parameters are in the unit of eV/Å^2 for the bond stretching interaction and in the unit of eV for the angle bending interaction. The fourth line gives the initial bond length (in the unit of Å) for the bond stretching interaction and the initial angle (in the unit of degrees) for the angle bending interaction. The angle θ_{ijk} has atom i as the apex.

Table 138. The VFF model for single-layer 1H-WSe_2.

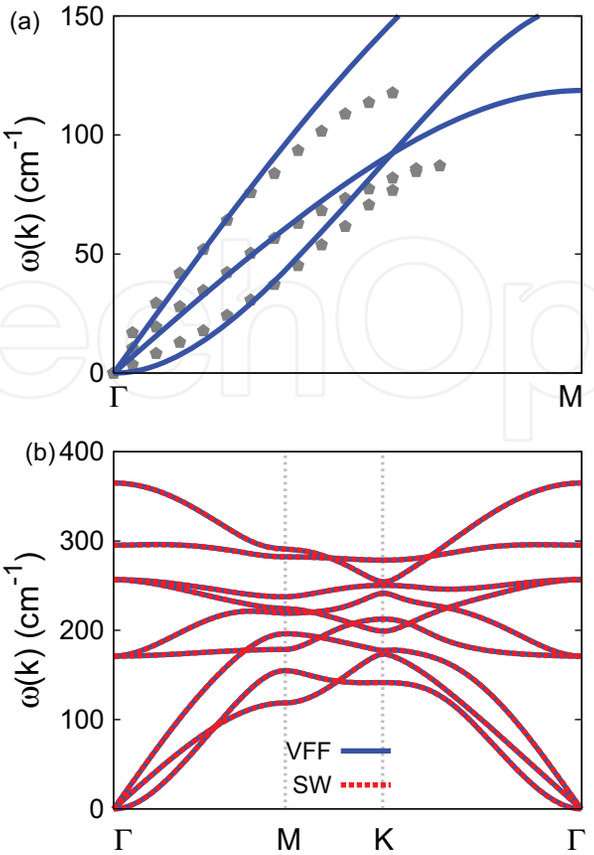

Figure 67. Phonon dispersion for single-layer 1H-WSe_2. (a) The VFF model is fitted to the three acoustic branches in the long wave limit along the ΓM direction. The *ab initio* results (gray pentagons) are from Ref. [31]. (b) The VFF model (blue lines) and the SW potential (red lines) give the same phonon dispersion for single-layer 1H-WSe_2 along ΓMΓ.

model and the SW potential give exactly the same phonon dispersion, as the SW potential is derived from the VFF model.

The parameters for the two-body SW potential used by GULP are shown in **Table 139**. The parameters for the three-body SW potential used by GULP are shown in **Table 140**. Parameters for the SW potential used by LAMMPS are listed in **Table 141**. We note that 12 atom types have been introduced for the simulation of the single-layer 1H-WSe_2 using LAMMPS, because the angles around atom W in **Figure 1** (with M = W and X = Se) are not distinguishable in LAMMPS. We have suggested two options to differentiate these angles by implementing some additional constraints in LAMMPS, which can be accomplished by modifying the source file of LAMMPS [13, 14]. According to our experience, it is not so convenient for some users to implement these constraints and recompile the LAMMPS package. Hence, in the present work, we differentiate the angles by introducing more atom types, so it is not necessary to modify the

	A (eV)	ρ (Å)	B (Å^4)	r_{min} (Å)	r_{max} (Å)
W—Se	5.476	0.706	16.273	0.0	3.308

Table 139. Two-body SW potential parameters for single-layer 1H-WSe_2 used by GULP [8] as expressed in Eq. (3).

	K (eV)	θ_0 (°)	ρ_1 (Å)	ρ_2 (Å)	r_{min12} (Å)	r_{max12} (Å)	r_{min13} (Å)	r_{max13} (Å)	r_{min23} (Å)	r_{max23} (Å)
$\theta_{W-Se-Se}$	25.607	80.693	0.706	0.706	0.0	3.308	0.0	3.308	0.0	3.953
$\theta_{W-Se-Se'}$	25.287	83.240	0.706	0.706	0.0	3.308	0.0	3.308	0.0	3.953
θ_{Se-W-W}	23.218	80.693	0.706	0.706	0.0	3.308	0.0	3.308	0.0	3.953

The angle θ_{ijk} in the first line indicates the bending energy for the angle with atom i as the apex.

Table 140. Three-body SW potential parameters for single-layer 1H-WSe_2 used by GULP [8] as expressed in Eq. (4).

	ϵ (eV)	σ (Å)	a	λ	γ	$\cos\theta_0$	A_L	B_L	p	q	Tol
W_1—Se_1—Se_1	1.000	0.706	4.689	0.000	1.000	0.000	5.476	65.662	4	0	0.0
W_1—Se_1—Se_3	1.000	0.000	0.000	25.607	1.000	0.162	0.000	0.000	4	0	0.0
W_1—Se_1—Se_2	1.000	0.000	0.000	25.287	1.000	0.118	0.000	0.000	4	0	0.0
Se_1—W_1—W_3	1.000	0.000	0.000	23.218	1.000	0.162	0.000	0.000	4	0	0.0

Atom types in the first column are displayed in **Figure 2** (with M = W and X = Se).

Table 141. SW potential parameters for single-layer 1H-WSe_2 used by LAMMPS [9] as expressed in Eqs. (9) and (10).

LAMMPS package. **Figure 2** (with M = W and X = Se) shows that, for 1H-WSe_2, we can differentiate these angles around the W atom by assigning these six neighboring Se atoms with different atom types. It can be found that 12 atom types are necessary for the purpose of differentiating all 6 neighbors around 1 W atom.

We use LAMMPS to perform MD simulations for the mechanical behavior of the single-layer 1H-WSe_2 under uniaxial tension at 1 and 300 K. **Figure 68** shows the stress-strain curve for the tension of a single-layer 1H-WSe_2 of dimension 100 × 100 Å. Periodic boundary conditions are applied in both armchair and zigzag directions. The single-layer 1H-WSe_2 is stretched uniaxially along the armchair or zigzag direction. The stress is calculated without involving

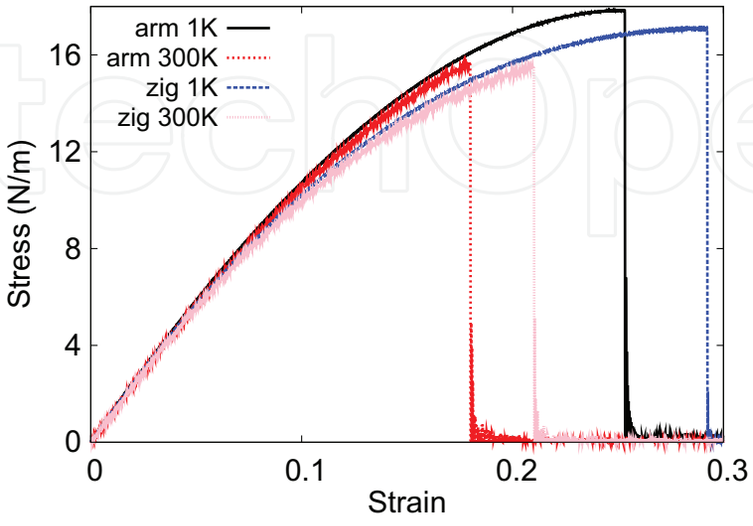

Figure 68. Stress-strain for single-layer 1H-WSe_2 of dimension 100 × 100 Å along the armchair and zigzag directions.

the actual thickness of the quasi-two-dimensional structure of the single-layer 1H-WSe_2. The Young's modulus can be obtained by a linear fitting of the stress-strain relation in the small strain range of [0, 0.01]. The Young's modulus is 124.1 and 123 N/m along the armchair and zigzag directions, respectively. The Young's modulus is essentially isotropic in the armchair and zigzag directions. These values are in reasonably agreement with the *ab initio* results, e.g., 116 N/m from [18], or 126.2 N/m from [35]. The Poisson's ratio from the VFF model and the SW potential is $\nu_{xy} = \nu_{yx} = 0.20$, which agrees with the *ab initio* value of 0.19 [18].

We have determined the nonlinear parameter to be $B = 0.41d^4$ in Eq. (5) by fitting to the third-order nonlinear elastic constant D from the *ab initio* calculations [17]. We have extracted the value of $D = -413.1$ N/m by fitting the stress-strain relation along the armchair direction in the *ab initio* calculations to the function $\sigma = E\epsilon + \frac{1}{2}D\epsilon^2$ with E as the Young's modulus. The values of D from the present SW potential are -400.4 and -444.3 N/m along the armchair and zigzag directions, respectively. The ultimate stress is about 17.8 N/m at the ultimate strain of 0.25 in the armchair direction at the low temperature of 1 K. The ultimate stress is about 17.1 N/m at the ultimate strain of 0.29 in the zigzag direction at the low temperature of 1 K.

36. 1H-WTe_2

Most existing theoretical studies on the single-layer 1H-WTe_2 are based on the first-principles calculations. In this section, we will develop both VFF model and the SW potential for the single-layer 1H-WTe_2.

The bulk WTe_2 has the trigonally coordinated H phase structure [43]. However, it has been predicted that the structure of the single-layer WTe_2 can be either the trigonally coordinated H phase [12] or the octahedrally coordinated T_d phase [44–47], with T_d phase as the more stable structure [42]. We will thus consider both phases in the present paper. This section is devoted to the H phase for the WTe_2 (1H-WTe_2), while the SW potential for the T_d-WTe_2 (1T-WTe_2) is presented in another section.

The structure for the single-layer 1H-WTe_2 is shown in **Figure 1** (with M = W and X = Te). Each W atom is surrounded by six Te atoms. These Te atoms are categorized into the top group (e.g., atoms 1, 3, and 5) and bottom group (e.g., atoms 2, 4, and 6). Each Te atom is connected to three W atoms. The structural parameters are from [42], including the lattice constant $a = 3.55$ Å and the bond length $d_{\mathrm{W-Te}} = 2.73$ Å. The resultant angles are $\theta_{\mathrm{WTeTe}} = \theta_{\mathrm{TeWW}} = 81.111^\circ$ and $\theta_{\mathrm{WTeTe'}} = 82.686^\circ$, in which atoms Te and Te′ are from different (top or bottom) groups.

Table 142 shows the VFF terms for the 1H-WTe_2; one of which is the bond stretching interaction shown by Eq. (1), while the other terms are the angle bending interaction shown by Eq. (2). These force constant parameters are determined by fitting to the three acoustic branches in the phonon dispersion along the ΓM as shown in **Figure 69(a)**. The *ab initio* calculations for the phonon dispersion are from [42]. Similar phonon dispersion can also be found in other *ab initio* calculations [12]. **Figure 69(b)** shows that the VFF model and the SW potential give exactly the same phonon dispersion, as the SW potential is derived from the VFF model.

VFF type	Bond stretching	Angle bending		
Expression	$\frac{1}{2}K_{\mathrm{W-Te}}(\Delta r)^2$	$\frac{1}{2}K_{\mathrm{W-Te-Te}}(\Delta\theta)^2$	$\frac{1}{2}K_{\mathrm{W-Te-Te'}}(\Delta\theta)^2$	$\frac{1}{2}K_{\mathrm{Te-W-W}}(\Delta\theta)^2$
Parameter	5.483	7.016	7.016	5.718
r_0 or θ_0	2.730	81.111	82.686	81.111

The second line gives an explicit expression for each VFF term. The third line is the force constant parameters. Parameters are in the unit of eV/Å^2 for the bond stretching interaction and in the unit of eV for the angle bending interaction. The fourth line gives the initial bond length (in the unit of Å) for the bond stretching interaction and the initial angle (in the unit of degrees) for the angle bending interaction. The angle θ_{ijk} has atom i as the apex.

Table 142. The VFF model for single-layer 1H-WTe_2.

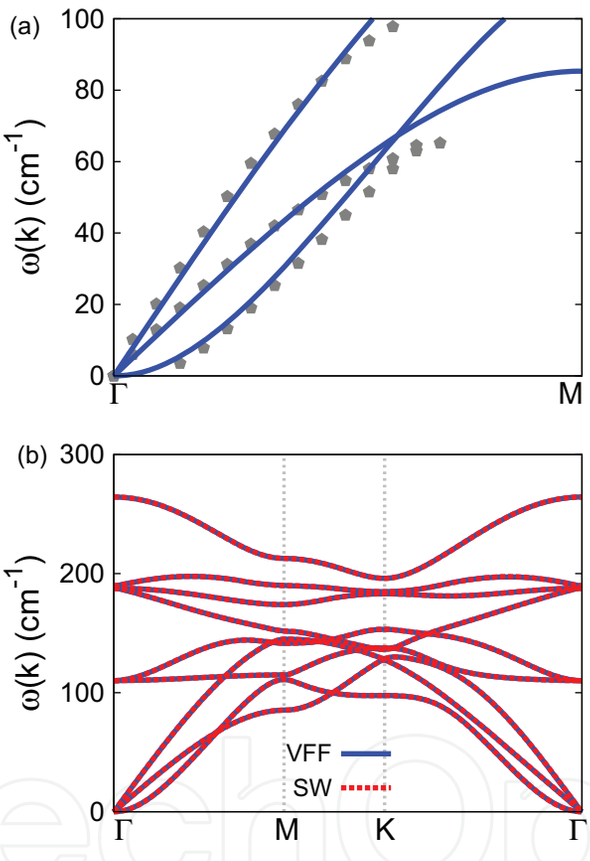

Figure 69. Phonon dispersion for single-layer 1H-WTe_2. (a) The VFF model is fitted to the three acoustic branches in the long wave limit along the ΓM direction. The *ab initio* results (gray pentagons) are from [42]. (b) The VFF model (blue lines) and the SW potential (red lines) give the same phonon dispersion for single-layer 1H-WTe_2 along ΓMKΓ.

The parameters for the two-body SW potential used by GULP are shown in **Table 143**. The parameters for the three-body SW potential used by GULP are shown in **Table 144**. Parameters for the SW potential used by LAMMPS are listed in **Table 145**. We note that 12 atom types have been introduced for the simulation of the single-layer 1H-WTe_2 using LAMMPS, because the angles around atom W in **Figure 1** (with M = W and X = Te) are not distinguishable in LAMMPS. We have suggested two options to differentiate these angles by implementing some additional constraints in LAMMPS, which can be accomplished by modifying the source file of

	A (eV)	ρ (Å)	B (Å^4)	$r_{\min}$ (Å)	$r_{\max}$ (Å)
W—Te	4.326	0.778	22.774	0.0	3.604

Table 143. Two-body SW potential parameters for single-layer 1H-WTe_2 used by GULP [8] as expressed in Eq. (3).

	K (eV)	θ_0 (°)	ρ_1 (Å)	ρ_2 (Å)	$r_{\min 12}$ (Å)	$r_{\max 12}$ (Å)	$r_{\min 13}$ (Å)	$r_{\max 13}$ (Å)	$r_{\min 23}$ (Å)	$r_{\max 23}$ (Å)
$\theta_{\mathrm{W-Te-Te}}$	21.313	81.111	0.778	0.778	0.0	3.604	0.0	3.604	0.0	4.305
$\theta_{\mathrm{W-Te-Te'}}$	21.147	82.686	0.778	0.778	0.0	3.604	0.0	3.604	0.0	4.305
$\theta_{\mathrm{Te-W-W}}$	17.370	81.111	0.778	0.778	0.0	3.604	0.0	3.604	0.0	4.305

The angle θ_{ijk} in the first line indicates the bending energy for the angle with atom i as the apex.

Table 144. Three-body SW potential parameters for single-layer 1H-WTe_2 used by GULP [8] as expressed in Eq. (4).

	ϵ (eV)	σ (Å)	a	λ	γ	$\cos\theta_0$	A_L	B_L	p	q	Tol
W_1—Te_1—Te_1	1.000	0.778	4.632	0.000	1.000	0.000	4.326	62.148	4	0	0.0
W_1—Te_1—Te_3	1.000	0.000	0.000	21.313	1.000	0.155	0.000	0.000	4	0	0.0
W_1—Te_1—Te_2	1.000	0.000	0.000	21.147	1.000	0.127	0.000	0.000	4	0	0.0
Te_1—W_1—W_3	1.000	0.000	0.000	17.370	1.000	0.155	0.000	0.000	4	0	0.0

Atom types in the first column are displayed in **Figure 2** (with M = W and X = Te).

Table 145. SW potential parameters for single-layer 1H-WTe_2 used by LAMMPS [9] as expressed in Eqs. (9) and (10).

LAMMPS [13, 14]. According to our experience, it is not so convenient for some users to implement these constraints and recompile the LAMMPS package. Hence, in the present work, we differentiate the angles by introducing more atom types, so it is not necessary to modify the LAMMPS package. **Figure 2** (with M = W and X = Te) shows that, for 1H-WTe_2, we can differentiate these angles around the W atom by assigning these six neighboring Te atoms with different atom types. It can be found that 12 atom types are necessary for the purpose of differentiating all 6 neighbors around 1 W atom.

We use LAMMPS to perform MD simulations for the mechanical behavior of the single-layer 1H-WTe_2 under uniaxial tension at 1 and 300 K. **Figure 70** shows the stress-strain curve for the tension of a single-layer 1H-WTe_2 of dimension 100 × 100 Å. Periodic boundary conditions are applied in both armchair and zigzag directions. The single-layer 1H-WTe_2 is stretched uniaxially along the armchair or zigzag direction. The stress is calculated without involving the actual thickness of the quasi-two-dimensional structure of the single-layer 1H-WTe_2. The Young's modulus can be obtained by a linear fitting of the stress-strain relation in the small strain range of [0, 0.01]. The Young's modulus is 82.7 and 81.9 N/m along the armchair and zigzag directions, respectively. The Young's modulus is essentially isotropic in the armchair and zigzag directions. These values are in reasonably agreement with the *ab initio* results, e.g., 86.4 N/m from [18] or 93.9 N/m from [35]. The Poisson's ratio from the VFF model and the SW potential is $\nu_{xy} = \nu_{yx} = 0.20$, which agrees with the *ab initio* value of 0.18 [18].

http://dx.doi.org/10.5772/intechopen.71929

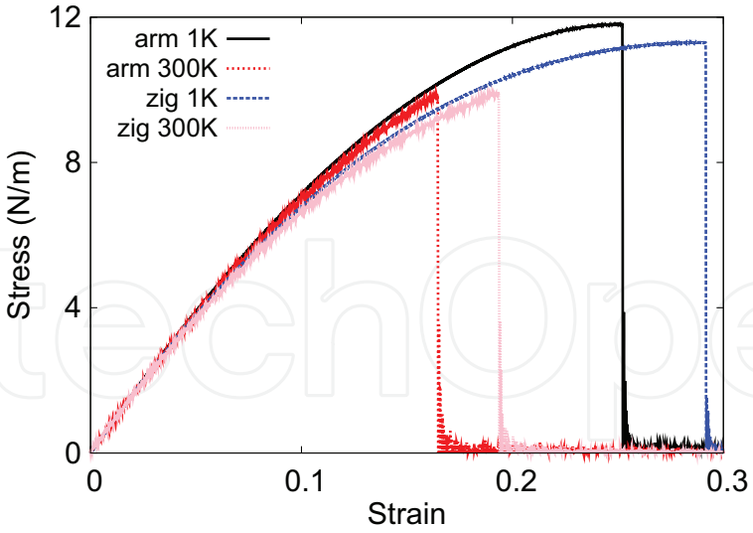

Figure 70. Stress-strain for single-layer 1H-WTe_2 of dimension 100 × 100 Å along the armchair and zigzag directions.

We have determined the nonlinear parameter to be $B = 0.41d^4$ in Eq. (5) by fitting to the third-order nonlinear elastic constant D from the *ab initio* calculations [35]. We have extracted the value of $D = -280.3$ N/m by fitting the stress-strain relation along the armchair direction in the *ab initio* calculations to the function $\sigma = E\epsilon + \frac{1}{2}D\epsilon^2$ with E as the Young's modulus. The values of D from the present SW potential are -269.4 and -297.9 N/m along the armchair and zigzag directions, respectively. The ultimate stress is about 11.8 N/m at the ultimate strain of 0.25 in the armchair direction at the low temperature of 1 K. The ultimate stress is about 11.3 N/m at the ultimate strain of 0.29 in the zigzag direction at the low temperature of 1 K.

37. 1T-ScO_2

Most existing theoretical studies on the single-layer 1T-ScO_2 are based on the first-principles calculations. In this section, we will develop the SW potential for the single-layer 1T-ScO_2.

The structure for the single-layer 1T-ScO_2 is shown in **Figure 71** (with M = Sc and X = O). Each Ni atom is surrounded by six O atoms. These O atoms are categorized into the top group (e.g., atoms 1, 3, and 5) and bottom group (e.g., atoms 2, 4, and 6). Each O atom is connected to three Sc atoms. The structural parameters are from the first-principles calculations [12], including the lattice constant $a = 3.22$ Å and the bond length $d_{Sc-O} = 2.07$ Å. The resultant angles are $\theta_{ScOO} = 102.115^\circ$ with O atoms from the same (top or bottom) group and $\theta_{OScSc} = 102.115^\circ$.

Table 146 shows three VFF terms for the single-layer 1T-ScO_2; one of which is the bond stretching interaction shown by Eq. (1), while the other two terms are the angle bending interaction shown by Eq. (2). We note that the angle bending term K_{Sc-O-O} is for the angle θ_{Sc-O-O} with both O atoms from the same (top or bottom) group. These force constant parameters are determined by fitting to the two in-plane acoustic branches in the phonon dispersion along the ΓM as shown in **Figure 72(a)**. The *ab initio* calculations for the phonon

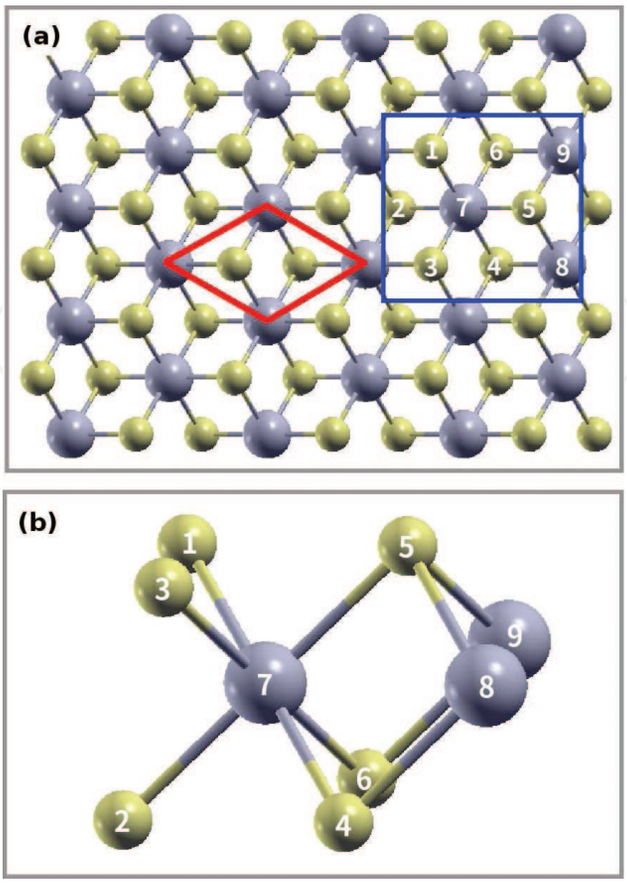

Figure 71. Configuration of the 1T-MX_2 in the 1T phase. (a) Top view. The unit cell is highlighted by a red parallelogram. The armchair direction is defined to be along the horizontal direction. The zigzag direction is along the vertical direction. (b) Enlarged view of atoms in the blue box in (a). Each M atom is surrounded by six X atoms, which are categorized into the top and bottom groups. Atoms X 1, 3, and 5 are from the top group, while atoms X 2, 4, and 6 are from the bottom group. M atoms are represented by larger gray balls. X atoms are represented by smaller yellow balls.

VFF type	Bond stretching	Angle bending	
Expression	$\frac{1}{2}K_{Sc-O}(\Delta r)^2$	$\frac{1}{2}K_{Sc-O-O}(\Delta\theta)^2$	$\frac{1}{2}K_{O-Sc-Sc}(\Delta\theta)^2$
Parameter	11.926	3.258	3.258
r_0 or θ_0	2.07	102.115	102.115

The second line gives an explicit expression for each VFF term. The third line is the force constant parameters. Parameters are in the unit of eV/Å^2 for the bond stretching interaction and in the unit of eV for the angle bending interaction. The fourth line gives the initial bond length (in the unit of Å) for the bond stretching interaction and the initial angle (in the unit of degrees) for the angle bending interaction. The angle θ_{ijk} has atom i as the apex.

Table 146. The VFF model for single-layer 1T-ScO_2.

dispersion are from [12]. **Figure 72(b)** shows that the VFF model and the SW potential give exactly the same phonon dispersion, as the SW potential is derived from the VFF model.

The parameters for the two-body SW potential used by GULP are shown in **Table 147**. The parameters for the three-body SW potential used by GULP are shown in **Table 148**. Some representative parameters for the SW potential used by LAMMPS are listed in **Table 149**.

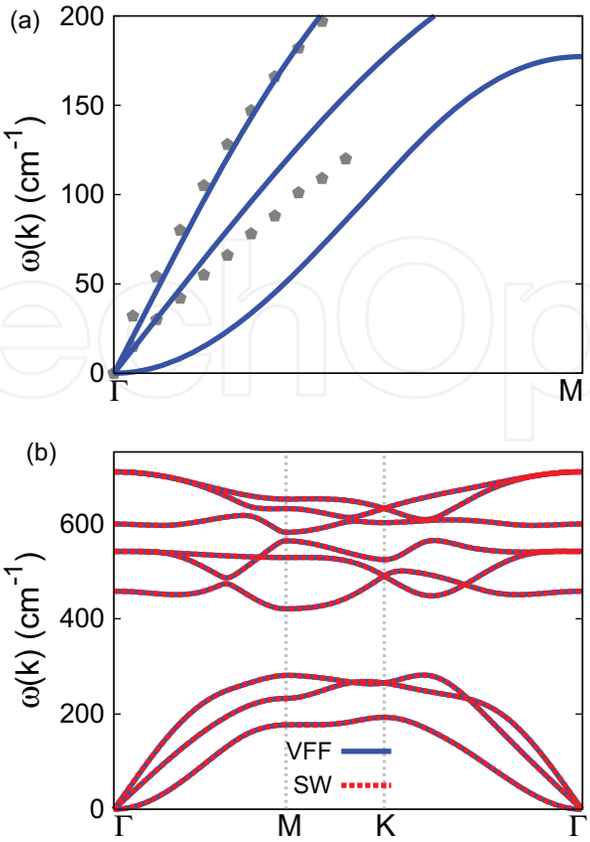

Figure 72. Phonon spectrum for single-layer 1T-ScO_2. (a) Phonon dispersion along the ΓM direction in the Brillouin zone. The results from the VFF model (lines) are comparable with the *ab initio* results (pentagons) from Ref. [12]. (b) The phonon dispersion from the SW potential is exactly the same as that from the VFF model.

	A (eV)	ρ(Å)	B (Å^4)	$r_{\min}$ (Å)	$r_{\max}$ (Å)
Sc—O	10.187	1.493	9.180	0.0	2.949

Table 147. Two-body SW potential parameters for single-layer 1T-ScO_2 used by GULP [8] as expressed in Eq. (3).

	K (eV)	θ_0 (°)	ρ_1 (Å)	ρ_2 (Å)	$r_{\min 12}$ (Å)	$r_{\max 12}$ (Å)	$r_{\min 13}$ (Å)	$r_{\max 13}$ (Å)	$r_{\min 23}$ (Å)	$r_{\max 23}$ (Å)
$\theta_{\text{Sc–O–O}}$	50.913	102.115	1.493	1.493	0.0	2.949	0.0	2.949	0.0	4.399
$\theta_{\text{O–Sc–Sc}}$	50.913	102.115	1.493	1.493	0.0	2.949	0.0	2.949	0.0	4.399

The angle θ_{ijk} in the first line indicates the bending energy for the angle with atom i as the apex.

Table 148. Three-body SW potential parameters for single-layer 1T-ScO_2 used by GULP [8] as expressed in Eq. (4).

	ϵ (eV)	σ (Å)	a	λ	γ	$\cos\theta_0$	A_L	B_L	p	q	Tol
Sc—O_1—O_1	1.000	1.493	1.975	50.913	1.000	−0.210	10.187	1.847	4	0	0.0

Table 149. SW potential parameters for single-layer 1T-ScO_2 used by LAMMPS [9] as expressed in Eqs. (9) and (10).

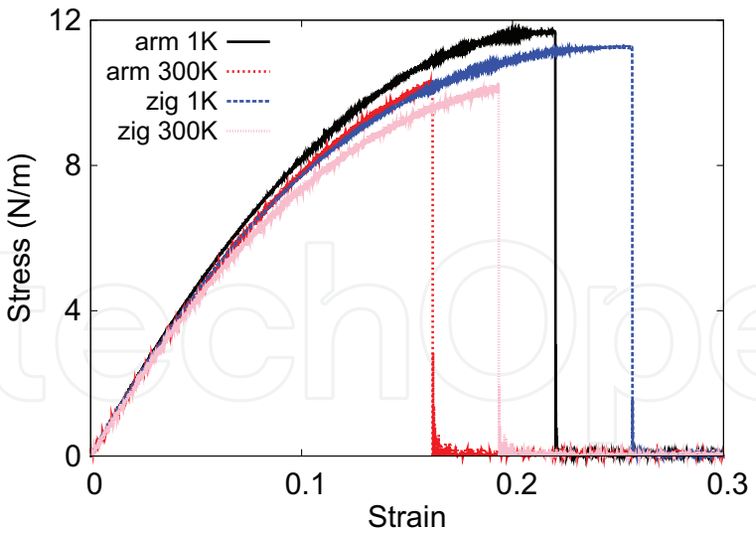

Figure 73. Stress-strain for single-layer 1T-ScO_2 of dimension 100 × 100 Å along the armchair and zigzag directions.

We use LAMMPS to perform MD simulations for the mechanical behavior of the single-layer 1T-ScO_2 under uniaxial tension at 1 and 300 K. **Figure 73** shows the stress-strain curve for the tension of a single-layer 1T-ScO_2 of dimension 100 × 100 Å. Periodic boundary conditions are applied in both armchair and zigzag directions. The single-layer 1T-ScO_2 is stretched uniaxially along the armchair or zigzag direction. The stress is calculated without involving the actual thickness of the quasi-two-dimensional structure of the single-layer 1T-ScO_2. The Young's modulus can be obtained by a linear fitting of the stress-strain relation in the small strain range of [0, 0.01]. The Young's modulus is 100.9 and 100.4 N/m along the armchair and zigzag directions, respectively. The Young's modulus is essentially isotropic in the armchair and zigzag directions. The Poisson's ratio from the VFF model and the SW potential is $\nu_{xy} = \nu_{yx} = 0.15$.

There is no available value for nonlinear quantities in the single-layer 1T-ScO_2. We have thus used the nonlinear parameter $B = 0.5d^4$ in Eq. (5), which is close to the value of B in most materials. The value of the third-order nonlinear elasticity D can be extracted by fitting the stress-strain relation to the function $\sigma = E\epsilon + \frac{1}{2}D\epsilon^2$ with E as the Young's modulus. The values of D from the present SW potential are −422.4 and −453.7 N/m along the armchair and zigzag directions, respectively. The ultimate stress is about 11.7 N/m at the ultimate strain of 0.22 in the armchair direction at the low temperature of 1 K. The ultimate stress is about 11.3 N/m at the ultimate strain of 0.25 in the zigzag direction at the low temperature of 1 K.

38. 1T-ScS_2

Most existing theoretical studies on the single-layer 1T-ScS_2 are based on the first-principles calculations. In this section, we will develop the SW potential for the single-layer 1T-ScS_2.

The structure for the single-layer 1T-ScS_2 is shown in **Figure 71** (with M = Sc and X = S). Each Sc atom is surrounded by six S atoms. These S atoms are categorized into the top group (e.g.,

atoms 1, 3, and 5) and bottom group (e.g., atoms 2, 4, and 6). Each S atom is connected to three Sc atoms. The structural parameters are from the first-principles calculations [12], including the lattice constant $a = 3.62$ Å and the bond length $d_{Sc-S} = 2.50$ Å. The resultant angle is $\theta_{SScSc} = 92.771^\circ$ and $\theta_{ScSS} = 92.771^\circ$ with S atoms from the same (top or bottom) group.

Table 150 shows three VFF terms for the single-layer 1T-ScS_2; one of which is the bond stretching interaction shown by Eq. (1), while the other two terms are the angle bending interaction shown by Eq. (2). We note that the angle bending term K_{Sc-S-S} is for the angle θ_{Sc-S-S} with both S atoms from the same (top or bottom) group. These force constant parameters are determined by fitting to the three acoustic branches in the phonon dispersion along the ΓM as shown in **Figure 74(a)**. The *ab initio* calculations for the phonon dispersion are from [12]. **Figure 74(b)** shows that the VFF model and the SW potential give exactly the same phonon dispersion, as the SW potential is derived from the VFF model.

The parameters for the two-body SW potential used by GULP are shown in **Table 151**. The parameters for the three-body SW potential used by GULP are shown in **Table 152**. Some representative parameters for the SW potential used by LAMMPS are listed in **Table 153**.

We use LAMMPS to perform MD simulations for the mechanical behavior of the single-layer 1T-ScS_2 under uniaxial tension at 1 and 300 K. **Figure 75** shows the stress-strain curve for the tension of a single-layer 1T-ScS_2 of dimension 100×100 Å. Periodic boundary conditions are applied in both armchair and zigzag directions. The single-layer 1T-ScS_2 is stretched uniaxially along the armchair or zigzag direction. The stress is calculated without involving the actual thickness of the quasi-two-dimensional structure of the single-layer 1T-ScS_2. The Young's modulus can be obtained by a linear fitting of the stress-strain relation in the small strain range of [0, 0.01]. The Young's modulus is 30 and 29.9 N/m along the armchair and zigzag directions, respectively. The Young's modulus is essentially isotropic in the armchair and zigzag directions. The Poisson's ratio from the VFF model and the SW potential is $\nu_{xy} = \nu_{yx} = 0.17$.

There is no available value for nonlinear quantities in the single-layer 1T-ScS_2. We have thus used the nonlinear parameter $B = 0.5d^4$ in Eq. (5), which is close to the value of B in most materials. The value of the third-order nonlinear elasticity D can be extracted by fitting the stress-strain relation to the function $\sigma = E\epsilon + \frac{1}{2}D\epsilon^2$ with E as the Young's modulus. The values of D from the present SW potential are −113.7 and −124.6 N/m along the armchair and zigzag

VFF type	**Bond stretching**	**Angle bending**	
Expression	$\frac{1}{2}K_{Sc-S}(\Delta r)^2$	$\frac{1}{2}K_{Sc-S-S}(\Delta\theta)^2$	$\frac{1}{2}K_{S-Sc-Sc}(\Delta\theta)^2$
Parameter	3.512	1.593	1.593
r_0 or θ_0	2.50	92.771	92.771

The second line gives an explicit expression for each VFF term. The third line is the force constant parameters. Parameters are in the unit of eV/Å^2 for the bond stretching interaction and in the unit of eV for the angle bending interaction. The fourth line gives the initial bond length (in the unit of Å) for the bond stretching interaction and the initial angle (in the unit of degrees) for the angle bending interaction. The angle θ_{ijk} has atom i as the apex.

Table 150. The VFF model for single-layer 1T-ScS_2.

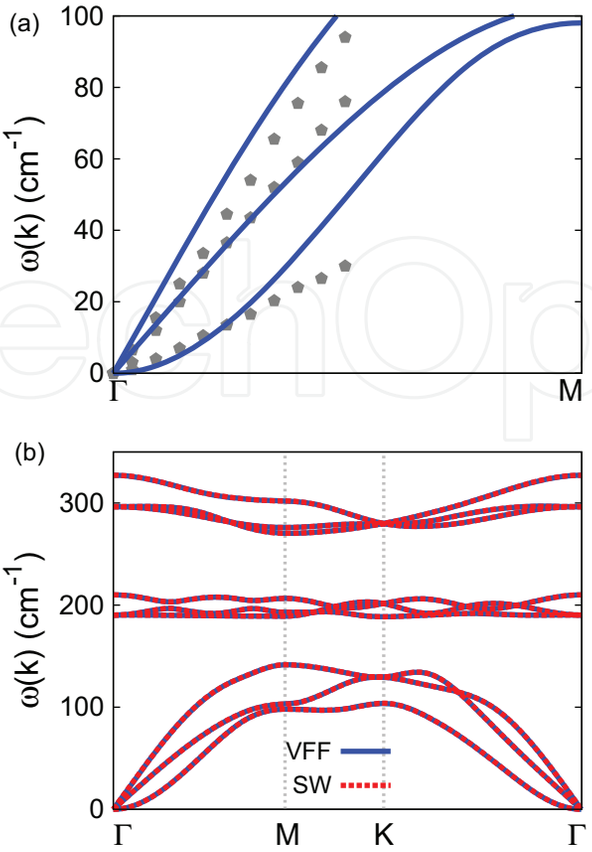

Figure 74. Phonon spectrum for single-layer 1T-ScS_2. (a) Phonon dispersion along the ΓM direction in the Brillouin zone. The results from the VFF model (lines) are comparable with the *ab initio* results (pentagons) from [12]. (b) The phonon dispersion from the SW potential is exactly the same as that from the VFF model.

	A (eV)	ρ (Å)	B (Å^4)	$r_{\min}$ (Å)	$r_{\max}$ (Å)
Sc—S	3.516	1.443	19.531	0.0	3.450

Table 151. Two-body SW potential parameters for single-layer 1T-ScS_2 used by GULP [8] as expressed in Eq. (3).

	K (eV)	θ_0 (°)	ρ_1 (Å)	ρ_2 (Å)	$r_{\min 12}$ (Å)	$r_{\max 12}$ (Å)	$r_{\min 13}$ (Å)	$r_{\max 13}$ (Å)	$r_{\min 23}$ (Å)	$r_{\max 23}$ (Å)
$\theta_{\text{Sc–S–S}}$	16.674	92.771	1.443	1.443	0.0	3.450	0.0	3.450	0.0	4.945
$\theta_{\text{S–Sc–Sc}}$	16.674	92.771	1.443	1.443	0.0	3.450	0.0	3.450	0.0	4.945

The angle θ_{ijk} in the first line indicates the bending energy for the angle with atom i as the apex.

Table 152. Three-body SW potential parameters for single-layer 1T-ScS_2 used by GULP [8] as expressed in Eq. (4).

	ϵ (eV)	σ (Å)	a	λ	γ	$\cos\theta_0$	A_L	B_L	p	q	Tol
Sc—S_1—S_1	1.000	1.443	2.390	16.674	1.000	−0.048	3.516	4.504	4	0	0.0

Table 153. SW potential parameters for single-layer 1T-ScS_2 used by LAMMPS [9] as expressed in Eqs. (9) and (10).

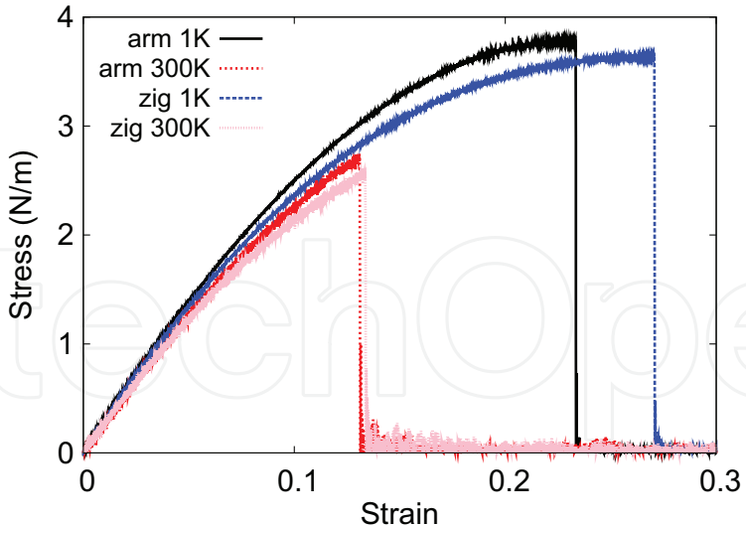

Figure 75. Stress-strain for single-layer 1T-ScS_2 of dimension 100 × 100 Å along the armchair and zigzag directions.

directions, respectively. The ultimate stress is about 3.8 N/m at the ultimate strain of 0.23 in the armchair direction at the low temperature of 1 K. The ultimate stress is about 3.6 N/m at the ultimate strain of 0.27 in the zigzag direction at the low temperature of 1 K.

39. 1T-$ScSe_2$

Most existing theoretical studies on the single-layer 1T-$ScSe_2$ are based on the first-principles calculations. In this section, we will develop the SW potential for the single-layer 1T-$ScSe_2$.

The structure for the single-layer 1T-$ScSe_2$ is shown in **Figure 71** (with M = Sc and X = Se). Each Sc atom is surrounded by six Se atoms. These Se atoms are categorized into the top group (e.g., atoms 1, 3, and 5) and bottom group (e.g., atoms 2, 4, and 6). Each Se atom is connected to three Sc atoms. The structural parameters are from the first-principles calculations [12], including the lattice constant $a = 3.52$ Å and the bond length $d_{Sc-Se} = 2.64$ Å. The resultant angle is $\theta_{SeScSc} = 83.621^\circ$ and $\theta_{ScSeSe} = 83.621^\circ$ with Se atoms from the same (top or bottom) group.

Table 154 shows three VFF terms for the single-layer 1T-$ScSe_2$, one of which is the bond stretching interaction shown by Eq. (1), while the other two terms are the angle bending interaction shown by Eq. (2). We note that the angle bending term $K_{Sc-Se-Se}$ is for the angle $\theta_{Sc-Se-Se}$ with both Se atoms from the same (top or bottom) group. These force constant parameters are determined by fitting to the three acoustic branches in the phonon dispersion along the ΓM as shown in **Figure 76(a)**. The *ab initio* calculations for the phonon dispersion are from [12]. We note that the lowest-frequency branch around the Γ point from the VFF model is lower than the *ab initio* results. This branch is the flexural branch, which should be a quadratic dispersion. However, the *ab initio* calculations give a linear dispersion for the flexural branch due to the violation of the rigid rotational invariance in the first-principles package [20], so *ab initio* calculations typically overestimate the frequency of this branch. **Figure 76(b)** shows that

VFF type	Bond stretching	Angle bending	
Expression	$\frac{1}{2}K_{Sc-Se}(\Delta r)^2$	$\frac{1}{2}K_{Sc-Se-Se}(\Delta\theta)^2$	$\frac{1}{2}K_{Se-Sc-Sc}(\Delta\theta)^2$
Parameter	4.407	2.399	2.399
r_0 or θ_0	2.64	83.621	83.621

The second line gives an explicit expression for each VFF term. The third line is the force constant parameters. Parameters are in the unit of eV/Å^2 for the bond stretching interaction and in the unit of eV for the angle bending interaction. The fourth line gives the initial bond length (in the unit of Å) for the bond stretching interaction and the initial angle (in the unit of degrees) for the angle bending interaction. The angle θ_{ijk} has atom i as the apex.

Table 154. The VFF model for single-layer 1T-$ScSe_2$.

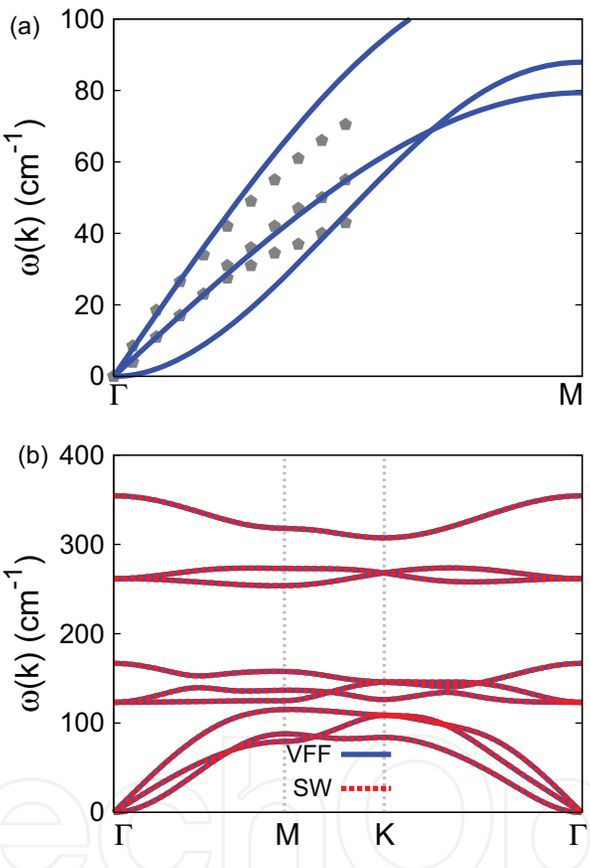

Figure 76. Phonon spectrum for single-layer 1T-$ScSe_2$. (a) Phonon dispersion along the ΓM direction in the Brillouin zone. The results from the VFF model (lines) are comparable with the *ab initio* results (pentagons) from [12]. (b) The phonon dispersion from the SW potential is exactly the same as that from the VFF model.

the VFF model and the SW potential give exactly the same phonon dispersion, as the SW potential is derived from the VFF model.

The parameters for the two-body SW potential used by GULP are shown in **Table 155**. The parameters for the three-body SW potential used by GULP are shown in **Table 156**. Some representative parameters for the SW potential used by LAMMPS are listed in **Table 157**.

	A (eV)	ρ (Å)	B (Å^4)	$r_{\min}$ (Å)	$r_{\max}$ (Å)
Sc—Se	3.884	1.173	24.288	0.0	3.520

Table 155. Two-body SW potential parameters for single-layer 1T-$ScSe_2$ used by GULP [8] as expressed in Eq. (3).

	K (eV)	θ_0 (°)	ρ_1 (Å)	ρ_2 (Å)	$r_{\min 12}$ (Å)	$r_{\max 12}$ (Å)	$r_{\min 13}$ (Å)	$r_{\max 13}$ (Å)	$r_{\min 23}$ (Å)	$r_{\max 23}$ (Å)
$\theta_{Sc-Se-Se}$	17.479	83.621	1.173	1.173	0.0	3.520	0.0	3.520	0.0	4.808
$\theta_{Se-Sc-Sc}$	17.479	83.621	1.173	1.173	0.0	3.520	0.0	3.520	0.0	4.808

The angle θ_{ijk} in the first line indicates the bending energy for the angle with atom i as the apex.

Table 156. Three-body SW potential parameters for single-layer 1T-$ScSe_2$ used by GULP [8] as expressed in Eq. (4).

	ϵ (eV)	σ (Å)	a	λ	γ	$\cos\theta_0$	A_L	B_L	p	q	Tol
$Sc—Se_1—Se_1$	1.000	1.173	3.000	17.479	1.000	0.111	3.884	12.814	4	0	0.0

Table 157. SW potential parameters for single-layer 1T-$ScSe_2$ used by LAMMPS [9] as expressed in Eqs. (9) and (10).

We use LAMMPS to perform MD simulations for the mechanical behavior of the single-layer 1T-$ScSe_2$ under uniaxial tension at 1 and 300 K. **Figure 77** shows the stress-strain curve for the tension of a single-layer 1T-$ScSe_2$ of dimension 100 × 100 Å. Periodic boundary conditions are applied in both armchair and zigzag directions. The single-layer 1T-$ScSe_2$ is stretched uniaxially along the armchair or zigzag direction. The stress is calculated without involving the actual thickness of the quasi-two-dimensional structure of the single-layer 1T-$ScSe_2$. The Young's modulus can be obtained by a linear fitting of the stress-strain relation in the small strain range of [0, 0.01]. The Young's modulus is 36.4 and 36.3 N/m along the armchair and

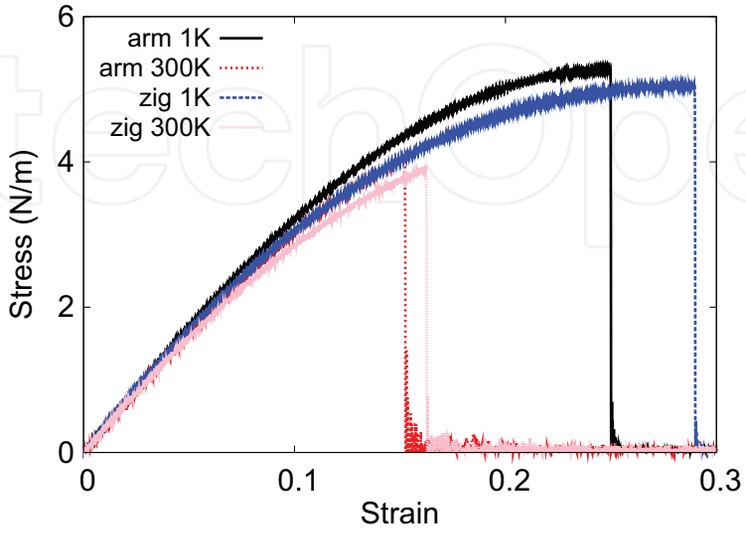

Figure 77. Stress-strain for single-layer 1T-$ScSe_2$ of dimension 100 × 100 Å along the armchair and zigzag directions.

zigzag directions, respectively. The Young's modulus is essentially isotropic in the armchair and zigzag directions. The Poisson's ratio from the VFF model and the SW potential is $\nu_{xy} = \nu_{yx} = 0.20$.

There is no available value for nonlinear quantities in the single-layer 1T-$ScSe_2$. We have thus used the nonlinear parameter $B = 0.5d^4$ in Eq. (5), which is close to the value of B in most materials. The value of the third-order nonlinear elasticity D can be extracted by fitting the stress-strain relation to the function $\sigma = E\epsilon + \frac{1}{2}D\epsilon^2$ with E as the Young's modulus. The values of D from the present SW potential are −113.7 and −130.3 N/m along the armchair and zigzag directions, respectively. The ultimate stress is about 5.3 N/m at the ultimate strain of 0.25 in the armchair direction at the low temperature of 1 K. The ultimate stress is about 5 N/m at the ultimate strain of 0.29 in the zigzag direction at the low temperature of 1 K.

40. 1T-$ScTe_2$

Most existing theoretical studies on the single-layer 1T-$ScTe_2$ are based on the first-principles calculations. In this section, we will develop the SW potential for the single-layer 1T-$ScTe_2$.

The structure for the single-layer 1T-$ScTe_2$ is shown in **Figure 71** (with M = Sc and X = Te). Each Sc atom is surrounded by six Te atoms. These Te atoms are categorized into the top group (e.g., atoms 1, 3, and 5) and bottom group (e.g., atoms 2, 4, and 6). Each Te atom is connected to three Sc atoms. The structural parameters are from the first-principles calculations [12], including the lattice constant $a = 3.72$ Å and the bond length $d_{Sc-Te} = 2.85$ Å. The resultant angle is $\theta_{TeScSc} = 81.481^\circ$ and $\theta_{ScTeTe} = 81.481^\circ$ with Se atoms from the same (top or bottom) group.

Table 158 shows three VFF terms for the single-layer 1T-$ScTe_2$; one of which is the bond stretching interaction shown by Eq. (1), while the other two terms are the angle bending interaction shown by Eq. (2). We note that the angle bending term $K_{Sc-Te-Te}$ is for the angle $\theta_{Sc-Te-Te}$ with both Te atoms from the same (top or bottom) group. These force constant parameters are determined by fitting to the two in-plane acoustic branches in the phonon dispersion along the ΓM as shown in **Figure 78(a)**. The *ab initio* calculations for the phonon dispersion are from [12]. **Figure 78(b)** shows that the VFF model and the SW potential give exactly the same phonon dispersion, as the SW potential is derived from the VFF model.

VFF type	Bond stretching	Angle bending	
Expression	$\frac{1}{2}K_{Sc-Te}(\Delta r)^2$	$\frac{1}{2}K_{Sc-Te-Te}(\Delta\theta)^2$	$\frac{1}{2}K_{Te-Sc-Sc}(\Delta\theta)^2$
Parameter	4.407	2.399	2.399
r_0 or θ_0	2.85	81.481	81.481

The second line gives an explicit expression for each VFF term. The third line is the force constant parameters. Parameters are in the unit of eV/Å^2 for the bond stretching interaction and in the unit of eV for the angle bending interaction. The fourth line gives the initial bond length (in the unit of Å) for the bond stretching interaction and the initial angle (in the unit of degrees) for the angle bending interaction. The angle θ_{ijk} has atom i as the apex.

Table 158. The VFF model for single-layer 1T-$ScTe_2$.

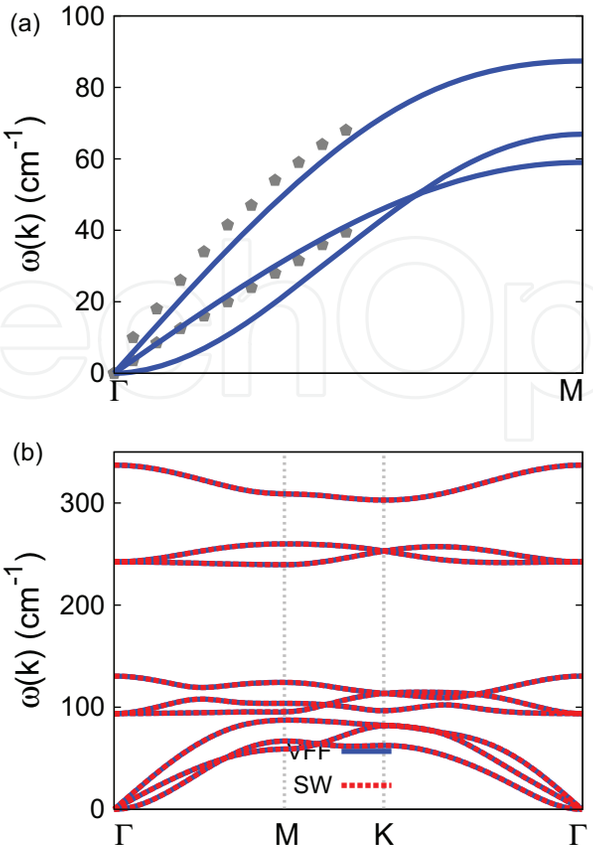

Figure 78. Phonon spectrum for single-layer 1T-$ScTe_2$. (a) Phonon dispersion along the ΓM direction in the Brillouin zone. The results from the VFF model (lines) are comparable with the *ab initio* results (pentagons) from [12]. (b) The phonon dispersion from the SW potential is exactly the same as that from the VFF model.

The parameters for the two-body SW potential used by GULP are shown in **Table 159**. The parameters for the three-body SW potential used by GULP are shown in **Table 160**. Some representative parameters for the SW potential used by LAMMPS are listed in **Table 161**.

	A (eV)	ρ (Å)	B (Å^4)	r_{min} (Å)	r_{max} (Å)
Sc—Te	4.269	1.183	32.988	0.0	3.768

Table 159. Two-body SW potential parameters for single-layer 1T-$ScTe_2$ used by GULP [8] as expressed in Eq. (3).

	K (eV)	θ_0 (°)	ρ_1 (Å)	ρ_2 (Å)	$r_{min\,12}$ (Å)	$r_{max\,12}$ (Å)	$r_{min\,13}$ (Å)	$r_{max\,13}$ (Å)	$r_{min\,23}$ (Å)	$r_{max\,23}$ (Å)
$\theta_{Sc-Te-Te}$	16.139	81.481	1.183	1.183	0.0	3.768	0.0	3.768	0.0	5.082
$\theta_{Te-Sc-Sc}$	16.139	81.481	1.183	1.183	0.0	3.768	0.0	3.768	0.0	5.082

The angle θ_{ijk} in the first line indicates the bending energy for the angle with atom i as the apex.

Table 160. Three-body SW potential parameters for single-layer 1T-$ScTe_2$ used by GULP [8] as expressed in Eq. (4).

	ϵ (eV)	σ (Å)	a	λ	γ	$\cos\theta_0$	A_L	B_L	p	q	Tol
Sc—Te_1—Te_1	1.000	1.183	3.185	16.139	1.000	0.148	4.269	16.841	4	0	0.0

Table 161. SW potential parameters for single-layer 1T-$ScTe_2$ used by LAMMPS [9] as expressed in Eqs. (9) and (10).

We use LAMMPS to perform MD simulations for the mechanical behavior of the single-layer 1T-$ScTe_2$ under uniaxial tension at 1 and 300 K. **Figure 79** shows the stress-strain curve for the tension of a single-layer 1T-$ScTe_2$ of dimension 100×100 Å. Periodic boundary conditions are applied in both armchair and zigzag directions. The single-layer 1T-$ScTe_2$ is stretched uniaxially along the armchair or zigzag direction. The stress is calculated without involving the actual thickness of the quasi-two-dimensional structure of the single-layer 1T-$ScTe_2$. The Young's modulus can be obtained by a linear fitting of the stress-strain relation in the small strain range of [0, 0.01]. The Young's modulus is 31.4 and 31.3 N/m along the armchair and zigzag directions, respectively. The Young's modulus is essentially isotropic in the armchair and zigzag directions. The Poisson's ratio from the VFF model and the SW potential is $\nu_{xy} = \nu_{yx} = 0.22$.

There is no available value for nonlinear quantities in the single-layer 1T-$ScTe_2$. We have thus used the nonlinear parameter $B = 0.5d^4$ in Eq. (5), which is close to the value of B in most materials. The value of the third-order nonlinear elasticity D can be extracted by fitting the stress-strain relation to the function $\sigma = E\epsilon + \frac{1}{2}D\epsilon^2$ with E as the Young's modulus. The values of D from the present SW potential are -81.2 and -96.7 N/m along the armchair and zigzag directions, respectively. The ultimate stress is about 5.2 N/m at the ultimate strain of 0.27 in the armchair direction at the low temperature of 1 K. The ultimate stress is about 5 N/m at the ultimate strain of 0.31 in the zigzag direction at the low temperature of 1 K.

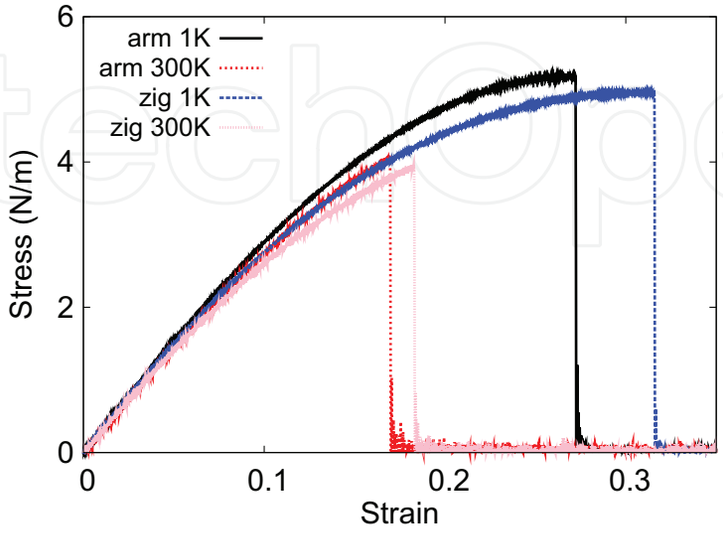

Figure 79. Stress-strain for single-layer 1T-$ScTe_2$ of dimension 100×100 Å along the armchair and zigzag directions.

41. 1T-TiS_2

Most existing theoretical studies on the single-layer 1T-TiS_2 are based on the first-principles calculations. In this section, we will develop the SW potential for the single-layer 1T-TiS_2.

The structure for the single-layer 1T-TiS_2 is shown in **Figure 71** (with M = Ti and X = S). Each Ti atom is surrounded by six S atoms. These S atoms are categorized into the top group (e.g., atoms 1, 3, and 5) and bottom group (e.g., atoms 2, 4, and 6). Each S atom is connected to three Ti atoms. The structural parameters are from the first-principles calculations [12], including the lattice constant $a = 3.32$ Å and the bond length $d_{\mathrm{Ti-S}} = 2.39$ Å. The resultant angles are $\theta_{\mathrm{TiSS}} = 87.984^\circ$ with S atoms from the same (top or bottom) group and $\theta_{\mathrm{STiTi}} = 87.984^\circ$.

Table 162 shows three VFF terms for the single-layer 1T-TiS_2; one of which is the bond stretching interaction shown by Eq. (1), while the other two terms are the angle bending interaction shown by Eq. (2). We note that the angle bending term $K_{\mathrm{Ti-S-S}}$ is for the angle $\theta_{\mathrm{Ti-S-S}}$ with both S atoms from the same (top or bottom) group. We find that there are actually only two parameters in the VFF model, so we can determine their value by fitting to the Young's modulus and the Poisson's ratio of the system. The *ab initio* calculations have predicted the Young's modulus to be 85 N/m and the Poisson's ratio as 0.20 [48].

The parameters for the two-body SW potential used by GULP are shown in **Table 163**. The parameters for the three-body SW potential used by GULP are shown in **Table 164**. Some representative parameters for the SW potential used by LAMMPS are listed in **Table 165**.

We use LAMMPS to perform MD simulations for the mechanical behavior of the single-layer 1T-TiS_2 under uniaxial tension at 1 and 300 K. **Figure 80** shows the stress-strain curve for the tension of a single-layer 1T-TiS_2 of dimension 100 × 100 Å. Periodic boundary conditions are applied in both armchair and zigzag directions. The single-layer 1T-TiS_2 is stretched uniaxially along the armchair or zigzag direction. The stress is calculated without involving the actual thickness of the quasi-two-dimensional structure of the single-layer 1T-TiS_2. The Young's modulus can be obtained by a linear fitting of the stress-strain relation in the small strain range of [0, 0.01]. The Young's modulus is 75 and 74.6 N/m along the armchair and zigzag directions, respectively. The Young's modulus is essentially isotropic in the armchair and zigzag directions. The Poisson's ratio from the VFF model and the SW potential is $\nu_{xy} = \nu_{yx} = 0.20$. The fitted Young's modulus

VFF type	**Bond stretching**	**Angle bending**	
Expression	$\frac{1}{2}K_{\mathrm{Ti-S}}(\Delta r)^2$	$\frac{1}{2}K_{\mathrm{Ti-S-S}}(\Delta\theta)^2$	$\frac{1}{2}K_{\mathrm{S-Ti-Ti}}(\Delta\theta)^2$
Parameter	9.815	3.754	3.754
r_0 or θ_0	2.390	87.984	87.984

The second line gives an explicit expression for each VFF term. The third line is the force constant parameters. Parameters are in the unit of eV/Å^2 for the bond stretching interaction and in the unit of eV for the angle bending interaction. The fourth line gives the initial bond length (in the unit of Å) for the bond stretching interaction and the initial angle (in the unit of degrees) for the angle bending interaction. The angle θ_{ijk} has atom i as the apex.

Table 162. The VFF model for single-layer 1T-TiS_2.

	A (eV)	ρ (Å)	B (Å^4)	$r_{\min}$ (Å)	$r_{\max}$ (Å)
Ti-S	7.958	1.210	16.314	0.0	3.240

Table 163. Two-body SW potential parameters for single-layer 1T-TiS_2 used by GULP [8] as expressed in Eq. (3).

	K (eV)	θ_0 (°)	ρ_1 (Å)	ρ_2 (Å)	$r_{\min 12}$ (Å)	$r_{\max 12}$ (Å)	$r_{\min 13}$ (Å)	$r_{\max 13}$ (Å)	$r_{\min 23}$ (Å)	$r_{\max 23}$ (Å)
$\theta_{\text{Ti–S–S}}$	32.377	87.984	1.210	1.210	0.0	3.240	0.0	3.240	0.0	4.535
$\theta_{\text{S–Ti–Ti}}$	32.377	87.984	1.210	1.210	0.0	3.240	0.0	3.240	0.0	4.535

The angle θ_{ijk} in the first line indicates the bending energy for the angle with atom i as the apex.

Table 164. Three-body SW potential parameters for single-layer 1T-TiS_2 used by GULP [8] as expressed in Eq. (4).

	ϵ (eV)	σ (Å)	a	λ	γ	$\cos\theta_0$	A_L	B_L	p	q	Tol
Ti—S—S	1.000	1.210	2.677	32.377	1.000	0.035	7.958	7.602	4	0	0.0

Table 165. SW potential parameters for single-layer 1T-TiS_2 used by LAMMPS [9] as expressed in Eqs. (9) and (10).

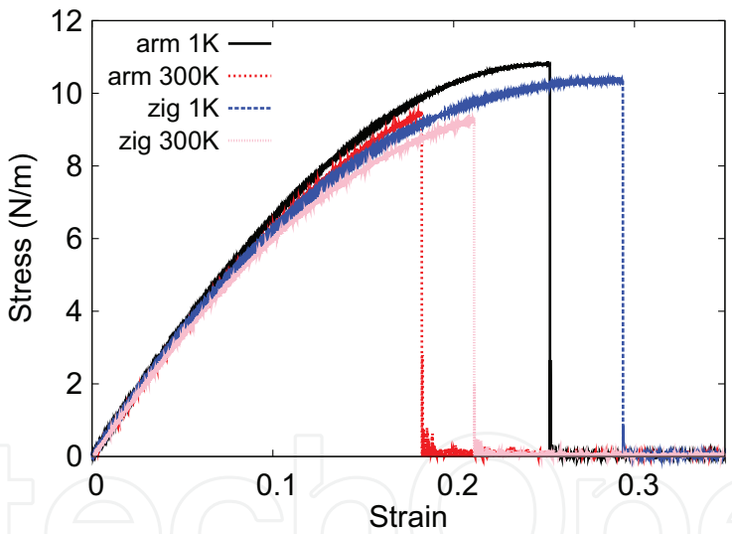

Figure 80. Stress-strain for single-layer 1T-TiS_2 of dimension 100 × 100 Å along the armchair and zigzag directions.

value is about 10% smaller than the *ab initio* result of 85 N/m [48], as only short-range interactions are considered in the present work. The long-range interactions are ignored, which typically leads to about 10% underestimation for the value of the Young's modulus.

There is no available value for nonlinear quantities in the single-layer 1T-TiS_2. We have thus used the nonlinear parameter $B = 0.5d^4$ in Eq. (5), which is close to the value of B in most materials. The value of the third-order nonlinear elasticity D can be extracted by fitting the stress-strain relation to the function $\sigma = E\epsilon + \frac{1}{2}D\epsilon^2$ with E as the Young's modulus. The values of D from the present SW potential are −220.8 and −264.4 N/m along the armchair and zigzag directions, respectively. The ultimate stress is about 10.8 N/m at the ultimate strain of 0.25 in

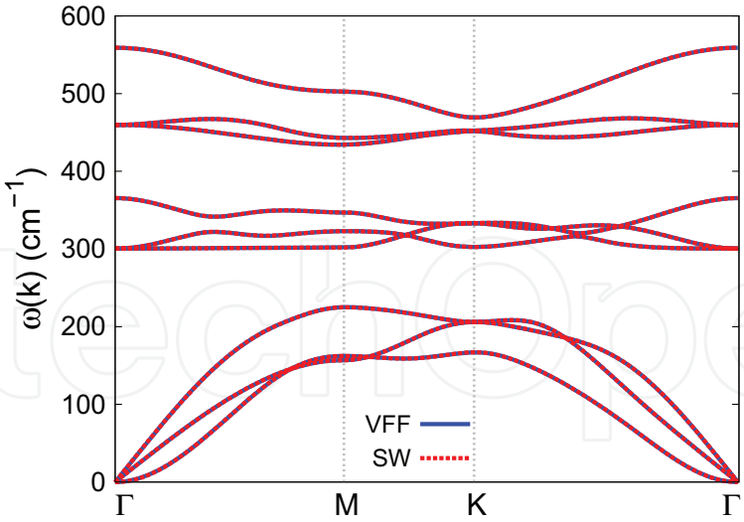

Figure 81. Phonon spectrum for single-layer 1T-TiS_2 along the ΓMKΓ direction in the Brillouin zone. The phonon dispersion from the SW potential is exactly the same as that from the VFF model.

the armchair direction at the low temperature of 1 K. The ultimate stress is about 10.4 N/m at the ultimate strain of 0.29 in the zigzag direction at the low temperature of 1 K.

Figure 81 shows that the VFF model and the SW potential give exactly the same phonon dispersion, as the SW potential is derived from the VFF model.

42. 1T-$TiSe_2$

Most existing theoretical studies on the single-layer 1T-$TiSe_2$ are based on the first-principles calculations. In this section, we will develop the SW potential for the single-layer 1T-$TiSe_2$.

The structure for the single-layer 1T-$TiSe_2$ is shown in **Figure 71** (with M = Ti and X = Se). Each Ti atom is surrounded by six Se atoms. These Se atoms are categorized into the top group (e.g., atoms 1, 3, and 5) and bottom group (e.g., atoms 2, 4, and 6). Each Se atom is connected to three Ti atoms. The structural parameters are from the first-principles calculations [12], including the lattice constant $a = 3.43$ Å and the bond length $d_{\mathrm{Ti-Se}} = 2.51$ Å. The resultant angles are $\theta_{\mathrm{TiSeSe}} = 86.199^\circ$ with Se atoms from the same (top or bottom) group and $\theta_{\mathrm{SeTiTi}} = 86.199^\circ$.

Table 166 shows three VFF terms for the single-layer 1T-$TiSe_2$; one of which is the bond stretching interaction shown by Eq. (1), while the other two terms are the angle bending interaction shown by Eq. (2). We note that the angle bending term $K_{\mathrm{Ti-Se-Se}}$ is for the angle $\theta_{\mathrm{Ti-Se-Se}}$ with both Se atoms from the same (top or bottom) group. We find that there are actually only two parameters in the VFF model, so we can determine their value by fitting to the Young's modulus and the Poisson's ratio of the system. The *ab initio* calculations have predicted the Young's modulus to be 70 N/m and the Poisson's ratio as 0.20 [48].

The parameters for the two-body SW potential used by GULP are shown in **Table 167**. The parameters for the three-body SW potential used by GULP are shown in **Table 168**. Some representative parameters for the SW potential used by LAMMPS are listed in **Table 169**.

VFF type	Bond stretching	Angle bending	
Expression	$\frac{1}{2}K_{\mathrm{Ti-Se}}(\Delta r)^2$	$\frac{1}{2}K_{\mathrm{Ti-Se-Se}}(\Delta\theta)^2$	$\frac{1}{2}K_{\mathrm{Se-Ti-Ti}}(\Delta\theta)^2$
Parameter	7.712	3.363	3.363
r_0 or θ_0	2.510	86.199	86.199

The second line gives an explicit expression for each VFF term. The third line is the force constant parameters. Parameters are in the unit of eV/Å^2 for the bond stretching interaction and in the unit of eV for the angle bending interaction. The fourth line gives the initial bond length (in the unit of Å) for the bond stretching interaction and the initial angle (in the unit of degrees) for the angle bending interaction. The angle θ_{ijk} has atom i as the apex.

Table 166. The VFF model for single-layer 1T-$TiSe_2$.

	A (eV)	ρ (Å)	B (Å^4)	r_{min} (Å)	r_{max} (Å)
Ti—Se	6.582	1.207	19.846	0.0	3.380

Table 167. Two-body SW potential parameters for single-layer 1T-$TiSe_2$ used by GULP [8] as expressed in Eq. (3).

	K (eV)	θ_0 (°)	ρ_1 (Å)	ρ_2 (Å)	$r_{\mathrm{min}\,12}$ (Å)	$r_{\mathrm{max}\,12}$ (Å)	$r_{\mathrm{min}\,13}$ (Å)	$r_{\mathrm{max}\,13}$ (Å)	$r_{\mathrm{min}\,23}$ (Å)	$r_{\mathrm{max}\,23}$ (Å)
$\theta_{\mathrm{Ti-Se-Se}}$	27.044	86.199	1.207	1.207	0.0	3.380	0.0	3.380	0.0	4.685
$\theta_{\mathrm{Se-Ti-Ti}}$	27.044	86.199	1.207	1.207	0.0	3.380	0.0	3.380	0.0	4.685

The angle θ_{ijk} in the first line indicates the bending energy for the angle with atom i as the apex.

Table 168. Three-body SW potential parameters for single-layer 1T-$TiSe_2$ used by GULP [8] as expressed in Eq. (4).

	ϵ (eV)	σ (Å)	a	λ	γ	$\cos\theta_0$	A_L	B_L	p	q	Tol
Ti—Se—Se	1.000	1.207	2.801	27.044	1.000	0.066	6.582	9.362	4	0	0.0

Table 169. SW potential parameters for single-layer 1T-$TiSe_2$ used by LAMMPS [9] as expressed in Eqs. (9) and (10).

We use LAMMPS to perform MD simulations for the mechanical behavior of the single-layer 1T-$TiSe_2$ under uniaxial tension at 1 and 300 K. **Figure 82** shows the stress-strain curve for the tension of a single-layer 1T-$TiSe_2$ of dimension 100×100 Å. Periodic boundary conditions are applied in both armchair and zigzag directions. The single-layer 1T-$TiSe_2$ is stretched uniaxially along the armchair or zigzag direction. The stress is calculated without involving the actual thickness of the quasi-two-dimensional structure of the single-layer 1T-$TiSe_2$. The Young's modulus can be obtained by a linear fitting of the stress-strain relation in the small strain range of [0, 0.01]. The Young's modulus is 59.2 and 58.9 N/m along the armchair and zigzag directions, respectively. The Young's modulus is essentially isotropic in the armchair and zigzag directions. The Poisson's ratio from the VFF model and the SW potential is $\nu_{xy} = \nu_{yx} = 0.20$. The fitted Young's modulus value is about 10% smaller than the *ab initio* result of 70 N/m [48], as only short-range interactions are considered in the present work. The long-range interactions are ignored, which typically leads to about 10% underestimation for the value of the Young's modulus.

http://dx.doi.org/10.5772/intechopen.71929

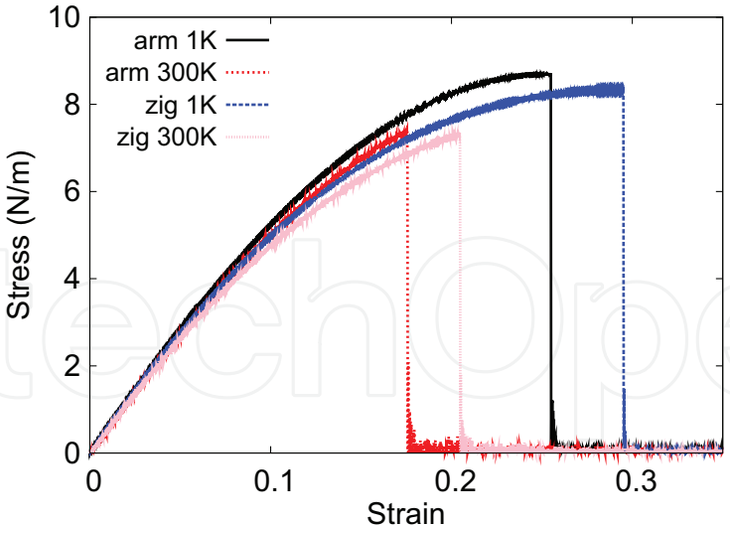

Figure 82. Stress-strain for single-layer 1T-$TiSe_2$ of dimension 100 × 100 Å along the armchair and zigzag directions.

There is no available value for nonlinear quantities in the single-layer 1T-$TiSe_2$. We have thus used the nonlinear parameter $B = 0.5d^4$ in Eq. (5), which is close to the value of B in most materials. The value of the third-order nonlinear elasticity D can be extracted by fitting the stress-strain relation to the function $\sigma = E\epsilon + \frac{1}{2}D\epsilon^2$ with E as the Young's modulus. The values of D from the present SW potential are −166.5 and −201.6 N/m along the armchair and zigzag directions, respectively. The ultimate stress is about 8.7 N/m at the ultimate strain of 0.25 in the armchair direction at the low temperature of 1 K. The ultimate stress is about 8.3 N/m at the ultimate strain of 0.29 in the zigzag direction at the low temperature of 1 K.

Figure 83 shows that the VFF model and the SW potential give exactly the same phonon dispersion, as the SW potential is derived from the VFF model.

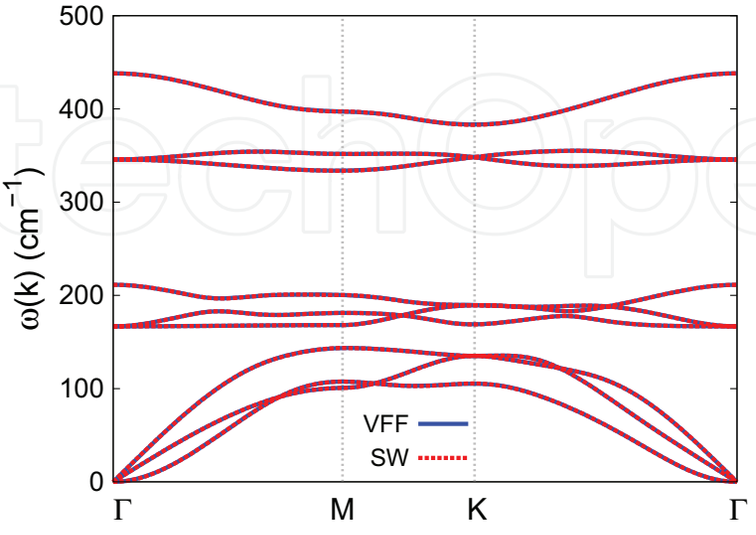

Figure 83. Phonon spectrum for single-layer 1T-$TiSe_2$ along the ΓMKΓ direction in the Brillouin zone. The phonon dispersion from the SW potential is exactly the same as that from the VFF model.

43. 1T-$TiTe_2$

Most existing theoretical studies on the single-layer 1T-$TiTe_2$ are based on the first-principles calculations. In this section, we will develop the SW potential for the single-layer 1T-$TiTe_2$.

The structure for the single-layer 1T-$TiTe_2$ is shown in **Figure 71** (with M = Ti and X = Te). Each Ti atom is surrounded by six Te atoms. These Te atoms are categorized into the top group (e.g., atoms 1, 3, and 5) and bottom group (e.g., atoms 2, 4, and 6). Each Te atom is connected to three Ti atoms. The structural parameters are from the first-principles calculations [12], including the lattice constant $a = 3.64$ Å and the bond length $d_{\mathrm{Ti-Te}} = 2.73$ Å. The resultant angles are $\theta_{\mathrm{TiTeTe}} = 83.621^\circ$ with Te atoms from the same (top or bottom) group and $\theta_{\mathrm{TeTiTi}} = 83.621^\circ$.

Table 170 shows three VFF terms for the single-layer 1T-$TiTe_2$; one of which is the bond stretching interaction shown by Eq. (1), while the other two terms are the angle bending interaction shown by Eq. (2). We note that the angle bending term $K_{\mathrm{Ti-Te-Te}}$ is for the angle $\theta_{\mathrm{Ti-Te-Te}}$ with both Te atoms from the same (top or bottom) group. We find that there are actually only two parameters in the VFF model, so we can determine their value by fitting to the Young's modulus and the Poisson's ratio of the system. The *ab initio* calculations have predicted the Young's modulus to be 46 N/m and the Poisson's ratio as 0.15 [48].

The parameters for the two-body SW potential used by GULP are shown in **Table 171**. The parameters for the three-body SW potential used by GULP are shown in **Table 172**. Some representative parameters for the SW potential used by LAMMPS are listed in **Table 173**.

We use LAMMPS to perform MD simulations for the mechanical behavior of the single-layer 1T-$TiTe_2$ under uniaxial tension at 1 and 300 K. **Figure 84** shows the stress-strain curve for the tension of a single-layer 1T-$TiTe_2$ of dimension 100 × 100 Å. Periodic boundary conditions are applied in both armchair and zigzag directions. The single-layer 1T-$TiTe_2$ is stretched uniaxially along the armchair or zigzag direction. The stress is calculated without involving

VFF type	Bond stretching	Angle bending	
Expression	$\frac{1}{2}K_{\mathrm{Ti-Te}}(\Delta r)^2$	$\frac{1}{2}K_{\mathrm{Ti-Te-Te}}(\Delta\theta)^2$	$\frac{1}{2}K_{\mathrm{Te-Ti-Ti}}(\Delta\theta)^2$
Parameter	3.758	3.217	3.217
r_0 or θ_0	2.730	83.621	83.621

The second line gives an explicit expression for each VFF term. The third line is the force constant parameters. Parameters are in the unit of eV/Å^2 for the bond stretching interaction and in the unit of eV for the angle bending interaction. The fourth line gives the initial bond length (in the unit of Å) for the bond stretching interaction and the initial angle (in the unit of degrees) for the angle bending interaction. The angle θ_{ijk} has atom i as the apex.

Table 170. The VFF model for single-layer 1T-$TiTe_2$.

	A (eV)	ρ (Å)	B (Å^4)	r_{min} (Å)	r_{max} (Å)
Ti—Te	3.542	1.213	27.773	0.0	3.640

Table 171. Two-body SW potential parameters for single-layer 1T-$TiTe_2$ used by GULP [8] as expressed in Eq. (3).

	K (eV)	θ_0 (°)	ρ_1 (Å)	ρ_2 (Å)	r_{min12} (Å)	r_{max12} (Å)	r_{min13} (Å)	r_{max13} (Å)	r_{min23} (Å)	r_{max23} (Å)
$\theta_{Ti-Te-Te}$	23.439	83.621	1.213	1.213	0.0	3.640	0.0	3.640	0.0	4.972
$\theta_{Te-Ti-Ti}$	23.439	83.621	1.213	1.213	0.0	3.640	0.0	3.640	0.0	4.972

The angle θ_{ijk} in the first line indicates the bending energy for the angle with atom i as the apex.

Table 172. Three-body SW potential parameters for single-layer 1T-$TiTe_2$ used by GULP [8] as expressed in Eq. (4).

	ϵ (eV)	σ (Å)	a	λ	γ	$\cos\theta_0$	A_L	B_L	p	q	Tol
Ti—Te—Te	1.000	1.213	3.000	23.439	1.000	0.111	3.542	12.814	4	0	0.0

Table 173. SW potential parameters for single-layer 1T-$TiTe_2$ used by LAMMPS [9] as expressed in Eqs. (9) and (10).

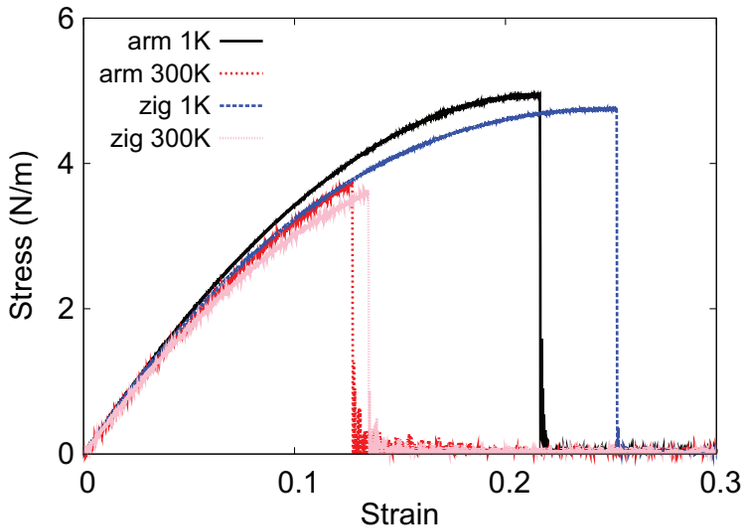

Figure 84. Stress-strain for single-layer 1T-$TiTe_2$ of dimension 100 × 100 Å along the armchair and zigzag directions.

the actual thickness of the quasi-two-dimensional structure of the single-layer 1T-$TiTe_2$. The Young's modulus can be obtained by a linear fitting of the stress-strain relation in the small strain range of [0, 0.01]. The Young's modulus is 41.4 and 41.2 N/m along the armchair and zigzag directions, respectively. The Young's modulus is essentially isotropic in the armchair and zigzag directions. The Poisson's ratio from the VFF model and the SW potential is $\nu_{xy} = \nu_{yx} = 0.15$. The fitted Young's modulus value is about 10% smaller than the *ab initio* result of 46 N/m [48], as only short-range interactions are considered in the present work. The long-range interactions are ignored, which typically leads to about 10% underestimation for the value of the Young's modulus.

There is no available value for nonlinear quantities in the single-layer 1T-$TiTe_2$. We have thus used the nonlinear parameter $B = 0.5d^4$ in Eq. (5), which is close to the value of B in most materials. The value of the third-order nonlinear elasticity D can be extracted by fitting the stress-strain relation to the function $\sigma = E\epsilon + \frac{1}{2}D\epsilon^2$ with E as the Young's modulus. The values

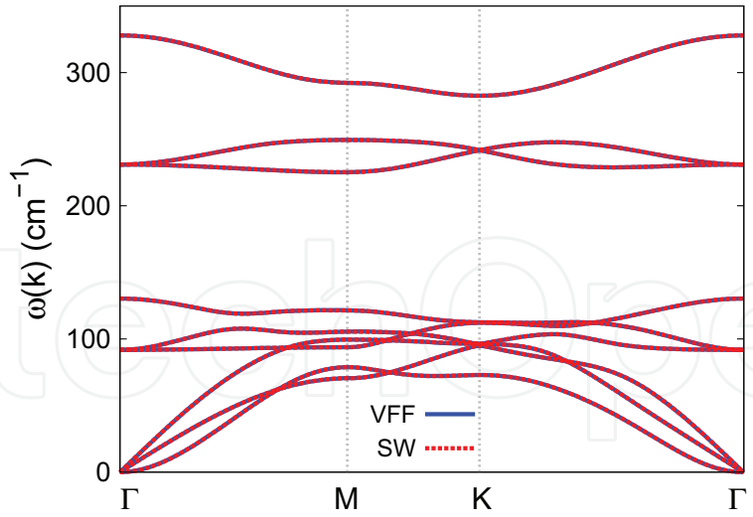

Figure 85. Phonon spectrum for single-layer 1T-$TiTe_2$ along the ΓMKΓ direction in the Brillouin zone. The phonon dispersion from the SW potential is exactly the same as that from the VFF model.

of D from the present SW potential are −161.3 and −181.4 N/m along the armchair and zigzag directions, respectively. The ultimate stress is about 4.9 N/m at the ultimate strain of 0.22 in the armchair direction at the low temperature of 1 K. The ultimate stress is about 4.7 N/m at the ultimate strain of 0.25 in the zigzag direction at the low temperature of 1 K.

Figure 85 shows that the VFF model and the SW potential give exactly the same phonon dispersion, as the SW potential is derived from the VFF model.

44. 1T-VS_2

Most existing theoretical studies on the single-layer 1T-VS_2 are based on the first-principles calculations. In this section, we will develop the SW potential for the single-layer 1T-VS_2.

The structure for the single-layer 1T-VS_2 is shown in **Figure 71** (with M = V and X = S). Each V atom is surrounded by six S atoms. These S atoms are categorized into the top group (e.g., atoms 1, 3, and 5) and bottom group (e.g., atoms 2, 4, and 6). Each S atom is connected to three V atoms. The structural parameters are from the first-principles calculations [12], including the lattice constant $a = 3.10$ Å and the bond length $d_{V-S} = 2.31$ Å. The resultant angles are $\theta_{VSS} = 84.288°$ with S atoms from the same (top or bottom) group and $\theta_{SVV} = 84.288°$.

Table 174 shows three VFF terms for the single-layer 1T-VS_2; one of which is the bond stretching interaction shown by Eq. (1), while the other two terms are the angle bending interaction shown by Eq. (2). We note that the angle bending term K_{V-S-S} is for the angle θ_{V-S-S} with both S atoms from the same (top or bottom) group. These force constant parameters are determined by fitting to the three acoustic branches in the phonon dispersion along the ΓM as shown in **Figure 86(a)**. The *ab initio* calculations for the phonon dispersion are from [12]. The lowest acoustic branch (flexural mode) is linear and very close to the in-plane

VFF type	Bond stretching	Angle bending	
Expression	$\frac{1}{2}K_{V-S}(\Delta r)^2$	$\frac{1}{2}K_{V-S-S}(\Delta\theta)^2$	$\frac{1}{2}K_{S-V-V}(\Delta\theta)^2$
Parameter	11.562	4.237	4.237
r_0 or θ_0	2.310	84.288	84.288

The second line gives an explicit expression for each VFF term. The third line is the force constant parameters. Parameters are in the unit of eV/Å^2 for the bond stretching interaction and in the unit of eV for the angle bending interaction. The fourth line gives the initial bond length (in the unit of Å) for the bond stretching interaction and the initial angle (in the unit of degrees) for the angle bending interaction. The angle θ_{ijk} has atom i as the apex.

Table 174. The VFF model for single-layer 1T-VS_2.

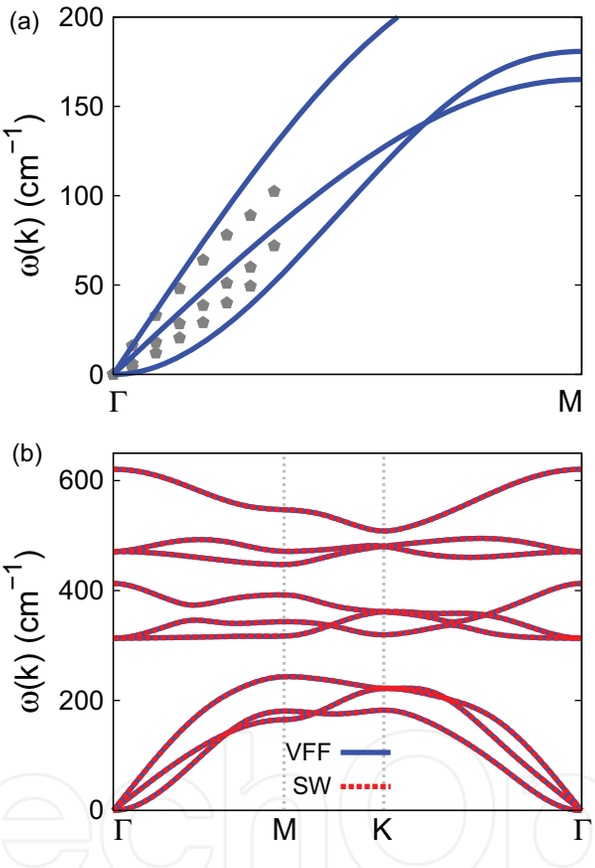

Figure 86. Phonon spectrum for single-layer 1T-VS_2. (a) Phonon dispersion along the ΓM direction in the Brillouin zone. The results from the VFF model (lines) are comparable with the *ab initio* results (pentagons) from [12]. (b) The phonon dispersion from the SW potential is exactly the same as that from the VFF model.

transverse acoustic branch in the *ab initio* calculations, which may be due to the violation of the rigid rotational invariance [20]. **Figure 86(b)** shows that the VFF model and the SW potential give exactly the same phonon dispersion, as the SW potential is derived from the VFF model.

The parameters for the two-body SW potential used by GULP are shown in **Table 175**. The parameters for the three-body SW potential used by GULP are shown in **Table 176**. Some representative parameters for the SW potential used by LAMMPS are listed in **Table 177**.

	A (eV)	ρ (Å)	B (Å^4)	r_{min} (Å)	r_{max} (Å)
V—S	7.943	1.048	14.237	0.0	3.088

Table 175. Two-body SW potential parameters for single-layer 1T-VS_2 used by GULP [8] as expressed in Eq. (3).

	K (eV)	θ_0 (°)	ρ_1 (Å)	ρ_2 (Å)	r_{min12} (Å)	r_{max12} (Å)	r_{min13} (Å)	r_{max13} (Å)	r_{min23} (Å)	r_{max23} (Å)
θ_{V-S-S}	31.659	84.288	1.048	1.048	0.0	3.088	0.0	3.088	0.0	4.235
θ_{S-V-V}	31.659	84.288	1.048	1.048	0.0	3.088	0.0	3.088	0.0	4.235

The angle θ_{ijk} in the first line indicates the bending energy for the angle with atom i as the apex.

Table 176. Three-body SW potential parameters for single-layer 1T-VS_2 used by GULP [8] as expressed in Eq. (4).

	ϵ (eV)	σ (Å)	a	λ	γ	$\cos\theta_0$	A_L	B_L	p	q	Tol
V—S_1—S_1	1.000	1.048	2.946	31.659	1.000	0.100	7.943	11.797	4	0	0.0

Table 177. SW potential parameters for single-layer 1T-VS_2 used by LAMMPS [9] as expressed in Eqs. (9) and (10).

We use LAMMPS to perform MD simulations for the mechanical behavior of the single-layer 1T-VS_2 under uniaxial tension at 1 and 300 K. **Figure 87** shows the stress-strain curve for the tension of a single-layer 1T-VS_2 of dimension 100 × 100 Å. Periodic boundary conditions are applied in both armchair and zigzag directions. The single-layer 1T-VS_2 is stretched uniaxially along the armchair or zigzag direction. The stress is calculated without involving the actual thickness of the quasi-two-dimensional structure of the single-layer 1T-VS_2. The Young's modulus can be obtained by a linear fitting of the stress-strain relation in the small strain range of [0, 0.01]. The Young's modulus is 87.1 and 86.8 N/m along the armchair and zigzag directions, respectively. The Young's modulus is essentially isotropic in the armchair and zigzag directions. The Poisson's ratio from the VFF model and the SW potential is $\nu_{xy} = \nu_{yx} = 0.21$.

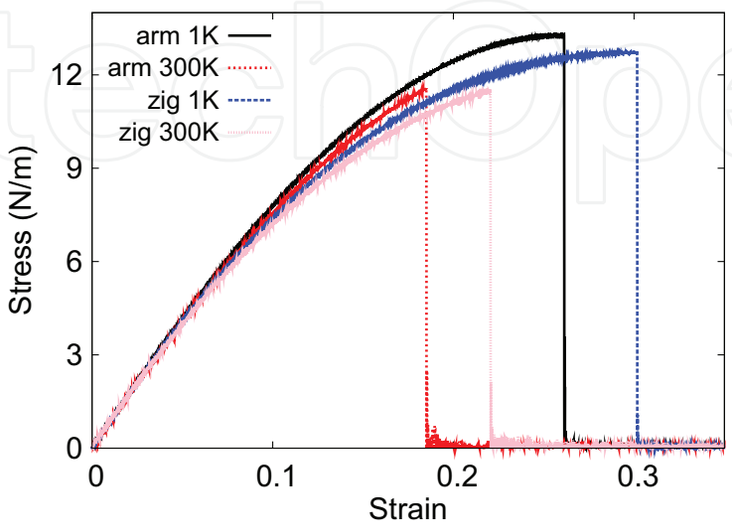

Figure 87. Stress-strain for single-layer 1T-VS_2 of dimension 100 × 100 Å along the armchair and zigzag directions.

There is no available value for nonlinear quantities in the single-layer 1T-VS_2. We have thus used the nonlinear parameter $B = 0.5d^4$ in Eq. (5), which is close to the value of B in most materials. The value of the third-order nonlinear elasticity D can be extracted by fitting the stress-strain relation to the function $\sigma = E\epsilon + \frac{1}{2}D\epsilon^2$ with E as the Young's modulus. The values of D from the present SW potential are -230.5 and -283.6 N/m along the armchair and zigzag directions, respectively. The ultimate stress is about 13.3 N/m at the ultimate strain of 0.26 in the armchair direction at the low temperature of 1 K. The ultimate stress is about 12.7 N/m at the ultimate strain of 0.30 in the zigzag direction at the low temperature of 1 K.

45. 1T-VSe_2

Most existing theoretical studies on the single-layer 1T-VSe_2 are based on the first-principles calculations. In this section, we will develop the SW potential for the single-layer 1T-VSe_2.

The structure for the single-layer 1T-VSe_2 is shown in **Figure 71** (with M = V and X = Se). Each V atom is surrounded by six Se atoms. These Se atoms are categorized into the top group (e.g., atoms 1, 3, and 5) and bottom group (e.g., atoms 2, 4, and 6). Each Se atom is connected to three V atoms. The structural parameters are from the first-principles calculations [12], including the lattice constant $a = 3.24$ Å and the bond length $d_{\mathrm{V-Se}} = 2.44$ Å. The resultant angles are $\theta_{\mathrm{VSeSe}} = 83.201^\circ$ with Se atoms from the same (top or bottom) group and $\theta_{\mathrm{SeVV}} = 83.201^\circ$.

Table 178 shows three VFF terms for the single-layer 1T-VSe_2; one of which is the bond stretching interaction shown by Eq. (1), while the other two terms are the angle bending interaction shown by Eq. (2). We note that the angle bending term $K_{\mathrm{V-Se-Se}}$ is for the angle $\theta_{\mathrm{V-Se-Se}}$ with both Se atoms from the same (top or bottom) group. These force constant parameters are determined by fitting to the three acoustic branches in the phonon dispersion along the ΓM as shown in **Figure 88(a)**. The *ab initio* calculations for the phonon dispersion are from [12]. The lowest acoustic branch (flexural mode) is almost linear in the *ab initio* calculations, which may be due to the violation of the rigid rotational invariance [20]. **Figure 88(b)** shows that the VFF model and the SW potential give exactly the same phonon dispersion, as the SW potential is derived from the VFF model.

VFF type	**Bond stretching**	**Angle bending**	
Expression	$\frac{1}{2}K_{\mathrm{V-Se}}(\Delta r)^2$	$\frac{1}{2}K_{\mathrm{V-Se-Se}}(\Delta\theta)^2$	$\frac{1}{2}K_{\mathrm{Se-V-V}}(\Delta\theta)^2$
Parameter	11.562	4.237	4.237
r_0 or θ_0	2.440	83.201	83.201

The second line gives an explicit expression for each VFF term. The third line is the force constant parameters. Parameters are in the unit of eV/Å^2 for the bond stretching interaction and in the unit of eV for the angle bending interaction. The fourth line gives the initial bond length (in the unit of Å) for the bond stretching interaction and the initial angle (in the unit of degrees) for the angle bending interaction. The angle θ_{ijk} has atom i as the apex.

Table 178. The VFF model for single-layer 1T-VSe_2.

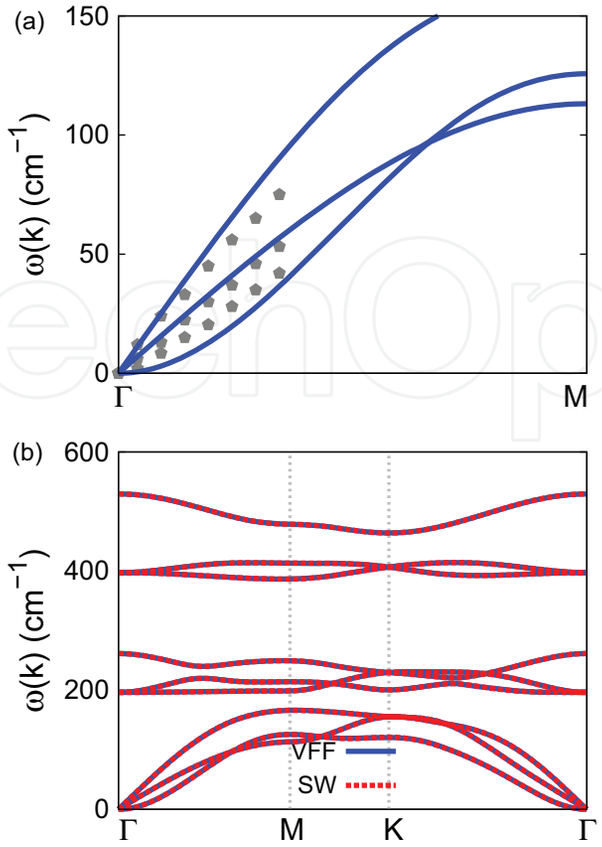

Figure 88. Phonon spectrum for single-layer 1T-VSe_2. (a) Phonon dispersion along the ΓM direction in the Brillouin zone. The results from the VFF model (lines) are comparable with the experiment data (pentagons) from [12]. (b) The phonon dispersion from the SW potential is exactly the same as that from the VFF model.

The parameters for the two-body SW potential used by GULP are shown in **Table 179**. The parameters for the three-body SW potential used by GULP are shown in **Table 180**. Some representative parameters for the SW potential used by LAMMPS are listed in **Table 181**.

We use LAMMPS to perform MD simulations for the mechanical behavior of the single-layer 1T-VSe_2 under uniaxial tension at 1 and 300 K. **Figure 89** shows the stress-strain curve for the tension of a single-layer 1T-VSe_2 of dimension 100 × 100 Å. Periodic boundary conditions are

	A (eV)	ρ (Å)	B (Å	r_{min} (Å)	r_{max} (Å)
V—Se	8.606	1.070	17.723	0.0	3.248

Table 179. Two-body SW potential parameters for single-layer 1T-VSe_2 used by GULP [8] as expressed in Eq. (3).

	K (eV)	θ_0 (°)	ρ_1 (Å)	ρ_2 (Å)	r_{min12} (Å)	r_{max12} (Å)	r_{min13} (Å)	r_{max13} (Å)	r_{min23} (Å)	r_{max23} (Å)
$\theta_{V-Se-Se}$	30.387	83.201	1.070	1.070	0.0	3.248	0.0	3.248	0.0	4.426
θ_{Se-V-V}	30.387	83.201	1.070	1.070	0.0	3.248	0.0	3.248	0.0	4.426

The angle θ_{ijk} in the first line indicates the bending energy for the angle with atom i as the apex.

Table 180. Three-body SW potential parameters for single-layer 1T-VSe_2 used by GULP [8] as expressed in Eq. (4).

	ϵ (eV)	σ (Å)	a	λ	γ	$\cos\theta_0$	A_L	B_L	p	q	Tol
V—Se_1—Se_1	1.000	1.070	3.035	30.387	1.000	0.118	8.606	13.507	4	0	0.0

Table 181. SW potential parameters for single-layer 1T-VSe_2 used by LAMMPS [9] as expressed in Eqs. (9) and (10).

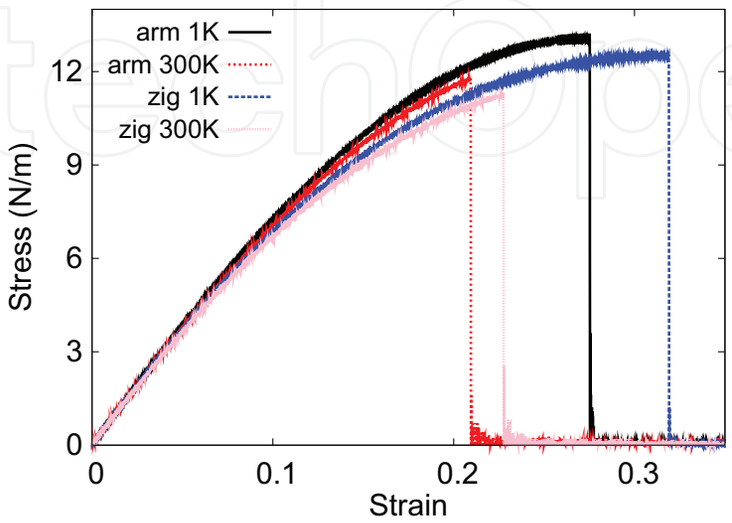

Figure 89. Stress-strain for single-layer 1T-VSe_2 of dimension 100 × 100 Å along the armchair and zigzag directions.

applied in both armchair and zigzag directions. The single-layer 1T-VSe_2 is stretched uniaxially along the armchair or zigzag direction. The stress is calculated without involving the actual thickness of the quasi-two-dimensional structure of the single-layer 1T-VSe_2. The Young's modulus can be obtained by a linear fitting of the stress-strain relation in the small strain range of [0, 0.01]. The Young's modulus is 78.4 and 78.1 N/m along the armchair and zigzag directions, respectively. The Young's modulus is essentially isotropic in the armchair and zigzag directions. The Poisson's ratio from the VFF model and the SW potential is $\nu_{xy} = \nu_{yx} = 0.22$.

There is no available value for nonlinear quantities in the single-layer 1T-VSe_2. We have thus used the nonlinear parameter $B = 0.5d^4$ in Eq. (5), which is close to the value of B in most materials. The value of the third-order nonlinear elasticity D can be extracted by fitting the stress-strain relation to the function $\sigma = E\epsilon + \frac{1}{2}D\epsilon^2$ with E as the Young's modulus. The values of D from the present SW potential are −168.5 and −218.6 N/m along the armchair and zigzag directions, respectively. The ultimate stress is about 13.1 N/m at the ultimate strain of 0.27 in the armchair direction at the low temperature of 1 K. The ultimate stress is about 12.5 N/m at the ultimate strain of 0.32 in the zigzag direction at the low temperature of 1 K.

46. 1T-VTe_2

Most existing theoretical studies on the single-layer 1T-VTe_2 are based on the first-principles calculations. In this section, we will develop the SW potential for the single-layer 1T-VTe_2.

The structure for the single-layer 1T-VTe_2 is shown in **Figure 71** (with M = V and X = Te). Each V atom is surrounded by six Te atoms. These Te atoms are categorized into the top group (e.g., atoms 1, 3, and 5) and bottom group (e.g., atoms 2, 4, and 6). Each Te atom is connected to three V atoms. The structural parameters are from the first-principles calculations [12], including the lattice constant $a = 3.46$ Å and the bond length $d_{\mathrm{V-Te}} = 2.64$ Å. The resultant angles are $\theta_{\mathrm{VTeTe}} = 81.885^\circ$ with Te atoms from the same (top or bottom) group and $\theta_{\mathrm{TeVV}} = 81.885^\circ$.

Table 182 shows three VFF terms for the single-layer 1T-VTe_2; one of which is the bond stretching interaction shown by Eq. (1), while the other two terms are the angle bending interaction shown by Eq. (2). We note that the angle bending term $K_{\mathrm{V-Te-Te}}$ is for the angle $\theta_{\mathrm{V-Te-Te}}$ with both Te atoms from the same (top or bottom) group. We find that there are actually only two parameters in the VFF model, so we can determine their value by fitting to the Young's modulus and the Poisson's ratio of the system. The *ab initio* calculations have predicted the Young's modulus to be 67 N/m and the Poisson's ratio as 0.24 [48].

The parameters for the two-body SW potential used by GULP are shown in **Table 183**. The parameters for the three-body SW potential used by GULP are shown in **Table 184**. Some representative parameters for the SW potential used by LAMMPS are listed in **Table 185**.

VFF type	**Bond stretching**	**Angle bending**	
Expression	$\frac{1}{2}K_{\mathrm{V-Te}}(\Delta r)^2$	$\frac{1}{2}K_{\mathrm{V-Te-Te}}(\Delta\theta)^2$	$\frac{1}{2}K_{\mathrm{Te-V-V}}(\Delta\theta)^2$
Parameter	10.476	3.814	3.814
r_0 or θ_0	2.640	81.885	81.885

The third line is the force constant parameters. Parameters are in the unit of eV/Å^2 for the bond stretching interaction and in the unit of eV for the angle bending interaction. The fourth line gives the initial bond length (in the unit of Å) for the bond stretching interaction and the initial angle (in the unit of degrees) for the angle bending interaction. The angle θ_{ijk} has atom i as the apex.

Table 182. The VFF model for single-layer 1T-VTe_2. The second line gives an explicit expression for each VFF term.

	A **(eV)**	ρ **(Å)**	B **(Å^4)**	r_{min} **(Å)**	r_{max} **(Å)**
V—Te	8.805	1.110	24.288	0.0	3.496

Table 183. Two-body SW potential parameters for single-layer 1T-VTe_2 used by GULP [8] as expressed in Eq. (3).

	K **(eV)**	θ_0 **(°)**	ρ_1 **(Å)**	ρ_2 **(Å)**	r_{min12} **(Å)**	r_{max12} **(Å)**	r_{min13} **(Å)**	r_{max13} **(Å)**	r_{min23} **(Å)**	r_{max23} **(Å)**
$\theta_{\mathrm{V-Te-Te}}$	26.043	81.885	1.110	1.110	0.0	3.496	0.0	3.496	0.0	4.726
$\theta_{\mathrm{Te-V-V}}$	26.043	81.885	1.110	1.110	0.0	3.496	0.0	3.496	0.0	4.726

The angle θ_{ijk} in the first line indicates the bending energy for the angle with atom i as the apex.

Table 184. Three-body SW potential parameters for single-layer 1T-VTe_2 used by GULP [8] as expressed in Eq. (4).

http://dx.doi.org/10.5772/intechopen.71929

	ϵ (eV)	σ (Å)	a	λ	γ	$\cos\theta_0$	A_L	B_L	p	q	Tol
V—Te_1—Te_1	1.000	1.110	3.149	26.043	1.000	0.141	8.805	15.980	4	0	0.0

Table 185. SW potential parameters for single-layer 1T-VTe_2 used by LAMMPS [9] as expressed in Eqs. (9) and (10).

We use LAMMPS to perform MD simulations for the mechanical behavior of the single-layer 1T-VTe_2 under uniaxial tension at 1 and 300 K. **Figure 90** shows the stress-strain curve for the tension of a single-layer 1T-VTe_2 of dimension 100×100 Å. Periodic boundary conditions are applied in both armchair and zigzag directions. The single-layer 1T-VTe_2 is stretched uniaxially along the armchair or zigzag direction. The stress is calculated without involving the actual thickness of the quasi-two-dimensional structure of the single-layer 1T-VTe_2. The Young's modulus can be obtained by a linear fitting of the stress-strain relation in the small strain range of [0, 0.01]. The Young's modulus is 61.2 and 61.0 N/m along the armchair and zigzag directions, respectively. The Young's modulus is essentially isotropic in the armchair and zigzag directions. The Poisson's ratio from the VFF model and the SW potential is $\nu_{xy} = \nu_{yx} = 0.24$. The fitted Young's modulus value is about 10% smaller than the *ab initio* result of 67 N/m [48], as only short-range interactions are considered in the present work. The long-range interactions are ignored, which typically leads to about 10% underestimation for the value of the Young's modulus.

There is no available value for nonlinear quantities in the single-layer 1T-VTe_2. We have thus used the nonlinear parameter $B = 0.5d^4$ in Eq. (5), which is close to the value of B in most materials. The value of the third-order nonlinear elasticity D can be extracted by fitting the stress-strain relation to the function $\sigma = E\epsilon + \frac{1}{2}D\epsilon^2$ with E as the Young's modulus. The values of D from the present SW potential are -95.8 and -135.6 N/m along the armchair and zigzag directions, respectively. The ultimate stress is about 11.5 N/m at the ultimate strain of 0.30 in the armchair direction at the low temperature of 1 K. The ultimate stress is about 11.0 N/m at the ultimate strain of 0.34 in the zigzag direction at the low temperature of 1 K.

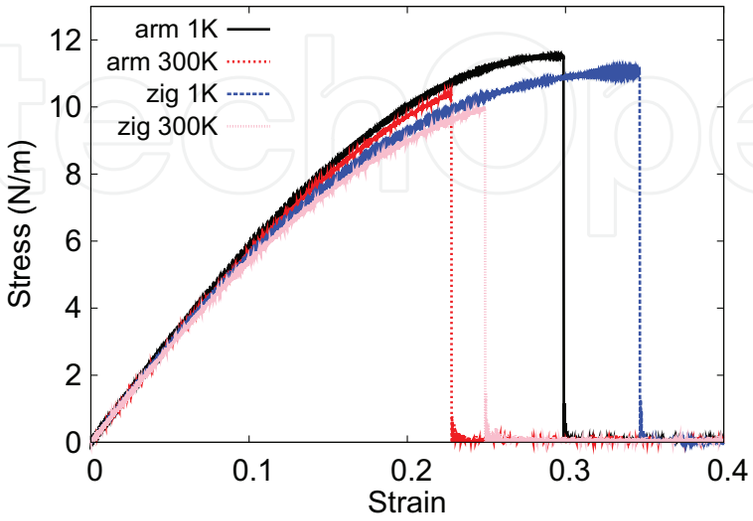

Figure 90. Stress-strain for single-layer 1T-VTe_2 of dimension 100×100 Å along the armchair and zigzag directions.

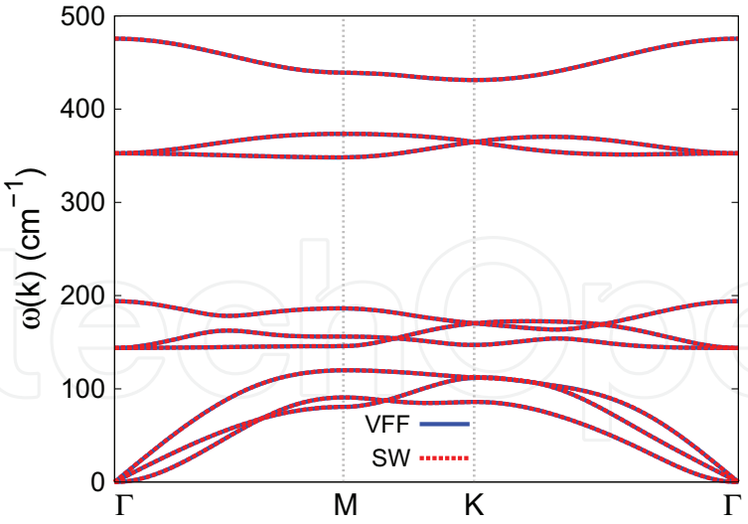

Figure 91. Phonon spectrum for single-layer 1T-VTe_2 along the ΓMKΓ direction in the Brillouin zone. The phonon dispersion from the SW potential is exactly the same as that from the VFF model.

Figure 91 shows that the VFF model and the SW potential give exactly the same phonon dispersion, as the SW potential is derived from the VFF model.

47. 1T-MnO_2

Most existing theoretical studies on the single-layer 1T-MnO_2 are based on the first-principles calculations. In this section, we will develop the SW potential for the single-layer 1T-MnO_2.

The structure for the single-layer 1T-MnO_2 is shown in **Figure 71** (with M = Mn and X = O). Each Mn atom is surrounded by six O atoms. These O atoms are categorized into the top group (e.g., atoms 1, 3, and 5) and bottom group (e.g., atoms 2, 4, and 6). Each O atom is connected to three Mn atoms. The structural parameters are from the first-principles calculations [12], including the lattice constant $a = 2.82$ Å and the bond length $d_{\mathrm{Mn-O}} = 1.88$ Å. The resultant angles are $\theta_{\mathrm{MnOO}} = 97.181^{\circ}$ with O atoms from the same (top or bottom) group and $\theta_{\mathrm{OMnMn}} = 97.181^{\circ}$.

Table 186 shows three VFF terms for the single-layer 1T-MnO_2; one of which is the bond stretching interaction shown by Eq. (1), while the other two terms are the angle bending interaction shown by Eq. (2). We note that the angle bending term $K_{\mathrm{Mn-O-O}}$ is for the angle $\theta_{\mathrm{Mn-O-O}}$ with both O atoms from the same (top or bottom) group. These force constant parameters are determined by fitting to the two in-plane acoustic branches in the phonon dispersion along the ΓM as shown in **Figure 92(a)**. The *ab initio* calculations for the phonon dispersion are from [12]. **Figure 92(b)** shows that the VFF model and the SW potential give exactly the same phonon dispersion, as the SW potential is derived from the VFF model.

The parameters for the two-body SW potential used by GULP are shown in **Table 187**. The parameters for the three-body SW potential used by GULP are shown in **Table 188**. Some representative parameters for the SW potential used by LAMMPS are listed in **Table 189**.

VFF type	Bond stretching	Angle bending	
Expression	$\frac{1}{2}K_{\mathrm{Mn-O}}(\Delta r)^2$	$\frac{1}{2}K_{\mathrm{Mn-O-O}}(\Delta\theta)^2$	$\frac{1}{2}K_{\mathrm{O-Mn-Mn}}(\Delta\theta)^2$
Parameter	15.371	4.822	4.822
r_0 or θ_0	1.88	97.181	97.181

The second line gives an explicit expression for each VFF term. The third line is the force constant parameters. Parameters are in the unit of eV/Å^2 for the bond stretching interaction and in the unit of eV for the angle bending interaction. The fourth line gives the initial bond length (in the unit of Å) for the bond stretching interaction and the initial angle (in the unit of degrees) for the angle bending interaction. The angle θ_{ijk} has atom i as the apex.

Table 186. The VFF model for single-layer 1T-MnO_2.

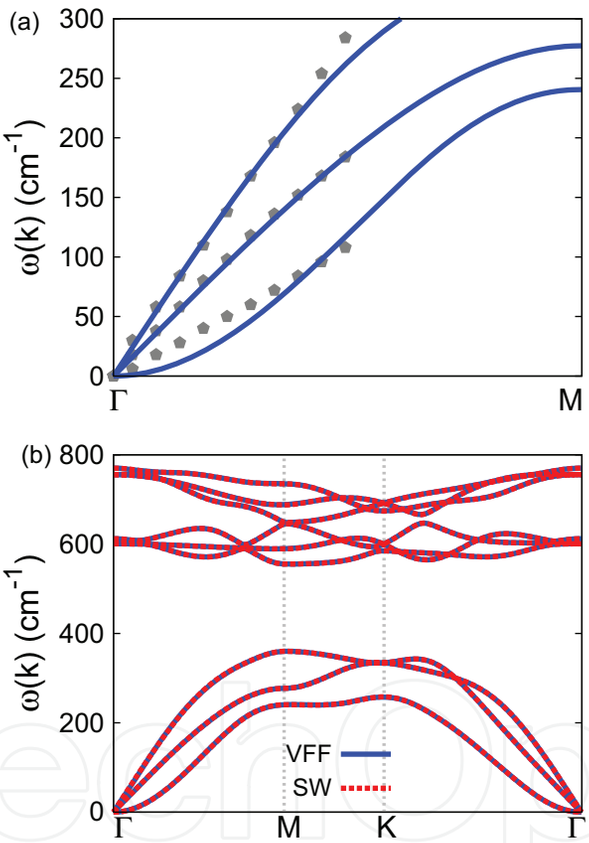

Figure 92. Phonon spectrum for single-layer 1T-MnO_2. (a) Phonon dispersion along the ΓM direction in the Brillouin zone. The results from the VFF model (lines) are comparable with the *ab initio* results (pentagons) from [12]. (b) The phonon dispersion from the SW potential is exactly the same as that from the VFF model.

	A (eV)	ρ (Å)	B (Å^4)	r_{min} (Å)	r_{max} (Å)
Mn—O	9.675	1.212	6.246	0.0	2.635

Table 187. Two-body SW potential parameters for single-layer 1T-MnO_2 used by GULP [8] as expressed in Eq. (3).

	K (eV)	θ_0 (°)	ρ_1 (Å)	ρ_2 (Å)	$r_{\min 12}$ (Å)	$r_{\max 12}$ (Å)	$r_{\min 13}$ (Å)	$r_{\max 13}$ (Å)	$r_{\min 23}$ (Å)	$r_{\max 23}$ (Å)
$\theta_{\mathrm{Mn-O-O}}$	60.755	97.181	1.212	1.212	0.0	2.635	0.0	2.635	0.0	3.852
$\theta_{\mathrm{O-Mn-Mn}}$	60.755	97.181	1.212	1.212	0.0	2.635	0.0	2.635	0.0	3.852

The angle θ_{ijk} in the first line indicates the bending energy for the angle with atom i as the apex.

Table 188. Three-body SW potential parameters for single-layer 1T-MnO_2 used by GULP [8] as expressed in Eq. (4).

	ε (eV)	σ (Å)	a	λ	γ	$\cos\theta_0$	A_L	B_L	p	q	Tol
Mn—O_1—O_1	1.000	1.212	2.175	60.755	1.000	-0.125	9.675	2.899	4	0	0.0

Table 189. SW potential parameters for single-layer 1T-MnO_2 used by LAMMPS [9] as expressed in Eqs. (9) and (10).

We use LAMMPS to perform MD simulations for the mechanical behavior of the single-layer 1T-MnO_2 under uniaxial tension at 1 and 300 K. **Figure 93** shows the stress-strain curve for the tension of a single-layer 1T-MnO_2 of dimension 100 × 100 Å. Periodic boundary conditions are applied in both armchair and zigzag directions. The single-layer 1T-MnO_2 is stretched uniaxially along the armchair or zigzag direction. The stress is calculated without involving the actual thickness of the quasi-two-dimensional structure of the single-layer 1T-MnO_2. The Young's modulus can be obtained by a linear fitting of the stress-strain relation in the small strain range of [0, 0.01]. The Young's modulus is 156.3 and 155.4 N/m along the armchair and zigzag directions, respectively. The Young's modulus is essentially isotropic in the armchair and zigzag directions. The Poisson's ratio from the VFF model and the SW potential is $\nu_{xy} = \nu_{yx} = 0.12$.

There is no available value for nonlinear quantities in the single-layer 1T-MnO_2. We have thus used the nonlinear parameter $B = 0.5d^4$ in Eq. (5), which is close to the value of B in most materials. The value of the third-order nonlinear elasticity D can be extracted by fitting the

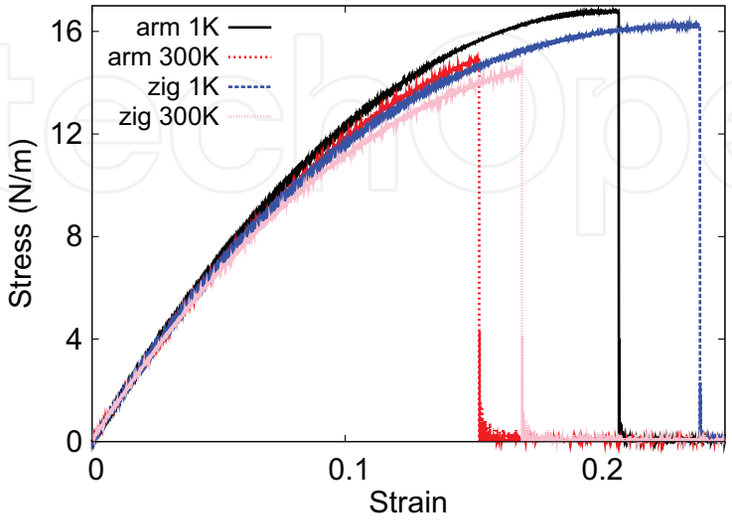

Figure 93. Stress-strain for single-layer 1T-MnO_2 of dimension 100 × 100 Å along the armchair and zigzag directions.

stress-strain relation to the function $\sigma = E\epsilon + \frac{1}{2}D\epsilon^2$ with E as the Young's modulus. The values of D from the present SW potential are -711.7 and -756.1 N/m along the armchair and zigzag directions, respectively. The ultimate stress is about 16.8 N/m at the ultimate strain of 0.21 in the armchair direction at the low temperature of 1 K. The ultimate stress is about 16.2 N/m at the ultimate strain of 0.24 in the zigzag direction at the low temperature of 1 K.

48. 1T-MnS_2

Most existing theoretical studies on the single-layer 1T-MnS_2 are based on the first-principles calculations. In this section, we will develop the SW potential for the single-layer 1T-MnS_2.

The structure for the single-layer 1T-MnS_2 is shown in **Figure 71** (with M = Mn and X = S). Each Mn atom is surrounded by six S atoms. These S atoms are categorized into the top group (e.g., atoms 1, 3, and 5) and bottom group (e.g., atoms 2, 4, and 6). Each S atom is connected to three Mn atoms. The structural parameters are from the first-principles calculations [12], including the lattice constant $a = 3.12$ Å and the bond length $d_{\mathrm{Mn-S}} = 2.27$ Å. The resultant angles are $\theta_{\mathrm{MnSS}} = 86.822^\circ$ with S atoms from the same (top or bottom) group and $\theta_{\mathrm{SMnMn}} = 86.822^\circ$.

Table 190 shows three VFF terms for the single-layer 1T-MnS_2; one of which is the bond stretching interaction shown by Eq. (1), while the other two terms are the angle bending interaction shown by Eq. (2). We note that the angle bending term $K_{\mathrm{Mn-S-S}}$ is for the angle $\theta_{\mathrm{Mn-S-S}}$ with both S atoms from the same (top or bottom) group. These force constant parameters are determined by fitting to the acoustic branches in the phonon dispersion along the ΓM as shown in **Figure 94(a)**. The *ab initio* calculations for the phonon dispersion are from [12]. **Figure 94(b)** shows that the VFF model and the SW potential give exactly the same phonon dispersion, as the SW potential is derived from the VFF model.

The parameters for the two-body SW potential used by GULP are shown in **Table 191**. The parameters for the three-body SW potential used by GULP are shown in **Table 192**. Some representative parameters for the SW potential used by LAMMPS are listed in **Table 193**.

We use LAMMPS to perform MD simulations for the mechanical behavior of the single-layer 1T-MnS_2 under uniaxial tension at 1 and 300 K. **Figure 95** shows the stress-strain curve for the

VFF type	**Bond stretching**	**Angle bending**	
Expression	$\frac{1}{2}K_{\mathrm{Mn-S}}(\Delta r)^2$	$\frac{1}{2}K_{\mathrm{Mn-S-S}}(\Delta\theta)^2$	$\frac{1}{2}K_{\mathrm{S-Mn-Mn}}(\Delta\theta)^2$
Parameter	4.407	2.399	2.399
r_0 or θ_0	2.27	86.822	86.822

The second line gives an explicit expression for each VFF term. The third line is the force constant parameters. Parameters are in the unit of eV/Å^2 for the bond stretching interaction and in the unit of eV for the angle bending interaction. The fourth line gives the initial bond length (in the unit of Å) for the bond stretching interaction and the initial angle (in the unit of degrees) for the angle bending interaction. The angle θ_{ijk} has atom i as the apex.

Table 190. The VFF model for single-layer 1T-MnS_2.

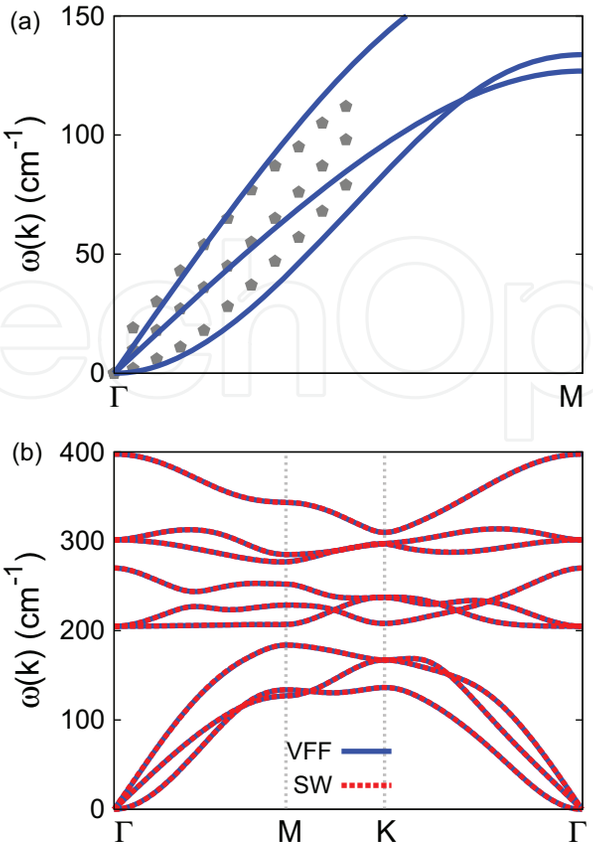

Figure 94. Phonon spectrum for single-layer 1T-MnS_2. (a) Phonon dispersion along the ΓM direction in the Brillouin zone. The results from the VFF model (lines) are comparable with the *ab initio* results (pentagons) from [12]. (b) The phonon dispersion from the SW potential is exactly the same as that from the VFF model.

	A (eV)	ρ (Å)	B (Å^4)	r_{min} (Å)	r_{max} (Å)
Mn—S	3.127	1.111	13.276	0.0	3.064

Table 191. Two-body SW potential parameters for single-layer 1T-MnS_2 used by GULP [8] as expressed in Eq. (3).

	K (eV)	θ_0 (°)	ρ_1 (Å)	ρ_2 (Å)	$r_{min\,12}$ (Å)	$r_{max\,12}$ (Å)	$r_{min\,13}$ (Å)	$r_{max\,13}$ (Å)	$r_{min\,23}$ (Å)	$r_{max\,23}$ (Å)
θ_{Mn-S-S}	19.765	86.822	1.111	1.111	0.0	3.064	0.0	3.064	0.0	4.262
$\theta_{S-Mn-Mn}$	19.765	86.822	1.111	1.111	0.0	3.064	0.0	3.064	0.0	4.262

The angle θ_{ijk} in the first line indicates the bending energy for the angle with atom i as the apex.

Table 192. Three-body SW potential parameters for single-layer 1T-MnS_2 used by GULP [8] as expressed in Eq. (4).

	ϵ (eV)	σ (Å)	a	λ	γ	$\cos\theta_0$	A_L	B_L	p	q	Tol
Mn—S_1—S_1	1.000	1.111	2.757	19.765	1.000	0.055	3.127	8.700	4	0	0.0

Table 193. SW potential parameters for single-layer 1T-MnS_2 used by LAMMPS [9] as expressed in Eqs. (9) and (10).

http://dx.doi.org/10.5772/intechopen.71929

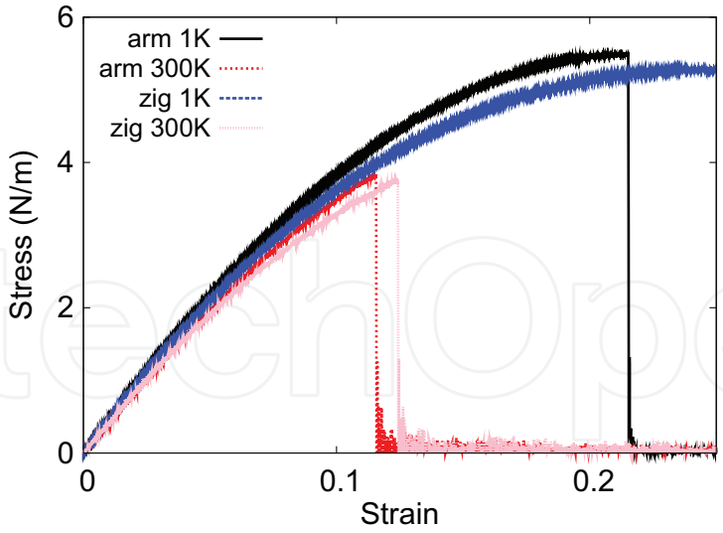

Figure 95. Stress-strain for single-layer 1T-MnS_2 of dimension 100 × 100 Å along the armchair and zigzag directions.

tension of a single-layer 1T-MnS_2 of dimension 100 × 100 Å. Periodic boundary conditions are applied in both armchair and zigzag directions. The single-layer 1T-MnS_2 is stretched uniaxially along the armchair or zigzag direction. The stress is calculated without involving the actual thickness of the quasi-two-dimensional structure of the single-layer 1T-MnS_2. The Young's modulus can be obtained by a linear fitting of the stress-strain relation in the small strain range of [0, 0.01]. The Young's modulus is 47.1 and 46.8 N/m along the armchair and zigzag directions, respectively. The Young's modulus is essentially isotropic in the armchair and zigzag directions. The Poisson's ratio from the VFF model and the SW potential is $\nu_{xy} = \nu_{yx} = 0.15$.

There is no available value for nonlinear quantities in the single-layer 1T-MnS_2. We have thus used the nonlinear parameter $B = 0.5d^4$ in Eq. (5), which is close to the value of B in most materials. The value of the third-order nonlinear elasticity D can be extracted by fitting the stress-strain relation to the function $\sigma = E\epsilon + \frac{1}{2}D\epsilon^2$ with E as the Young's modulus. The values of D from the present SW potential are −193.8 and −210.1 N/m along the armchair and zigzag directions, respectively. The ultimate stress is about 5.5 N/m at the ultimate strain of 0.21 in the armchair direction at the low temperature of 1 K. The ultimate stress is about 5.3 N/m at the ultimate strain of 0.25 in the zigzag direction at the low temperature of 1 K.

49. 1T-$MnSe_2$

Most existing theoretical studies on the single-layer 1T-$MnSe_2$ are based on the first-principles calculations. In this section, we will develop the SW potential for the single-layer 1T-$MnSe_2$.

The structure for the single-layer 1T-$MnSe_2$ is shown in **Figure 71** (with M = Mn and X = Se). Each Mn atom is surrounded by six Se atoms. These Se atoms are categorized into the top group (e.g., atoms 1, 3, and 5) and bottom group (e.g., atoms 2, 4, and 6). Each Se atom is

connected to three Mn atoms. The structural parameters are from the first-principles calculations [12], including the lattice constant $a = 3.27$ Å and the bond length $d_{\mathrm{Mn-Se}} = 2.39$ Å. The resultant angles are $\theta_{\mathrm{MnSeSe}} = 86.330^\circ$ with Se atoms from the same (top or bottom) group and $\theta_{\mathrm{SeMnMn}} = 86.330^\circ$.

Table 194 shows three VFF terms for the single-layer 1T-$MnSe_2$; one of which is the bond stretching interaction shown by Eq. (1), while the other two terms are the angle bending interaction shown by Eq. (2). We note that the angle bending term $K_{\mathrm{Mn-Se-Se}}$ is for the angle $\theta_{\mathrm{Mn-Se-Se}}$ with both Se atoms from the same (top or bottom) group. These force constant parameters are determined by fitting to the acoustic branches in the phonon dispersion along the ΓM as shown in **Figure 96(a)**. The *ab initio* calculations for the phonon dispersion are from [12]. **Figure 96(b)** shows that the VFF model and the SW potential give exactly the same phonon dispersion, as the SW potential is derived from the VFF model.

The parameters for the two-body SW potential used by GULP are shown in **Table 195**. The parameters for the three-body SW potential used by GULP are shown in **Table 196**. Some representative parameters for the SW potential used by LAMMPS are listed in **Table 197**.

We use LAMMPS to perform MD simulations for the mechanical behavior of the single-layer 1T-$MnSe_2$ under uniaxial tension at 1 and 300 K. **Figure 97** shows the stress-strain curve for the tension of a single-layer 1T-$MnSe_2$ of dimension 100 × 100 Å. Periodic boundary conditions are applied in both armchair and zigzag directions. The single-layer 1T-$MnSe_2$ is stretched uniaxially along the armchair or zigzag direction. The stress is calculated without involving the actual thickness of the quasi-two-dimensional structure of the single-layer 1T-$MnSe_2$. The Young's modulus can be obtained by a linear fitting of the stress-strain relation in the small strain range of [0, 0.01]. The Young's modulus is 43.2 and 42.9 N/m along the armchair and zigzag directions, respectively. The Young's modulus is essentially isotropic in the armchair and zigzag directions. The Poisson's ratio from the VFF model and the SW potential is $\nu_{xy} = \nu_{yx} = 0.17$.

There is no available value for nonlinear quantities in the single-layer 1T-$MnSe_2$. We have thus used the nonlinear parameter $B = 0.5d^4$ in Eq. (5), which is close to the value of B in most materials. The value of the third-order nonlinear elasticity D can be extracted by fitting the stress-strain relation to the function $\sigma = E\epsilon + \frac{1}{2}D\epsilon^2$ with E as the Young's modulus. The values

VFF type	Bond stretching	Angle bending	
Expression	$\frac{1}{2}K_{\mathrm{Mn-Se}}(\Delta r)^2$	$\frac{1}{2}K_{\mathrm{Mn-Se-Se}}(\Delta\theta)^2$	$\frac{1}{2}K_{\mathrm{Se-Mn-Mn}}(\Delta\theta)^2$
Parameter	4.407	2.399	2.399
r_0 or θ_0	2.39	86.330	86.330

The second line gives an explicit expression for each VFF term. The third line is the force constant parameters. Parameters are in the unit of eV/Å^2 for the bond stretching interaction and in the unit of eV for the angle bending interaction. The fourth line gives the initial bond length (in the unit of Å) for the bond stretching interaction and the initial angle (in the unit of degrees) for the angle bending interaction. The angle θ_{ijk} has atom i as the apex.

Table 194. The VFF model for single-layer 1T-$MnSe_2$.

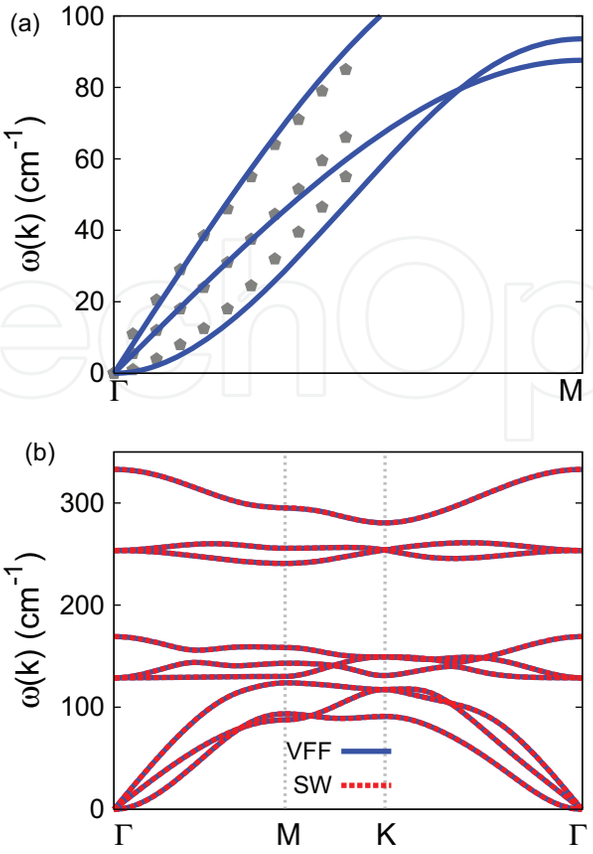

Figure 96. Phonon spectrum for single-layer 1T-$MnSe_2$. (a) Phonon dispersion along the ΓM direction in the Brillouin zone. The results from the VFF model (lines) are comparable with the *ab initio* results (pentagons) from [12]. (b) The phonon dispersion from the SW potential is exactly the same as that from the VFF model.

	A (eV)	ρ (Å)	B (Å^4)	r_{min} (Å)	r_{max} (Å)
Mn—Se	3.422	1.153	16.314	0.0	3.220

Table 195. Two-body SW potential parameters for single-layer 1T-$MnSe_2$ used by GULP [8] as expressed in Eq. (3).

	K (eV)	θ_0 (°)	ρ_1 (Å)	ρ_2 (Å)	$r_{min\,12}$ (Å)	$r_{max\,12}$ (Å)	$r_{min\,13}$ (Å)	$r_{max\,13}$ (Å)	$r_{min\,23}$ (Å)	$r_{max\,23}$ (Å)
$\theta_{Mn-Se-Se}$	19.390	86.330	1.153	1.153	0.0	3.220	0.0	3.220	0.0	4.467
$\theta_{Se-Mn-Mn}$	19.390	86.330	1.153	1.153	0.0	3.220	0.0	3.220	0.0	4.467

The angle θ_{ijk} in the first line indicates the bending energy for the angle with atom i as the apex.

Table 196. Three-body SW potential parameters for single-layer 1T-$MnSe_2$ used by GULP [8] as expressed in Eq. (4).

	ϵ (eV)	σ (Å)	a	λ	γ	$\cos\theta_0$	A_L	B_L	p	q	Tol
$Mn—Se_1—Se_1$	1.000	1.153	2.792	19.390	1.000	0.064	3.422	9.219	4	0	0.0

Table 197. SW potential parameters for single-layer 1T-$MnSe_2$ used by LAMMPS [9] as expressed in Eqs. (9) and (10).

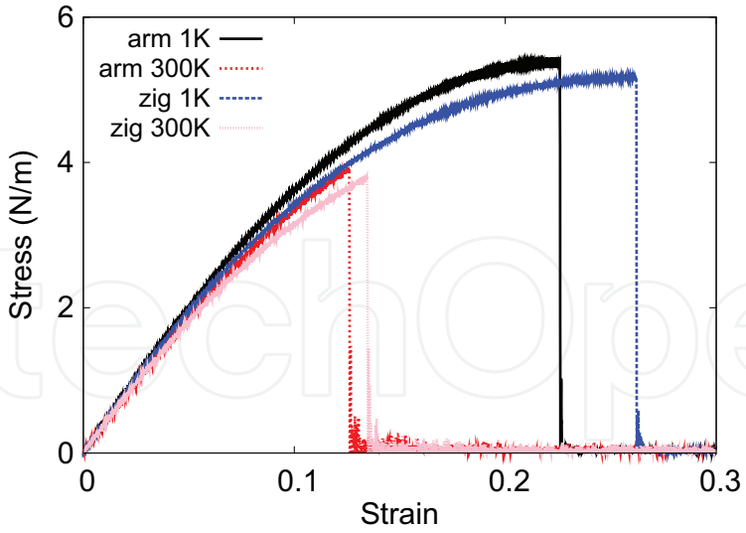

Figure 97. Stress-strain for single-layer 1T-$MnSe_2$ of dimension 100 × 100 Å along the armchair and zigzag directions.

of D from the present SW potential are −163.4 and −179.4 N/m along the armchair and zigzag directions, respectively. The ultimate stress is about 5.4 N/m at the ultimate strain of 0.22 in the armchair direction at the low temperature of 1 K. The ultimate stress is about 5.2 N/m at the ultimate strain of 0.26 in the zigzag direction at the low temperature of 1 K.

50. 1T-$MnTe_2$

Most existing theoretical studies on the single-layer 1T-$MnTe_2$ are based on the first-principles calculations. In this section, we will develop the SW potential for the single-layer 1T-$MnTe_2$.

The structure for the single-layer 1T-$MnTe_2$ is shown in **Figure 71** (with M = Mn and X = Te). Each Mn atom is surrounded by six Te atoms. These Te atoms are categorized into the top group (e.g., atoms 1, 3, and 5) and bottom group (e.g., atoms 2, 4, and 6). Each Te atom is connected to three Mn atoms. The structural parameters are from the first-principles calculations [12], including the lattice constant $a = 3.54$ Å and the bond length $d_{\mathrm{Mn-Te}} = 2.59$ Å. The resultant angles are $\theta_{\mathrm{MnTeTe}} = 86.219^\circ$ with Te atoms from the same (top or bottom) group and $\theta_{\mathrm{TeMnMn}} = 86.219^\circ$.

Table 198 shows three VFF terms for the single-layer 1T-$MnTe_2$; one of which is the bond stretching interaction shown by Eq. (1), while the other two terms are the angle bending interaction shown by Eq. (2). We note that the angle bending term $K_{\mathrm{Mn-Te-Te}}$ is for the angle $\theta_{\mathrm{Mn-Te-Te}}$ with both Se atoms from the same (top or bottom) group. These force constant parameters are determined by fitting to the acoustic branches in the phonon dispersion along the ΓM as shown in **Figure 98(a)**. The *ab initio* calculations for the phonon dispersion are from [12]. **Figure 98(b)** shows that the VFF model and the SW potential give exactly the same phonon dispersion, as the SW potential is derived from the VFF model.

VFF type	Bond stretching	Angle bending	
Expression	$\frac{1}{2}K_{\mathrm{Mn-Te}}(\Delta r)^2$	$\frac{1}{2}K_{\mathrm{Mn-Te-Te}}(\Delta\theta)^2$	$\frac{1}{2}K_{\mathrm{Te-Mn-Mn}}(\Delta\theta)^2$
Parameter	4.407	2.399	2.399
r_0 or θ_0	2.59	86.219	86.219

The second line gives an explicit expression for each VFF term. The third line is the force constant parameters. Parameters are in the unit of eV/Å^2 for the bond stretching interaction and in the unit of eV for the angle bending interaction. The fourth line gives the initial bond length (in the unit of Å) for the bond stretching interaction and the initial angle (in the unit of degrees) for the angle bending interaction. The angle θ_{ijk} has atom i as the apex.

Table 198. The VFF model for single-layer 1T-$MnTe_2$.

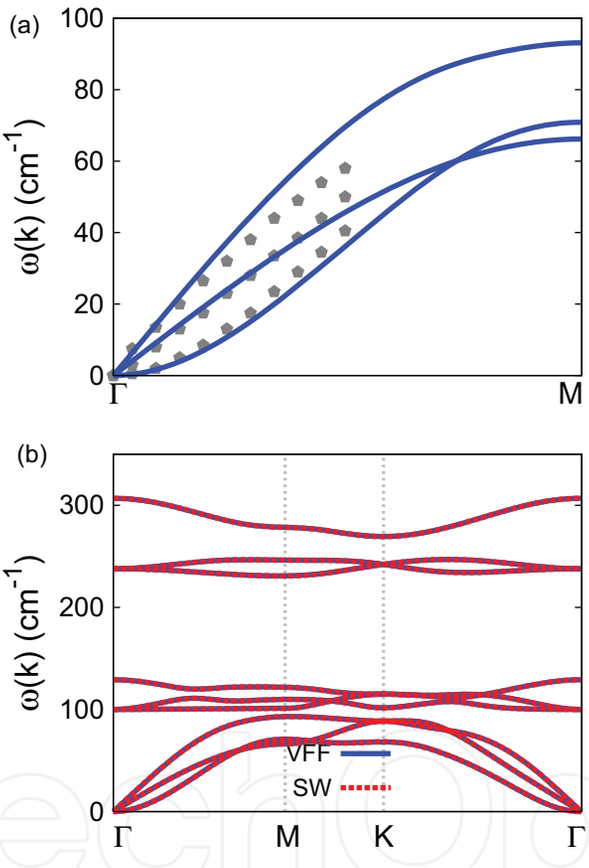

Figure 98. Phonon spectrum for single-layer 1T-$MnTe_2$. (a) Phonon dispersion along the ΓM direction in the Brillouin zone. The results from the VFF model (lines) are comparable with the *ab initio* results (pentagons) from [12]. (b) The phonon dispersion from the SW potential is exactly the same as that from the VFF model.

The parameters for the two-body SW potential used by GULP are shown in **Table 199**. The parameters for the three-body SW potential used by GULP are shown in **Table 200**. Some representative parameters for the SW potential used by LAMMPS are listed in **Table 201**.

We use LAMMPS to perform MD simulations for the mechanical behavior of the single-layer 1T-$MnTe_2$ under uniaxial tension at 1 and 300 K. **Figure 99** shows the stress-strain curve for the tension of a single-layer 1T-$MnTe_2$ of dimension 100 × 100 Å. Periodic boundary conditions are

	A (eV)	ρ (Å)	B (Å^4)	$r_{\min}$ (Å)	$r_{\max}$ (Å)
Mn—Te	4.007	1.246	22.499	0.0	3.488

Table 199. Two-body SW potential parameters for single-layer 1T-$MnTe_2$ used by GULP [8] as expressed in Eq. (3).

	K (eV)	θ_0 (°)	ρ_1 (Å)	ρ_2 (Å)	$r_{\min 12}$ (Å)	$r_{\max 12}$ (Å)	$r_{\min 13}$ (Å)	$r_{\max 13}$ (Å)	$r_{\min 23}$ (Å)	$r_{\max 23}$ (Å)
$\theta_{\text{Mn-Te-Te}}$	19.307	86.219	1.246	1.246	0.0	3.488	0.0	3.488	0.0	4.836
$\theta_{\text{Te-Mn-Mn}}$	19.307	86.219	1.246	1.246	0.0	3.488	0.0	3.488	0.0	4.836

The angle θ_{ijk} in the first line indicates the bending energy for the angle with atom i as the apex.

Table 200. Three-body SW potential parameters for single-layer 1T-$MnTe_2$ used by GULP [8] as expressed in Eq. (4).

	ϵ (eV)	σ (Å)	a	λ	γ	$\cos\theta_0$	A_L	B_L	p	q	Tol
Mn—Te_1—Te_1	1.000	1.246	2.800	19.307	1.000	0.066	4.007	9.340	4	0	0.0

Table 201. SW potential parameters for single-layer 1T-$MnTe_2$ used by LAMMPS [9] as expressed in Eqs. (9) and (10).

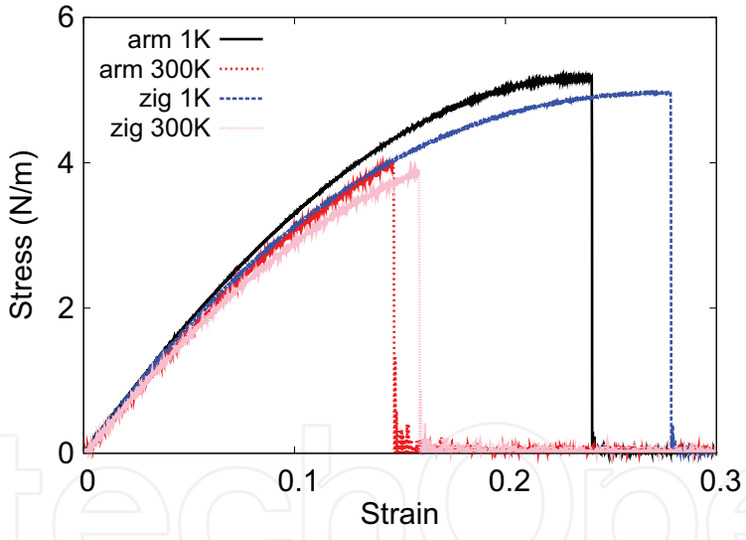

Figure 99. Stress-strain for single-layer 1T-$MnTe_2$ of dimension 100 × 100 Å along the armchair and zigzag directions.

applied in both armchair and zigzag directions. The single-layer 1T-$MnTe_2$ is stretched uniaxially along the armchair or zigzag direction. The stress is calculated without involving the actual thickness of the quasi-two-dimensional structure of the single-layer 1T-$MnTe_2$. The Young's modulus can be obtained by a linear fitting of the stress-strain relation in the small strain range of [0, 0.01]. The Young's modulus is 38.5 and 38.4 N/m along the armchair and zigzag directions, respectively. The Young's modulus is essentially isotropic in the armchair and zigzag directions. The Poisson's ratio from the VFF model and the SW potential is $\nu_{xy} = \nu_{yx} = 0.19$.

There is no available value for nonlinear quantities in the single-layer 1T-$MnTe_2$. We have thus used the nonlinear parameter $B = 0.5d^4$ in Eq. (5), which is close to the value of B in most materials. The value of the third-order nonlinear elasticity D can be extracted by fitting the stress-strain relation to the function $\sigma = E\epsilon + \frac{1}{2}D\epsilon^2$ with E as the Young's modulus. The values of D from the present SW potential are -133.5 and -149.5 N/m along the armchair and zigzag directions, respectively. The ultimate stress is about 5.2 N/m at the ultimate strain of 0.24 in the armchair direction at the low temperature of 1 K. The ultimate stress is about 5.0 N/m at the ultimate strain of 0.28 in the zigzag direction at the low temperature of 1 K.

51. 1T-$CoTe_2$

Most existing theoretical studies on the single-layer 1T-$CoTe_2$ are based on the first-principles calculations. In this section, we will develop the SW potential for the single-layer 1T-$CoTe_2$.

The structure for the single-layer 1T-$CoTe_2$ is shown in **Figure 71** (with M = Co and X = Te). Each Co atom is surrounded by six Te atoms. These Te atoms are categorized into the top group (e.g., atoms 1, 3, and 5) and bottom group (e.g., atoms 2, 4, and 6). Each Te atom is connected to three Co atoms. The structural parameters are from the first-principles calculations [48], including the lattice constant $a = 3.5983$ Å and the bond length $d_{\mathrm{Co-Te}} = 2.5117$ Å, which are derived from the angle $\theta_{\mathrm{TeCoCo}} = 91.5^\circ$. The other angle is $\theta_{\mathrm{CoTeTe}} = 91.5^\circ$ with Te atoms from the same (top or bottom) group.

Table 202 shows three VFF terms for the single-layer 1T-$CoTe_2$; one of which is the bond stretching interaction shown by Eq. (1), while the other two terms are the angle bending interaction shown by Eq. (2). We note that the angle bending term $K_{\mathrm{Co-Te-Te}}$ is for the angle $\theta_{\mathrm{Co-Te-Te}}$ with both Te atoms from the same (top or bottom) group. We find that there are actually only two parameters in the VFF model, so we can determine their value by fitting to the Young's modulus and the Poisson's ratio of the system. The *ab initio* calculations have predicted the Young's modulus to be 59 N/m and the Poisson's ratio as 0.14 [48].

The parameters for the two-body SW potential used by GULP are shown in **Table 203**. The parameters for the three-body SW potential used by GULP are shown in **Table 204**. Some representative parameters for the SW potential used by LAMMPS are listed in **Table 205**.

VFF type	Bond stretching	Angle bending	
Expression	$\frac{1}{2}K_{\mathrm{Co-Te}}(\Delta r)^2$	$\frac{1}{2}K_{\mathrm{Co-Te-Te}}(\Delta\theta)^2$	$\frac{1}{2}K_{\mathrm{Te-Co-Co}}(\Delta\theta)^2$
Parameter	4.726	3.035	3.035
r_0 or θ_0	2.512	91.501	91.501

The second line gives an explicit expression for each VFF term. The third line is the force constant parameters. Parameters are in the unit of eV/Å^2 for the bond stretching interaction and in the unit of eV for the angle bending interaction. The fourth line gives the initial bond length (in the unit of Å) for the bond stretching interaction and the initial angle (in the unit of degrees) for the angle bending interaction. The angle θ_{ijk} has atom i as the apex.

Table 202. The VFF model for single-layer 1T-$CoTe_2$.

	A (eV)	ρ (Å)	B (Å^4)	$r_{\min}$ (Å)	$r_{\max}$ (Å)
Co—Te	4.628	1.402	19.899	0.0	3.450

Table 203. Two-body SW potential parameters for single-layer 1T-$CoTe_2$ used by GULP [8] as expressed in Eq. (3).

	K (eV)	θ_0 (°)	ρ_1 (Å)	ρ_2 (Å)	$r_{\min 12}$ (Å)	$r_{\max 12}$ (Å)	$r_{\min 13}$ (Å)	$r_{\max 13}$ (Å)	$r_{\min 23}$ (Å)	$r_{\max 23}$ (Å)
$\theta_{\text{Co–Te–Te}}$	30.149	91.501	1.402	1.402	0.0	3.450	0.0	3.450	0.0	4.915
$\theta_{\text{Te–Co–Co}}$	30.149	91.501	1.402	1.402	0.0	3.450	0.0	3.450	0.0	4.915

The angle θ_{ijk} in the first line indicates the bending energy for the angle with atom i as the apex.

Table 204. Three-body SW potential parameters for single-layer 1T-$CoTe_2$ used by GULP [8] as expressed in Eq. (4).

	ϵ (eV)	σ (Å)	a	λ	γ	$\cos\theta_0$	A_L	B_L	p	q	Tol
Co—Te_1—Te_1	1.000	1.402	2.461	30.149	1.000	-0.026	4.628	5.151	4	0	0.0

Table 205. SW potential parameters for single-layer 1T-$CoTe_2$ used by LAMMPS [9] as expressed in Eqs. (9) and (10).

We use LAMMPS to perform MD simulations for the mechanical behavior of the single-layer 1T-$CoTe_2$ under uniaxial tension at 1 and 300 K. **Figure 100** shows the stress-strain curve for the tension of a single-layer 1T-$CoTe_2$ of dimension 100 × 100 Å. Periodic boundary conditions are applied in both armchair and zigzag directions. The single-layer 1T-$CoTe_2$ is stretched uniaxially along the armchair or zigzag direction. The stress is calculated without involving the actual thickness of the quasi-two-dimensional structure of the single-layer 1T-$CoTe_2$. The Young's modulus can be obtained by a linear fitting of the stress-strain relation in the small strain range of [0, 0.01]. The Young's modulus is 50.5 and 50.3 N/m along the armchair and zigzag directions, respectively. The Young's modulus is essentially isotropic in the armchair

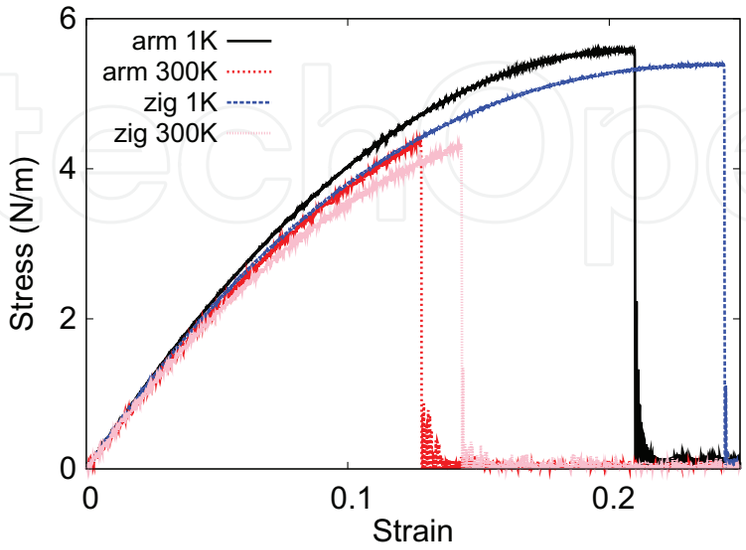

Figure 100. Stress-strain for single-layer 1T-$CoTe_2$ of dimension 100 × 100 Å along the armchair and zigzag directions.

http://dx.doi.org/10.5772/intechopen.71929

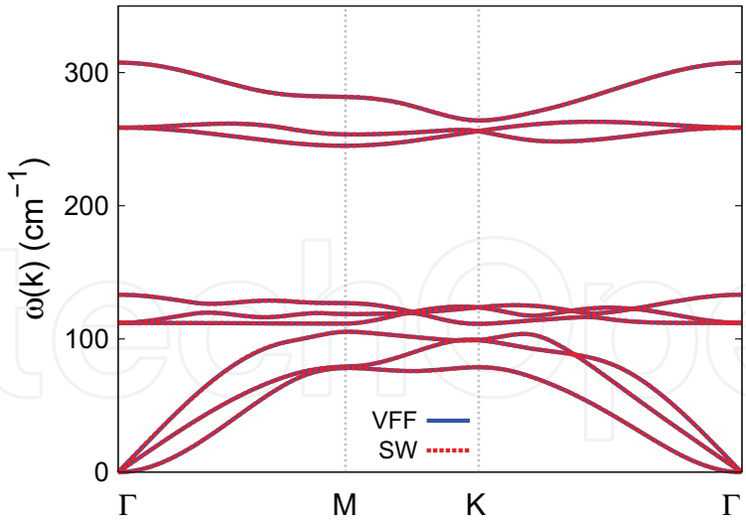

Figure 101. Phonon spectrum for single-layer 1T-$CoTe_2$ along the ΓMKΓ direction in the Brillouin zone. The phonon dispersion from the SW potential is exactly the same as that from the VFF model

and zigzag directions. The Poisson's ratio from the VFF model and the SW potential is $\nu_{xy} = \nu_{yx} = 0.13$. The fitted Young's modulus value is about 10% smaller than the *ab initio* result of 59 N/m [48], as only short-range interactions are considered in the present work. The long-range interactions are ignored, which typically leads to about 10% underestimation for the value of the Young's modulus.

There is no available value for nonlinear quantities in the single-layer 1T-$CoTe_2$. We have thus used the nonlinear parameter $B = 0.5d^4$ in Eq. (5), which is close to the value of B in most materials. The value of the third-order nonlinear elasticity D can be extracted by fitting the stress-strain relation to the function $\sigma = E\epsilon + \frac{1}{2}D\epsilon^2$ with E as the Young's modulus. The values of D from the present SW potential are -221.5 and -238.3 N/m along the armchair and zigzag directions, respectively. The ultimate stress is about 5.6 N/m at the ultimate strain of 0.21 in the armchair direction at the low temperature of 1 K. The ultimate stress is about 5.4 N/m at the ultimate strain of 0.24 in the zigzag direction at the low temperature of 1 K.

Figure 101 shows that the VFF model and the SW potential give exactly the same phonon dispersion, as the SW potential is derived from the VFF model.

52. 1T-NiO_2

Most existing theoretical studies on the single-layer 1T-NiO_2 are based on the first-principles calculations. In this section, we will develop the SW potential for the single-layer 1T-NiO_2.

The structure for the single-layer 1T-NiO_2 is shown in **Figure 71** (with M = Ni and X = O). Each Ni atom is surrounded by six O atoms. These O atoms are categorized into the top group (e.g., atoms 1, 3, and 5) and bottom group (e.g., atoms 2, 4, and 6). Each O atom is connected to three

Ni atoms. The structural parameters are from the first-principles calculations [12], including the lattice constant $a = 2.77$ Å and the bond length $d_{\mathrm{Ni-O}} = 1.84$ Å. The resultant angles are $\theta_{\mathrm{NiOO}} = 97.653^\circ$ with O atoms from the same (top or bottom) group and $\theta_{\mathrm{ONiNi}} = 97.653^\circ$.

Table 206 shows three VFF terms for the single-layer 1T-NiO_2; one of which is the bond stretching interaction shown by Eq. (1), while the other two terms are the angle bending interaction shown by Eq. (2). We note that the angle bending term $K_{\mathrm{Ni-O-O}}$ is for the angle $\theta_{\mathrm{Ni-O-O}}$ with both O atoms from the same (top or bottom) group. These force constant parameters are determined by fitting to the two in-plane acoustic branches in the phonon dispersion along the ΓM as shown in **Figure 102(a)**. The *ab initio* calculations for the phonon dispersion are from [12]. **Figure 102(b)** shows that the VFF model and the SW potential give exactly the same phonon dispersion, as the SW potential is derived from the VFF model.

The parameters for the two-body SW potential used by GULP are shown in **Table 207**. The parameters for the three-body SW potential used by GULP are shown in **Table 208**. Some representative parameters for the SW potential used by LAMMPS are listed in **Table 209**.

We use LAMMPS to perform MD simulations for the mechanical behavior of the single-layer 1T-NiO_2 under uniaxial tension at 1 and 300 K. **Figure 103** shows the stress-strain curve for the tension of a single-layer 1T-NiO_2 of dimension 100×100 Å. Periodic boundary conditions are applied in both armchair and zigzag directions. The single-layer 1T-NiO_2 is stretched uniaxially along the armchair or zigzag direction. The stress is calculated without involving the actual thickness of the quasi-two-dimensional structure of the single-layer 1T-NiO_2. The Young's modulus can be obtained by a linear fitting of the stress-strain relation in the small strain range of [0, 0.01]. The Young's modulus is 163.3 and 162.4 N/m along the armchair and zigzag directions, respectively. The Young's modulus is essentially isotropic in the armchair and zigzag directions. The Poisson's ratio from the VFF model and the SW potential is $\nu_{xy} = \nu_{yx} = 0.12$.

There is no available value for nonlinear quantities in the single-layer 1T-NiO_2. We have thus used the nonlinear parameter $B = 0.5d^4$ in Eq. (5), which is close to the value of B in most materials. The value of the third-order nonlinear elasticity D can be extracted by fitting the stress-strain relation to the function $\sigma = E\epsilon + \frac{1}{2}D\epsilon^2$ with E as the Young's modulus. The values of D from the present SW potential are -748.7 and -796.0 N/m along the armchair and zigzag directions, respectively. The ultimate stress is about 17.4 N/m at the ultimate strain of 0.20 in

VFF type	Bond stretching	Angle bending	
Expression	$\frac{1}{2}K_{\mathrm{Ni-O}}(\Delta r)^2$	$\frac{1}{2}K_{\mathrm{Ni-O-O}}(\Delta\theta)^2$	$\frac{1}{2}K_{\mathrm{O-Ni-Ni}}(\Delta\theta)^2$
Parameter	15.925	4.847	4.847
r_0 or θ_0		97.653	97.653

The third line is the force constant parameters. Parameters are in the unit of eV/Å^2 for the bond stretching interaction and in the unit of eV for the angle bending interaction. The fourth line gives the initial bond length (in the unit of Å) for the bond stretching interaction and the initial angle (in the unit of degrees) for the angle bending interaction. The angle θ_{ijk} has atom i as the apex.

Table 206. The VFF model for single-layer 1T-NiO_2. The second line gives an explicit expression for each VFF term.

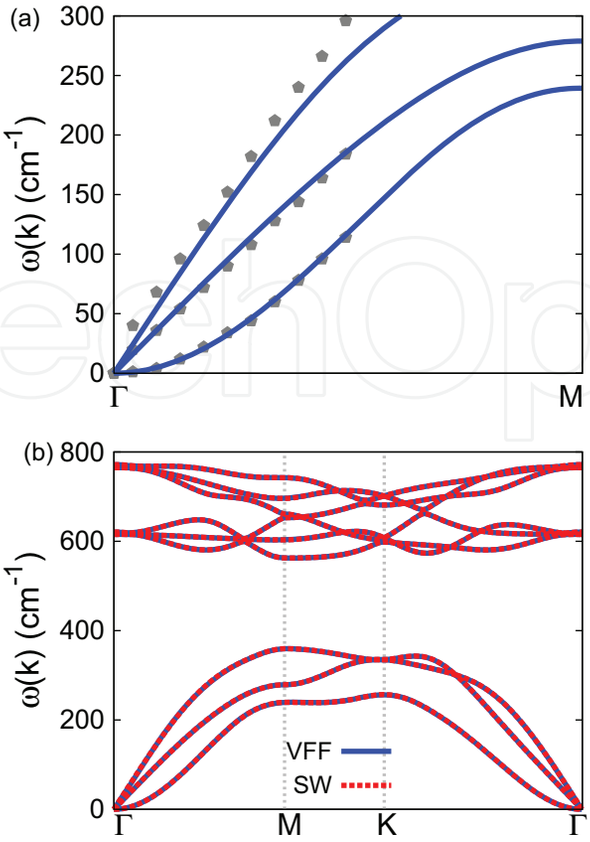

Figure 102. Phonon spectrum for single-layer 1T-NiO_2. (a) Phonon dispersion along the ΓM direction in the Brillouin zone. The results from the VFF model (lines) are comparable with the *ab initio* results (pentagons) from [12]. (b) The phonon dispersion from the SW potential is exactly the same as that from the VFF model.

	A (eV)	ρ(Å)	B (Å^4)	r_{min} (Å)	r_{max} (Å)
Ni-O	9.709	1.199	5.731	0.0	2.583

Table 207. Two-body SW potential parameters for single-layer 1T-NiO_2 used by GULP [8] as expressed in Eq. (3).

	K (eV)	θ_0 (°)	ρ_1 (Å)	ρ_2 (Å)	$r_{min\,12}$ (Å)	$r_{max\,12}$ (Å)	$r_{min\,13}$ (Å)	$r_{max\,13}$ (Å)	$r_{min\,23}$ (Å)	$r_{max\,23}$ (Å)
θ_{Ni-O-O}	62.317	97.653	1.199	1.199	0.0	2.583	0.0	2.583	0.0	3.784
$\theta_{O-Ni-Ni}$	62.317	97.653	1.199	1.199	0.0	2.583	0.0	2.583	0.0	3.784

The angle θ_{ijk} in the first line indicates the bending energy for the angle with atom i as the apex.

Table 208. Three-body SW potential parameters for single-layer 1T-NiO_2 used by GULP [8] as expressed in Eq. (4).

	ϵ (eV)	σ (Å)	a	λ	γ	$\cos\theta_0$	A_L	B_L	p	q	Tol
Ni—O_1—O_1	1.000	1.199	2.154	62.317	1.000	-0.133	9.709	2.772	4	0	0.0

Table 209. SW potential parameters for single-layer 1T-NiO_2 used by LAMMPS [9] as expressed in Eqs. (9) and (10).

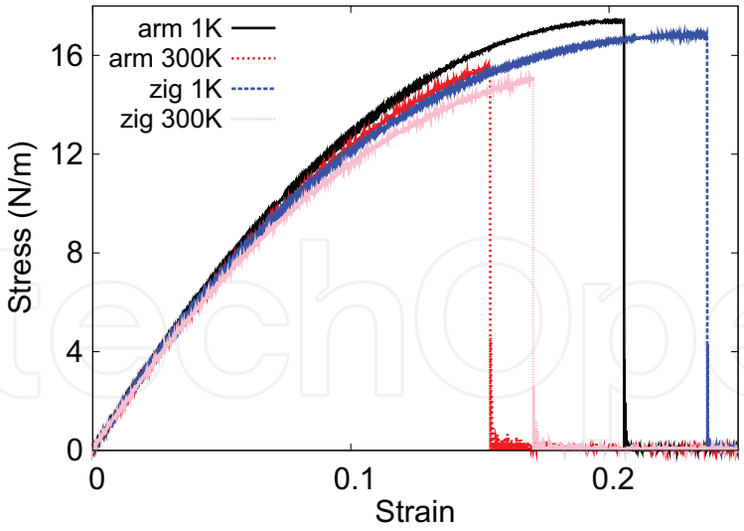

Figure 103. Stress-strain for single-layer 1T-NiO_2 of dimension 100 × 100 Å along the armchair and zigzag directions.

the armchair direction at the low temperature of 1 K. The ultimate stress is about 16.8 N/m at the ultimate strain of 0.24 in the zigzag direction at the low temperature of 1 K.

53. 1T-NiS_2

Most existing theoretical studies on the single-layer 1T-NiS_2 are based on the first-principles calculations. In this section, we will develop the SW potential for the single-layer 1T-NiS_2.

The structure for the single-layer 1T-NiS_2 is shown in **Figure 71** (with M = Ni and X = S). Each Ni atom is surrounded by six S atoms. These S atoms are categorized into the top group (e.g., atoms 1, 3, and 5) and bottom group (e.g., atoms 2, 4, and 6). Each S atom is connected to three Ni atoms. The structural parameters are from the first-principles calculations [48], including the lattice constant $a = 3.3174$ Å and the bond length $d_{\mathrm{Ni-S}} = 2.2320$ Å, which are derived from the angle $\theta_{\mathrm{SNiNi}} = 96^\circ$. The other angle is $\theta_{\mathrm{NiSS}} = 96^\circ$ with S atoms from the same (top or bottom) group.

Table 210 shows three VFF terms for the single-layer 1T-NiS_2; one of which is the bond stretching interaction shown by Eq. (1), while the other two terms are the angle bending

VFF type	Bond stretching	Angle bending	
Expression	$\frac{1}{2}K_{\mathrm{Ni-S}}(\Delta r)^2$	$\frac{1}{2}K_{\mathrm{Ni-S-S}}(\Delta\theta)^2$	$\frac{1}{2}K_{\mathrm{S-Ni-Ni}}(\Delta\theta)^2$
Parameter	9.385	2.952	2.952
r_0 or θ_0	2.232	96.000	96.000

The third line is the force constant parameters. Parameters are in the unit of eV/Å^2 for the bond stretching interaction and in the unit of eV for the angle bending interaction. The fourth line gives the initial bond length (in the unit of Å) for the bond stretching interaction and the initial angle (in the unit of degrees) for the angle bending interaction. The angle θ_{ijk} has atom i as the apex.

Table 210. The VFF model for single-layer 1T-NiS_2. The second line gives an explicit expression for each VFF term.

interaction shown by Eq. (2). We note that the angle bending term $K_{\mathrm{Ni-S-S}}$ is for the angle $\theta_{\mathrm{Ni-S-S}}$ with both S atoms from the same (top or bottom) group. These force constant parameters are determined by fitting to the two in-plane acoustic branches in the phonon dispersion along the ΓM as shown in **Figure 104(a)**. The *ab initio* calculations for the phonon dispersion are from [12]. **Figure 104(b)** shows that the VFF model and the SW potential give exactly the same phonon dispersion, as the SW potential is derived from the VFF model.

The parameters for the two-body SW potential used by GULP are shown in **Table 211**. The parameters for the three-body SW potential used by GULP are shown in **Table 212**. Some representative parameters for the SW potential used by LAMMPS are listed in **Table 213**.

We use LAMMPS to perform MD simulations for the mechanical behavior of the single-layer 1T-NiS_2 under uniaxial tension at 1 and 300 K. **Figure 105** shows the stress-strain curve for the tension of a single-layer 1T-NiS_2 of dimension 100 × 100 Å. Periodic boundary conditions are

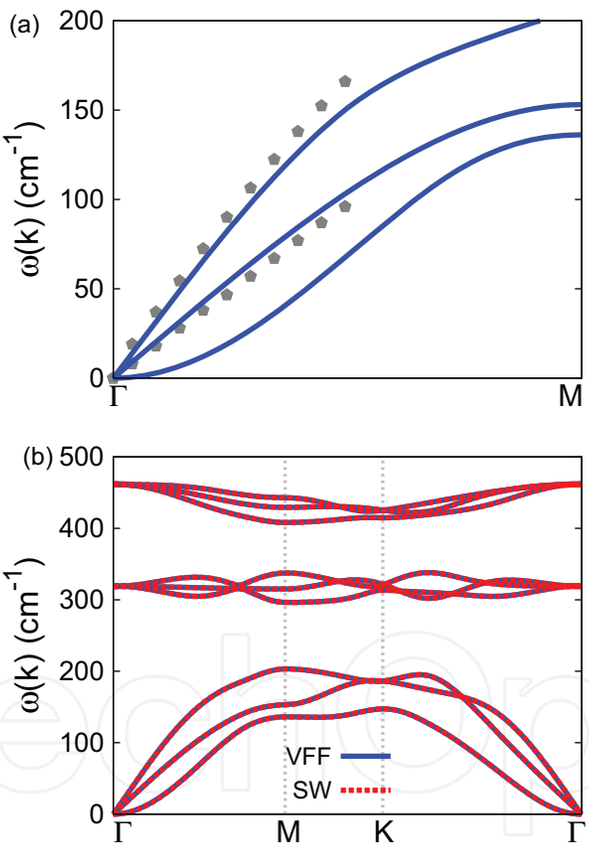

Figure 104. Phonon spectrum for single-layer 1T-NiS_2. (a) Phonon dispersion along the ΓM direction in the Brillouin zone. The results from the VFF model (lines) are comparable with the *ab initio* results (pentagons) from [12]. (b) The phonon dispersion from the SW potential is exactly the same as that from the VFF model.

	A (eV)	ρ(Å)	B (Å^4)	r_{min} (Å)	r_{max} (Å)
Ni-S	8.098	1.398	12.409	0.0	3.115

Table 211. Two-body SW potential parameters for single-layer 1T-NiS_2 used by GULP [8] as expressed in Eq. (3).

	K (eV)	θ_0 (°)	ρ_1 (Å)	ρ_2 (Å)	$r_{\min 12}$ (Å)	$r_{\max 12}$ (Å)	$r_{\min 13}$ (Å)	$r_{\max 13}$ (Å)	$r_{\min 23}$ (Å)	$r_{\max 23}$ (Å)
$\theta_{\text{Ni–S–S}}$	35.372	96.000	1.398	1.398	0.0	3.115	0.0	3.115	0.0	4.532
$\theta_{\text{S–Ni–Ni}}$	35.372	96.000	1.398	1.398	0.0	3.115	0.0	3.115	0.0	4.532

The angle θ_{ijk} in the first line indicates the bending energy for the angle with atom i as the apex.

Table 212. Three-body SW potential parameters for single-layer 1T-NiS_2 used by GULP [8] as expressed in Eq. (4).

	ϵ (eV)	σ (Å)	a	λ	γ	$\cos\theta_0$	A_L	B_L	p	q	Tol
Ni—S_1—S_1	1.000	1.398	2.228	35.372	1.000	-0.105	8.098	3.249	4	0	0.0

Table 213. SW potential parameters for single-layer 1T-NiS_2 used by LAMMPS [9] as expressed in Eqs. (9) and (10).

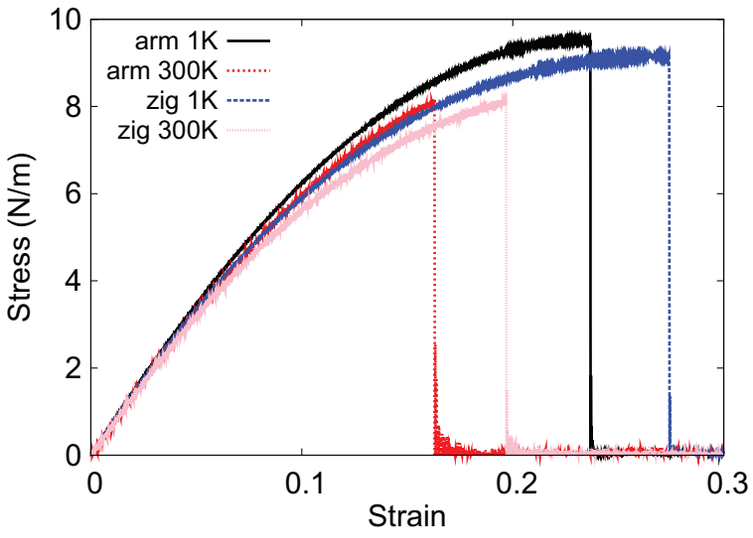

Figure 105. Stress-strain for single-layer 1T-NiS_2 of dimension 100 × 100 Å along the armchair and zigzag directions.

applied in both armchair and zigzag directions. The single-layer 1T-NiS_2 is stretched uniaxially along the armchair or zigzag direction. The stress is calculated without involving the actual thickness of the quasi-two-dimensional structure of the single-layer 1T-NiS_2. The Young's modulus can be obtained by a linear fitting of the stress-strain relation in the small strain range of [0, 0.01]. The Young's modulus is 74.2 and 73.9 N/m along the armchair and zigzag directions, respectively. The Young's modulus is essentially isotropic in the armchair and zigzag directions. The Poisson's ratio from the VFF model and the SW potential is $\nu_{xy} = \nu_{yx} = 0.17$.

There is no available value for nonlinear quantities in the single-layer 1T-NiS_2. We have thus used the nonlinear parameter $B = 0.5d^4$ in Eq. (5), which is close to the value of B in most materials. The value of the third-order nonlinear elasticity D can be extracted by fitting the stress-strain relation to the function $\sigma = E\epsilon + \frac{1}{2}D\epsilon^2$ with E as the Young's modulus. The values of D from the present SW potential are -274.5 and -301.4 N/m along the armchair and zigzag directions, respectively. The ultimate stress is about 9.5 N/m at the ultimate strain of 0.23 in the

armchair direction at the low temperature of 1 K. The ultimate stress is about 9.2 N/m at the ultimate strain of 0.27 in the zigzag direction at the low temperature of 1 K.

54. 1T-$NiSe_2$

Most existing theoretical studies on the single-layer 1T-$NiSe_2$ are based on the first-principles calculations. In this section, we will develop the SW potential for the single-layer 1T-$NiSe_2$.

The structure for the single-layer 1T-$NiSe_2$ is shown in **Figure 71** (with M = Ni and X = Se). Each Ni atom is surrounded by six Se atoms. These Se atoms are categorized into the top group (e.g., atoms 1, 3, and 5) and bottom group (e.g., atoms 2, 4, and 6). Each Se atom is connected to three Ni atoms. The structural parameters are from the first-principles calculations [48], including the lattice constant $a = 3.4712$ Å and the bond length $d_{\mathrm{Ni-Se}} = 2.3392$ Å, which are derived from the angle $\theta_{\mathrm{SeNiNi}} = 95.8^\circ$. The other angle is $\theta_{\mathrm{NiSeSe}} = 95.8^\circ$ with Se atoms from the same (top or bottom) group.

Table 214 shows three VFF terms for the single-layer 1T-$NiSe_2$; one of which is the bond stretching interaction shown by Eq. (1), while the other two terms are the angle bending interaction shown by Eq. (2). We note that the angle bending term $K_{\mathrm{Ni-Se-Se}}$ is for the angle $\theta_{\mathrm{Ni-Se-Se}}$ with both Se atoms from the same (top or bottom) group. These force constant parameters are determined by fitting to the two in-plane acoustic branches in the phonon dispersion along the ΓM as shown in **Figure 106(a)**. The *ab initio* calculations for the phonon dispersion are from [12]. **Figure 106(b)** shows that the VFF model and the SW potential give exactly the same phonon dispersion, as the SW potential is derived from the VFF model.

The parameters for the two-body SW potential used by GULP are shown in **Table 215**. The parameters for the three-body SW potential used by GULP are shown in **Table 216**. Some representative parameters for the SW potential used by LAMMPS are listed in **Table 217**.

We use LAMMPS to perform MD simulations for the mechanical behavior of the single-layer 1T-$NiSe_2$ under uniaxial tension at 1 and 300 K. **Figure 107** shows the stress-strain curve for the tension of a single-layer 1T-$NiSe_2$ of dimension 100 × 100 Å. Periodic boundary conditions are applied in both armchair and zigzag directions. The single-layer 1T-$NiSe_2$ is stretched uniaxially along the armchair or zigzag direction. The stress is calculated without involving

VFF type	Bond stretching	Angle bending	
Expression	$\frac{1}{2}K_{\mathrm{Ni-Se}}(\Delta r)^2$	$\frac{1}{2}K_{\mathrm{Ni-Se-Se}}(\Delta\theta)^2$	$\frac{1}{2}K_{\mathrm{Se-Ni-Ni}}(\Delta\theta)^2$
Parameter	8.814	3.149	3.149
r_0 or θ_0	2.339	95.798	95.798

The second line gives an explicit expression for each VFF term. The third line is the force constant parameters. Parameters are in the unit of eV/Å^2 for the bond stretching interaction and in the unit of eV for the angle bending interaction. The fourth line gives the initial bond length (in the unit of Å) for the bond stretching interaction and the initial angle (in the unit of degrees) for the angle bending interaction. The angle θ_{ijk} has atom i as the apex.

Table 214. The VFF model for single-layer 1T-$NiSe_2$.

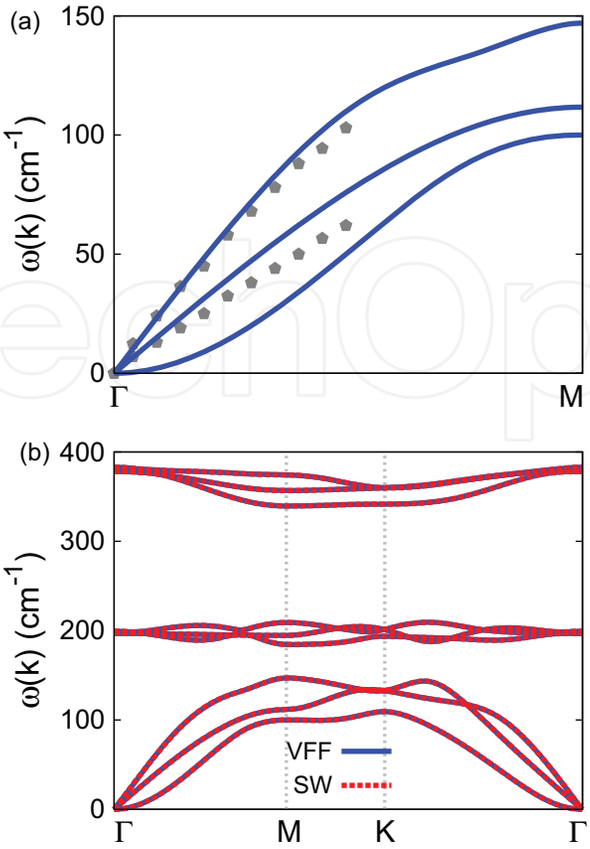

Figure 106. Phonon spectrum for single-layer 1T-$NiSe_2$. (a) Phonon dispersion along the ΓM direction in the Brillouin zone. The results from the VFF model (lines) are comparable with the *ab initio* results (pentagons) from [12]. (b) The phonon dispersion from the SW potential is exactly the same as that from the VFF model.

	A (eV)	ρ (Å)	B (Å^4)	r_{min} (Å)	r_{max} (Å)
Ni—Se	8.313	1.458	14.971	0.0	3.263

Table 215. Two-body SW potential parameters for single-layer 1T-$NiSe_2$ used by GULP [8] as expressed in Eq. (3).

	K (eV)	θ_0 (°)	ρ_1 (Å)	ρ_2 (Å)	$r_{min\,12}$ (Å)	$r_{max\,12}$ (Å)	$r_{min\,13}$ (Å)	$r_{max\,13}$ (Å)	$r_{min\,23}$ (Å)	$r_{max\,23}$ (Å)
$\theta_{Ni-Se-Se}$	37.407	95.798	1.458	1.458	0.0	3.263	0.0	3.263	0.0	4.742
$\theta_{Se-Ni-Ni}$	37.407	95.798	1.458	1.458	0.0	3.263	0.0	3.263	0.0	4.742

The angle θ_{ijk} in the first line indicates the bending energy for the angle with atom i as the apex.

Table 216. Three-body SW potential parameters for single-layer 1T-$NiSe_2$ used by GULP [8] as expressed in Eq. (4).

	ϵ (eV)	σ (Å)	a	λ	γ	$\cos\theta_0$	A_L	B_L	p	q	Tol
$Ni—Se_1—Se_1$	1.000	1.458	2.238	37.407	1.000	-0.101	8.313	3.315	4	0	0.0

Table 217. SW potential parameters for single-layer 1T-$NiSe_2$ used by LAMMPS [9] as expressed in Eqs. (9) and (10).

http://dx.doi.org/10.5772/intechopen.71929

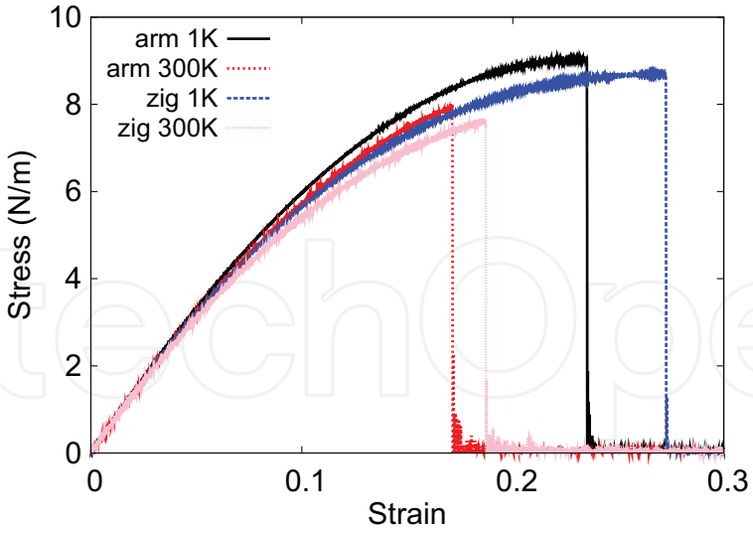

Figure 107. Stress-strain for single-layer 1T-$NiSe_2$ of dimension 100 × 100 Å along the armchair and zigzag directions.

the actual thickness of the quasi-two-dimensional structure of the single-layer 1T-$NiSe_2$. The Young's modulus can be obtained by a linear fitting of the stress-strain relation in the small strain range of [0, 0.01]. The Young's modulus is 70.9 and 70.6 N/m along the armchair and zigzag directions, respectively. The Young's modulus is essentially isotropic in the armchair and zigzag directions. The Poisson's ratio from the VFF model and the SW potential is $\nu_{xy} = \nu_{yx} = 0.17$.

There is no available value for nonlinear quantities in the single-layer 1T-$NiSe_2$. We have thus used the nonlinear parameter $B = 0.5d^4$ in Eq. (5), which is close to the value of B in most materials. The value of the third-order nonlinear elasticity D can be extracted by fitting the stress-strain relation to the function $\sigma = E\epsilon + \frac{1}{2}D\epsilon^2$ with E as the Young's modulus. The values of D from the present SW potential are −263.7 and −289.5 N/m along the armchair and zigzag directions, respectively. The ultimate stress is about 9.0 N/m at the ultimate strain of 0.23 in the armchair direction at the low temperature of 1 K. The ultimate stress is about 8.7 N/m at the ultimate strain of 0.27 in the zigzag direction at the low temperature of 1 K.

55. 1T-$NiTe_2$

Most existing theoretical studies on the single-layer 1T-$NiTe_2$ are based on the first-principles calculations. In this section, we will develop the SW potential for the single-layer 1T-$NiTe_2$.

The structure for the single-layer 1T-$NiTe_2$ is shown in **Figure 71** (with M = Ni and X = Te). Each Ni atom is surrounded by six Te atoms. These Te atoms are categorized into the top group (e.g., atoms 1, 3, and 5) and bottom group (e.g., atoms 2, 4, and 6). Each Te atom is connected to three Ni atoms. The structural parameters are from the first-principles calculations [48], including the lattice constant $a = 3.7248$ Å and the bond length $d_{\mathrm{Ni-Te}} = 2.5321$ Å,

which are derived from the angle $\theta_{\mathrm{TeNiNi}} = 94.7^{\circ}$. The other angle is $\theta_{\mathrm{NiTeTe}} = 94.7^{\circ}$ with Te atoms from the same (top or bottom) group.

Table 218 shows three VFF terms for the single-layer 1T-$NiTe_2$; one of which is the bond stretching interaction shown by Eq. (1), while the other two terms are the angle bending interaction shown by Eq. (2). We note that the angle bending term $K_{\mathrm{Ni-Te-Te}}$ is for the angle $\theta_{\mathrm{Ni-Te-Te}}$ with both Te atoms from the same (top or bottom) group. We find that there are actually only two parameters in the VFF model, so we can determine their value by fitting to the Young's modulus and the Poisson's ratio of the system. The *ab initio* calculations have predicted the Young's modulus to be 44 N/m and the Poisson's ratio as 0.14 [48].

The parameters for the two-body SW potential used by GULP are shown in **Table 219**. The parameters for the three-body SW potential used by GULP are shown in **Table 220**. Some representative parameters for the SW potential used by LAMMPS are listed in **Table 221**.

VFF type	Bond stretching	Angle bending	
Expression	$\frac{1}{2}K_{\mathrm{Ni-Te}}(\Delta r)^2$	$\frac{1}{2}K_{\mathrm{Ni-Te-Te}}(\Delta\theta)^2$	$\frac{1}{2}K_{\mathrm{Te-Ni-Ni}}(\Delta\theta)^2$
Parameter	4.230	2.429	2.429
r_0 or θ_0	2.532	94.702	94.702
or θ_0	2.635	95.999	95.999

The second line gives an explicit expression for each VFF term. The third line is the force constant parameters. Parameters are in the unit of eV/Å^2 for the bond stretching interaction and in the unit of eV for the angle bending interaction. The fourth line gives the initial bond length (in the unit of Å) for the bond stretching interaction and the initial angle (in the unit of degrees) for the angle bending interaction. The angle θ_{ijk} has atom i as the apex.

Table 218. The VFF model for single-layer 1T-$NiTe_2$.

	A (eV)	ρ (Å)	B (Å^4)	r_{min} (Å)	r_{max} (Å)
Ni—Te	4.554	1.536	20.554	0.0	3.518

Table 219. Two-body SW potential parameters for single-layer 1T-$NiTe_2$ used by GULP [8] as expressed in Eq. (3).

	K (eV)	θ_0 (°)	ρ_1 (Å)	ρ_2 (Å)	$r_{\mathrm{min}\,12}$ (Å)	$r_{\mathrm{max}\,12}$ (Å)	$r_{\mathrm{min}\,13}$ (Å)	$r_{\mathrm{max}\,13}$ (Å)	$r_{\mathrm{min}\,23}$ (Å)	$r_{\mathrm{max}\,23}$ (Å)
$\theta_{\mathrm{Ni-Te-Te}}$	27.553	94.702	1.536	1.536	0.0	3.518	0.0	3.518	0.0	5.088
$\theta_{\mathrm{Te-Ni-Ni}}$	27.553	94.702	1.536	1.536	0.0	3.518	0.0	3.518	0.0	5.088

The angle θ_{ijk} in the first line indicates the bending energy for the angle with atom i as the apex.

Table 220. Three-body SW potential parameters for single-layer 1T-$NiTe_2$ used by GULP [8] as expressed in Eq. (4).

	ϵ (eV)	σ (Å)	a	λ	γ	$\cos\theta_0$	A_L	B_L	p	q	Tol
Ni—Te_1—Te_1	1.000	1.536	2.291	27.553	1.000	−0.082	4.554	3.696	4	0	0.0

Table 221. SW potential parameters for single-layer 1T-$NiTe_2$ used by LAMMPS [9] as expressed in Eqs. (9) and (10).

http://dx.doi.org/10.5772/intechopen.71929

We use LAMMPS to perform MD simulations for the mechanical behavior of the single-layer 1T-$NiTe_2$ under uniaxial tension at 1 and 300 K. **Figure 108** shows the stress-strain curve for the tension of a single-layer 1T-$NiTe_2$ of dimension 100 × 100 Å. Periodic boundary conditions are applied in both armchair and zigzag directions. The single-layer 1T-$NiTe_2$ is stretched uniaxially along the armchair or zigzag direction. The stress is calculated without involving the actual thickness of the quasi-two-dimensional structure of the single-layer 1T-$NiTe_2$. The Young's modulus can be obtained by a linear fitting of the stress-strain relation in the small strain range of [0, 0.01]. The Young's modulus is 42.6 and 42.4 N/m along the armchair and zigzag directions, respectively. The Young's modulus is essentially isotropic in the armchair

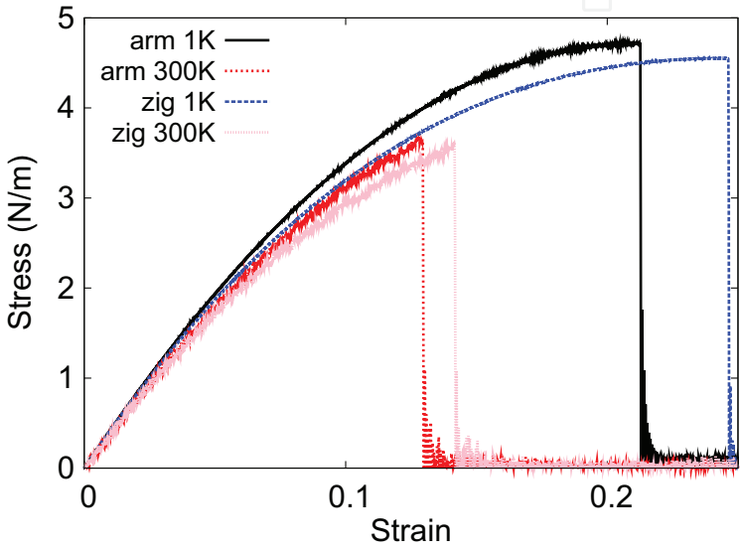

Figure 108. Stress-strain for single-layer 1T-$NiTe_2$ of dimension 100 × 100 Å along the armchair and zigzag directions.

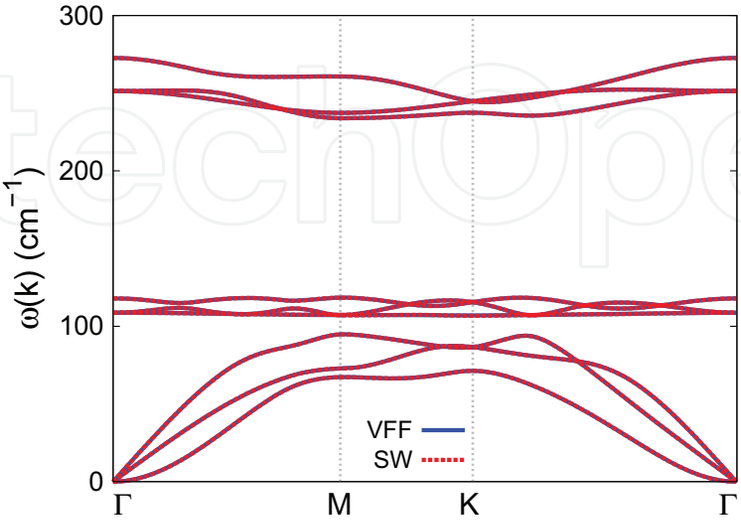

Figure 109. Phonon spectrum for single-layer 1T-$NiTe_2$ along the ΓMKΓ direction in the Brillouin zone. The phonon dispersion from the SW potential is exactly the same as that from the VFF model.

and zigzag directions. The Poisson's ratio from the VFF model and the SW potential is $\nu_{xy} = \nu_{yx} = 0.14$.

There is no available value for nonlinear quantities in the single-layer 1T-$NiTe_2$. We have thus used the nonlinear parameter $B = 0.5d^4$ in Eq. (5), which is close to the value of B in most materials. The value of the third-order nonlinear elasticity D can be extracted by fitting the stress-strain relation to the function $\sigma = E\epsilon + \frac{1}{2}D\epsilon^2$ with E as the Young's modulus. The values of D from the present SW potential are -187.6 and -200.6 N/m along the armchair and zigzag directions, respectively. The ultimate stress is about 4.7 N/m at the ultimate strain of 0.21 in the armchair direction at the low temperature of 1 K. The ultimate stress is about 4.6 N/m at the ultimate strain of 0.24 in the zigzag direction at the low temperature of 1 K.

Figure 109 shows that the VFF model and the SW potential give exactly the same phonon dispersion, as the SW potential is derived from the VFF model.

56. 1T-ZrS_2

Most existing theoretical studies on the single-layer 1T-ZrS_2 are based on the first-principles calculations. In this section, we will develop the SW potential for the single-layer 1T-ZrS_2.

The structure for the single-layer 1T-ZrS_2 is shown in **Figure 71** (with M = Zr and X = S). Each Zr atom is surrounded by six S atoms. These S atoms are categorized into the top group (e.g., atoms 1, 3, and 5) and bottom group (e.g., atoms 2, 4, and 6). Each S atom is connected to three Zr atoms. The structural parameters are from the first-principles calculations [49], including the lattice constant $a = 3.690$ Å and the bond length $d_{\mathrm{Zr-S}} = 2.58$ Å. The resultant angles are $\theta_{\mathrm{ZrSS}} = 91.305^\circ$ with S atoms from the same (top or bottom) group and $\theta_{\mathrm{SZrZr}} = 91.305^\circ$.

Table 222 shows three VFF terms for the single-layer 1T-ZrS_2; one of which is the bond stretching interaction shown by Eq. (1), while the other two terms are the angle bending interaction shown by Eq. (2). We note that the angle bending term $K_{\mathrm{Zr-S-S}}$ is for the angle $\theta_{\mathrm{Zr-S-S}}$ with both S atoms from the same (top or bottom) group. These force constant parameters are determined by fitting to the three acoustic branches in the phonon dispersion along the ΓM as shown in **Figure 110(a)**. The *ab initio* calculations for the phonon dispersion are

VFF type	Bond stretching	Angle bending	
Expression	$\frac{1}{2}K_{\mathrm{Zr-S}}(\Delta r)^2$	$\frac{1}{2}K_{\mathrm{Zr-S-S}}(\Delta\theta)^2$	$\frac{1}{2}K_{\mathrm{S-Zr-Zr}}(\Delta\theta)^2$
Parameter	7.930	4.283	4.283
r_0 or θ_0	2.580	91.305	91.305

The second line gives an explicit expression for each VFF term. The third line is the force constant parameters. Parameters are in the unit of eV/Å^2 for the bond stretching interaction and in the unit of eV for the angle bending interaction. The fourth line gives the initial bond length (in the unit of Å) for the bond stretching interaction and the initial angle (in the unit of degrees) for the angle bending interaction. The angle θ_{ijk} has atom i as the apex.

Table 222. The VFF model for single-layer 1T-ZrS_2.

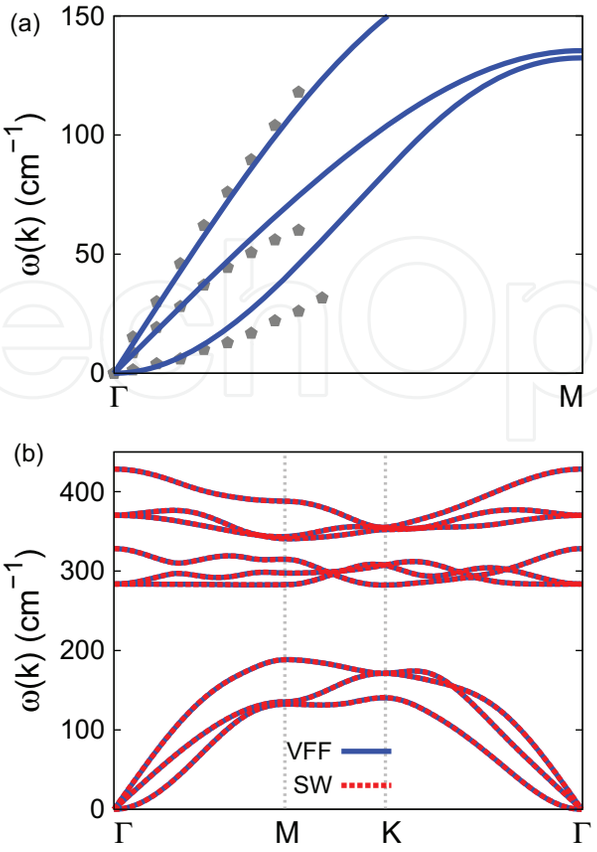

Figure 110. Phonon spectrum for single-layer 1T-ZrS_2. (a) Phonon dispersion along the ΓM direction in the Brillouin zone. The results from the VFF model (lines) are comparable with the experiment data (pentagons) from [38]. (b) The phonon dispersion from the SW potential is exactly the same as that from the VFF model.

from [38]. Similar phonon dispersion can also be found in other *ab initio* calculations [34]. **Figure 110(b)** shows that the VFF model and the SW potential give exactly the same phonon dispersion, as the SW potential is derived from the VFF model.

The parameters for the two-body SW potential used by GULP are shown in **Table 223**. The parameters for the three-body SW potential used by GULP are shown in **Table 224**. Some representative parameters for the SW potential used by LAMMPS are listed in **Table 225**.

We use LAMMPS to perform MD simulations for the mechanical behavior of the single-layer 1T-ZrS_2 under uniaxial tension at 1 and 300 K. **Figure 111** shows the stress-strain curve for the tension of a single-layer 1T-ZrS_2 of dimension 100 × 100 Å. Periodic boundary conditions are applied in both armchair and zigzag directions. The single-layer 1T-ZrS_2 is stretched uniaxially along the armchair or zigzag direction. The stress is calculated without involving the actual thickness of the quasi-two-dimensional structure of the single-layer 1T-ZrS_2. The Young's

	A (eV)	ρ (Å)	B (Å^4)	r_{min} (Å)	r_{max} (Å)
Zr—S	8.149	1.432	22.154	0.0	3.541

Table 223. Two-body SW potential parameters for single-layer 1T-ZrS_2 used by GULP [8] as expressed in Eq. (3).

	K (eV)	θ_0 (°)	ρ_1 (Å)	ρ_2 (Å)	$r_{\min 12}$ (Å)	$r_{\max 12}$ (Å)	$r_{\min 13}$ (Å)	$r_{\max 13}$ (Å)	$r_{\min 23}$ (Å)	$r_{\max 23}$ (Å)
$\theta_{\text{Zr–S–S}}$	42.170	91.305	1.432	1.432	0.0	3.541	0.0	3.541	0.0	5.041
$\theta_{\text{S–Zr–Zr}}$	42.170	91.305	1.432	1.432	0.0	3.541	0.0	3.541	0.0	5.041

The angle θ_{ijk} in the first line indicates the bending energy for the angle with atom i as the apex.

Table 224. Three-body SW potential parameters for single-layer 1T-ZrS_2 used by GULP [8] as expressed in Eq. (4).

	ϵ (eV)	σ (Å)	a	λ	γ	$\cos\theta_0$	A_L	B_L	p	q	Tol
Zr—S1—S1	1.000	1.432	2.473	42.177	1.000	−0.023	8.149	5.268	4	0	0.0
S1—Zr—Zr	1.000	1.432	2.473	42.177	1.000	−0.023	8.149	5.268	4	0	0.0

Table 225. SW potential parameters for single-layer 1T-ZrS_2 used by LAMMPS [9] as expressed in Eqs. (9) and (10).

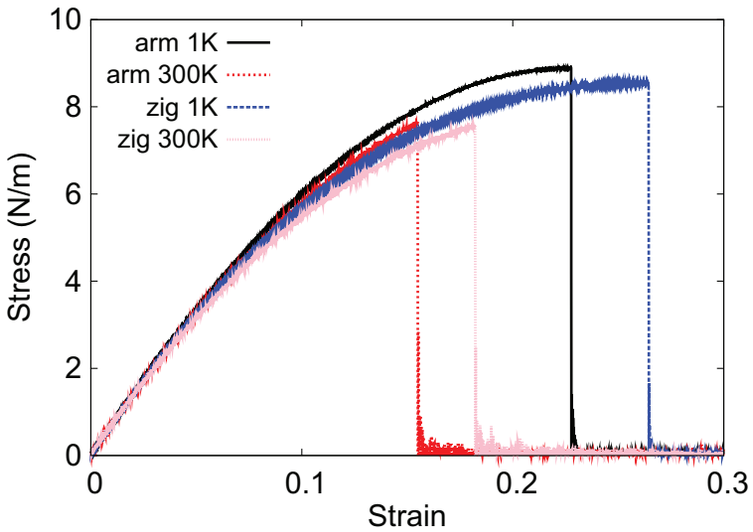

Figure 111. Stress-strain for single-layer 1T-ZrS_2 of dimension 100 × 100 Å along the armchair and zigzag directions.

modulus can be obtained by a linear fitting of the stress-strain relation in the small strain range of [0, 0.01]. The Young's modulus is 71.8 and 71.5 N/m along the armchair and zigzag directions, respectively. The Young's modulus is essentially isotropic in the armchair and zigzag directions. These values are close to the *ab initio* results at 0 K temperature, e.g., 75.74 N/m in [49]. The Poisson's ratio from the VFF model and the SW potential is $\nu_{xy} = \nu_{yx} = 0.16$, which are comparable with the *ab initio* result [49] of 0.22.

There is no available value for nonlinear quantities in the single-layer 1T-ZrS_2. We have thus used the nonlinear parameter $B = 0.5d^4$ in Eq. (5), which is close to the value of B in most materials. The value of the third-order nonlinear elasticity D can be extracted by fitting the stress-strain relation to the function $\sigma = E\epsilon + \frac{1}{2}D\epsilon^2$ with E as the Young's modulus. The values of D from the present SW potential are −268.9 and −305.2 N/m along the armchair and zigzag directions, respectively. The ultimate stress is about 8.9 N/m at the ultimate strain of 0.23 in the

armchair direction at the low temperature of 1 K. The ultimate stress is about 8.5 N/m at the ultimate strain of 0.26 in the zigzag direction at the low temperature of 1 K.

57. 1T-$ZrSe_2$

Most existing theoretical studies on the single-layer 1T-$ZrSe_2$ are based on the first-principles calculations. In this section, we will develop the SW potential for the single-layer 1T-$ZrSe_2$.

The structure for the single-layer 1T-$ZrSe_2$ is shown in **Figure 71** (with M = Zr and X = Se). Each Zr atom is surrounded by six Se atoms. These Se atoms are categorized into the top group (e.g., atoms 1, 3, and 5) and bottom group (e.g., atoms 2, 4, and 6). Each Se atom is connected to three Zr atoms. The structural parameters are from the first-principles calculations [51], including the lattice constant $a = 3.707$ Å and the position of the Se atom with respect to the Zr atomic plane $h = 1.591$ Å. The resultant angles are $\theta_{\mathrm{ZrSeSe}} = 88.058^\circ$ with Se atoms from the same (top or bottom) group and $\theta_{\mathrm{SeZrZr}} = 88.058^\circ$.

Table 226 shows three VFF terms for the single-layer 1T-$ZrSe_2$; one of which is the bond stretching interaction shown by Eq. (1), while the other two terms are the angle bending interaction shown by Eq. (2). We note that the angle bending term $K_{\mathrm{Zr-Se-Se}}$ is for the angle $\theta_{\mathrm{Zr-Se-Se}}$ with both Se atoms from the same (top or bottom) group. These force constant parameters are determined by fitting to the three acoustic branches in the phonon dispersion along the ΓM as shown in **Figure 112(a)**. The *ab initio* calculations for the phonon dispersion are from [50]. Similar phonon dispersion can also be found in other *ab initio* calculations [34]. **Figure 112(b)** shows that the VFF model and the SW potential give exactly the same phonon dispersion, as the SW potential is derived from the VFF model.

The parameters for the two-body SW potential used by GULP are shown in **Table 227**. The parameters for the three-body SW potential used by GULP are shown in **Table 228**. Some representative parameters for the SW potential used by LAMMPS are listed in **Table 229**.

We use LAMMPS to perform MD simulations for the mechanical behavior of the single-layer 1T-$ZrSe_2$ under uniaxial tension at 1 and 300 K. **Figure 113** shows the stress-strain curve for the tension of a single-layer 1T-$ZrSe_2$ of dimension 100×100 Å. Periodic boundary conditions are applied in both armchair and zigzag directions. The single-layer 1T-$ZrSe_2$ is stretched

VFF type	Bond stretching	Angle bending	
Expression	$\frac{1}{2}K_{\mathrm{Zr-Se}}(\Delta r)^2$	$\frac{1}{2}K_{\mathrm{Zr-Se-Se}}(\Delta\theta)^2$	$\frac{1}{2}K_{\mathrm{Se-Zr-Zr}}(\Delta\theta)^2$
Parameter	7.930	4.283	4.283
r_0 or θ_0	2.667	88.058	88.058

The second line gives an explicit expression for each VFF term. The third line is the force constant parameters. Parameters are in the unit of eV/Å^2 for the bond stretching interaction and in the unit of eV for the angle bending interaction. The fourth line gives the initial bond length (in the unit of Å) for the bond stretching interaction and the initial angle (in the unit of degrees) for the angle bending interaction. The angle θ_{ijk} has atom i as the apex.

Table 226. The VFF model for single-layer 1T-$ZrSe_2$.

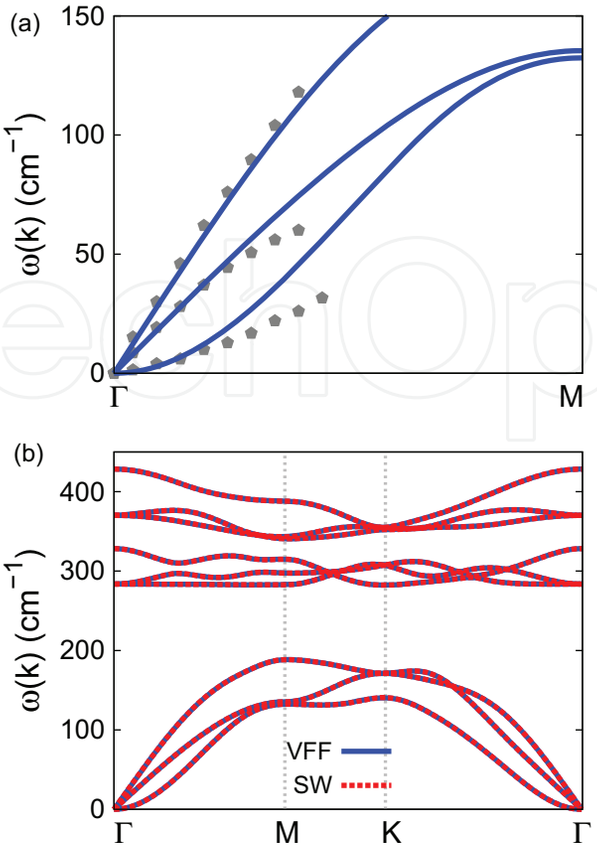

Figure 112. Phonon spectrum for single-layer 1T-$ZrSe_2$. (a) Phonon dispersion along the ΓM direction in the Brillouin zone. The results from the VFF model (lines) are comparable with the experiment data (pentagons) from [50]. (b) The phonon dispersion from the SW potential is exactly the same as that from the VFF model.

	A (eV)	ρ (Å)	B (Å^4)	$r_{\min}$ (Å)	$r_{\max}$ (Å)
Zr—Se	8.022	1.354	25.297	0.0	3.617

Table 227. Two-body SW potential parameters for single-layer 1T-$ZrSe_2$ used by GULP [8] as expressed in Eq. (3).

	K (eV)	θ_0 (°)	ρ_1 (Å)	ρ_2 (Å)	$r_{\min 12}$ (Å)	$r_{\max 12}$ (Å)	$r_{\min 13}$ (Å)	$r_{\max 13}$ (Å)	$r_{\min 23}$ (Å)	$r_{\max 23}$ (Å)
$\theta_{\text{Zr–Se–Se}}$	37.051	88.058	1.354	1.354	0.0	3.617	0.0	3.617	0.0	5.064
$\theta_{\text{Se–Zr–Zr}}$	37.051	88.058	1.354	1.354	0.0	3.617	0.0	3.617	0.0	5.064

The angle θ_{ijk} in the first line indicates the bending energy for the angle with atom i as the apex.

Table 228. Three-body SW potential parameters for single-layer 1T-$ZrSe_2$ used by GULP [8] as expressed in Eq. (4).

	ϵ (eV)	σ (Å)	a	λ	γ	$\cos\theta_0$	A_L	B_L	p	q	Tol
Zr—Se—Se	1.000	1.354	2.671	37.051	1.000	0.034	8.022	7.527	4	0	0.0
Se—Zr—Zr	1.000	1.354	2.671	37.051	1.000	0.034	8.022	7.527	4	0	0.0

Table 229. SW potential parameters for single-layer 1T-$ZrSe_2$ used by LAMMPS[9] as expressed in Eqs. (9) and (10).

http://dx.doi.org/10.5772/intechopen.71929

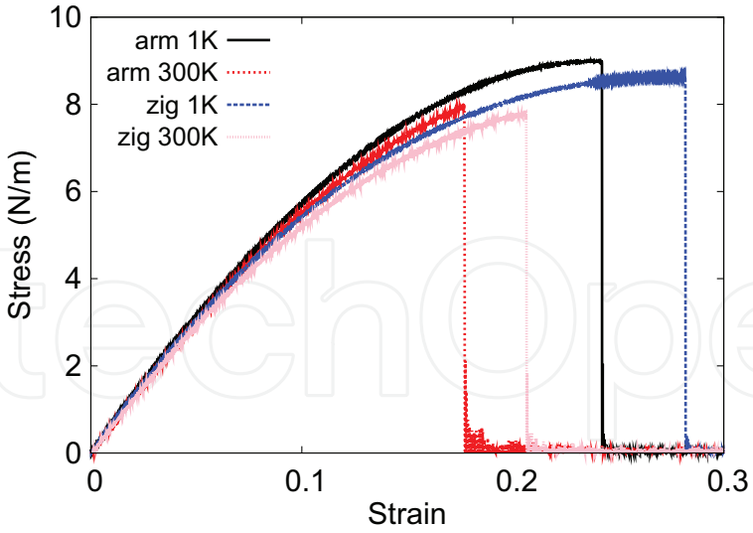

Figure 113. Stress-strain for single-layer 1T-$ZrSe_2$ of dimension 100 × 100 Å along the armchair and zigzag directions.

uniaxially along the armchair or zigzag direction. The stress is calculated without involving the actual thickness of the quasi-two-dimensional structure of the single-layer 1T-$ZrSe_2$. The Young's modulus can be obtained by a linear fitting of the stress-strain relation in the small strain range of [0, 0.01]. The Young's modulus is 66.7 and 66.4 N/m along the armchair and zigzag directions, respectively. The Young's modulus is essentially isotropic in the armchair and zigzag directions. The Poisson's ratio from the VFF model and the SW potential is $\nu_{xy} = \nu_{yx} = 0.19$.

There is no available value for nonlinear quantities in the single-layer 1T-$ZrSe_2$. We have thus used the nonlinear parameter $B = 0.5d^4$ in Eq. (5), which is close to the value of B in most materials. The value of the third-order nonlinear elasticity D can be extracted by fitting the stress-strain relation to the function $\sigma = E\epsilon + \frac{1}{2}D\epsilon^2$ with E as the Young's modulus. The values of D from the present SW potential are -219.6 and -256.6 N/m along the armchair and zigzag directions, respectively. The ultimate stress is about 9.0 N/m at the ultimate strain of 0.24 in the armchair direction at the low temperature of 1 K. The ultimate stress is about 8.6 N/m at the ultimate strain of 0.28 in the zigzag direction at the low temperature of 1 K.

58. 1T-$ZrTe_2$

Most existing theoretical studies on the single-layer 1T-$ZrTe_2$ are based on the first-principles calculations. In this section, we will develop the SW potential for the single-layer 1T-$ZrTe_2$.

The structure for the single-layer 1T-$ZrTe_2$ is shown in **Figure 71** (with M=Zr and X=Te). Each Zr atom is surrounded by six Te atoms. These Te atoms are categorized into the top group (e.g., atoms 1, 3, and 5) and bottom group (e.g., atoms 2, 4, and 6). Each Te atom is connected to three Zr atoms. The structural parameters are from the first-principles calculations [48], including the lattice constant $a = 4.0064$ Å and the bond length $d_{Zr-Te} = 2.9021$ Å, which are derived

from the angle $\theta_{\mathrm{TeZrZr}} = 87.3^\circ$. The other angle is $\theta_{\mathrm{ZrTeTe}} = 87.3^\circ$ with Te atoms from the same (top or bottom) group.

Table 230 shows three VFF terms for the single-layer 1T-$ZrTe_2$; one of which is the bond stretching interaction shown by Eq. (1), while the other two terms are the angle bending interaction shown by Eq. (2). We note that the angle bending term $K_{\mathrm{Zr-Te-Te}}$ is for the angle $\theta_{\mathrm{Zr-Te-Te}}$ with both Te atoms from the same (top or bottom) group. We find that there are actually only two parameters in the VFF model, so we can determine their value by fitting to the Young's modulus and the Poisson's ratio of the system. The *ab initio* calculations have predicted the Young's modulus to be 44 N/m and the Poisson's ratio as 0.13 [48].

The parameters for the two-body SW potential used by GULP are shown in **Table 231**. The parameters for the three-body SW potential used by GULP are shown in **Table 232**. Some representative parameters for the SW potential used by LAMMPS are listed in **Table 233**.

VFF type	**Bond stretching**	**Angle bending**	
Expression	$\frac{1}{2}K_{\mathrm{Zr-Te}}(\Delta r)^2$	$\frac{1}{2}K_{\mathrm{Zr-Te-Te}}(\Delta\theta)^2$	$\frac{1}{2}K_{\mathrm{Te-Zr-Zr}}(\Delta\theta)^2$
Parameter	2.974	3.681	3.681
r_0 or θ_0	2.902	87.301	87.301

The second line gives an explicit expression for each VFF term. The third line is the force constant parameters. Parameters are in the unit of eV/Å^2 for the bond stretching interaction and in the unit of eV for the angle bending interaction. The fourth line gives the initial bond length (in the unit of Å) for the bond stretching interaction and the initial angle (in the unit of degrees) for the angle bending interaction. The angle θ_{ijk} has atom i as the apex.

Table 230. The VFF model for single-layer 1T-$ZrTe_2$.

	A **(eV)**	ρ **(Å)**	B **(Å^4)**	r_{min} **(Å)**	r_{max} **(Å)**
Zr—Te	3.493	1.441	35.467	0.0	3.925

Table 231. Two-body SW potential parameters for single-layer 1T-$ZrTe_2$ used by GULP [8] as expressed in Eq. (3).

	K **(eV)**	θ_0 **(°)**	ρ_1 **(Å)**	ρ_2 **(Å)**	$r_{\mathrm{min}\,12}$ **(Å)**	$r_{\mathrm{max}\,12}$ **(Å)**	$r_{\mathrm{min}\,13}$ **(Å)**	$r_{\mathrm{max}\,13}$ **(Å)**	$r_{\mathrm{min}\,23}$ **(Å)**	$r_{\mathrm{max}\,23}$ **(Å)**
$\theta_{\mathrm{Zr-Te-Te}}$	30.905	87.301	1.441	1.441	0.0	3.925	0.0	3.925	0.0	5.473
$\theta_{\mathrm{Te-Zr-Zr}}$	30.905	87.301	1.441	1.441	0.0	3.925	0.0	3.925	0.0	5.473

The angle θ_{ijk} in the first line indicates the bending energy for the angle with atom i as the apex.

Table 232. Three-body SW potential parameters for single-layer 1T-$ZrTe_2$ used by GULP [8] as expressed in Eq. (4).

	ϵ **(eV)**	σ **(Å)**	a	λ	γ	$\cos\theta_0$	A_L	B_L	p	q	**Tol**
Zr—Te_1—Te_1	1.000	1.441	2.723	30.905	1.000	0.047	3.493	8.225	4	0	0.0

Table 233. SW potential parameters for single-layer 1T-$ZrTe_2$ used by LAMMPS [9] as expressed in Eqs. (9) and (10).

http://dx.doi.org/10.5772/intechopen.71929

We use LAMMPS to perform MD simulations for the mechanical behavior of the single-layer 1T-$ZrTe_2$ under uniaxial tension at 1 and 300 K. **Figure 114** shows the stress-strain curve for the tension of a single-layer 1T-$ZrTe_2$ of dimension 100×100 Å. Periodic boundary conditions are applied in both armchair and zigzag directions. The single-layer 1T-$ZrTe_2$ is stretched uniaxially along the armchair or zigzag direction. The stress is calculated without involving the actual thickness of the quasi-two-dimensional structure of the single-layer 1T-$ZrTe_2$. The Young's modulus can be obtained by a linear fitting of the stress-strain relation in the small strain range of [0, 0.01]. The Young's modulus is 39.2 and 39.1 N/m along the armchair and zigzag directions, respectively. The Young's modulus is essentially isotropic in the armchair and zigzag directions. The Poisson's ratio from the VFF model and the SW potential is $\nu_{xy} = \nu_{yx} = 0.10$. The fitted Young's modulus value is about 10% smaller than the *ab initio* result of 44 N/m [48], as only short-range interactions are considered in the present work. The long-range interactions are ignored, which typically leads to about 10% underestimation for the value of the Young's modulus.

There is no available value for nonlinear quantities in the single-layer 1T-$ZrTe_2$. We have thus used the nonlinear parameter $B = 0.5d^4$ in Eq. (5), which is close to the value of B in most materials. The value of the third-order nonlinear elasticity D can be extracted by fitting the stress-strain relation to the function $\sigma = E\epsilon + \frac{1}{2}D\epsilon^2$ with E as the Young's modulus. The values of D from the present SW potential are -187.2 and -201.1 N/m along the armchair and zigzag directions, respectively. The ultimate stress is about 4.0 N/m at the ultimate strain of 0.19 in the armchair direction at the low temperature of 1 K. The ultimate stress is about 3.9 N/m at the ultimate strain of 0.22 in the zigzag direction at the low temperature of 1 K.

Figure 115 shows that the VFF model and the SW potential give exactly the same phonon dispersion, as the SW potential is derived from the VFF model.

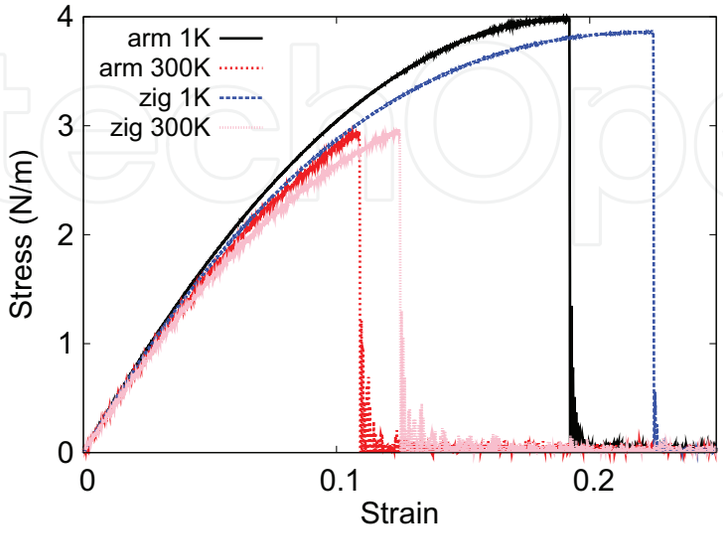

Figure 114. Stress-strain for single-layer 1T-$ZrTe_2$ of dimension 100×100 Å along the armchair and zigzag directions.

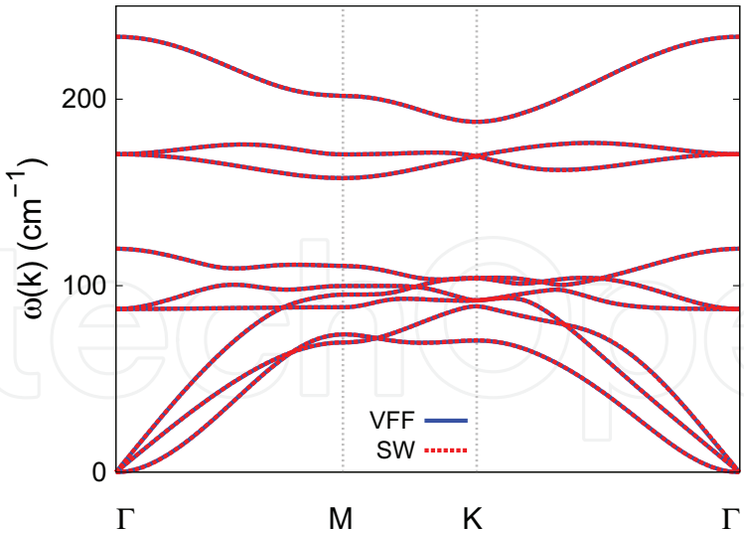

Figure 115. Phonon spectrum for single-layer 1T-$ZrTe_2$ along the ΓMKΓ direction in the Brillouin zone. The phonon dispersion from the SW potential is exactly the same as that from the VFF model.

59. 1T-NbS_2

Most existing theoretical studies on the single-layer 1T-NbS_2 are based on the first-principles calculations. In this section, we will develop the SW potential for the single-layer 1T-NbS_2.

The structure for the single-layer 1T-NbS_2 is shown in **Figure 71** (with M=Nb and X=S). Each Nb atom is surrounded by six S atoms. These S atoms are categorized into the top group (e.g., atoms 1, 3, and 5) and bottom group (e.g., atoms 2, 4, and 6). Each S atom is connected to three Nb atoms. The structural parameters are from the first-principles calculations [12], including the lattice constant $a = 3.30$ Å and the bond length $d_{\mathrm{Nb-S}} = 2.45$ Å. The resultant angles are $\theta_{\mathrm{NbSS}} = 84.671^\circ$ with S atoms from the same (top or bottom) group and $\theta_{\mathrm{SNbNb}} = 84.671^\circ$.

Table 234 shows three VFF terms for the single-layer 1T-NbS_2; one of which is the bond stretching interaction shown by Eq. (1), while the other two terms are the angle bending interaction shown by Eq. (2). We note that the angle bending term $K_{\mathrm{Nb-S-S}}$ is for the angle $\theta_{\mathrm{Nb-S-S}}$ with both S atoms from the same (top or bottom) group. These force constant

VFF type	Bond stretching	Angle bending	
Expression	$\frac{1}{2}K_{\mathrm{Nb-S}}(\Delta r)^2$	$\frac{1}{2}K_{\mathrm{Nb-S-S}}(\Delta\theta)^2$	$\frac{1}{2}K_{\mathrm{S-Nb-Nb}}(\Delta\theta)^2$
Parameter	7.930	4.283	4.283
r_0 or θ_0	2.450	84.671	84.671

The second line gives an explicit expression for each VFF term. The third line is the force constant parameters. Parameters are in the unit of eV/Å^2 for the bond stretching interaction and in the unit of eV for the angle bending interaction. The fourth line gives the initial bond length (in the unit of Å) for the bond stretching interaction and the initial angle (in the unit of degrees) for the angle bending interaction. The angle θ_{ijk} has atom i as the apex.

Table 234. The VFF model for single-layer 1T-NbS_2.

parameters are determined by fitting to the three acoustic branches in the phonon dispersion along the ΓM as shown in **Figure 116(a)**. The *ab initio* calculations for the phonon dispersion are from [12]. The lowest acoustic branch (flexural mode) is linear and very close to the in-plane transverse acoustic branch in the *ab initio* calculations, which may be due to the violation of the rigid rotational invariance [20]. **Figure 116(b)** shows that the VFF model and the SW potential give exactly the same phonon dispersion, as the SW potential is derived from the VFF model.

The parameters for the two-body SW potential used by GULP are shown in **Table 235**. The parameters for the three-body SW potential used by GULP are shown in **Table 236**. Some representative parameters for the SW potential used by LAMMPS are listed in **Table 237**.

We use LAMMPS to perform MD simulations for the mechanical behavior of the single-layer 1T-NbS_2 under uniaxial tension at 1 and 300 K. **Figure 117** shows the stress-strain curve for the

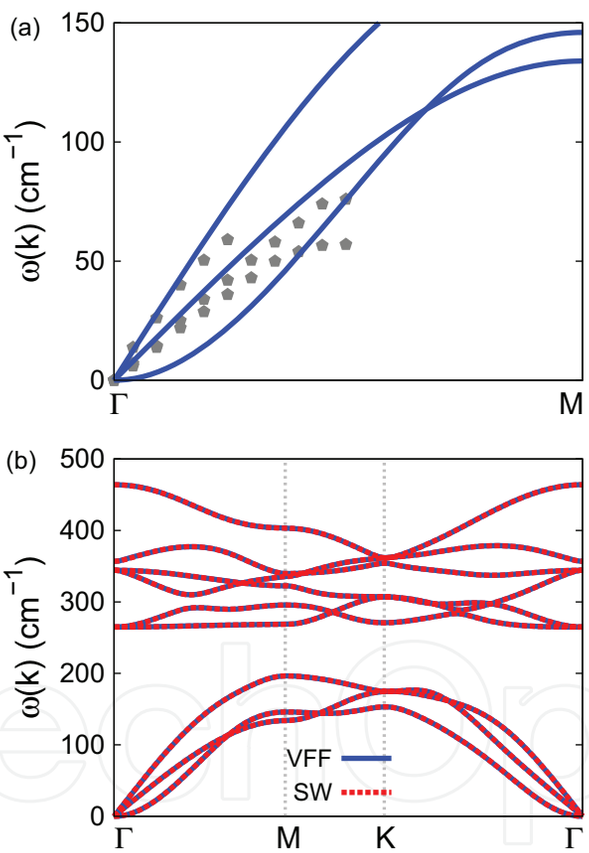

Figure 116. Phonon spectrum for single-layer 1T-NbS_2. (a) Phonon dispersion along the ΓM direction in the Brillouin zone. The results from the VFF model (lines) are comparable with the experiment data (pentagons) from [12]. (b) The phonon dispersion from the SW potential is exactly the same as that from the VFF model.

	A (eV)	ρ (Å)	B (Å^4)	r_{min} (Å)	r_{max} (Å)
Nb—S	6.192	1.125	18.015	0.0	3.280

Table 235. Two-body SW potential parameters for single-layer 1T-NbS_2 used by GULP [8] as expressed in Eq. (3).

	K (eV)	θ_0 (°)	ρ_1 (Å)	ρ_2 (Å)	$r_{\min 12}$ (Å)	$r_{\max 12}$ (Å)	$r_{\min 13}$ (Å)	$r_{\max 13}$ (Å)	$r_{\min 23}$ (Å)	$r_{\max 23}$ (Å)
$\theta_{\mathrm{Nb-S-S}}$	32.472	84.671	1.125	1.125	0.0	3.280	0.0	3.280	0.0	4.508
$\theta_{\mathrm{S-Nb-Nb}}$	32.472	84.671	1.125	1.125	0.0	3.280	0.0	3.280	0.0	4.508

The angle θ_{ijk} in the first line indicates the bending energy for the angle with atom i as the apex.

Table 236. Three-body SW potential parameters for single-layer 1T-NbS_2 used by GULP [8] as expressed in Eq. (4).

	ϵ (eV)	σ (Å)	a	λ	γ	$\cos\theta_0$	A_L	B_L	p	q	Tol
$Nb—S_1—S_1$	1.000	1.125	2.916	32.472	1.000	0.093	6.192	11.247	4	0	0.0
$S_1—Nb—Nb$	1.000	1.125	2.916	32.472	1.000	0.093	6.192	11.247	4	0	0.0

Table 237. SW potential parameters for single-layer 1T-NbS_2 used by LAMMPS [9] as expressed in Eqs. (9) and (10).

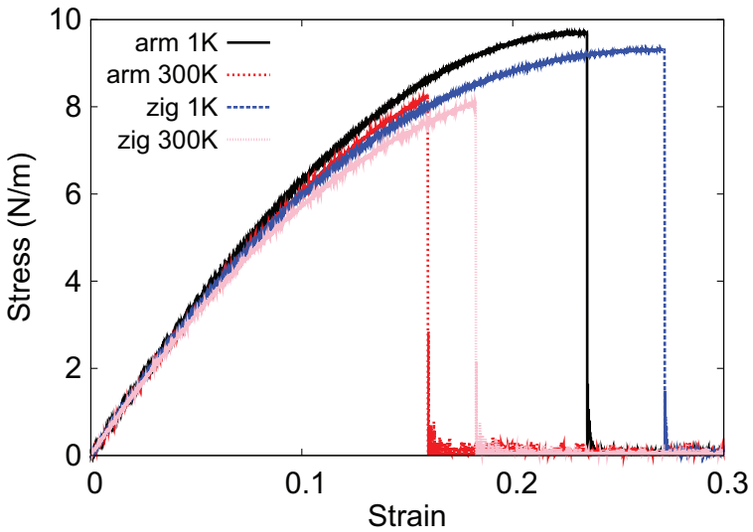

Figure 117. Stress-strain for single-layer 1T-NbS_2 of dimension 100 × 100 Å along the armchair and zigzag directions.

tension of a single-layer 1T-NbS_2 of dimension 100 × 100 Å. Periodic boundary conditions are applied in both armchair and zigzag directions. The single-layer 1T-NbS_2 is stretched uniaxially along the armchair or zigzag direction. The stress is calculated without involving the actual thickness of the quasi-two-dimensional structure of the single-layer 1T-NbS_2. The Young's modulus can be obtained by a linear fitting of the stress-strain relation in the small strain range of [0, 0.01]. The Young's modulus is 73.8 and 73.4 N/m along the armchair and zigzag directions, respectively. The Young's modulus is essentially isotropic in the armchair and zigzag directions. The Poisson's ratio from the VFF model and the SW potential is $\nu_{xy} = \nu_{yx} = 0.18$.

There is no available value for nonlinear quantities in the single-layer 1T-NbS_2. We have thus used the nonlinear parameter $B = 0.5d^4$ in Eq. (5), which is close to the value of B in most materials. The value of the third-order nonlinear elasticity D can be extracted by fitting the stress-strain relation to the function $\sigma = E\epsilon + \frac{1}{2}D\epsilon^2$ with E as the Young's modulus. The values

of D from the present SW potential are −250.5 and −290.4 N/m along the armchair and zigzag directions, respectively. The ultimate stress is about 9.7 N/m at the ultimate strain of 0.23 in the armchair direction at the low temperature of 1 K. The ultimate stress is about 9.4 N/m at the ultimate strain of 0.27 in the zigzag direction at the low temperature of 1 K.

60. 1T-$NbSe_2$

Most existing theoretical studies on the single-layer 1T-$NbSe_2$ are based on the first-principles calculations. In this section, we will develop the SW potential for the single-layer 1T-$NbSe_2$.

The structure for the single-layer 1T-$NbSe_2$ is shown in **Figure 71** (with M=Nb and X=Se). Each Nb atom is surrounded by six Se atoms. These Se atoms are categorized into the top group (e.g., atoms 1, 3, and 5) and bottom group (e.g., atoms 2, 4, and 6). Each Se atom is connected to three Nb atoms. The structural parameters are from the first-principles calculations [12], including the lattice constant $a = 3.39$ Å and the bond length $d_{\mathrm{Nb-Se}} = 2.57$ Å. The resultant angles are $\theta_{\mathrm{NbSeSe}} = 82.529^\circ$ with Se atoms from the same (top or bottom) group and $\theta_{\mathrm{SeNbNb}} = 82.529^\circ$.

Table 238 shows three VFF terms for the single-layer 1T-$NbSe_2$; one of which is the bond stretching interaction shown by Eq. (1), while the other two terms are the angle bending interaction shown by Eq. (2). We note that the angle bending term $K_{\mathrm{Nb-Se-Se}}$ is for the angle $\theta_{\mathrm{Nb-Se-Se}}$ with both Se atoms from the same (top or bottom) group. We find that there are actually only two parameters in the VFF model, so we can determine their value by fitting to the Young's modulus and the Poisson's ratio of the system. The *ab initio* calculations have predicted the Young's modulus to be 73 N/m and the Poisson's ratio as 0.20 [48].

The parameters for the two-body SW potential used by GULP are shown in **Table 239**. The parameters for the three-body SW potential used by GULP are shown in **Table 240**. Some representative parameters for the SW potential used by LAMMPS are listed in **Table 241**.

VFF type	**Bond stretching**	**Angle bending**	
Expression	$\frac{1}{2}K_{\mathrm{Nb-Se}}(\Delta r)^2$	$\frac{1}{2}K_{\mathrm{Nb-Se-Se}}(\Delta\theta)^2$	$\frac{1}{2}K_{\mathrm{Se-Nb-Nb}}(\Delta\theta)^2$
Parameter	7.930	4.283	4.283
r_0 or θ_0	2.570	82.529	82.529

The second line gives an explicit expression for each VFF term. The third line is the force constant parameters. Parameters are in the unit of eV/Å^2 for the bond stretching interaction and in the unit of eV for the angle bending interaction. The fourth line gives the initial bond length (in the unit of Å) for the bond stretching interaction and the initial angle (in the unit of degrees) for the angle bending interaction. The angle θ_{ijk} has atom i as the apex.

Table 238. The VFF model for single-layer 1T-$NbSe_2$.

	A **(eV)**	ρ **(Å)**	B **(Å^4)**	r_{min} **(Å)**	r_{max} **(Å)**
Nb—Se	6.430	1.104	21.812	0.0	3.412

Table 239. Two-body SW potential parameters for single-layer 1T-$NbSe_2$ used by GULP [8] as expressed in Eq. (3).

	K (eV)	θ_0 (°)	ρ_1 (Å)	ρ_2 (Å)	$r_{\min 12}$ (Å)	$r_{\max 12}$ (Å)	$r_{\min 13}$ (Å)	$r_{\max 13}$ (Å)	$r_{\min 23}$ (Å)	$r_{\max 23}$ (Å)
$\theta_{\text{Nb-Se-Se}}$	29.956	82.528	1.104	1.104	0.0	3.412	0.0	3.412	0.0	4.631
$\theta_{\text{Se-Nb-Nb}}$	29.956	82.528	1.104	1.104	0.0	3.412	0.0	3.412	0.0	4.631

The angle θ_{ijk} in the first line indicates the bending energy for the angle with atom i as the apex.

Table 240. Three-body SW potential parameters for single-layer 1T-$NbSe_2$ used by GULP [8] as expressed in Eq. (4).

	ϵ (eV)	σ (Å)	a	λ	γ	$\cos\theta_0$	A_L	B_L	p	q	Tol
Nb—Se_1—Se_1	1.000	1.104	3.092	29.956	1.000	0.130	6.430	14.706	4	0	0.0

Table 241. SW potential parameters for single-layer 1T-$NbSe_2$ used by LAMMPS [9] as expressed in Eqs. (9) and (10).

We use LAMMPS to perform MD simulations for the mechanical behavior of the single-layer 1T-$NbSe_2$ under uniaxial tension at 1 and 300 K. **Figure 118** shows the stress-strain curve for the tension of a single-layer 1T-$NbSe_2$ of dimension 100 × 100 Å. Periodic boundary conditions are applied in both armchair and zigzag directions. The single-layer 1T-$NbSe_2$ is stretched uniaxially along the armchair or zigzag direction. The stress is calculated without involving the actual thickness of the quasi-two-dimensional structure of the single-layer 1T-$NbSe_2$. The Young's modulus can be obtained by a linear fitting of the stress-strain relation in the small strain range of [0, 0.01]. The Young's modulus is 67.1 and 66.8 N/m along the armchair and zigzag directions, respectively. The Young's modulus is essentially isotropic in the armchair and zigzag directions. The Poisson's ratio from the VFF model and the SW potential is $\nu_{xy} = \nu_{yx} = 0.20$. The fitted Young's modulus value is about 10% smaller than the *ab initio* result of 73 N/m [48], as only short-range interactions are considered in the present work. The long-range interactions are ignored, which typically lead to about 10% underestimation for the Young's modulus value.

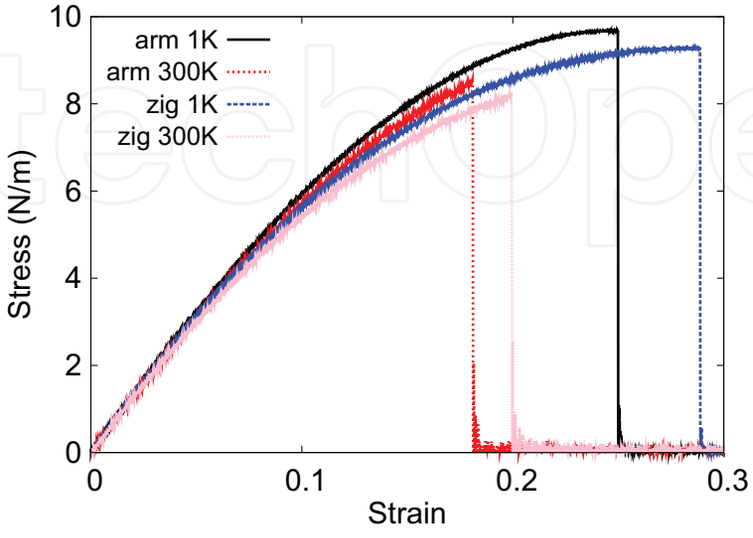

Figure 118. Stress-strain for single-layer 1T-$NbSe_2$ of dimension 100 × 100 Å along the armchair and zigzag directions.

http://dx.doi.org/10.5772/intechopen.71929

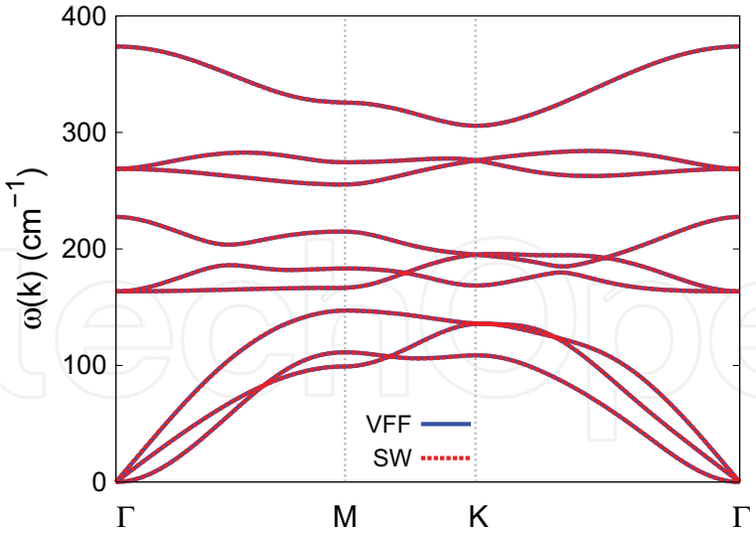

Figure 119. Phonon spectrum for single-layer 1T-$NbSe_2$ along the ΓMKΓ direction in the Brillouin zone. The phonon dispersion from the SW potential is exactly the same as that from the VFF model.

There is no available value for nonlinear quantities in the single-layer 1T-$NbSe_2$. We have thus used the nonlinear parameter $B = 0.5d^4$ in Eq. (5), which is close to the value of B in most materials. The value of the third-order nonlinear elasticity D can be extracted by fitting the stress-strain relation to the function $\sigma = E\epsilon + \frac{1}{2}D\epsilon^2$ with E as the Young's modulus. The values of D from the present SW potential are -193.5 N/m and -233.4 N/m along the armchair and zigzag directions, respectively. The ultimate stress is about 9.7 N/m at the ultimate strain of 0.25 in the armchair direction at the low temperature of 1 K. The ultimate stress is about 9.3 N/m at the ultimate strain of 0.29 in the zigzag direction at the low temperature of 1 K.

Figure 119 shows that the VFF model and the SW potential give exactly the same phonon dispersion, as the SW potential is derived from the VFF model.

61. 1T-$NbTe_2$

Most existing theoretical studies on the single-layer 1T-$NbTe_2$ are based on the first-principles calculations. In this section, we will develop the SW potential for the single-layer 1T-$NbTe_2$.

The structure for the single-layer 1T-$NbTe_2$ is shown in **Figure 71** (with M=Nb and X=Te). Each Nb atom is surrounded by six Te atoms. These Te atoms are categorized into the top group (e.g., atoms 1, 3, and 5) and bottom group (e.g., atoms 2, 4, and 6). Each Te atom is connected to three Nb atoms. The structural parameters are from the first-principles calculations [12], including the lattice constant $a = 3.56$ Å and the bond length $d_{\mathrm{Nb-Te}} = 2.77$ Å. The resultant angles are $\theta_{\mathrm{NbTeTe}} = 79.972^\circ$ with Te atoms from the same (top or bottom) group and $\theta_{\mathrm{TeNbNb}} = 79.972^\circ$.

Table 242 shows three VFF terms for the single-layer 1T-$NbTe_2$; one of which is the bond stretching interaction shown by Eq. (1), while the other two terms are the angle bending

VFF type	Bond stretching	Angle bending	
Expression	$\frac{1}{2}K_{\mathrm{Nb-Te}}(\Delta r)^2$	$\frac{1}{2}K_{\mathrm{Nb-Te-Te}}(\Delta\theta)^2$	$\frac{1}{2}K_{\mathrm{Te-Nb-Nb}}(\Delta\theta)^2$
Parameter	3.559	4.863	4.863
r_0 or θ_0	2.770	79.972	79.972

The second line gives an explicit expression for each VFF term. The third line is the force constant parameters. Parameters are in the unit of eV/Å^2 for the bond stretching interaction and in the unit of eV for the angle bending interaction. The fourth line gives the initial bond length (in the unit of Å) for the bond stretching interaction and the initial angle (in the unit of degrees) for the angle bending interaction. The angle θ_{ijk} has atom i as the apex.

Table 242. The VFF model for single-layer 1T-$NbTe_2$.

interaction shown by Eq. (2). We note that the angle bending term $K_{\mathrm{Nb-Te-Te}}$ is for the angle $\theta_{\mathrm{Nb-Te-Te}}$ with both Te atoms from the same (top or bottom) group. We find that there are actually only two parameters in the VFF model, so we can determine their value by fitting to the Young's modulus and the Poisson's ratio of the system. The *ab initio* calculations have predicted the Young's modulus to be 56 N/m and the Poisson's ratio as 0.11 [48].

The parameters for the two-body SW potential used by GULP are shown in **Table 243**. The parameters for the three-body SW potential used by GULP are shown in **Table 244**. Some representative parameters for the SW potential used by LAMMPS are listed in **Table 245**.

We use LAMMPS to perform MD simulations for the mechanical behavior of the single-layer 1T-$NbTe_2$ under uniaxial tension at 1 and 300 K. **Figure 120** shows the stress-strain curve for the tension of a single-layer 1T-$NbTe_2$ of dimension 100 × 100 Å. Periodic boundary conditions are applied in both armchair and zigzag directions. The single-layer 1T-$NbTe_2$ is stretched uniaxially along the armchair or zigzag direction. The stress is calculated without involving

	A (eV)	ρ (Å)	B (Å^4)	r_{min} (Å)	r_{max} (Å)
Nb—Te	3.123	1.094	29.437	0.0	3.640

Table 243. Two-body SW potential parameters for single-layer 1T-$NbTe_2$ used by GULP [8] as expressed in Eq. (3).

	K (eV)	θ_0 (°)	ρ_1 (Å)	ρ_2 (Å)	$r_{\mathrm{min}\,12}$ (Å)	$r_{\mathrm{max}\,12}$ (Å)	$r_{\mathrm{min}\,13}$ (Å)	$r_{\mathrm{max}\,13}$ (Å)	$r_{\mathrm{min}\,23}$ (Å)	$r_{\mathrm{max}\,23}$ (Å)
$\theta_{\mathrm{Nb-Te-Te}}$	30.968	79.972	1.094	1.094	0.0	3.640	0.0	3.640	0.0	4.863
$\theta_{\mathrm{Te-Nb-Nb}}$	30.968	79.972	1.094	1.094	0.0	3.640	0.0	3.640	0.0	4.863

The angle θ_{ijk} in the first line indicates the bending energy for the angle with atom i as the apex.

Table 244. Three-body SW potential parameters for single-layer 1T-$NbTe_2$ used by GULP [8] as expressed in Eq. (4).

	ϵ (eV)	σ (Å)	a	λ	γ	$\cos\theta_0$	A_L	B_L	p	q	Tol
Nb—Te_1—Te_1	1.000	1.094	3.328	30.968	1.000	0.174	3.123	20.560	4	0	0.0

Table 245. SW potential parameters for single-layer 1T-$NbTe_2$ used by LAMMPS [9] as expressed in Eqs. (9) and (10).

http://dx.doi.org/10.5772/intechopen.71929

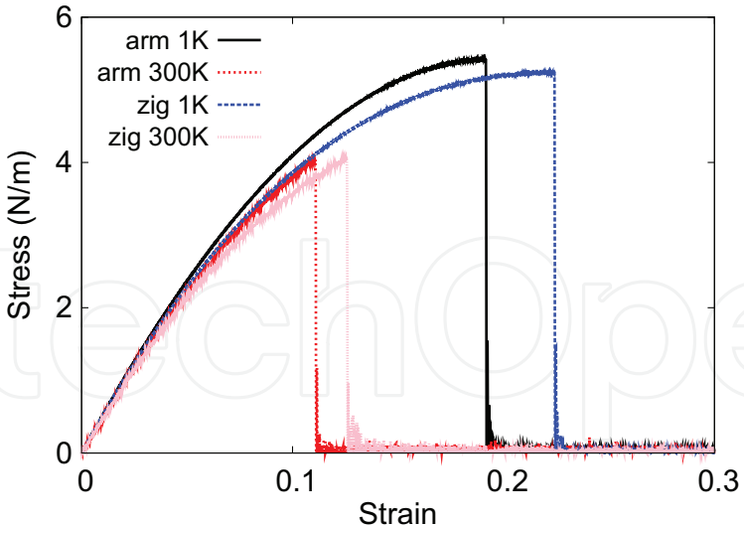

Figure 120. Stress-strain for single-layer 1T-$NbTe_2$ of dimension 100×100 Å along the armchair and zigzag directions.

the actual thickness of the quasi-two-dimensional structure of the single-layer 1T-$NbTe_2$. The Young's modulus can be obtained by a linear fitting of the stress-strain relation in the small strain range of [0, 0.01]. The Young's modulus is 52.2 and 51.9 N/m along the armchair and zigzag directions, respectively. The Young's modulus is essentially isotropic in the armchair and zigzag directions. The Poisson's ratio from the VFF model and the SW potential is $\nu_{xy} = \nu_{yx} = 0.11$. The fitted Young's modulus value is about 10% smaller than the *ab initio* result of 56 N/m [48], as only short-range interactions are considered in the present work. The long-range interactions are ignored, which typically leads to about 10% underestimation for the value of the Young's modulus.

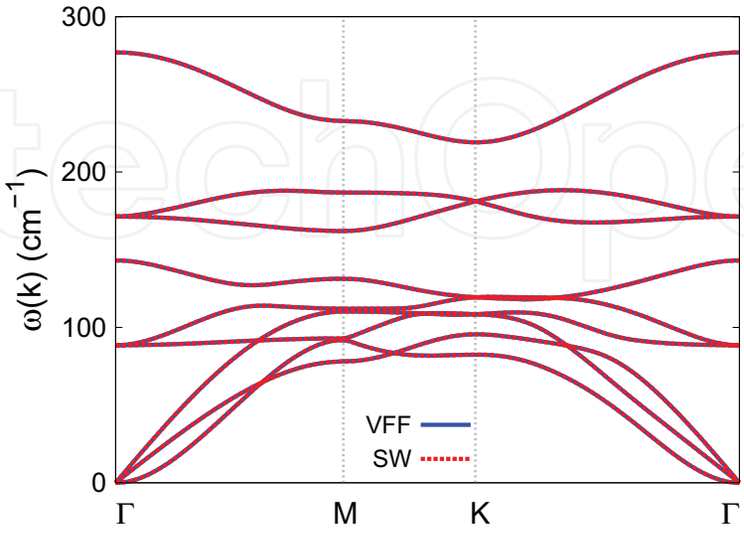

Figure 121. Phonon spectrum for single-layer 1T-$NbTe_2$ along the ΓMKΓ direction in the Brillouin zone. The phonon dispersion from the SW potential is exactly the same as that from the VFF model.

There is no available value for nonlinear quantities in the single-layer 1T-$NbTe_2$. We have thus used the nonlinear parameter $B = 0.5d^4$ in Eq. (5), which is close to the value of B in most materials. The value of the third-order nonlinear elasticity D can be extracted by fitting the stress-strain relation to the function $\sigma = E\epsilon + \frac{1}{2}D\epsilon^2$ with E as the Young's modulus. The values of D from the present SW potential are -237.7 and -265.0 N/m along the armchair and zigzag directions, respectively. The ultimate stress is about 5.4 N/m at the ultimate strain of 0.19 in the armchair direction at the low temperature of 1 K. The ultimate stress is about 5.2 N/m at the ultimate strain of 0.22 in the zigzag direction at the low temperature of 1 K.

Figure 121 shows that the VFF model and the SW potential give exactly the same phonon dispersion, as the SW potential is derived from the VFF model.

62. 1T-MoS_2

Most existing theoretical studies on the single-layer 1T-MoS_2 are based on the first-principles calculations. In this section, we will develop the SW potential for the single-layer 1T-MoS_2.

The structure for the single-layer 1T-MoS_2 is shown in **Figure 71** (with M=Mo and X=S). Each Mo atom is surrounded by six S atoms. These S atoms are categorized into the top group (e.g., atoms 1, 3, and 5) and bottom group (e.g., atoms 2, 4, and 6). Each S atom is connected to three Mo atoms. The structural parameters are from the first-principles calculations [48], including the lattice constant $a = 3.1998$ Å and the bond length $d_{\mathrm{Mo-S}} = 2.4193$ Å, which are derived from the angle $\theta_{\mathrm{SMoMo}} = 82.8^\circ$. The other angle is $\theta_{\mathrm{MoSS}} = 82.8^\circ$ with S atoms from the same (top or bottom) group.

Table 246 shows three VFF terms for the single-layer 1T-MoS_2; one of which is the bond stretching interaction shown by Eq. (1), while the other two terms are the angle bending interaction shown by Eq. (2). We note that the angle bending term $K_{\mathrm{Mo-S-S}}$ is for the angle $\theta_{\mathrm{Mo-S-S}}$ with both S atoms from the same (top or bottom) group. We find that there are actually only two parameters in the VFF model, so we can determine their value by fitting to the Young's modulus and the Poisson's ratio of the system. The *ab initio* calculations have predicted the Young's modulus to be 103 N/m and the Poisson's ratio as -0.07 [48]. The *ab*

VFF type	Bond stretching	Angle bending	
Expression	$\frac{1}{2}K_{\mathrm{Mo-S}}(\Delta r)^2$	$\frac{1}{2}K_{\mathrm{Mo-S-S}}(\Delta\theta)^2$	$\frac{1}{2}K_{\mathrm{S-Mo-Mo}}(\Delta\theta)^2$
Parameter	3.523	10.394	10.394
r_0 or θ_0	2.419	82.799	82.799

The second line gives an explicit expression for each VFF term. The third line is the force constant parameters. Parameters are in the unit of eV/Å^2 for the bond stretching interaction and in the unit of eV for the angle bending interaction. The fourth line gives the initial bond length (in the unit of Å) for the bond stretching interaction and the initial angle (in the unit of degrees) for the angle bending interaction. The angle θ_{ijk} has atom i as the apex.

Table 246. The VFF model for single-layer 1T-MoS_2.

initio calculations have predicted a negative Poisson's ratio in the 1T-MoS_2, which was attributed to the orbital coupling in this material. The orbital coupling enhances the angle bending interaction in the VFF model. As a result, the value of the angle bending parameter is much larger than the bond stretching force constant parameter, which is typical in auxetic materials with negative Poisson's ratio [52].

The parameters for the two-body SW potential used by GULP are shown in **Table 247**. The parameters for the three-body SW potential used by GULP are shown in **Table 248**. Some representative parameters for the SW potential used by LAMMPS are listed in **Table 249**.

We use LAMMPS to perform MD simulations for the mechanical behavior of the single-layer 1T-MoS_2 under uniaxial tension at 1 and 300 K. **Figure 122** shows the stress-strain curve for the tension of a single-layer 1T-MoS_2 of dimension 100×100 Å. Periodic boundary conditions are applied in both armchair and zigzag directions. The single-layer 1T-MoS_2 is stretched uniaxially along the armchair or zigzag direction. The stress is calculated without involving the actual thickness of the quasi-two-dimensional structure of the single-layer 1T-MoS_2. The Young's modulus can be obtained by a linear fitting of the stress-strain relation in the small strain range of [0, 0.01]. The Young's modulus is 88.7 and 88.3 N/m along the armchair and zigzag directions, respectively. The Young's modulus is essentially isotropic in the armchair and zigzag directions. The Poisson's ratio from the VFF model and the SW potential is $\nu_{xy} = \nu_{yx} = -0.07$. The fitted Young's modulus value is about 10% smaller than the *ab initio* result of 103 N/m [48], as only short-range interactions are considered in the present work. The long-range interactions are ignored, which typically leads to about 10% underestimation for the value of the Young's modulus.

	A (eV)	ρ (Å)	B (Å^4)	$r_{\min}$ (Å)	$r_{\max}$ (Å)
Mo—S	2.550	1.048	17.129	0.0	3.215

Table 247. Two-body SW potential parameters for single-layer 1T-MoS_2 used by GULP [8] as expressed in Eq. (3).

	K (eV)	θ_0 (degree)	ρ_1 (Å)	ρ_2 (Å)	$r_{\min 12}$ (Å)	$r_{\max 12}$ (Å)	$r_{\min 13}$ (Å)	$r_{\max 13}$ (Å)	$r_{\min 23}$ (Å)	$r_{\max 23}$ (Å)
$\theta_{\mathrm{Mo-S-S}}$	73.436	82.799	1.048	1.048	0.0	3.215	0.0	3.215	0.0	4.371
$\theta_{\mathrm{S-Mo-Mo}}$	73.436	82.799	1.048	1.048	0.0	3.215	0.0	3.215	0.0	4.371

The angle θ_{ijk} in the first line indicates the bending energy for the angle with atom i as the apex.

Table 248. Three-body SW potential parameters for single-layer 1T-MoS_2 used by GULP [8] as expressed in Eq. (4).

	ϵ (eV)	σ (Å)	a	λ	γ	$\cos\theta_0$	A_L	B_L	p	q	Tol
Mo—S_1—S_1	1.000	1.048	3.069	73.436	1.000	0.125	2.550	14.207	4	0	0.0

Table 249. SW potential parameters for single-layer 1T-MoS_2 used by LAMMPS [9] as expressed in Eqs. (9) and (10).

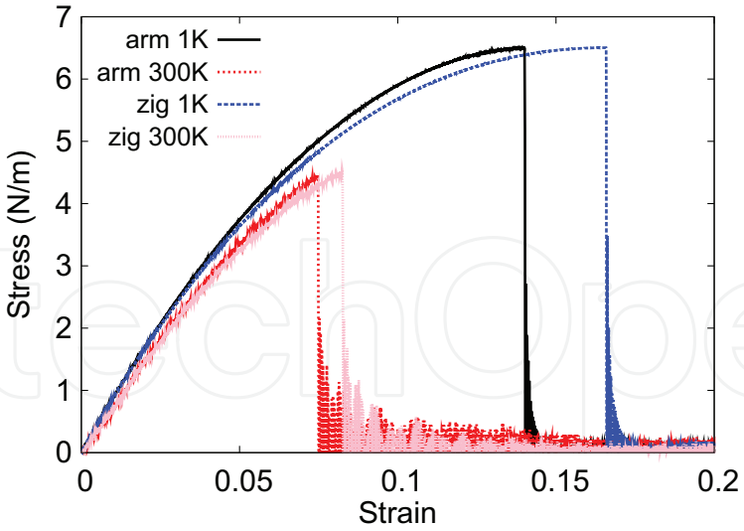

Figure 122. Stress-strain for single-layer 1T-MoS_2 of dimension 100 × 100 Å along the armchair and zigzag directions.

There is no available value for nonlinear quantities in the single-layer 1T-MoS_2. We have thus used the nonlinear parameter $B = 0.5d^4$ in Eq. (5), which is close to the value of B in most materials. The value of the third-order nonlinear elasticity D can be extracted by fitting the stress-strain relation to the function $\sigma = E\epsilon + \frac{1}{2}D\epsilon^2$ with E as the Young's modulus. The values of D from the present SW potential are −595.2 and −624.1 N/m along the armchair and zigzag directions, respectively. The ultimate stress is about 6.5 N/m at the ultimate strain of 0.14 in the armchair direction at the low temperature of 1 K. The ultimate stress is about 6.5 N/m at the ultimate strain of 0.16 in the zigzag direction at the low temperature of 1 K.

Figure 123 shows that the VFF model and the SW potential give exactly the same phonon dispersion, as the SW potential is derived from the VFF model.

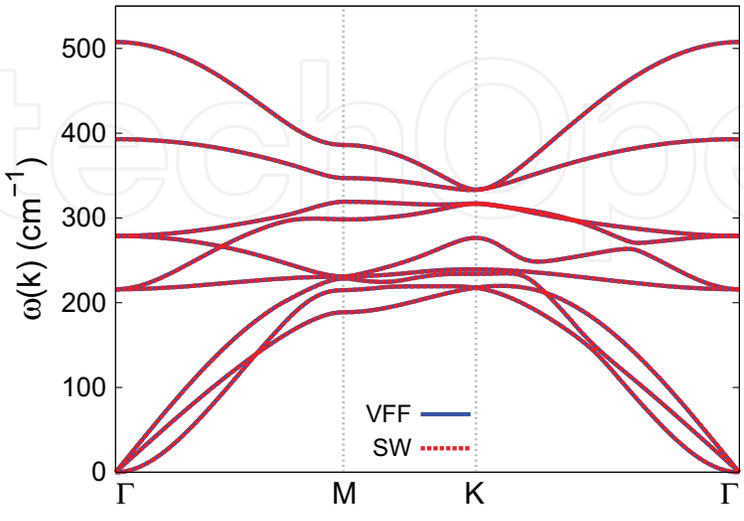

Figure 123. Phonon spectrum for single-layer 1T-MoS_2 along the ΓMKΓ direction in the Brillouin zone. The phonon dispersion from the SW potential is exactly the same as that from the VFF model.

63. 1T-$MoSe_2$

Most existing theoretical studies on the single-layer 1T-$MoSe_2$ are based on the first-principles calculations. In this section, we will develop the SW potential for the single-layer 1T-$MoSe_2$.

The structure for the single-layer 1T-$MoSe_2$ is shown in **Figure 71** (with M=Mo and X=Se). Each Mo atom is surrounded by six Se atoms. These Se atoms are categorized into the top group (e.g., atoms 1, 3, and 5) and bottom group (e.g., atoms 2, 4, and 6). Each Se atom is connected to three Mo atoms. The structural parameters are from the first-principles calculations [48], including the lattice constant $a = 3.2685$ Å and the bond length $d_{\mathrm{Mo-Se}} = 2.5293$ Å, which are derived from the angle $\theta_{\mathrm{SeMoMo}} = 80.5^\circ$. The other angle is $\theta_{\mathrm{MoSeSe}} = 80.5^\circ$ with Se atoms from the same (top or bottom) group.

Table 250 shows three VFF terms for the single-layer 1T-$MoSe_2$; one of which is the bond stretching interaction shown by Eq. (1), while the other two terms are the angle bending interaction shown by Eq. (2). We note that the angle bending term $K_{\mathrm{Mo-Se-Se}}$ is for the angle $\theta_{\mathrm{Mo-Se-Se}}$ with both Se atoms from the same (top or bottom) group. We find that there are actually only two parameters in the VFF model, so we can determine their value by fitting to the Young's modulus and the Poisson's ratio of the system. The *ab initio* calculations have predicted the Young's modulus to be 104 N/m and the Poisson's ratio as -0.13 [48]. The *ab initio* calculations have predicted a negative Poisson's ratio in the 1T-$MoSe_2$, which was attributed to the orbital coupling in this material. The orbital coupling enhances the angle bending interaction in the VFF model. As a result, the value of the angle bending parameter is much larger than the bond stretching force constant parameter, which is typical in auxetic materials with negative Poisson's ratio [52].

The parameters for the two-body SW potential used by GULP are shown in **Table 251**. The parameters for the three-body SW potential used by GULP are shown in **Table 252**. Some representative parameters for the SW potential used by LAMMPS are listed in **Table 253**.

We use LAMMPS to perform MD simulations for the mechanical behavior of the single-layer 1T-$MoSe_2$ under uniaxial tension at 1 and 300 K. **Figure 124** shows the stress-strain curve for the tension of a single-layer 1T-$MoSe_2$ of dimension 100×100 Å. Periodic boundary conditions are applied in both armchair and zigzag directions. The single-layer 1T-$MoSe_2$ is stretched

VFF type	Bond stretching	Angle bending	
Expression	$\frac{1}{2}K_{\mathrm{Mo-Se}}(\Delta r)^2$	$\frac{1}{2}K_{\mathrm{Mo-Se-Se}}(\Delta\theta)^2$	$\frac{1}{2}K_{\mathrm{Se-Mo-Mo}}(\Delta\theta)^2$
Parameter	2.964	14.753	14.753
r_0 or θ_0	2.529	80.501	80.501

The second line gives an explicit expression for each VFF term. The third line is the force constant parameters. Parameters are in the unit of eV/Å^2 for the bond stretching interaction and in the unit of eV for the angle bending interaction. The fourth line gives the initial bond length (in the unit of Å) for the bond stretching interaction and the initial angle (in the unit of degrees) for the angle bending interaction. The angle θ_{ijk} has atom i as the apex.

Table 250. The VFF model for single-layer 1T-$MoSe_2$.

	A (eV)	ρ (Å)	B (Å^4)	$r_{\min}$ (Å)	$r_{\max}$ (Å)
Mo—Se	2.201	1.017	20.463	0.0	3.331

Table 251. Two-body SW potential parameters for single-layer 1T-$MoSe_2$ used by GULP [8] as expressed in Eq. (3).

	K (eV)	θ_0 (°)	ρ_1 (Å)	ρ_2 (Å)	$r_{\min 12}$ (Å)	$r_{\max 12}$ (Å)	$r_{\min 13}$ (Å)	$r_{\max 13}$ (Å)	$r_{\min 23}$ (Å)	$r_{\max 23}$ (Å)
$\theta_{\text{Mo-Se-Se}}$	95.770	80.501	1.017	1.017	0.0	3.331	0.0	3.331	0.0	4.465
$\theta_{\text{Se-Mo-Mo}}$	95.770	80.501	1.017	1.017	0.0	3.331	0.0	3.331	0.0	4.465

The angle θ_{ijk} in the first line indicates the bending energy for the angle with atom i as the apex.

Table 252. Three-body SW potential parameters for single-layer 1T-$MoSe_2$ used by GULP [8] as expressed in Eq. (4).

	ϵ (eV)	σ (Å)	a	λ	γ	$\cos\theta_0$	A_L	B_L	p	q	Tol
Mo—Se_1—Se_1	1.000	1.017	3.276	95.770	1.000	0.165	2.201	19.152	4	0	0.0

Table 253. SW potential parameters for single-layer 1T-$MoSe_2$ used by LAMMPS [9] as expressed in Eqs. (9) and (10).

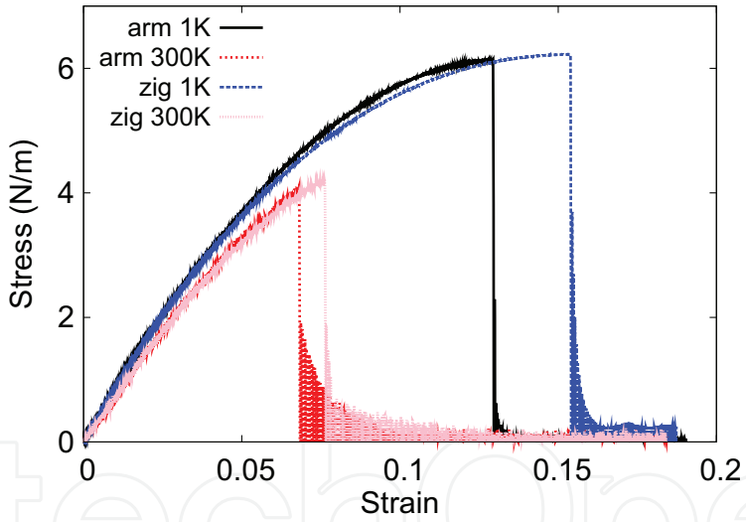

Figure 124. Stress-strain for single-layer 1T-$MoSe_2$ of dimension 100 × 100 Å along the armchair and zigzag directions.

uniaxially along the armchair or zigzag direction. The stress is calculated without involving the actual thickness of the quasi-two-dimensional structure of the single-layer 1T-$MoSe_2$. The Young's modulus can be obtained by a linear fitting of the stress-strain relation in the small strain range of [0, 0.01]. The Young's modulus is 88.2 and 87.9 N/m along the armchair and zigzag directions, respectively. The Young's modulus is essentially isotropic in the armchair and zigzag directions. The Poisson's ratio from the VFF model and the SW potential is $\nu_{xy} = \nu_{yx} = -0.13$. The fitted Young's modulus value is about 10% smaller than the *ab initio* result of 104 N/m [48], as only short-range interactions are considered in the present work. The

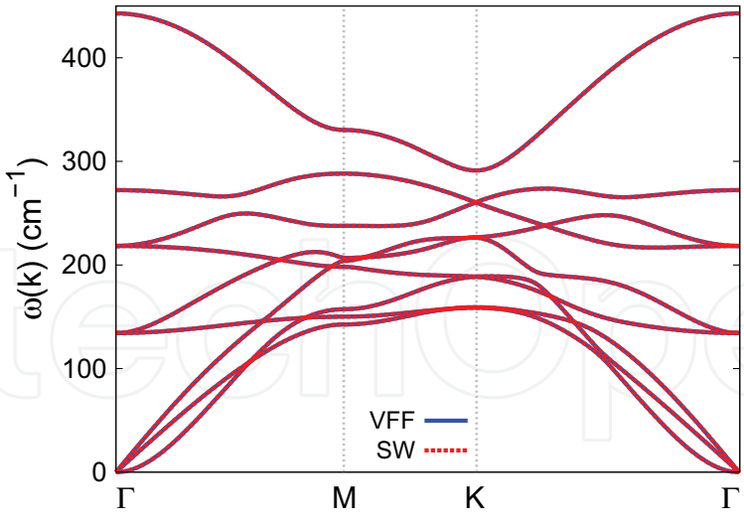

Figure 125. Phonon spectrum for single-layer 1T-$MoSe_2$ along the ΓMKΓ direction in the Brillouin zone. The phonon dispersion from the SW potential is exactly the same as that from the VFF model.

long-range interactions are ignored, which typically leads to about 10% underestimation for the value of the Young's modulus.

There is no available value for nonlinear quantities in the single-layer 1T-$MoSe_2$. We have thus used the nonlinear parameter $B = 0.5d^4$ in Eq. (5), which is close to the value of B in most materials. The value of the third-order nonlinear elasticity D can be extracted by fitting the stress-strain relation to the function $\sigma = E\epsilon + \frac{1}{2}D\epsilon^2$ with E as the Young's modulus. The values of D from the present SW potential are -632.6 and -629.7 N/m along the armchair and zigzag directions, respectively. The ultimate stress is about 6.1 N/m at the ultimate strain of 0.13 in the armchair direction at the low temperature of 1 K. The ultimate stress is about 6.2 N/m at the ultimate strain of 0.15 in the zigzag direction at the low temperature of 1 K.

Figure 125 shows that the VFF model and the SW potential give exactly the same phonon dispersion, as the SW potential is derived from the VFF model.

64. 1T-$MoTe_2$

Most existing theoretical studies on the single-layer 1T-$MoTe_2$ are based on the first-principles calculations. In this section, we will develop the SW potential for the single-layer 1T-$MoTe_2$.

The structure for the single-layer 1T-$MoTe_2$ is shown in **Figure 71** (with M=Mo and X=Te). Each Mo atom is surrounded by six Te atoms. These Te atoms are categorized into the top group (e.g., atoms 1, 3, and 5) and bottom group (e.g., atoms 2, 4, and 6). Each Te atom is connected to three Mo atoms. The structural parameters are from the first-principles calculations [48], including the lattice constant $a = 3.4970$ Å and the bond length $d_{\mathrm{Mo-Te}} = 2.7287$ Å, which are derived from the angle $\theta_{\mathrm{TeMoMo}} = 79.7°$. The other angle is $\theta_{\mathrm{MoTeTe}} = 79.7°$ with Te atoms from the same (top or bottom) group.

Table 254 shows three VFF terms for the single-layer 1T-$MoTe_2$; one of which is the bond stretching interaction shown by Eq. (1), while the other two terms are the angle bending interaction shown by Eq. (2). We note that the angle bending term $K_{\mathrm{Mo-Te-Te}}$ is for the angle $\theta_{\mathrm{Mo-Te-Te}}$ with both Te atoms from the same (top or bottom) group. We find that there are actually only two parameters in the VFF model, so we can determine their value by fitting to the Young's modulus and the Poisson's ratio of the system. The *ab initio* calculations have predicted the Young's modulus to be 92 N/m and the Poisson's ratio as −0.07 [48]. The *ab initio* calculations have predicted a negative Poisson's ratio in the 1T-$MoTe_2$, which was attributed to the orbital coupling in this material. The orbital coupling enhances the angle bending interaction in the VFF model. As a result, the value of the angle bending parameter is much larger than the bond stretching force constant parameter, which is typical in auxetic materials with negative Poisson's ratio [52].

The parameters for the two-body SW potential used by GULP are shown in **Table 255**. The parameters for the three-body SW potential used by GULP are shown in **Table 256**. Some representative parameters for the SW potential used by LAMMPS are listed in **Table 257**.

We use LAMMPS to perform MD simulations for the mechanical behavior of the single-layer 1T-$MoTe_2$ under uniaxial tension at 1 and 300 K. **Figure 126** shows the stress-strain curve for the tension of a single-layer 1T-$MoTe_2$ of dimension 100 × 100 Å. Periodic boundary conditions

VFF type	Bond stretching	Angle bending	
Expression	$\frac{1}{2}K_{\mathrm{Mo-Te}}(\Delta r)^2$	$\frac{1}{2}K_{\mathrm{Mo-Te-Te}}(\Delta\theta)^2$	$\frac{1}{2}K_{\mathrm{Te-Mo-Mo}}(\Delta\theta)^2$
Parameter	3.074	12.516	12.516
r_0 or θ_0	2.729	79.700	79.700

The second line gives an explicit expression for each VFF term. The third line is the force constant parameters. Parameters are in the unit of eV/Å^2 for the bond stretching interaction and in the unit of eV for the angle bending interaction. The fourth line gives the initial bond length (in the unit of Å) for the bond stretching interaction and the initial angle (in the unit of degrees) for the angle bending interaction. The angle θ_{ijk} has atom i as the apex.

Table 254. The VFF model for single-layer 1T-$MoTe_2$.

	A (eV)	ρ (Å)	B (Å^4)	r_{min} (Å)	r_{max} (Å)
Mo—Te	2.597	1.068	27.720	0.0	3.582

Table 255. Two-body SW potential parameters for single-layer 1T-$MoTe_2$ used by GULP [8] as expressed in Eq. (3).

	K (eV)	θ_0 (°)	ρ_1 (Å)	ρ_2 (Å)	$r_{\mathrm{min}\,12}$ (Å)	$r_{\mathrm{max}\,12}$ (Å)	$r_{\mathrm{min}\,13}$ (Å)	$r_{\mathrm{max}\,13}$ (Å)	$r_{\mathrm{min}\,23}$ (Å)	$r_{\mathrm{max}\,23}$ (Å)
$\theta_{\mathrm{Mo-Te-Te}}$	78.925	79.700	1.068	1.068	0.0	3.582	0.0	3.582	0.0	4.777
$\theta_{\mathrm{Te-Mo-Mo}}$	78.925	79.700	1.068	1.068	0.0	3.582	0.0	3.582	0.0	4.777

The angle θ_{ijk} in the first line indicates the bending energy for the angle with atom i as the apex.

Table 256. Three-body SW potential parameters for single-layer 1T-$MoTe_2$ used by GULP [8] as expressed in Eq. (4).

	ϵ (eV)	σ (Å)	a	λ	γ	$\cos\theta_0$	A_L	B_L	p	q	Tol
Mo—Te_1—Te_1	1.000	1.068	3.355	78.925	1.000	0.179	2.597	21.328	4	0	0.0

Table 257. SW potential parameters for single-layer 1T-$MoTe_2$ used by LAMMPS [9] as expressed in Eqs. (9) and (10).

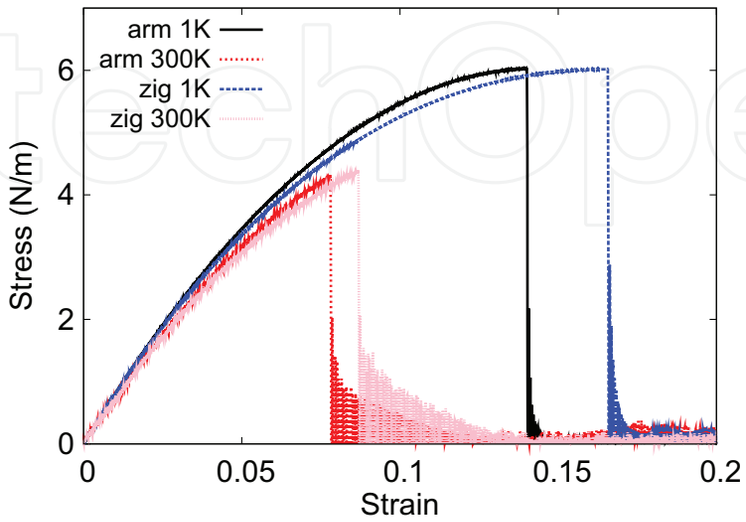

Figure 126. Stress-strain for single-layer 1T-$MoTe_2$ of dimension 100 × 100 Å along the armchair and zigzag directions.

are applied in both armchair and zigzag directions. The single-layer 1T-$MoTe_2$ is stretched uniaxially along the armchair or zigzag direction. The stress is calculated without involving the actual thickness of the quasi-two-dimensional structure of the single-layer 1T-$MoTe_2$. The Young's modulus can be obtained by a linear fitting of the stress-strain relation in the small strain range of [0, 0.01]. The Young's modulus is 81.6 and 81.2 N/m along the armchair and zigzag directions, respectively. The Young's modulus is essentially isotropic in the armchair and zigzag directions. The Poisson's ratio from the VFF model and the SW potential is $\nu_{xy} = \nu_{yx} = -0.07$. The fitted Young's modulus value is about 10% smaller than the *ab initio* result of 92 N/m [48], as only short-range interactions are considered in the present work. The long-range interactions are ignored, which typically leads to about 10% underestimation for the value of the Young's modulus.

There is no available value for nonlinear quantities in the single-layer 1T-$MoTe_2$. We have thus used the nonlinear parameter $B = 0.5d^4$ in Eq. (5), which is close to the value of B in most materials. The value of the third-order nonlinear elasticity D can be extracted by fitting the stress-strain relation to the function $\sigma = E\epsilon + \frac{1}{2}D\epsilon^2$ with E as the Young's modulus. The values of D from the present SW potential are −543.1 and −558.6 N/m along the armchair and zigzag directions, respectively. The ultimate stress is about 6.0 N/m at the ultimate strain of 0.14 in the armchair direction at the low temperature of 1 K. The ultimate stress is about 6.0 N/m at the ultimate strain of 0.16 in the zigzag direction at the low temperature of 1 K.

Figure 127 shows that the VFF model and the SW potential give exactly the same phonon dispersion, as the SW potential is derived from the VFF model.

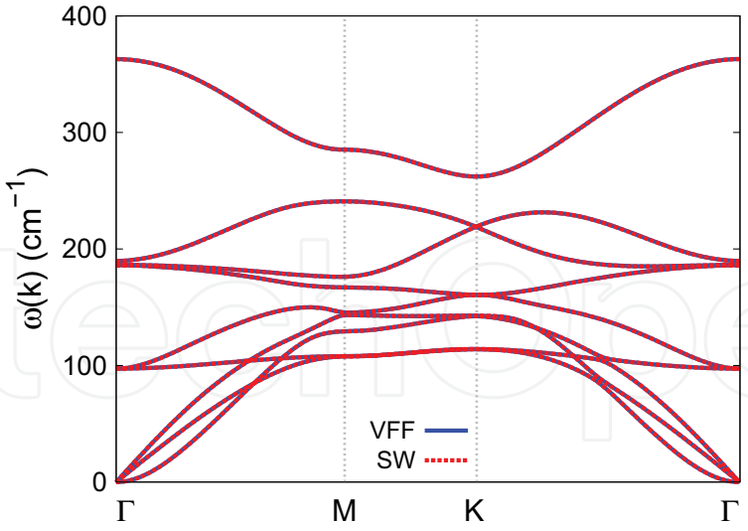

Figure 127. Phonon spectrum for single-layer 1T-$MoTe_2$ along the ΓMKΓ direction in the Brillouin zone. The phonon dispersion from the SW potential is exactly the same as that from the VFF model.

65. 1T-TcS_2

Most existing theoretical studies on the single-layer 1T-TcS_2 are based on the first-principles calculations. In this section, we will develop the SW potential for the single-layer 1T-TcS_2.

The structure for the single-layer 1T-TcS_2 is shown in **Figure 71** (with M = Tc and X = S). Each Tc atom is surrounded by six S atoms. These S atoms are categorized into the top group (e.g., atoms 1, 3, and 5) and bottom group (e.g., atoms 2, 4, and 6). Each S atom is connected to three Tc atoms. The structural parameters are from the first-principles calculations [48] including the lattice constant $a = 3.0692$ Å and the bond length $d_{\mathrm{Tc-S}} = 2.3924$ Å, which are derived from the angle $\theta_{\mathrm{STcTc}} = 79.8^\circ$. The other angle is $\theta_{\mathrm{TcSS}} = 79.8^\circ$ with S atoms from the same (top or bottom) group.

Table 258 shows three VFF terms for the single-layer 1T-TcS_2; one of which is the bond stretching interaction shown by Eq. (1), while the other two terms are the angle bending interaction shown by Eq. (2). We note that the angle bending term $K_{\mathrm{Tc-S-S}}$ is for the angle $\theta_{\mathrm{Tc-S-S}}$ with both S atoms from the same (top or bottom) group. We find that there are actually

VFF type	Bond stretching	Angle bending	
Expression	$\frac{1}{2}K_{\mathrm{Tc-S}}(\Delta r)^2$	$\frac{1}{2}K_{\mathrm{Tc-S-S}}(\Delta\theta)^2$	$\frac{1}{2}K_{\mathrm{S-Tc-Tc}}(\Delta\theta)^2$
Parameter	2.986	11.141	11.141
r_0 or θ_0	2.392	79.800	79.800

The second line gives an explicit expression for each VFF term. The third line is the force constant parameters. Parameters are in the unit of ev/Å^2 for the bond stretching interaction and in the unit of eV for the angle bending interaction. The fourth line gives the initial bond length (in the unit of Å) for the bond stretching interaction and the initial angle (in the unit of degrees) for the angle bending interaction. The angle θ_{ijk} has atom i as the apex.

Table 258. The VFF model for single-layer 1T-TcS_2.

only two parameters in the VFF model, so we can determine their value by fitting to the Young's modulus and the Poisson's ratio of the system. The *ab initio* calculations have predicted the Young's modulus to be 94 N/m and the Poisson's ratio as −0.10 [48]. The *ab initio* calculations have predicted a negative Poisson's ratio in the 1T-TcS_2, which was attributed to the orbital coupling in this material. The orbital coupling enhances the angle bending interaction in the VFF model. As a result, the value of the angle bending parameter is much larger than the bond stretching force constant parameter, which is typical in auxetic materials with negative Poisson's ratio [52].

The parameters for the two-body SW potential used by GULP are shown in **Table 259**. The parameters for the three-body SW potential used by GULP are shown in **Table 260**. Some representative parameters for the SW potential used by LAMMPS are listed in **Table 261**.

We use LAMMPS to perform MD simulations for the mechanical behavior of the single-layer 1T-TcS_2 under uniaxial tension at 1 and 300 K. **Figure 128** shows the stress-strain curve for the tension of a single-layer 1T-TcS_2 of dimension 100 × 100 Å. Periodic boundary conditions are applied in both armchair and zigzag directions. The single-layer 1T-TcS_2 is stretched uniaxially along the armchair or zigzag direction. The stress is calculated without involving the actual thickness of the quasi-two-dimensional structure of the single-layer 1T-TcS_2. The Young's modulus can be obtained by a linear fitting of the stress-strain relation in the small strain range of [0, 0.01]. The Young's modulus is 84.3 and 84.0 N/m along the armchair and zigzag directions, respectively. The Young's modulus is essentially isotropic in the armchair and zigzag directions. The Poisson's ratio from the VFF model and the SW potential is $\nu_{xy} = \nu_{yx} = -0.10$. The fitted Young's modulus value is about 10% smaller than the *ab initio* result of 94 N/m [48], as only short-range interactions are considered in the present work. The long-range interactions are ignored, which typically leads to about 10% underestimation for the value of the Young's modulus.

	A (eV)	ρ (Å)	B (Å^4)	$r_{\min}$ (Å)	$r_{\max}$ (Å)
Tc—S	1.945	0.939	16.380	0.0	3.142

Table 259. Two-body SW potential parameters for single-layer 1T-TcS_2 used by GULP [8] as expressed in Eq. (3).

	K (eV)	θ_0 (°)	ρ_1 (Å)	ρ_2 (Å)	$r_{\min 12}$ (Å)	$r_{\max 12}$ (Å)	$r_{\min 13}$ (Å)	$r_{\max 13}$ (Å)	$r_{\min 23}$ (Å)	$r_{\max 23}$ (Å)
$\theta_{\mathrm{Tc-S-S}}$	70.512	79.800	0.939	0.939	0.0	3.142	0.0	3.142	0.0	4.193
$\theta_{\mathrm{S-Tc-Tc}}$	70.512	79.800	0.939	0.939	0.0	3.142	0.0	3.142	0.0	4.193

The angle θ_{ijk} in the first line indicates the bending energy for the angle with atom i as the apex.

Table 260. Three-body SW potential parameters for single-layer 1T-TcS_2 used by GULP [8] as expressed in Eq. (4).

	ϵ (eV)	σ (Å)	a	λ	γ	$\cos\theta_0$	A_L	B_L	p	q	Tol
Tc—S_1—S_1	1.000	0.939	3.345	70.512	1.000	0.177	1.945	21.038	4	0	0.0

Table 261. SW potential parameters for single-layer 1T-TcS_2 used by LAMMPS [9] as expressed in Eqs. (9) and (10).

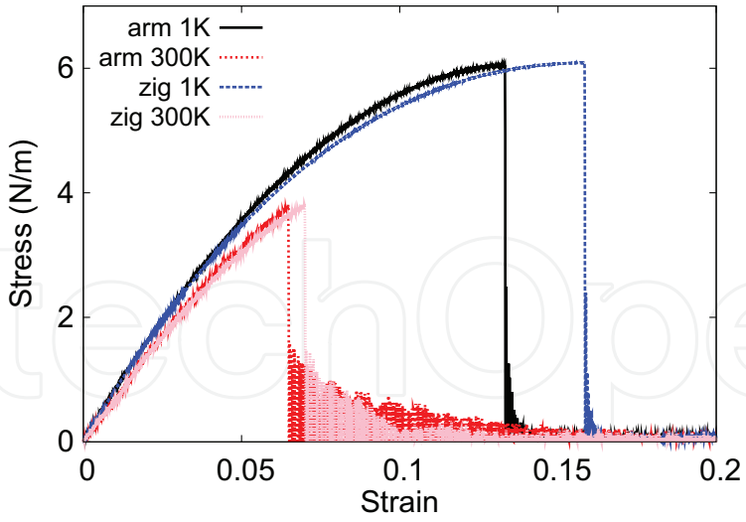

Figure 128. Stress-strain for single-layer 1T-TcS_2 of dimension 100 × 100 Å along the armchair and zigzag directions.

There is no available value for nonlinear quantities in the single-layer 1T-TcS_2. We have thus used the nonlinear parameter $B = 0.5d^4$ in Eq. (5), which is close to the value of B in most materials. The value of the third-order nonlinear elasticity D can be extracted by fitting the stress-strain relation to the function $\sigma = E\epsilon + \frac{1}{2}D\epsilon^2$ with E as the Young's modulus. The values of D from the present SW potential are −572.0 and −588.6 N/m along the armchair and zigzag directions, respectively. The ultimate stress is about 6.0 N/m at the ultimate strain of 0.13 in the armchair direction at the low temperature of 1 K. The ultimate stress is about 6.1 N/m at the ultimate strain of 0.16 in the zigzag direction at the low temperature of 1 K.

Figure 129 shows that the VFF model and the SW potential give exactly the same phonon dispersion, as the SW potential is derived from the VFF model.

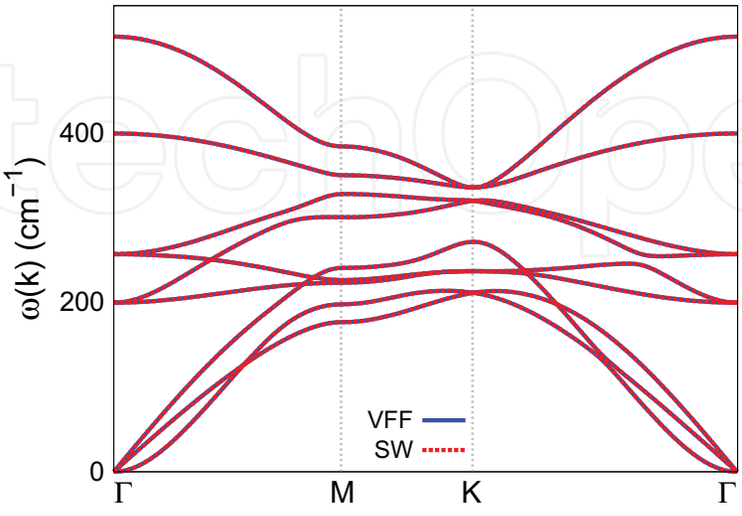

Figure 129. Phonon spectrum for single-layer 1T-TcS_2 along the ΓMKΓ direction in the Brillouin zone. The phonon dispersion from the SW potential is exactly the same as that from the VFF model.

66. 1T-$TcSe_2$

Most existing theoretical studies on the single-layer 1T-$TcSe_2$ are based on the first-principles calculations. In this section, we will develop the SW potential for the single-layer 1T-$TcSe_2$.

The structure for the single-layer 1T-$TcSe_2$ is shown in **Figure 71** (with M=Tc and X=Se). Each Tc atom is surrounded by six Se atoms. These Se atoms are categorized into the top group (e.g., atoms 1, 3, and 5) and bottom group (e.g., atoms 2, 4, and 6). Each Se atom is connected to three Tc atoms. The structural parameters are from the first-principles calculations [48], including the lattice constant $a = 3.1543$ Å and the bond length $d_{\mathrm{Tc-Se}} = 2.5061$ Å, which are derived from the angle $\theta_{\mathrm{SeTcTc}} = 78^\circ$. The other angle is $\theta_{\mathrm{TcSeSe}} = 78^\circ$ with Se atoms from the same (top or bottom) group.

Table 262 shows three VFF terms for the single-layer 1T-$TcSe_2$; one of which is the bond stretching interaction shown by Eq. (1), while the other two terms are the angle bending interaction shown by Eq. (2). We note that the angle bending term $K_{\mathrm{Tc-Se-Se}}$ is for the angle $\theta_{\mathrm{Tc-Se-Se}}$ with both Se atoms from the same (top or bottom) group. We find that there are actually only two parameters in the VFF model, so we can determine their value by fitting to the Young's modulus and the Poisson's ratio of the system. The *ab initio* calculations have predicted the Young's modulus to be 104 N/m and the Poisson's ratio as -0.04 [48]. The *ab initio* calculations have predicted a negative Poisson's ratio in the 1T-$TcSe_2$, which was attributed to the orbital coupling in this material. The orbital coupling enhances the angle bending interaction in the VFF model. As a result, the value of the angle bending parameter is much larger than the bond stretching force constant parameter, which is typical in auxetic materials with negative Poisson's ratio [52].

The parameters for the two-body SW potential used by GULP are shown in **Table 263**. The parameters for the three-body SW potential used by GULP are shown in **Table 264**. Some representative parameters for the SW potential used by LAMMPS are listed in **Table 265**.

VFF type	Bond stretching	Angle bending	
Expression	$\frac{1}{2}K_{\mathrm{Tc-Se}}(\Delta r)^2$	$\frac{1}{2}K_{\mathrm{Tc-Se-Se}}(\Delta\theta)^2$	$\frac{1}{2}K_{\mathrm{Se-Tc-Tc}}(\Delta\theta)^2$
Parameter	3.467	10.636	10.636
r_0 or θ_0	2.506	78.001	78.001

The second line gives an explicit expression for each VFF term. The third line is the force constant parameters. Parameters are in the unit of ev/Å^2 for the bond stretching interaction and in the unit of eV for the angle bending interaction. The fourth line gives the initial bond length (in the unit of Å) for the bond stretching interaction and the initial angle (in the unit of degrees) for the angle bending interaction. The angle θ_{ijk} has atom i as the apex.

Table 262. The VFF model for single-layer 1T-$TcSe_2$.

	A (eV)	ρ (Å)	B (Å^4)	r_{min} (Å)	r_{max} (Å)
Tc—Se	2.355	0.925	19.723	0.0	3.267

Table 263. Two-body SW potential parameters for single-layer 1T-$TcSe_2$ used by GULP [8] as expressed in Eq. (3).

	K (eV)	θ_0 (°)	ρ_1 (Å)	ρ_2 (Å)	$r_{\min 12}$ (Å)	$r_{\max 12}$ (Å)	$r_{\min 13}$ (Å)	$r_{\max 13}$ (Å)	$r_{\min 23}$ (Å)	$r_{\max 23}$ (Å)
$\theta_{\text{Tc–Se–Se}}$	63.150	78.001	0.925	0.925	0.0	3.267	0.0	3.267	0.0	4.309
$\theta_{\text{Se–Tc–Tc}}$	63.150	78.001	0.925	0.925	0.0	3.267	0.0	3.267	0.0	4.309

The angle θ_{ijk} in the first line indicates the bending energy for the angle with atom i as the apex.

Table 264. Three-body SW potential parameters for single-layer 1T-$TcSe_2$ used by GULP [8] as expressed in Eq. (4).

	ϵ (eV)	σ (Å)	a	λ	γ	$\cos\theta_0$	A_L	B_L	p	q	Tol
$Tc—Se_1—Se_1$	1.000	0.925	3.532	63.150	1.000	0.208	2.355	26.932	4	0	0.0

Table 265. SW potential parameters for single-layer 1T-$TcSe_2$ used by LAMMPS [9] as expressed in Eqs. (9) and (10).

We use LAMMPS to perform MD simulations for the mechanical behavior of the single-layer 1T-$TcSe_2$ under uniaxial tension at 1 and 300 K. **Figure 130** shows the stress-strain curve for the tension of a single-layer 1T-$TcSe_2$ of dimension 100 × 100 Å. Periodic boundary conditions are applied in both armchair and zigzag directions. The single-layer 1T-$TcSe_2$ is stretched uniaxially along the armchair or zigzag direction. The stress is calculated without involving the actual thickness of the quasi-two-dimensional structure of the single-layer 1T-$TcSe_2$. The Young's modulus can be obtained by a linear fitting of the stress-strain relation in the small strain range of [0, 0.01]. The Young's modulus is 88.8 and 88.3 N/m along the armchair and zigzag directions, respectively. The Young's modulus is essentially isotropic in the armchair and zigzag directions. The Poisson's ratio from the VFF model and the SW potential is $\nu_{xy} = \nu_{yx} = -0.04$. The fitted Young's modulus value is about 10% smaller than the *ab initio* result of 104 N/m [48], as only short-range interactions are considered in the present work. The long-range interactions are ignored, which typically leads to about 10% underestimation for the value of the Young's modulus.

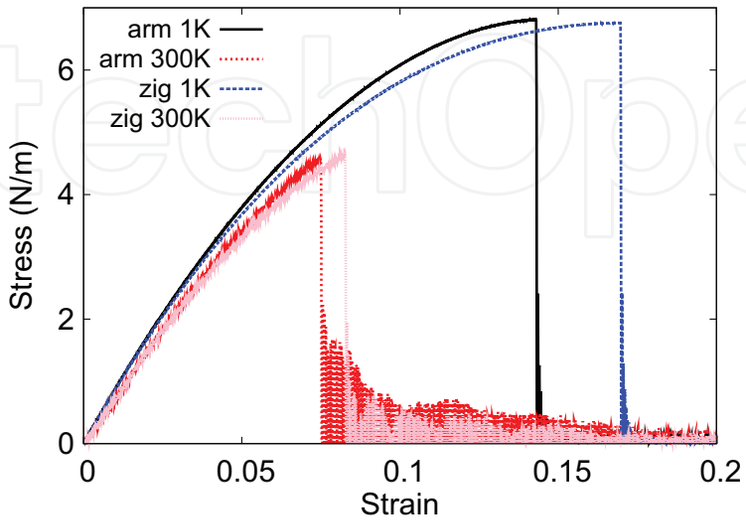

Figure 130. Stress-strain for single-layer 1T-$TcSe_2$ of dimension 100 × 100 Å along the armchair and zigzag directions.

http://dx.doi.org/10.5772/intechopen.71929

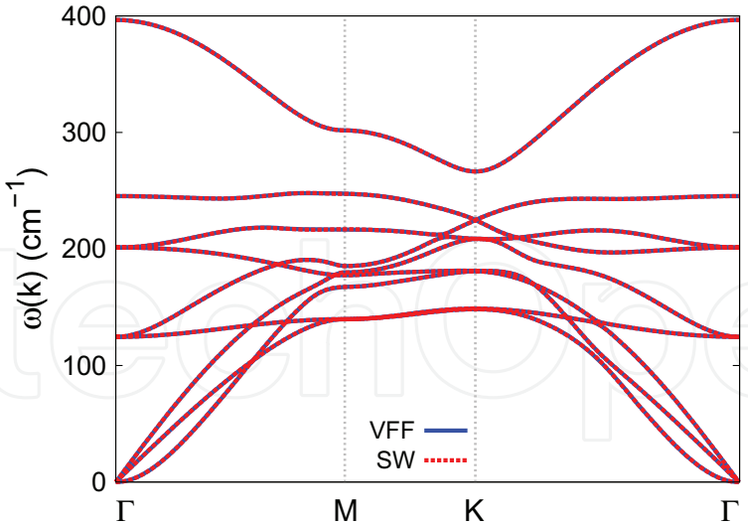

Figure 131. Phonon spectrum for single-layer 1T-$TcSe_2$ along the ΓMKΓ direction in the Brillouin zone. The phonon dispersion from the SW potential is exactly the same as that from the VFF model.

There is no available value for nonlinear quantities in the single-layer 1T-$TcSe_2$. We have thus used the nonlinear parameter $B = 0.5d^4$ in Eq. (5), which is close to the value of B in most materials. The value of the third-order nonlinear elasticity D can be extracted by fitting the stress-strain relation to the function $\sigma = E\epsilon + \frac{1}{2}D\epsilon^2$ with E as the Young's modulus. The values of D from the present SW potential are -565.7 and -587.3 N/m along the armchair and zigzag directions, respectively. The ultimate stress is about 6.8 N/m at the ultimate strain of 0.14 in the armchair direction at the low temperature of 1 K. The ultimate stress is about 6.8 N/m at the ultimate strain of 0.17 in the zigzag direction at the low temperature of 1 K.

Figure 131 shows that the VFF model and the SW potential give exactly the same phonon dispersion, as the SW potential is derived from the VFF model.

67. 1T-$TcTe_2$

Most existing theoretical studies on the single-layer 1T-$TcTe_2$ are based on the first-principles calculations. In this section, we will develop the SW potential for the single-layer 1T-$TcTe_2$.

The structure for the single-layer 1T-$TcTe_2$ is shown in **Figure 71** (with M=Tc and X=Te). Each Tc atom is surrounded by six Te atoms. These Te atoms are categorized into the top group (e.g., atoms 1, 3, and 5) and bottom group (e.g., atoms 2, 4, and 6). Each Te atom is connected to three Tc atoms. The structural parameters are from the first-principles calculations [48], including the lattice constant $a = 3.4149$ Å and the bond length $d_{\mathrm{Tc-Te}} = 2.6900$ Å, which are derived from the angle $\theta_{\mathrm{TeTcTc}} = 78.8^\circ$. The other angle is $\theta_{\mathrm{TcTeTe}} = 78.8^\circ$ with Te atoms from the same (top or bottom) group.

Table 266 shows three VFF terms for the single-layer 1T-$TcTe_2$; one of which is the bond stretching interaction shown by Eq. (1), while the other two terms are the angle bending

VFF type	Bond stretching	Angle bending	
Expression	$\frac{1}{2}K_{\mathrm{Tc-Te}}(\Delta r)^2$	$\frac{1}{2}K_{\mathrm{Tc-Te-Te}}(\Delta\theta)^2$	$\frac{1}{2}K_{\mathrm{Te-Tc-Tc}}(\Delta\theta)^2$
Parameter	0.785	8.894	8.894
r_0 or θ_0	2.690	78.801	78.801

The second line gives an explicit expression for each VFF term. The third line is the force constant parameters. Parameters are in the unit of ev/Å^2 for the bond stretching interaction and in the unit of eV for the angle bending interaction. The fourth line gives the initial bond length (in the unit of Å) for the bond stretching interaction and the initial angle (in the unit of degrees) for the angle bending interaction. The angle θ_{ijk} has atom i as the apex.

Table 266. The VFF model for single-layer 1T-$TcTe_2$.

interaction shown by Eq. (2). We note that the angle bending term $K_{\mathrm{Tc-Te-Te}}$ is for the angle $\theta_{\mathrm{Tc-Te-Te}}$ with both Te atoms from the same (top or bottom) group. We find that there are actually only two parameters in the VFF model, so we can determine their value by fitting to the Young's modulus and the Poisson's ratio of the system. The *ab initio* calculations have predicted the Young's modulus to be 34 N/m and the Poisson's ratio as −0.36 [48]. The *ab initio* calculations have predicted a negative Poisson's ratio in the 1T-$TcTe_2$, which was attributed to the orbital coupling in this material. The orbital coupling enhances the angle bending interaction in the VFF model. As a result, the value of the angle bending parameter is much larger than the bond stretching force constant parameter, which is typical in auxetic materials with negative Poisson's ratio [52].

The parameters for the two-body SW potential used by GULP are shown in **Table 267**. The parameters for the three-body SW potential used by GULP are shown in **Table 268**. Some representative parameters for the SW potential used by LAMMPS are listed in **Table 269**.

	A (eV)	ρ (Å)	B (Å^4)	r_{min} (Å)	r_{max} (Å)
Tc—Te	0.628	1.021	26.181	0.0	3.519

Table 267. Two-body SW potential parameters for single-layer 1T-$TcTe_2$ used by GULP [8] as expressed in Eq. (3).

	K (eV)	θ_0 (°)	ρ_1 (Å)	ρ_2 (Å)	$r_{\mathrm{min\,12}}$ (Å)	$r_{\mathrm{max\,12}}$ (Å)	$r_{\mathrm{min\,13}}$ (Å)	$r_{\mathrm{max\,13}}$ (Å)	$r_{\mathrm{min\,23}}$ (Å)	$r_{\mathrm{max\,23}}$ (Å)
$\theta_{\mathrm{Tc-Te-Te}}$	54.313	78.801	1.021	1.021	0.0	3.519	0.0	3.519	0.0	4.665
$\theta_{\mathrm{Te-Tc-Tc}}$	54.313	78.801	1.021	1.021	0.0	3.519	0.0	3.519	0.0	4.665

The angle θ_{ijk} in the first line indicates the bending energy for the angle with atom i as the apex.

Table 268. Three-body SW potential parameters for single-layer 1T-$TcTe_2$ used by GULP [8] as expressed in Eq. (4).

	ϵ (eV)	σ (Å)	a	λ	γ	$\cos\theta_0$	A_L	B_L	p	q	Tol
Tc—Te_1—Te_1	1.000	1.021	3.447	54.313	1.000	0.194	0.628	24.110	4	0	0.0

Table 269. SW potential parameters for single-layer 1T-$TcTe_2$ used by LAMMPS [9] as expressed in Eqs. (9) and (10).

http://dx.doi.org/10.5772/intechopen.71929

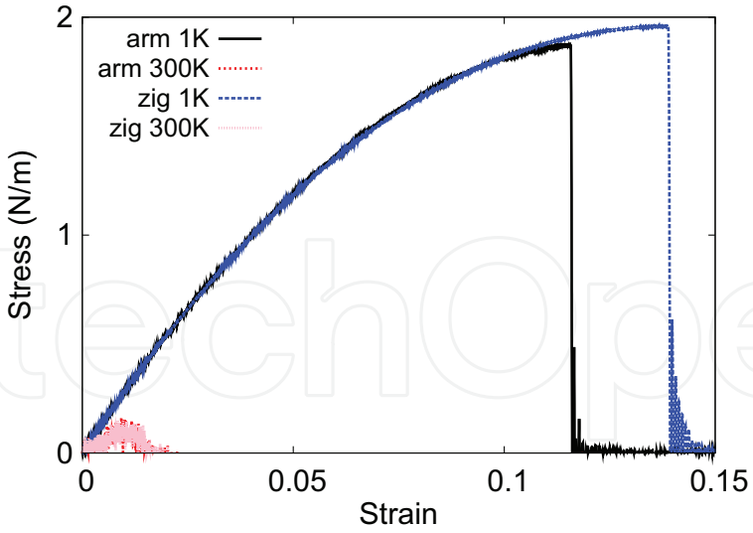

Figure 132. Stress-strain for single-layer 1T-$TcTe_2$ of dimension 100 × 100 Å along the armchair and zigzag directions.

We use LAMMPS to perform MD simulations for the mechanical behavior of the single-layer 1T-$TcTe_2$ under uniaxial tension at 1 and 300 K. **Figure 132** shows the stress-strain curve for the tension of a single-layer 1T-$TcTe_2$ of dimension 100 × 100 Å. Periodic boundary conditions are applied in both armchair and zigzag directions. The single-layer 1T-$TcTe_2$ is stretched uniaxially along the armchair or zigzag direction. The stress is calculated without involving the actual thickness of the quasi-two-dimensional structure of the single-layer 1T-$TcTe_2$. The Young's modulus can be obtained by a linear fitting of the stress-strain relation in the small strain range of [0, 0.01]. The Young's modulus is 28.6 N/m along the armchair and zigzag directions. The Poisson's ratio from the VFF model and the SW potential is $\nu_{xy} = \nu_{yx} = -0.21$. The fitted Young's modulus value is about 10% smaller than the *ab initio* result of 34 N/m [48], as only short-range interactions are considered in the present work. The long-range interactions are ignored, which typically leads to about 10% underestimation for the value of the Young's modulus.

There is no available value for nonlinear quantities in the single-layer 1T-$TcTe_2$. We have thus used the nonlinear parameter $B = 0.5d^4$ in Eq. (5), which is close to the value of B in most materials. The value of the third-order nonlinear elasticity D can be extracted by fitting the stress-strain relation to the function $\sigma = E\epsilon + \frac{1}{2}D\epsilon^2$ with E as the Young's modulus. The values of D from the present SW potential are −207.8 and −208.7 N/m along the armchair and zigzag directions, respectively. The ultimate stress is about 1.9 N/m at the ultimate strain of 0.11 in the armchair direction at the low temperature of 1 K. The ultimate stress is about 2.0 N/m at the ultimate strain of 0.14 in the zigzag direction at the low temperature of 1 K. The ultimate strain decreases to be about 0.01 at 300 K, so the single-layer 1T-$TcTe_2$ is not very stable at higher temperature. It is because this material is very soft and the Poisson's ratio is very small (negative value).

Figure 133 shows that the VFF model and the SW potential give exactly the same phonon dispersion, as the SW potential is derived from the VFF model.

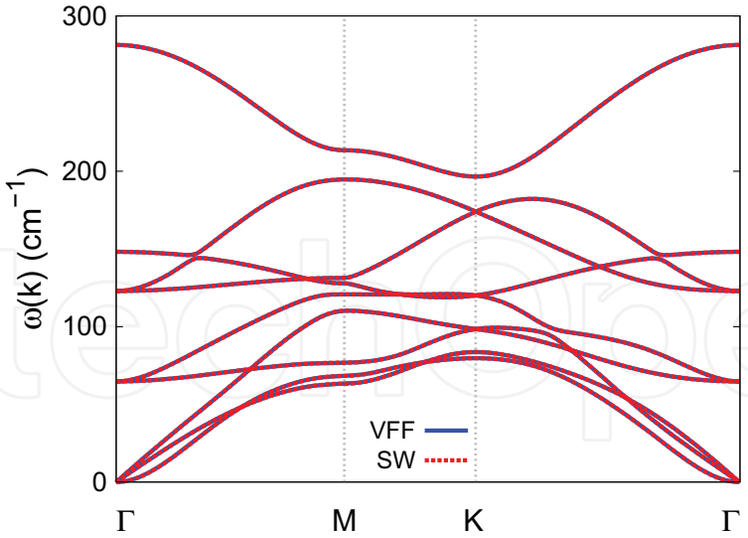

Figure 133. Phonon spectrum for single-layer 1T-$TcTe_2$ along the ΓMKΓ direction in the Brillouin zone. The phonon dispersion from the SW potential is exactly the same as that from the VFF model.

68. 1T-$RhTe_2$

Most existing theoretical studies on the single-layer 1T-$RhTe_2$ are based on the first-principles calculations. In this section, we will develop the SW potential for the single-layer 1T-$RhTe_2$.

The structure for the single-layer 1T-$RhTe_2$ is shown in **Figure 71** (with M=Rh and X=Te). Each Rh atom is surrounded by six Te atoms. These Te atoms are categorized into the top group (e.g., atoms 1, 3, and 5) and bottom group (e.g., atoms 2, 4, and 6). Each Te atom is connected to three Rh atoms. The structural parameters are from the first-principles calculations [48], including the lattice constant $a = 3.7563$ Å and the bond length $d_{\mathrm{Rh-Te}} = 2.6332$ Å, which are derived from the angle $\theta_{\mathrm{TeRhRh}} = 91^\circ$. The other angle is $\theta_{\mathrm{RhTeTe}} = 91^\circ$ with Te atoms from the same (top or bottom) group.

Table 270 shows three VFF terms for the single-layer 1T-$RhTe_2$; one of which is the bond stretching interaction shown by Eq. (1), while the other two terms are the angle bending

VFF type	Bond stretching	Angle bending	
Expression	$\frac{1}{2}K_{\mathrm{Rh-Te}}(\Delta r)^2$	$\frac{1}{2}K_{\mathrm{Rh-Te-Te}}(\Delta\theta)^2$	$\frac{1}{2}K_{\mathrm{Te-Rh-Rh}}(\Delta\theta)^2$
Parameter	4.366	1.869	1.869
r_0 or θ_0	2.633	91.001	91.001

The second line gives an explicit expression for each VFF term. The third line is the force constant parameters. Parameters are in the unit of ev/Å^2 for the bond stretching interaction and in the unit of eV for the angle bending interaction. The fourth line gives the initial bond length (in the unit of Å) for the bond stretching interaction and the initial angle (in the unit of degrees) for the angle bending interaction. The angle θ_{ijk} has atom i as the apex.

Table 270. The VFF model for single-layer 1T-$RhTe_2$.

interaction shown by Eq. (2). We note that the angle bending term $K_{\mathrm{Rh-Te-Te}}$ is for the angle $\theta_{\mathrm{Rh-Te-Te}}$ with both Te atoms from the same (top or bottom) group. We find that there are actually only two parameters in the VFF model, so we can determine their value by fitting to the Young's modulus and the Poisson's ratio of the system. The *ab initio* calculations have predicted the Young's modulus to be 37 N/m and the Poisson's ratio as 0.20 [48].

The parameters for the two-body SW potential used by GULP are shown in **Table 271**. The parameters for the three-body SW potential used by GULP are shown in **Table 272**. Some representative parameters for the SW potential used by LAMMPS are listed in **Table 273**.

We use LAMMPS to perform MD simulations for the mechanical behavior of the single-layer 1T-$RhTe_2$ under uniaxial tension at 1 and 300 K. **Figure 134** shows the stress-strain curve for the tension of a single-layer 1T-$RhTe_2$ of dimension 100 × 100 Å. Periodic boundary conditions are applied in both armchair and zigzag directions. The single-layer 1T-$RhTe_2$ is stretched uniaxially along the armchair or zigzag direction. The stress is calculated without involving the actual thickness of the quasi-two-dimensional structure of the single-layer 1T-$RhTe_2$. The Young's modulus can be obtained by a linear fitting of the stress-strain relation in the small strain range of [0, 0.01]. The Young's modulus is 32.1 and 32.0 N/m along the armchair and zigzag directions, respectively. The Young's modulus is essentially isotropic in the armchair and zigzag directions. The Poisson's ratio from the VFF model and the SW potential is $\nu_{xy} = \nu_{yx} = 0.20$. The fitted Young's modulus value is about 10% smaller than the *ab initio* result of 37 N/m [48], as only short-range interactions are considered in the present work. The long-range interactions are ignored, which typically leads to about 10% underestimation for the value of the Young's modulus.

	A (eV)	ρ (Å)	B (Å^4)	$r_{\min}$ (Å)	$r_{\max}$ (Å)
Rh—Te	4.640	1.450	24.038	0.0	3.610

Table 271. Two-body SW potential parameters for single-layer 1T-$RhTe_2$ used by GULP [8] as expressed in Eq. (3).

	K (eV)	θ_0 (°)	ρ_1 (Å)	ρ_2 (Å)	$r_{\min 12}$ (Å)	$r_{\max 12}$ (Å)	$r_{\min 13}$ (Å)	$r_{\max 13}$ (Å)	$r_{\min 23}$ (Å)	$r_{\max 23}$ (Å)
$\theta_{\mathrm{Rh-Te-Te}}$ 18.192	18.192	91.001	1.450	1.450	0.0	3.610	0.0	3.610	0.0	5.131
$\theta_{\mathrm{Te-Rh-Rh}}$ 18.192	18.192	91.001	1.450	1.450	0.0	3.610	0.0	3.610	0.0	5.131

The angle θ_{ijk} in the first line indicates the bending energy for the angle with atom i as the apex.

Table 272. Three-body SW potential parameters for single-layer 1T-$RhTe_2$ used by GULP [8] as expressed in Eq. (4).

	ϵ (eV)	σ (Å)	a	λ	γ	$\cos\theta_0$	A_L	B_L	p	q	Tol
Rh—Te_1—Te_1	1.000	1.450	2.490	18.192	1.000	−0.017	4.640	5.436	4	0	0.0

Table 273. SW potential parameters for single-layer 1T-$RhTe_2$ used by LAMMPS [9] as expressed in Eqs. (9) and (10).

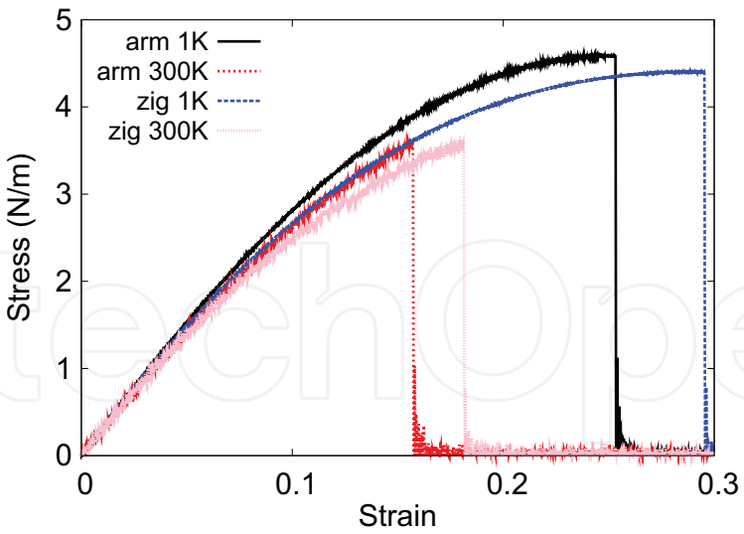

Figure 134. Stress-strain for single-layer 1T-$RhTe_2$ of dimension 100 × 100 Å along the armchair and zigzag directions.

There is no available value for nonlinear quantities in the single-layer 1T-$RhTe_2$. We have thus used the nonlinear parameter $B = 0.5d^4$ in Eq. (5), which is close to the value of B in most materials. The value of the third-order nonlinear elasticity D can be extracted by fitting the stress-strain relation to the function $\sigma = E\epsilon + \frac{1}{2}D\epsilon^2$ with E as the Young's modulus. The values of D from the present SW potential are -103.1 and -116.5 N/m along the armchair and zigzag directions, respectively. The ultimate stress is about 4.6 N/m at the ultimate strain of 0.25 in the armchair direction at the low temperature of 1 K. The ultimate stress is about 4.4 N/m at the ultimate strain of 0.29 in the zigzag direction at the low temperature of 1 K.

Figure 135 shows that the VFF model and the SW potential give exactly the same phonon dispersion, as the SW potential is derived from the VFF model.

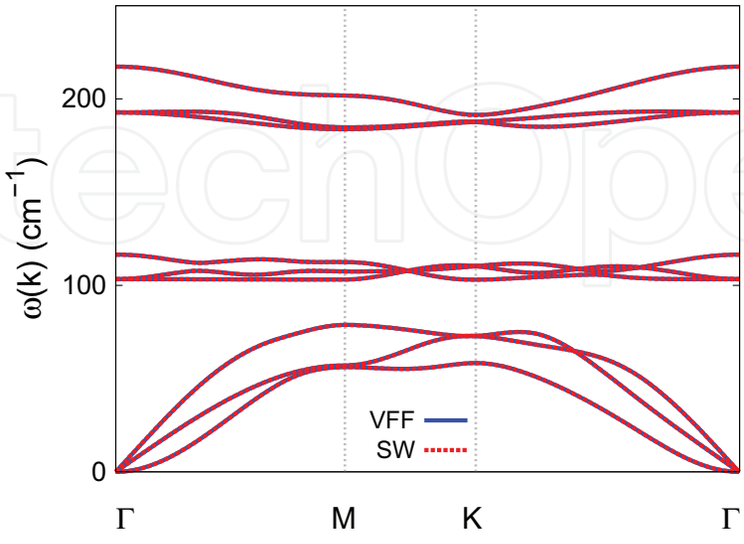

Figure 135. Phonon spectrum for single-layer 1T-$RhTe_2$ along the ΓMKΓ direction in the Brillouin zone. The phonon dispersion from the SW potential is exactly the same as that from the VFF model.

69. 1T-PdS_2

Most existing theoretical studies on the single-layer 1T-PdS_2 are based on the first-principles calculations. In this section, we will develop the SW potential for the single-layer 1T-PdS_2.

The structure for the single-layer 1T-PdS_2 is shown in **Figure 71** (with M=Pd and X=S). Each Pd atom is surrounded by six S atoms. These S atoms are categorized into the top group (e.g., atoms 1, 3, and 5) and bottom group (e.g., atoms 2, 4, and 6). Each S atom is connected to three Pd atoms. The structural parameters are from the first-principles calculations [48], including the lattice constant $a = 3.5408$ Å and the bond length $d_{\mathrm{Pd-S}} = 2.4013$ Å, which are derived from the angle $\theta_{\mathrm{SPdPd}} = 95^{\circ}$. The other angle is $\theta_{\mathrm{PdSS}} = 95^{\circ}$ with S atoms from the same (top or bottom) group.

Table 274 shows three VFF terms for the single-layer 1T-PdS_2; one of which is the bond stretching interaction shown by Eq. (1), while the other two terms are the angle bending interaction shown by Eq. (2). We note that the angle bending term $K_{\mathrm{Pd-S-S}}$ is for the angle $\theta_{\mathrm{Pd-S-S}}$ with both S atoms from the same (top or bottom) group. We find that there are actually only two parameters in the VFF model, so we can determine their value by fitting to the Young's modulus and the Poisson's ratio of the system. The *ab initio* calculations have predicted the Young's modulus to be 77 N/m and the Poisson's ratio as 0.53 [48].

The parameters for the two-body SW potential used by GULP are shown in **Table 275**. The parameters for the three-body SW potential used by GULP are shown in **Table 276**. Some representative parameters for the SW potential used by LAMMPS are listed in **Table 277**.

We use LAMMPS to perform MD simulations for the mechanical behavior of the single-layer 1T-PdS_2 under uniaxial tension at 1 and 300 K. **Figure 136** shows the stress-strain curve for the tension of a single-layer 1T-PdS_2 of dimension 100×100 Å. Periodic boundary conditions are applied in both armchair and zigzag directions. The single-layer 1T-PdS_2 is stretched

VFF type	**Bond stretching**	**Angle bending**	
Expression	$\frac{1}{2}K_{\mathrm{Pd-S}}(\Delta r)^2$	$\frac{1}{2}K_{\mathrm{Pd-S-S}}(\Delta\theta)^2$	$\frac{1}{2}K_{\mathrm{S-Pd-Pd}}(\Delta\theta)^2$
Parameter	10.374	3.122	3.122
r_0 or θ_0	2.401	94.998	94.998

The second line gives an explicit expression for each VFF term. The third line is the force constant parameters. Parameters are in the unit of ev/Å^2 for the bond stretching interaction and in the unit of eV for the angle bending interaction. The fourth line gives the initial bond length (in the unit of Å) for the bond stretching interaction and the initial angle (in the unit of degrees) for the angle bending interaction. The angle θ_{ijk} has atom i as the apex.

Table 274. The VFF model for single-layer 1T-PdS_2.

	A **(eV)**	ρ **(Å)**	B **(Å^4)**	r_{min} **(Å)**	r_{max} **(Å)**
Pd—S	10.116	1.467	16.625	0.0	3.340

Table 275. Two-body SW potential parameters for single-layer 1T-PdS_2 used by GULP [8] as expressed in Eq. (3).

	K (eV)	θ_0 (°)	ρ_1 (Å)	ρ_2 (Å)	$r_{\min 12}$ (Å)	$r_{\max 12}$ (Å)	$r_{\min 13}$ (Å)	$r_{\max 13}$ (Å)	$r_{\min 23}$ (Å)	$r_{\max 23}$ (Å)
$\theta_{\mathrm{Pd-S-S}}$	35.859	94.998	1.467	1.467	0.0	3.340	0.0	3.340	0.0	4.837
$\theta_{\mathrm{S-Pd-Pd}}$	35.859	94.998	1.467	1.467	0.0	3.340	0.0	3.340	0.0	4.837

The angle θ_{ijk} in the first line indicates the bending energy for the angle with atom i as the apex.

Table 276. Three-body SW potential parameters for single-layer 1T-PdS_2 used by GULP [8] as expressed in Eq. (4).

	ϵ (eV)	σ (Å)	a	λ	γ	$\cos\theta_0$	A_L	B_L	p	q	Tol
$\mathrm{Pd—S_1—S_1}$	1.000	1.467	2.276	35.859	1.000	−0.087	10.116	3.588	4	0	0.0

Table 277. SW potential parameters for single-layer 1T-PdS_2 used by LAMMPS [9] as expressed in Eqs. (9) and (10).

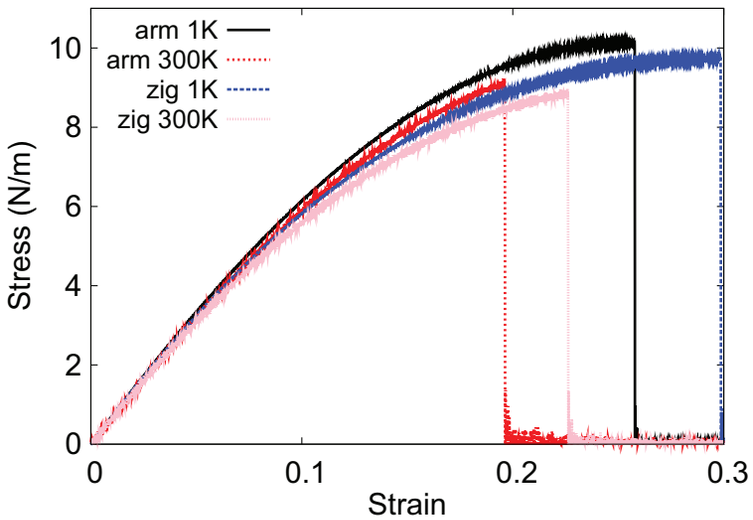

Figure 136. Stress-strain for single-layer 1T-PdS_2 of dimension 100 × 100 Å along the armchair and zigzag directions.

uniaxially along the armchair or zigzag direction. The stress is calculated without involving the actual thickness of the quasi-two-dimensional structure of the single-layer 1T-PdS_2. The Young's modulus can be obtained by a linear fitting of the stress-strain relation in the small strain range of [0, 0.01]. The Young's modulus is 69.9 and 69.5 N/m along the armchair and zigzag directions, respectively. The Young's modulus is essentially isotropic in the armchair and zigzag directions. The Poisson's ratio from the VFF model and the SW potential is $\nu_{xy} = \nu_{yx} = 0.20$. The fitted Young's modulus value is about 10% smaller than the *ab initio* result of 77 N/m [48], as only short-range interactions are considered in the present work. The long-range interactions are ignored, which typically leads to about 10% underestimation for the value of the Young's modulus.

There is no available value for nonlinear quantities in the single-layer 1T-PdS_2. We have thus used the nonlinear parameter $B = 0.5d^4$ in Eq. (5), which is close to the value of B in most materials. The value of the third-order nonlinear elasticity D can be extracted by fitting the stress-strain relation to the function $\sigma = E\epsilon + \frac{1}{2}D\epsilon^2$ with E as the Young's modulus. The values

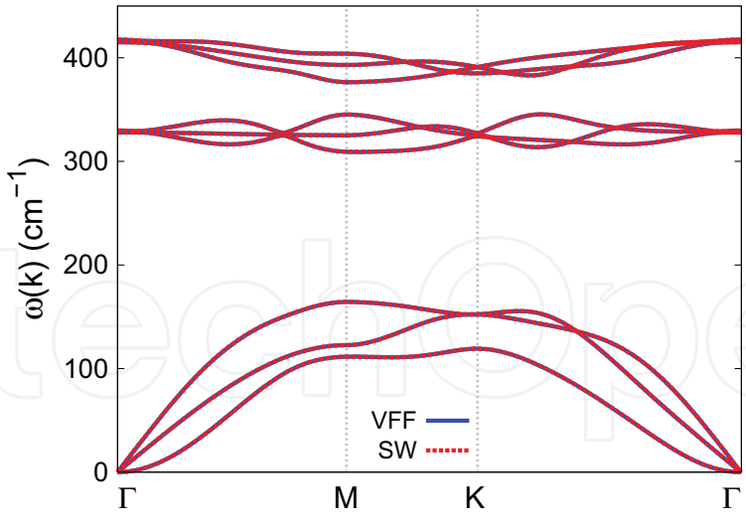

Figure 137. Phonon spectrum for single-layer 1T-PdS_2 along the ΓMKΓ direction in the Brillouin zone. The phonon dispersion from the SW potential is exactly the same as that from the VFF model.

of D from the present SW potential are −222.0 and −248.8 N/m along the armchair and zigzag directions, respectively. The ultimate stress is about 10.1 N/m at the ultimate strain of 0.25 in the armchair direction at the low temperature of 1 K. The ultimate stress is about 9.7 N/m at the ultimate strain of 0.30 in the zigzag direction at the low temperature of 1 K.

Figure 137 shows that the VFF model and the SW potential give exactly the same phonon dispersion, as the SW potential is derived from the VFF model.

70. 1T-$PdSe_2$

Most existing theoretical studies on the single-layer 1T-$PdSe_2$ are based on the first-principles calculations. In this section, we will develop the SW potential for the single-layer 1T-$PdSe_2$.

The structure for the single-layer 1T-$PdSe_2$ is shown in **Figure 71** (with M=Pd and X=Se). Each Pd atom is surrounded by six Se atoms. These Se atoms are categorized into the top group (e.g., atoms 1, 3, and 5) and bottom group (e.g., atoms 2, 4, and 6). Each Se atom is connected to three Pd atoms. The structural parameters are from the first-principles calculations [48], including the lattice constant $a = 3.6759$ Å and the bond length $d_{\mathrm{Pd-Se}} = 2.4929$ Å, which are derived from the angle $\theta_{\mathrm{SePdPd}} = 95°$. The other angle is $\theta_{\mathrm{PdSeSe}} = 95°$ with Se atoms from the same (top or bottom) group.

Table 278 shows three VFF terms for the single-layer 1T-$PdSe_2$; one of which is the bond stretching interaction shown by Eq. (1), while the other two terms are the angle bending interaction shown by Eq. (2). We note that the angle bending term $K_{\mathrm{Pd-Se-Se}}$ is for the angle $\theta_{\mathrm{Pd-Se-Se}}$ with both Se atoms from the same (top or bottom) group. We find that there are actually only two parameters in the VFF model, so we can determine their value by fitting to the Young's modulus and the Poisson's ratio of the system. The *ab initio* calculations have predicted the Young's modulus to be 66 N/m and the Poisson's ratio as 0.45 [48].

VFF type	Bond stretching	Angle bending	
Expression	$\frac{1}{2}K_{\mathrm{Pd-Se}}(\Delta r)^2$	$\frac{1}{2}K_{\mathrm{Pd-Se-Se}}(\Delta\theta)^2$	$\frac{1}{2}K_{\mathrm{Se-Pd-Pd}}(\Delta\theta)^2$
Parameter	10.374	3.122	3.122
r_0 or θ_0	2.493	94.999	94.999

The second line gives an explicit expression for each VFF term. The third line is the force constant parameters. Parameters are in the unit of ev/Å^2 for the bond stretching interaction and in the unit of eV for the angle bending interaction. The fourth line gives the initial bond length (in the unit of Å) for the bond stretching interaction and the initial angle (in the unit of degrees) for the angle bending interaction. The angle θ_{ijk} has atom i as the apex.

Table 278. The VFF model for single-layer 1T-$PdSe_2$.

The parameters for the two-body SW potential used by GULP are shown in **Table 279**. The parameters for the three-body SW potential used by GULP are shown in **Table 280**. Some representative parameters for the SW potential used by LAMMPS are listed in **Table 281**.

We use LAMMPS to perform MD simulations for the mechanical behavior of the single-layer 1T-$PdSe_2$ under uniaxial tension at 1 and 300 K. **Figure 138** shows the stress-strain curve for the tension of a single-layer 1T-$PdSe_2$ of dimension 100×100 Å. Periodic boundary conditions are applied in both armchair and zigzag directions. The single-layer 1T-$PdSe_2$ is stretched uniaxially along the armchair or zigzag direction. The stress is calculated without involving the actual thickness of the quasi-two-dimensional structure of the single-layer 1T-$PdSe_2$. The Young's modulus can be obtained by a linear fitting of the stress-strain relation in the small strain range of [0, 0.01]. The Young's modulus is 65.5 and 65.3 N/m along the armchair and zigzag directions, respectively. The Young's modulus is essentially isotropic in the armchair and zigzag directions. The Poisson's ratio from the VFF model and the SW potential is $\nu_{xy} = \nu_{yx} = 0.21$.

	A (eV)	ρ (Å)	B (Å^4)	r_{min} (Å)	r_{max} (Å)
Pd—Se	10.902	1.523	19.310	0.0	3.467

Table 279. Two-body SW potential parameters for single-layer 1T-$PdSe_2$ used by GULP [8] as expressed in Eq. (3).

	K (eV)	θ_0 (°)	ρ_1 (Å)	ρ_2 (Å)	$r_{\mathrm{min}\,12}$ (Å)	$r_{\mathrm{max}\,12}$ (Å)	$r_{\mathrm{min}\,13}$ (Å)	$r_{\mathrm{max}\,13}$ (Å)	$r_{\mathrm{min}\,23}$ (Å)	$r_{\mathrm{max}\,23}$ (Å)
$\theta_{\mathrm{Pd-Se-Se}}$	35.859	94.999	1.523	1.523	0.0	3.467	0.0	3.467	0.0	5.021
$\theta_{\mathrm{Se-Pd-Pd}}$	35.859	94.999	1.523	1.523	0.0	3.467	0.0	3.467	0.0	5.021

The angle θ_{ijk} in the first line indicates the bending energy for the angle with atom i as the apex.

Table 280. Three-body SW potential parameters for single-layer 1T-$PdSe_2$ used by GULP [8] as expressed in Eq. (4).

	ϵ (eV)	σ (Å)	a	λ	γ	$\cos\theta_0$	A_L	B_L	p	q	Tol
Pd—Se_1—Se_1	1.000	1.523	2.276	35.859	1.000	−0.087	10.902	3.588	4	0	0.0

Table 281. SW potential parameters for single-layer 1T-$PdSe_2$ used by LAMMPS [9] as expressed in Eqs. (9) and (10).

http://dx.doi.org/10.5772/intechopen.71929

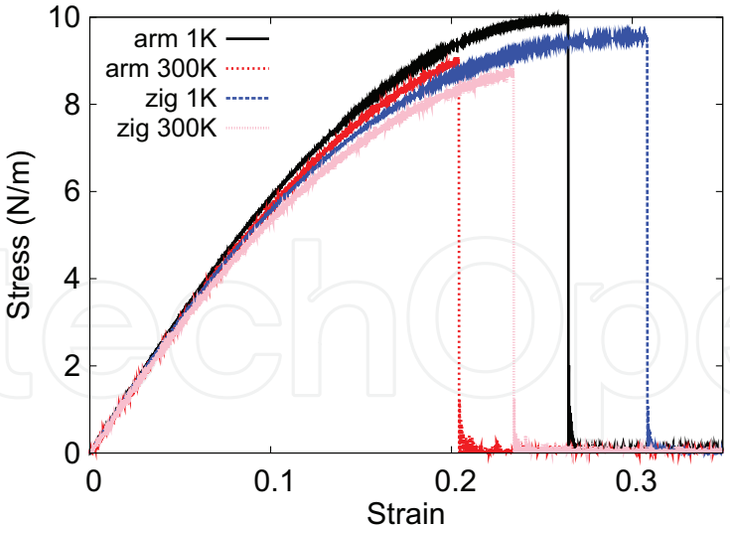

Figure 138. Stress-strain for single-layer 1T-$PdSe_2$ of dimension 100 × 100 Å along the armchair and zigzag directions.

There is no available value for nonlinear quantities in the single-layer 1T-$PdSe_2$. We have thus used the nonlinear parameter $B = 0.5d^4$ in Eq. (5), which is close to the value of B in most materials. The value of the third-order nonlinear elasticity D can be extracted by fitting the stress-strain relation to the function $\sigma = E\epsilon + \frac{1}{2}D\epsilon^2$ with E as the Young's modulus. The values of D from the present SW potential are −194.7 and −222.8 N/m along the armchair and zigzag directions, respectively. The ultimate stress is about 9.9 N/m at the ultimate strain of 0.26 in the armchair direction at the low temperature of 1 K. The ultimate stress is about 9.5 N/m at the ultimate strain of 0.31 in the zigzag direction at the low temperature of 1 K.

Figure 139 shows that the VFF model and the SW potential give exactly the same phonon dispersion, as the SW potential is derived from the VFF model.

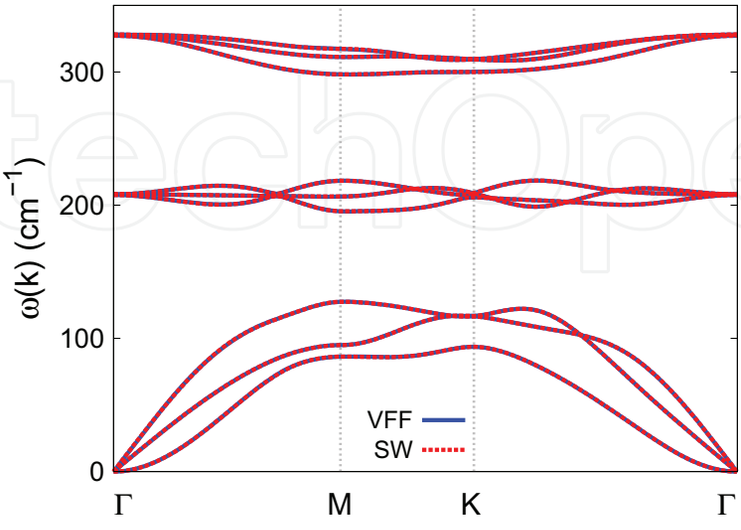

Figure 139. Phonon spectrum for single-layer 1T-$PdSe_2$ along the ΓMKΓ direction in the Brillouin zone. The phonon dispersion from the SW potential is exactly the same as that from the VFF model.

71. 1T-$PdTe_2$

Most existing theoretical studies on the single-layer 1T-$PdTe_2$ are based on the first-principles calculations. In this section, we will develop the SW potential for the single-layer 1T-$PdTe_2$.

The structure for the single-layer 1T-$PdTe_2$ is shown in **Figure 71** (with M=Pd and X=Te). Each Pd atom is surrounded by six Te atoms. These Te atoms are categorized into the top group (e.g., atoms 1, 3, and 5) and bottom group (e.g., atoms 2, 4, and 6). Each Te atom is connected to three Pd atoms. The structural parameters are from the first-principles calculations [48], including the lattice constant $a = 3.9162$ Å and the bond length $d_{\mathrm{Pd-Te}} = 2.6349$ Å, which are derived from the angle $\theta_{\mathrm{TePdPd}} = 96^\circ$. The other angle is $\theta_{\mathrm{PdTeTe}} = 96^\circ$ with Te atoms from the same (top or bottom) group.

Table 282 shows three VFF terms for the single-layer 1T-$PdTe_2$; one of which is the bond stretching interaction shown by Eq. (1), while the other two terms are the angle bending interaction shown by Eq. (2). We note that the angle bending term $K_{\mathrm{Pd-Te-Te}}$ is for the angle $\theta_{\mathrm{Pd-Te-Te}}$ with both Te atoms from the same (top or bottom) group. We find that there are actually only two parameters in the VFF model, so we can determine their value by fitting to the Young's modulus and the Poisson's ratio of the system. The *ab initio* calculations have predicted the Young's modulus to be 63 N/m and the Poisson's ratio as 0.35 [48].

The parameters for the two-body SW potential used by GULP are shown in **Table 283**. The parameters for the three-body SW potential used by GULP are shown in **Table 284**. Some representative parameters for the SW potential used by LAMMPS are listed in **Table 285**.

We use LAMMPS to perform MD simulations for the mechanical behavior of the single-layer 1T-$PdTe_2$ under uniaxial tension at 1 and 300 K. **Figure 140** shows the stress-strain curve for the tension of a single-layer 1T-$PdTe_2$ of dimension 100 × 100 Å. Periodic boundary conditions are applied in both armchair and zigzag directions. The single-layer 1T-$PdTe_2$ is stretched

VFF type	Bond stretching	Angle bending	
Expression	$\frac{1}{2}K_{\mathrm{Pd-Te}}(\Delta r)^2$	$\frac{1}{2}K_{\mathrm{Pd-Te-Te}}(\Delta\theta)^2$	$\frac{1}{2}K_{\mathrm{Te-Pd-Pd}}(\Delta\theta)^2$
Parameter	10.374	3.122	3.122
r_0 or θ_0	2.635	95.999	95.999

The second line gives an explicit expression for each VFF term. The third line is the force constant parameters. Parameters are in the unit of ev/Å^2 for the bond stretching interaction and in the unit of eV for the angle bending interaction. The fourth line gives the initial bond length (in the unit of Å) for the bond stretching interaction and the initial angle (in the unit of degrees) for the angle bending interaction. The angle θ_{ijk} has atom i as the apex.

Table 282. The VFF model for single-layer 1T-$PdTe_2$.

	A (eV)	ρ (Å)	B (Å^4)	r_{min} (Å)	r_{max} (Å)
Pd—Te	12.474	1.650	24.101	0.0	3.678

Table 283. Two-body SW potential parameters for single-layer 1T-$PdTe_2$ used by GULP [8] as expressed in Eq. (3).

	K (eV)	θ_0 (°)	ρ_1 (Å)	ρ_2 (Å)	$r_{\min 12}$ (Å)	$r_{\max 12}$ (Å)	$r_{\min 13}$ (Å)	$r_{\max 13}$ (Å)	$r_{\min 23}$ (Å)	$r_{\max 23}$ (Å)
$\theta_{\text{Pd-Te-Te}}$	37.406	95.999	1.650	1.650	0.0	3.678	0.0	3.678	0.0	5.350
$\theta_{\text{Te-Pd-Pd}}$	37.406	95.999	1.650	1.650	0.0	3.678	0.0	3.678	0.0	5.350

The angle θ_{ijk} in the first line indicates the bending energy for the angle with atom i as the apex.

Table 284. Three-body SW potential parameters for single-layer 1T-$PdTe_2$ used by GULP [8] as expressed in Eq. (4).

	ϵ (eV)	σ (Å)	a	λ	γ	$\cos\theta_0$	A_L	B_L	p	q	Tol
Pd—Te_1—Te_1	1.000	1.650	2.229	37.406	1.000	−0.105	12.474	3.250	4	0	0.0

Table 285. SW potential parameters for single-layer 1T-$PdTe_2$ used by LAMMPS [9] as expressed in Eqs. (9) and (10).

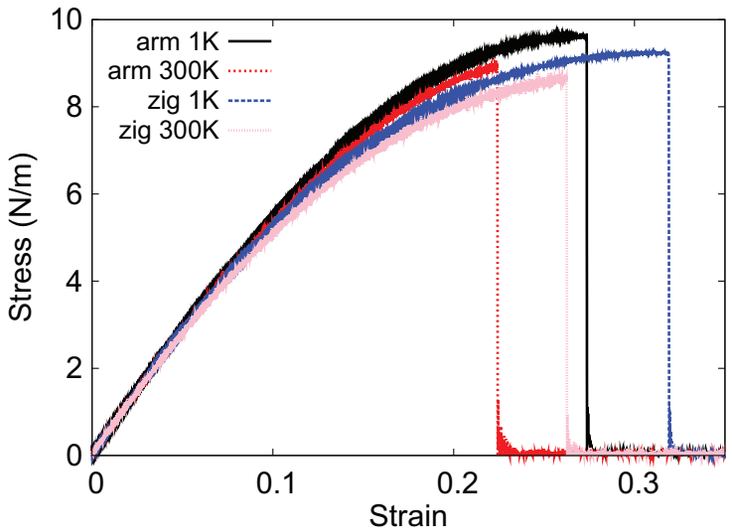

Figure 140. Stress-strain for single-layer 1T-$PdTe_2$ of dimension 100 × 100 Å along the armchair and zigzag directions.

uniaxially along the armchair or zigzag direction. The stress is calculated without involving the actual thickness of the quasi-two-dimensional structure of the single-layer 1T-$PdTe_2$. The Young's modulus can be obtained by a linear fitting of the stress-strain relation in the small strain range of [0, 0.01]. The Young's modulus is 61.6 and 61.4 N/m along the armchair and zigzag directions, respectively. The Young's modulus is essentially isotropic in the armchair and zigzag directions. The Poisson's ratio from the VFF model and the SW potential is $\nu_{xy} = \nu_{yx} = 0.22$.

There is no available value for nonlinear quantities in the single-layer 1T-$PdTe_2$. We have thus used the nonlinear parameter $B = 0.5d^4$ in Eq. (5), which is close to the value of B in most materials. The value of the third-order nonlinear elasticity D can be extracted by fitting the stress-strain relation to the function $\sigma = E\epsilon + \frac{1}{2}D\epsilon^2$ with E as the Young's modulus. The values of D from the present SW potential are −178.8 and −203.8 N/m along the armchair and zigzag

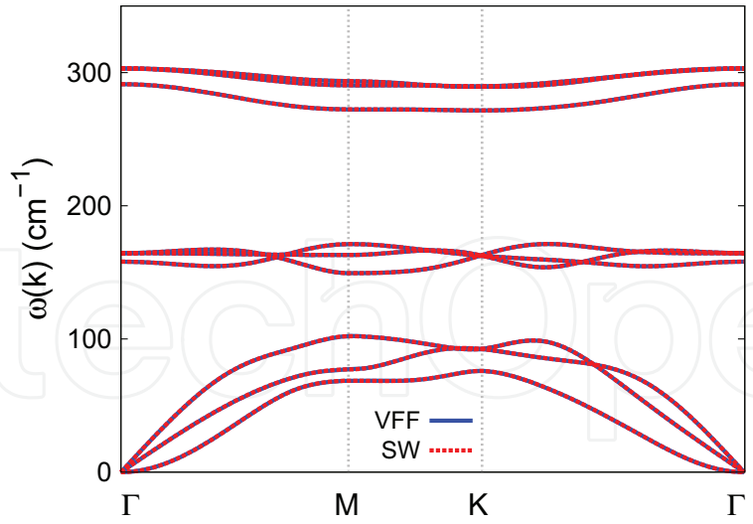

Figure 141. Phonon spectrum for single-layer 1T-$PdTe_2$ along the ΓMKΓ direction in the Brillouin zone. The phonon dispersion from the SW potential is exactly the same as that from the VFF model.

directions, respectively. The ultimate stress is about 9.6 N/m at the ultimate strain of 0.27 in the armchair direction at the low temperature of 1 K. The ultimate stress is about 9.2 N/m at the ultimate strain of 0.32 in the zigzag direction at the low temperature of 1 K.

Figure 141 shows that the VFF model and the SW potential give exactly the same phonon dispersion, as the SW potential is derived from the VFF model.

72. 1T-SnS_2

Most existing theoretical studies on the single-layer 1T-SnS_2 are based on the first-principles calculations. In this section, we will develop the SW potential for the single-layer 1T-SnS_2.

The structure for the single-layer 1T-SnS_2 is shown in **Figure 71** (with M=Sn and X=S). Each Sn atom is surrounded by six S atoms. These S atoms are categorized into the top group (e.g., atoms 1, 3, and 5) and bottom group (e.g., atoms 2, 4, and 6). Each S atom is connected to three Sn atoms. The structural parameters are from the first-principles calculations [34], including the lattice constant $a = 3.640$ Å and the bond length $d_{\mathrm{Sn-S}} = 2.570$ Å. The resultant angles are $\theta_{\mathrm{SSnSn}} = 90.173^\circ$ and $\theta_{\mathrm{SnSS}} = 90.173^\circ$ with S atoms from the same (top or bottom) group.

Table 286 shows three VFF terms for the single-layer 1T-SnS_2; one of which is the bond stretching interaction shown by Eq. (1), while the other two terms are the angle bending interaction shown by Eq. (2). We note that the angle bending term $K_{\mathrm{Sn-S-S}}$ is for the angle $\theta_{\mathrm{Sn-S-S}}$ with both S atoms from the same (top or bottom) group. These force constant parameters are determined by fitting to the acoustic branches in the phonon dispersion along the ΓM as shown in **Figure 142(a)**. The *ab initio* calculations for the phonon dispersion are from Ref. [34]. The lowest acoustic branch (flexural mode) is almost linear in the *ab initio* calculations, which may be due to the violation of the rigid rotational invariance [20]. **Figure 142(b)** shows

VFF type	Bond stretching	Angle bending	
Expression	$\frac{1}{2}K_{\mathrm{Sn-S}}(\Delta r)^2$	$\frac{1}{2}K_{\mathrm{Sn-S-S}}(\Delta\theta)^2$	$\frac{1}{2}K_{\mathrm{S-Sn-Sn}}(\Delta\theta)^2$
Parameter	7.872	5.817	5.817
r_0 or θ_0	2.570	90.173	90.173

The second line gives an explicit expression for each VFF term. The third line is the force constant parameters. Parameters are in the unit of ev/Å^2 for the bond stretching interaction and in the unit of eV for the angle bending interaction. The fourth line gives the initial bond length (in the unit of Å) for the bond stretching interaction and the initial angle (in the unit of degrees) for the angle bending interaction. The angle θ_{ijk} has atom i as the apex.

Table 286. The VFF model for single-layer 1T-SnS_2.

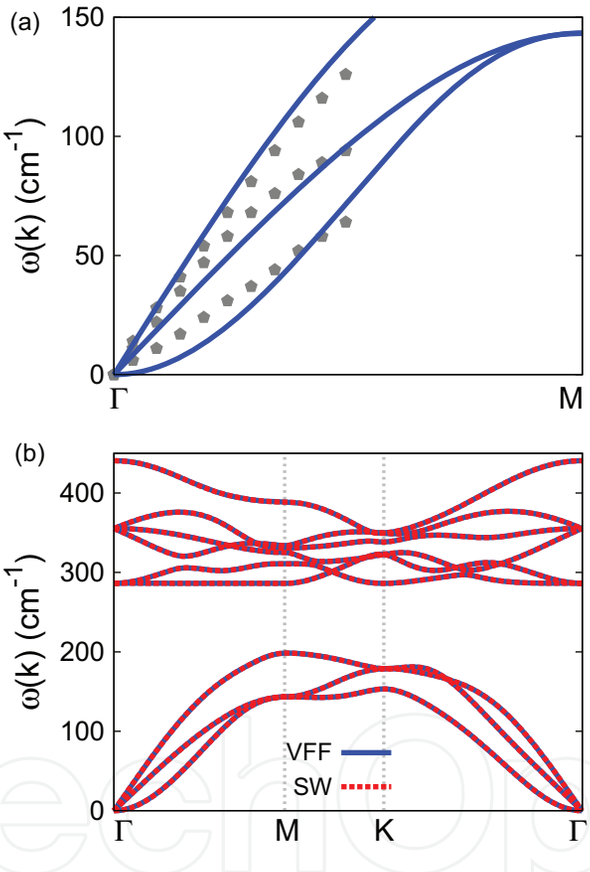

Figure 142. Phonon spectrum for single-layer 1T-SnS_2. (a) Phonon dispersion along the ΓM direction in the Brillouin zone. The results from the VFF model (lines) are comparable with the *ab initio* results (pentagons) from Ref. [34]. (b) The phonon dispersion from the SW potential is exactly the same as that from the VFF model.

that the VFF model and the SW potential give exactly the same phonon dispersion, as the SW potential is derived from the VFF model.

The parameters for the two-body SW potential used by GULP are shown in **Table 287**. The parameters for the three-body SW potential used by GULP are shown in **Table 288**. Some representative parameters for the SW potential used by LAMMPS are listed in **Table 289**.

	A (eV)	ρ (Å)	B (Å^4)	$r_{\min}$ (Å)	$r_{\max}$ (Å)
Sn—S	7.805	1.384	21.812	0.0	3.513

Table 287. Two-body SW potential parameters for single-layer 1T-SnS_2 used by GULP [8] as expressed in Eq. (3).

	K (eV)	θ_0 (°)	ρ_1 (Å)	ρ_2 (Å)	$r_{\min 12}$ (Å)	$r_{\max 12}$ (Å)	$r_{\min 13}$ (Å)	$r_{\max 13}$ (Å)	$r_{\min 23}$ (Å)	$r_{\max 23}$ (Å)
$\theta_{\text{Sn–S–S}}$	54.748	90.173	1.384	1.384	0.0	3.513	0.0	3.513	0.0	4.972
$\theta_{\text{S–Sn–Sn}}$	54.748	90.173	1.384	1.384	0.0	3.513	0.0	3.513	0.0	4.972

The angle θ_{ijk} in the first line indicates the bending energy for the angle with atom i as the apex.

Table 288. Three-body SW potential parameters for single-layer 1T-SnS_2 used by GULP [8] as expressed in Eq. (4).

	ϵ (eV)	σ (Å)	a	λ	γ	$\cos\theta_0$	A_L	B_L	p	q	Tol
Sn—S_1—S_1	1.000	1.384	2.539	54.748	1.000	−0.003	7.805	5.949	4	0	0.0

Table 289. SW potential parameters for single-layer 1T-SnS_2 used by LAMMPS [9] as expressed in Eqs. (9) and (10).

We use LAMMPS to perform MD simulations for the mechanical behavior of the single-layer 1T-SnS_2 under uniaxial tension at 1 and 300 K. **Figure 143** shows the stress-strain curve for the tension of a single-layer 1T-SnS_2 of dimension 100 × 100 Å. Periodic boundary conditions are applied in both armchair and zigzag directions. The single-layer 1T-SnS_2 is stretched uniaxially along the armchair or zigzag direction. The stress is calculated without involving the actual thickness of the quasi-two-dimensional structure of the single-layer 1T-SnS_2. The Young's modulus can be obtained by a linear fitting of the stress-strain relation in the small strain range of [0, 0.01]. The Young's modulus is 88.4 and 87.9 N/m along the armchair and zigzag

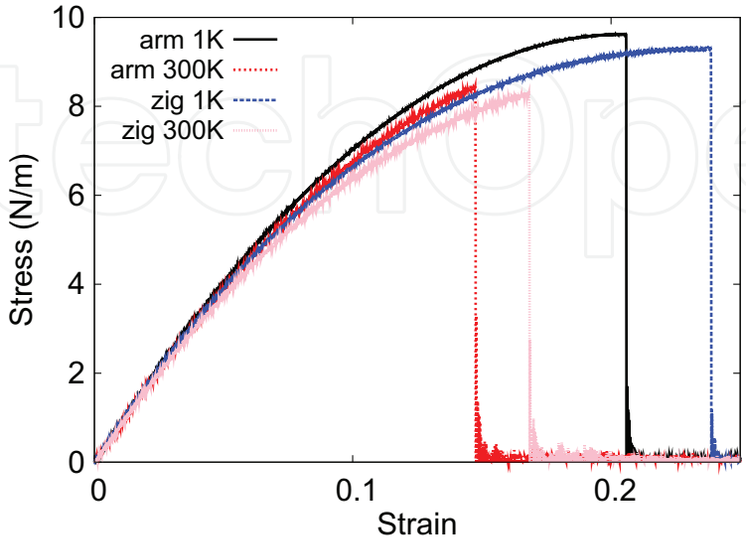

Figure 143. Stress-strain for single-layer 1T-SnS_2 of dimension 100 × 100 Å along the armchair and zigzag directions.

directions, respectively. The Young's modulus is essentially isotropic in the armchair and zigzag directions. The Poisson's ratio from the VFF model and the SW potential is $\nu_{xy} = \nu_{yx} = 0.13$.

There is no available value for nonlinear quantities in the single-layer 1T-SnS_2. We have thus used the nonlinear parameter $B = 0.5d^4$ in Eq. (5), which is close to the value of B in most materials. The value of the third-order nonlinear elasticity D can be extracted by fitting the stress-strain relation to the function $\sigma = E\epsilon + \frac{1}{2}D\epsilon^2$ with E as the Young's modulus. The values of D from the present SW potential are -392.8 and -421.6 N/m along the armchair and zigzag directions, respectively. The ultimate stress is about 9.6 N/m at the ultimate strain of 0.20 in the armchair direction at the low temperature of 1 K. The ultimate stress is about 9.3 N/m at the ultimate strain of 0.24 in the zigzag direction at the low temperature of 1 K.

73. 1T-$SnSe_2$

Most existing theoretical studies on the single-layer 1T-$SnSe_2$ are based on the first-principles calculations. In this section, we will develop the SW potential for the single-layer 1T-$SnSe_2$.

The structure for the single-layer 1T-$SnSe_2$ is shown in **Figure 71** (with M=Sn and X=Se). Each Sn atom is surrounded by six Se atoms. These Se atoms are categorized into the top group (e.g., atoms 1, 3, and 5) and bottom group (e.g., atoms 2, 4, and 6). Each Se atom is connected to three Sn atoms. The structural parameters are from the first-principles calculations [34] including the lattice constant $a = 3.792$ Å and the bond length $d_{\mathrm{Sn-Se}} = 2.704$ Å. The resultant angles are $\theta_{\mathrm{SeSnSn}} = 89.044^\circ$ and $\theta_{\mathrm{SnSeSe}} = 89.044^\circ$ with Se atoms from the same (top or bottom) group.

Table 290 shows three VFF terms for the single-layer 1T-$SnSe_2$; one of which is the bond stretching interaction shown by Eq. (1), while the other two terms are the angle bending interaction shown by Eq. (2). We note that the angle bending term $K_{\mathrm{Sn-Se-Se}}$ is for the angle $\theta_{\mathrm{Sn-Se-Se}}$ with both Se atoms from the same (top or bottom) group. These force constant parameters are determined by fitting to the acoustic branches in the phonon dispersion along the ΓM as shown in **Figure 144(a)**. The *ab initio* calculations for the phonon dispersion are from Ref. [34]. The lowest acoustic branch (flexural mode) is almost linear in the *ab initio*

VFF type	Bond stretching	Angle bending	
Expression	$\frac{1}{2}K_{\mathrm{Sn-Se}}(\Delta r)^2$	$\frac{1}{2}K_{\mathrm{Sn-Se-Se}}(\Delta\theta)^2$	$\frac{1}{2}K_{\mathrm{Se-Sn-Sn}}(\Delta\theta)^2$
Parameter	7.872	5.817	5.817
r_0 or θ_0	2.704	89.044	89.044

The second line gives an explicit expression for each VFF term. The third line is the force constant parameters. Parameters are in the unit of ev/Å^2 for the bond stretching interaction and in the unit of eV for the angle bending interaction. The fourth line gives the initial bond length (in the unit of Å) for the bond stretching interaction and the initial angle (in the unit of degrees) for the angle bending interaction. The angle θ_{ijk} has atom i as the apex.

Table 290. The VFF model for single-layer 1T-$SnSe_2$.

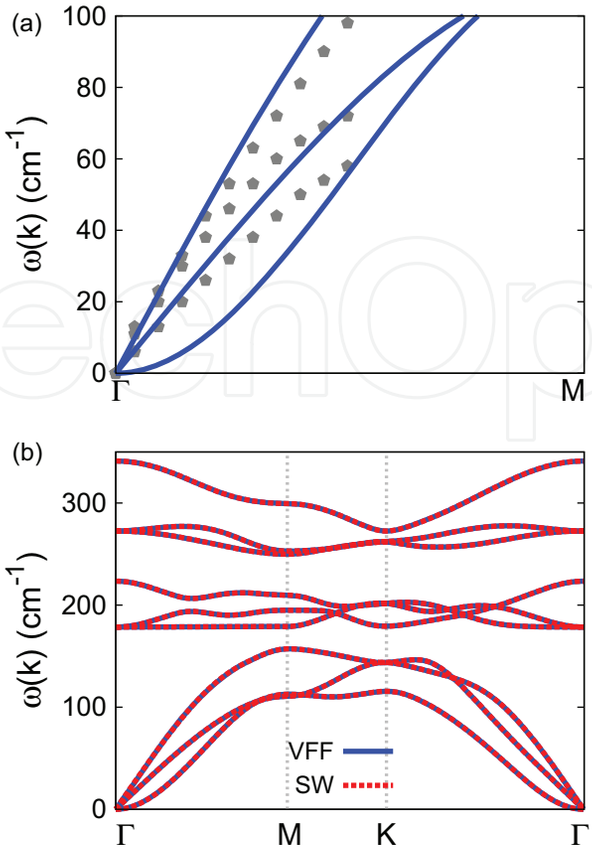

Figure 144. Phonon spectrum for single-layer 1T-$SnSe_2$. (a) Phonon dispersion along the ΓM direction in the Brillouin zone. The results from the VFF model (lines) are comparable with the *ab initio* results (pentagons) from Ref. [34]. (b) The phonon dispersion from the SW potential is exactly the same as that from the VFF model.

calculations, which may be due to the violation of the rigid rotational invariance [20]. **Figure 144(b)** shows that the VFF model and the SW potential give exactly the same phonon dispersion, as the SW potential is derived from the VFF model.

The parameters for the two-body SW potential used by GULP are shown in **Table 291**. The parameters for the three-body SW potential used by GULP are shown in **Table 292**. Some representative parameters for the SW potential used by LAMMPS are listed in **Table 293**.

We use LAMMPS to perform MD simulations for the mechanical behavior of the single-layer 1T-$SnSe_2$ under uniaxial tension at 1 and 300 K. **Figure 145** shows the stress-strain curve for the tension of a single-layer 1T-$SnSe_2$ of dimension 100 × 100 Å. Periodic boundary conditions are applied in both armchair and zigzag directions. The single-layer 1T-$SnSe_2$ is stretched uniaxially along the armchair or zigzag direction. The stress is calculated without involving the actual thickness of the quasi-two-dimensional structure of the single-layer 1T-$SnSe_2$. The

	A (eV)	ρ (Å)	B (Å^4)	r_{min} (Å)	r_{max} (Å)
Sn—Se	8.395	1.411	26.730	0.0	3.681

Table 291. Two-body SW potential parameters for single-layer 1T-$SnSe_2$ used by GULP [8] as expressed in Eq. (3).

	K (eV)	θ_0 (°)	ρ_1 (Å)	ρ_2 (Å)	$r_{\min 12}$ (Å)	$r_{\max 12}$ (Å)	$r_{\min 13}$ (Å)	$r_{\max 13}$ (Å)	$r_{\min 23}$ (Å)	$r_{\max 23}$ (Å)
$\theta_{\text{Sn-Se-Se}}$	52.322	89.044	1.411	1.411	0.0	3.681	0.0	3.681	0.0	5.180
$\theta_{\text{Se-Sn-Sn}}$	52.322	89.044	1.411	1.411	0.0	3.681	0.0	3.681	0.0	5.180

The angle θ_{ijk} in the first line indicates the bending energy for the angle with atom i as the apex.

Table 292. Three-body SW potential parameters for single-layer 1T-$SnSe_2$ used by GULP [8] as expressed in Eq. (4).

	ϵ (eV)	σ (Å)	a	λ	γ	$\cos\theta_0$	A_L	B_L	p	q	Tol
Sn—Se_1—Se_1	1.000	1.411	2.609	52.322	1.000	0.017	8.395	6.743	4	0	0.0

Table 293. SW potential parameters for single-layer 1T-$SnSe_2$ used by LAMMPS [9] as expressed in Eqs. (9) and (10).

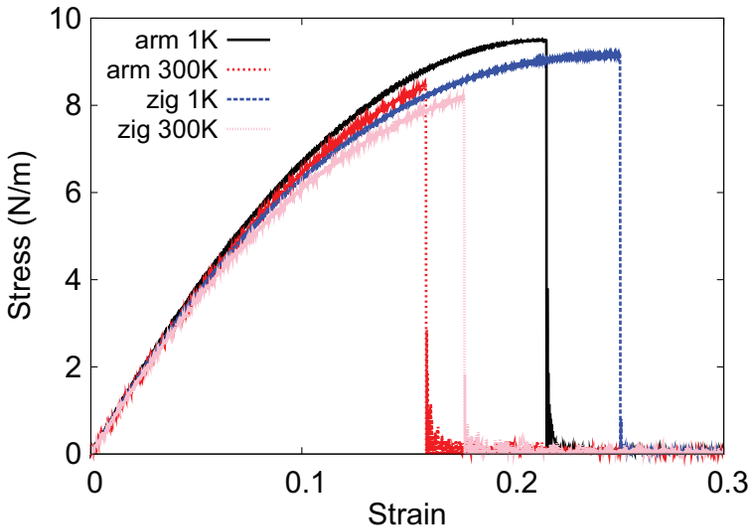

Figure 145. Stress-strain for single-layer 1T-$SnSe_2$ of dimension 100 × 100 Å along the armchair and zigzag directions.

Young's modulus can be obtained by a linear fitting of the stress-strain relation in the small strain range of [0, 0.01]. The Young's modulus is 82.0 and 81.6 N/m along the armchair and zigzag directions, respectively. The Young's modulus is essentially isotropic in the armchair and zigzag directions. The Poisson's ratio from the VFF model and the SW potential is $\nu_{xy} = \nu_{yx} = 0.15$.

There is no available value for nonlinear quantities in the single-layer 1T-$SnSe_2$. We have thus used the nonlinear parameter $B = 0.5d^4$ in Eq. (5), which is close to the value of B in most materials. The value of the third-order nonlinear elasticity D can be extracted by fitting the stress-strain relation to the function $\sigma = E\epsilon + \frac{1}{2}D\epsilon^2$ with E as the Young's modulus. The values of D from the present SW potential are −339.2 and −368.3 N/m along the armchair and zigzag directions, respectively. The ultimate stress is about 9.5 N/m at the ultimate strain of 0.21 in the armchair direction at the low temperature of 1 K. The ultimate stress is about 9.1 N/m at the ultimate strain of 0.25 in the zigzag direction at the low temperature of 1 K.

74. 1T-HfS_2

Most existing theoretical studies on the single-layer 1T-HfS_2 are based on the first-principles calculations. In this section, we will develop the SW potential for the single-layer 1T-HfS_2.

The structure for the single-layer 1T-HfS_2 is shown in **Figure 71** (with M=Hf and X=S). Each Hf atom is surrounded by six S atoms. These S atoms are categorized into the top group (e.g., atoms 1, 3, and 5) and bottom group (e.g., atoms 2, 4, and 6). Each S atom is connected to three Hf atoms. The structural parameters are from the first-principles calculations [53], including the lattice constant $a = 3.64$ Å and the bond length $d_{\mathrm{Hf-S}} = 2.55$ Å. The resultant angles are $\theta_{\mathrm{HfSS}} = 91.078^\circ$ with S atoms from the same (top or bottom) group and $\theta_{\mathrm{SHfHf}} = 91.078^\circ$.

Table 294 shows three VFF terms for the single-layer 1T-HfS_2; one of which is the bond stretching interaction shown by Eq. (1), while the other two terms are the angle bending interaction shown by Eq. (2). We note that the angle bending term $K_{\mathrm{Hf-S-S}}$ is for the angle $\theta_{\mathrm{Hf-S-S}}$ with both S atoms from the same (top or bottom) group. These force constant parameters are determined by fitting to the three acoustic branches in the phonon dispersion along the ΓM as shown in **Figure 146(a)**. The *ab initio* calculations for the phonon dispersion are from Ref. [38]. Similar phonon dispersion can also be found in other *ab initio* calculations [34, 35]. **Figure 146(b)** shows that the VFF model and the SW potential give exactly the same phonon dispersion, as the SW potential is derived from the VFF model.

The parameters for the two-body SW potential used by GULP are shown in **Table 295**. The parameters for the three-body SW potential used by GULP are shown in **Table 296**. Some representative parameters for the SW potential used by LAMMPS are listed in **Table 297**.

We use LAMMPS to perform MD simulations for the mechanical behavior of the single-layer 1T-HfS_2 under uniaxial tension at 1 and 300 K. **Figure 147** shows the stress-strain curve for the tension of a single-layer 1T-HfS_2 of dimension 100 × 100 Å. Periodic boundary conditions are applied in both armchair and zigzag directions. The single-layer 1T-HfS_2 is stretched uniaxially along the armchair or zigzag direction. The stress is calculated without involving the actual thickness of the quasi-two-dimensional structure of the single-layer 1T-HfS_2. The Young's modulus can be obtained by a linear fitting of the stress-strain relation in the small strain range of [0, 0.01]. The Young's modulus is 73.3 and 72.9 N/m along the armchair and zigzag

VFF type	Bond stretching	Angle bending	
Expression	$\frac{1}{2}K_{\mathrm{Hf-S}}(\Delta r)^2$	$\frac{1}{2}K_{\mathrm{Hf-S-S}}(\Delta\theta)^2$	$\frac{1}{2}K_{\mathrm{S-Hf-Hf}}(\Delta\theta)^2$
Parameter	7.930	4.283	4.283
r_0 or θ_0	2.550	91.078	91.078

The second line gives an explicit expression for each VFF term. The third line is the force constant parameters. Parameters are in the unit of ev/Å^2 for the bond stretching interaction and in the unit of eV for the angle bending interaction. The fourth line gives the initial bond length (in the unit of Å) for the bond stretching interaction and the initial angle (in the unit of degrees) for the angle bending interaction. The angle θ_{ijk} has atom i as the apex.

Table 294. The VFF model for single-layer 1T-HfS_2.

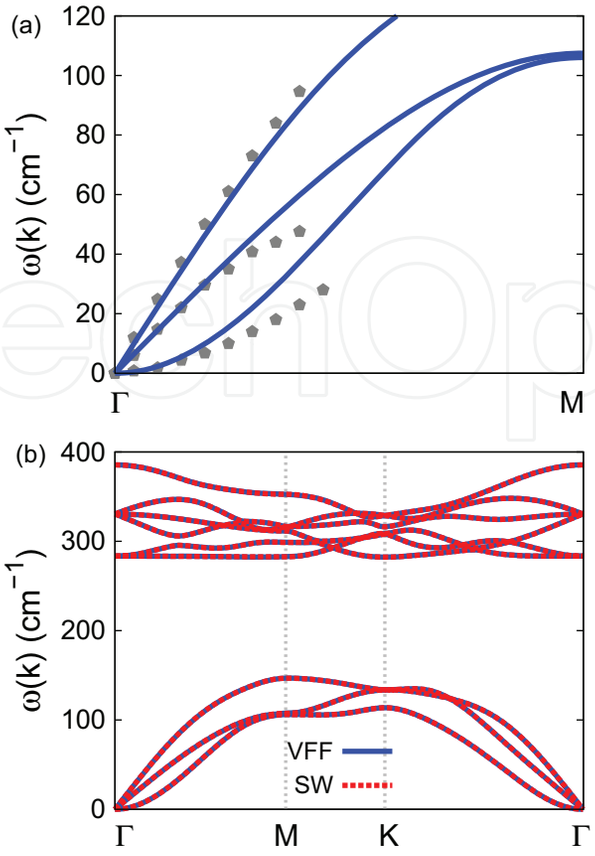

Figure 146. Phonon spectrum for single-layer 1T-HfS_2. (a) Phonon dispersion along the ΓM direction in the Brillouin zone. The results from the VFF model (lines) are comparable with the experiment data (pentagons) from Ref. [38]. (b) The phonon dispersion from the SW potential is exactly the same as that from the VFF model.

	A (eV)	ρ (Å)	B (Å^4)	r_{min} (Å)	r_{max} (Å)
Hf—S	7.917	1.407	21.141	0.0	3.497

Table 295. Two-body SW potential parameters for single-layer 1T-HfS2 used by GULP [8] as expressed in Eq. (3).

	K (eV)	θ_0 (°)	ρ_1 (Å)	ρ_2 (Å)	$r_{min\,12}$ (Å)	$r_{max\,12}$ (Å)	$r_{min\,13}$ (Å)	$r_{max\,13}$ (Å)	$r_{min\,23}$ (Å)	$r_{max\,23}$ (Å)
θ_{Hf-S-S} (Å)	41.798	91.078	1.407	1.407	0.0	3.497	0.0	3.497	0.0	4.973
$\theta_{S-Hf-Hf}$ (Å)	41.798	91.078	1.407	1.407	0.0	3.497	0.0	3.497	0.0	4.973

The angle θ_{ijk} in the first line indicates the bending energy for the angle with atom i as the apex.

Table 296. Three-body SW potential parameters for single-layer 1T-HfS_2 used by GULP [8] as expressed in Eq. (4).

	ϵ (eV)	σ (Å)	a	λ	γ	cos θ_0	A_L	B_L	p	q	Tol
Hf—S—S	1.000	1.407	2.485	41.798	1.000	−0.019	7.917	5.394	4	0	0.0
S—Hf—Hf	1.000	1.407	2.485	41.798	1.000	−0.019	7.917	5.394	4	0	0.0

Table 297. SW potential parameters for single-layer 1T-HfS2 used by LAMMPS [9] as expressed in Eqs. (9) and (10).

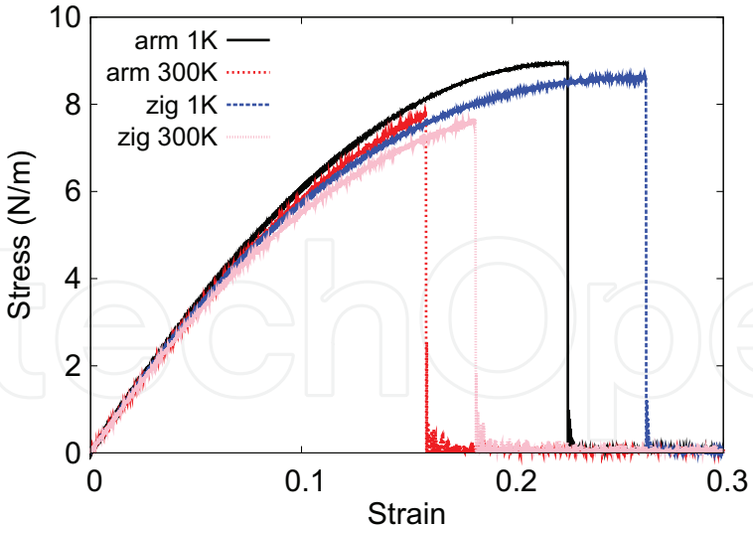

Figure 147. Stress-strain for single-layer 1T-HfS_2 of dimension 100 × 100 Å along the armchair and zigzag directions.

directions, respectively. The Young's modulus is essentially isotropic in the armchair and zigzag directions. These values are close to the *ab initio* results at 0 K temperature, e.g., 79.86 N/m in Ref. [53]. The Poisson's ratio from the VFF model and the SW potential is $\nu_{xy} = \nu_{yx} = 0.16$, which agrees reasonably with the *ab initio* result [54] of 0.19.

There is no available value for nonlinear quantities in the single-layer 1T-HfS_2. We have thus used the nonlinear parameter $B = 0.5d^4$ in Eq. (5), which is close to the value of B in most materials. The value of the third-order nonlinear elasticity D can be extracted by fitting the stress-strain relation to the function $\sigma = E\epsilon + \frac{1}{2}D\epsilon^2$ with E as the Young's modulus. The values of D from the present SW potential are −280.9 and −317.2 N/m along the armchair and zigzag directions, respectively. The ultimate stress is about 8.9 N/m at the ultimate strain of 0.22 in the armchair direction at the low temperature of 1 K. The ultimate stress is about 8.6 N/m at the ultimate strain of 0.26 in the zigzag direction at the low temperature of 1 K.

75. 1T-$HfSe_2$

Most existing theoretical studies on the single-layer 1T-$HfSe_2$ are based on the first-principles calculations. In this section, we will develop the SW potential for the single-layer 1T-$HfSe_2$.

The structure for the single-layer 1T-$HfSe_2$ is shown in **Figure 71** (with M=Hf and X=Se). Each Hf atom is surrounded by six Se atoms. These Se atoms are categorized into the top group (e.g., atoms 1, 3, and 5) and bottom group (e.g., atoms 2, 4, and 6). Each Se atom is connected to three Hf atoms. The structural parameters are from the first-principles calculations [51], including the lattice constant $a = 3.673$ Å and the position of the Se atom with respect to the Hf atomic plane $h = 1.575$ Å. The resultant angles are $\theta_{\mathrm{HfSeSe}} = 88.093^\circ$ with S atoms from the same (top or bottom) group and $\theta_{\mathrm{SeHfHf}} = 88.093^\circ$.

http://dx.doi.org/10.5772/intechopen.71929

Table 298 shows three VFF terms for the single-layer 1T-$HfSe_2$; one of which is the bond stretching interaction shown by Eq. (1), while the other two terms are the angle bending interaction shown by Eq. (2). We note that the angle bending term $K_{Hf-Se-Se}$ is for the angle $\theta_{Hf-Se-Se}$ with both Se atoms from the same (top or bottom) group. These force constant parameters are determined by fitting to the three acoustic branches in the phonon dispersion along the ΓM as shown in **Figure 148(a)**. The *ab initio* calculations for the phonon dispersion are from Ref. [50]. Similar phonon dispersion can also be found in other *ab initio*

VFF type	**Bond stretching**	**Angle bending**	
Expression	$\frac{1}{2}K_{Hf-Se}(\Delta r)^2$	$\frac{1}{2}K_{Hf-Se-Se}(\Delta\theta)^2$	$\frac{1}{2}K_{Se-Hf-Hf}(\Delta\theta)^2$
Parameter	7.930	4.283	4.283
r_0 or θ_0	2.642	88.093	88.093

The second line gives an explicit expression for each VFF term. The third line is the force constant parameters. Parameters are in the unit of ev/Å^2 for the bond stretching interaction and in the unit of eV for the angle bending interaction. The fourth line gives the initial bond length (in the unit of Å) for the bond stretching interaction and the initial angle (in the unit of degrees) for the angle bending interaction. The angle θ_{ijk} has atom i as the apex.

Table 298. The VFF model for single-layer 1T-$HfSe_2$.

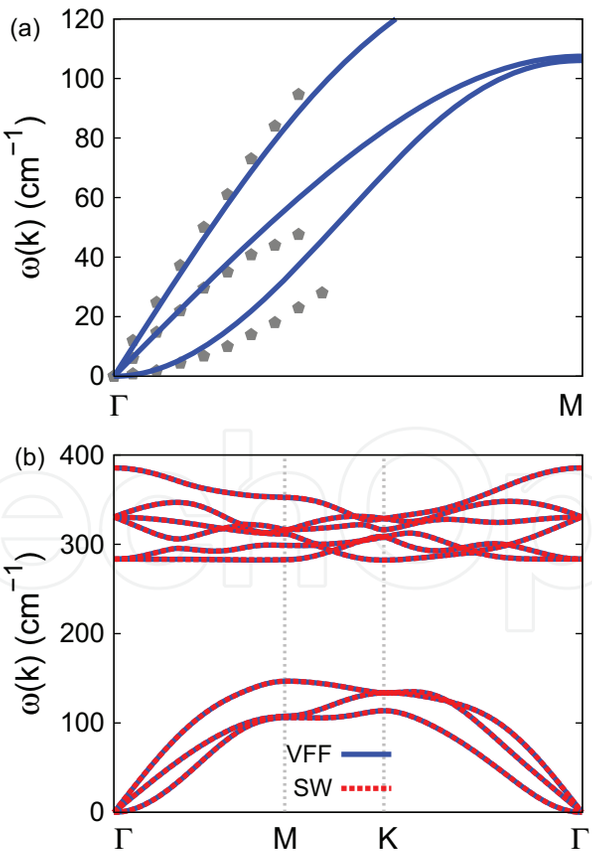

Figure 148. Phonon spectrum for single-layer 1T-$HfSe_2$. (a) Phonon dispersion along the ΓM direction in the Brillouin zone. The results from the VFF model (lines) are comparable with the experiment data (pentagons) from Ref. [50]. (b) The phonon dispersion from the SW potential is exactly the same as that from the VFF model.

calculations [34]. **Figure 148(b)** shows that the VFF model and the SW potential give exactly the same phonon dispersion, as the SW potential is derived from the VFF model.

The parameters for the two-body SW potential used by GULP are shown in **Table 299**. The parameters for the three-body SW potential used by GULP are shown in **Table 300**. Some representative parameters for the SW potential used by LAMMPS are listed in **Table 301**.

We use LAMMPS to perform MD simulations for the mechanical behavior of the single-layer 1T-$HfSe_2$ under uniaxial tension at 1 and 300 K. **Figure 149** shows the stress-strain curve for the tension of a single-layer 1T-$HfSe_2$ of dimension 100×100 Å. Periodic boundary conditions are applied in both armchair and zigzag directions. The single-layer 1T-$HfSe_2$ is stretched uniaxially along the armchair or zigzag direction. The stress is calculated without involving the actual thickness of the quasi-two-dimensional structure of the single-layer 1T-$HfSe_2$. The Young's modulus can be obtained by a linear fitting of the stress-strain relation in the small strain range of [0, 0.01]. The Young's modulus is 67.3 and 67.0 N/m along the armchair and zigzag directions, respectively. The Young's modulus is essentially isotropic in the armchair and zigzag directions. The Poisson's ratio from the VFF model and the SW potential is $\nu_{xy} = \nu_{yx} = 0.18$.

There is no available value for nonlinear quantities in the single-layer 1T-$HfSe_2$. We have thus used the nonlinear parameter $B = 0.5d^4$ in Eq. (5), which is close to the value of B in most materials. The value of the third-order nonlinear elasticity D can be extracted by fitting the stress-strain relation to the function $\sigma = E\epsilon + \frac{1}{2}D\epsilon^2$ with E as the Young's modulus. The values of D from the present SW potential are -221.5 and -258.6 N/m along the armchair and zigzag directions, respectively. The ultimate stress is about 9.0 N/m at the ultimate strain of 0.24 in the

	A (eV)	ρ (Å)	B (Å^4)	$r_{\min}$ (Å)	$r_{\max}$ (Å)
Hf—Se	7.871	1.341	24.361	0.0	3.583

Table 299. Two-body SW potential parameters for single-layer 1T-$HfSe_2$ used by GULP [8] as expressed in Eq. (3).

	K (eV)	θ_0 (°)	ρ_1 (Å)	ρ_2 (Å)	$r_{\min 12}$ (Å)	$r_{\max 12}$ (Å)	$r_{\min 13}$ (Å)	$r_{\max 13}$ (Å)	$r_{\min 23}$ (Å)	$r_{\max 23}$ (Å)
$\theta_{\text{Hf–Se–Se}}$	37.039	88.093	1.341	1.341	0.0	3.583	0.0	3.583	0.0	5.018
$\theta_{\text{Se–Hf–Hf}}$	37.039	88.093	1.341	1.341	0.0	3.583	0.0	3.583	0.0	5.018

The angle θ_{ijk} in the first line indicates the bending energy for the angle with atom i as the apex.

Table 300. Three-body SW potential parameters for single-layer 1T-$HfSe_2$ used by GULP [8] as expressed in Eq. (4).

	ϵ (eV)	σ (Å)	a	λ	γ	$\cos\theta_0$	A_L	B_L	p	q	Tol
Hf—Se—Se	1.000	1.341	2.672	37.039	1.000	0.033	7.871	7.533	4	0	0.0
Se—Hf—Hf	1.000	1.341	2.672	37.039	1.000	0.033	7.871	7.533	4	0	0.0

Table 301. SW potential parameters for single-layer 1T-$HfSe_2$ used by LAMMPS [9] as expressed in Eqs. (9) and (10).

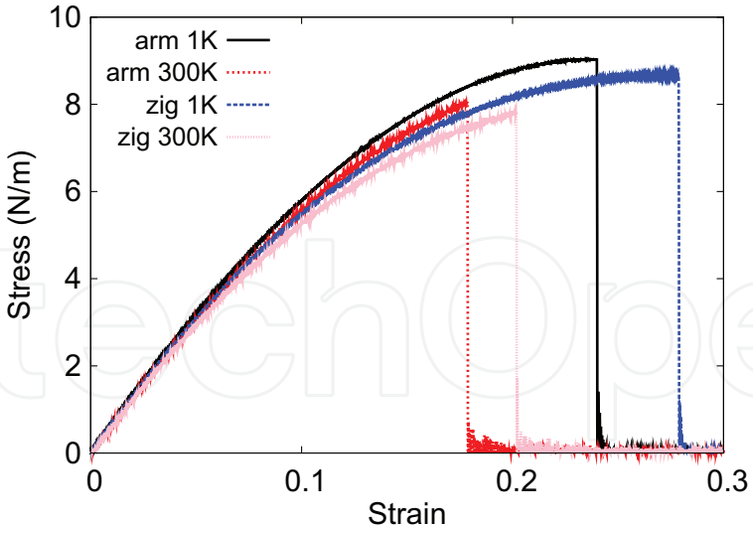

Figure 149. Stress-strain for single-layer 1T-$HfSe_2$ of dimension 100 × 100 Å along the armchair and zigzag directions.

armchair direction at the low temperature of 1 K. The ultimate stress is about 8.7 N/m at the ultimate strain of 0.28 in the zigzag direction at the low temperature of 1 K.

76. 1T-$HfTe_2$

Most existing theoretical studies on the single-layer 1T-$HfTe_2$ are based on the first-principles calculations. In this section, we will develop the SW potential for the single-layer 1T-$HfTe_2$.

The structure for the single-layer 1T-$HfTe_2$ is shown in **Figure 71** (with M = Hf and X = Te). Each Hf atom is surrounded by six Te atoms. These Te atoms are categorized into the top group (e.g., atoms 1, 3, and 5) and bottom group (e.g., atoms 2, 4, and 6). Each Te atom is connected to three Hf atoms. The structural parameters are from the first-principles calculations [48], including the lattice constant $a = 3.9606$ Å and the bond length $d_{\mathrm{Hf-Te}} = 2.8559$ Å, which are derived from the angle $\theta_{\mathrm{TeHfHf}} = 87.8^{\circ}$. The other angle is $\theta_{\mathrm{HfTeTe}} = 87.8^{\circ}$ with Te atoms from the same (top or bottom) group.

Table 302 shows three VFF terms for the single-layer 1T-$HfTe_2$; one of which is the bond stretching interaction shown by Eq. (1), while the other two terms are the angle bending interaction shown by Eq. (2). We note that the angle bending term $K_{\mathrm{Hf-Te-Te}}$ is for the angle $\theta_{\mathrm{Hf-Te-Te}}$ with both Te atoms from the same (top or bottom) group. We find that there are actually only two parameters in the VFF model, so we can determine their value by fitting to the Young's modulus and the Poisson's ratio of the system. The *ab initio* calculations have predicted the Young's modulus to be 50 N/m and the Poisson's ratio as 0.10 [48].

The parameters for the two-body SW potential used by GULP are shown in **Table 303**. The parameters for the three-body SW potential used by GULP are shown in **Table 304**. Some representative parameters for the SW potential used by LAMMPS are listed in **Table 305**.

VFF type	Bond stretching	Angle bending	
Expression	$\frac{1}{2}K_{\mathrm{Hf-Te}}(\Delta r)^2$	$\frac{1}{2}K_{\mathrm{Hf-Te-Te}}(\Delta\theta)^2$	$\frac{1}{2}K_{\mathrm{Te-Hf-Hf}}(\Delta\theta)^2$
Parameter	3.328	3.877	3.877
r_0 or θ_0	2.856	87.801	87.801

The second line gives an explicit expression for each VFF term. The third line is the force constant parameters. Parameters are in the unit of ev/Å^2 for the bond stretching interaction and in the unit of eV for the angle bending interaction. The fourth line gives the initial bond length (in the unit of Å) for the bond stretching interaction and the initial angle (in the unit of degrees) for the angle bending interaction. The angle θ_{ijk} has atom i as the apex.

Table 302. The VFF model for single-layer 1T-$HfTe_2$.

	A (eV)	ρ (Å)	B (Å^4)	$r_{\min}$ (Å)	$r_{\max}$ (Å)
Hf—Te	3.835	1.439	33.262	0.0	3.869

Table 303. Two-body SW potential parameters for single-layer 1T-$HfTe_2$ used by GULP [8] as expressed in Eq. (3).

	K (eV)	θ_0 (°)	ρ_1 (Å)	ρ_2 (Å)	$r_{\min 12}$ (Å)	$r_{\max 12}$ (Å)	$r_{\min 13}$ (Å)	$r_{\max 13}$ (Å)	$r_{\min 23}$ (Å)	$r_{\max 23}$ (Å)
$\theta_{\mathrm{Hf-Te-Te}}$	33.196	87.801	1.439	1.439	0.0	3.869	0.0	3.869	0.0	5.410
$\theta_{\mathrm{Te-Hf-Hf}}$	33.196	87.801	1.439	1.439	0.0	3.869	0.0	3.869	0.0	5.410

The angle θ_{ijk} in the first line indicates the bending energy for the angle with atom i as the apex.

Table 304. Three-body SW potential parameters for single-layer 1T-$HfTe_2$ used by GULP [8] as expressed in Eq. (4).

	ϵ (eV)	σ (Å)	a	λ	γ	$\cos\theta_0$	A_L	B_L	p	q	Tol
Hf—Te_1—Te_1	1.000	1.439	2.690	33.196	1.000	0.038	3.835	7.764	4	0	0.0

Table 305. SW potential parameters for single-layer 1T-$HfTe_2$ used by LAMMPS [9] as expressed in Eqs. (9) and (10).

We use LAMMPS to perform MD simulations for the mechanical behavior of the single-layer 1T-$HfTe_2$ under uniaxial tension at 1 and 300 K. **Figure 150** shows the stress-strain curve for the tension of a single-layer 1T-$HfTe_2$ of dimension 100 × 100 Å. Periodic boundary conditions are applied in both armchair and zigzag directions. The single-layer 1T-$HfTe_2$ is stretched uniaxially along the armchair or zigzag direction. The stress is calculated without involving the actual thickness of the quasi-two-dimensional structure of the single-layer 1T-$HfTe_2$. The Young's modulus can be obtained by a linear fitting of the stress-strain relation in the small strain range of [0, 0.01]. The Young's modulus is 43.1 N/m along the armchair and zigzag directions. The Poisson's ratio from the VFF model and the SW potential is $\nu_{xy} = \nu_{yx} = 0.10$. The fitted Young's modulus value is about 10% smaller than the *ab initio* result of 50 N/m [48], as only short-range interactions are considered in the present work. The long-range interactions are ignored, which typically lead to about 10% underestimation for the value of the Young's modulus.

http://dx.doi.org/10.5772/intechopen.71929

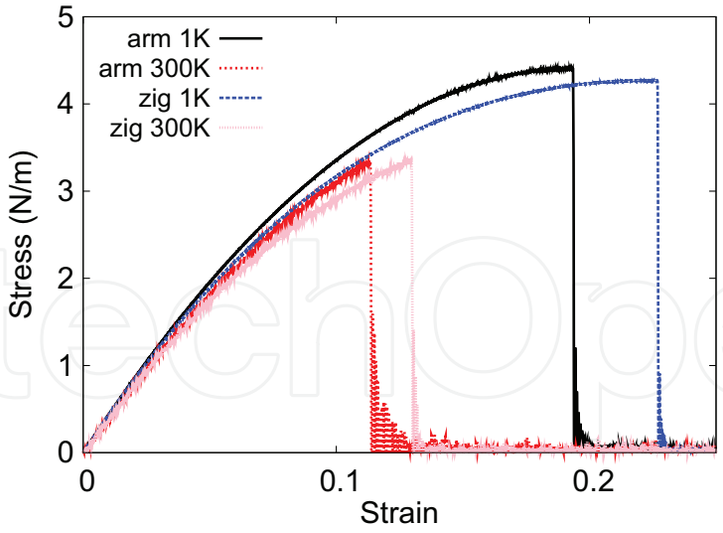

Figure 150. Stress-strain for single-layer 1T-$HfTe_2$ of dimension 100 × 100 Å along the armchair and zigzag directions.

There is no available value for nonlinear quantities in the single-layer 1T-$HfTe_2$. We have thus used the nonlinear parameter $B = 0.5d^4$ in Eq. (5), which is close to the value of B in most materials. The value of the third-order nonlinear elasticity D can be extracted by fitting the stress-strain relation to the function $\sigma = E\epsilon + \frac{1}{2}D\epsilon^2$ with E as the Young's modulus. The values of D from the present SW potential are −204.3 and −220.7 N/m along the armchair and zigzag directions, respectively. The ultimate stress is about 4.4 N/m at the ultimate strain of 0.19 in the armchair direction at the low temperature of 1 K. The ultimate stress is about 4.3 N/m at the ultimate strain of 0.22 in the zigzag direction at the low temperature of 1 K.

Figure 151 shows that the VFF model and the SW potential give exactly the same phonon dispersion, as the SW potential is derived from the VFF model.

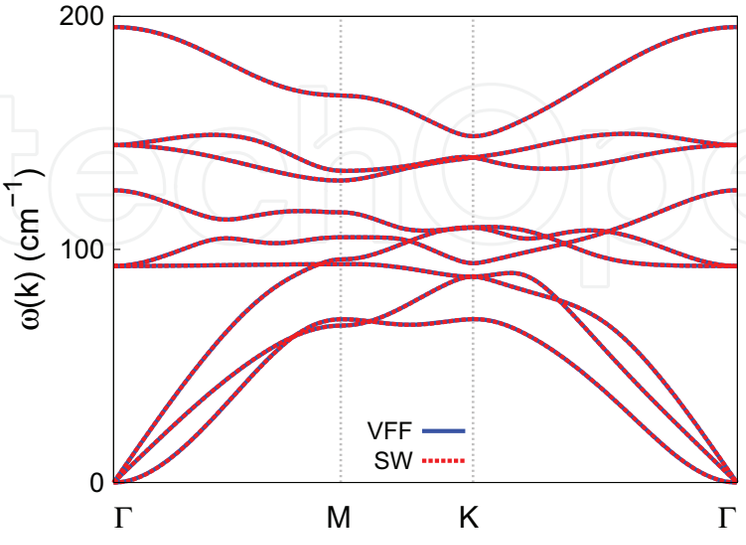

Figure 151. Phonon spectrum for single-layer 1T-$HfTe_2$ along the ΓMKΓ direction in the Brillouin zone. The phonon dispersion from the SW potential is exactly the same as that from the VFF model.

77. 1T-TaS_2

Most existing theoretical studies on the single-layer 1T-TaS_2 are based on the first-principles calculations. In this section, we will develop the SW potential for the single-layer 1T-TaS_2.

The structure for the single-layer 1T-TaS_2 is shown in **Figure 71** (with M=Ta and X=S). Each Ta atom is surrounded by six S atoms. These S atoms are categorized into the top group (e.g., atoms 1, 3, and 5) and bottom group (e.g., atoms 2, 4, and 6). Each S atom is connected to three Ta atoms. The structural parameters are from the first-principles calculations [48], including the lattice constant $a = 3.3524$ Å and the bond length $d_{\mathrm{Ta-S}} = 2.4578$ Å, which are derived from the angle $\theta_{\mathrm{STaTa}} = 86^\circ$. The other angle is $\theta_{\mathrm{TaSS}} = 86^\circ$ with S atoms from the same (top or bottom) group.

Table 306 shows three VFF terms for the single-layer 1T-TaS_2; one of which is the bond stretching interaction shown by Eq. (1), while the other two terms are the angle bending interaction shown by Eq. (2). We note that the angle bending term $K_{\mathrm{Ta-S-S}}$ is for the angle $\theta_{\mathrm{Ta-S-S}}$ with both S atoms from the same (top or bottom) group. We find that there are actually only two parameters in the VFF model, so we can determine their value by fitting to the Young's modulus and the Poisson's ratio of the system. The *ab initio* calculations have predicted the Young's modulus to be 101 N/m and the Poisson's ratio as 0.20 [48].

The parameters for the two-body SW potential used by GULP are shown in **Table 307**. The parameters for the three-body SW potential used by GULP are shown in **Table 308**. Some representative parameters for the SW potential used by LAMMPS are listed in **Table 309**.

We use LAMMPS to perform MD simulations for the mechanical behavior of the single-layer 1T-TaS_2 under uniaxial tension at 1 and 300 K. **Figure 152** shows the stress-strain curve for the tension of a single-layer 1T-TaS_2 of dimension 100×100 Å. Periodic boundary conditions are applied in both armchair and zigzag directions. The single-layer 1T-TaS_2 is stretched uniaxially

VFF type	Bond stretching	Angle bending	
Expression	$\frac{1}{2}K_{\mathrm{Ta-S}}(\Delta r)^2$	$\frac{1}{2}K_{\mathrm{Ta-S-S}}(\Delta\theta)^2$	$\frac{1}{2}K_{\mathrm{S-Ta-Ta}}(\Delta\theta)^2$
Parameter	11.192	4.774	4.774
r_0 or θ_0	2.458	85.999	85.999

The second line gives an explicit expression for each VFF term. The third line is the force constant parameters. Parameters are in the unit of ev/Å^2 for the bond stretching interaction and in the unit of eV for the angle bending interaction. The fourth line gives the initial bond length (in the unit of Å) for the bond stretching interaction and the initial angle (in the unit of degrees) for the angle bending interaction. The angle θ_{ijk} has atom i as the apex.

Table 306. The VFF model for single-layer 1T-TaS_2.

	A (eV)	ρ (Å)	B (Å^4)	r_{min} (Å)	r_{max} (Å)
Ta—S	9.110	1.174	18.246	0.0	3.307

Table 307. Two-body SW potential parameters for single-layer 1T-TaS_2 used by GULP [8] as expressed in Eq. (3).

	K (eV)	θ_0 (°)	ρ_1 (Å)	ρ_2 (Å)	$r_{\min 12}$ (Å)	$r_{\max 12}$ (Å)	$r_{\min 13}$ (Å)	$r_{\max 13}$ (Å)	$r_{\min 23}$ (Å)	$r_{\max 23}$ (Å)
$\theta_{\text{Ta–S–S}}$	38.092	85.999	1.174	1.174	0.0	3.307	0.0	3.307	0.0	4.579
$\theta_{\text{S–Ta–Ta}}$	38.092	85.999	1.174	1.174	0.0	3.307	0.0	3.307	0.0	4.579

The angle θ_{ijk} in the first line indicates the bending energy for the angle with atom i as the apex.

Table 308. Three-body SW potential parameters for single-layer 1T-TaS_2 used by GULP [8] as expressed in Eq. (4).

	ϵ (eV)	σ (Å)	a	λ	γ	$\cos\theta_0$	A_L	B_L	p	q	Tol
Ta—S_1—S_1	1.000	1.174	2.816	38.092	1.000	0.070	9.110	9.589	4	0	0.0

Table 309. SW potential parameters for single-layer 1T-TaS_2 used by LAMMPS [9] as expressed in Eqs. (9) and (10).

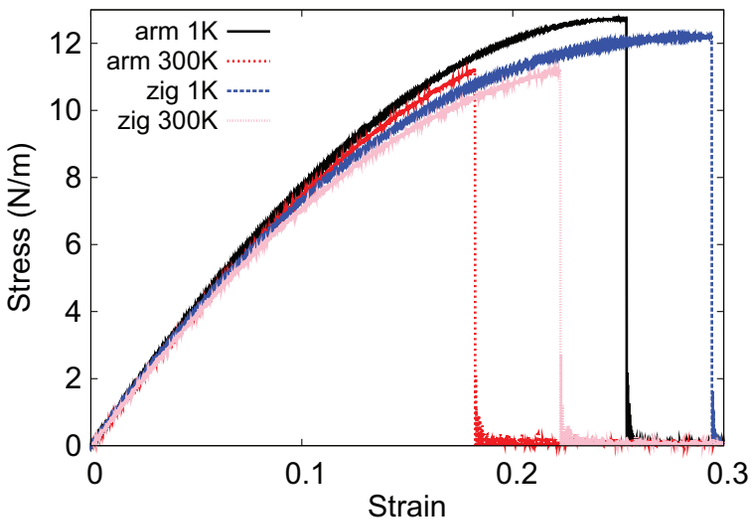

Figure 152. Stress-strain for single-layer 1T-TaS_2 of dimension 100 × 100 Å along the armchair and zigzag directions.

along the armchair or zigzag direction. The stress is calculated without involving the actual thickness of the quasi-two-dimensional structure of the single-layer 1T-TaS_2. The Young's modulus can be obtained by a linear fitting of the stress-strain relation in the small strain range of [0, 0.01]. The Young's modulus is 87.8 and 87.4 N/m along the armchair and zigzag directions, respectively. The Young's modulus is essentially isotropic in the armchair and zigzag directions. The Poisson's ratio from the VFF model and the SW potential is $\nu_{xy} = \nu_{yx} = 0.20$. The fitted Young's modulus value is about 10% smaller than the *ab initio* result of 101 N/m [48], as only short-range interactions are considered in the present work. The long-range interactions are ignored, which typically lead to about 10% underestimation for the value of the Young's modulus.

There is no available value for nonlinear quantities in the single-layer 1T-TaS_2. We have thus used the nonlinear parameter $B = 0.5d^4$ in Eq. (5), which is close to the value of B in most materials. The value of the third-order nonlinear elasticity D can be extracted by fitting the

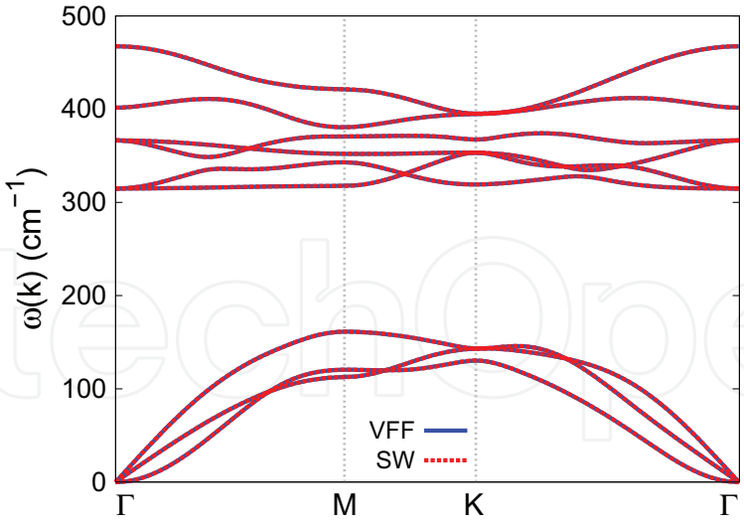

Figure 153. Phonon spectrum for single-layer 1T-TaS_2 along the ΓMKΓ direction in the Brillouin zone. The phonon dispersion from the SW potential is exactly the same as that from the VFF model.

stress-strain relation to the function $\sigma = E\epsilon + \frac{1}{2}D\epsilon^2$ with E as the Young's modulus. The values of D from the present SW potential are -276.3 and -313.0 N/m along the armchair and zigzag directions, respectively. The ultimate stress is about 12.7 N/m at the ultimate strain of 0.25 in the armchair direction at the low temperature of 1 K. The ultimate stress is about 12.2 N/m at the ultimate strain of 0.29 in the zigzag direction at the low temperature of 1 K.

Figure 153 shows that the VFF model and the SW potential give exactly the same phonon dispersion, as the SW potential is derived from the VFF model.

78. 1T-$TaSe_2$

Most existing theoretical studies on the single-layer 1T-$TaSe_2$ are based on the first-principles calculations. In this section, we will develop the SW potential for the single-layer 1T-$TaSe_2$.

The structure for the single-layer 1T-$TaSe_2$ is shown in **Figure 71** (with M=Ta and X=Se). Each Ta atom is surrounded by six Se atoms. These Se atoms are categorized into the top group (e.g., atoms 1, 3, and 5) and bottom group (e.g., atoms 2, 4, and 6). Each Se atom is connected to three Ta atoms. The structural parameters are from the first-principles calculations [48], including the lattice constant $a = 3.4602$ Å and the bond length $d_{\mathrm{Ta-Se}} = 2.5609$ Å, which are derived from the angle $\theta_{\mathrm{SeTaTa}} = 85^\circ$. The other angle is $\theta_{\mathrm{TaSeSe}} = 85^\circ$ with Se atoms from the same (top or bottom) group.

Table 310 shows three VFF terms for the single-layer 1T-$TaSe_2$; one of which is the bond stretching interaction shown by Eq. (1), while the other two terms are the angle bending interaction shown by Eq. (2). We note that the angle bending term $K_{\mathrm{Ta-Se-Se}}$ is for the angle $\theta_{\mathrm{Ta-Se-Se}}$ with both Se atoms from the same (top or bottom) group. We find that there are

VFF type	Bond stretching	Angle bending	
Expression	$\frac{1}{2}K_{\mathrm{Ta-Se}}(\Delta r)^2$	$\frac{1}{2}K_{\mathrm{Ta-Se-Se}}(\Delta\theta)^2$	$\frac{1}{2}K_{\mathrm{Se-Ta-Ta}}(\Delta\theta)^2$
Parameter	9.348	4.535	4.535
r_0 or θ_0	2.561	84.999	84.999

The second line gives an explicit expression for each VFF term. The third line is the force constant parameters. Parameters are in the unit of ev/Å^2 for the bond stretching interaction and in the unit of eV for the angle bending interaction. The fourth line gives the initial bond length (in the unit of Å) for the bond stretching interaction and the initial angle (in the unit of degrees) for the angle bending interaction. The angle θ_{ijk} has atom i as the apex.

Table 310. The VFF model for single-layer 1T-$TaSe_2$.

actually only two parameters in the VFF model, so we can determine their value by fitting to the Young's modulus and the Poisson's ratio of the system. The *ab initio* calculations have predicted the Young's modulus to be 85 N/m and the Poisson's ratio as 0.20 [48].

The parameters for the two-body SW potential used by GULP are shown in **Table 311**. The parameters for the three-body SW potential used by GULP are shown in **Table 312**. Some representative parameters for the SW potential used by LAMMPS are listed in **Table 313**.

We use LAMMPS to perform MD simulations for the mechanical behavior of the single-layer 1T-$TaSe_2$ under uniaxial tension at 1 and 300 K. **Figure 154** shows the stress-strain curve for the tension of a single-layer 1T-$TaSe_2$ of dimension 100 × 100 Å. Periodic boundary conditions are applied in both armchair and zigzag directions. The single-layer 1T-$TaSe_2$ is stretched uniaxially along the armchair or zigzag direction. The stress is calculated without involving the actual thickness of the quasi-two-dimensional structure of the single-layer 1T-$TaSe_2$. The Young's modulus can be obtained by a linear fitting of the stress-strain relation in the small

	A (eV)	ρ (Å)	B (Å^4)	r_{min} (Å)	r_{max} (Å)
Ta—Se	8.045	1.188	21.505	0.0	3.433

Table 311. Two-body SW potential parameters for single-layer 1T-$TaSe_2$ used by GULP [8] as expressed in Eq. (3).

	K (eV)	θ_0 (°)	ρ_1 (Å)	ρ_2 (Å)	$r_{\mathrm{min}\,12}$ (Å)	$r_{\mathrm{max}\,12}$ (Å)	$r_{\mathrm{min}\,13}$ (Å)	$r_{\mathrm{max}\,13}$ (Å)	$r_{\mathrm{min}\,23}$ (Å)	$r_{\mathrm{max}\,23}$ (Å)
$\theta_{\mathrm{Ta-Se-Se}}$	34.820	84.999	1.188	1.188	0.0	3.433	0.0	3.3433	0.0	4.727
$\theta_{\mathrm{Se-Ta-Ta}}$	34.820	84.999	1.188	1.188	0.0	3.433	0.0	3.3433	0.0	4.727

The angle θ_{ijk} in the first line indicates the bending energy for the angle with atom i as the apex.

Table 312. Three-body SW potential parameters for single-layer 1T-$TaSe_2$ used by GULP [8] as expressed in Eq. (4).

	ϵ (eV)	σ (Å)	a	λ	γ	$\cos\theta_0$	A_L	B_L	p	q	Tol
Ta—Se_1—Se_1	1.000	1.188	2.891	34.820	1.000	0.087	8.045	10.813	4	0	0.0

Table 313. SW potential parameters for single-layer 1T-$TaSe_2$ used by LAMMPS [9] as expressed in Eqs. (9) and (10).

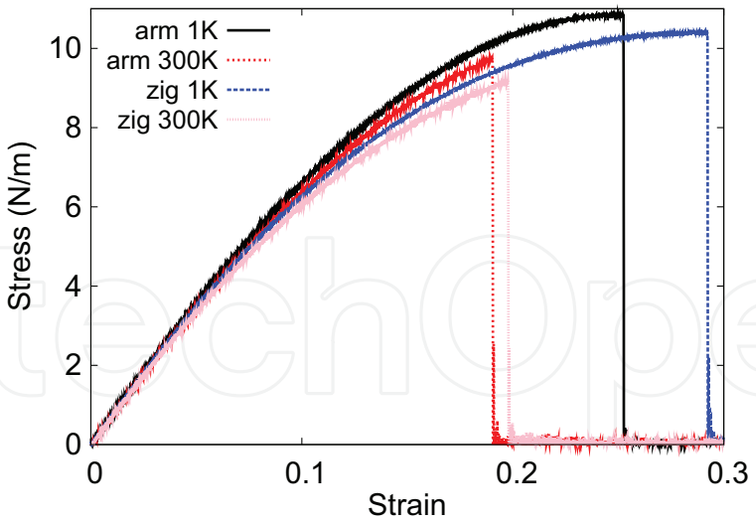

Figure 154. Stress-strain for single-layer 1T-$TaSe_2$ of dimension 100×100 Å along the armchair and zigzag directions.

strain range of [0, 0.01]. The Young's modulus is 74.6 and 74.4 N/m along the armchair and zigzag directions, respectively. The Young's modulus is essentially isotropic in the armchair and zigzag directions. The Poisson's ratio from the VFF model and the SW potential is $\nu_{xy} = \nu_{yx} = 0.20$. The fitted Young's modulus value is about 10% smaller than the *ab initio* result of 85 N/m [48], as only short-range interactions are considered in the present work. The long-range interactions are ignored, which typically leads to about 10% underestimation for the value of the Young's modulus.

There is no available value for nonlinear quantities in the single-layer 1T-$TaSe_2$. We have thus used the nonlinear parameter $B = 0.5d^4$ in Eq. (5), which is close to the value of B in most materials. The value of the third-order nonlinear elasticity D can be extracted by fitting the stress-strain relation to the function $\sigma = E\epsilon + \frac{1}{2}D\epsilon^2$ with E as the Young's modulus. The values

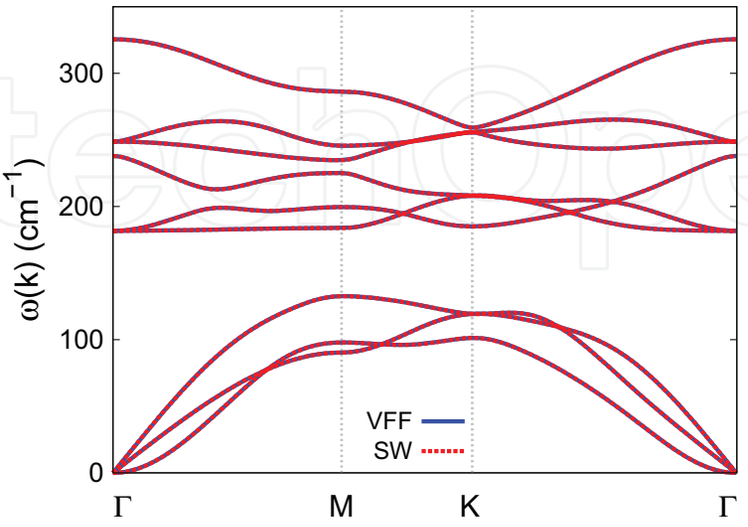

Figure 155. Phonon spectrum for single-layer 1T-$TaSe_2$ along the ΓMKΓ direction in the Brillouin zone. The phonon dispersion from the SW potential is exactly the same as that from the VFF model.

of D from the present SW potential are -231.7 and -265.4 N/m along the armchair and zigzag directions, respectively. The ultimate stress is about 10.8 N/m at the ultimate strain of 0.25 in the armchair direction at the low temperature of 1 K. The ultimate stress is about 10.4 N/m at the ultimate strain of 0.29 in the zigzag direction at the low temperature of 1 K.

Figure 155 shows that the VFF model and the SW potential give exactly the same phonon dispersion, as the SW potential is derived from the VFF model.

79. 1T-$TaTe_2$

Most existing theoretical studies on the single-layer 1T-$TaTe_2$ are based on the first-principles calculations. In this section, we will develop the SW potential for the single-layer 1T-$TaTe_2$.

The structure for the single-layer 1T-$TaTe_2$ is shown in **Figure 71** (with M=Ta and X=Te). Each Ta atom is surrounded by six Te atoms. These Te atoms are categorized into the top group (e.g., atoms 1, 3, and 5) and bottom group (e.g., atoms 2, 4, and 6). Each Te atom is connected to three Ta atoms. The structural parameters are from the first-principles calculations [48], including the lattice constant $a = 3.6702$ Å and the bond length $d_{\mathrm{Ta-Te}} = 2.7695$ Å, which are derived from the angle $\theta_{\mathrm{TeTaTa}} = 83^\circ$. The other angle is $\theta_{\mathrm{TaTeTe}} = 83^\circ$ with Te atoms from the same (top or bottom) group.

Table 314 shows three VFF terms for the single-layer 1T-$TaTe_2$; one of which is the bond stretching interaction shown by Eq. (1), while the other two terms are the angle bending interaction shown by Eq. (2). We note that the angle bending term $K_{\mathrm{Ta-Te-Te}}$ is for the angle $\theta_{\mathrm{Ta-Te-Te}}$ with both Te atoms from the same (top or bottom) group. We find that there are actually only two parameters in the VFF model, so we can determine their value by fitting to the Young's modulus and the Poisson's ratio of the system. The *ab initio* calculations have predicted the Young's modulus to be 57 N/m and the Poisson's ratio as 0.10 [48].

The parameters for the two-body SW potential used by GULP are shown in **Table 315**. The parameters for the three-body SW potential used by GULP are shown in **Table 316**. Some representative parameters for the SW potential used by LAMMPS are listed in **Table 317**.

VFF type	Bond stretching	Angle bending	
Expression	$\frac{1}{2}K_{\mathrm{Ta-Te}}(\Delta r)^2$	$\frac{1}{2}K_{\mathrm{Ta-Te-Te}}(\Delta\theta)^2$	$\frac{1}{2}K_{\mathrm{Te-Ta-Ta}}(\Delta\theta)^2$
Parameter	3.442	4.516	4.516
r_0 or θ_0	2.770	82.999	82.999

The second line gives an explicit expression for each VFF term. The third line is the force constant parameters. Parameters are in the unit of ev/Å^2 for the bond stretching interaction and in the unit of eV for the angle bending interaction. The fourth line gives the initial bond length (in the unit of Å) for the bond stretching interaction and the initial angle (in the unit of degrees) for the angle bending interaction. The angle θ_{ijk} has atom i as the apex.

Table 314. The VFF model for single-layer 1T-$TaTe_2$.

	A (eV)	ρ (Å)	B (Å^4)	$r_{\min}$ (Å)	$r_{\max}$ (Å)
Ta—Te	3.283	1.207	29.415	0.0	3.684

Table 315. Two-body SW potential parameters for single-layer 1T-$TaTe_2$ used by GULP [8] as expressed in Eq. (3).

	K (eV)	θ_0 (°)	ρ_1 (Å)	ρ_2 (Å)	$r_{\min 12}$ (Å)	$r_{\max 12}$ (Å)	$r_{\min 13}$ (Å)	$r_{\max 13}$ (Å)	$r_{\min 23}$ (Å)	$r_{\max 23}$ (Å)
$\theta_{\text{Ta–Te–Te}}$	32.144	82.999	1.207	1.207	0.0	3.684	0.0	3.684	0.0	5.014
$\theta_{\text{Te–Ta–Ta}}$	32.144	82.999	1.207	1.207	0.0	3.684	0.0	3.684	0.0	5.014

The angle θ_{ijk} in the first line indicates the bending energy for the angle with atom i as the apex.

Table 316. Three-body SW potential parameters for single-layer 1T-$TaTe_2$ used by GULP [8] as expressed in Eq. (4).

	ϵ (eV)	σ (Å)	a	λ	γ	$\cos\theta_0$	A_L	B_L	p	q	Tol
Ta—Se_1—Se_1	1.000	1.188	2.891	34.820	1.000	0.087	8.045	10.813	4	0	0.0

Table 317. SW potential parameters for single-layer 1T-$TaTe_2$ used by LAMMPS [9] as expressed in Eqs. (9) and (10).

We use LAMMPS to perform MD simulations for the mechanical behavior of the single-layer 1T-$TaTe_2$ under uniaxial tension at 1 and 300 K. **Figure 156** shows the stress-strain curve for the tension of a single-layer 1T-$TaTe_2$ of dimension 100 × 100 Å. Periodic boundary conditions are applied in both armchair and zigzag directions. The single-layer 1T-$TaTe_2$ is stretched uniaxially along the armchair or zigzag direction. The stress is calculated without involving the actual thickness of the quasi-two-dimensional structure of the single-layer 1T-$TaTe_2$. The Young's modulus can be obtained by a linear fitting of the stress-strain relation in the small strain range of [0, 0.01]. The Young's modulus is 50.3 and 50.0 N/m along the armchair and

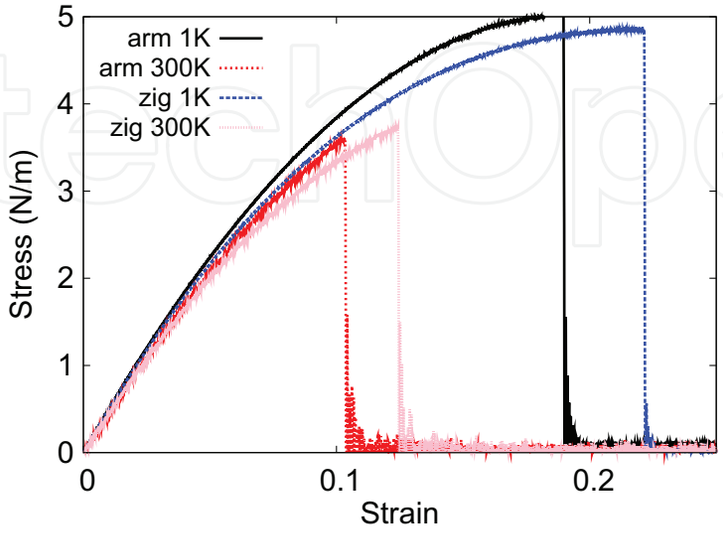

Figure 156. Stress-strain for single-layer 1T-$TaTe_2$ of dimension 100 × 100 Å along the armchair and zigzag directions.

http://dx.doi.org/10.5772/intechopen.71929

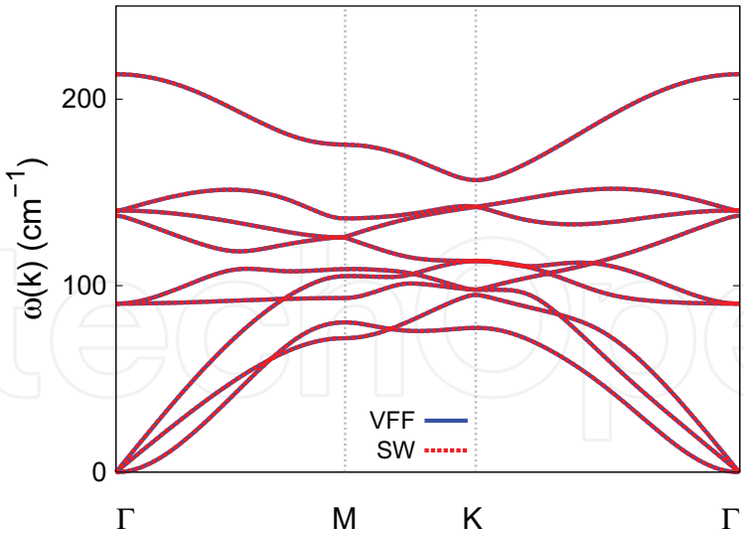

Figure 157. Phonon spectrum for single-layer 1T-$TaTe_2$ along the ΓMKΓ direction in the Brillouin zone. The phonon dispersion from the SW potential is exactly the same as that from the VFF model.

zigzag directions, respectively. The Young's modulus is essentially isotropic in the armchair and zigzag directions. The Poisson's ratio from the VFF model and the SW potential is $\nu_{xy} = \nu_{yx} = 0.10$. The fitted Young's modulus value is about 10% smaller than the *ab initio* result of 57 N/m [48], as only short-range interactions are considered in the present work. The long-range interactions are ignored, which typically lead to about 10% underestimation for the value of the Young's modulus.

There is no available value for nonlinear quantities in the single-layer 1T-$TaTe_2$. We have thus used the nonlinear parameter $B = 0.5d^4$ in Eq. (5), which is close to the value of B in most materials. The value of the third-order nonlinear elasticity D can be extracted by fitting the stress-strain relation to the function $\sigma = E\epsilon + \frac{1}{2}D\epsilon^2$ with E as the Young's modulus. The values of D from the present SW potential are -247.1 and -262.2 N/m along the armchair and zigzag directions, respectively. The ultimate stress is about 5.0 N/m at the ultimate strain of 0.19 in the armchair direction at the low temperature of 1 K. The ultimate stress is about 4.9 N/m at the ultimate strain of 0.22 in the zigzag direction at the low temperature of 1 K.

Figure 157 shows that the VFF model and the SW potential give exactly the same phonon dispersion, as the SW potential is derived from the VFF model.

80. 1T-WS_2

Most existing theoretical studies on the single-layer 1T-WS_2 are based on the first-principles calculations. In this section, we will develop the SW potential for the single-layer 1T-WS_2.

The structure for the single-layer 1T-WS_2 is shown in **Figure 71** (with M=W and X=S). Each W atom is surrounded by six S atoms. These S atoms are categorized into the top group

(e.g., atoms 1, 3, and 5) and bottom group (e.g., atoms 2, 4, and 6). Each S atom is connected to three W atoms. The structural parameters are from the first-principles calculations [48], including the lattice constant $a = 3.1908$ Å and the bond length $d_{W-S} = 2.4125$ Å, which are derived from the angle $\theta_{SWW} = 82.8^\circ$. The other angle is $\theta_{WSS} = 82.8^\circ$ with S atoms from the same (top or bottom) group.

Table 318 shows three VFF terms for the single-layer 1T-WS_2; one of which is the bond stretching interaction shown by Eq. (1), while the other two terms are the angle bending interaction shown by Eq. (2). We note that the angle bending term K_{W-S-S} is for the angle θ_{W-S-S} with both S atoms from the same (top or bottom) group. We find that there are actually only two parameters in the VFF model, so we can determine their value by fitting to the Young's modulus and the Poisson's ratio of the system. The *ab initio* calculations have predicted the Young's modulus to be 113 N/m and the Poisson's ratio as −0.03 [48]. The *ab initio* calculations have predicted a negative Poisson's ratio in the 1T-WS_2, which was attributed to the orbital coupling in this material. The orbital coupling enhances the angle bending interaction in the VFF model. As a result, the value of the angle bending parameter is much larger than the bond stretching force constant parameter, which is typical in auxetic materials with negative Poisson's ratio [52].

The parameters for the two-body SW potential used by GULP are shown in **Table 319**. The parameters for the three-body SW potential used by GULP are shown in **Table 320**. Some representative parameters for the SW potential used by LAMMPS are listed in **Table 321**.

We use LAMMPS to perform MD simulations for the mechanical behavior of the single-layer 1T-WS_2 under uniaxial tension at 1 and 300 K. **Figure 158** shows the stress-strain curve for the tension of a single-layer 1T-WS_2 of dimension 100 × 100 Å. Periodic boundary conditions are applied in both armchair and zigzag directions. The single-layer 1T-WS_2 is stretched uniaxially along the armchair or zigzag direction. The stress is calculated without involving the actual

VFF type	**Bond stretching**	**Angle bending**	
Expression	$\frac{1}{2}K_{W-S}(\Delta r)^2$	$\frac{1}{2}K_{W-S-S}(\Delta\theta)^2$	$\frac{1}{2}K_{S-W-W}(\Delta\theta)^2$
Parameter	4.395	10.087	10.087
r_0 or θ_0	2.413	82.799	82.799

The second line gives an explicit expression for each VFF term. The third line is the force constant parameters. Parameters are in the unit of ev/Å^2 for the bond stretching interaction and in the unit of eV for the angle bending interaction. The fourth line gives the initial bond length (in the unit of Å) for the bond stretching interaction and the initial angle (in the unit of degrees) for the angle bending interaction. The angle θ_{ijk} has atom i as the apex.

Table 318. The VFF model for single-layer 1T-WS_2.

	A **(eV)**	ρ **(Å)**	B **(Å^4)**	r_{min} **(Å)**	r_{max} **(Å)**
W—S	3.163	1.045	16.937	0.0	3.206

Table 319. Two-body SW potential parameters for single-layer 1T-WS_2 used by GULP [8] as expressed in Eq. (3).

	K (eV)	θ_0 (°)	ρ_1 (Å)	ρ_2 (Å)	$r_{\min 12}$ (Å)	$r_{\max 12}$ (Å)	$r_{\min 13}$ (Å)	$r_{\max 13}$ (Å)	$r_{\min 23}$ (Å)	$r_{\max 23}$ (Å)
θ_{W-S-S}	71.264	82.799	1.045	1.045	0.0	3.206	0.0	3.206	0.0	4.359
θ_{S-W-W}	71.264	82.799	1.045	1.045	0.0	3.206	0.0	3.206	0.0	4.359

The angle θ_{ijk} in the first line indicates the bending energy for the angle with atom i as the apex.

Table 320. Three-body SW potential parameters for single-layer 1T-WS_2 used by GULP [8] as expressed in Eq. (4).

	ϵ (eV)	σ (Å)	a	λ	γ	$\cos\theta_0$	A_L	B_L	p	q	Tol
W—S_1—S_1	1.000	1.045	3.069	71.264	1.000	0.125	3.163	14.209	4	0	0.0

Table 321. SW potential parameters for single-layer 1T-WS_2 used by LAMMPS [9] as expressed in Eqs. (9) and (10).

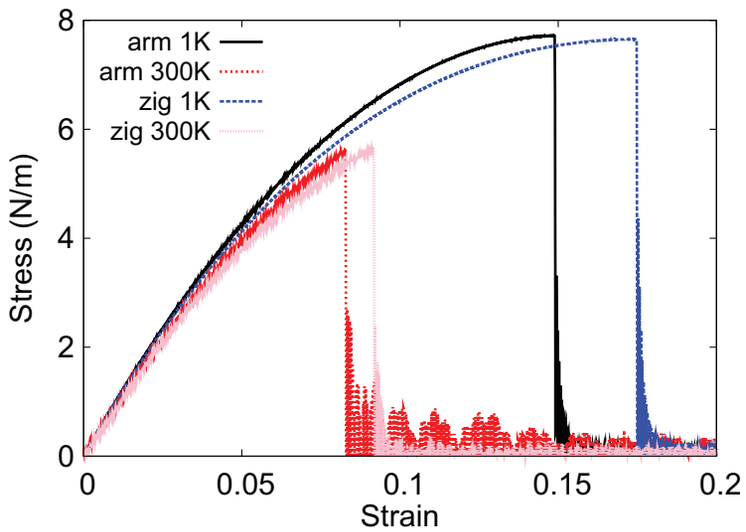

Figure 158. Stress-strain for single-layer 1T-WS_2 of dimension 100 × 100 Å along the armchair and zigzag directions.

thickness of the quasi-two-dimensional structure of the single-layer 1T-WS_2. The Young's modulus can be obtained by a linear fitting of the stress-strain relation in the small strain range of [0, 0.01]. The Young's modulus is 100.2 and 99.5 N/m along the armchair and zigzag directions, respectively. The Young's modulus is essentially isotropic in the armchair and zigzag directions. The Poisson's ratio from the VFF model and the SW potential is $\nu_{xy} = \nu_{yx} = -0.03$. The fitted Young's modulus value is about 10% smaller than the *ab initio* result of 113 N/m [48], as only short-range interactions are considered in the present work. The long-range interactions are ignored, which typically lead to about 10% underestimation for the value of the Young's modulus.

There is no available value for nonlinear quantities in the single-layer 1T-WS_2. We have thus used the nonlinear parameter $B = 0.5d^4$ in Eq. (5), which is close to the value of B in most materials. The value of the third-order nonlinear elasticity D can be extracted by fitting the stress-strain relation to the function $\sigma = E\epsilon + \frac{1}{2}D\epsilon^2$ with E as the Young's modulus. The values

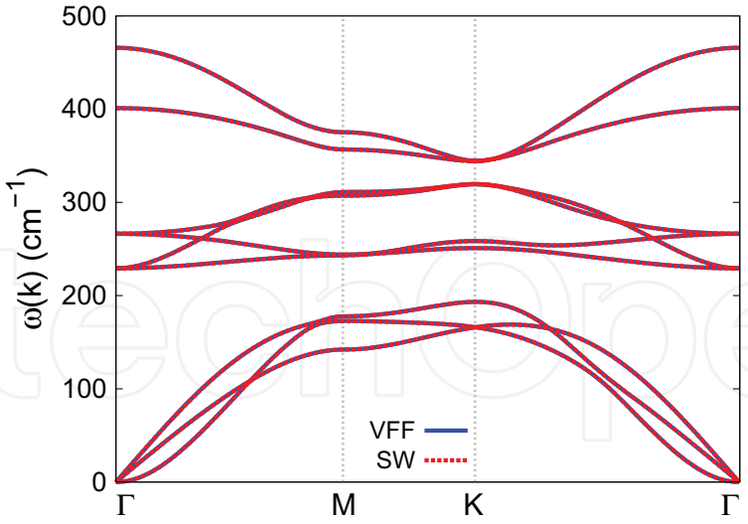

Figure 159. Phonon spectrum for single-layer 1T-WS_2 along the ΓMKΓ direction in the Brillouin zone. The phonon dispersion from the SW potential is exactly the same as that from the VFF model.

of D from the present SW potential are −666.6 and −660.6 N/m along the armchair and zigzag directions, respectively. The ultimate stress is about 7.7 N/m at the ultimate strain of 0.15 in the armchair direction at the low temperature of 1 K. The ultimate stress is about 7.7 N/m at the ultimate strain of 0.17 in the zigzag direction at the low temperature of 1 K.

Figure 159 shows that the VFF model and the SW potential give exactly the same phonon dispersion, as the SW potential is derived from the VFF model.

81. 1T-WSe_2

Most existing theoretical studies on the single-layer 1T-WSe_2 are based on the first-principles calculations. In this section, we will develop the SW potential for the single-layer 1T-WSe_2.

The structure for the single-layer 1T-WSe_2 is shown in **Figure 71** (with M=W and X=Se). Each W atom is surrounded by six Se atoms. These Se atoms are categorized into the top group (e.g., atoms 1, 3, and 5) and bottom group (e.g., atoms 2, 4, and 6). Each Se atom is connected to three W atoms. The structural parameters are from the first-principles calculations [48], including the lattice constant $a = 3.2574$ Å and the bond length $d_{W-Se} = 2.5207$ Å, which are derived from the angle $\theta_{SeWW} = 80.5^\circ$. The other angle is $\theta_{WSeSe} = 80.5^\circ$ with Se atoms from the same (top or bottom) group.

Table 322 shows three VFF terms for the single-layer 1T-WSe_2; one of which is the bond stretching interaction shown by Eq. (1), while the other two terms are the angle bending interaction shown by Eq. (2). We note that the angle bending term $K_{W-Se-Se}$ is for the angle $\theta_{W-Se-Se}$ with both Se atoms from the same (top or bottom) group. We find that there are actually only two parameters in the VFF model, so we can determine their value by fitting to the Young's modulus and the Poisson's ratio of the system. The *ab initio* calculations have

VFF type	Bond stretching	Angle bending	
Expression	$\frac{1}{2}K_{W-Se}(\Delta r)^2$	$\frac{1}{2}K_{W-Se-Se}(\Delta\theta)^2$	$\frac{1}{2}K_{Se-W-W}(\Delta\theta)^2$
Parameter	2.556	15.375	15.375
r_0 or θ_0	2.521	80.501	80.501

The second line gives an explicit expression for each VFF term. The third line is the force constant parameters. Parameters are in the unit of ev/Å^2 for the bond stretching interaction and in the unit of eV for the angle bending interaction. The fourth line gives the initial bond length (in the unit of Å) for the bond stretching interaction and the initial angle (in the unit of degrees) for the angle bending interaction. The angle θ_{ijk} has atom i as the apex.

Table 322. The VFF model for single-layer 1T-WSe_2.

predicted the Young's modulus to be 94 N/m and the Poisson's ratio as −0.15 [48]. The *ab initio* calculations have predicted a negative Poisson's ratio in the 1T-WSe_2, which was attributed to the orbital coupling in this material. The orbital coupling enhances the angle bending interaction in the VFF model. As a result, the value of the angle bending parameter is much larger than the bond stretching force constant parameter, which is typical in auxetic materials with negative Poisson's ratio [52].

The parameters for the two-body SW potential used by GULP are shown in **Table 323**. The parameters for the three-body SW potential used by GULP are shown in **Table 324**. Some representative parameters for the SW potential used by LAMMPS are listed in **Table 325**.

We use LAMMPS to perform MD simulations for the mechanical behavior of the single-layer 1T-WSe_2 under uniaxial tension at 1 and 300 K. **Figure 160** shows the stress-strain curve for the tension of a single-layer 1T-WSe_2 of dimension 100 × 100 Å. Periodic boundary conditions are applied in both armchair and zigzag directions. The single-layer 1T-WSe_2 is stretched

	A (eV)	ρ (Å)	B (Å^4)	r_{min} (Å)	r_{max} (Å)
W—Se	1.885	1.013	20.186	0.0	3.320

Table 323. Two-body SW potential parameters for single-layer 1T-WSe_2 used by GULP [8] as expressed in Eq. (3).

	K (eV)	θ_0 (°)	ρ_1 (Å)	ρ_2 (Å)	$r_{min\,12}$ (Å)	$r_{max\,12}$ (Å)	$r_{min\,13}$ (Å)	$r_{max\,13}$ (Å)	$r_{min\,23}$ (Å)	$r_{max\,23}$ (Å)
$\theta_{W-Se-Se}$	99.800	80.501	1.013	1.013	0.0	3.320	0.0	3.320	0.0	4.450
θ_{Se-W-W}	99.800	80.501	1.013	1.013	0.0	3.320	0.0	3.320	0.0	4.450

The angle θ_{ijk} in the first line indicates the bending energy for the angle with atom i as the apex.

Table 324. Three-body SW potential parameters for single-layer 1T-WSe_2 used by GULP [8] as expressed in Eq. (4).

	ϵ (eV)	σ (Å)	a	λ	γ	$\cos\theta_0$	A_L	B_L	p	q	Tol
W—Se_1—Se_1	1.000	1.013	3.277	99.800	1.000	0.165	1.885	19.156	4	0	0.0

Table 325. SW potential parameters for single-layer 1T-WSe_2 used by LAMMPS [9] as expressed in Eqs. (9) and (10).

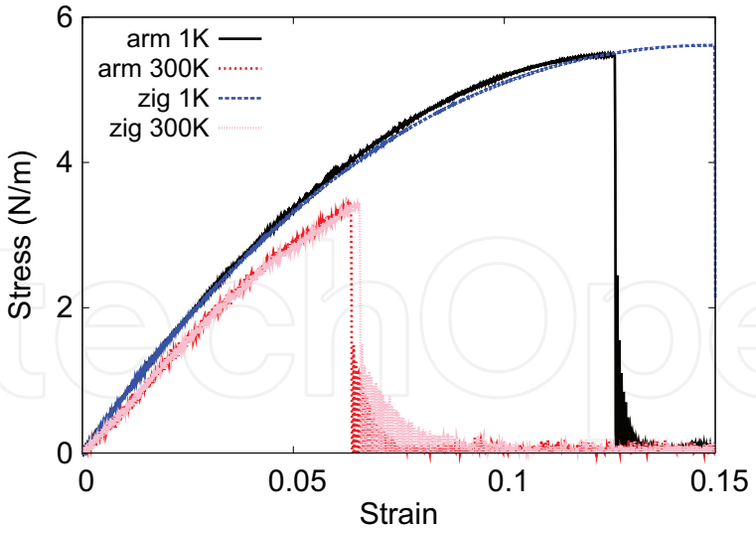

Figure 160. Stress-strain for single-layer 1T-WSe_2 of dimension 100 × 100 Å along the armchair and zigzag directions.

uniaxially along the armchair or zigzag direction. The stress is calculated without involving the actual thickness of the quasi-two-dimensional structure of the single-layer 1T-WSe_2. The Young's modulus can be obtained by a linear fitting of the stress-strain relation in the small strain range of [0, 0.01]. The Young's modulus is 80.5 and 80.3 N/m along the armchair and zigzag directions, respectively. The Young's modulus is essentially isotropic in the armchair and zigzag directions. The Poisson's ratio from the VFF model and the SW potential is $\nu_{xy} = \nu_{yx} = -0.15$. The fitted Young's modulus value is about 10% smaller than the *ab initio* result of 94 N/m [48], as only short-range interactions are considered in the present work. The long-range interactions are ignored, which typically lead to about 10% underestimation for the value of the Young's modulus.

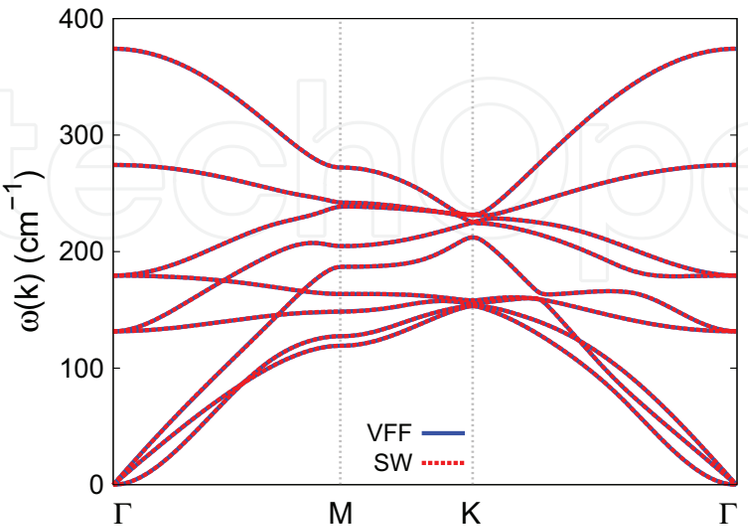

Figure 161. Phonon spectrum for single-layer 1T-WSe_2 along the ΓMKΓ direction in the Brillouin zone. The phonon dispersion from the SW potential is exactly the same as that from the VFF model.

There is no available value for nonlinear quantities in the single-layer 1T-WSe_2. We have thus used the nonlinear parameter $B = 0.5d^4$ in Eq. (5), which is close to the value of B in most materials. The value of the third-order nonlinear elasticity D can be extracted by fitting the stress-strain relation to the function $\sigma = E\epsilon + \frac{1}{2}D\epsilon^2$ with E as the Young's modulus. The values of D from the present SW potential are -666.1 and -580.1 N/m along the armchair and zigzag directions, respectively. The ultimate stress is about 5.5 N/m at the ultimate strain of 0.13 in the armchair direction at the low temperature of 1 K. The ultimate stress is about 5.6 N/m at the ultimate strain of 0.15 in the zigzag direction at the low temperature of 1 K.

Figure 161 shows that the VFF model and the SW potential give exactly the same phonon dispersion, as the SW potential is derived from the VFF model.

82. 1T-WTe_2

Most existing theoretical studies on the single-layer 1T-WTe_2 are based on the first-principles calculations. In this section, we will develop the SW potential for the single-layer 1T-WTe_2.

The structure for the single-layer 1T-WTe_2 is shown in **Figure 71** (with M=W and X=Te). Each W atom is surrounded by six Te atoms. These Te atoms are categorized into the top group (e.g., atoms 1, 3, and 5) and bottom group (e.g., atoms 2, 4, and 6). Each Te atom is connected to three W atoms. The structural parameters are from the first-principles calculations [48], including the lattice constant $a = 3.4970$ Å and the bond length $d_{\mathrm{W-Te}} = 2.7202$ Å, which are derived from the angle $\theta_{\mathrm{TeWW}} = 80.0^\circ$. The other angle is $\theta_{\mathrm{WTeTe}} = 80.0^\circ$ with Te atoms from the same (top or bottom) group.

Table 326 shows three VFF terms for the single-layer 1T-WTe_2; one of which is the bond stretching interaction shown by Eq. (1), while the other two terms are the angle bending interaction shown by Eq. (2). We note that the angle bending term $K_{\mathrm{W-Te-Te}}$ is for the angle $\theta_{\mathrm{W-Te-Te}}$ with both Te atoms from the same (top or bottom) group. We find that there are actually only two parameters in the VFF model, so we can determine their value by fitting to the Young's modulus and the Poisson's ratio of the system. The *ab initio* calculations have predicted the Young's modulus to be 88 N/m and the Poisson's ratio as -0.18 [48]. The *ab initio*

VFF type	Bond stretching	Angle bending	
Expression	$\frac{1}{2}K_{\mathrm{W-Te}}(\Delta r)^2$	$\frac{1}{2}K_{\mathrm{W-Te-Te}}(\Delta\theta)^2$	$\frac{1}{2}K_{\mathrm{Te-W-W}}(\Delta\theta)^2$
Parameter	2.272	19.437	19.437
r_0 or θ_0	2.720	79.999	79.999

The second line gives an explicit expression for each VFF term. The third line is the force constant parameters. Parameters are in the unit of ev/Å^2 for the bond stretching interaction and in the unit of eV for the angle bending interaction. The fourth line gives the initial bond length (in the unit of Å) for the bond stretching interaction and the initial angle (in the unit of degrees) for the angle bending interaction. The angle θ_{ijk} has atom i as the apex.

Table 326. The VFF model for single-layer 1T-WTe_2.

calculations have predicted a negative Poisson's ratio in the 1T-WTe_2, which was attributed to the orbital coupling in this material. The orbital coupling enhances the angle bending interaction in the VFF model. As a result, the value of the angle bending parameter is much larger than the bond stretching force constant parameter, which is typical in auxetic materials with negative Poisson's ratio [52].

The parameters for the two-body SW potential used by GULP are shown in **Table 327**. The parameters for the three-body SW potential used by GULP are shown in **Table 328**. Some representative parameters for the SW potential used by LAMMPS are listed in **Table 329**.

We use LAMMPS to perform MD simulations for the mechanical behavior of the single-layer 1T-WTe_2 under uniaxial tension at 1 and 300 K. **Figure 162** shows the stress-strain curve for the tension of a single-layer 1T-WTe_2 of dimension 100 × 100 Å. Periodic boundary conditions are applied in both armchair and zigzag directions. The single-layer 1T-WTe_2 is stretched uniaxially along the armchair or zigzag direction. The stress is calculated without involving the actual thickness of the quasi-two-dimensional structure of the single-layer 1T-WTe_2. The Young's modulus can be obtained by a linear fitting of the stress-strain relation in the small strain range of [0, 0.01]. The Young's modulus is 75.9 and 75.8 N/m along the armchair and zigzag directions, respectively. The Young's modulus is essentially isotropic in the armchair and zigzag directions. The Poisson's ratio from the VFF model and the SW potential is $\nu_{xy} = \nu_{yx} = -0.18$. The fitted Young's modulus value is about 10% smaller than the *ab initio* result of 88 N/m [48], as only short-range interactions are considered in the present work. The long-range interactions are ignored, which typically leads to about 10% underestimation for the value of the Young's modulus.

	A (eV)	ρ (Å)	B (Å^4)	r_{min} (Å)	r_{max} (Å)
W—Te	1.924	1.075	27.376	0.0	3.575

Table 327. Two-body SW potential parameters for single-layer 1T-WTe_2 used by GULP [8] as expressed in Eq. (3).

	K (eV)	θ_0 (°)	ρ_1 (Å)	ρ_2 (Å)	r_{min12} (Å)	r_{max12} (Å)	r_{min13} (Å)	r_{max13} (Å)	r_{min23} (Å)	r_{max23} (Å)
$\theta_{W-Te-Te}$	123.899	79.999	1.075	1.075	0.0	3.575	0.0	3.575	0.0	4.777
θ_{Te-W-W}	123.899	79.999	1.075	1.075	0.0	3.575	0.0	3.575	0.0	4.777

The angle θ_{ijk} in the first line indicates the bending energy for the angle with atom i as the apex.

Table 328. Three-body SW potential parameters for single-layer 1T-WTe_2 used by GULP [8] as expressed in Eq. (4).

	ϵ (eV)	σ (Å)	a	λ	γ	$\cos\theta_0$	A_L	B_L	p	q	Tol
W—Te_1—Te_1	1.000	1.075	3.325	123.899	1.000	0.174	1.924	20.483	4	0	0.0

Table 329. SW potential parameters for single-layer 1T-WTe_2 used by LAMMPS [9] as expressed in Eqs. (9) and (10).

http://dx.doi.org/10.5772/intechopen.71929

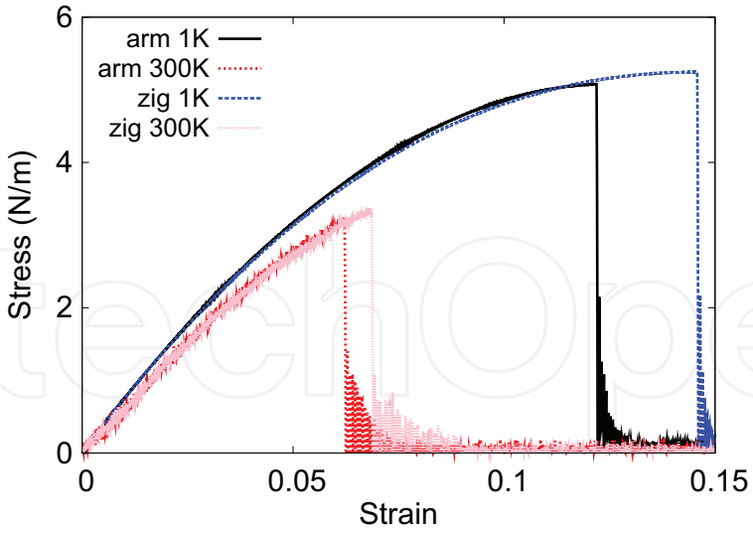

Figure 162. Stress-strain for single-layer 1T-WTe_2 of dimension 100 × 100 Å along the armchair and zigzag directions.

There is no available value for nonlinear quantities in the single-layer 1T-WTe_2. We have thus used the nonlinear parameter $B = 0.5d^4$ in Eq. (5), which is close to the value of B in most materials. The value of the third-order nonlinear elasticity D can be extracted by fitting the stress-strain relation to the function $\sigma = E\epsilon + \frac{1}{2}D\epsilon^2$ with E as the Young's modulus. The values of D from the present SW potential are −546.0 and −551.5 N/m along the armchair and zigzag directions, respectively. The ultimate stress is about 5.1 N/m at the ultimate strain of 0.12 in the armchair direction at the low temperature of 1 K. The ultimate stress is about 5.2 N/m at the ultimate strain of 0.14 in the zigzag direction at the low temperature of 1 K.

Figure 163 shows that the VFF model and the SW potential give exactly the same phonon dispersion, as the SW potential is derived from the VFF model.

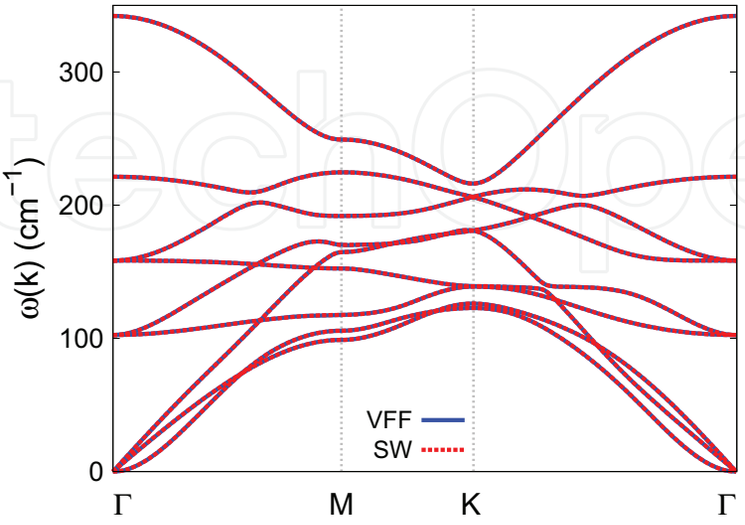

Figure 163. Phonon spectrum for single-layer 1T-WTe_2 along the ΓMKΓ direction in the Brillouin zone. The phonon dispersion from the SW potential is exactly the same as that from the VFF model.

83. 1T-ReS_2

Most existing theoretical studies on the single-layer 1T-ReS_2 are based on the first-principles calculations. In this section, we will develop the SW potential for the single-layer 1T-ReS_2.

The structure for the single-layer 1T-ReS_2 is shown in **Figure 71** (with M=Re and X=S). Each Re atom is surrounded by six S atoms. These S atoms are categorized into the top group (e.g., atoms 1, 3, and 5) and bottom group (e.g., atoms 2, 4, and 6). Each S atom is connected to three Re atoms. The structural parameters are from the first-principles calculations [48], including the lattice constant $a = 3.0750$ Å and the bond length $d_{\mathrm{Re-S}} = 2.4045$ Å, which are derived from the angle $\theta_{\mathrm{SReRe}} = 79.5^\circ$. The other angle is $\theta_{\mathrm{ReSS}} = 79.5^\circ$ with S atoms from the same (top or bottom) group.

Table 330 shows three VFF terms for the single-layer 1T-ReS_2; one of which is the bond stretching interaction shown by Eq. (1), while the other two terms are the angle bending interaction shown by Eq. (2). We note that the angle bending term $K_{\mathrm{Re-S-S}}$ is for the angle $\theta_{\mathrm{Re-S-S}}$ with both S atoms from the same (top or bottom) group. We find that there are actually only two parameters in the VFF model, so we can determine their value by fitting to the Young's modulus and the Poisson's ratio of the system. The *ab initio* calculations have predicted the Young's modulus to be 90 N/m and the Poisson's ratio as -0.11 [48]. The *ab initio* calculations have predicted a negative Poisson's ratio in the 1T-ReS_2, which was attributed to the orbital coupling in this material. The orbital coupling enhances the angle bending interaction in the VFF model. As a result, the value of the angle bending parameter is much larger than the bond stretching force constant parameter, which is typical in auxetic materials with negative Poisson's ratio [52].

The parameters for the two-body SW potential used by GULP are shown in **Table 331**. The parameters for the three-body SW potential used by GULP are shown in **Table 332**. Some representative parameters for the SW potential used by LAMMPS are listed in **Table 333**.

VFF type	**Bond stretching**	**Angle bending**	
Expression	$\frac{1}{2}K_{\mathrm{Re-S}}(\Delta r)^2$	$\frac{1}{2}K_{\mathrm{Re-S-S}}(\Delta\theta)^2$	$\frac{1}{2}K_{\mathrm{S-Re-Re}}(\Delta\theta)^2$
Parameter	2.684	10.829	10.829
r_0 or θ_0	2.405	79.498	79.498

The second line gives an explicit expression for each VFF term. The third line is the force constant parameters. Parameters are in the unit of ev/Å^2 for the bond stretching interaction and in the unit of eV for the angle bending interaction. The fourth line gives the initial bond length (in the unit of Å) for the bond stretching interaction and the initial angle (in the unit of degrees) for the angle bending interaction. The angle θ_{ijk} has atom i as the apex.

Table 330. The VFF model for single-layer 1T-ReS_2.

	A **(eV)**	ρ **(Å)**	B **(Å^4)**	r_{min} **(Å)**	r_{max} **(Å)**
Re—S	1.751	0.934	16.714	0.0	3.154

Table 331. Two-body SW potential parameters for single-layer 1T-ReS_2 used by GULP [8] as expressed in Eq. (3).

	K (eV)	θ_0 (°)	ρ_1 (Å)	ρ_2 (Å)	$r_{\min 12}$ (Å)	$r_{\max 12}$ (Å)	$r_{\min 13}$ (Å)	$r_{\max 13}$ (Å)	$r_{\min 23}$ (Å)	$r_{\max 23}$ (Å)
$\theta_{\text{Re}-\text{S}-\text{S}}$	67.797	79.498	0.934	0.934	0.0	3.154	0.0	3.154	0.0	4.201
$\theta_{\text{S}-\text{Re}-\text{Re}}$	67.797	79.498	0.934	0.934	0.0	3.154	0.0	3.154	0.0	4.201

The angle θ_{ijk} in the first line indicates the bending energy for the angle with atom i as the apex.

Table 332. Three-body SW potential parameters for single-layer 1T-ReS_2 used by GULP [8] as expressed in Eq. (4).

	ϵ (eV)	σ (Å)	a	λ	γ	$\cos\theta_0$	A_L	B_L	p	q	Tol
$\text{Re}—\text{S}_1—\text{S}_1$	1.000	0.934	3.375	67.797	1.000	0.182	1.751	21.916	4	0	0.0

Table 333. SW potential parameters for single-layer 1T-ReS_2 used by LAMMPS [9] as expressed in Eqs. (9) and (10).

We use LAMMPS to perform MD simulations for the mechanical behavior of the single-layer 1T-ReS_2 under uniaxial tension at 1 and 300 K. **Figure 164** shows the stress-strain curve for the tension of a single-layer 1T-ReS_2 of dimension 100 × 100 Å. Periodic boundary conditions are applied in both armchair and zigzag directions. The single-layer 1T-ReS_2 is stretched uniaxially along the armchair or zigzag direction. The stress is calculated without involving the actual thickness of the quasi-two-dimensional structure of the single-layer 1T-ReS_2. The Young's modulus can be obtained by a linear fitting of the stress-strain relation in the small strain range of [0, 0.01]. The Young's modulus is 78.1 and 77.8 N/m along the armchair and zigzag directions, respectively. The Young's modulus is essentially isotropic in the armchair and zigzag directions. The Poisson's ratio from the VFF model and the SW potential is $\nu_{xy} = \nu_{yx} = -0.11$. The fitted Young's modulus value is about 10% smaller than the *ab initio* result of 90 N/m [48], as only short-range interactions are considered in the present work. The long-range interactions are ignored, which typically leads to about 10% underestimation for the value of the Young's modulus.

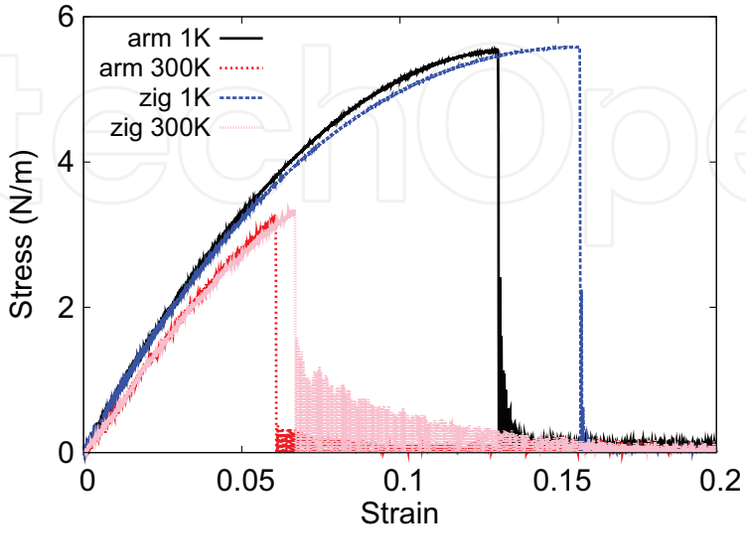

Figure 164. Stress-strain for single-layer 1T-ReS_2 of dimension 100 × 100 Å along the armchair and zigzag directions.

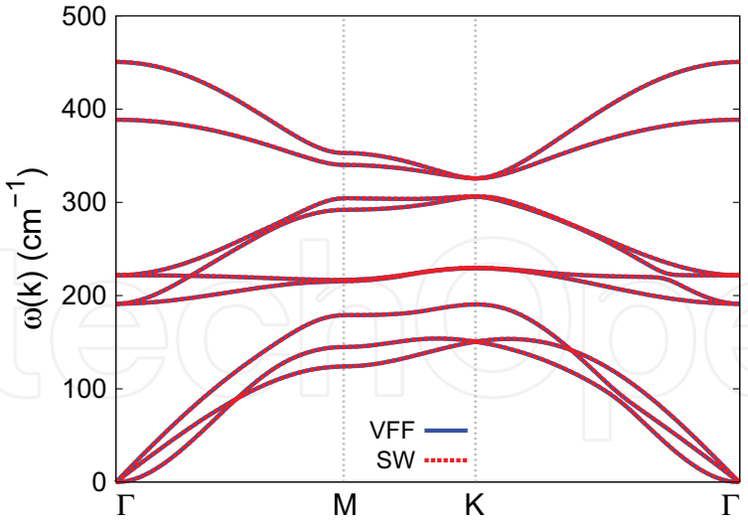

Figure 165. Phonon spectrum for single-layer 1T-ReS_2 along the ΓMKΓ direction in the Brillouin zone. The phonon dispersion from the SW potential is exactly the same as that from the VFF model.

There is no available value for nonlinear quantities in the single-layer 1T-ReS_2. We have thus used the nonlinear parameter $B = 0.5d^4$ in Eq. (5), which is close to the value of B in most materials. The value of the third-order nonlinear elasticity D can be extracted by fitting the stress-strain relation to the function $\sigma = E\epsilon + \frac{1}{2}D\epsilon^2$ with E as the Young's modulus. The values of D from the present SW potential are -537.1 and -550.7 N/m along the armchair and zigzag directions, respectively. The ultimate stress is about 5.5 N/m at the ultimate strain of 0.13 in the armchair direction at the low temperature of 1 K. The ultimate stress is about 5.6 N/m at the ultimate strain of 0.15 in the zigzag direction at the low temperature of 1 K.

Figure 165 shows that the VFF model and the SW potential give exactly the same phonon dispersion, as the SW potential is derived from the VFF model.

84. 1T-$ReSe_2$

Most existing theoretical studies on the single-layer 1T-$ReSe_2$ are based on the first-principles calculations. In this section, we will develop the SW potential for the single-layer 1T-$ReSe_2$.

The structure for the single-layer 1T-$ReSe_2$ is shown in **Figure 71** (with M=Re and X=Se). Each Re atom is surrounded by six Se atoms. These Se atoms are categorized into the top group (e.g., atoms 1, 3, and 5) and bottom group (e.g., atoms 2, 4, and 6). Each Se atom is connected to three Re atoms. The structural parameters are from the first-principles calculations [48], including the lattice constant $a = 3.1311$ Å and the bond length $d_{\text{Re}-\text{Se}} = 2.5149$ Å, which are derived from the angle $\theta_{\text{SeReRe}} = 77^\circ$. The other angle is $\theta_{\text{ReSeSe}} = 77^\circ$ with Se atoms from the same (top or bottom) group.

Table 334 shows three VFF terms for the single-layer 1T-$ReSe_2$; one of which is the bond stretching interaction shown by Eq. (1), while the other two terms are the angle bending

VFF type	Bond stretching	Angle bending	
Expression	$\frac{1}{2}K_{\mathrm{Re-Se}}(\Delta r)^2$	$\frac{1}{2}K_{\mathrm{Re-Se-Se}}(\Delta\theta)^2$	$\frac{1}{2}K_{\mathrm{Se-Re-Re}}(\Delta\theta)^2$
Parameter	4.313	12.674	12.674
r_0 or θ_0	2.515	76.999	76.999

The second line gives an explicit expression for each VFF term. The third line is the force constant parameters. Parameters are in the unit of ev/Å^2 for the bond stretching interaction and in the unit of eV for the angle bending interaction. The fourth line gives the initial bond length (in the unit of Å) for the bond stretching interaction and the initial angle (in the unit of degrees) for the angle bending interaction. The angle θ_{ijk} has atom i as the apex.

Table 334. The VFF model for single-layer 1T-$ReSe_2$.

interaction shown by Eq. (2). We note that the angle bending term $K_{\mathrm{Re-Se-Se}}$ is for the angle $\theta_{\mathrm{Re-Se-Se}}$ with both Se atoms from the same (top or bottom) group. We find that there are actually only two parameters in the VFF model, so we can determine their value by fitting to the Young's modulus and the Poisson's ratio of the system. The *ab initio* calculations have predicted the Young's modulus to be 123 N/m and the Poisson's ratio as −0.03 [48]. The *ab initio* calculations have predicted a negative Poisson's ratio in the 1T-$ReSe_2$, which was attributed to the orbital coupling in this material. The orbital coupling enhances the angle bending interaction in the VFF model. As a result, the value of the angle bending parameter is much larger than the bond stretching force constant parameter, which is typical in auxetic materials with negative Poisson's ratio [52].

The parameters for the two-body SW potential used by GULP are shown in **Table 335**. The parameters for the three-body SW potential used by GULP are shown in **Table 336**. Some representative parameters for the SW potential used by LAMMPS are listed in **Table 337**.

	A (eV)	ρ (Å)	B (Å^4)	r_{min} (Å)	r_{max} (Å)
Re—Se	2.866	0.896	20.001	0.0	3.265

Table 335. Two-body SW potential parameters for single-layer 1T-$ReSe_2$ used by GULP [8] as expressed in Eq. (3).

	K (eV)	θ_0 (°)	ρ_1 (Å)	ρ_2 (Å)	$r_{\mathrm{min\,12}}$ (Å)	$r_{\mathrm{max\,12}}$ (Å)	$r_{\mathrm{min\,13}}$ (Å)	$r_{\mathrm{max\,13}}$ (Å)	$r_{\mathrm{min\,23}}$ (Å)	$r_{\mathrm{max\,23}}$ (Å)
$\theta_{\mathrm{Re-Se-Se}}$	72.666	76.999	0.896	0.896	0.0	3.265	0.0	3.265	0.0	4.277
$\theta_{\mathrm{Se-Re-Re}}$	72.666	76.999	0.896	0.896	0.0	3.265	0.0	3.265	0.0	4.277

The angle θ_{ijk} in the first line indicates the bending energy for the angle with atom i as the apex.

Table 336. Three-body SW potential parameters for single-layer 1T-$ReSe_2$ used by GULP [8] as expressed in Eq. (4).

	ϵ (eV)	σ (Å)	a	λ	γ	$\cos\theta_0$	A_L	B_L	p	q	Tol
Re—Se_1—Se_1	1.000	0.896	3.645	72.666	1.000	0.225	2.866	31.036	4	0	0.0

Table 337. SW potential parameters for single-layer 1T-$ReSe_2$ used by LAMMPS [9] as expressed in Eqs. (9) and (10).

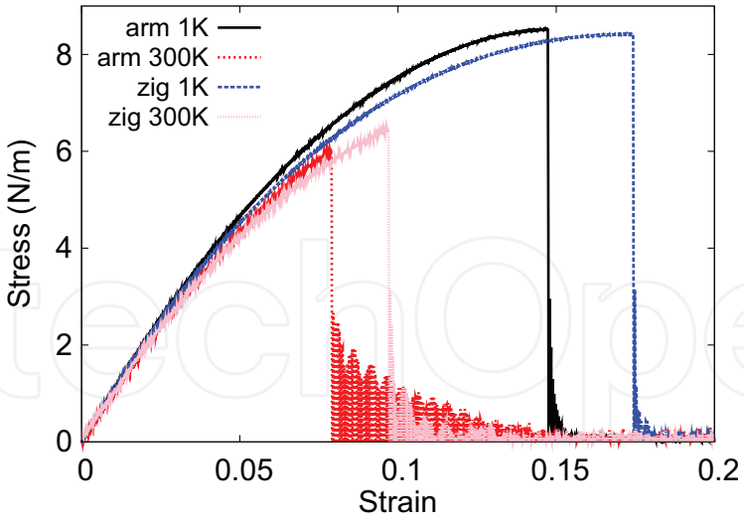

Figure 166. Stress-strain for single-layer 1T-$ReSe_2$ of dimension 100 × 100 Å along the armchair and zigzag directions.

We use LAMMPS to perform MD simulations for the mechanical behavior of the single-layer 1T-$ReSe_2$ under uniaxial tension at 1 and 300 K. **Figure 166** shows the stress-strain curve for the tension of a single-layer 1T-$ReSe_2$ of dimension 100 × 100 Å. Periodic boundary conditions are applied in both armchair and zigzag directions. The single-layer 1T-$ReSe_2$ is stretched uniaxially along the armchair or zigzag direction. The stress is calculated without involving the actual thickness of the quasi-two-dimensional structure of the single-layer 1T-$ReSe_2$. The Young's modulus can be obtained by a linear fitting of the stress-strain relation in the small strain range of [0, 0.01]. The Young's modulus is 108.2 and 107.7 N/m along the armchair and zigzag directions, respectively. The Young's modulus is essentially isotropic in the armchair and zigzag directions. The Poisson's ratio from the VFF model and the SW potential is $\nu_{xy} = \nu_{yx} = -0.03$. The fitted Young's modulus value is about 10% smaller than the *ab initio* result of 123 N/m [48], as only short-range interactions are considered in the present work. The long-range interactions are ignored, which typically lead to about 10% underestimation for the value of the Young's modulus.

There is no available value for nonlinear quantities in the single-layer 1T-$ReSe_2$. We have thus used the nonlinear parameter $B = 0.5d^4$ in Eq. (5), which is close to the value of B in most materials. The value of the third-order nonlinear elasticity D can be extracted by fitting the stress-strain relation to the function $\sigma = E\epsilon + \frac{1}{2}D\epsilon^2$ with E as the Young's modulus. The values of D from the present SW potential are −669.3 and −699.9 N/m along the armchair and zigzag directions, respectively. The ultimate stress is about 8.5 N/m at the ultimate strain of 0.14 in the armchair direction at the low temperature of 1 K. The ultimate stress is about 8.4 N/m at the ultimate strain of 0.17 in the zigzag direction at the low temperature of 1 K.

Figure 167 shows that the VFF model and the SW potential give exactly the same phonon dispersion, as the SW potential is derived from the VFF model.

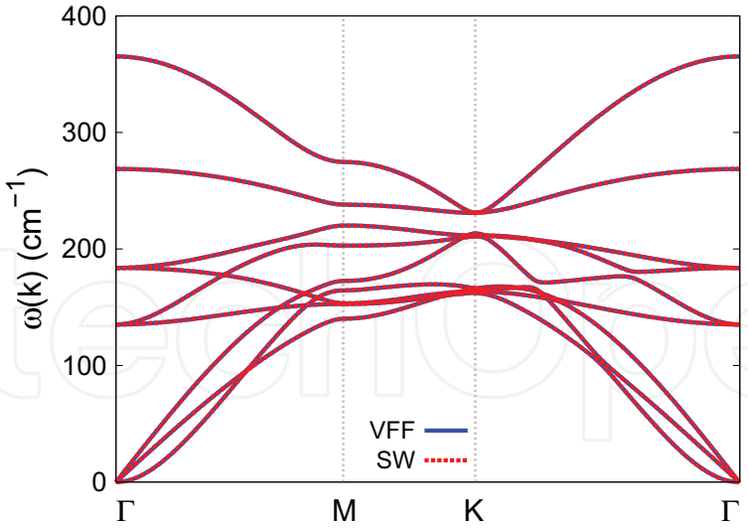

Figure 167. Phonon spectrum for single-layer 1T-$ReSe_2$ along the ΓMKΓ direction in the Brillouin zone. The phonon dispersion from the SW potential is exactly the same as that from the VFF model.

85. 1T-$ReTe_2$

Most existing theoretical studies on the single-layer 1T-$ReTe_2$ are based on the first-principles calculations. In this section, we will develop the SW potential for the single-layer 1T-$ReTe_2$.

The structure for the single-layer 1T-$ReTe_2$ is shown in **Figure 71** (with M=Re and X=Te). Each Re atom is surrounded by six Te atoms. These Te atoms are categorized into the top group (e.g., atoms 1, 3, and 5) and bottom group (e.g., atoms 2, 4, and 6). Each Te atom is connected to three Re atoms. The structural parameters are from the first-principles calculations [48], including the lattice constant $a = 3.3834$ Å and the bond length $d_{\mathrm{Re-Te}} = 2.7027$ Å, which are derived from the angle $\theta_{\mathrm{TeReRe}} = 77.5^\circ$. The other angle is $\theta_{\mathrm{ReTeTe}} = 77.5^\circ$ with Te atoms from the same (top or bottom) group.

Table 338 shows three VFF terms for the single-layer 1T-$ReTe_2$; one of which is the bond stretching interaction shown by Eq. (1), while the other two terms are the angle bending

VFF type	Bond stretching	Angle bending	
Expression	$\frac{1}{2}K_{\mathrm{Re-Te}}(\Delta r)^2$	$\frac{1}{2}K_{\mathrm{Re-Te-Te}}(\Delta\theta)^2$	$\frac{1}{2}K_{\mathrm{Te-Re-Re}}(\Delta\theta)^2$
Parameter	1.724	14.812	14.812
r_0 or θ_0	2.703	77.501	77.501

The second line gives an explicit expression for each VFF term. The third line is the force constant parameters. Parameters are in the unit of ev/Å^2 for the bond stretching interaction and in the unit of eV for the angle bending interaction. The fourth line gives the initial bond length (in the unit of Å) for the bond stretching interaction and the initial angle (in the unit of degrees) for the angle bending interaction. The angle θ_{ijk} has atom i as the apex.

Table 338. The VFF model for single-layer 1T-$ReTe_2$.

interaction shown by Eq. (2). We note that the angle bending term $K_{\mathrm{Re-Te-Te}}$ is for the angle $\theta_{\mathrm{Re-Te-Te}}$ with both Te atoms from the same (top or bottom) group. We find that there are actually only two parameters in the VFF model, so we can determine their value by fitting to the Young's modulus and the Poisson's ratio of the system. The *ab initio* calculations have predicted the Young's modulus to be 71 N/m and the Poisson's ratio as −0.22 [48]. The *ab initio* calculations have predicted a negative Poisson's ratio in the 1T-$ReTe_2$, which was attributed to the orbital coupling in this material. The orbital coupling enhances the angle bending interaction in the VFF model. As a result, the value of the angle bending parameter is much larger than the bond stretching force constant parameter, which is typical in auxetic materials with negative Poisson's ratio [52].

The parameters for the two-body SW potential used by GULP are shown in **Table 339**. The parameters for the three-body SW potential used by GULP are shown in **Table 340**. Some representative parameters for the SW potential used by LAMMPS are listed in **Table 341**.

We use LAMMPS to perform MD simulations for the mechanical behavior of the single-layer 1T-$ReTe_2$ under uniaxial tension at 1 and 300 K. **Figure 168** shows the stress-strain curve for the tension of a single-layer 1T-$ReTe_2$ of dimension 100 × 100 Å. Periodic boundary conditions are applied in both armchair and zigzag directions. The single-layer 1T-$ReTe_2$ is stretched uniaxially along the armchair or zigzag direction. The stress is calculated without involving the actual thickness of the quasi-two-dimensional structure of the single-layer 1T-$ReTe_2$. The Young's modulus can be obtained by a linear fitting of the stress-strain relation in the small strain range of [0, 0.01]. The Young's modulus is 59.4 and 59.3 N/m along the armchair and zigzag directions, respectively. The Young's modulus is essentially isotropic in the armchair and zigzag directions. The Poisson's ratio from the VFF model and the SW potential is $\nu_{xy} = \nu_{yx} = -0.17$. The fitted Young's modulus value is about 10% smaller than the *ab initio*

	A (eV)	ρ (Å)	B (Å^4)	r_{min} (Å)	r_{max} (Å)
Re—Te	1.343	0.980	26.678	0.0	3.517

Table 339. Two-body SW potential parameters for single-layer 1T-$ReTe_2$ used by GULP [8] as expressed in Eq. (3).

	K (eV)	θ_0 (°)	ρ_1 (Å)	ρ_2 (Å)	$r_{\mathrm{min}\,12}$ (Å)	$r_{\mathrm{max}\,12}$ (Å)	$r_{\mathrm{min}\,13}$ (Å)	$r_{\mathrm{max}\,13}$ (Å)	$r_{\mathrm{min}\,23}$ (Å)	$r_{\mathrm{max}\,23}$ (Å)
$\theta_{\mathrm{Re-Te-Te}}$	86.424	77.501	0.980	0.980	0.0	3.517	0.0	3.517	0.0	4.622
$\theta_{\mathrm{Te-Re-Re}}$	86.424	77.501	0.980	0.980	0.0	3.517	0.0	3.517	0.0	4.622

The angle θ_{ijk} in the first line indicates the bending energy for the angle with atom i as the apex.

Table 340. Three-body SW potential parameters for single-layer 1T-$ReTe_2$ used by GULP [8] as expressed in Eq. (4).

	ϵ (eV)	σ (Å)	a	λ	γ	$\cos\theta_0$	A_L	B_L	p	q	Tol
Re—Te_1—Te_1	1.000	0.980	3.587	86.424	1.000	0.216	1.343	28.891	4	0	0.0

Table 341. SW potential parameters for single-layer 1T-$ReTe_2$ used by LAMMPS [9] as expressed in Eqs. (9) and (10).

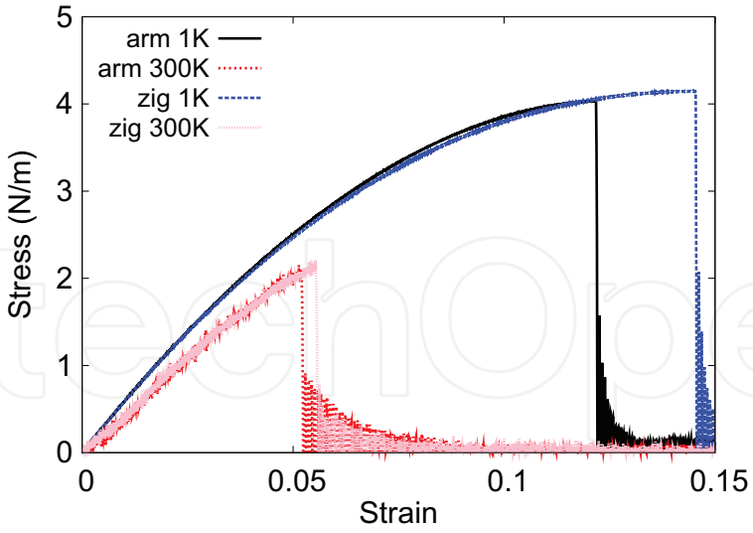

Figure 168. Stress-strain for single-layer 1T-$ReTe_2$ of dimension 100 × 100 Å along the armchair and zigzag directions.

result of 71 N/m [48], as only short-range interactions are considered in the present work. The long-range interactions are ignored, which typically lead to about 10% underestimation for the value of the Young's modulus.

There is no available value for nonlinear quantities in the single-layer 1T-$ReTe_2$. We have thus used the nonlinear parameter $B = 0.5d^4$ in Eq. (5), which is close to the value of B in most materials. The value of the third-order nonlinear elasticity D can be extracted by fitting the stress-strain relation to the function $\sigma = E\epsilon + \frac{1}{2}D\epsilon^2$ with E as the Young's modulus. The values of D from the present SW potential are −416.1 and −425.1 N/m along the armchair and zigzag directions, respectively. The ultimate stress is about 4.0 N/m at the ultimate strain of 0.12 in the

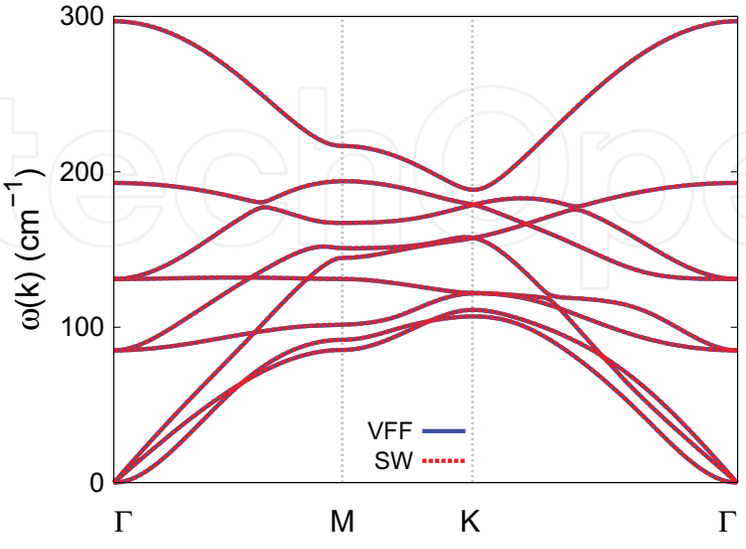

Figure 169. Phonon spectrum for single-layer 1T-$ReTe_2$ along the ΓMKΓ direction in the Brillouin zone. The phonon dispersion from the SW potential is exactly the same as that from the VFF model.

armchair direction at the low temperature of 1 K. The ultimate stress is about 4.1 N/m at the ultimate strain of 0.14 in the zigzag direction at the low temperature of 1 K.

Figure 169 shows that the VFF model and the SW potential give exactly the same phonon dispersion, as the SW potential is derived from the VFF model.

86. 1T-$IrTe_2$

Most existing theoretical studies on the single-layer 1T-$IrTe_2$ are based on the first-principles calculations. In this section, we will develop the SW potential for the single-layer 1T-$IrTe_2$.

The structure for the single-layer 1T-$IrTe_2$ is shown in **Figure 71** (with M = Ir and X = Te). Each Ir atom is surrounded by six Te atoms. These Te atoms are categorized into the top group (e.g., atoms 1, 3, and 5) and bottom group (e.g., atoms 2, 4, and 6). Each Te atom is connected to three Ir atoms. The structural parameters are from the first-principles calculations [48], including the lattice constant $a = 3.8431$ Å and the bond length $d_{\mathrm{Ir-Te}} = 2.6490$ Å, which are derived from the angle $\theta_{\mathrm{TeIrIr}} = 93^\circ$. The other angle is $\theta_{\mathrm{IrTeTe}} = 93^\circ$ with Te atoms from the same (top or bottom) group.

Table 342 shows three VFF terms for the single-layer 1T-$IrTe_2$; one of which is the bond stretching interaction shown by Eq. (1), while the other two terms are the angle bending interaction shown by Eq. (2). We note that the angle bending term $K_{\mathrm{Ir-Te-Te}}$ is for the angle $\theta_{\mathrm{Ir-Te-Te}}$ with both Te atoms from the same (top or bottom) group. We find that there are actually only two parameters in the VFF model, so we can determine their value by fitting to the Young's modulus and the Poisson's ratio of the system. The *ab initio* calculations have predicted the Young's modulus to be 45 N/m and the Poisson's ratio as 0.22 [48].

The parameters for the two-body SW potential used by GULP are shown in **Table 343**. The parameters for the three-body SW potential used by GULP are shown in **Table 344**. Some representative parameters for the SW potential used by LAMMPS are listed in **Table 345**.

We use LAMMPS to perform MD simulations for the mechanical behavior of the single-layer 1T-$IrTe_2$ under uniaxial tension at 1 and 300 K. **Figure 170** shows the stress-strain curve for the tension of a single-layer 1T-$IrTe_2$ of dimension 100×100 Å. Periodic boundary conditions are

VFF type	Bond stretching	Angle bending	
Expression	$\frac{1}{2}K_{\mathrm{Ir-Te}}(\Delta r)^2$	$\frac{1}{2}K_{\mathrm{Ir-Te-Te}}(\Delta\theta)^2$	$\frac{1}{2}K_{\mathrm{Te-Ir-Ir}}(\Delta\theta)^2$
Parameter	5.334	2.182	2.182
r_0 or θ_0	2.649	93.002	93.002

The second line gives an explicit expression for each VFF term. The third line is the force constant parameters. Parameters are in the unit of eV/Å^2 for the bond stretching interaction and in the unit of eV for the angle bending interaction. The fourth line gives the initial bond length (in the unit of Å) for the bond stretching interaction and the initial angle (in the unit of degrees) for the angle bending interaction. The angle θ_{ijk} has atom i as the apex.

Table 342. The VFF model for single-layer 1T-$IrTe_2$.

	A (eV)	ρ (Å)	B (Å^4)	$r_{\min}$ (Å)	$r_{\max}$ (Å)
Ir—Te	6.030	1.538	24.621	0.0	3.658

Table 343. Two-body SW potential parameters for single-layer 1T-$IrTe_2$ used by GULP [8] as expressed in Eq. (3).

	K (eV)	θ_0 (°)	ρ_1 (Å)	ρ_2 (Å)	$r_{\min 12}$ (Å)	$r_{\max 12}$ (Å)	$r_{\min 13}$ (Å)	$r_{\max 13}$ (Å)	$r_{\min 23}$ (Å)	$r_{\max 23}$ (Å)
$\theta_{\text{Ir–Te–Te}}$	23.056	93.002	1.538	1.538	0.0	3.658	0.0	3.658	0.0	5.250
$\theta_{\text{Te–Ir–Ir}}$	23.056	93.002	1.538	1.538	0.0	3.658	0.0	3.658	0.0	5.250

The angle θ_{ijk} in the first line indicates the bending energy for the angle with atom i as the apex.

Table 344. Three-body SW potential parameters for single-layer 1T-$IrTe_2$ used by GULP [8] as expressed in Eq. (4).

	ϵ (eV)	σ (Å)	a	λ	γ	$\cos\theta_0$	A_L	B_L	p	q	Tol
Ir—Te_1—Te_1	1.000	1.538	2.370	23.056	1.000	−0.052	6.030	4.398	4	0	0.0

Table 345. SW potential parameters for single-layer 1T-$IrTe_2$ used by LAMMPS [9] as expressed in Eqs. (9) and (10).

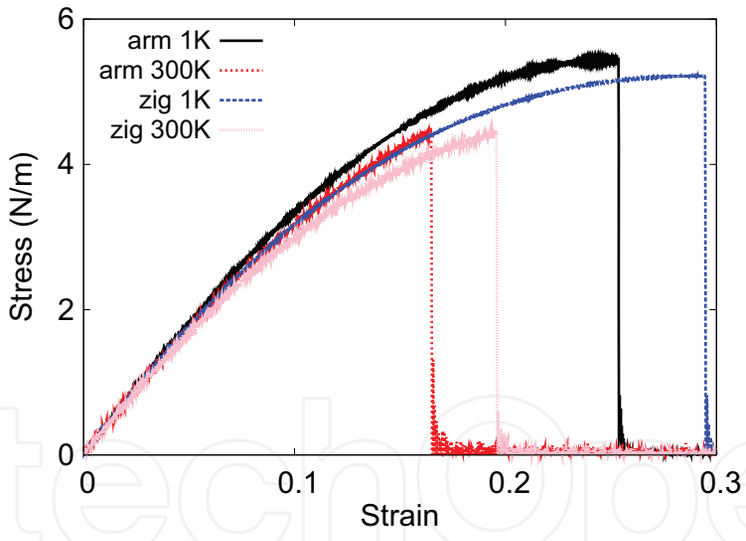

Figure 170. Stress-strain for single-layer 1T-$IrTe_2$ of dimension 100×100 Å along the armchair and zigzag directions.

applied in both armchair and zigzag directions. The single-layer 1T-$IrTe_2$ is stretched uniaxially along the armchair or zigzag direction. The stress is calculated without involving the actual thickness of the quasi-two-dimensional structure of the single-layer 1T-$IrTe_2$. The Young's modulus can be obtained by a linear fitting of the stress-strain relation in the small strain range of [0, 0.01]. The Young's modulus is 38.6 and 38.4 N/m along the armchair and zigzag directions, respectively. The Young's modulus is essentially isotropic in the armchair and zigzag directions. The Poisson's ratio from the VFF model and the SW potential is $\nu_{xy} = \nu_{yx} = 0.20$. The fitted Young's modulus value is about 10% smaller than the *ab initio* result

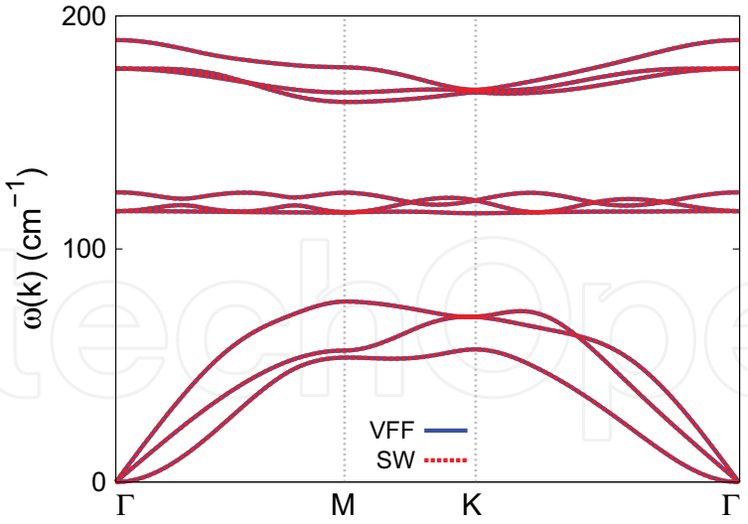

Figure 171. Phonon spectrum for single-layer 1T-$IrTe_2$ along the ΓMKΓ direction in the Brillouin zone. The phonon dispersion from the SW potential is exactly the same as that from the VFF model.

of 45 N/m [48], as only short-range interactions are considered in the present work. The long-range interactions are ignored, which typically leads to about 10% underestimation for the value of the Young's modulus.

There is no available value for nonlinear quantities in the single-layer 1T-$IrTe_2$. We have thus used the nonlinear parameter $B = 0.5d^4$ in Eq. (5), which is close to the value of B in most materials. The value of the third-order nonlinear elasticity D can be extracted by fitting the stress-strain relation to the function $\sigma = E\epsilon + \frac{1}{2}D\epsilon^2$ with E as the Young's modulus. The values of D from the present SW potential are -127.7 and -142 N/m along the armchair and zigzag directions, respectively. The ultimate stress is about 5.4 N/m at the ultimate strain of 0.25 in the armchair direction at the low temperature of 1 K. The ultimate stress is about 5.2 N/m at the ultimate strain of 0.29 in the zigzag direction at the low temperature of 1 K.

Figure 171 shows that the VFF model and the SW potential give exactly the same phonon dispersion, as the SW potential is derived from the VFF model.

87. 1T-PtS_2

Most existing theoretical studies on the single-layer 1T-PtS_2 are based on the first-principles calculations. In this section, we will develop the SW potential for the single-layer 1T-PtS_2.

The structure for the single-layer 1T-PtS_2 is shown in **Figure 71** (with M = Pt and X = S). Each Pt atom is surrounded by six S atoms. These S atoms are categorized into the top group (e.g., atoms 1, 3, and 5) and bottom group (e.g., atoms 2, 4, and 6). Each S atom is connected to three Pt atoms. The structural parameters are from the first-principles calculations [48], including the lattice constant $a = 3.5237$ Å and the bond length $d_{\mathrm{Pt-S}} = 2.3708$ Å, which are derived from the angle $\theta_{\mathrm{SPtPt}} = 96^\circ$. The other angle is $\theta_{\mathrm{PtSS}} = 96^\circ$ with S atoms from the same (top or bottom) group.

VFF type	Bond stretching	Angle bending	
Expression	$\frac{1}{2}K_{\mathrm{Pt-S}}(\Delta r)^2$	$\frac{1}{2}K_{\mathrm{Pt-S-S}}(\Delta\theta)^2$	$\frac{1}{2}K_{\mathrm{S-Pt-Pt}}(\Delta\theta)^2$
Parameter	12.128	4.975	4.975
r_0 or θ_0	2.371	96.00	96.00

The second line gives an explicit expression for each VFF term. The third line is the force constant parameters. Parameters are in the unit of eV/Å^2 for the bond stretching interaction and in the unit of eV for the angle bending interaction. The fourth line gives the initial bond length (in the unit of Å) for the bond stretching interaction and the initial angle (in the unit of degrees) for the angle bending interaction. The angle θ_{ijk} has atom i as the apex.

Table 346. The VFF model for single-layer 1T-PtS_2.

Table 346 shows three VFF terms for the single-layer 1T-PtS_2; one of which is the bond stretching interaction shown by Eq. (1), while the other two terms are the angle bending interaction shown by Eq. (2). We note that the angle bending term $K_{\mathrm{Pt-S-S}}$ is for the angle $\theta_{\mathrm{Pt-S-S}}$ with both S atoms from the same (top or bottom) group. These force constant parameters are determined by fitting to the three acoustic branches in the phonon dispersion along the ΓM as shown in **Figure 172(a)**. The *ab initio* calculations for the phonon dispersion are from [34]. The lowest acoustic branch (flexural mode) is almost linear in the *ab initio*

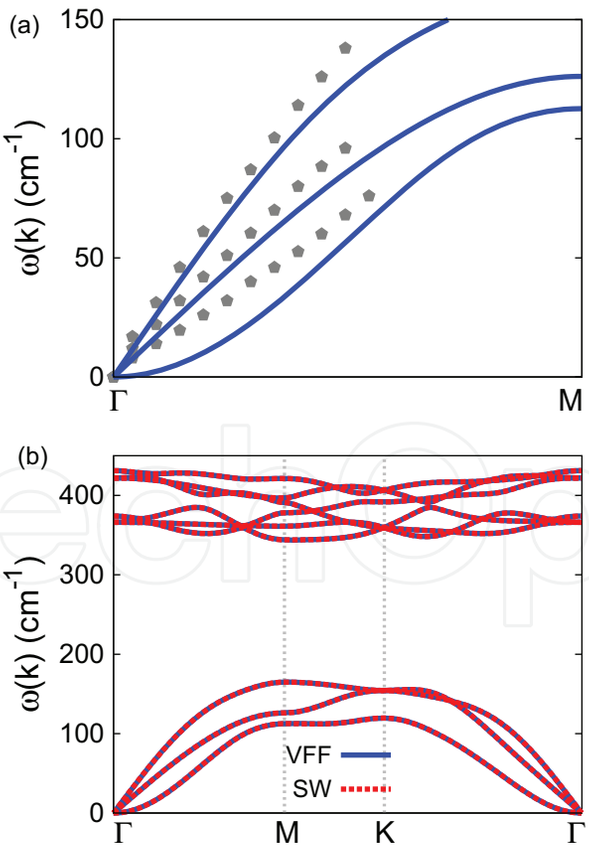

Figure 172. Phonon spectrum for single-layer 1T-PtS_2. (a) Phonon dispersion along the ΓM direction in the Brillouin zone. The results from the VFF model (lines) are comparable with the *ab initio* results (pentagons) from [34]. (b) The phonon dispersion from the SW potential is exactly the same as that from the VFF model.

calculations, which may be due to the violation of the rigid rotational invariance [20]. **Figure 172(b)** shows that the VFF model and the SW potential give exactly the same phonon dispersion, as the SW potential is derived from the VFF model.

The parameters for the two-body SW potential used by GULP are shown in **Table 347**. The parameters for the three-body SW potential used by GULP are shown in **Table 348**. Some representative parameters for the SW potential used by LAMMPS are listed in **Table 349**.

We use LAMMPS to perform MD simulations for the mechanical behavior of the single-layer 1T-PtS_2 under uniaxial tension at 1 and 300 K. **Figure 173** shows the stress-strain curve for the tension of a single-layer 1T-PtS_2 of dimension 100×100 Å. Periodic boundary conditions are applied in both armchair and zigzag directions. The single-layer 1T-PtS_2 is stretched uniaxially along the armchair or zigzag direction. The stress is calculated without involving the actual thickness of the quasi-two-dimensional structure of the single-layer 1T-PtS_2. The Young's modulus can be obtained by a linear fitting of the stress-strain relation in the small strain range of [0, 0.01]. The Young's modulus is 105.9 and 105.4 N/m along the armchair and zigzag directions, respectively. The Young's modulus is essentially isotropic in the armchair and zigzag directions. The Poisson's ratio from the VFF model and the SW potential is $\nu_{xy} = \nu_{yx} = 0.16$.

There is no available value for nonlinear quantities in the single-layer 1T-PtS_2. We have thus used the nonlinear parameter $B = 0.5d^4$ in Eq. (5), which is close to the value of B in most materials. The value of the third-order nonlinear elasticity D can be extracted by fitting the stress-strain relation to the function $\sigma = E\epsilon + \frac{1}{2}D\epsilon^2$ with E as the Young's modulus. The values of D from the present SW potential are -420.6 and -457.1 N/m along the armchair and zigzag directions, respectively. The ultimate stress is about 12.8 N/m at the ultimate strain of 0.22 in

	A (eV)	ρ (Å)	B (Å^4)	$r_{\min}$ (Å)	$r_{\max}$ (Å)
Pt—S	11.806	1.485	15.796	0.0	3.309

Table 347. Two-body SW potential parameters for single-layer 1T-PtS_2 used by GULP [8] as expressed in Eq. (3).

	K (eV)	θ_0 (°)	ρ_1 (Å)	ρ_2 (Å)	$r_{\min 12}$ (Å)	$r_{\max 12}$ (Å)	$r_{\min 13}$ (Å)	$r_{\max 13}$ (Å)	$r_{\min 23}$ (Å)	$r_{\max 23}$ (Å)
$\theta_{\text{Pt–S–S}}$	59.607	96.00	1.485	1.485	0.0	3.309	0.0	3.309	0.0	4.813
$\theta_{\text{S–Pt–Pt}}$	59.607	96.00	1.485	1.485	0.0	3.309	0.0	3.309	0.0	4.813

The angle θ_{ijk} in the first line indicates the bending energy for the angle with atom i as the apex.

Table 348. Three-body SW potential parameters for single-layer 1T-PtS_2 used by GULP [8] as expressed in Eq. (4).

	ϵ (eV)	σ (Å)	a	λ	γ	$\cos\theta_0$	A_L	B_L	p	q	Tol
Pt—S_1—S_1	1.000	1.485	2.229	59.607	1.000	−0.105	11.806	3.250	4	0	0.0

Table 349. SW potential parameters for single-layer 1T-PtS_2 used by LAMMPS [9] as expressed in Eqs. (9) and (10).

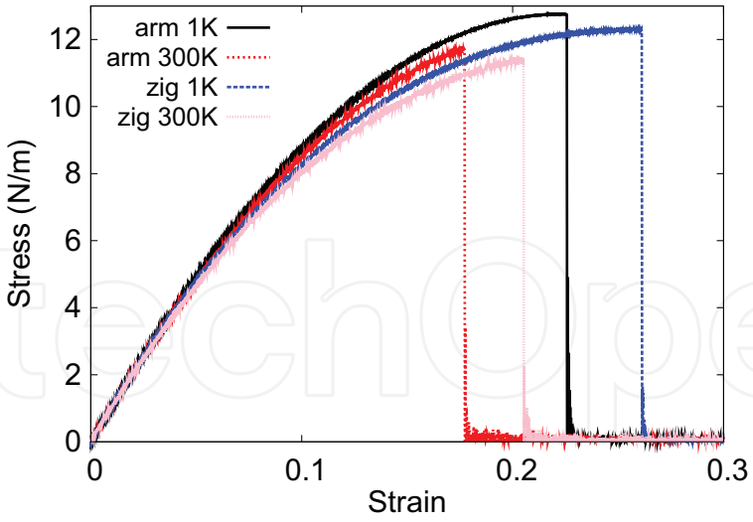

Figure 173. Stress-strain for single-layer 1T-PtS_2 of dimension 100×100 Å along the armchair and zigzag directions.

the armchair direction at the low temperature of 1 K. The ultimate stress is about 12.3 N/m at the ultimate strain of 0.26 in the zigzag direction at the low temperature of 1 K.

88. 1T-$PtSe_2$

Most existing theoretical studies on the single-layer 1T-$PtSe_2$ are based on the first-principles calculations. In this section, we will develop the SW potential for the single-layer 1T-$PtSe_2$.

The structure for the single-layer 1T-$PtSe_2$ is shown in **Figure 71** (with M = Pt and X = Se). Each Pt atom is surrounded by six Se atoms. These Se atoms are categorized into the top group (e.g., atoms 1, 3, and 5) and bottom group (e.g., atoms 2, 4, and 6). Each Se atom is connected to three Pt atoms. The structural parameters are from the first-principles calculations [48], including the lattice constant $a = 3.6662$ Å and the bond length $d_{\mathrm{Pt-Se}} = 2.4667$ Å, which are derived from the angle $\theta_{\mathrm{SePtPt}} = 96^\circ$. The other angle is $\theta_{\mathrm{PtSeSe}} = 96^\circ$ with Se atoms from the same (top or bottom) group.

Table 350 shows three VFF terms for the single-layer 1T-$PtSe_2$; one of which is the bond stretching interaction shown by Eq. (1), while the other two terms are the angle bending

VFF type	Bond stretching	Angle bending	
Expression	$\frac{1}{2}K_{\mathrm{Pt-Se}}(\Delta r)^2$	$\frac{1}{2}K_{\mathrm{Pt-Se-Se}}(\Delta\theta)^2$	$\frac{1}{2}K_{\mathrm{Se-Pt-Pt}}(\Delta\theta)^2$
Parameter	12.128	4.975	4.975
r_0 or θ_0	2.467	95.999	95.999

The second line gives an explicit expression for each VFF term. The third line is the force constant parameters. Parameters are in the unit of eV/Å^2 for the bond stretching interaction and in the unit of eV for the angle bending interaction. The fourth line gives the initial bond length (in the unit of Å) for the bond stretching interaction and the initial angle (in the unit of degrees) for the angle bending interaction. The angle θ_{ijk} has atom i as the apex.

Table 350. The VFF model for single-layer 1T-$PtSe_2$.

interaction shown by Eq. (2). We note that the angle bending term $K_{Pt-Se-Se}$ is for the angle $\theta_{Pt-Se-Se}$ with both Se atoms from the same (top or bottom) group. These force constant parameters are determined by fitting to the three acoustic branches in the phonon dispersion along the ΓM as shown in **Figure 174(a)**. The *ab initio* calculations for the phonon dispersion are from [34]. The lowest acoustic branch (flexural mode) is almost linear in the *ab initio* calculations, which may be due to the violation of the rigid rotational invariance [20]. **Figure 174(b)** shows that the VFF model and the SW potential give exactly the same phonon dispersion, as the SW potential is derived from the VFF model.

The parameters for the two-body SW potential used by GULP are shown in **Table 351**. The parameters for the three-body SW potential used by GULP are shown in **Table 352**. Some representative parameters for the SW potential used by LAMMPS are listed in **Table 353**.

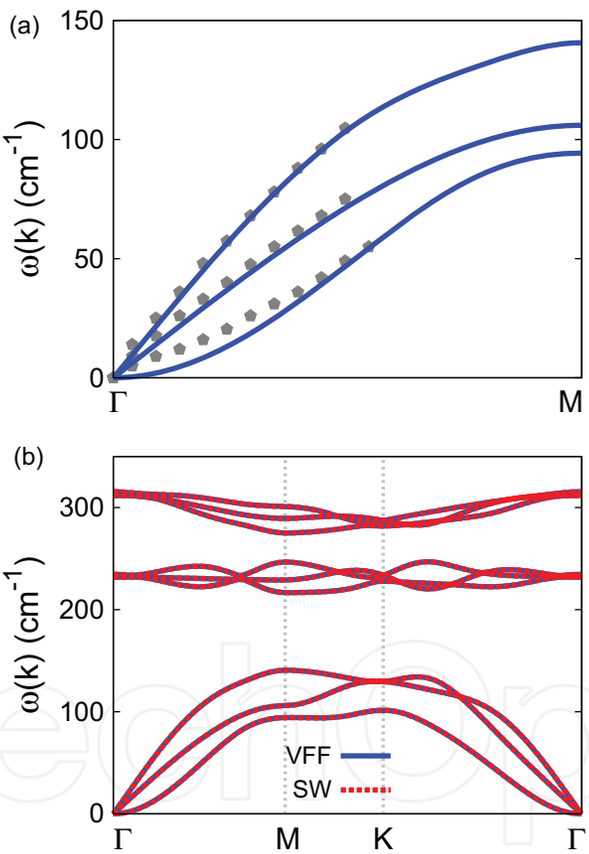

Figure 174. Phonon spectrum for single-layer 1T-$PtSe_2$. (a) Phonon dispersion along the ΓM direction in the Brillouin zone. The results from the VFF model (lines) are comparable with the *ab initio* results (pentagons) from [34]. (b) The phonon dispersion from the SW potential is exactly the same as that from the VFF model.

	A (eV)	ρ (Å)	B (Å^4)	r_{min} (Å)	r_{max} (Å)
Pt—Se	12.781	1.545	18.511	0.0	3.443

Table 351. Two-body SW potential parameters for single-layer 1T-$PtSe_2$ used by GULP [8] as expressed in Eq. (3).

	K (eV)	θ_0 (°)	ρ_1 (Å)	ρ_2 (Å)	$r_{\min 12}$ (Å)	$r_{\max 12}$ (Å)	$r_{\min 13}$ (Å)	$r_{\max 13}$ (Å)	$r_{\min 23}$ (Å)	$r_{\max 23}$ (Å)
$\theta_{\text{Pt–Se–Se}}$	59.608	95.999	1.545	1.545	0.0	3.443	0.0	3.443	0.0	5.008
$\theta_{\text{Se–Pt–Pt}}$	59.608	95.999	1.545	1.545	0.0	3.443	0.0	3.443	0.0	5.008

The angle θ_{ijk} in the first line indicates the bending energy for the angle with atom i as the apex.

Table 352. Three-body SW potential parameters for single-layer 1T-$PtSe_2$ used by GULP [8] as expressed in Eq. (4).

	ϵ (eV)	σ (Å)	a	λ	γ	$\cos\theta_0$	A_L	B_L	p	q	Tol
Pt—Se_1—Se_1	1.000	1.545	2.229	59.608	1.000	−0.105	12.781	3.250	4	0	0.0

Table 353. SW potential parameters for single-layer 1T-$PtSe_2$ used by LAMMPS [9] as expressed in Eqs. (9) and (10).

We use LAMMPS to perform MD simulations for the mechanical behavior of the single-layer 1T-$PtSe_2$ under uniaxial tension at 1 and 300 K. **Figure 175** shows the stress-strain curve for the tension of a single-layer 1T-$PtSe_2$ of dimension 100 × 100 Å. Periodic boundary conditions are applied in both armchair and zigzag directions. The single-layer 1T-$PtSe_2$ is stretched uniaxially along the armchair or zigzag direction. The stress is calculated without involving the actual thickness of the quasi-two-dimensional structure of the single-layer 1T-$PtSe_2$. The Young's modulus can be obtained by a linear fitting of the stress-strain relation in the small strain range of [0, 0.01]. The Young's modulus is 101.1 and 100.5 N/m along the armchair and zigzag directions, respectively. The Young's modulus is essentially isotropic in the armchair and zigzag directions. The Poisson's ratio from the VFF model and the SW potential is $\nu_{xy} = \nu_{yx} = 0.17$.

There is no available value for nonlinear quantities in the single-layer 1T-$PtSe_2$. We have thus used the nonlinear parameter $B = 0.5d^4$ in Eq. (5), which is close to the value of B in most materials. The value of the third-order nonlinear elasticity D can be extracted by fitting the

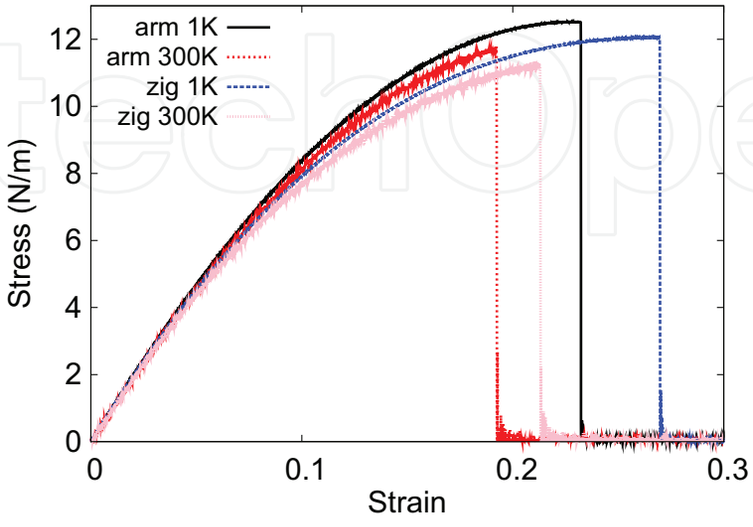

Figure 175. Stress-strain for single-layer 1T-$PtSe_2$ of dimension 100 × 100 Å along the armchair and zigzag directions.

stress-strain relation to the function $\sigma = E\epsilon + \frac{1}{2}D\epsilon^2$ with E as the Young's modulus. The values of D from the present SW potential are -391.4 and -424 N/m along the armchair and zigzag directions, respectively. The ultimate stress is about 12.5 N/m at the ultimate strain of 0.23 in the armchair direction at the low temperature of 1 K. The ultimate stress is about 12.1 N/m at the ultimate strain of 0.27 in the zigzag direction at the low temperature of 1 K.

89. 1T-$PtTe_2$

Most existing theoretical studies on the single-layer 1T-$PtTe_2$ are based on the first-principles calculations. In this section, we will develop the SW potential for the single-layer 1T-$PtTe_2$.

The structure for the single-layer 1T-$PtTe_2$ is shown in **Figure 71** (with M = Pt and X = Te). Each Pt atom is surrounded by six Te atoms. These Te atoms are categorized into the top group (e.g., atoms 1, 3, and 5) and bottom group (e.g., atoms 2, 4, and 6). Each Te atom is connected to three Pt atoms. The structural parameters are from the first-principles calculations [48], including the lattice constant $a = 3.9554$ Å and the bond length $d_{\mathrm{Pt-Te}} = 2.6613$ Å, which are derived from the angle $\theta_{\mathrm{TePtPt}} = 96^\circ$. The other angle is $\theta_{\mathrm{PtTeTe}} = 96^\circ$ with Te atoms from the same (top or bottom) group.

Table 354 shows three VFF terms for the single-layer 1T-$PtTe_2$; one of which is the bond stretching interaction shown by Eq. (1), while the other two terms are the angle bending interaction shown by Eq. (2). We note that the angle bending term $K_{\mathrm{Pt-Te-Te}}$ is for the angle $\theta_{\mathrm{Pt-Te-Te}}$ with both Te atoms from the same (top or bottom) group. These force constant parameters are determined by fitting to the three acoustic branches in the phonon dispersion along the ΓM as shown in **Figure 176(a)**. The *ab initio* calculations for the phonon dispersion are from [34]. **Figure 176(b)** shows that the VFF model and the SW potential give exactly the same phonon dispersion, as the SW potential is derived from the VFF model.

The parameters for the two-body SW potential used by GULP are shown in **Table 355**. The parameters for the three-body SW potential used by GULP are shown in **Table 356**. Some representative parameters for the SW potential used by LAMMPS are listed in **Table 357**.

VFF type	Bond stretching	Angle bending	
Expression	$\frac{1}{2}K_{\mathrm{Pt-Te}}(\Delta r)^2$	$\frac{1}{2}K_{\mathrm{Pt-Te-Te}}(\Delta\theta)^2$	$\frac{1}{2}K_{\mathrm{Te-Pt-Pt}}(\Delta\theta)^2$
Parameter	12.128	4.975	4.975
r_0 or θ_0	2.661	95.998	95.998

The second line gives an explicit expression for each VFF term. The third line is the force constant parameters. Parameters are in the unit of eV/Å^2 for the bond stretching interaction and in the unit of eV for the angle bending interaction. The fourth line gives the initial bond length (in the unit of Å) for the bond stretching interaction and the initial angle (in the unit of degrees) for the angle bending interaction. The angle θ_{ijk} has atom i as the apex.

Table 354. The VFF model for single-layer 1T-$PtTe_2$.

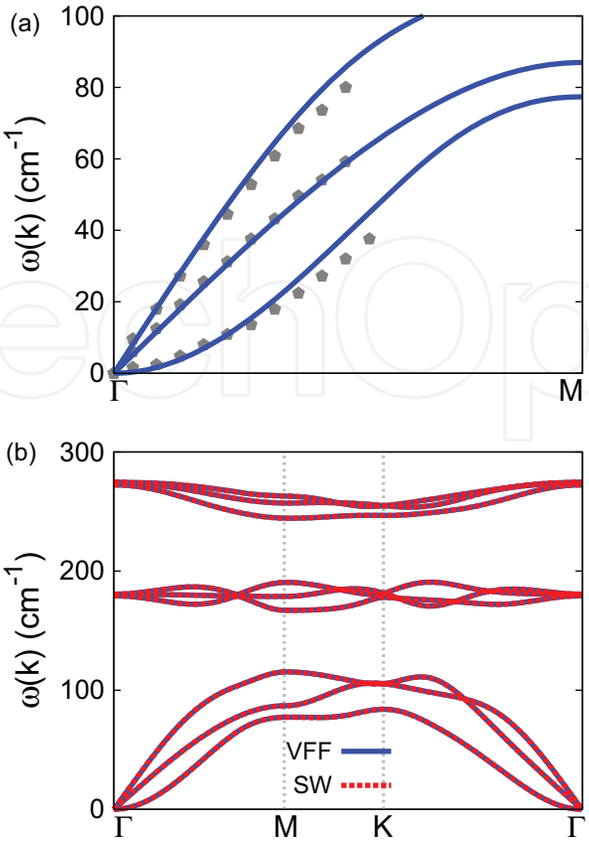

Figure 176. Phonon spectrum for single-layer 1T-$PtTe_2$. (a) Phonon dispersion along the ΓM direction in the Brillouin zone. The results from the VFF model (lines) are comparable with the *ab initio* results (pentagons) from [34]. (b) The phonon dispersion from the SW potential is exactly the same as that from the VFF model.

	A (eV)	ρ (Å)	B (Å^4)	$r_{\min}$ (Å)	$r_{\max}$ (Å)
Pt—Te	14.877	1.667	25.081	0.0	3.714

Table 355. Two-body SW potential parameters for single-layer 1T-$PtTe_2$ used by GULP [8] as expressed in Eq. (3).

	K (eV)	θ_0 (°)	ρ_1 (Å)	ρ_2 (Å)	$r_{\min 12}$ (Å)	$r_{\max 12}$ (Å)	$r_{\min 13}$ (Å)	$r_{\max 13}$ (Å)	$r_{\min 23}$ (Å)	$r_{\max 23}$ (Å)
$\theta_{\mathrm{Pt-Te-Te}}$	59.607	95.998	1.667	1.667	0.0	3.714	0.0	3.714	0.0	5.403
$\theta_{\mathrm{Te-Pt-Pt}}$	59.607	95.998	1.667	1.667	0.0	3.714	0.0	3.714	0.0	5.403

The angle θ_{ijk} in the first line indicates the bending energy for the angle with atom i as the apex.

Table 356. Three-body SW potential parameters for single-layer 1T-$PtTe_2$ used by GULP [8] as expressed in Eq. (4).

	ϵ (eV)	σ (Å)	a	λ	γ	$\cos\theta_0$	A_L	B_L	p	q	Tol
Pt—Te_1—Te_1	1.000	1.667	2.229	59.607	1.000	−0.104	14.877	3.250	4	0	0.0

Table 357. SW potential parameters for single-layer 1T-$PtTe_2$ used by LAMMPS [9] as expressed in Eqs. (9) and (10).

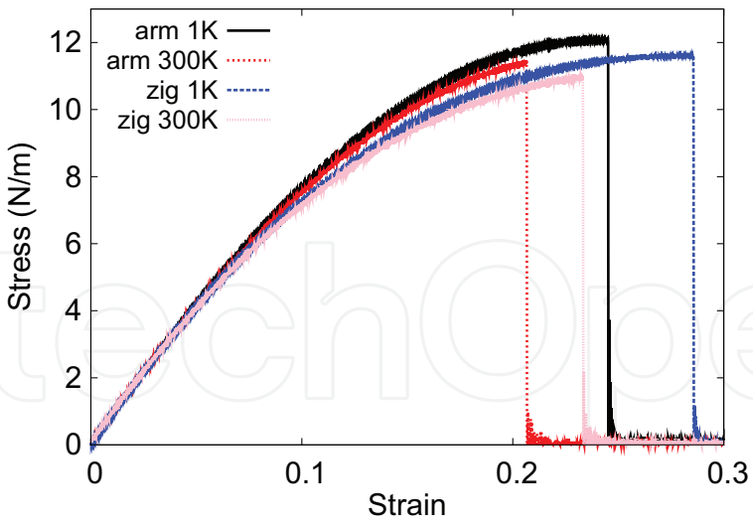

Figure 177. Stress-strain for single-layer 1T-$PtTe_2$ of dimension 100 × 100 Å along the armchair and zigzag directions.

We use LAMMPS to perform MD simulations for the mechanical behavior of the single-layer 1T-$PtTe_2$ under uniaxial tension at 1 and 300 K. **Figure 177** shows the stress-strain curve for the tension of a single-layer 1T-$PtTe_2$ of dimension 100 × 100 Å. Periodic boundary conditions are applied in both armchair and zigzag directions. The single-layer 1T-$PtTe_2$ is stretched uniaxially along the armchair or zigzag direction. The stress is calculated without involving the actual thickness of the quasi-two-dimensional structure of the single-layer 1T-$PtTe_2$. The Young's modulus can be obtained by a linear fitting of the stress-strain relation in the small strain range of [0, 0.01]. The Young's modulus is 89.1 and 88.7 N/m along the armchair and zigzag directions, respectively. The Young's modulus is essentially isotropic in the armchair and zigzag directions. The Poisson's ratio from the VFF model and the SW potential is $\nu_{xy} = \nu_{yx} = 0.19$.

There is no available value for nonlinear quantities in the single-layer 1T-$PtTe_2$. We have thus used the nonlinear parameter $B = 0.5d^4$ in Eq. (5), which is close to the value of B in most materials. The value of the third-order nonlinear elasticity D can be extracted by fitting the stress-strain relation to the function $\sigma = E\epsilon + \frac{1}{2}D\epsilon^2$ with E as the Young's modulus. The values of D from the present SW potential are −306.8 and −340.9 N/m along the armchair and zigzag directions, respectively. The ultimate stress is about 12.1 N/m at the ultimate strain of 0.24 in the armchair direction at the low temperature of 1 K. The ultimate stress is about 11.6 N/m at the ultimate strain of 0.28 in the zigzag direction at the low temperature of 1 K.

90. Black phosphorus

The black phosphorus is also named the α phosphorus. There are several empirical potentials available for the atomic interaction in the black phosphorus. A VFF model was proposed for the single-layer black phosphorus in 1982 [56]. One of the present authors (J.W.J.) simplified this VFF model by ignoring some angle-angle crossing terms and using the simplified VFF

model to develop the SW potential for the black phosphorus [7]. However, the mechanical properties from this SW potential are smaller than first-principles calculations, as some angle-angle crossing VFF terms cannot be implemented in the SW potential. We will thus propose a new set of SW potential for the single-layer black phosphorus in this section.

The structure of the single-layer black phosphorus is shown in **Figure 178**, with structural parameters from the *ab initio* calculations [57]. The black phosphorus has a puckered configuration as shown in **Figure 178(b)**, where the pucker is perpendicular to the x-direction. The bases for the rectangular unit cell are $a_1 = 4.422$ Å and $a_2 = 3.348$ Å. For bulk black phosphorus, the basis lattice vector in the third direction is $a_3 = 10.587$ Å. There are four phosphorus atoms in the basic unit cell, and their relative coordinates are $(-u, 0, -v)$, $(u, 0, v)$, $(0.5 - u, 0.5, v)$, and $(0.5 + u, 0.5, -v)$ with $u = 0.0821$ and $v = 0.1011$. Atoms are categorized into the top and bottom groups. Atoms in the top group are denoted by P_1, while atoms in the bottom group are denoted by P_2.

Table 358 shows four VFF terms for the single-layer black phosphorus; two of which are the bond stretching interactions shown by Eq. (1), while the other two terms are the angle bending interaction shown by Eq. (2). The force constant parameters are reasonably chosen to be the same for the two bond stretching terms denoted by r_{12} and r_{14}, as these two bonds have very

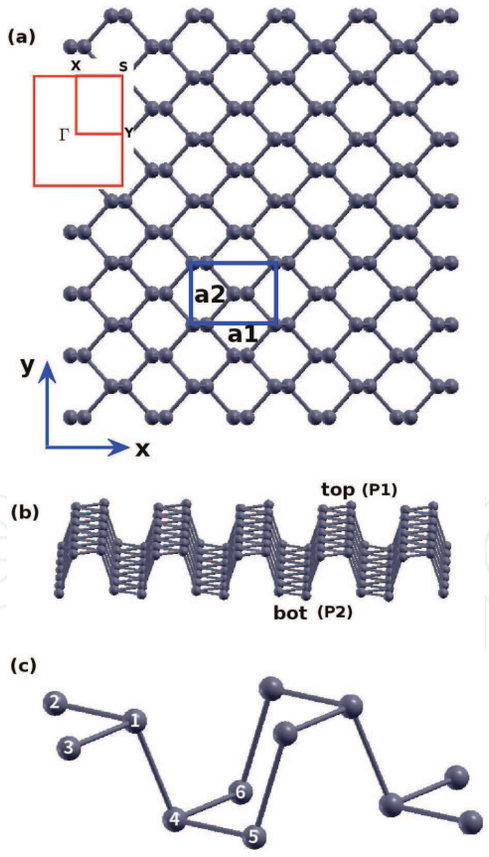

Figure 178. Structure for single-layer black phosphorus. (a) Top view. The armchair direction is along the x-axis, while the zigzag direction is along the y-axis. Inset shows the first Brillouin zone. (b) Perspective view illustrates the puckered configuration. The pucker is perpendicular to the x-axis and is parallel with the y-axis. Atoms are divided into the top (denoted by P_1) and the bottom (denoted by P_2) groups. (c) Atomic configuration.

VFF type	Bond stretching		Angle bending	
Expression	$\frac{1}{2}K_{12}(\Delta r_{12})^2$	$\frac{1}{2}K_{14}(\Delta r_{14})^2$	$\frac{1}{2}K_{123}(\Delta\theta_{123})^2$	$\frac{1}{2}K_{134}(\Delta\theta_{134})^2$
Parameter	10.542	10.542	7.048	7.048
r_0 or θ_0	2.238	2.260	96.581	102.307

The second line gives an explicit expression for each VFF term, where atom indexes are from **Figure 178(c)**. The third line is the force constant parameters. Parameters are in the unit of eV/Å^2 for the bond stretching interaction and in the unit of eV for the angle bending interaction. The fourth line gives the initial bond length (in the unit of Å) for the bond stretching interaction and the initial angle (in the unit of degrees) for the angle bending interaction. The angle θ_{ijk} has atom i as the apex.

Table 358. The VFF model for black phosphorus.

close bond length value. The force constant parameters are the same for the two angle bending terms θ_{123} and θ_{134}, which have very similar chemical environment. These force constant parameters are determined by fitting to the three acoustic branches in the phonon dispersion along the ΓX as shown in **Figure 179(a)**. The *ab initio* calculations for the phonon dispersion are from [55]. Similar phonon dispersion can also be found in other *ab initio* calculations [58–64].

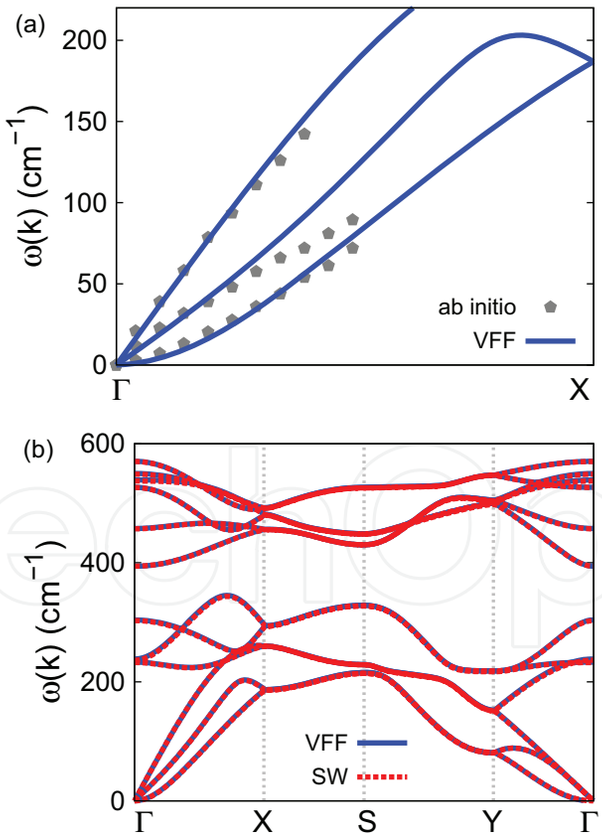

Figure 179. Phonon dispersion for the single-layer black phosphorus. (a) The VFF model is fitted to the three acoustic branches in the long wave limit along the ΓX direction. The *ab initio* results (gray pentagons) are from [55]. (b) The VFF model (blue lines) and the SW potential (red lines) give the same phonon dispersion for the black phosphorus along ΓXSYΓ.

Figure 179(b) shows that the VFF model and the SW potential give exactly the same phonon dispersion, as the SW potential is derived from the VFF model.

The parameters for the two-body SW potential used by GULP are shown in **Table 359**. The parameters for the three-body SW potential used by GULP are shown in **Table 360**. Parameters for the SW potential used by LAMMPS are listed in **Table 361**.

Figure 180 shows the stress-strain relations for the black phosphorus of size 100 × 100 Å. The structure is uniaxially stretched in the armchair or zigzag directions at 1 and 300 K. The Young's modulus is 24.3 and 90.5 N/m in the armchair and zigzag directions, respectively, at 1 K, which is obtained by linear fitting of the stress-strain relations in [0, 0.01]. These values agree quite well with previously reported *ab initio* results, e.g., 28.9 and 101.6 N/m from [65] or 24.4 and 92.1 N/m from [66] or 24.3 and 80.2 N/m from [58]. The ultimate stress is about 4.27 N/m at the critical strain of 0.33 in the armchair direction at the low temperature of 1 K. The ultimate stress is about 8 N/m at the critical strain of 0.19 in the zigzag direction at the low temperature of 1 K. These values agree quite well with the *ab initio* results at 0 K [66].

It should be noted that the Poisson's ratios from the VFF model and the SW potential are $\nu_{xy} = 0.058$ and $\nu_{yx} = 0.22$. These values are obviously smaller than first-principles calculations

	A (eV)	ρ (Å)	B (Å^4)	$r_{\min}$ (Å)	$r_{\max}$ (Å)
r_{12}	4.172	0.551	12.543	0.0	2.793
r_{14}	4.976	0.685	13.044	0.0	2.882

The quantity (r_{ij}) in the first line lists one representative term for the two-body SW potential between atoms i and j. Atom indexes are from **Figure 178(c)**.

Table 359. Two-body SW potential parameters for black phosphorus used by GULP [8] as expressed in Eq. (3).

	K (eV)	θ_0 (°)	ρ_1 (Å)	ρ_2 (Å)	$r_{\min 12}$ (Å)	$r_{\max 12}$ (Å)	$r_{\min 13}$ (Å)	$r_{\max 13}$ (Å)	$r_{\min 23}$ (Å)	$r_{\max 23}$ (Å)
θ_{123}	25.965	96.581	0.551	0.551	0.0	2.793	0.0	2.793	2.793	3.365
θ_{134}	29.932	102.307	0.551	0.685	0.0	2.793	0.0	2.882	2.882	3.772

The first line (θ_{ijk}) presents one representative term for the three-body SW potential. The angle θ_{ijk} has the atom i as the apex. Atom indexes are from **Figure 178(c)**.

Table 360. Three-body SW potential parameters for black phosphorus used by GULP [8] as expressed in Eq. (4).

	ϵ (eV)	σ (Å)	a	λ	γ	$\cos\theta_0$	A_L	B_L	p	q	Tol
P_1—P_1—P_1	1.000	0.551	5.069	25.965	1.000	−0.115	4.172	136.080	4	0	0.0
P_1—P_2—P_2	1.000	0.685	4.207	0.000	1.000	0.000	4.976	59.245	4	0	0.0
P_1—P_1—P_2	1.000	0.000	0.000	29.932	1.000	−0.213	0.000	0.000	4	0	0.0

Atom types (P_1 and P_2) in the first column are displayed in **Figure 178**.

Table 361. SW potential parameters for black phosphorus used by LAMMPS [9] as expressed in Eqs. (9) and (10).

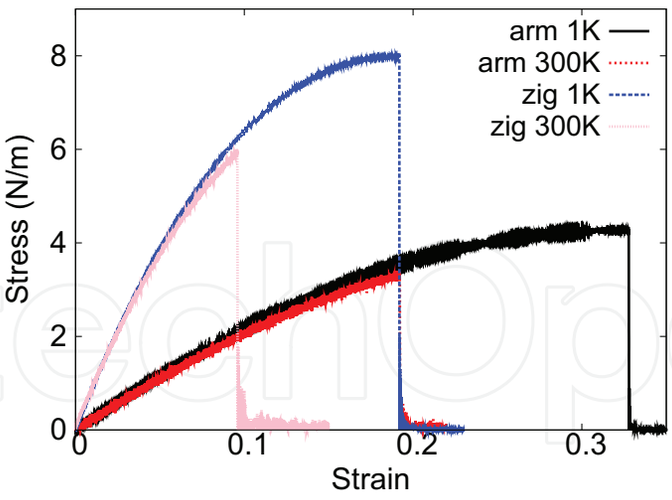

Figure 180. Stress-strain relations for the black phosphorus of size 100×100 Å. The black phosphorus is uniaxially stretched along the armchair or zigzag directions at temperatures 1 and 300 K.

results, e.g., 0.4 and 0.93 from [67] or 0.17 and 0.62 from [58] or 0.24 and 0.81 from [59]. The Poisson's ratio cannot be obtained correctly by the VFF model proposed in 1982 [56] and the SW potential [7] either [68]. These failures are due to the missing of one angle-angle crossing term [69], which has not been implemented in the package LAMMPS and is not included in the present work.

91. p-Arsenene

Present studies on the puckered (p-) arsenene, also named α arsenene, are based on first-principles calculations, and no empirical potential has been proposed for the p-arsenene. We will thus parametrize a set of VFF model for the single-layer p-arsenene in this section. We will also derive the SW potential based on the VFF model for the single-layer p-arsenene.

The structure of the single-layer p-arsenene is exactly the same as that of the black phosphorus as shown in **Figure 178**. Structural parameters for p-arsenene are from the *ab initio* calculations [70]. The pucker of the p-arsenene is perpendicular to the x (armchair)-direction. The bases for the rectangular unit cell are $a_1 = 4.77$ Å and $a_2 = 3.68$ Å. There are four As atoms in the basic unit cell, and their relative coordinates are $(-u, 0, -v)$, $(u, , v)$, $(0.5 - u, 0.5, v)$, and $(0.5 + u, 0.5, -v)$ with $u = 0.0714$ and $v = 0.108$. The value of the dimensionless parameter u is extracted from the geometrical parameters provided in [70]. The other dimensionless parameter v is a ratio based on the lattice constant in the out-of-plane z-direction, so the other basis $a_3 = 11.11$ Å from [71] is also adopted in extracting the value of v. We note that the main purpose of the usage of u and v in representing atomic coordinates is to follow the same convention for all puckered structures. The resultant atomic coordinates are the same as that in [70].

Table 362 shows four VFF terms for the single-layer p-arsenene; two of which are the bond stretching interactions shown by Eq. (1), while the other two terms are the angle bending

VFF type	Bond stretching		Angle bending	
Expression	$\frac{1}{2}K_{12}(\Delta r_{12})^2$	$\frac{1}{2}K_{14}(\Delta r_{14})^2$	$\frac{1}{2}K_{123}(\Delta\theta_{123})^2$	$\frac{1}{2}K_{134}(\Delta\theta_{134})^2$
Parameter	7.936	7.936	7.456	7.456
r_0 or θ_0	2.508	2.495	94.400	100.692

The second line gives an explicit expression for each VFF term, where atom indexes are from **Figure 178(c)**. The third line is the force constant parameters. Parameters are in the unit of eV/Å^2 for the bond stretching interaction and in the unit of eV for the angle bending interaction. The fourth line gives the initial bond length (in the unit of Å) for the bond stretching interaction and the initial angle (in the unit of degrees) for the angle bending interaction. The angle θ_{ijk} has atom i as the apex.

Table 362. The VFF model for p-arsenene.

interaction shown by Eq. (2). The force constant parameters are reasonably chosen to be the same for the two bond stretching terms denoted by r_{12} and r_{14}, as these two bonds have very close bond length value. The force constant parameters happen to be the same for the two angle bending terms θ_{123} and θ_{134}. These force constant parameters are determined by fitting to the three acoustic branches in the phonon dispersion along the ΓX as shown in **Figure 181(a)**. The *ab initio* calculations for the phonon dispersion are from [70]. Similar phonon dispersion

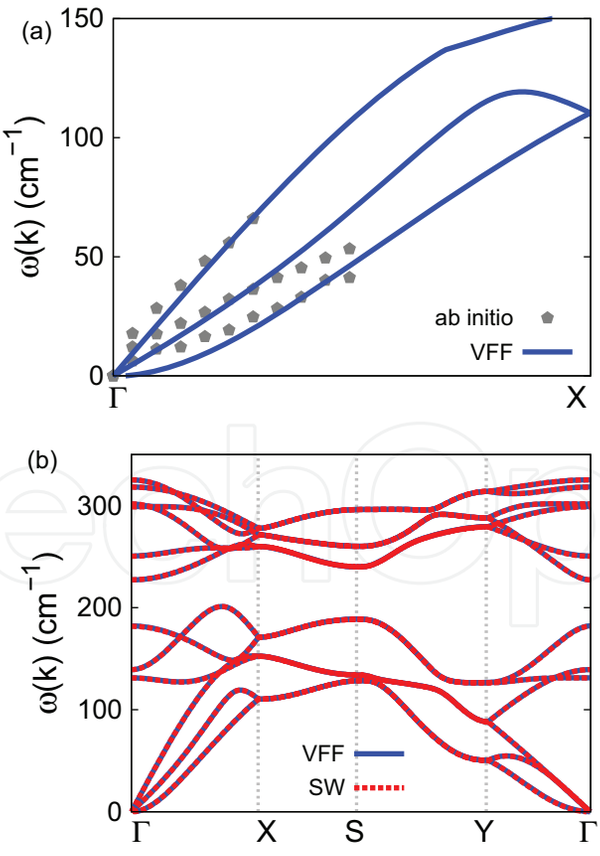

Figure 181. Phonon dispersion for the single-layer p-arsenene. (a) The VFF model is fitted to the three acoustic branches in the long wave limit along the ΓX direction. The *ab initio* results (gray pentagons) are from [70]. (b) The VFF model (blue lines) and the SW potential (red lines) give the same phonon dispersion for the p-arsenene along ΓXSYΓ.

can also be found in other *ab initio* calculations [64, 72–74]. We note that the lowest frequency branch around the Γ point from the VFF model is lower than the *ab initio* results. This branch is the flexural branch, which should be a quadratic dispersion. However, the *ab initio* calculations give a linear dispersion for the flexural branch due to the violation of the rigid rotational invariance in the first-principles package [20] so *ab initio* calculations typically overestimate the frequency of this branch. **Figure 181(b)** shows that the VFF model and the SW potential give exactly the same phonon dispersion, as the SW potential is derived from the VFF model.

The parameters for the two-body SW potential used by GULP are shown in **Table 363**. The parameters for the three-body SW potential used by GULP are shown in **Table 364**. Parameters for the SW potential used by LAMMPS are listed in **Table 365**.

Figure 182 shows the stress-strain relations for the p-arsenene of size 100 × 100 Å. The structure is uniaxially stretched in the armchair or zigzag directions at 1 and 300 K. The Young's modulus is 20.7 and 73 N/m in the armchair and zigzag directions, respectively, at 1 K, which is obtained by linear fitting of the stress-strain relations in [0, 0.01]. The third-order nonlinear elastic constant D can be obtained by fitting the stress-strain relation to $\sigma = E\epsilon + \frac{1}{2}D\epsilon^2$ with E as the Young's modulus. The values of D are −56.4 and −415.5 N/m at 1 K along the armchair

	A (eV)	ρ (Å)	B (Å^4)	$r_{\min}$ (Å)	$r_{\max}$ (Å)
r_{12}	3.180	0.455	19.782	0.0	3.042
r_{14}	4.477	0.737	19.375	0.0	3.173

The quantity (r_{ij}) in the first line lists one representative term for the two-body SW potential between atoms i and j. Atom indexes are from **Figure 178(c)**.

Table 363. Two-body SW potential parameters for p-arsenene used by GULP [8] as expressed in Eq. (3).

	K (eV)	θ_0 (°)	ρ_1 (Å)	ρ_2 (Å)	$r_{\min 12}$ (Å)	$r_{\max 12}$ (Å)	$r_{\min 13}$ (Å)	$r_{\max 13}$ (Å)	$r_{\min 23}$ (Å)	$r_{\max 23}$ (Å)
θ_{123}	20.597	94.400	0.455	0.455	0.0	3.042	0.0	3.042	3.628	4.225
θ_{134}	26.831	100.692	0.455	0.737	0.0	3.042	0.0	3.173	3.173	4.149

The first line (θ_{ijk}) presents one representative term for the three-body SW potential. The angle θ_{ijk} has the atom i as the apex. Atom indexes are from **Figure 178(c)**.

Table 364. Three-body SW potential parameters for p-arsenene used by GULP [8] as expressed in Eq. (4).

	ϵ (eV)	σ (Å)	a	λ	γ	$\cos\theta_0$	A_L	B_L	p	q	Tol
As_1—As_1—As_1	1.000	0.455	6.686	20.597	1.000	−0.077	3.180	461.556	4	0	0.0
As_1—As_2—As_2	1.000	0.737	4.305	0.000	1.000	0.000	4.477	65.671	4	0	0.0
As_1—As_1—As_2	1.000	0.000	0.000	26.831	1.000	−0.186	0.000	0.000	4	0	0.0

Atom types in the first column are displayed in **Figure 178(b)**, with element symbol P substituted by As.

Table 365. SW potential parameters for p-arsenene used by LAMMPS [9] as expressed in Eqs. (9) and (10).

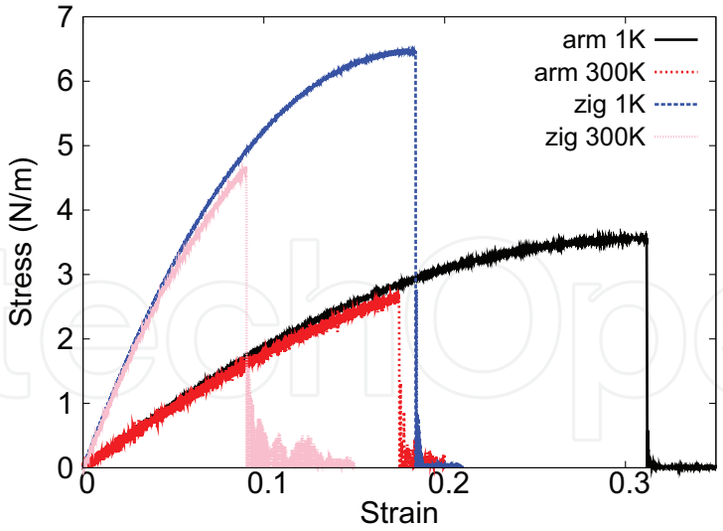

Figure 182. Stress-strain relations for the p-arsenene of size 100 × 100 Å. The p-arsenene is uniaxially stretched along the armchair or zigzag directions at temperatures 1 and 300 K.

and zigzag directions, respectively. The ultimate stress is about 3.5 N/m at the critical strain of 0.31 in the armchair direction at the low temperature of 1 K. The ultimate stress is about 6.5 N/m at the critical strain of 0.18 in the zigzag direction at the low temperature of 1 K.

92. p-Antimonene

Present studies on the puckered (p-) antimonene, also named α antimonene, are based on first-principles calculations, and no empirical potential has been proposed for the p-antimonene. We will thus parametrize a set of VFF model for the single-layer p-antimonene in this section. We will also derive the SW potential based on the VFF model for the single-layer p-antimonene.

The structure of the single-layer p-antimonene is shown in **Figure 183**, which is similar as that of the black phosphorus as shown in **Figure 178**. Structural parameters for p-antimonene are from the *ab initio* calculations [70]. The pucker of the p-antimonene is perpendicular to the x (armchair)-direction. The bases for the rectangular unit cell are $a_1 = 4.73$ Å and $a_2 = 4.36$ Å. There are four Sb atoms in the basic unit cell, and their relative coordinates are $(-u, 0, -v)$, $(u, 0, v)$, $(0.5 - u, 0.5, v + w)$, and $(0.5 + u, 0.5, -v + w)$ with $u = 0.044$, $v = 0.128$, and $w = 0.0338$. The value of the dimensionless parameter u is extracted from the geometrical parameters (bond lengths and bond angles) provided in [70]. The dimensionless parameters v and w are ratios based on the lattice constant in the out-of-plane z-direction, so an arbitrary value of $a_3 = 11.11$ Å is adopted in extracting the values of v and w. The value of a_3 has no effect on the actual position of each Sb atom. We note that the main purpose of the usage of u, v, and w in representing atomic coordinates is to follow the same convention of black phosphorus. The resultant atomic coordinates are the same as that in [70].

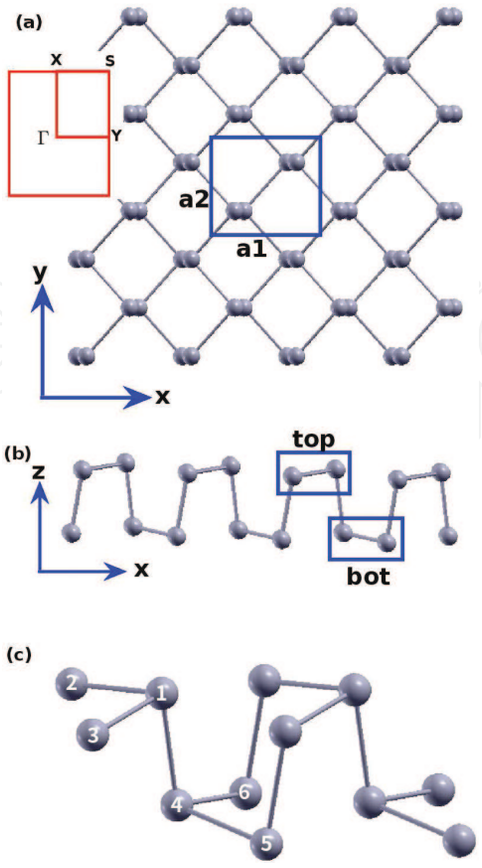

Figure 183. Structure for single-layer p-antimonene. (a) Top view illustrates the armchair direction is along the x-axis, while the zigzag direction is along the y-axis. The first Brillouin zone is shown in the inset. (b) Side view illustrates the puckered configuration. The pucker is perpendicular to the x-axis and is parallel with the y-axis. Sb atoms in the top/bottom group have different z-coordinates. (c) Atomic configuration.

As shown in **Figure 183(b)**, a specific feature in the puckered configuration of the p-antimonene is that Sb atoms in the top/bottom group are further divided into two subgroups with different z-coordinates. Specifically, in **Figure 183(c)**, there is a difference of wa_3 between the z-coordinate of atom 1 and the z-coordinates of atoms 2 and 3. Similarly, atom 4 is higher than atoms 5 and 6 for wa_3 along the z-direction. As a result of the nonzero value of w, there are two different intergroup angles, i.e., θ_{134}= 88.3° and θ_{415}= 102.8°. We have $w = 0$ for the ideal puckered configuration of the black phosphorus.

Table 366 shows five VFF terms for the single-layer p-antimonene; two of which are the bond stretching interactions shown by Eq. (1), while the other three terms are the angle bending interaction shown by Eq. (2). The force constant parameters are reasonably chosen to be the same for the two bond stretching terms denoted by r_{12} and r_{14}, as these two bonds have very close bond length value. The force constant parameters are the same for the two angle bending terms θ_{134} and θ_{415}, which have the same arm lengths. As a result, there are only three force constant parameters, i.e., $K_{12} = K_{14}$, K_{123}, and $K_{134} = K_{415}$. These three force constant parameters are determined by fitting to the three acoustic branches in the phonon dispersion along the ΓX as shown in **Figure 185(a)**. The *ab initio* calculations for the phonon dispersion are from [70].

VFF type	Bond stretching		Angle bending		
Expression	$\frac{1}{2}K_{12}(\Delta r_{12})^2$	$\frac{1}{2}K_{14}(\Delta r_{14})^2$	$\frac{1}{2}K_{123}(\Delta\theta_{123})^2$	$\frac{1}{2}K_{134}(\Delta\theta_{134})^2$	$\frac{1}{2}K_{415}(\Delta\theta_{415})^2$
Parameter	7.675	7.675	6.534	12.068	12.068
r_0 or θ_0	2.950	2.870	95.380	88.300	102.800

The second line gives an explicit expression for each VFF term, where atom indexes are from **Figure 183(c)**. The third line is the force constant parameters. Parameters are in the unit of eV/Å^2 for the bond stretching interaction and in the unit of eV for the angle bending interaction. The fourth line gives the initial bond length (in the unit of Å) for the bond stretching interaction and the initial angle (in the unit of degrees) for the angle bending interaction. The angle θ_{ijk} has atom i as the apex.

Table 366. The VFF model for p-antimonene.

Similar phonon dispersion can also be found in other *ab initio* calculations [64, 75, 76]. We note that the lowest frequency branch around the Γ point from the VFF model is lower than the *ab initio* results. This branch is the flexural branch, which should be a quadratic dispersion. However, the *ab initio* calculations give a linear dispersion for the flexural branch due to the violation of the rigid rotational invariance in the first-principles package [20], so *ab initio* calculations typically overestimate the frequency of this branch. **Figure 185(b)** shows that the VFF model and the SW potential give exactly the same phonon dispersion, as the SW potential is derived from the VFF model.

The parameters for the two-body SW potential used by GULP are shown in **Table 367**. The parameters for the three-body SW potential used by GULP are shown in **Table 368**. Parameters for the SW potential used by LAMMPS are listed in **Table 369**. Eight atom types have been introduced for writing the SW potential script used by LAMMPS as shown in **Figure 184**,

	A (eV)	ρ (Å)	B (Å^4)	$r_{\min}$ (Å)	$r_{\max}$ (Å)
r_{12}	1.750	0.122	37.867	0.0	3.250
r_{14}	11.221	1.843	33.923	0.0	4.020

The quantity (r_{ij}) in the first line lists one representative term for the two-body SW potential between atoms i and j. Atom indexes are from **Figure 183(c)**.

Table 367. Two-body SW potential parameters for p-antimonene used by GULP [8] as expressed in Eq. (3).

	K (eV)	θ_0 (°)	ρ_1 (Å)	ρ_2 (Å)	$r_{\min 12}$ (Å)	$r_{\max 12}$ (Å)	$r_{\min 13}$ (Å)	$r_{\max 13}$ (Å)	$r_{\min 23}$ (Å)	$r_{\max 23}$ (Å)
θ_{123}	7.435	95.380	0.122	0.122	0.0	3.250	0.0	3.250	0.0	4.545
θ_{134}	45.054	88.380	1.843	0.122	0.0	4.020	0.0	3.250	0.0	5.715
θ_{415}	47.338	102.800	1.843	0.122	0.0	4.020	0.0	3.250	0.0	6.105

The first line (θ_{ijk}) presents one representative term for the three-body SW potential. The angle θ_{ijk} has the atom i as the apex. Atom indexes are from **Figure 183(c)**.

Table 368. Three-body SW potential parameters for p-antimonene used by GULP [8] as expressed in Eq. (4).

	ϵ (eV)	σ (Å)	a	λ	γ	$\cos\theta_0$	A_L	B_L	p	q	Tol
Sb_5—Sb_4—Sb_4	1.000	5.103	0.958	635.059	1.000	−0.094	38.498	0.056	4	0	0.0
Sb_1—Sb_2—Sb_2	1.000	1.924	2.102	0.000	1.000	0.000	11.708	2.476	4	0	0.0
Sb_5—Sb_4—Sb_6	1.000	0.000	0.000	431.139	1.000	0.030	0.000	0.000	4	0	0.0
Sb_2—Sb_3—Sb_1	1.000	0.000	0.000	452.994	1.000	−0.222	0.000	0.000	4	0	0.0

Atom types in the first column are displayed in **Figure 184**.

Table 369. SW potential parameters for p-antimonene used by LAMMPS [9] as expressed in Eqs. (9) and (10).

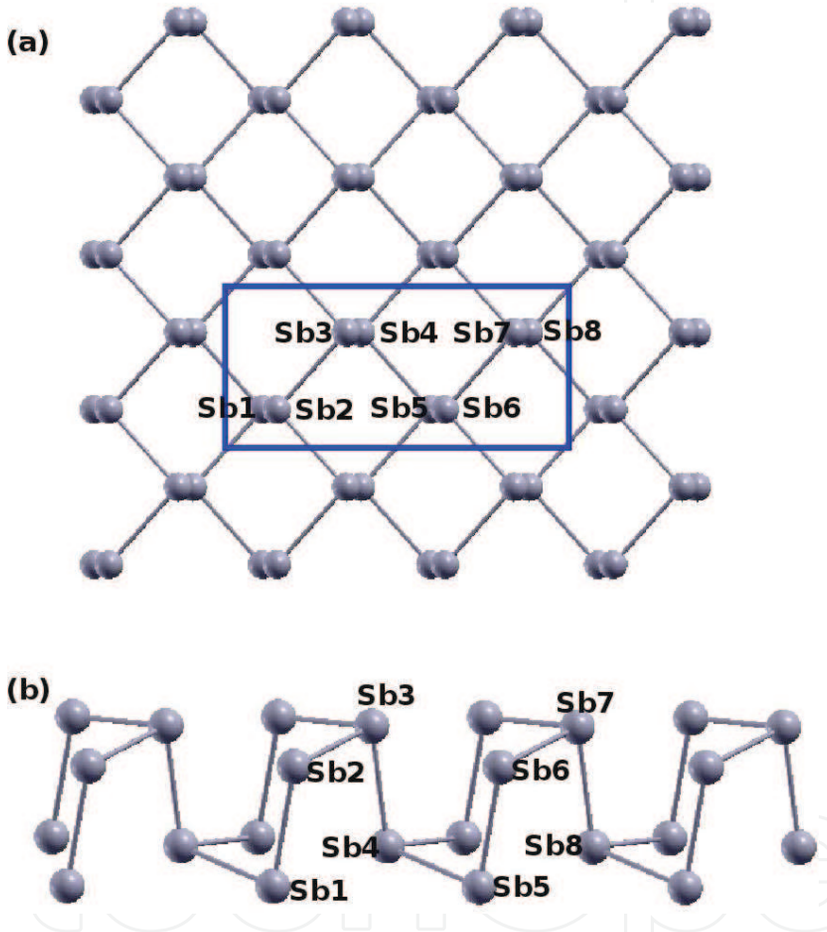

Figure 184. Eight atom types are introduced for the Sb atoms in the p-antimonene. (a) Top view and (b) side view.

which technically increases the cutoff for the bond stretching interaction between atom 1 and atom 2 in **Figure 183(c)**.

Figure 186 shows the stress-strain relations for the p-antimonene of size 100×100 Å. The structure is uniaxially stretched in the armchair or zigzag directions at 1 and 300 K. The Young's modulus is 18.3 and 65.2 N/m in the armchair and zigzag directions, respectively, at 1 K, which is obtained by linear fitting of the stress-strain relations in [0, 0.01]. The Poisson's ratios from the VFF model and the SW potential are $\nu_{xy} = 0.08$ and $\nu_{yx} = 0.29$. The third-order nonlinear elastic

http://dx.doi.org/10.5772/intechopen.71929

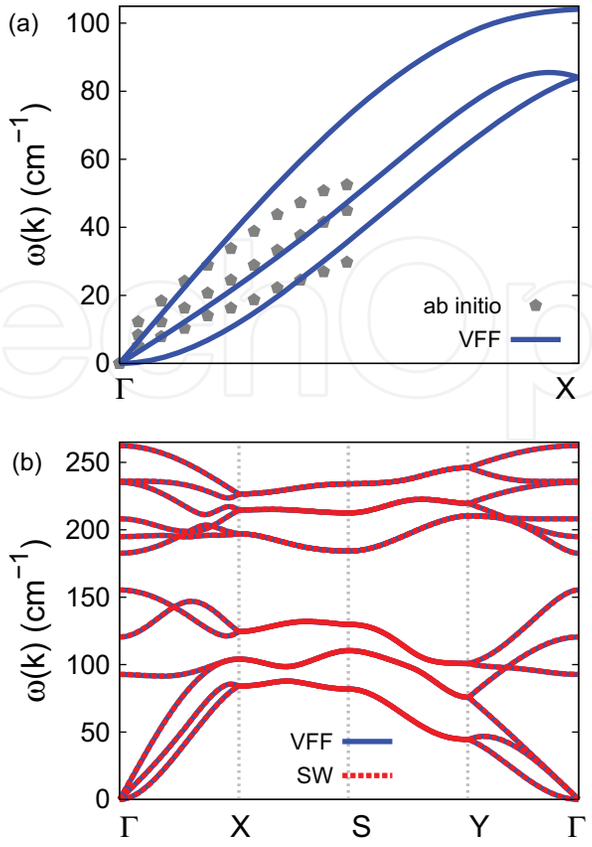

Figure 185. Phonon dispersion for the single-layer p-antimonene. (a) The VFF model is fitted to the three acoustic branches in the long wave limit along the ΓX direction. The *ab initio* results (gray pentagons) are from [70]. (b) The VFF model (blue lines) and the SW potential (red lines) give the same phonon dispersion for the p-antimonene along ΓXSYΓ.

constant D can be obtained by fitting the stress-strain relation to $\sigma = E\epsilon + \frac{1}{2}D\epsilon^2$ with E as the Young's modulus. The values of D are -22.1 and -354.1 N/m at 1 K along the armchair and zigzag directions, respectively. The ultimate stress is about 3.7 N/m at the critical strain of 0.37 in

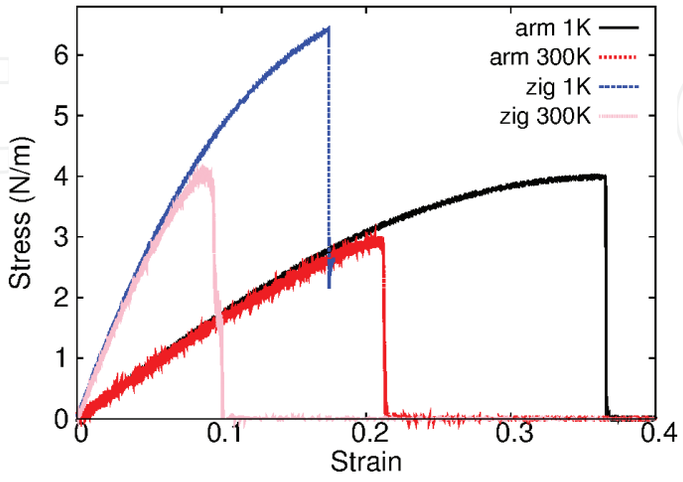

Figure 186. Stress-strain relations for the p-antimonene of size 100 × 100 Å. The p-antimonene is uniaxially stretched along the armchair or zigzag directions at temperatures 1 and 300 K.

the armchair direction at the low temperature of 1 K. The ultimate stress is about 6.4 N/m at the critical strain of 0.17 in the zigzag direction at the low temperature of 1 K.

93. p-Bismuthene

Present studies on the puckered (p-) bismuthene, which is also named α bismuthene, are based on first-principles calculations, and no empirical potential has been proposed for the p-bismuthene. We will thus parametrize a set of VFF model for the single-layer p-bismuthene in this section. We will also derive the SW potential based on the VFF model for the single-layer p-bismuthene.

The structure of the single-layer p-bismuthene is the same as p-antimonene as shown in **Figure 183**. Structural parameters for p-bismuthene are from the *ab initio* calculations [77]. The pucker of the p-bismuthene is perpendicular to the x (armchair)-direction. The bases for the rectangular unit cell are $a_1 = 4.94$ Å and $a_2 = 4.55$ Å. There are four Bi atoms in the basic unit cell, and their relative coordinates are $(-u, 0, -v)$, $(u, 0, v)$, $(0.5 - u, 0.5, v + w)$, and $(0.5 + u, 0.5, -v + w)$ with $u = 0.0405$, $v = 0.130$, and $w = 0.0391$. The value of the dimensionless parameter u is extracted from the geometrical parameters provided in [77]. The dimensionless parameters v and w are ratios based on the lattice constant in the out-of-plane z-direction, so an arbitrary value of $a_3 = 11.81$ Å is adopted in extracting the values of v and w. The value of a_3 has no effect on the actual position of each Bi atom. We note that the main purpose of the usage of u, v, and w in representing atomic coordinates is to follow the same convention of black phosphorus. The resultant atomic coordinates are the same as that in [77].

As shown in **Figure 183(b)**, a specific feature in the puckered configuration of the p-bismuthene is that Bi atoms in the top/bottom group are further divided into two subgroups with different z-coordinates. Specifically, in **Figure 183(c)**, there is a difference of wa_3 between the z-coordinate of atom 1 and the z-coordinates of atoms 2 and 3. Similarly, atom 4 is higher than atoms 5 and 6 for wa_3 along the z-direction. As a result of the nonzero value of w, there are two different intergroup angles, i.e., $\theta_{134} = 86.486^\circ$ and $\theta_{415} = 103.491^\circ$. We have $w = 0$ for the ideal puckered configuration of the black phosphorus.

Table 370 shows five VFF terms for the single-layer p-bismuthene; two of which are the bond stretching interactions shown by Eq. (1), while the other three terms are the angle bending interaction shown by Eq. (2). The force constant parameters are reasonably chosen to be the same for the two bond stretching terms denoted by r_{12} and r_{14}, as these two bonds have very close bond length value. The force constant parameters are the same for the two angle bending terms θ_{134} and θ_{415}, which have the same arm lengths. As a result, there are only three force constant parameters, i.e., $K_{12} = K_{14}$, K_{123}, and $K_{134} = K_{415}$. These three force constant parameters are determined by fitting to the three acoustic branches in the phonon dispersion along the ΓX as shown in **Figure 187(a)**. The *ab initio* calculations for the phonon dispersion are from [77]. Similar phonon dispersion can also be found in other *ab initio* calculations [64]. **Figure 187(b)** shows that the VFF model and the SW potential give exactly the same phonon dispersion, as the SW potential is derived from the VFF model.

VFF type	Bond stretching		Angle bending		
Expression	$\frac{1}{2}K_{12}(\Delta r_{12})^2$	$\frac{1}{2}K_{14}(\Delta r_{14})^2$	$\frac{1}{2}K_{123}(\Delta\theta_{123})^2$	$\frac{1}{2}K_{134}(\Delta\theta_{134})^2$	$\frac{1}{2}K_{415}(\Delta\theta_{415})^2$
Parameter	7.675	7.675	2.267	8.347	8.347
r_0 or θ_0	3.110	3.097	94.018	86.486	103.491

The second line gives an explicit expression for each VFF term, where atom indexes are from **Figure 183(c)**. The third line is the force constant parameters. Parameters are in the unit of eV/Å^2 for the bond stretching interaction and in the unit of eV for the angle bending interaction. The fourth line gives the initial bond length (in the unit of Å) for the bond stretching interaction and the initial angle (in the unit of degrees) for the angle bending interaction. The angle θ_{ijk} has atom i as the apex.

Table 370. The VFF model for p-bismuthene.

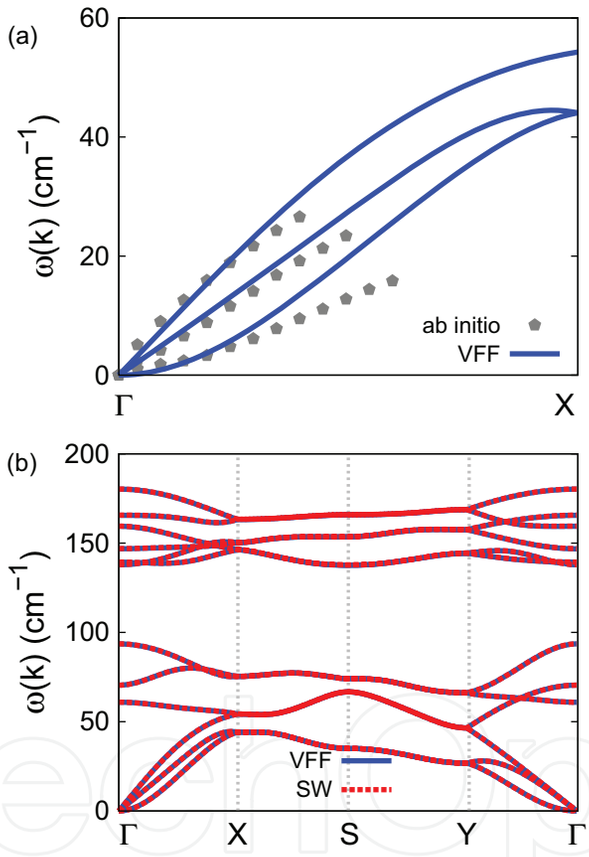

Figure 187. Phonon dispersion for the single-layer p-bismuthene. (a) The VFF model is fitted to the three acoustic branches in the long wave limit along the ΓX direction. The *ab initio* results (gray pentagons) are from [77]. (b) The VFF model (blue lines) and the SW potential (red lines) give the same phonon dispersion for the p-bismuthene along ΓXSYΓ.

The parameters for the two-body SW potential used by GULP are shown in **Table 371**. The parameters for the three-body SW potential used by GULP are shown in **Table 372**. Parameters for the SW potential used by LAMMPS are listed in **Table 373**. Eight atom types have been introduced for writing the SW potential script used by LAMMPS as shown in **Figure 184**, which helps to increase the cutoff for the bond stretching interaction between atoms like 1 and 2 in **Figure 183(c)**.

	A (eV)	ρ (Å)	B (Å^4)	$r_{\min}$ (Å)	$r_{\max}$ (Å)
r_{12}	1.777	0.109	46.775	0.0	3.401
r_{14}	12.322	1.872	45.998	0.0	4.301

The quantity (r_{ij}) in the first line lists one representative term for the two-body SW potential between atoms i and j. Atom indexes are from **Figure 183(c)**.

Table 371. Two-body SW potential parameters for p-bismuthene used by GULP [8] as expressed in Eq. (3).

	K (eV)	θ_0 (°)	ρ_1 (Å)	ρ_2 (Å)	$r_{\min 12}$ (Å)	$r_{\max 12}$ (Å)	$r_{\min 13}$ (Å)	$r_{\max 13}$ (Å)	$r_{\min 23}$ (Å)	$r_{\max 23}$ (Å)
θ_{123}	2.408	94.018	0.109	0.109	0.0	3.401	0.0	3.401	0.0	4.745
θ_{134}	28.842	86.486	1.872	0.109	0.0	4.301	0.0	3.401	0.0	5.982
θ_{415}	30.388	103.491	1.872	0.109	0.0	4.301	0.0	3.401	0.0	6.473

The first line (θ_{ijk}) presents one representative term for the three-body SW potential. The angle θ_{ijk} has the atom i as the apex. Atom indexes are from **Figure 183(c)**.

Table 372. Three-body SW potential parameters for p-bismuthene used by GULP [8] as expressed in Eq. (4).

	ϵ (eV)	σ (Å)	a	λ	γ	$\cos\theta_0$	A_L	B_L	p	q	Tol
Bi_1—Bi_8—Bi_8	1.000	2.737	1.571	112.813	1.000	−0.070	18.974	1.000	4	0	0.0
Bi_1—Bi_2—Bi_2	1.000	2.808	1.532	0.000	1.000	0.000	19.577	0.888	4	0	0.0
Bi_1—Bi_8—Bi_2	1.000	0.000	0.000	429.598	1.000	0.061	0.000	0.000	4	0	0.0
Bi_2—Bi_3—Bi_1	1.000	0.000	0.000	452.618	1.000	−0.233	0.000	0.000	4	0	0.0

Atom types in the first column are displayed in **Figure 184** with elemental symbol Sb substituted by Bi.

Table 373. SW potential parameters for p-bismuthene used by LAMMPS [9] as expressed in Eqs. (9) and (10).

Figure 188 shows the stress-strain relations for the p-bismuthene of size 100×100 Å. The structure is uniaxially stretched in the armchair or zigzag directions at 1 and 300 K. The Young's modulus is 10.2 and 26.2 N/m in the armchair and zigzag directions, respectively, at 1 K, which is obtained by linear fitting of the stress-strain relations in [0, 0.01]. The Poisson's ratios from the VFF model and the SW potential are $\nu_{xy} = 0.24$ and $\nu_{yx} = 0.61$. These values are very close to the *ab initio* calculations, e.g., $\nu_{xy} = 0.261$ and $\nu_{yx} = 0.648$ in [77]. The third-order nonlinear elastic constant D can be obtained by fitting the stress-strain relation to $\sigma = E\epsilon + \frac{1}{2}D\epsilon^2$ with E as the Young's modulus. The values of D are −12.4 and −86.4 N/m at 1 K along the armchair and zigzag directions, respectively. The ultimate stress is about 2.6 N/m at the critical strain of 0.38 in the armchair direction at the low temperature of 1 K. The ultimate stress is about 3.9 N/m at the critical strain of 0.29 in the zigzag direction at the low temperature of 1 K.

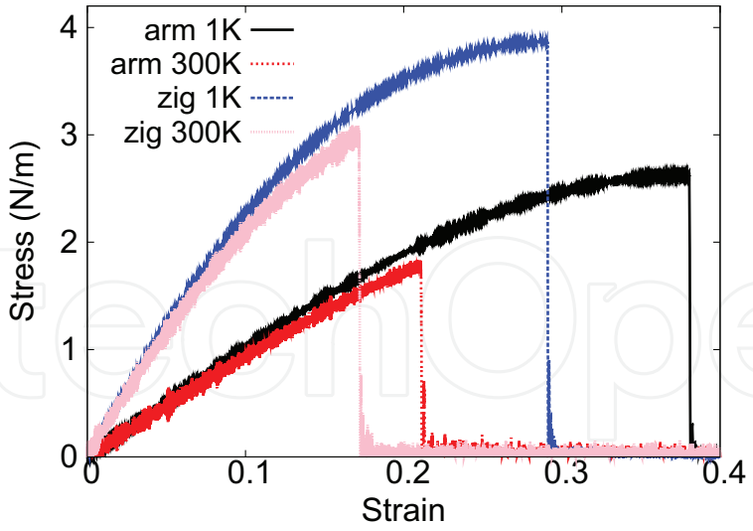

Figure 188. Stress-strain relations for the p-bismuthene of size 100×100 Å. The p-bismuthene is uniaxially stretched along the armchair or zigzag directions at temperatures 1 and 300 K.

94. p-SiO

Present studies on the puckered (p-) SiO are based on first-principles calculations, and no empirical potential has been proposed for the p-SiO. We will thus parametrize the SW potential for the single-layer p-SiO in this section.

The structure of the single-layer p-SiO is shown in **Figure 189**, with M = Si and X = O. Structural parameters for p-SiO are from the *ab initio* calculations [78]. There are four atoms in the unit cell with relative coordinates as $(-u, 0, -v)$, $(u, 0, v)$, $(0.5-u, 0.5, v+w)$, and $(0.5+u, 0.5, -v+w)$ with $u = 0.1501$, $v = 0.0605$, and $w = 0.0800$. The value of these dimensionless parameters are extracted from the geometrical parameters provided in [78], including lattice constants $a_1 = 4.701$ Å and $a_2 = 2.739$ Å, bond lengths $d_{12} = 1.843$ Å and $d_{14} = 2.859$ Å, and the angle $\theta_{145} = 96.0^\circ$. The dimensionless parameters v and w are ratios based on the lattice constant in the out-of-plane z-direction, which are arbitrarily chosen as $a_3 = 10.0$ Å. We note that the main purpose of the usage of u, v, and w in representing atomic coordinates is to follow the same convention for all puckered structures in the present work. The resultant atomic coordinates are the same as that in [78].

As shown in **Figure 189**, a specific feature in the puckered configuration of the p-SiO is that there is a small difference of wa_3 between the z-coordinate of atom 1 and the z-coordinates of atoms 2 and 3. Similarly, atom 4 is higher than atoms 5 and 6 for wa_3 along the z-direction. The sign of w determines which types of atoms take the out-most positions, e.g., atoms 1, 5, and 6 are the out-most atoms if $w > 0$ in **Figure 189(c)**, while atoms 2, 3, and 4 will take the out-most positions for $w < 0$. The p-SiO has a zigzag configuration as shown in **Figure 191**, which is a specific case of the puckered structure shown in **Figure 189**.

Table 374 shows five VFF terms for the single-layer p-SiO; two of which are the bond stretching interactions shown by Eq. (1), while the other three terms are the angle bending

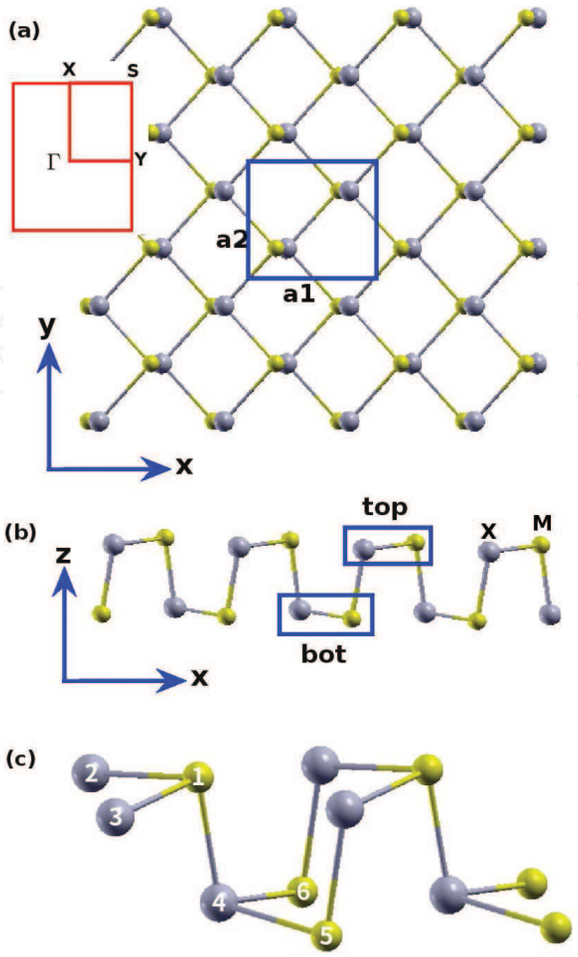

Figure 189. Structure for single-layer p-MX, with M from group IV and X from group VI. (a) Top view. The armchair direction is along the x-axis, while the zigzag direction is along the y-axis. Red inset shows the first Brillouin zone. (b) Side view illustrates the puckered configuration. The pucker is perpendicular to the x-axis and is parallel with the y-axis. (c) Atomic configuration. Atom M (X) is represented by yellow smaller (gray larger) balls.

interaction shown by Eq. (2). The force constant parameters are the same for the two angle bending terms θ_{134} and θ_{415}, which have the same arm lengths. All force constant parameters are determined by fitting to the acoustic branches in the phonon dispersion along the ΓX as shown in **Figure 192(a)**. The *ab initio* calculations for the phonon dispersion are calculated from the SIESTA package [79]. The generalized gradients approximation is applied to account for the exchange-correlation function with Perdew, Burke, and Ernzerhof parameterization [80], and the double-ζ orbital basis set is adopted. **Figure 192(b)** shows that the VFF model and the SW potential give exactly the same phonon dispersion.

The parameters for the two-body SW potential used by GULP are shown in **Table 375**. The parameters for the three-body SW potential used by GULP are shown in **Table 376**. Parameters for the SW potential used by LAMMPS are listed in **Table 377**.

Figure 193 shows the stress-strain relations for the single-layer p-SiO of size 100 × 100 Å. The structure is uniaxially stretched in the armchair or zigzag directions at 1 and 300 K. The structure of p-SiO is so soft along the armchair direction that the Young's modulus is almost

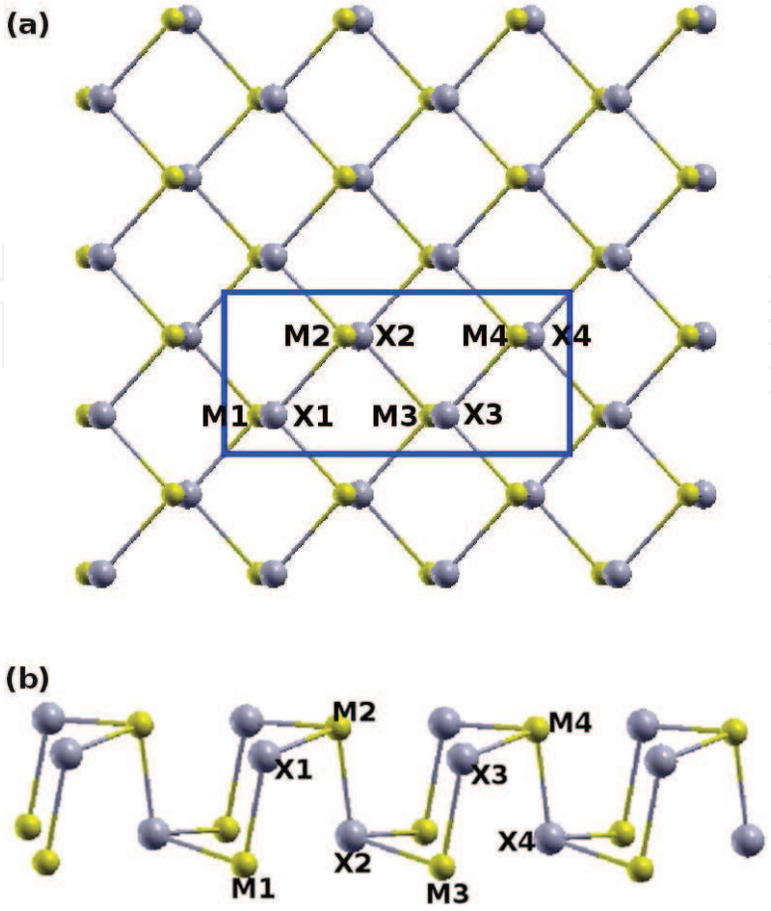

Figure 190. Eight atom types are introduced for atoms in the p-MX, with M from group IV and X from group VI. (a) Top view and (b) side view.

zero in the armchair direction. The Young's modulus is 81.3 N/m in the zigzag direction at 1 K, which is obtained by linear fitting of the stress-strain relations in [0, 0.01]. The third-order nonlinear elastic constant D can be obtained by fitting the stress-strain relation to $\sigma = E\epsilon + \frac{1}{2}D\epsilon^2$ with E as the Young's modulus. The value of D is -432.4 N/m at 1 K along the zigzag direction. The ultimate stress is about 5.3 N/m at the critical strain of 0.29 in the armchair direction at the low temperature of 1 K. The ultimate stress is about 7.8 N/m at the critical strain of 0.23 in the zigzag direction at the low temperature of 1 K.

95. P-GeO

Present studies on the puckered (p-) GeO are based on first-principles calculations, and no empirical potential has been proposed for the p-GeO. We will thus parametrize the SW potential for the single-layer p-GeO in this section.

The structure of the single-layer p-GeO is shown in **Figure 189**, with M=Ge and X=O. Structural parameters for p-GeO are from the *ab initio* calculations [78]. There are four atoms in the

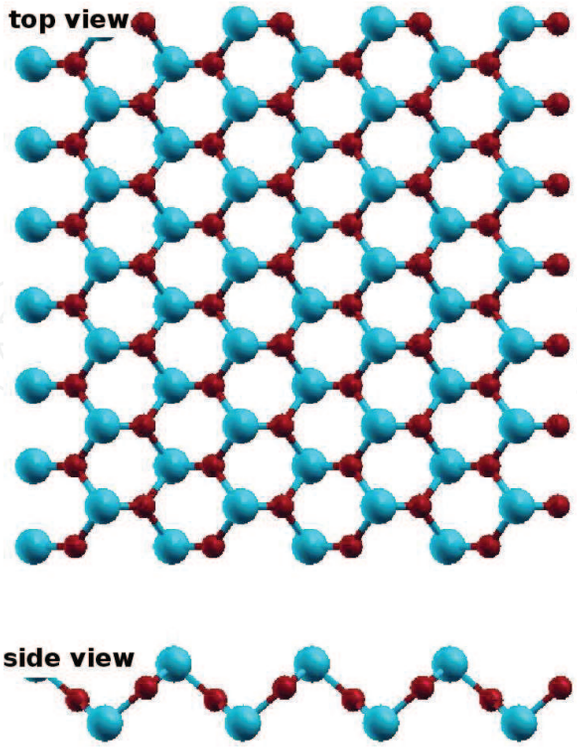

Figure 191. Zigzag configuration of single-layer p-MX, with M from group IV and X = O. Atom M (O) is represented by purple larger (red smaller) balls.

VFF type	**Bond stretching**		**Angle bending**		
Expression	$\frac{1}{2}K_{12}(\Delta r_{12})^2$	$\frac{1}{2}K_{14}(\Delta r_{14})^2$	$\frac{1}{2}K_{123}(\Delta\theta_{123})^2$	$\frac{1}{2}K_{134}(\Delta\theta_{134})^2$	$\frac{1}{2}K_{415}(\Delta\theta_{415})^2$
Parameter	12.191	12.191	4.817	3.123	3.123
r_0 or θ_0	1.843	1.859	95.989	96.000	132.005

The second line gives an explicit expression for each VFF term, where atom indexes are from **Figure 189(c)**. The third line is the force constant parameters. Parameters are in the unit of eV/Å^2 for the bond stretching interaction and in the unit of eV for the angle bending interaction. The fourth line gives the initial bond length (in the unit of Å) for the bond stretching interaction and the initial angle (in the unit of degrees) for the angle bending interaction. The angle θ_{ijk} has atom i as the apex.

Table 374. The VFF model for the single-layer p-SiO.

	A **(eV)**	ρ **(Å)**	B **(Å^4)**	$r_{\min}$ **(Å)**	$r_{\max}$ **(Å)**
r_{12}	19.127	2.720	5.769	0.0	2.962
r_{14}	7.105	1.133	5.972	0.0	2.585

The quantity (r_{ij}) in the first line lists one representative term for the two-body SW potential between atoms i and j. Atom indexes are from **Figure 189(c)**.

Table 375. Two-body SW potential parameters for the single-layer p-SiO used by GULP [8] as expressed in Eq. (3).

	K (eV)	θ_0 (°)	ρ_1 (Å)	ρ_2 (Å)	$r_{\min 12}$ (Å)	$r_{\max 12}$ (Å)	$r_{\min 13}$ (Å)	$r_{\max 13}$ (Å)	$r_{\min 23}$ (Å)	$r_{\max 23}$ (Å)
θ_{123}	314.008	95.989	2.720	2.720	0.0	2.962	0.0	2.962	0.0	3.720
θ_{134}	85.406	96.000	1.133	2.720	0.0	2.585	0.0	2.962	0.0	3.875
θ_{415}	152.982	132.005	1.133	2.720	0.0	2.585	0.0	2.962	0.0	4.194

The first line (θ_{ijk}) presents one representative term for the three-body SW potential. The angle θ_{ijk} has the atom i as the apex. Atom indexes are from **Figure 189(c)**.

Table 376. Three-body SW potential parameters for the single-layer p-SiO used by GULP [8] as expressed in Eq. (4).

	ϵ (eV)	σ (Å)	a	λ	γ	$\cos\theta_0$	A_L	B_L	p	q	Tol
Sn_1—O_2—O_2	1.000	2.720	1.089	314.008	1.000	−0.104	19.127	0.105	4	0	0.0
Sn_1—O_1—O_1	1.000	1.133	2.282	0.000	1.000	0.000	7.105	3.630	4	0	0.0
Sn_1—O_1—O_2	1.000	0.000	0.000	85.406	1.000	−0.105	0.000	0.000	4	0	0.0
O_1—Sn_1—Sn_2	1.000	0.000	0.000	152.982	1.000	−0.669	0.000	0.000	4	0	0.0

Atom types in the first column are displayed in **Figure 190**, with M=Si and X=O.

Table 377. SW potential parameters for p-SiO used by LAMMPS [9], as expressed in Eqs. (9) and (10).

unit cell with relative coordinates such as $(-u, 0, -v)$, $(u, 0, v)$, $(0.5-u, 0.5, v+w)$, and $(0.5+u, 0.5, -v+w)$ with $u = 0.1622$, $v = 0.0616$, and $w = 0.0884$. The values of these dimensionless parameters are extracted from the geometrical parameters provided in Ref. [78], including lattice constants $a_1 = 4.801$ Å and $a_2 = 3.055$ Å, bond lengths $d_{12} = 1.956$ Å and $d_{14} = 1.986$ Å, and the angle $\theta_{145} = 93.3°$. The dimensionless parameters v and w are ratios based on the lattice constant in the out-of-plane z-direction, which is arbitrarily chosen as $a_3 = 10.0$ Å. We note that the main purpose of the usage of u, v, and w in representing atomic coordinates is to follow the same convention for all puckered structures in the present work. The resultant atomic coordinates are the same as that in Ref. [78].

As shown in **Figure 189**, a specific feature in the puckered configuration of the p-GeO is that there is a small difference of wa_3 between the z-coordinate of atom 1 and the z-coordinates of atoms 2 and 3. Similarly, atom 4 is higher than atoms 5 and 6 for wa_3 along the z-direction. The sign of w determines which types of atoms take the outmost positions, e.g., atoms 1, 5, and 6 are the outmost atoms if $w > 0$ in **Figure 189(c)**, while atoms 2, 3, and 4 will take the outmost positions for $w < 0$. The p-GeO has a zigzag configuration as shown in **Figure 191**, which is a specific case of the puckered structure shown in **Figure 189**.

Table 378 shows five VFF terms for the single-layer p-GeO; two of which are the bond stretching interactions shown in Eq. (1), while the other three terms are the angle bending interaction shown in Eq. (2). The force constant parameters are the same for the two angle bending terms θ_{134} and θ_{415}, which have the same arm lengths. All force constant parameters are determined by fitting to the acoustic branches in the phonon dispersion along the ΓX as

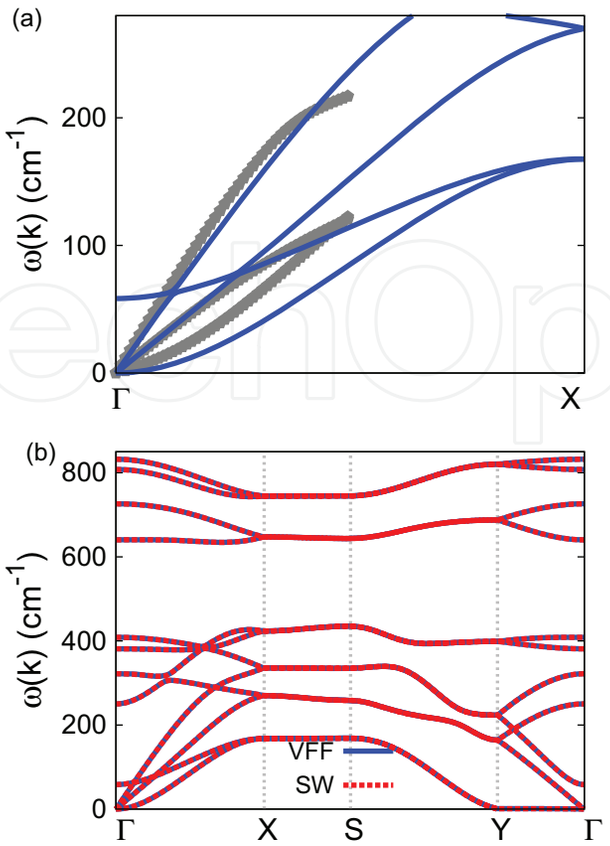

Figure 192. Phonon dispersion for the single-layer p-SiO. (a) The VFF model is fitted to the acoustic branches in the long wave limit along the ΓX direction. The *ab initio* calculations are calculated from SIESTA. (b) The VFF model (blue lines) and the SW potential (red lines) give the same phonon dispersion for the p-SiO along ΓXSYΓ.

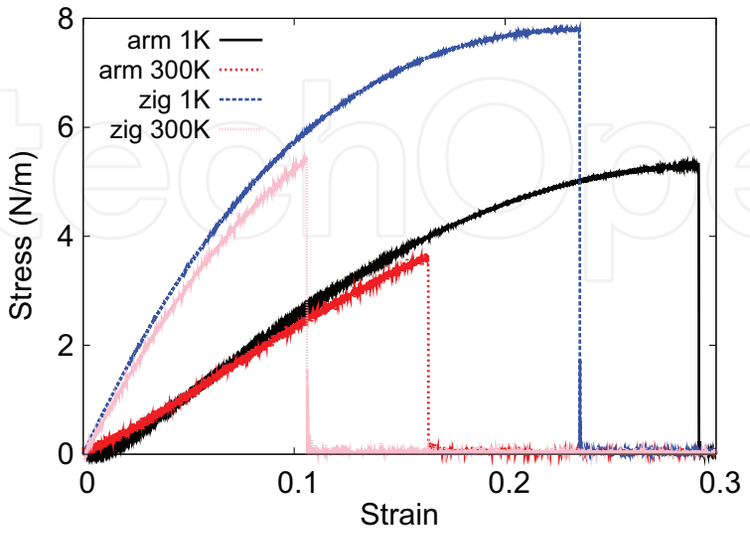

Figure 193. Stress-strain relations for the single-layer p-SiO of size 100 × 100 Å. The single-layer p-SiO is uniaxially stretched along the armchair or zigzag directions at temperatures 1 and 300 K.

VFF type	Bond stretching	Angle bending			
Expression	$\frac{1}{2}K_{12}(\Delta r_{12})^2$	$\frac{1}{2}K_{14}(\Delta r_{14})^2$	$\frac{1}{2}K_{123}(\Delta\theta_{123})^2$	$\frac{1}{2}K_{134}(\Delta\theta_{134})^2$	$\frac{1}{2}K_{415}(\Delta\theta_{415})^2$
Parameter	12.191	12.191	4.817	3.123	3.123
r_0 or θ_0	1.956	1.986	102.692	93.300	128.213

The second line gives an explicit expression for each VFF term, where atom indexes are from **Figure 189(c)**. The third line is the force constant parameters. Parameters are in the unit of eV/Å^2 for the bond stretching interaction and in the unit of eV for the angle bending interaction. The fourth line gives the initial bond length (in the unit of Å) for the bond stretching interaction and the initial angle (in the unit of degrees) for the angle bending interaction. The angle θ_{ijk} has atom i as the apex.

Table 378. The VFF model for the single-layer p-GeO.

shown in **Figure 194(a)**. The *ab initio* calculations for the phonon dispersion are calculated from the SIESTA package [79]. The generalized gradients approximation is applied to account for the exchange-correlation function with Perdew, Burke, and Ernzerhof parameterization [80], and the double-ζ orbital basis set is adopted. **Figure 194(b)** shows that the VFF model and the SW potential give exactly the same phonon dispersion.

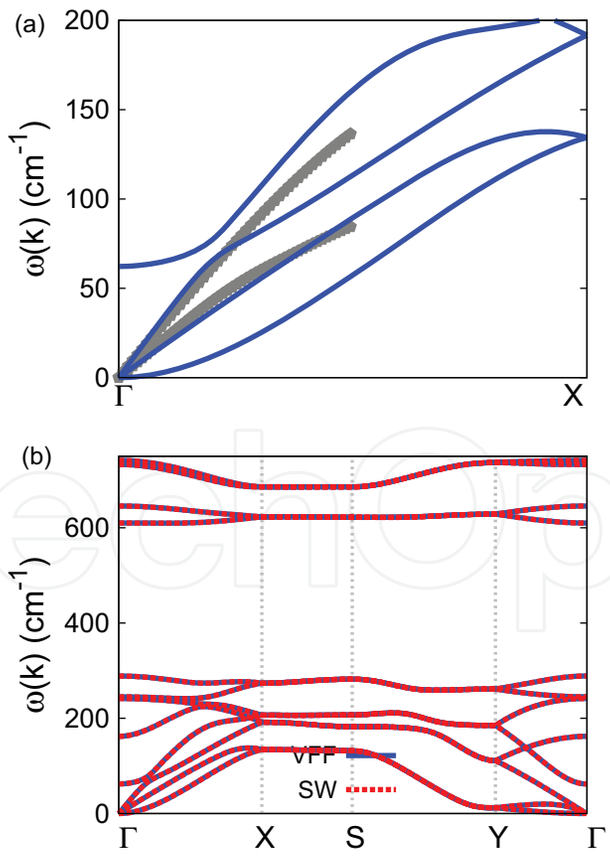

Figure 194. Phonon dispersion for the single-layer p-GeO. (a) The VFF model is fitted to the acoustic branches in the long wave limit along the ΓX direction. The *ab initio* calculations are calculated from SIESTA. (b) The VFF model (blue lines) and the SW potential (red lines) give the same phonon dispersion for the p-GeO along ΓXSYΓ.

The parameters for the two-body SW potential used by GULP are shown in **Table 379**. The parameters for the three-body SW potential used by GULP are shown in **Table 380**. Parameters for the SW potential used by LAMMPS are listed in **Table 381**.

Figure 195 shows the stress-strain relations for the single-layer p-GeO of size 100 × 100 Å. The structure is uniaxially stretched in the armchair or zigzag directions at 1 and 300 K. The structure of p-GeO is so soft along the armchair direction that the Young's modulus is almost zero in the armchair direction. The Young's modulus is 14.5 and 78.9 N/m in the armchair and zigzag directions at 1 K, which are obtained by linear fitting of the stress-strain relations in [0, 0.01]. The Poisson's ratios from the VFF model and the SW potential are $\nu_{xy} = 0.09$ and $\nu_{yx} = 0.65$. The third-order nonlinear elastic constant D can be obtained by fitting the stress-strain relation to $\sigma = E\epsilon + \frac{1}{2}D\epsilon^2$ with E as the Young's modulus. The values of D are 22.0 and −383.3 N/m at 1 K along the armchair and zigzag directions, respectively. The ultimate stress is about 4.8 N/m at the critical strain of 0.32 in the armchair direction at the low temperature of 1 K.

	A (eV)	ρ (Å)	B (Å^4)	$r_{\min}$ (Å)	$r_{\max}$ (Å)
r_{12}	21.562	2.889	7.319	0.0	3.144
r_{14}	9.258	1.384	7.778	0.0	2.815

The quantity (r_{ij}) in the first line lists one representative term for the two-body SW potential between atoms i and j. Atom indexes are from **Figure 189(c)**.

Table 379. Two-body SW potential parameters for the single-layer p-GeO used by GULP [8], as expressed in Eq. (3).

	K (eV)	θ_0 (°)	ρ_1 (Å)	ρ_2 (Å)	$r_{\min 12}$ (Å)	$r_{\max 12}$ (Å)	$r_{\min 13}$ (Å)	$r_{\max 13}$ (Å)	$r_{\min 23}$ (Å)	$r_{\max 23}$ (Å)
θ_{123}	326.824	102.692	2.889	2.889	0.0	3.144	0.0	3.144	0.0	3.928
θ_{134}	94.550	93.300	1.384	2.889	0.0	2.815	0.0	3.144	0.0	3.933
θ_{415}	152.646	128.213	1.384	2.889	0.0	2.815	0.0	3.144	0.0	4.284

The first line (θ_{ijk}) presents one representative term for the three-body SW potential. The angle θ_{ijk} has the atom i as the apex. Atom indexes are from **Figure 189(c)**.

Table 380. Three-body SW potential parameters for the single-layer p-GeO used by GULP [8], as expressed in Eq. (4).

	ϵ (eV)	σ (Å)	a	λ	γ	$\cos\theta_0$	A_L	B_L	p	q	Tol
Ge_1—O_2—O_2	1.000	2.889	1.089	326.824	1.000	−0.220	21.562	0.105	4	0	0.0
Ge_1—O_1—O_1	1.000	1.384	2.034	0.000	1.000	0.000	9.258	2.119	4	0	0.0
Ge_1—O_1—O_2	1.000	0.000	0.000	94.550	1.000	−0.058	0.000	0.000	4	0	0.0
O_1—Ge_1—Ge_2	1.000	0.000	0.000	152.646	1.000	−0.619	0.000	0.000	4	0	0.0

Atom types in the first column are displayed in **Figure 190**, with M = Ge and X = O.

Table 381. SW potential parameters for p-GeO used by LAMMPS [9], as expressed in Eqs. (9) and (10).

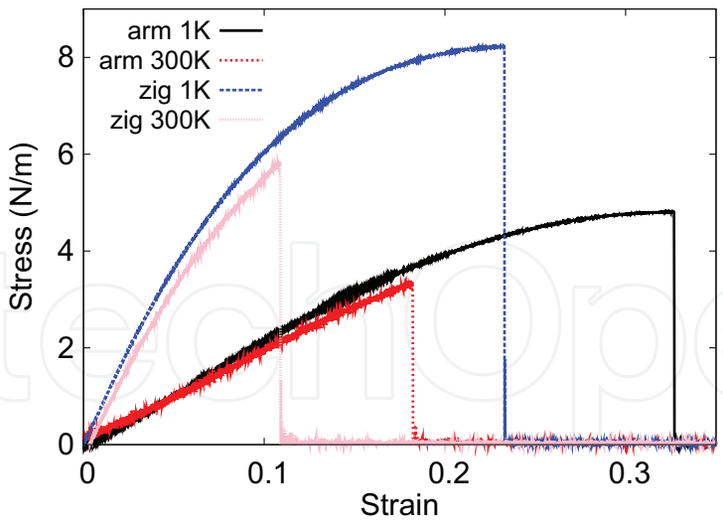

Figure 195. Stress-strain relations for the single-layer p-GeO of size 100 × 100 Å. The single-layer p-GeO is uniaxially stretched along the armchair or zigzag directions at temperatures 1 and 300 K.

The ultimate stress is about 8.2 N/m at the critical strain of 0.23 in the zigzag direction at the low temperature of 1 K.

96. P-SnO

Present studies on the puckered (p-) SnO are based on first-principles calculations, and no empirical potential has been proposed for the p-SnO. We will thus parametrize the SW potential for the single-layer p-SnO in this section.

The structure of the single-layer p-SnO is shown in **Figure 189**, with M = Sn and X = O. Structural parameters for p-SnO are from the *ab initio* calculations [78]. There are four atoms in the unit cell with relative coordinates such as $(-u, 0, -v)$, $(u, 0, v)$, $(0.5 - u, 0.5, v + w)$, and $(0.5 + u, 0.5, -v + w)$ with $u = 0.1485$, $v = 0.0818$, and $w = 0.0836$. The values of these dimensionless parameters are extracted from the geometrical parameters provided in Ref. [78], including lattice constants $a_1 = 4.764$ Å and $a_2 = 3.400$ Å, bond lengths $d_{12} = 2.127$ Å and $d_{14} = 2.163$ Å, and the angle $\theta_{145} = 90.0^\circ$. The dimensionless parameters v and w are ratios based on the lattice constant in the out-of-plane z-direction, which is arbitrarily chosen as $a_3 = 10.0$ Å. We note that the main purpose of the usage of u, v, and w in representing atomic coordinates is to follow the same convention for all puckered structures in the present work. The resultant atomic coordinates are the same as that in Ref. [78].

As shown in **Figure 189**, a specific feature in the puckered configuration of the p-SnO is that there is a small difference of wa_3 between the z-coordinate of atom 1 and the z-coordinates of atoms 2 and 3. Similarly, atom 4 is higher than atoms 5 and 6 for wa_3 along the z-direction. The sign of w determines which types of atoms take the outmost positions, e.g., atoms 1, 5, and 6 are the outmost atoms if $w > 0$ in **Figure 189(c)**, while atoms 2, 3, and 4 will take the outmost

positions for $w < 0$. The p-SnO has a zigzag configuration as shown in **Figure 191**, which is a specific case of the puckered structure shown in **Figure 189**.

Table 382 shows five VFF terms for the single-layer p-SnO; two of which are the bond stretching interactions shown in Eq. (1), while the other three terms are the angle bending interaction shown in Eq. (2). The force constant parameters are the same for the two angle

VFF type	**Bond stretching**	**Angle bending**		
Expression	$\frac{1}{2}K_{12}(\Delta r_{12})^2$	$\frac{1}{2}K_{14}(\Delta r_{14})^2$	$\frac{1}{2}K_{123}(\Delta\theta_{123})^2$	$\frac{1}{2}K_{134}(\Delta\theta_{134})^2$	$\frac{1}{2}K_{415}(\Delta\theta_{415})^2$
Parameter	9.208	9.208	2.835	3.023	3.023
r_0 or θ_0	2.127	2.163	106.117	90.000	126.496

The second line gives an explicit expression for each VFF term, where atom indexes are from **Figure 189(c)**. The third line is the force constant parameters. Parameters are in the unit of eV/Å^2 for the bond stretching interaction and in the unit of eV for the angle bending interaction. The fourth line gives the initial bond length (in the unit of Å) for the bond stretching interaction and the initial angle (in the unit of degrees) for the angle bending interaction. The angle θ_{ijk} has atom i as the apex.

Table 382. The VFF model for the single-layer p-SnO.

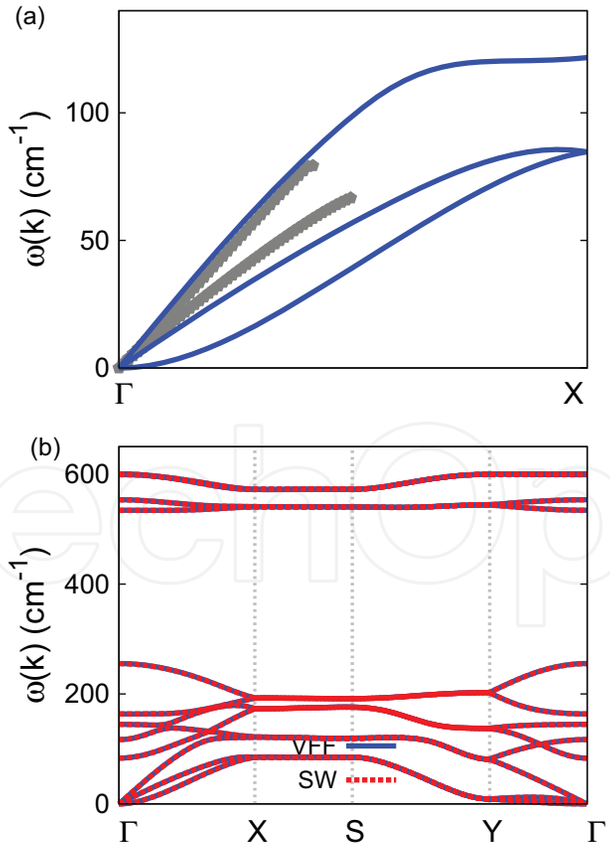

Figure 196. Phonon dispersion for the single-layer p-SnO. (a) The VFF model is fitted to the acoustic branches in the long wave limit along the ΓX direction. The *ab initio* calculations are calculated from SIESTA. (b) The VFF model (blue lines) and the SW potential (red lines) give the same phonon dispersion for the p-SnO along ΓXSYΓ.

bending terms θ_{134} and θ_{415}, which have the same arm lengths. All force constant parameters are determined by fitting to the acoustic branches in the phonon dispersion along the ΓX as shown in **Figure 196(a)**. The *ab initio* calculations for the phonon dispersion are calculated from the SIESTA package [79]. The generalized gradients approximation is applied to account for the exchange-correlation function with Perdew, Burke, and Ernzerhof parameterization [80], and the double-ζ orbital basis set is adopted. **Figure 196(b)** shows that the VFF model and the SW potential give exactly the same phonon dispersion.

The parameters for the two-body SW potential used by GULP are shown in **Table 383**. The parameters for the three-body SW potential used by GULP are shown in **Table 384**. Parameters for the SW potential used by LAMMPS are listed in **Table 385**.

Figure 197 shows the stress-strain relations for the single-layer p-SnO of size 100 × 100 Å. The structure is uniaxially stretched in the armchair or zigzag directions at 1 and 300 K. The structure of p-SnO is so soft along the armchair direction that the Young's modulus is almost

	A (eV)	ρ (Å)	B (Å^4)	$r_{\min}$ (Å)	$r_{\max}$ (Å)
r_{12}	11.711	2.107	10.234	0.0	3.185
r_{14}	8.879	1.612	10.945	0.0	3.096

The quantity (r_{ij}) in the first line lists one representative term for the two-body SW potential between atoms i and j. Atom indexes are from **Figure 189(c)**.

Table 383. Two-body SW potential parameters for the single-layer p-SnO used by GULP [8], as expressed in Eq. (3).

	K (eV)	θ_0 (°)	ρ_1 (Å)	ρ_2 (Å)	$r_{\min 12}$ (Å)	$r_{\max 12}$ (Å)	$r_{\min 13}$ (Å)	$r_{\max 13}$ (Å)	$r_{\min 23}$ (Å)	$r_{\max 23}$ (Å)
θ_{123}	82.293	106.117	2.107	2.107	0.0	3.185	0.0	3.185	0.0	4.082
θ_{134}	62.178	90.000	1.612	2.107	0.0	3.096	0.0	3.185	0.0	4.017
θ_{415}	96.214	126.496	1.612	2.107	0.0	3.096	0.0	3.185	0.0	4.426

The first line (θ_{ijk}) presents one representative term for the three-body SW potential. The angle θ_{ijk} has the atom i as the apex. Atom indexes are from **Figure 189(c)**.

Table 384. Three-body SW potential parameters for the single-layer p-SnO used by GULP [8], as expressed in Eq. (4).

	ϵ (eV)	σ (Å)	a	λ	γ	$\cos\theta_0$	A_L	B_L	p	q	Tol
Sn_1—O_2—O_2	1.000	2.107	1.512	82.293	1.000	−0.278	11.711	0.519	4	0	0.0
Sn_1—O_1—O_1	1.000	1.612	1.921	0.000	1.000	0.000	8.879	1.623	4	0	0.0
Sn_1—O_1—O_2	1.000	0.000	0.000	62.178	1.000	0.000	0.000	0.000	4	0	0.0
O_1—Sn_1—Sn_2	1.000	0.000	0.000	96.214	1.000	−0.595	0.000	0.000	4	0	0.0

Atom types in the first column are displayed in **Figure 190**, with M=Sn and X=O.

Table 385. SW potential parameters for p-SnO used by LAMMPS [9], as expressed in Eqs. (9) and (10).

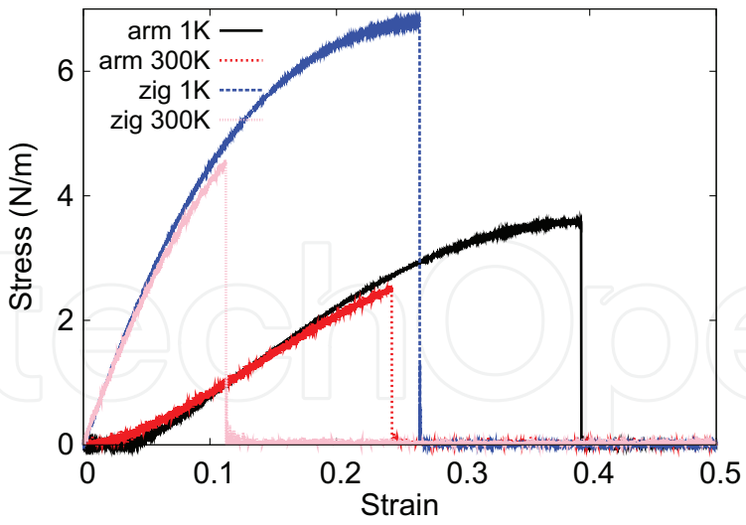

Figure 197. Stress-strain relations for the single-layer p-SnO of size 100 × 100 Å. The single-layer p-SnO is uniaxially stretched along the armchair or zigzag directions at temperatures 1 and 300 K.

zero in the armchair direction. The Young's modulus is 52.8 N/m in the zigzag direction at 1 K, which is obtained by linear fitting of the stress-strain relations in [0, 0.01]. The third-order nonlinear elastic constant D can be obtained by fitting the stress-strain relation to $\sigma = E\epsilon + \frac{1}{2}D\epsilon^2$ with E as the Young's modulus. The value of D is −204.5 N/m at 1 K along the zigzag direction. The ultimate stress is about 3.8 N/m at the critical strain of 0.38 in the armchair direction at the low temperature of 1 K. The ultimate stress is about 6.8 N/m at the critical strain of 0.26 in the zigzag direction at the low temperature of 1 K.

97. P-CS

Present studies on the puckered (p-) CS are based on first-principles calculations, and no empirical potential has been proposed for the p-CS. We will thus parametrize the SW potential for the single-layer p-CS in this section.

The structure of the single-layer p-CS is shown in **Figure 189**, with M = C and X = S. Structural parameters for p-CS are from the *ab initio* calculations [78]. There are four atoms in the unit cell with relative coordinates such as $(-u, 0, -v)$, $(u, 0, v)$, $(0.5-u, 0.5, v+w)$, and $(0.5+u, 0.5, -v+w)$ with $u = 0.1302$, $v = 0.0733$, and $w = -0.0248$. The values of these dimensionless parameters are extracted from the geometrical parameters provided in Ref. [78], including lattice constants $a_1 = 4.323$ Å and $a_2 = 2.795$ Å, bond lengths $d_{12} = 1.757$ Å and $d_{14} = 1.849$ Å, and the angle $\theta_{145} = 118.1^\circ$. The dimensionless parameters v and w are ratios based on the lattice constant in the out-of-plane z-direction, which is arbitrarily chosen as $a_3 = 10.0$ Å. We note that the main purpose of the usage of u, v, and w in representing atomic coordinates is to follow the same convention for all puckered structures in the present work. The resultant atomic coordinates are the same as that in Ref. [78].

As shown in **Figure 189**, a specific feature in the puckered configuration of the p-CS is that there is a small difference of wa_3 between the z-coordinate of atom 1 and the z-coordinates of atoms 2 and 3. Similarly, atom 4 is higher than atoms 5 and 6 for wa_3 along the z-direction. The sign of w determines which types of atoms take the outmost positions, e.g., atoms 1, 5, and 6 are the outmost atoms if $w > 0$ in **Figure 189(c)**, while atoms 2, 3, and 4 will take the outmost positions for $w < 0$.

Table 386 shows five VFF terms for the single-layer p-CS; two of which are the bond stretching interactions shown in Eq. (1), while the other three terms are the angle bending interaction shown in Eq. (2). The force constant parameters are the same for the two angle bending terms θ_{134} and θ_{415}, which have the same arm lengths. All force constant parameters are determined by fitting to the acoustic branches in the phonon dispersion along the ΓX as shown in **Figure 198(a)**. The *ab initio* calculations for the phonon dispersion are calculated from the SIESTA package [79]. The generalized gradients approximation is applied to account for the exchange-correlation function with Perdew, Burke, and Ernzerhof parameterization [80], and the double-ζ orbital basis set is adopted. **Figure 198(b)** shows that the VFF model and the SW potential give exactly the same phonon dispersion.

The parameters for the two-body SW potential used by GULP are shown in **Table 387**. The parameters for the three-body SW potential used by GULP are shown in **Table 388**. Parameters for the SW potential used by LAMMPS are listed in **Table 389**.

Figure 199 shows the stress-strain relations for the single-layer p-CS of size 100 × 100 Å. The structure is uniaxially stretched in the armchair or zigzag directions at 1 and 300 K. There is a structural transition around 0.16 at 1 K, where the C atom is twisted. The Young's modulus is 16.2 and 70.5 N/m in the armchair and zigzag directions, respectively, at 1 K, which is obtained by linear fitting of the stress-strain relations in [0, 0.01]. The Poisson's ratios from the VFF model and the SW potential are $\nu_{xy} = -0.06$ and $\nu_{yx} = -0.27$. The third-order nonlinear elastic constant D can be obtained by fitting the stress-strain relation to $\sigma = E\epsilon + \frac{1}{2}D\epsilon^2$ with E as the Young's modulus. The values of D are −27.3 and −447.2 N/m at 1 K along the armchair and zigzag directions, respectively. The ultimate stress is about 4.3 N/m at the critical strain of 0.38 in the armchair direction at the low temperature of 1 K. The ultimate stress is about 5.2 N/m at the critical strain of 0.22 in the zigzag direction at the low temperature of 1 K.

VFF type	**Bond stretching**	**Angle bending**			
Expression	$\frac{1}{2}K_{12}(\Delta r_{12})^2$	$\frac{1}{2}K_{14}(\Delta r_{14})^2$	$\frac{1}{2}K_{123}(\Delta\theta_{123})^2$	$\frac{1}{2}K_{134}(\Delta\theta_{134})^2$	$\frac{1}{2}K_{415}(\Delta\theta_{415})^2$
Parameter	9.291	9.291	3.933	3.075	3.075
r_0 or θ_0	1.757	1.849	105.384	118.100	104.288

The second line gives an explicit expression for each VFF term, where atom indexes are from **Figure 189(c)**. The third line is the force constant parameters. Parameters are in the unit of eV/Å^2 for the bond stretching interaction and in the unit of eV for the angle bending interaction. The fourth line gives the initial bond length (in the unit of Å) for the bond stretching interaction and the initial angle (in the unit of degrees) for the angle bending interaction. The angle θ_{ijk} has atom i as the apex.

Table 386. The VFF model for the single-layer p-CS.

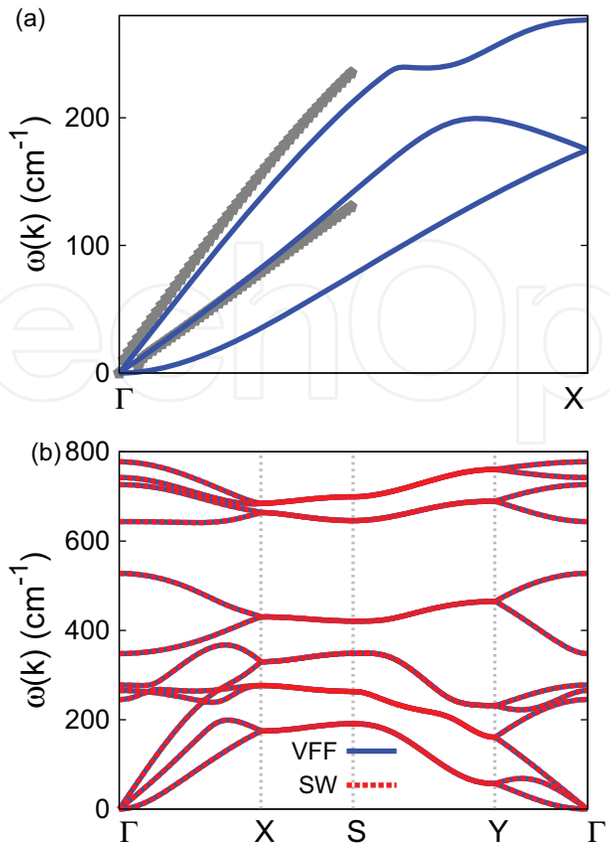

Figure 198. Phonon dispersion for the single-layer p-CS. (a) The VFF model is fitted to the acoustic branches in the long wave limit along the ΓX direction. The *ab initio* calculations are calculated from SIESTA. (b) The VFF model (blue lines) and the SW potential (red lines) give the same phonon dispersion for the p-CS along ΓXSYΓ.

	A (eV)	ρ (Å)	B (Å^4)	r_{min} (Å)	r_{max} (Å)
r_{12}	8.898	1.894	4.765	0.0	2.669
r_{14}	5.791	1.220	5.844	0.0	2.600

The quantity (r_{ij}) in the first line lists one representative term for the two-body SW potential between atoms i and j. Atom indexes are from **Figure 189(c)**.

Table 387. Two-body SW potential parameters for the single-layer p-CS used by GULP [8], as expressed in Eq. (3).

	K (eV)	θ_0 (°)	ρ_1 (Å)	ρ_2 (Å)	$r_{min\,12}$ (Å)	r_{max12} (Å)	$r_{min\,13}$ (Å)	$r_{max\,13}$ (Å)	$r_{min\,23}$ (Å)	$r_{max\,23}$ (Å)
θ_{123}	134.527	105.384	1.894	1.894	0.0	2.669	0.0	2.669	0.0	3.559
θ_{134}	79.992	118.100	1.220	1.894	0.0	2.600	0.0	2.669	0.0	4.046
θ_{415}	66.283	104.288	1.220	1.894	0.0	2.600	0.0	2.669	0.0	3.921

The first line (θ_{ijk}) presents one representative term for the three-body SW potential. The angle θ_{ijk} has the atom i as the apex. Atom indexes are from **Figure 189(c)**.

Table 388. Three-body SW potential parameters for the single-layer p-CS used by GULP [8], as expressed in Eq. (4).

	ϵ (eV)	σ (Å)	a	λ	γ	$\cos\theta_0$	A_L	B_L	p	q	Tol
C_1—S_2—S_2	1.000	1.894	1.410	134.527	1.000	−0.265	8.898	0.371	4	0	0.0
C_1—S_1—S_1	1.000	1.220	2.131	0.000	1.000	0.000	5.791	2.637	4	0	0.0
C_1—S_1—S_2	1.000	0.000	0.000	79.992	1.000	−0.471	0.000	0.000	4	0	0.0
S_1—C_1—C_2	1.000	0.000	0.000	66.283	1.000	−0.247	0.000	0.000	4	0	0.0

Atom types in the first column are displayed in **Figure 190**, with M=C and X=S.

Table 389. SW potential parameters for p-CS used by LAMMPS [9], as expressed in Eqs. (9) and (10)

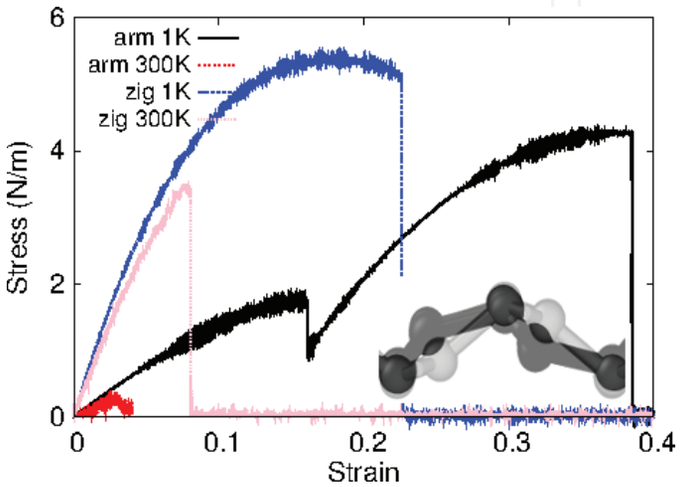

Figure 199. Stress-strain relations for the single-layer p-CS of size 100×100 Å. The single-layer p-CS is uniaxially stretched along the armchair or zigzag directions at temperatures 1 and 300 K. Inset shows the structure before (light) and after (dark) the structural transition around 0.16.

98. P-SiS

Present studies on the puckered (p-) SiS are based on first-principles calculations, and no empirical potential has been proposed for the p-SiS. We will thus parametrize the SW potential for the single-layer p-SiS in this section.

The structure of the single-layer p-SiS is shown in **Figure 189**, with M = Si and X = S. Structural parameters for p-SiS are from the *ab initio* calculations [78]. There are four atoms in the unit cell with relative coordinates such as $(-u, 0, -v)$, $(u, 0, v)$, $(0.5-u, 0.5, v+w)$, and $(0.5+u, 0.5, -v+w)$ with $u = 0.0884$, $v = 0.1093$, and $w = 0.0316$. The values of these dimensionless parameters are extracted from the geometrical parameters provided in Ref. [78], including lattice constants $a_1 = 4.774$ Å and $a_2 = 3.352$ Å, bond lengths $d_{12} = 2.300$ Å and $d_{14} = 2.344$ Å, and the angle $\theta_{145} = 96.5^\circ$. The dimensionless parameters v and w are ratios based on the lattice constant in the out-of-plane z-direction, which is arbitrarily chosen as $a_3 = 10.0$ Å. We note that the main purpose of the usage of u, v, and w in representing atomic coordinates is to follow the same convention for all puckered structures in the present work. The resultant atomic coordinates are the same as that in Ref. [78].

As shown in **Figure 189**, a specific feature in the puckered configuration of the p-SiS is that there is a small difference of wa_3 between the z-coordinate of atom 1 and the z-coordinates of atoms 2 and 3. Similarly, atom 4 is higher than atoms 5 and 6 for wa_3 along the z-direction. The sign of w determines which types of atoms take the outmost positions, e.g., atoms 1, 5, and 6 are the outmost atoms if $w > 0$ in **Figure 189(c)**, while atoms 2, 3, and 4 will take the outmost positions for $w < 0$.

Table 390 shows five VFF terms for the single-layer p-SiS; two of which are the bond stretching interactions shown in Eq. (1), while the other three terms are the angle bending interaction shown in Eq. (2). The force constant parameters are the same for the two angle bending terms θ_{134} and θ_{415}, which have the same arm lengths. All force constant parameters are determined by fitting to the acoustic branches in the phonon dispersion along the ΓX as shown in **Figure 200(a)**. The *ab initio* calculations for the phonon dispersion are calculated from the SIESTA package [79]. The generalized gradients approximation is applied to account for the exchange-correlation function with Perdew, Burke, and Ernzerhof parameterization [80], and the double-ζ orbital basis set is adopted. **Figure 200(b)** shows that the VFF model and the SW potential give exactly the same phonon dispersion.

The parameters for the two-body SW potential used by GULP are shown in **Table 391**. The parameters for the three-body SW potential used by GULP are shown in **Table 392**. Parameters for the SW potential used by LAMMPS are listed in **Table 393**.

Figure 201 shows the stress-strain relations for the single-layer p-SiS of size 100 × 100 Å. The structure is uniaxially stretched in the armchair or zigzag directions at 1 and 300 K. The Young's modulus is 10.9 and 34.8 N/m in the armchair and zigzag directions, respectively, at 1 K, which is obtained by linear fitting of the stress-strain relations in [0, 0.01]. The Poisson's ratios from the VFF model and the SW potential are $\nu_{xy} = 0.04$ and $\nu_{yx} = 0.12$. The third-order nonlinear elastic constant D can be obtained by fitting the stress-strain relation to $\sigma = E\epsilon + \frac{1}{2}D\epsilon^2$ with E as the Young's modulus. The values of D are −24.1 and −145.2 N/m at 1 K along the armchair and zigzag directions, respectively. The ultimate stress is about 2.3 N/m at the critical strain of 0.39 in the armchair direction at the low temperature of 1 K. The ultimate stress is about 4.2 N/m at the critical strain of 0.25 in the zigzag direction at the low temperature of 1 K.

VFF type	**Bond stretching**	**Angle bending**			
Expression	$\frac{1}{2}K_{12}(\Delta r_{12})^2$	$\frac{1}{2}K_{14}(\Delta r_{14})^2$	$\frac{1}{2}K_{123}(\Delta\theta_{123})^2$	$\frac{1}{2}K_{134}(\Delta\theta_{134})^2$	$\frac{1}{2}K_{415}(\Delta\theta_{415})^2$
Parameter	7.135	7.135	2.512	2.922	2.922
r_0 or θ_0	2.300	2.344	93.554	96.500	111.710

The second line gives an explicit expression for each VFF term, where atom indexes are from **Figure 189(c)**. The third line is the force constant parameters. Parameters are in the unit of eV/Å^2 for the bond stretching interaction and in the unit of eV for the angle bending interaction. The fourth line gives the initial bond length (in the unit of Å) for the bond stretching interaction and the initial angle (in the unit of degrees) for the angle bending interaction. The angle θ_{ijk} has atom i as the apex.

Table 390. The VFF model for the single-layer p-SiS.

http://dx.doi.org/10.5772/intechopen.71929

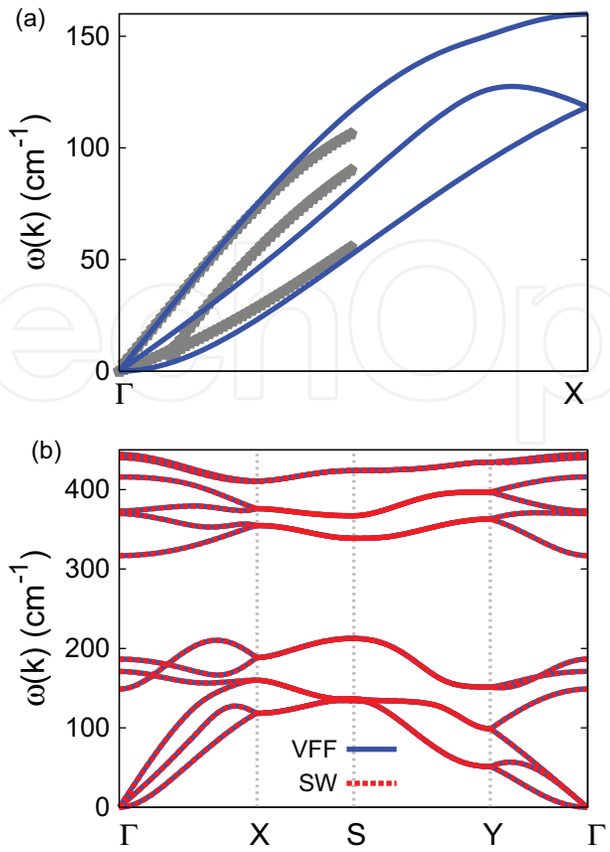

Figure 200. Phonon dispersion for the single-layer p-SiS. (a) The VFF model is fitted to the acoustic branches in the long wave limit along the ΓX direction. The *ab initio* calculations are calculated from SIESTA. (b) The VFF model (blue lines) and the SW potential (red lines) give the same phonon dispersion for the p-SiS along ΓXSYΓ.

	A (eV)	ρ (Å)	B (Å^4)	$r_{\min}$ (Å)	$r_{\max}$ (Å)
r_{12}	3.878	0.797	13.992	0.0	2.977
r_{14}	6.051	1.301	15.094	0.0	3.217

The quantity (r_{ij}) in the first line lists one representative term for the two-body SW potential between atoms i and j. Atom indexes are from **Figure 189(c)**.

Table 391. Two-body SW potential parameters for the single-layer p-SiS used by GULP [8], as expressed in Eq. (3).

	K (eV)	θ_0 (°)	ρ_1 (Å)	ρ_2 (Å)	$r_{\min 12}$ (Å)	$r_{\max 12}$ (Å)	$r_{\min 13}$ (Å)	$r_{\max 13}$ (Å)	$r_{\min 23}$ (Å)	$r_{\max 23}$ (Å)
θ_{123}	13.284	93.554	0.797	0.797	0.0	2.977	0.0	2.977	0.0	4.063
θ_{134}	21.310	96.500	1.301	0.797	0.0	3.217	0.0	2.977	0.0	4.232
θ_{415}	24.372	111.710	1.301	0.797	0.0	3.217	0.0	2.977	0.0	4.423

The first line (θ_{ijk}) presents one representative term for the three-body SW potential. The angle θ_{ijk} has the atom i as the apex. Atom indexes are from **Figure 189(c)**.

Table 392. Three-body SW potential parameters for the single-layer p-SiS used by GULP [8], as expressed in Eq. (4).

	ϵ (eV)	σ (Å)	a	λ	γ	$\cos\theta_0$	A_L	B_L	p	q	Tol
Si_1—S_2—S_2	1.000	0.797	3.735	13.284	1.000	−0.062	3.878	34.661	4	0	0.0
Si_1—S_1—S_1	1.000	1.301	2.474	0.000	1.000	0.000	6.051	5.276	4	0	0.0
Si_1—S_1—S_2	1.000	0.000	0.000	21.310	1.000	−0.113	0.000	0.000	4	0	0.0
S_1—Si_1—Si_2	1.000	0.000	0.000	24.372	1.000	−0.370	0.000	0.000	4	0	0.0

Atom types in the first column are displayed in **Figure 190**, with M=Si and X=S.

Table 393. SW potential parameters for p-SiS used by LAMMPS [9], as expressed in Eqs. (9) and (10).

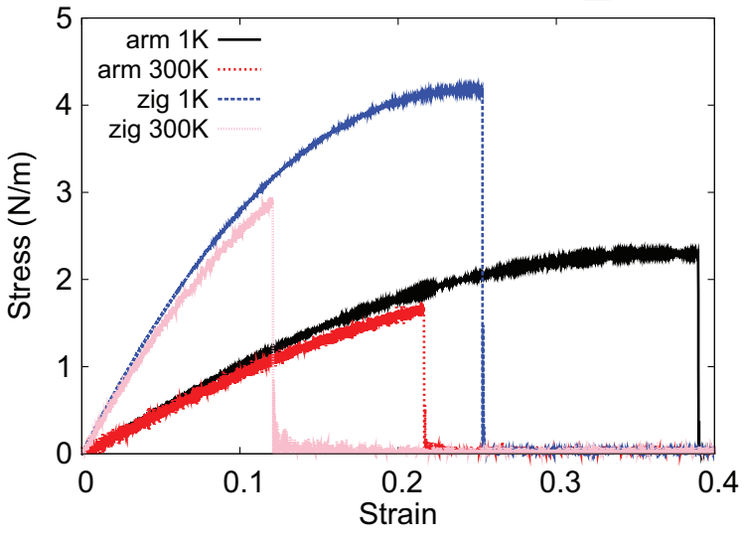

Figure 201. Stress-strain relations for the single-layer p-SiS of size 100×100 Å. The single-layer p-SiS is uniaxially stretched along the armchair or zigzag directions at temperatures 1 and 300 K.

99. P-GeS

Present studies on the puckered (p-) GeS are based on first-principles calculations, and no empirical potential has been proposed for the p-GeS. We will thus parametrize the SW potential for the single-layer p-GeS in this section.

The structure of the single-layer p-GeS is shown in **Figure 189**, with M = Ge and X = S. Structural parameters for p-GeS are from the *ab initio* calculations [78]. There are four atoms in the unit cell with relative coordinates such as $(-u, 0, -v)$, $(u, 0, v)$, $(0.5-u, 0.5, v+w)$, and $(0.5+u, 0.5, -v+w)$ with $u = 0.0673$, $v = 0.1173$, and $w = 0.0228$. The values of these dimensionless parameters are extracted from the geometrical parameters provided in Ref. [78], including lattice constants $a_1 = 4.492$ Å and $a_2 = 3.642$ Å, bond lengths $d_{12} = 2.462$ Å and $d_{14} = 2.423$ Å, and the angle $\theta_{145} = 94.4^\circ$. The dimensionless parameters v and w are ratios based on the lattice constant in the out-of-plane z-direction, which is arbitrarily chosen as $a_3 = 10.0$ Å. We note that the main purpose of the usage of u, v, and w in representing atomic

coordinates is to follow the same convention for all puckered structures in the present work. The resultant atomic coordinates are the same as that in Ref. [78].

As shown in **Figure 189**, a specific feature in the puckered configuration of the p-GeS is that there is a small difference of wa_3 between the z-coordinate of atom 1 and the z-coordinates of atoms 2 and 3. Similarly, atom 4 is higher than atoms 5 and 6 for wa_3 along the z-direction. The sign of w determines which types of atoms take the outmost positions, e.g., atoms 1, 5, and 6 are the outmost atoms if $w > 0$ in **Figure 189(c)**, while atoms 2, 3, and 4 will take the outmost positions for $w < 0$.

Table 394 shows five VFF terms for the single-layer p-GeS; two of which are the bond stretching interactions shown in Eq. (1), while the other three terms are the angle bending interaction shown in Eq. (2). The force constant parameters are the same for the two angle bending terms θ_{134} and θ_{415}, which have the same arm lengths. All force constant parameters are determined by fitting to the acoustic branches in the phonon dispersion along the ΓX as shown in **Figure 202(a)**. The *ab initio* calculations are from Ref. [81]. **Figure 202(b)** shows that the VFF model and the SW potential give exactly the same phonon dispersion.

The parameters for the two-body SW potential used by GULP are shown in **Table 395**. The parameters for the three-body SW potential used by GULP are shown in **Table 396**. Parameters for the SW potential used by LAMMPS are listed in **Table 397**. Eight atom types have been introduced for writing the SW potential script used by LAMMPS as shown in **Figure 190** with M = Ge and X = S, which helps to increase the cutoff for the bond stretching interaction between atom 1 and atom 2 in **Figure 189(c)**.

Figure 203 shows the stress-strain relations for the single-layer p-GeS of size 100 × 100 Å. The structure is uniaxially stretched in the armchair or zigzag directions at 1 and 300 K. The Young's modulus is 10.6 and 32.1 N/m in the armchair and zigzag directions, respectively, at 1 K, which is obtained by linear fitting of the stress-strain relations in [0, 0.01]. The Poisson's ratios from the VFF model and the SW potential are $\nu_{xy} = 0.10$ and $\nu_{yx} = 0.29$. The third-order nonlinear elastic constant D can be obtained by fitting the stress-strain relation to $\sigma = E\epsilon + \frac{1}{2}D\epsilon^2$ with E as the Young's modulus. The values of D are −20.4 and −118.8 N/m at 1 K along the armchair and zigzag directions, respectively. The ultimate stress is about 2.4 N/m at the critical strain of 0.39 in the armchair direction at the low temperature of 1 K. The ultimate

VFF type	**Bond stretching**	**Angle bending**			
Expression	$\frac{1}{2}K_{12}(\Delta r_{12})^2$	$\frac{1}{2}K_{14}(\Delta r_{14})^2$	$\frac{1}{2}K_{123}(\Delta\theta_{123})^2$	$\frac{1}{2}K_{134}(\Delta\theta_{134})^2$	$\frac{1}{2}K_{415}(\Delta\theta_{415})^2$
Parameter	6.364	6.364	2.153	3.896	3.896
r_0 or θ_0	2.462	2.423	95.402	94.400	104.837

The second line gives an explicit expression for each VFF term, where atom indexes are from **Figure 189(c)**. The third line is the force constant parameters. Parameters are in the unit of eV/Å^2 for the bond stretching interaction and in the unit of eV for the angle bending interaction. The fourth line gives the initial bond length (in the unit of Å) for the bond stretching interaction and the initial angle (in the unit of degrees) for the angle bending interaction. The angle θ_{ijk} has atom i as the apex.

Table 394. The VFF model for the single-layer p-GeS.

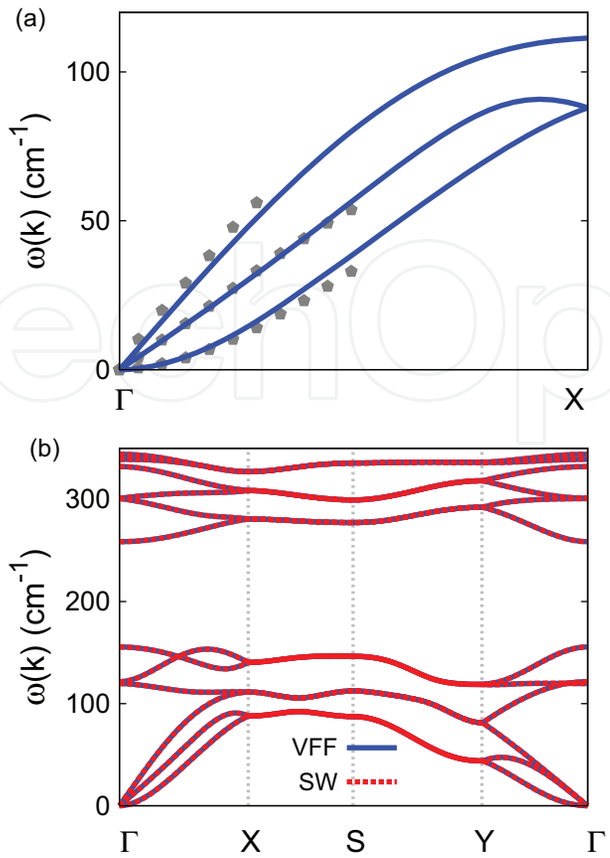

Figure 202. Phonon dispersion for the single-layer p-GeS. (a) The VFF model is fitted to the acoustic branches in the long wave limit along the ΓX direction. The *ab initio* calculations are from Ref. 81. (b) The VFF model (blue lines) and the SW potential (red lines) give the same phonon dispersion for the p-GeS along ΓXSYΓ.

	A (eV)	ρ (Å)	B (Å^4)	$r_{\min}$ (Å)	$r_{\max}$ (Å)
r_{12}	2.096	0.351	18.371	0.0	2.926
r_{14}	6.694	1.571	17.234	0.0	3.398

The quantity (r_{ij}) in the first line lists one representative term for the two-body SW potential between atoms i and j. Atom indexes are from **Figure 189(c)**.

Table 395. Two-body SW potential parameters for the single-layer p-GeS used by GULP [8], as expressed in Eq. (3).

	K (eV)	θ_0 (°)	ρ_1 (Å)	ρ_2 (Å)	$r_{\min 12}$ (Å)	$r_{\max 12}$ (Å)	$r_{\min 13}$ (Å)	$r_{\max 13}$ (Å)	$r_{\min 23}$ (Å)	$r_{\max 23}$ (Å)
θ_{123}	4.905	95.402	0.350	0.350	0.0	2.926	0.0	2.926	0.0	4.067
θ_{134}	20.842	94.400	1.571	0.350	0.0	3.398	0.0	2.926	0.0	4.292
θ_{415}	22.173	104.837	1.571	0.350	0.0	3.398	0.0	2.296	0.0	4.438

The first line (θ_{ijk}) presents one representative term for the three-body SW potential. The angle θ_{ijk} has the atom i as the apex. Atom indexes are from **Figure 189(c)**.

Table 396. Three-body SW potential parameters for the single-layer p-GeS used by GULP [8], as expressed in Eq. (4).

	ϵ (eV)	σ (Å)	a	λ	γ	$\cos\theta_0$	A_L	B_L	p	q	Tol
Ge_1—S_4—S_4	1.000	0.351	8.332	4.905	1.000	−0.094	2.096	1227.130	4	0	0.0
Ge_1—S_1—S_1	1.000	1.571	2.163	0.000	1.000	0.000	6.694	2.830	4	0	0.0
Ge_1—S_1—S_4	1.000	0.000	0.000	20.842	1.000	−0.077	0.000	0.000	4	0	0.0
S_1—Ge_1—Ge_2	1.000	0.000	0.000	22.173	1.000	−0.256	0.000	0.000	4	0	0.0

Atom types in the first column are displayed in **Figure 190**, with M=Ge and X=S.

Table 397. SW potential parameters for p-GeS used by LAMMPS [9], as expressed in Eqs. (9) and (10).

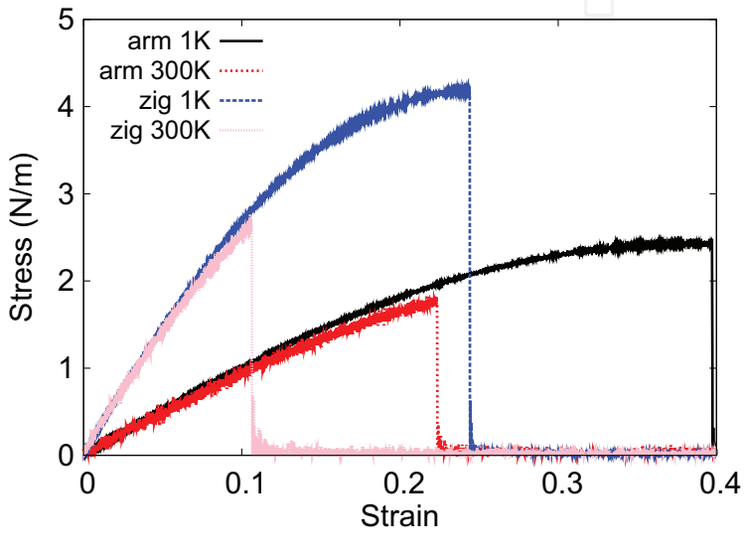

Figure 203. Stress-strain relations for the single-layer p-GeS of size 100 × 100 Å. The single-layer p-GeS is uniaxially stretched along the armchair or zigzag directions at temperatures 1 and 300 K.

stress is about 4.2 N/m at the critical strain of 0.24 in the zigzag direction at the low temperature of 1 K.

100. P-SnS

Present studies on the puckered (p-) SnS are based on first-principles calculations, and no empirical potential has been proposed for the p-SnS. We will thus parametrize the SW potential for the single-layer p-SnS in this section.

The structure of the single-layer p-SnS is shown in **Figure 189**, with M = Sn and X = S. Structural parameters for p-SnS are from the *ab initio* calculations [78]. There are four atoms in the unit cell with relative coordinates such as $(-u, 0, -v)$, $(u, 0, v)$, $(0.5-u, 0.5, v+w)$, and $(0.5+u, 0.5, -v+w)$ with $u = 0.0426$, $v = 0.1284$, and $w = 0.0308$. The values of these dimensionless parameters are extracted from the geometrical parameters provided in Ref. [78], including lattice constants $a_1 = 4.347$ Å and $a_2 = 4.047$ Å, bond lengths $d_{12} = 2.728$ Å and

$d_{14} = 2.595$ Å, and the angle $\theta_{145} = 89.0^\circ$. The dimensionless parameters v and w are ratios based on the lattice constant in the out-of-plane z-direction, which is arbitrarily chosen as $a_3 = 10.0$ Å. We note that the main purpose of the usage of u, v, and w in representing atomic coordinates is to follow the same convention for all puckered structures in the present work. The resultant atomic coordinates are the same as that in Ref. [78].

As shown in **Figure 189**, a specific feature in the puckered configuration of the p-SnS is that there is a small difference of wa_3 between the z-coordinate of atom 1 and the z-coordinates of atoms 2 and 3. Similarly, atom 4 is higher than atoms 5 and 6 for wa_3 along the z-direction. The sign of w determines which types of atoms take the outmost positions, e.g., atoms 1, 5, and 6 are the outmost atoms if $w > 0$ in **Figure 189(c)**, while atoms 2, 3, and 4 will take the outmost positions for $w < 0$.

Table 398 shows five VFF terms for the single-layer p-SnS; two of which are the bond stretching interactions shown in Eq. (1), while the other three terms are the angle bending interaction shown in Eq. (2). The force constant parameters are the same for the two angle bending terms θ_{134} and θ_{415}, which have the same arm lengths. All force constant parameters are determined by fitting to the acoustic branches in the phonon dispersion along the ΓX as shown in **Figure 204(a)**. The *ab initio* calculations are from Ref. [81]. **Figure 204(b)** shows that the VFF model and the SW potential give exactly the same phonon dispersion.

The parameters for the two-body SW potential used by GULP are shown in **Table 399**. The parameters for the three-body SW potential used by GULP are shown in **Table 400**. Parameters for the SW potential used by LAMMPS are listed in **Table 401**. Eight atom types have been introduced for writing the SW potential script used by LAMMPS as shown in **Figure 190** with M = Sn and X = S, which helps to increase the cutoff for the bond stretching interaction between atom 1 and atom 2 in **Figure 189(c)**.

Figure 205 shows the stress-strain relations for the single-layer p-SnS of size 100 × 100 Å. The structure is uniaxially stretched in the armchair or zigzag directions at 1 and 300 K. The Young's modulus is 9.6 and 24.5 N/m in the armchair and zigzag directions, respectively, at 1 K, which is obtained by linear fitting of the stress-strain relations in [0, 0.01]. The Poisson's ratios from the VFF model and the SW potential are $\nu_{xy} = 0.18$ and $\nu_{yx} = 0.47$. The third-order nonlinear elastic constant D can be obtained by fitting the stress-strain relation to

VFF type	**Bond stretching**	**Angle bending**			
Expression	$\frac{1}{2}K_{12}(\Delta r_{12})^2$	$\frac{1}{2}K_{14}(\Delta r_{14})^2$	$\frac{1}{2}K_{123}(\Delta\theta_{123})^2$	$\frac{1}{2}K_{134}(\Delta\theta_{134})^2$	$\frac{1}{2}K_{415}(\Delta\theta_{415})^2$
Parameter	4.163	4.163	1.776	5.841	5.841
r_0 or θ_0	2.728	2.595	95.762	89.000	101.887

The second line gives an explicit expression for each VFF term, where atom indexes are from **Figure 189(c)**. The third line is the force constant parameters. Parameters are in the unit of eV/Å^2 for the bond stretching interaction and in the unit of eV for the angle bending interaction. The fourth line gives the initial bond length (in the unit of Å) for the bond stretching interaction and the initial angle (in the unit of degrees) for the angle bending interaction. The angle θ_{ijk} has atom i as the apex.

Table 398. The VFF model for the single-layer p-SnS

http://dx.doi.org/10.5772/intechopen.71929

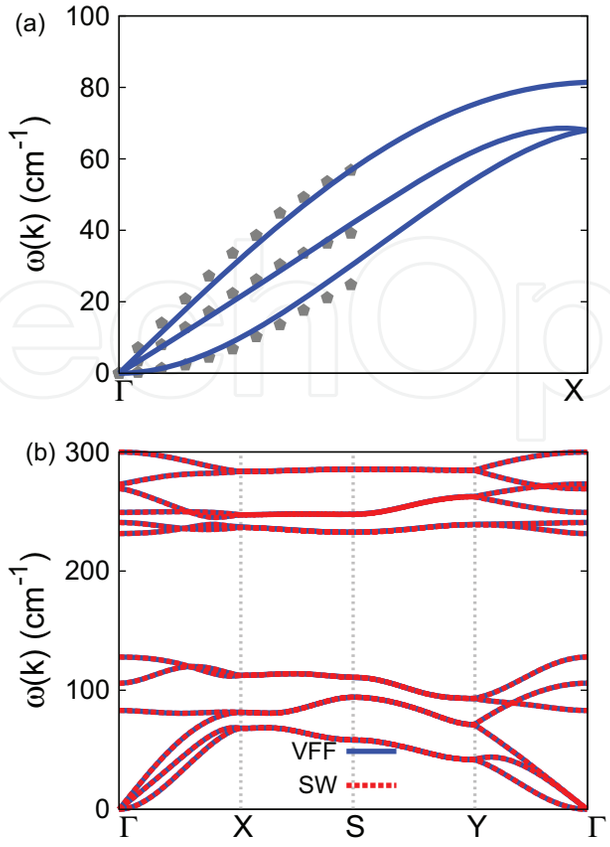

Figure 204. Phonon dispersion for the single-layer p-SnS. (a) The VFF model is fitted to the acoustic branches in the long wave limit along the ΓX direction. The *ab initio* calculations are from Ref. [81]. (b) The VFF model (blue lines) and the SW potential (red lines) give the same phonon dispersion for the p-SnS along ΓXSYΓ.

	A (eV)	ρ (Å)	B (Å^4)	r_{min} (Å)	r_{max} (Å)
r_{12}	0.782	0.106	27.692	0.0	2.997
r_{14}	5.636	1.887	22.674	0.0	3.702

The quantity (r_{ij}) in the first line lists one representative term for the two-body SW potential between atoms i and j. Atom indexes are from **Figure 189(c)**.

Table 399. Two-body SW potential parameters for the single-layer p-SnS used by GULP [8], as expressed in Eq. (3).

	K (eV)	θ_0 (°)	ρ_1 (Å)	ρ_2 (Å)	r_{min12} (Å)	r_{max12} (Å)	r_{min13} (Å)	r_{max13} (Å)	r_{min23} (Å)	r_{max23} (Å)
θ_{123}	1.968	95.762	0.106	0.106	0.0	2.997	0.0	2.997	0.0	4.197
θ_{134}	23.839	89.000	1.887	0.106	0.0	3.702	0.0	2.997	0.0	4.366
θ_{415}	24.888	101.887	1.887	0.106	0.0	3.702	0.0	2.997	0.0	4.566

The first line (θ_{ijk}) presents one representative term for the three-body SW potential. The angle θ_{ijk} has the atom i as the apex. Atom indexes are from **Figure 189(c)**.

Table 400. Three-body SW potential parameters for the single-layer p-SnS used by GULP [8], as expressed in Eq. (4).

	ϵ (eV)	σ (Å)	a	λ	γ	$\cos\theta_0$	A_L	B_L	p	q	Tol
Sn_1—S_4—S_4	1.000	0.106	28.347	1.971	1.000	−0.100	0.783	221784.222	4	0	0.0
Sn_1—S_1—S_1	1.000	1.887	1.961	0.000	1.000	0.000	5.636	1.787	4	0	0.0
Sn_1—S_1—S_4	1.000	0.000	0.000	23.839	1.000	0.017	0.000	0.000	4	0	0.0
S_1—Sn_1—Sn_2	1.000	0.000	0.000	24.888	1.000	−0.206	0.000	0.000	4	0	0.0

Atom types in the first column are displayed in **Figure 190**, with M=Sn and X=S.

Table 401. SW potential parameters for p-SnS used by LAMMPS [9], as expressed in Eqs. (9) and (10).

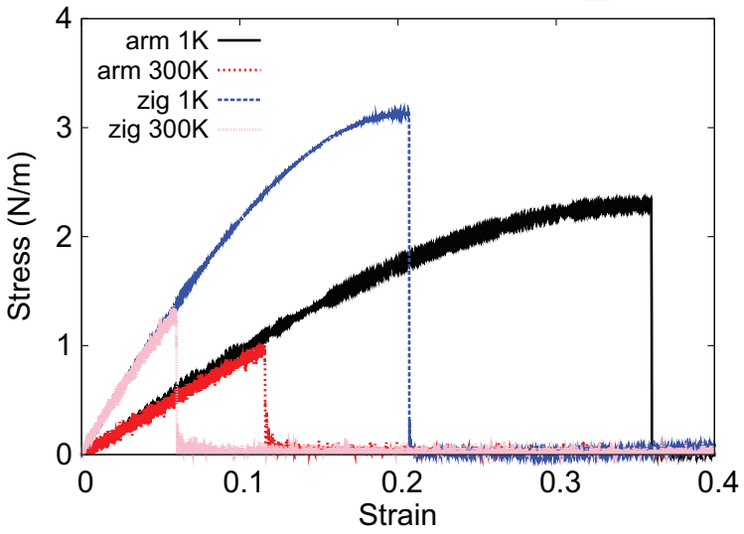

Figure 205. Stress-strain relations for the single-layer p-SnS of size 100 × 100 Å. The single-layer p-SnS is uniaxially stretched along the armchair or zigzag directions at temperatures 1 and 300 K.

$\sigma = E\epsilon + \frac{1}{2}D\epsilon^2$ with E as the Young's modulus. The values of D are −14.7 and −80.3 N/m at 1 K along the armchair and zigzag directions, respectively. The ultimate stress is about 2.3 N/m at the critical strain of 0.36 in the armchair direction at the low temperature of 1 K. The ultimate stress is about 3.1 N/m at the critical strain of 0.20 in the zigzag direction at the low temperature of 1 K.

101. P-CSe

Present studies on the puckered (p-) CSe are based on first-principles calculations, and no empirical potential has been proposed for the p-CSe. We will thus parametrize the SW potential for the single-layer p-CSe in this section.

The structure of the single-layer p-CSe is shown in **Figure 189**, with M = C and X = Se. Structural parameters for p-CSe are from the *ab initio* calculations [78]. There are four atoms

in the unit cell with relative coordinates such as $(-u, 0, -v)$, $(u, 0, v)$, $(0.5-u, 0.5, v+w)$, and $(0.5+u, 0.5, -v+w)$ with $u = 0.1079$, $v = 0.0894$, and $w = -0.0229$. The values of these dimensionless parameters are extracted from the geometrical parameters provided in Ref. [78], including lattice constants $a_1 = 4.299$ Å and $a_2 = 3.034$ Å, bond lengths $d_{12} = 1.961$ Å and $d_{14} = 2.014$ Å, and the angle $\theta_{145} = 113.0^\circ$. The dimensionless parameters v and w are ratios based on the lattice constant in the out-of-plane z-direction, which is arbitrarily chosen as $a_3 = 10.0$ Å. We note that the main purpose of the usage of u, v, and w in representing atomic coordinates is to follow the same convention for all puckered structures in the present work. The resultant atomic coordinates are the same as that in Ref. [78].

As shown in **Figure 189**, a specific feature in the puckered configuration of the p-CSe is that there is a small difference of wa_3 between the z-coordinate of atom 1 and the z-coordinates of atoms 2 and 3. Similarly, atom 4 is higher than atoms 5 and 6 for wa_3 along the z-direction. The sign of w determines which types of atoms take the outmost positions, e.g., atoms 1, 5, and 6 are the outmost atoms if $w > 0$ in **Figure 189(c)**, while atoms 2, 3, and 4 will take the outmost positions for $w < 0$.

Table 402 shows five VFF terms for the single-layer p-CSe; two of which are the bond stretching interactions shown in Eq. (1), while the other three terms are the angle bending interaction shown in Eq. (2). The force constant parameters are the same for the two angle bending terms θ_{134} and θ_{415}, which have the same arm lengths. All force constant parameters are determined by fitting to the acoustic branches in the phonon dispersion along the ΓX as shown in **Figure 206(a)**. The *ab initio* calculations for the phonon dispersion are calculated from the SIESTA package [79]. The generalized gradients approximation is applied to account for the exchange-correlation function with Perdew, Burke, and Ernzerhof parameterization [80], and the double-ζ orbital basis set is adopted. **Figure 206(b)** shows that the VFF model and the SW potential give exactly the same phonon dispersion.

The parameters for the two-body SW potential used by GULP are shown in **Table 403**. The parameters for the three-body SW potential used by GULP are shown in **Table 404**. Parameters for the SW potential used by LAMMPS are listed in **Table 405**. Eight atom types have been introduced for writing the SW potential script used by LAMMPS as shown in **Figure 190** with M = C and X = Se, which helps to increase the cutoff for the bond stretching interaction between atom 1 and atom 2 in **Figure 189(c)**.

VFF type	**Bond stretching**	**Angle bending**			
Expression	$\frac{1}{2}K_{12}(\Delta r_{12})^2$	$\frac{1}{2}K_{14}(\Delta r_{14})^2$	$\frac{1}{2}K_{123}(\Delta\theta_{123})^2$	$\frac{1}{2}K_{134}(\Delta\theta_{134})^2$	$\frac{1}{2}K_{415}(\Delta\theta_{415})^2$
Parameter	10.120	10.120	4.505	3.910	3.910
r_0 or θ_0	1.961	2.014	101.354	113.000	100.563

The second line gives an explicit expression for each VFF term, where atom indexes are from **Figure 189(c)**. The third line is the force constant parameters. Parameters are in the unit of eV/Å^2 for the bond stretching interaction and in the unit of eV for the angle bending interaction. The fourth line gives the initial bond length (in the unit of Å) for the bond stretching interaction and the initial angle (in the unit of degrees) for the angle bending interaction. The angle θ_{ijk} has atom i as the apex.

Table 402. The VFF model for the single-layer p-CSe.

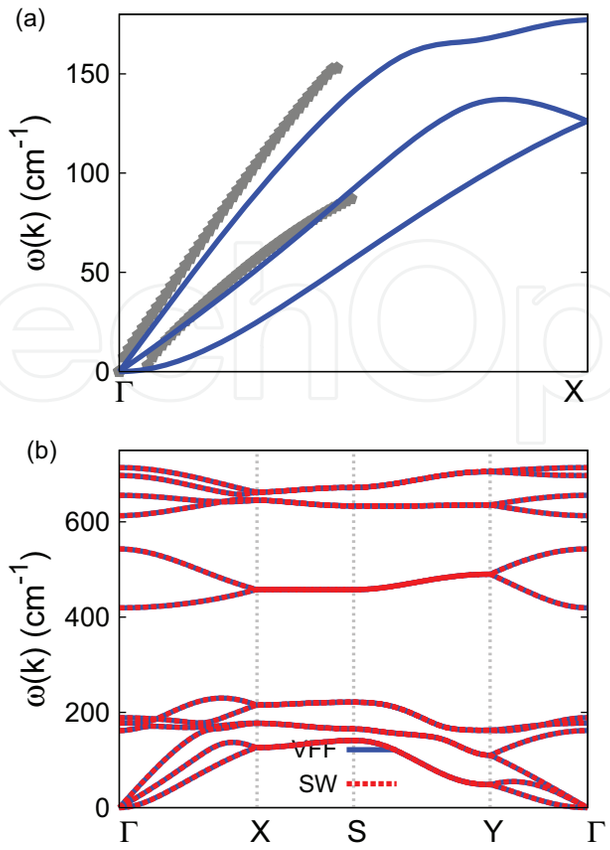

Figure 206. Phonon dispersion for the single-layer p-CSe. (a) The VFF model is fitted to the acoustic branches in the long wave limit along the ΓX direction. The *ab initio* calculations are calculated from SIESTA. (b) The VFF model (blue lines) and the SW potential (red lines) give the same phonon dispersion for the p-CSe along ΓXSYΓ.

	A (eV)	ρ (Å)	B (Å^4)	r_{min} (Å)	r_{max} (Å)
r_{12}	6.141	1.114	7.394	0.0	2.700
r_{14}	7.411	1.316	8.226	0.0	2.828

The quantity (r_{ij}) in the first line lists one representative term for the two-body SW potential between atoms i and j. Atom indexes are from **Figure 189(c)**.

Table 403. Two-body SW potential parameters for the single-layer p-CSe used by GULP [8], as expressed in Eq. (3).

	K (eV)	θ_0 (°)	ρ_1 (Å)	ρ_2 (Å)	r_{min12} (Å)	r_{max12} (Å)	r_{min13} (Å)	r_{max13} (Å)	r_{min23} (Å)	r_{max23} (Å)
θ_{123}	47.768	101.354	1.114	1.114	0.0	2.700	0.0	2.700	0.0	3.667
θ_{134}	52.464	113.000	1.316	1.114	0.0	2.828	0.0	2.700	0.0	4.157
θ_{415}	46.000	100.563	1.316	1.114	0.0	2.828	0.0	2.700	0.0	4.032

The first line (θ_{ijk}) presents one representative term for the three-body SW potential. The angle θ_{ijk} has the atom i as the apex. Atom indexes are from **Figure 189(c)**.

Table 404. Three-body SW potential parameters for the single-layer p-CSe used by GULP [8], as expressed in Eq. (4).

	ϵ (eV)	σ (Å)	a	λ	γ	$\cos\theta_0$	A_L	B_L	p	q	Tol
C_1—Se_4—Se_4	1.000	1.114	2.424	47.768	1.000	−0.197	6.141	4.802	4	0	0.0
C_1—Se_1—Se_1	1.000	1.316	2.149	0.000	1.000	0.000	7.411	2.743	4	0	0.0
C_1—Se_1—Se_4	1.000	0.000	0.000	52.464	1.000	−0.391	0.000	0.000	4	0	0.0
Se_1—C_1—C_2	1.000	0.000	0.000	46.000	1.000	−0.183	0.000	0.000	4	0	0.0

Atom types in the first column are displayed in **Figure 190**, with M=C and X=Se.

Table 405. SW potential parameters for p-CSe used by LAMMPS [9], as expressed in Eqs. (9) and (10).

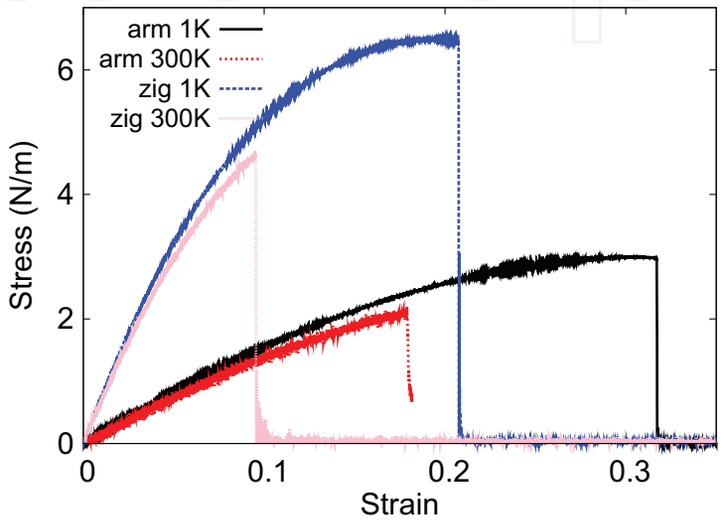

Figure 207. Stress-strain relations for the single-layer p-CSe of size 100 × 100 Å. The single-layer p-CSe is uniaxially stretched along the armchair or zigzag directions at temperatures 1 and 300 K.

Figure 207 shows the stress-strain relations for the single-layer p-CSe of size 100 × 100 Å. The structure is uniaxially stretched in the armchair or zigzag directions at 1 and 300 K. The Young's modulus is 17.2 and 75.4 N/m in the armchair and zigzag directions, respectively, at 1 K, which is obtained by linear fitting of the stress-strain relations in [0, 0.01]. The Poisson's ratios from the VFF model and the SW potential are $\nu_{xy} = -0.02$ and $\nu_{yx} = -0.11$. The third-order nonlinear elastic constant D can be obtained by fitting the stress-strain relation to $\sigma = E\epsilon + \frac{1}{2}D\epsilon^2$ with E as the Young's modulus. The values of D are −46.3 and −442.0 N/m at 1 K along the armchair and zigzag directions, respectively. The ultimate stress is about 3.0 N/m at the critical strain of 0.31 in the armchair direction at the low temperature of 1 K. The ultimate stress is about 6.5 N/m at the critical strain of 0.20 in the zigzag direction at the low temperature of 1 K.

102. P-SiSe

Present studies on the puckered (p-) SiSe are based on first-principles calculations, and no empirical potential has been proposed for the p-SiSe. We will thus parametrize the SW potential for the single-layer p-SiSe in this section.

The structure of the single-layer p-SiSe is shown in **Figure 189**, with M = Si and X = Se. Structural parameters for p-SiSe are from the *ab initio* calculations [78]. There are four atoms in the unit cell with relative coordinates such as $(-u, 0, -v)$, $(u, 0, v)$, $(0.5-u, 0.5, v+w)$, and $(0.5+u, 0.5, -v+w)$ with $u = 0.0572$, $v = 0.1198$, and $w = -0.0011$. The values of these dimensionless parameters are extracted from the geometrical parameters provided in Ref. [78], including lattice constants $a_1 = 4.400$ Å and $a_2 = 3.737$ Å, bond lengths $d_{12} = 2.524$ Å and $d_{14} = 2.448$ Å, and the angle $\theta_{145} = 98.2^\circ$. The dimensionless parameters v and w are ratios based on the lattice constant in the out-of-plane z-direction, which is arbitrarily chosen as $a_3 = 10.0$ Å. We note that the main purpose of the usage of u, v, and w in representing atomic coordinates is to follow the same convention for all puckered structures in the present work. The resultant atomic coordinates are the same as that in Ref. [78].

As shown in **Figure 189**, a specific feature in the puckered configuration of the p-SiSe is that there is a small difference of wa_3 between the z-coordinate of atom 1 and the z-coordinates of atoms 2 and 3. Similarly, atom 4 is higher than atoms 5 and 6 for wa_3 along the z-direction. The sign of w determines which types of atoms take the outmost positions, e.g., atoms 1, 5, and 6 are the outmost atoms if $w > 0$ in **Figure 189(c)**, while atoms 2, 3, and 4 will take the outmost positions for $w < 0$.

Table 406 shows five VFF terms for the single-layer p-SiSe; two of which are the bond stretching interactions shown in Eq. (1), while the other three terms are the angle bending interaction shown in Eq. (2). The force constant parameters are the same for the two angle bending terms θ_{134} and θ_{415}, which have the same arm lengths. All force constant parameters are determined by fitting to the acoustic branches in the phonon dispersion along the ΓX as shown in **Figure 208(a)**. The *ab initio* calculations for the phonon dispersion are calculated from the SIESTA package [79]. The generalized gradients approximation is applied to account for the exchange-correlation function with Perdew, Burke, and Ernzerhof parameterization [80], and the double-ζ orbital basis set is adopted. **Figure 208(b)** shows that the VFF model and the SW potential give exactly the same phonon dispersion.

The parameters for the two-body SW potential used by GULP are shown in **Table 407**. The parameters for the three-body SW potential used by GULP are shown in **Table 408**. Parameters for the SW potential used by LAMMPS are listed in **Table 409**. Eight atom types have been

VFF type	**Bond stretching**	**Angle bending**			
Expression	$\frac{1}{2}K_{12}(\Delta r_{12})^2$	$\frac{1}{2}K_{14}(\Delta r_{14})^2$	$\frac{1}{2}K_{123}(\Delta\theta_{123})^2$	$\frac{1}{2}K_{134}(\Delta\theta_{134})^2$	$\frac{1}{2}K_{415}(\Delta\theta_{415})^2$
Parameter	7.192	7.192	3.222	5.890	5.890
r_0 or θ_0	2.524	2.448	95.513	98.200	97.686

The second line gives an explicit expression for each VFF term, where atom indexes are from **Figure 189(c)**. The third line is the force constant parameters. Parameters are in the unit of eV/Å^2 for the bond stretching interaction and in the unit of eV for the angle bending interaction. The fourth line gives the initial bond length (in the unit of Å) for the bond stretching interaction and the initial angle (in the unit of degrees) for the angle bending interaction. The angle θ_{ijk} has atom i as the apex.

Table 406. The VFF model for the single-layer p-SiSe.

http://dx.doi.org/10.5772/intechopen.71929

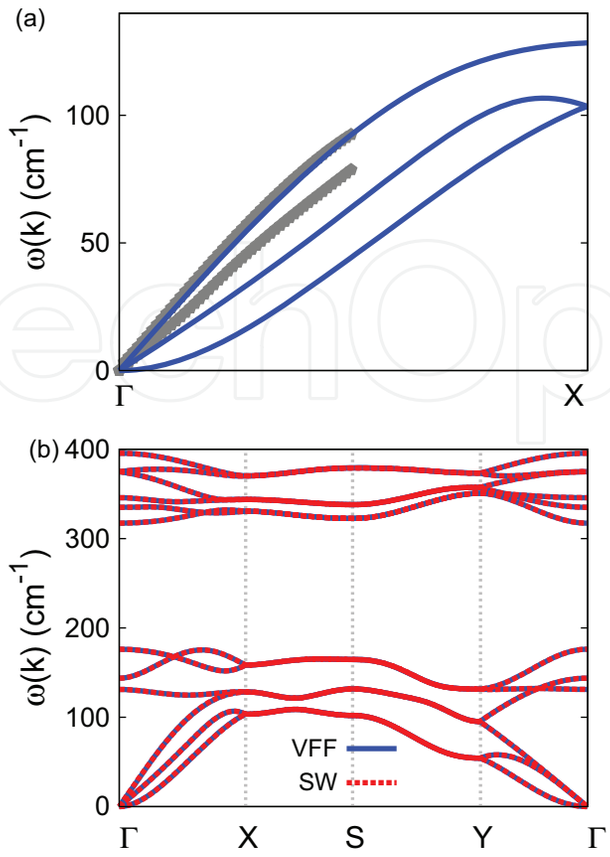

Figure 208. Phonon dispersion for the single-layer p-SiSe. (a) The VFF model is fitted to the acoustic branches in the long wave limit along the ΓX direction. The *ab initio* calculations are calculated from SIESTA. (b) The VFF model (blue lines) and the SW potential (red lines) give the same phonon dispersion for the p-SiSe along ΓXSYΓ.

	A (eV)	ρ (Å)	B (Å^4)	r_{min} (Å)	r_{max} (Å)
r_{12}	1.883	0.230	20.292	0.0	2.905
r_{14}	8.098	1.665	17.956	0.0	3.457

The quantity (r_{ij}) in the first line lists one representative term for the two-body SW potential between atoms i and j. Atom indexes are from **Figure 189(c)**.

Table 407. Two-body SW potential parameters for the single-layer p-SiSe used by GULP [8], as expressed in Eq. (3).

	K (eV)	θ_0 (°)	ρ_1 (Å)	ρ_2 (Å)	r_{min12} (Å)	r_{max12} (Å)	r_{min13} (Å)	r_{max13} (Å)	r_{min23} (Å)	r_{max23} (Å)
θ_{123}	5.440	95.513	0.230	0.230	0.0	2.905	0.0	2.905	0.0	4.069
θ_{134}	28.616	98.200	1.665	0.230	0.0	3.457	0.0	2.905	0.0	4.379
θ_{415}	28.545	97.686	1.665	0.230	0.0	3.457	0.0	2.905	0.0	4.369

The first line (θ_{ijk}) presents one representative term for the three-body SW potential. The angle θ_{ijk} has the atom i as the apex. Atom indexes are from **Figure 189(c)**.

Table 408. Three-body SW potential parameters for the single-layer p-SiSe used by GULP [8], as expressed in Eq. (4).

	ϵ (eV)	σ (Å)	a	λ	γ	$\cos\theta_0$	A_L	B_L	p	q	Tol
Si_1—Se_4—Se_4	1.000	0.230	12.628	5.440	1.000	−0.096	1.883	7245.111	4	0	0.0
Si_1—Se_1—Se_1	1.000	1.665	2.076	0.000	1.000	0.000	8.098	2.335	4	0	0.0
Si_1—Se_1—Se_4	1.000	0.000	0.000	28.616	1.000	−0.143	0.000	0.000	4	0	0.0
Se_1—Si_1—Si_2	1.000	0.000	0.000	28.545	1.000	−0.134	0.000	0.000	4	0	0.0

Atom types in the first column are displayed in **Figure 190**, with M=Si and X=Se.

Table 409. SW potential parameters for p-SiSe used by LAMMPS [9], as expressed in Eqs. (9) and (10).

introduced for writing the SW potential script used by LAMMPS as shown in **Figure 190** with M=Si and X=Se, which helps to increase the cutoff for the bond stretching interaction between atom 1 and atom 2 in **Figure 189(c)**.

Figure 209 shows the stress-strain relations for the single-layer p-SiSe of size 100 × 100 Å. The structure is uniaxially stretched in the armchair or zigzag directions at 1 and 300 K. The Young's modulus is 14.4 and 44.6 N/m in the armchair and zigzag directions, respectively, at 1 K, which is obtained by linear fitting of the stress-strain relations in [0, 0.01]. The Poisson's ratios from the VFF model and the SW potential are $\nu_{xy} = 0.09$ and $\nu_{yx} = 0.30$. The third-order nonlinear elastic constant D can be obtained by fitting the stress-strain relation to $\sigma = E\epsilon + \frac{1}{2}D\epsilon^2$ with E as the Young's modulus. The values of D are −28.8 and −176.6 N/m at 1 K along the armchair and zigzag directions, respectively. The ultimate stress is about 3.1 N/m at the critical strain of 0.37 in the armchair direction at the low temperature of 1 K. The ultimate stress is about 5.3 N/m at the critical strain of 0.21 in the zigzag direction at the low temperature of 1 K.

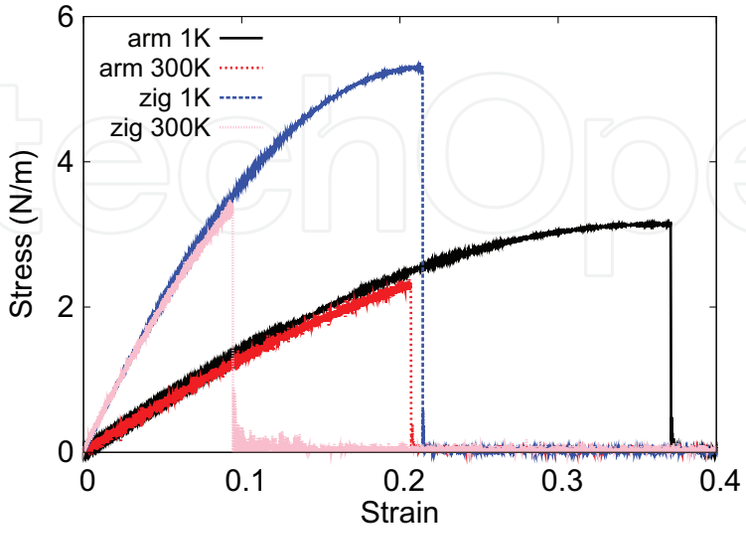

Figure 209. Stress-strain relations for the single-layer p-SiSe of size 100 × 100 Å. The single-layer p-SiSe is uniaxially stretched along the armchair or zigzag directions at temperatures 1 and 300 K.

103. P-GeSe

Present studies on the puckered (p-) GeSe are based on first-principles calculations, and no empirical potential has been proposed for the p-GeSe. We will thus parametrize the SW potential for the single-layer p-GeSe in this section.

The structure of the single-layer p-GeSe is shown in **Figure 189**, with M = Ge and X = Se. Structural parameters for p-GeSe are from the *ab initio* calculations [78]. There are four atoms in the unit cell with relative coordinates such as $(-u, 0, -v)$, $(u, 0, v)$, $(0.5-u, 0.5, v+w)$, and $(0.5+u, 0.5, -v+w)$ with $u = 0.0439$, $v = 0.1258$, and $w = -0.0080$. The values of these dimensionless parameters are extracted from the geometrical parameters provided in Ref. [78], including lattice constants $a_1 = 4.302$ Å and $a_2 = 3.965$ Å, bond lengths $d_{12} = 2.661$ Å and $d_{14} = 2.544$ Å, and the angle $\theta_{145} = 97.4^\circ$. The dimensionless parameters v and w are ratios based on the lattice constant in the out-of-plane z-direction, which is arbitrarily chosen as $a_3 = 10.0$ Å. We note that the main purpose of the usage of u, v, and w in representing atomic coordinates is to follow the same convention for all puckered structures in the present work. The resultant atomic coordinates are the same as that in Ref. [78].

As shown in **Figure 189**, a specific feature in the puckered configuration of the p-GeSe is that there is a small difference of wa_3 between the z-coordinate of atom 1 and the z-coordinates of atoms 2 and 3. Similarly, atom 4 is higher than atoms 5 and 6 for wa_3 along the z-direction. The sign of w determines which types of atoms take the outmost positions, e.g., atoms 1, 5, and 6 are the outmost atoms if $w > 0$ in **Figure 189(c)**, while atoms 2, 3, and 4 will take the outmost positions for $w < 0$.

Table 410 shows five VFF terms for the single-layer p-GeSe; two of which are the bond stretching interactions shown in Eq. (1), while the other three terms are the angle bending interaction shown in Eq. (2). The force constant parameters are the same for the two angle bending terms θ_{134} and θ_{415}, which have the same arm lengths. All force constant parameters are determined by fitting to the acoustic branches in the phonon dispersion along the ΓX as shown in **Figure 210(a)**. The *ab initio* calculations are from Ref. [81]. **Figure 210(b)** shows that the VFF model and the SW potential give exactly the same phonon dispersion.

VFF type	**Bond stretching**	**Angle bending**			
Expression	$\frac{1}{2}K_{12}(\Delta r_{12})^2$	$\frac{1}{2}K_{14}(\Delta r_{14})^2$	$\frac{1}{2}K_{123}(\Delta\theta_{123})^2$	$\frac{1}{2}K_{134}(\Delta\theta_{134})^2$	$\frac{1}{2}K_{415}(\Delta\theta_{415})^2$
Parameter	5.063	5.063	2.249	5.927	5.927
r_0 or θ_0	2.661	2.544	96.322	97.000	93.964

The second line gives an explicit expression for each VFF term, where atom indexes are from **Figure 189(c)**. The third line is the force constant parameters. Parameters are in the unit of eV/Å^2 for the bond stretching interaction and in the unit of eV for the angle bending interaction. The fourth line gives the initial bond length (in the unit of Å) for the bond stretching interaction and the initial angle (in the unit of degrees) for the angle bending interaction. The angle θ_{ijk} has atom i as the apex.

Table 410. The VFF model for the single-layer p-GeSe.

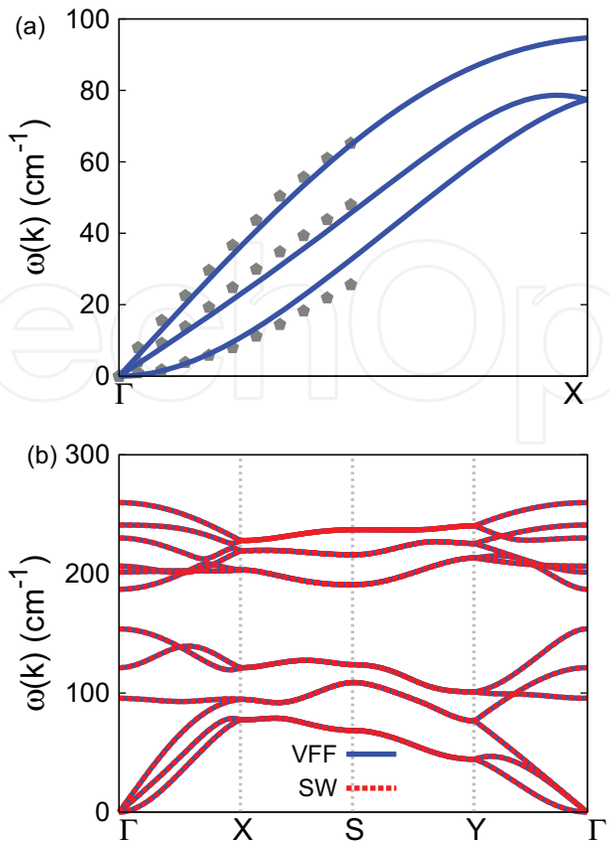

Figure 210. Phonon dispersion for the single-layer p-GeSe. (a) The VFF model is fitted to the acoustic branches in the long wave limit along the ΓX direction. The *ab initio* calculations are from Ref. [81]. (b) The VFF model (blue lines) and the SW potential (red lines) give the same phonon dispersion for the p-GeSe along ΓXSYΓ.

The parameters for the two-body SW potential used by GULP are shown in **Table 411**. The parameters for the three-body SW potential used by GULP are shown in **Table 412**. Parameters for the SW potential used by LAMMPS are listed in **Table 413**. Eight atom types have been introduced for writing the SW potential script used by LAMMPS as shown in **Figure 190** with M = Ge and X = Se, which helps to increase the cutoff for the bond stretching interaction between atom 1 and atom 2 in **Figure 189(c)**.

Figure 211 shows the stress-strain relations for the single-layer p-GeSe of size 100 × 100 Å. The structure is uniaxially stretched in the armchair or zigzag directions at 1 and 300 K. The Young's modulus is 11.1 and 32.0 N/m in the armchair and zigzag directions, respectively, at

	A (eV)	ρ (Å)	B (Å^4)	r_{min} (Å)	r_{max} (Å)
r_{12}	0.962	0.115	25.070	0.0	2.938
r_{14}	6.572	1.846	20.943	0.0	3.628

The quantity (r_{ij}) in the first line lists one representative term for the two-body SW potential between atoms i and j. Atom indexes are from **Figure 189(c)**.

Table 411. Two-body SW potential parameters for the single-layer p-GeSe used by GULP [8], as expressed in Eq. (3).

	K (eV)	θ_0 (°)	ρ_1 (Å)	ρ_2 (Å)	r_{min12} (Å)	r_{max12} (Å)	r_{min13} (Å)	r_{max13} (Å)	r_{min23} (Å)	r_{max23} (Å)
θ_{123}	2.614	96.322	0.115	0.115	0.0	2.938	0.0	2.938	0.0	4.133
θ_{134}	25.087	97.400	1.846	0.115	0.0	3.628	0.0	2.938	0.0	4.455
θ_{415}	24.789	93.964	1.846	0.155	0.0	3.628	0.0	2.938	0.0	4.404

The first line (θ_{ijk}) presents one representative term for the three-body SW potential. The angle θ_{ijk} has the atom i as the apex. Atom indexes are from **Figure 189(c)**.

Table 412. Three-body SW potential parameters for the single-layer p-GeSe used by GULP [8], as expressed in Eq. (4).

	ϵ (eV)	σ (Å)	a	λ	γ	$\cos\theta_0$	A_L	B_L	p	q	Tol
Ge_1—Se_4—Se_4	1.000	0.115	25.561	2.614	1.000	−0.110	0.962	143723.555	4	0	0.0
Ge_1—Se_1—Se_1	1.000	1.846	1.965	0.000	1.000	0.000	6.572	1.804	4	0	0.0
Ge_1—Se_1—Se_4	1.000	0.000	0.000	25.087	1.000	−0.129	0.000	0.000	4	0	0.0
Se_1—Ge_1—Ge_2	1.000	0.000	0.000	24.789	1.000	−0.069	0.000	0.000	4	0	0.0

Atom types in the first column are displayed in **Figure 190**, with M=Ge and X=Se.

Table 413. SW potential parameters for p-GeSe used by LAMMPS [9], as expressed in Eqs. (9) and (10).

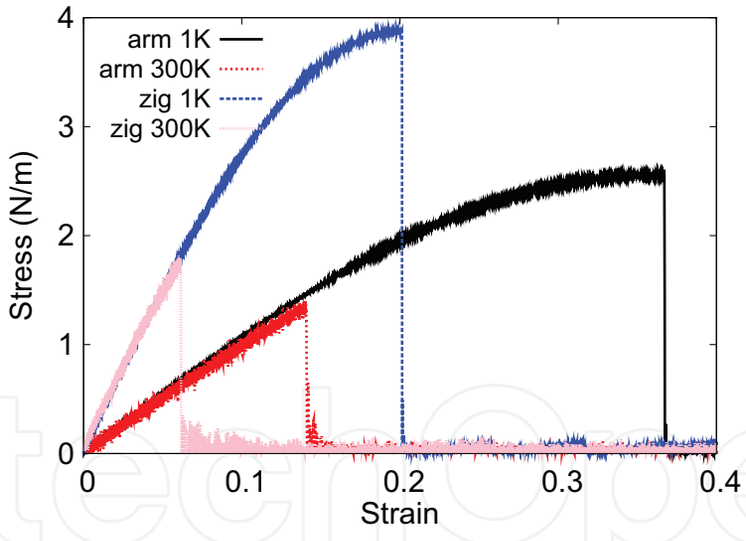

Figure 211. Stress-strain relations for the single-layer p-GeSe of size 100 × 100 Å. The single-layer p-GeSe is uniaxially stretched along the armchair or zigzag directions at temperatures 1 and 300 K.

1 K, which is obtained by linear fitting of the stress-strain relations in [0, 0.01]. The Poisson's ratios from the VFF model and the SW potential are $\nu_{xy} = 0.14$ and $\nu_{yx} = 0.42$. The third-order nonlinear elastic constant D can be obtained by fitting the stress-strain relation to $\sigma = E\epsilon + \frac{1}{2}D\epsilon^2$ with E as the Young's modulus. The values of D are −19.3 and −114.7 N/m at 1 K along the armchair and zigzag directions, respectively. The ultimate stress is about 2.6 N/m at the critical strain of 0.36 in the armchair direction at the low temperature of 1 K. The ultimate

stress is about 3.9 N/m at the critical strain of 0.20 in the zigzag direction at the low temperature of 1 K.

104. P-SnSe

Present studies on the puckered (p-) SnSe are based on first-principles calculations, and no empirical potential has been proposed for the p-SnSe. We will thus parametrize the SW potential for the single-layer p-SnSe in this section.

The structure of the single-layer p-SnSe is shown in **Figure 189**, with M = Sn and X = Se. Structural parameters for p-SnSe are from the *ab initio* calculations [78]. There are four atoms in the unit cell with relative coordinates such as $(-u, 0, -v)$, $(u, 0, v)$, $(0.5-u, 0.5, v+w)$, and $(0.5+u, 0.5, -v+w)$ with $u = 0.0313$, $v = 0.1358$, and $w = 0.0074$. The values of these dimensionless parameters are extracted from the geometrical parameters provided in Ref. [78], including lattice constants $a_1 = 4.453$ Å and $a_2 = 4.260$ Å, bond lengths $d_{12} = 2.887$ Å and $d_{14} = 2.730$ Å, and the angle $\theta_{145} = 92.5^\circ$. The dimensionless parameters v and w are ratios based on the lattice constant in the out-of-plane z-direction, which is arbitrarily chosen as $a_3 = 10.0$ Å. We note that the main purpose of the usage of u, v, and w in representing atomic coordinates is to follow the same convention for all puckered structures in the present work. The resultant atomic coordinates are the same as that in Ref. [78].

As shown in **Figure 189**, a specific feature in the puckered configuration of the p-SnSe is that there is a small difference of wa_3 between the z-coordinate of atom 1 and the z-coordinates of atoms 2 and 3. Similarly, atom 4 is higher than atoms 5 and 6 for wa_3 along the z-direction. The sign of w determines which types of atoms take the outmost positions, e.g., atoms 1, 5, and 6 are the outmost atoms if $w > 0$ in **Figure 189(c)**, while atoms 2, 3, and 4 will take the outmost positions for $w < 0$.

Table 414 shows five VFF terms for the single-layer p-SnSe; two of which are the bond stretching interactions shown in Eq. (1), while the other three terms are the angle bending interaction shown in Eq. (2). The force constant parameters are the same for the two angle bending terms θ_{134} and θ_{415}, which have the same arm lengths. All force constant parameters

VFF type	Bond stretching		Angle bending		
Expression	$\frac{1}{2}K_{12}(\Delta r_{12})^2$	$\frac{1}{2}K_{14}(\Delta r_{14})^2$	$\frac{1}{2}K_{123}(\Delta\theta_{123})^2$	$\frac{1}{2}K_{134}(\Delta\theta_{134})^2$	$\frac{1}{2}K_{415}(\Delta\theta_{415})^2$
Parameter	3.872	3.872	3.157	7.674	7.674
r_0 or θ_0	2.887	2.730	95.087	92.500	95.411

The second line gives an explicit expression for each VFF term, where atom indexes are from **Figure 189(c)**. The third line is the force constant parameters. Parameters are in the unit of eV/Å^2 for the bond stretching interaction and in the unit of eV for the angle bending interaction. The fourth line gives the initial bond length (in the unit of Å) for the bond stretching interaction and the initial angle (in the unit of degrees) for the angle bending interaction. The angle θ_{ijk} has atom i as the apex.

Table 414. The VFF model for the single-layer p-SnSe.

are determined by fitting to the acoustic branches in the phonon dispersion along the ΓX as shown in **Figure 212(a)**. The *ab initio* calculations are from Ref. [82]. **Figure 212(b)** shows that the VFF model and the SW potential give exactly the same phonon dispersion.

The parameters for the two-body SW potential used by GULP are shown in **Table 415**. The parameters for the three-body SW potential used by GULP are shown in **Table 416**. Parameters for the SW potential used by LAMMPS are listed in **Table 417**. Eight atom types have been introduced for writing the SW potential script used by LAMMPS as shown in **Figure 190** with M = Sn and X = Se, which helps to increase the cutoff for the bond stretching interaction between atom 1 and atom 2 in **Figure 189(c)**.

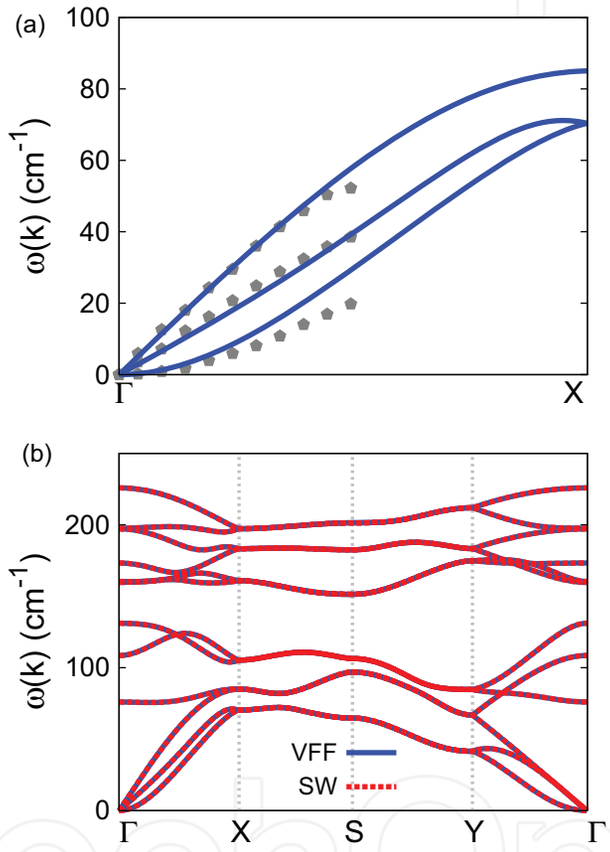

Figure 212. Phonon dispersion for the single-layer p-SnSe. (a) The VFF model is fitted to the acoustic branches in the long wave limit along the ΓX direction. The *ab initio* calculations are from Ref. [82]. (b) The VFF model (blue lines) and the SW potential (red lines) give the same phonon dispersion for the p-SnSe along ΓXSYΓ.

	A (eV)	ρ (Å)	B (Å^4)	$r_{\min}$ (Å)	$r_{\max}$ (Å)
r_{12}	0.565	0.056	34.734	0.0	3.088
r_{14}	5.811	1.989	27.773	0.0	3.895

The quantity (r_{ij}) in the first line lists one representative term for the two-body SW potential between atoms i and j. Atom indexes are from **Figure 189(c)**.

Table 415. Two-body SW potential parameters for the single-layer p-SnSe used by GULP [8], as expressed in Eq. (3).

	K (eV)	θ_0 (°)	ρ_1 (Å)	ρ_2 (Å)	$r_{\min 12}$ (Å)	$r_{\max 12}$ (Å)	$r_{\min 13}$ (Å)	$r_{\max 13}$ (Å)	$r_{\min 23}$ (Å)	$r_{\max 23}$ (Å)
θ_{123}	2.777	95.087	0.056	0.056	0.0	3.088	0.0	3.088	0.0	4.357
θ_{134}	27.996	92.500	1.989	0.056	0.0	3.895	0.0	3.088	0.0	4.530
θ_{415}	28.193	95.411	1.989	0.056	0.0	3.895	0.0	3.088	0.0	4.576

The first line (θ_{ijk}) presents one representative term for the three-body SW potential. The angle θ_{ijk} has the atom i as the apex. Atom indexes are from **Figure 189(c)**.

Table 416. Three-body SW potential parameters for the single-layer p-SnSe used by GULP [8], as expressed in Eq. (4).

	ϵ (eV)	σ (Å)	a	λ	γ	$\cos\theta_0$	A_L	B_L	p	q	Tol
Sn_1—Se_4—Se_4	1.000	0.056	55.166	2.777	1.000	−0.089	0.565	3537820.961	4	0	0.0
Sn_1—Se_1—Se_1	1.000	1.989	1.959	0.000	1.000	0.000	5.811	1.776	4	0	0.0
Sn_1—Se_1—Se_4	1.000	0.000	0.000	27.996	1.000	−0.044	0.000	0.000	4	0	0.0
Se_1—Sn_1—Sn_2	1.000	0.000	0.000	28.193	1.000	−0.094	0.000	0.000	4	0	0.0

Atom types in the first column are displayed in **Figure 190**, with M = Sn and X = Se.

Table 417. SW potential parameters for p-SnSe used by LAMMPS [9], as expressed in Eqs. (9) and (10).

Figure 213 shows the stress-strain relations for the single-layer p-SnSe of size 100 × 100 Å. The structure is uniaxially stretched in the armchair or zigzag directions at 1 and 300 K. The Young's modulus is 11.4 and 34.1 Nm^{-1} in the armchair and zigzag directions, respectively, at 1 K, which is obtained by linear fitting of the stress-strain relations in [0, 0.01]. The Poisson's ratios from the VFF model and the SW potential are $\nu_{xy} = 0.11$ and $\nu_{yx} = 0.33$. The third-order nonlinear elastic constant D can be obtained by fitting the stress-strain relation to $\sigma = E\epsilon + \frac{1}{2}D\epsilon^2$ with E as the Young's modulus. The values of D are −22.0 and −128.8 Nm^{-1} at

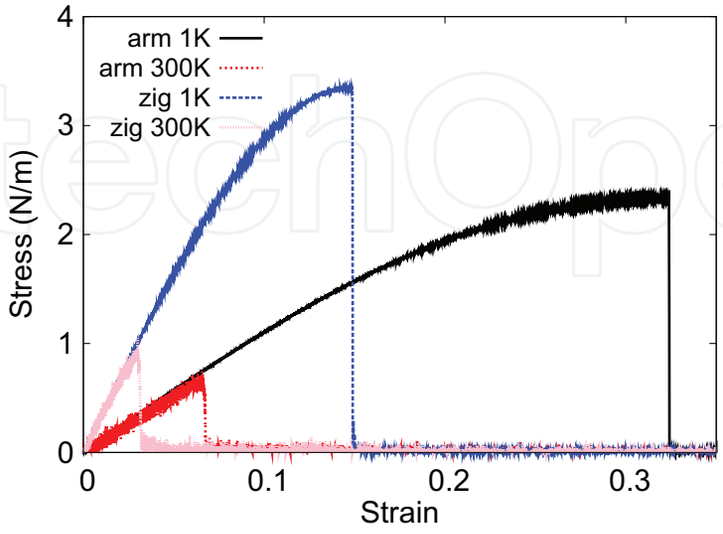

Figure 213. Stress-strain relations for the single-layer p-SnSe of size 100 × 100 Å. The single-layer p-SnSe is uniaxially stretched along the armchair or zigzag directions at temperatures 1 and 300 K.

1 K along the armchair and zigzag directions, respectively. The ultimate stress is about 2.3 Nm^{-1} at the critical strain of 0.32 in the armchair direction at the low temperature of 1 K. The ultimate stress is about 3.3 Nm^{-1} at the critical strain of 0.15 in the zigzag direction at the low temperature of 1 K.

105. P-CTe

Present studies on the puckered (p-) CTe are based on first-principles calculations, and no empirical potential has been proposed for the p-CTe. We will thus parametrize the SW potential for the single-layer p-CTe in this section.

The structure of the single-layer p-CTe is shown in **Figure 189**, with M = C and X = Te. Structural parameters for p-CTe are from the *ab initio* calculations [78]. There are four atoms in the unit cell with relative coordinates such as $(-u, 0, -v)$, $(u, 0, v)$, $(0.5-u, 0.5, v+w)$, and $(0.5+u, 0.5, -v+w)$ with $u = 0.0837$, $v = 0.1041$, and $w = -0.0371$. The values of these dimensionless parameters are extracted from the geometrical parameters provided in Ref. [78], including lattice constants $a_1 = 3.889$ Å and $a_2 = 3.390$ Å, bond lengths $d_{12} = 2.164$ Å and $d_{14} = 2.181$ Å, and the angle $\theta_{145} = 110.0°$. The dimensionless parameters v and w are ratios based on the lattice constant in the out-of-plane z-direction, which is arbitrarily chosen as $a_3 = 10.0$ Å. We note that the main purpose of the usage of u, v, and w in representing atomic coordinates is to follow the same convention for all puckered structures in the present work. The resultant atomic coordinates are the same as that in Ref. [78].

As shown in **Figure 189**, a specific feature in the puckered configuration of the p-CTe is that there is a small difference of wa_3 between the z-coordinate of atom 1 and the z-coordinates of atoms 2 and 3. Similarly, atom 4 is higher than atoms 5 and 6 for wa_3 along the z-direction. The sign of w determines which types of atoms take the outmost positions, e.g., atoms 1, 5, and 6 are the outmost atoms if $w > 0$ in **Figure 189(c)**, while atoms 2, 3, and 4 will take the outmost positions for $w < 0$.

Table 418 shows five VFF terms for the single-layer p-CTe; two of which are the bond stretching interactions shown in Eq. (1), while the other three terms are the angle bending

VFF type	Bond stretching		Angle bending		
Expression	$\frac{1}{2}K_{12}(\Delta r_{12})^2$	$\frac{1}{2}K_{14}(\Delta r_{14})^2$	$\frac{1}{2}K_{123}(\Delta\theta_{123})^2$	$\frac{1}{2}K_{134}(\Delta\theta_{134})^2$	$\frac{1}{2}K_{415}(\Delta\theta_{415})^2$
Parameter	13.235	13.235	4.210	3.901	3.901
r_0 or θ_0	2.164	2.181	103.122	110.000	90.854

The second line gives an explicit expression for each VFF term, where atom indexes are from **Figure 189(c)**. The third line is the force constant parameters. Parameters are in the unit of eV/Å^2 for the bond stretching interaction and in the unit of eV for the angle bending interaction. The fourth line gives the initial bond length (in the unit of Å) for the bond stretching interaction and the initial angle (in the unit of degrees) for the angle bending interaction. The angle θ_{ijk} has atom i as the apex.

Table 418. The VFF model for the single-layer p-CTe.

interaction shown in Eq. (2). The force constant parameters are the same for the two angle bending terms θ_{134} and θ_{415}, which have the same arm lengths. All force constant parameters are determined by fitting to the acoustic branches in the phonon dispersion along the ΓX as shown in **Figure 214(a)**. The *ab initio* calculations for the phonon dispersion are calculated from the SIESTA package [79]. The generalized gradients approximation is applied to account for the exchange-correlation function with Perdew et al. parameterization [80], and the double-ζ orbital basis set is adopted. **Figure 214(b)** shows that the VFF model and the SW potential give exactly the same phonon dispersion.

The parameters for the two-body SW potential used by GULP are shown in **Table 419**. The parameters for the three-body SW potential used by GULP are shown in **Table 420**. Parameters for the SW potential used by LAMMPS are listed in **Table 421**. Eight atom types have been introduced for writing the SW potential script used by LAMMPS as shown in **Figure 190** with M = C and X = Te, which helps to increase the cutoff for the bond stretching interaction between atom 1 and 2 in **Figure 189(c)**.

Figure 215 shows the stress-strain relations for the single-layer p-CTe of size 100 × 100 Å. The structure is uniaxially stretched in the armchair or zigzag directions at 1 and 300 K. The Young's modulus is 10.8 and 89.1 Nm^{-1} in the armchair and zigzag directions, respectively, at

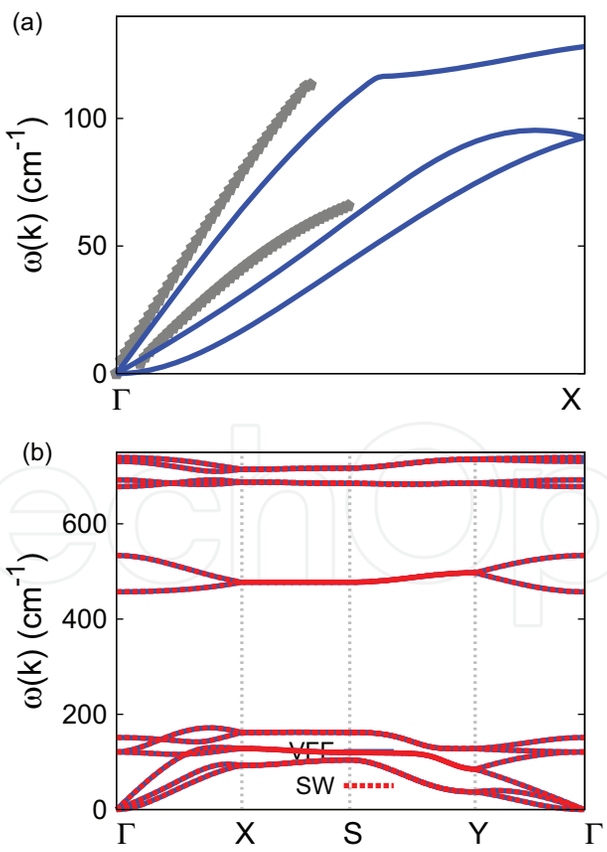

Figure 214. Phonon dispersion for the single-layer p-CTe. (a) The VFF model is fitted to the acoustic branches in the long wave limit along the ΓX direction. The *ab initio* calculations are calculated from SIESTA. (b) The VFF model (blue lines) and the SW potential (red lines) give the same phonon dispersion for the p-CTe along ΓXSYΓ.

	A (eV)	ρ (Å)	B (Å^4)	$r_{\min}$ (Å)	$r_{\max}$ (Å)
r_{12}	4.165	0.424	10.965	0.0	2.643
r_{14}	12.519	1.569	11.313	0.0	3.106

The quantity (r_{ij}) in the first line lists one representative term for the two-body SW potential between atoms i and j. Atom indexes are from **Figure 189(c)**.

Table 419. Two-body SW potential parameters for the single-layer p-CTe used by GULP [8], as expressed in Eq. (3).

	K (eV)	θ_0 (°)	ρ_1 (Å)	ρ_2 (Å)	$r_{\min 12}$ (Å)	$r_{\max 12}$ (Å)	$r_{\min 13}$ (Å)	$r_{\max 13}$ (Å)	$r_{\min 23}$ (Å)	$r_{\max 23}$ (Å)
θ_{123}	13.040	103.122	0.424	0.424	0.0	2.643	0.0	2.643	0.0	3.639
θ_{134}	29.206	110.000	1.569	0.424	0.0	3.106	0.0	2.643	0.0	4.280
θ_{415}	25.795	90.854	1.569	0.424	0.0	3.106	0.0	2.643	0.0	4.043

The first line (θ_{ijk}) presents one representative term for the three-body SW potential. The angle θ_{ijk} has the atom i as the apex. Atom indexes are from **Figure 189(c)**.

Table 420. Three-body SW potential parameters for the single-layer p-CTe used by GULP [8], as expressed in Eq. (4).

	ϵ (eV)	σ (Å)	a	λ	γ	$\cos\theta_0$	A_L	B_L	p	q	Tol
C_1—Te_4—Te_4	1.000	0.424	6.232	13.040	1.000	−0.227	4.165	338.925	4	0	0.0
C_1—Te_1—Te_1	1.000	1.569	1.979	0.000	1.000	0.000	12.519	1.866	4	0	0.0
C_1—Te_1—Te_4	1.000	0.000	0.000	29.206	1.000	−0.342	0.000	0.000	4	0	0.0
Te_1—C_1—C_2	1.000	0.000	0.000	25.795	1.000	−0.015	0.000	0.000	4	0	0.0

Atom types in the first column are displayed in **Figure 190**, with M = C and X = Te.

Table 421. SW potential parameters for p-CTe used by LAMMPS [9], as expressed in Eqs. (9) and (10).

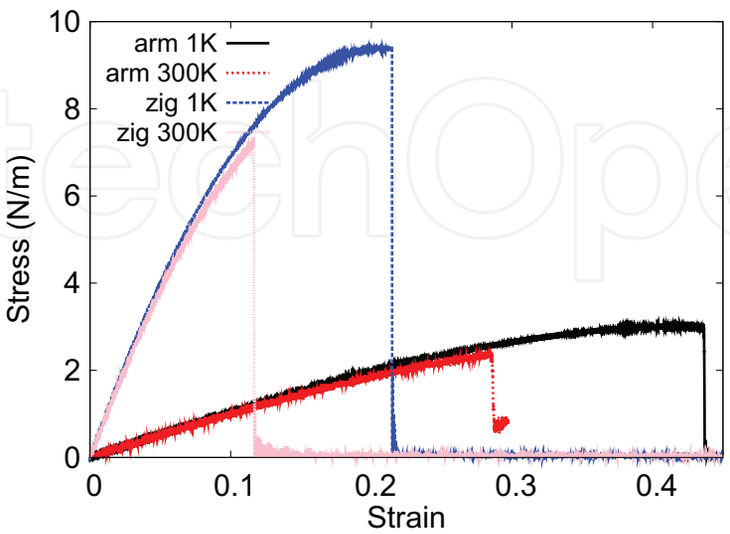

Figure 215. Stress-strain relations for the single-layer p-CTe of size 100 × 100 Å. The single-layer p-CTe is uniaxially stretched along the armchair or zigzag directions at temperatures 1 and 300 K.

1 K, which is obtained by linear fitting of the stress-strain relations in [0, 0.01]. The Poisson's ratios from the VFF model and the SW potential are $\nu_{xy} = 0.02$ and $\nu_{yx} = 0.20$. The third-order nonlinear elastic constant D can be obtained by fitting the stress-strain relation to $\sigma = E\epsilon + \frac{1}{2}D\epsilon^2$ with E as the Young's modulus. The values of D are -15.3 and -419.6 Nm^{-1} at 1 K along the armchair and zigzag directions, respectively. The ultimate stress is about 3.0 Nm^{-1} at the critical strain of 0.43 in the armchair direction at the low temperature of 1 K. The ultimate stress is about 9.4 Nm^{-1} at the critical strain of 0.21 in the zigzag direction at the low temperature of 1 K.

106. P-SiTe

Present studies on the puckered (p-) SiTe are based on first-principles calculations, and no empirical potential has been proposed for the p-SiTe. We will thus parametrize the SW potential for the single-layer p-SiTe in this section.

The structure of the single-layer p-SiTe is shown in **Figure 189**, with M = Si and X = Te. Structural parameters for p-SiTe are from the *ab initio* calculations [78]. There are four atoms in the unit cell with relative coordinates such as $(-u, 0, -v)$, $(u, 0, v)$, $(0.5 - u, 0.5, v + w)$, and $(0.5 + u, 0.5, -v + w)$ with $u = 0.0581$, $v = 0.1363$, and $w = -0.0173$. The values of these dimensionless parameters are extracted from the geometrical parameters provided in Ref. [78], including lattice constants $a_1 = 4.300$ Å and $a_2 = 4.109$ Å, bond lengths $d_{12} = 2.641$ Å and $d_{14} = 2.772$ Å, and the angle $\theta_{145} = 100.200°$. The dimensionless parameters v and w are ratios based on the lattice constant in the out-of-plane z-direction, which is arbitrarily chosen as $a_3 = 10.0$ Å. We note that the main purpose of the usage of u, v, and w in representing atomic coordinates is to follow the same convention for all puckered structures in the present work. The resultant atomic coordinates are the same as that in Ref. [78].

As shown in **Figure 189**, a specific feature in the puckered configuration of the p-SiTe is that there is a small difference of wa_3 between the z-coordinate of atom 1 and the z-coordinates of atoms 2 and 3. Similarly, atom 4 is higher than atoms 5 and 6 for wa_3 along the z-direction. The sign of w determines which types of atoms take the outmost positions, e.g., atoms 1, 5, and 6 are the outmost atoms if $w > 0$ in **Figure 189(c)**, while atoms 2, 3, and 4 will take the outmost positions for $w < 0$.

Table 422 shows five VFF terms for the single-layer p-SiTe; two of which are the bond stretching interactions shown in Eq. (1), while the other three terms are the angle bending interaction shown in Eq. (2). The force constant parameters are the same for the two angle bending terms θ_{134} and θ_{415}, which have the same arm lengths. All force constant parameters are determined by fitting to the acoustic branches in the phonon dispersion along the ΓX as shown in **Figure 216(a)**. The *ab initio* calculations are from Ref. [83]. **Figure 216(b)** shows that the VFF model and the SW potential give exactly the same phonon dispersion.

The parameters for the two-body SW potential used by GULP are shown in **Table 423**. The parameters for the three-body SW potential used by GULP are shown in **Table 424**. Parameters for the SW potential used by LAMMPS are listed in **Table 425**. Eight atom types have been

VFF type	Bond stretching		Angle bending		
Expression	$\frac{1}{2}K_{12}(\Delta r_{12})^2$	$\frac{1}{2}K_{14}(\Delta r_{14})^2$	$\frac{1}{2}K_{123}(\Delta\theta_{123})^2$	$\frac{1}{2}K_{134}(\Delta\theta_{134})^2$	$\frac{1}{2}K_{415}(\Delta\theta_{415})^2$
Parameter	9.479	2.892	3.145	10.111	10.111
r_0 or θ_0	2.641	2.772	102.142	100.200	92.760

The second line gives an explicit expression for each VFF term, where atom indexes are from **Figure 189(c)**. The third line is the force constant parameters. Parameters are in the unit of eV/Å^2 for the bond stretching interaction and in the unit of eV for the angle bending interaction. The fourth line gives the initial bond length (in the unit of Å) for the bond stretching interaction and the initial angle (in the unit of degrees) for the angle bending interaction. The angle θ_{ijk} has atom i as the apex.

Table 422. The VFF model for the single-layer p-SiTe.

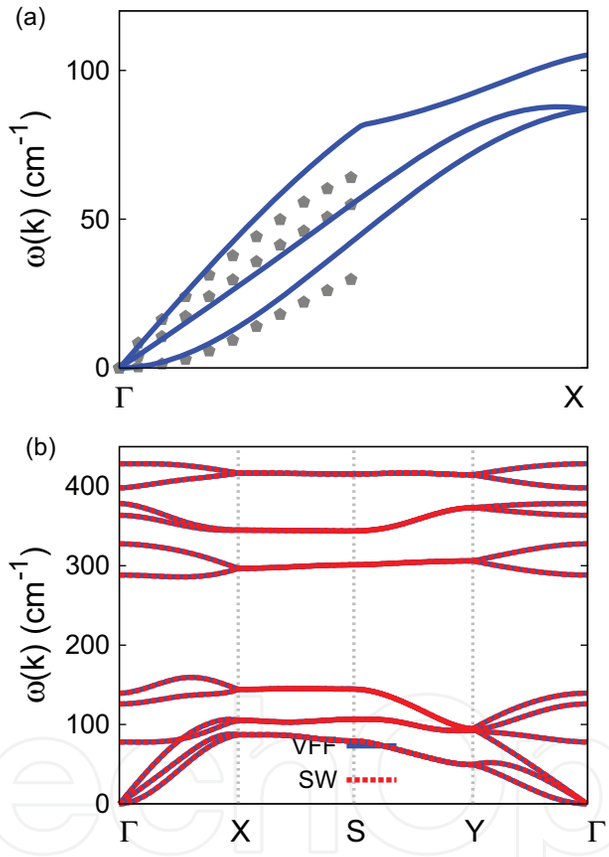

Figure 216. Phonon dispersion for the single-layer p-SiTe. (a) The VFF model is fitted to the acoustic branches in the long wave limit along the ΓX direction. The *ab initio* calculations are from Ref. [83]. (b) The VFF model (blue lines) and the SW potential (red lines) give the same phonon dispersion for the p-SiTe along ΓXSYΓ.

introduced for writing the SW potential script used by LAMMPS as shown in **Figure 190** with M = Si and X = Te, which helps to increase the cutoff for the bond stretching interaction between atom 1 and 2 in **Figure 189(c)**.

Figure 217 shows the stress-strain relations for the single-layer p-SiTe of size 100 × 100 Å. The structure is uniaxially stretched in the armchair or zigzag directions at 1 and 300 K. The

	A (eV)	ρ (Å)	B (Å^4)	$r_{\min}$ (Å)	$r_{\max}$ (Å)
r_{12}	2.394	0.194	24.324	0.0	2.999
r_{14}	3.818	1.722	29.522	0.0	3.864

The quantity (r_{ij}) in the first line lists one representative term for the two-body SW potential between atoms i and j. Atom indexes are from **Figure 189(c)**.

Table 423. Two-body SW potential parameters for the single-layer p-SiTe used by GULP [8], as expressed in Eq. (3).

	K (eV)	θ_0 (°)	ρ_1 (Å)	ρ_2 (Å)	$r_{\min 12}$ (Å)	$r_{\max 12}$ (Å)	$r_{\min 13}$ (Å)	$r_{\max 13}$ (Å)	$r_{\min 23}$ (Å)	$r_{\max 23}$ (Å)
θ_{123}	4.868	102.142	0.194	0.194	0.0	2.999	0.0	2.999	0.0	4.204
θ_{134}	43.419	100.200	1.722	0.194	0.0	3.864	0.0	2.999	0.0	4.577
θ_{415}	42.155	92.760	1.722	0.194	0.0	3.864	0.0	2.999	0.0	4.289

The first line (θ_{ijk}) presents one representative term for the three-body SW potential. The angle θ_{ijk} has the atom i as the apex. Atom indexes are from **Figure 189(c)**.

Table 424. Three-body SW potential parameters for the single-layer p-SiTe used by GULP [8], as expressed in Eq. (4).

	ϵ (eV)	σ (Å)	a	λ	γ	$\cos\theta_0$	A_L	B_L	p	q	Tol
Si_1—Te_4—Te_4	1.000	0.194	15.442	4.868	1.000	−0.210	2.394	17093.960	4	0	0.0
Si_1—Te_1—Te_1	1.000	1.722	2.245	0.000	1.000	0.000	3.818	3.360	4	0	0.0
Si_1—Te_1—Te_4	1.000	0.000	0.000	43.419	1.000	−0.177	0.000	0.000	4	0	0.0
Te_1—Si_1—Si_2	1.000	0.000	0.000	42.155	1.000	−0.048	0.000	0.000	4	0	0.0

Atom types in the first column are displayed in **Figure 190**, with M = Si and X = Te.

Table 425. SW potential parameters for p-SiTe used by LAMMPS [9], as expressed in Eqs. (9) and (10).

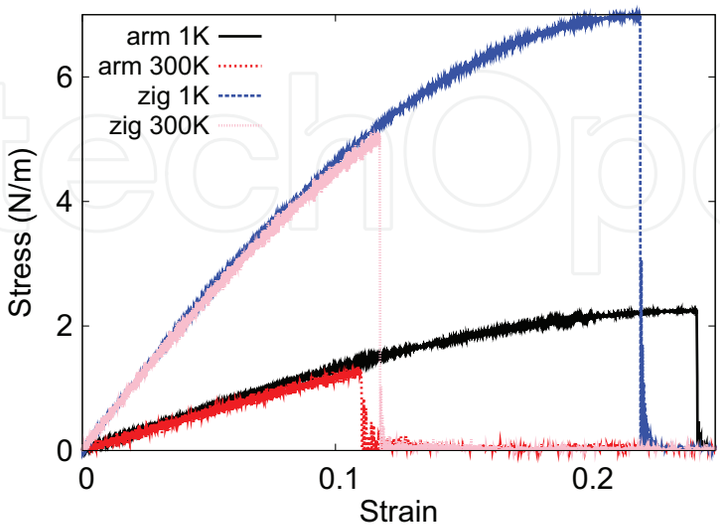

Figure 217. Stress-strain relations for the single-layer p-SiTe of size 100 × 100 Å. The single-layer p-SiTe is uniaxially stretched along the armchair or zigzag directions at temperatures 1 and 300 K.

Young's modulus is 14.0 and 53.6 Nm^{-1} in the armchair and zigzag directions, respectively, at 1 K, which is obtained by linear fitting of the stress-strain relations in [0, 0.01]. The Poisson's ratios from the VFF model and the SW potential are $\nu_{xy} = 0.12$ and $\nu_{yx} = 0.47$. The third-order nonlinear elastic constant D can be obtained by fitting the stress-strain relation to $\sigma = E\epsilon + \frac{1}{2}D\epsilon^2$ with E as the Young's modulus. The values of D are -32.9 and -183.2 Nm^{-1} at 1 K along the armchair and zigzag directions, respectively. The ultimate stress is about 2.2 Nm^{-1} at the critical strain of 0.24 in the armchair direction at the low temperature of 1 K. The ultimate stress is about 7.0 Nm^{-1} at the critical strain of 0.22 in the zigzag direction at the low temperature of 1 K.

107. P-GeTe

Present studies on the puckered (p-) GeTe are based on first-principles calculations, and no empirical potential has been proposed for the p-GeTe. We will thus parametrize the SW potential for the single-layer p-GeTe in this section.

The structure of the single-layer p-GeTe is shown in **Figure 189**, with M = Ge and X = Te. Structural parameters for p-GeTe are from the *ab initio* calculations [78]. There are four atoms in the unit cell with relative coordinates such as $(-u, 0, -v)$, $(u, 0, v)$, $(0.5 - u, 0.5, v + w)$, and $(0.5 + u, 0.5, -v + w)$ with $u = 0.0538$, $v = 0.1422$, and $w = -0.0216$. The values of these dimensionless parameters are extracted from the geometrical parameters provided in Ref. [78], including lattice constants $a_1 = 4.376$ Å and $a_2 = 4.238$ Å, bond lengths $d_{12} = 2.736$ Å and $d_{14} = 2.883$ Å, and the angle $\theta_{145} = 100.4^\circ$. The dimensionless parameters v and w are ratios based on the lattice constant in the out-of-plane z-direction, which is arbitrarily chosen as $a_3 = 10.0$ Å. We note that the main purpose of the usage of u, v, and w in representing atomic coordinates is to follow the same convention for all puckered structures in the present work. The resultant atomic coordinates are the same as that in Ref. [78].

As shown in **Figure 189**, a specific feature in the puckered configuration of the p-GeTe is that there is a small difference of wa_3 between the z-coordinate of atom 1 and the z-coordinates of atoms 2 and 3. Similarly, atom 4 is higher than atoms 5 and 6 for wa_3 along the z-direction. The sign of w determines which types of atoms take the outmost positions, e.g., atoms 1, 5, and 6 are the outmost atoms if $w > 0$ in **Figure 189(c)**, while atoms 2, 3, and 4 will take the outmost positions for $w < 0$.

Table 426 shows five VFF terms for the single-layer p-GeTe; two of which are the bond stretching interactions shown in Eq. (1), while the other three terms are the angle bending interaction shown by Eq. (2). The force constant parameters are the same for the two angle bending terms θ_{134} and θ_{415}, which have the same arm lengths. All force constant parameters are determined by fitting to the acoustic branches in the phonon dispersion along the ΓX as shown in **Figure 218(a)**. The *ab initio* calculations for the phonon dispersion are calculated from the SIESTA package [79]. The generalized gradients approximation is applied to account for the exchange-correlation function with Perdew et al. parameterization [80], and the double-ζ

VFF type	Bond stretching		Angle bending		
Expression	$\frac{1}{2}K_{12}(\Delta r_{12})^2$	$\frac{1}{2}K_{14}(\Delta r_{14})^2$	$\frac{1}{2}K_{123}(\Delta\theta_{123})^2$	$\frac{1}{2}K_{134}(\Delta\theta_{134})^2$	$\frac{1}{2}K_{415}(\Delta\theta_{415})^2$
Parameter	7.074	7.074	2.611	5.876	5.876
r_0 or θ_0	2.736	2.883	101.517	100.400	91.402

The second line gives an explicit expression for each VFF term, where atom indexes are from **Figure 189(c)**. The third line is the force constant parameters. Parameters are in the unit of eV/Å^2 for the bond stretching interaction and in the unit of eV for the angle bending interaction. The fourth line gives the initial bond length (in the unit of Å) for the bond stretching interaction and the initial angle (in the unit of degrees) for the angle bending interaction. The angle θ_{ijk} has atom i as the apex.

Table 426. The VFF model for the single-layer p-GeTe.

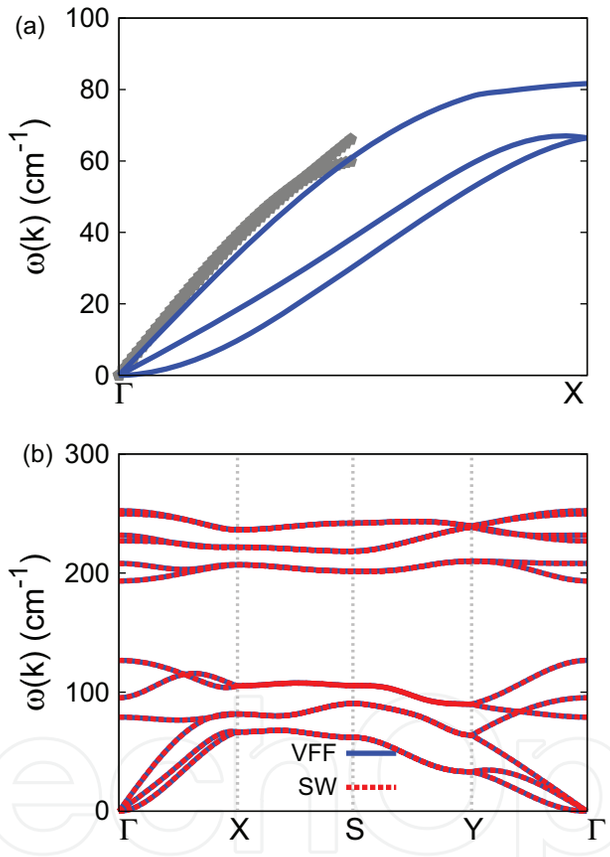

Figure 218. Phonon dispersion for the single-layer p-GeTe. (a) The VFF model is fitted to the acoustic branches in the long wave limit along the ΓX direction. The *ab initio* calculations are calculated from SIESTA. (b) The VFF model (blue lines) and the SW potential (red lines) give the same phonon dispersion for the p-GeTe along ΓXSYΓ.

orbital basis set is adopted. **Figure 218(b)** shows that the VFF model and the SW potential give exactly the same phonon dispersion.

The parameters for the two-body SW potential used by GULP are shown in **Table 427**. The parameters for the three-body SW potential used by GULP are shown in **Table 428**. Parameters for the SW potential used by LAMMPS are listed in **Table 429**. Eight atom types have been

	A (eV)	ρ (Å)	B (Å^4)	$r_{\min}$ (Å)	$r_{\max}$ (Å)
r_{12}	1.708	0.165	28.018	0.0	3.072
r_{14}	9.854	1.745	34.542	0.0	4.005

The quantity (r_{ij}) in the first line lists one representative term for the two-body SW potential between atoms i and j. Atom indexes are from **Figure 189(c)**.

Table 427. Two-body SW potential parameters for the single-layer p-GeTe used by GULP [8], as expressed in Eq. (3).

	K (eV)	θ_0 (°)	ρ_1 (Å)	ρ_2 (Å)	$r_{\min 12}$ (Å)	$r_{\max 12}$ (Å)	$r_{\min 13}$ (Å)	$r_{\max 13}$ (Å)	$r_{\min 23}$ (Å)	$r_{\max 23}$ (Å)
θ_{123}	3.626	101.517	0.165	0.165	0.0	3.072	0.0	3.072	0.0	4.307
θ_{134}	23.509	100.400	1.745	0.165	0.0	4.005	0.0	3.072	0.0	4.659
θ_{415}	22.756	91.402	1.745	0.165	0.0	4.005	0.0	3.072	0.0	4.434

The first line (θ_{ijk}) presents one representative term for the three-body SW potential. The angle θ_{ijk} has the atom i as the apex. Atom indexes are from **Figure 189(c)**.

Table 428. Three-body SW potential parameters for the single-layer p-GeTe used by GULP [8], as expressed in Eq. (4).

	ϵ (eV)	σ (Å)	a	λ	γ	$\cos\theta_0$	A_L	B_L	p	q	Tol
Ge_1—Te_4—Te_4	1.000	0.165	18.665	3.626	1.000	−0.200	1.708	38204.858	4	0	0.0
Ge_1—Te_1—Te_1	1.000	1.745	2.295	0.000	1.000	0.000	9.854	3.725	4	0	0.0
Ge_1—Te_1—Te_4	1.000	0.000	0.000	23.509	1.000	−0.181	0.000	0.000	4	0	0.0
Te_1—Ge_1—Ge_2	1.000	0.000	0.000	22.756	1.000	−0.024	0.000	0.000	4	0	0.0

Atom types in the first column are displayed in **Figure 190**, with M = Ge and X = Te.

Table 429. SW potential parameters for p-GeTe used by LAMMPS [9], as expressed in Eqs. (9) and (10).

introduced for writing the SW potential script used by LAMMPS as shown in **Figure 190** with M = Ge and X = Te, which helps to increase the cutoff for the bond stretching interaction between atom 1 and 2 in **Figure 189(c)**.

Figure 219 shows the stress-strain relations for the single-layer p-GeTe of size 100 × 100 Å. The structure is uniaxially stretched in the armchair or zigzag directions at 1 and 300 K. The Young's modulus is 8.1 and 41.6 N/m in the armchair and zigzag directions, respectively, at 1 K, which is obtained by linear fitting of the stress-strain relations in [0, 0.01]. The Poisson's ratios from the VFF model and the SW potential are $\nu_{xy} = 0.09$ and $\nu_{yx} = 0.49$. The third-order nonlinear elastic constant D can be obtained by fitting the stress-strain relation to $\sigma = E\epsilon + \frac{1}{2}D\epsilon^2$ with E as the Young's modulus. The values of D are −10.5 and −143.7 N/m at 1 K along the armchair and zigzag directions, respectively. The ultimate stress is about 2.6 N/m at the critical strain of 0.53 in the armchair direction at the low temperature of 1 K. The ultimate stress is about 5.3 N/m at the critical strain of 0.21 in the zigzag direction at the low temperature of 1 K.

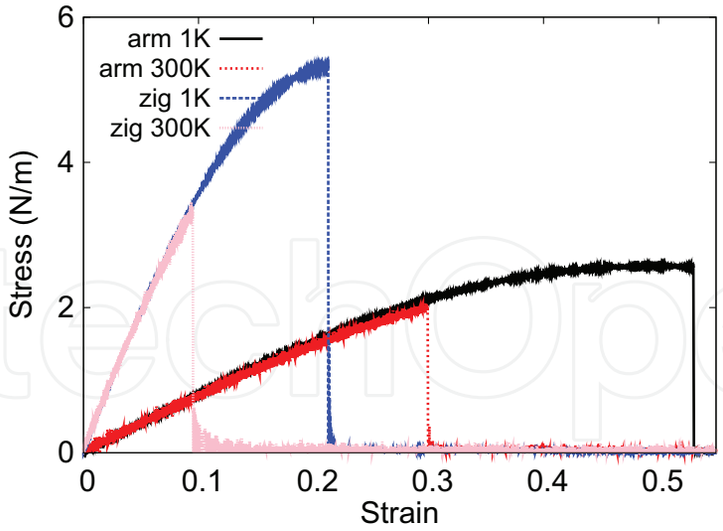

Figure 219. Stress-strain relations for the single-layer p-GeTe of size 100 × 100 Å. The single-layer p-GeTe is uniaxially stretched along the armchair or zigzag directions at temperatures 1 and 300 K.

108. P-SnTe

Present studies on the puckered (p-) SnTe are based on first-principles calculations, and no empirical potential has been proposed for the p-SnTe. We will thus parametrize the SW potential for the single-layer p-SnTe in this section.

The structure of the single-layer p-SnTe is shown in **Figure 189**, with M = Sn and X = Te. Structural parameters for p-SnTe are from the *ab initio* calculations [78]. There are four atoms in the unit cell with relative coordinates such as $(-u, 0, -v)$, $(u, 0, v)$, $(0.5-u, 0.5, v+w)$, and $(0.5+u, 0.5, -v+w)$ with $u = 0.0478$, $v = 0.1567$, and $w = -0.0050$. The values of these dimensionless parameters are extracted from the geometrical parameters provided in Ref. [78], including lattice constants $a_1 = 4.581$ Å and $a_2 = 4.542$ Å, bond lengths $d_{12} = 2.931$ Å and $d_{14} = 3.164$ Å, and the angle $\theta_{145} = 96.0°$. The dimensionless parameters v and w are ratios based on the lattice constant in the out-of-plane z-direction, which is arbitrarily chosen as $a_3 = 10.0$ Å. We note that the main purpose of the usage of u, v, and w in representing atomic coordinates is to follow the same convention for all puckered structures in the present work. The resultant atomic coordinates are the same as that in Ref. [78].

As shown in **Figure 189**, a specific feature in the puckered configuration of the p-SnTe is that there is a small difference of wa_3 between the z-coordinate of atom 1 and the z-coordinates of atoms 2 and 3. Similarly, atom 4 is higher than atoms 5 and 6 for wa_3 along the z-direction. The sign of w determines which types of atoms take the outmost positions, e.g., atoms 1, 5, and 6 are the outmost atoms if $w > 0$ in **Figure 189(c)**, while atoms 2, 3, and 4 will take the outmost positions for $w < 0$.

Table 430 shows five VFF terms for the single-layer p-SnTe; two of which are the bond stretching interactions shown in Eq. (1), while the other three terms are the angle bending interaction shown in Eq. (2). The force constant parameters are the same for the two angle

VFF type	Bond stretching		Angle bending		
Expression	$\frac{1}{2}K_{12}(\Delta r_{12})^2$	$\frac{1}{2}K_{14}(\Delta r_{14})^2$	$\frac{1}{2}K_{123}(\Delta\theta_{123})^2$	$\frac{1}{2}K_{134}(\Delta\theta_{134})^2$	$\frac{1}{2}K_{415}(\Delta\theta_{415})^2$
Parameter	7.074	7.074	2.611	2.611	5.876
r_0 or θ_0	2.931	3.164	101.578	96.000	94.045

The second line gives an explicit expression for each VFF term, where atom indexes are from **Figure 189(c)**. The third line is the force constant parameters. Parameters are in the unit of eV/Å^2 for the bond stretching interaction and in the unit of eV for the angle bending interaction. The fourth line gives the initial bond length (in the unit of Å) for the bond stretching interaction and the initial angle (in the unit of degrees) for the angle bending interaction. The angle θ_{ijk} has atom i as the apex.

Table 430. The VFF model for the single-layer p-SnTe.

bending terms θ_{134} and θ_{415}, which have the same arm lengths. All force constant parameters are determined by fitting to the acoustic branches in the phonon dispersion along the ΓX as shown in **Figure 220(a)**. The *ab initio* calculations for the phonon dispersion are calculated from the SIESTA package [79]. The generalized gradients approximation is applied to account for the exchange-correlation function with Perdew et al. parameterization [80], and the double-ζ orbital basis set is adopted. **Figure 220(b)** shows that the VFF model and the SW potential give exactly the same phonon dispersion.

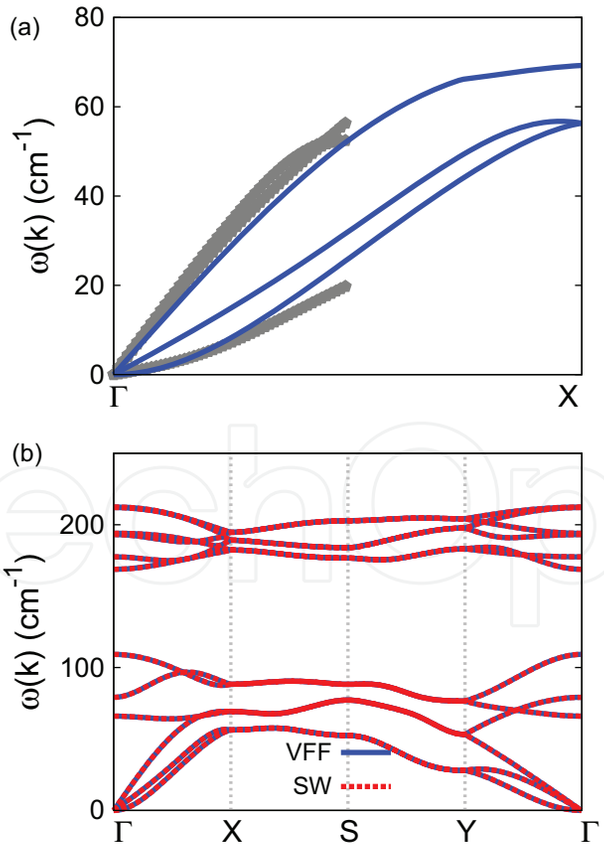

Figure 220. Phonon dispersion for the single-layer p-SnTe. (a) The VFF model is fitted to the acoustic branches in the long wave limit along the ΓX direction. The *ab initio* calculations are calculated from SIESTA. (b) The VFF model (blue lines) and the SW potential (red lines) give the same phonon dispersion for the p-SnTe along ΓXSYΓ.

The parameters for the two-body SW potential used by GULP are shown in **Table 431**. The parameters for the three-body SW potential used by GULP are shown in **Table 432**. Parameters for the SW potential used by LAMMPS are listed in **Table 433**. Eight atom types have been introduced for writing the SW potential script used by LAMMPS as shown in **Figure 190** with M = Sn and X = Te, which helps to increase the cutoff for the bond stretching interaction between atom 1 and 2 in **Figure 189(c)**.

Figure 221 shows the stress-strain relations for the single-layer p-SnTe of size 100 × 100 Å. The structure is uniaxially stretched in the armchair or zigzag directions at 1 and 300 K. The Young's modulus is 6.6 and 38.5 Nm^{-1} in the armchair and zigzag directions, respectively, at 1 K, which is obtained by linear fitting of the stress-strain relations in [0, 0.01]. The Poisson's ratios from the VFF model and the SW potential are $\nu_{xy} = 0.10$ and $\nu_{yx} = 0.57$. The third-order nonlinear elastic constant D can be obtained by fitting the stress-strain relation to $\sigma = E\epsilon + \frac{1}{2}D\epsilon^2$ with E as the Young's modulus. The values of D are −7.2 and −114.5 N/m at 1 K along the armchair and zigzag directions, respectively. The ultimate stress is about 2.4 Nm^{-1} at the critical strain of 0.61 in the armchair direction at the low temperature of 1 K. The ultimate

	A (eV)	ρ (Å)	B (Å^4)	r_{min} (Å)	r_{max} (Å)
r_{12}	1.662	0.131	36.901	0.0	3.241
r_{14}	11.054	1.777	50.109	0.0	4.349

The quantity (r_{ij}) in the first line lists one representative term for the two-body SW potential between atoms i and j. Atom indexes are from **Figure 189(c)**.

Table 431. Two-body SW potential parameters for the single-layer p-SnTe used by GULP [8], as expressed in Eq. (3).

	K (eV)	θ_0 (°)	ρ_1 (Å)	ρ_2 (Å)	$r_{min\,12}$ (Å)	$r_{max\,12}$ (Å)	$r_{min\,13}$ (Å)	$r_{max\,13}$ (Å)	$r_{min\,23}$ (Å)	$r_{max\,23}$ (Å)
θ_{123}	3.170	101.578	0.131	0.131	0.0	3.241	0.0	3.241	0.0	4.562
θ_{134}	20.298	96.000	1.777	0.131	0.0	4.349	0.0	3.241	0.0	4.766
θ_{415}	20.176	94.045	1.777	0.131	0.0	4.349	0.0	3.241	0.0	4.595

The first line (θ_{ijk}) presents one representative term for the three-body SW potential. The angle θ_{ijk} has the atom i as the apex. Atom indexes are from **Figure 189(c)**.

Table 432. Three-body SW potential parameters for the single-layer p-SnTe used by GULP [8], as expressed in Eq. (4).

	ϵ (eV)	σ (Å)	a	λ	γ	$\cos\theta_0$	A_L	B_L	p	q	Tol
Sn_1—Te_4—Te_4	1.000	0.131	24.712	3.170	1.000	−0.201	1.662	124727.735	4	0	0.0
Sn_1—Te_1—Te_1	1.000	1.777	2.448	0.000	1.000	0.000	11.054	5.028	4	0	0.0
Sn_1—Te_1—Te_4	1.000	0.000	0.000	20.298	1.000	−0.105	0.000	0.000	4	0	0.0
Te_1—Sn_1—Sn_2	1.000	0.000	0.000	20.176	1.000	−0.071	0.000	0.000	4	0	0.0

Atom types in the first column are displayed in **Figure 190**, with M = Sn and X = Te.

Table 433. SW potential parameters for p-SnTe used by LAMMPS [9], as expressed in Eqs. (9) and (10).

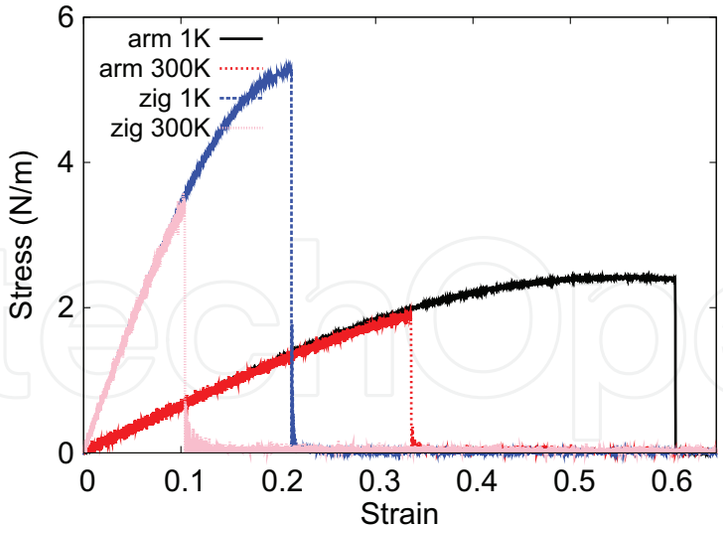

Figure 221. Stress-strain relations for the single-layer p-SnTe of size 100 × 100 Å. The single-layer p-SnTe is uniaxially stretched along the armchair or zigzag directions at temperatures 1 and 300 K.

stress is about 5.3 N/m at the critical strain of 0.21 in the zigzag direction at the low temperature of 1 K.

109. Silicene

There have been several empirical potentials available for the silicene. A many-body potential based on the Lennard-Jones and Axilrod-Teller functions was used to describe the interaction within the single-layer silicene [85]. The modified embedded-atom potential [86] was used by Pei et al. to simulate the thermal transport in the single-layer silicene in 2013 [87]. The environment-dependent interatomic potential [88] was also used to simulate the silicene [89]. In particular, the original set of SW parameters [4] for the silicon was found to be not suitable for the planar silicene, so two sets of optimized parameters for the SW potential were proposed to simulate the thermal conductivity in the single-layer silicene in 2014 [90]. We will develop a new SW potential to describe the interaction within the silicene in this section, with specific focus on the mechanical properties of the silicene.

The structure of the silicene is shown in **Figure 222**, with structural parameters from the *ab initio* calculations [84]. The silicene has a buckled configuration as shown in **Figure 222(b)**, where the buckle is along the zigzag direction. The height of the buckle is $h = 0.45$ Å and the lattice constant is 3.87 Å, which results in a bond length of 2.279 Å.

Table 434 shows the VFF model for the silicene. The force constant parameters are determined by fitting to the three acoustic branches in the phonon dispersion along the ΓM as shown in **Figure 223(a)**. The *ab initio* calculations for the phonon dispersion are from Ref. [84]. Similar phonon dispersion can also be found in other *ab initio* calculations [84, 91–102]. **Figure 223(b)** shows that the VFF model and the SW potential give exactly the same phonon dispersion, as the SW potential is derived from the VFF model.

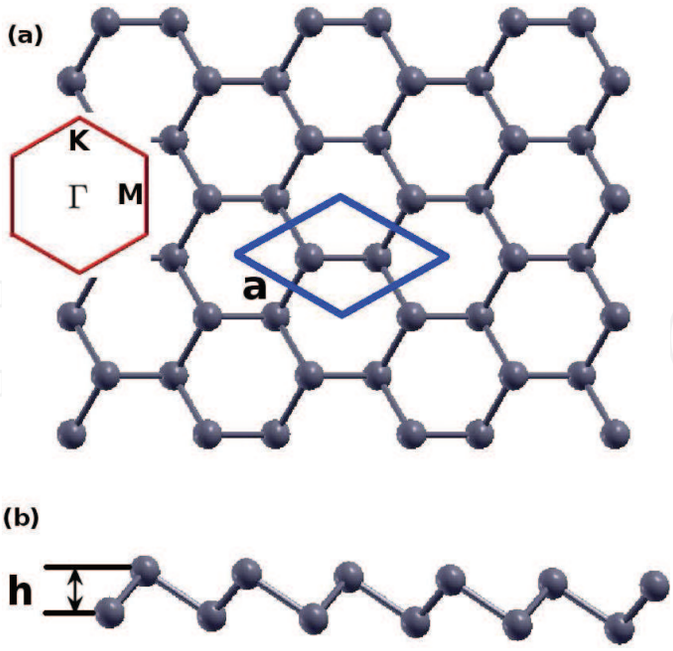

Figure 222. Structure for the buckled M, with M from group V. (a) Top view. The armchair direction is along the horizontal direction, while the zigzag direction is along the vertical direction. The unit cell is displayed by the blue rhombus. Inset shows the first Brillouin zone. (b) Side view illustrates the buckled configuration of height h.

VFF type	Bond stretching	Angle bending
Expression	$\frac{1}{2}K_r(\Delta r)^2$	$\frac{1}{2}K_\theta(\Delta\theta)^2$
Parameter	18.387	3.465
r_0 or θ_0	2.279	116.218

The second line gives an explicit expression for each VFF term. The third line is the force constant parameters. Parameters are in the unit of eV/Å^2 for the bond stretching interaction and in the unit of eV for the angle bending interaction. The fourth line gives the initial bond length (in the unit of Å) for the bond stretching interaction and the initial angle (in the unit of degrees) for the angle bending interaction.

Table 434. The VFF model for silicene.

We note that the present SW potential is fitted perfectly to the three acoustic phonon branches, so it can give a nice description for the elastic deformation of the silicene. As a trade off, the optical phonons are overestimated by the present SW potential. Hence, the present SW potential is in particular suitable for the simulation of mechanical or thermal processes, which are dominated by acoustic phonons, while the present SW potential may cause a systematic error for the optical absorption process, which mainly involves the optical phonons. One can introduce the long-range interactions (e.g., the second-nearest-neighboring interaction) to give a good description for both acoustic and optical phonon branches, see one such example for borophene in Ref. [14]. It is because the long-range interaction mainly contributes to the acoustic phonon branches, while it makes only neglectable contribution to the optical phonon branches. As another solution, the SW potential can give reasonable descriptions for the optical

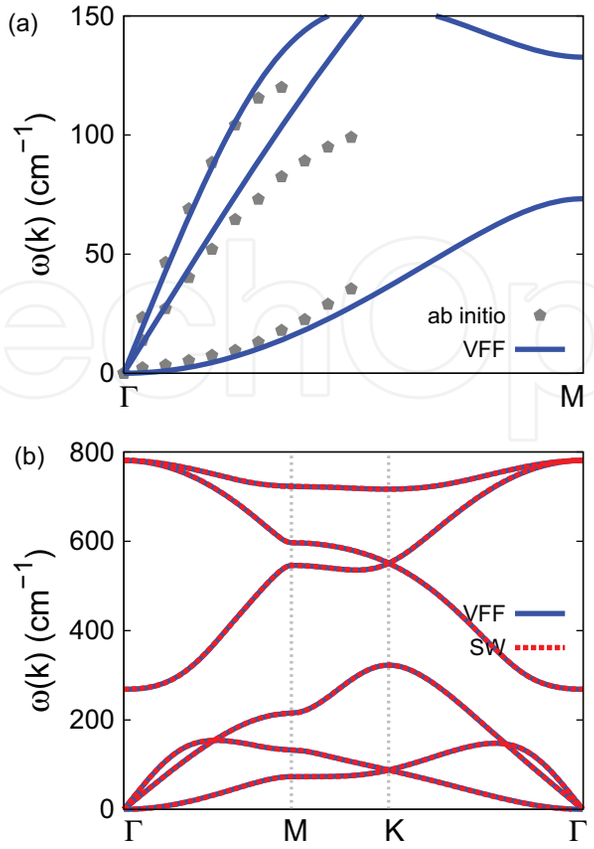

Figure 223. Phonon dispersion for the silicene. (a) The VFF model is fitted to the three acoustic branches in the long wave limit along the ΓM direction. The *ab initio* results (gray pentagons) are from Ref. [84]. (b) The VFF model (blue lines) and the SW potential (red lines) give the same phonon dispersion for the silicene along ΓMKΓ.

phonon branches by reducing its accuracy in describing acoustic phonon branches as done in Ref. [90].

The parameters for the two-body SW potential used by GULP are shown in **Table 435**. The parameters for the three-body SW potential used by GULP are shown in **Table 436**. Parameters for the SW potential used by LAMMPS are listed in **Table 437**.

	A (eV)	ρ (Å)	B (Å^4)	$r_{\min}$ (Å)	$r_{\max}$ (Å)
Si—Si	19.343	1.668	16.186	0.0	3.075

Table 435. Two-body SW potential parameters for silicene used by GULP [8], as expressed in Eq. (3).

	K (eV)	θ_0 (°)	ρ_1 (Å)	ρ_2 (Å)	$r_{\min 12}$ (Å)	$r_{\max 12}$ (Å)	$r_{\min 13}$ (Å)	$r_{\max 13}$ (Å)	$r_{\min 23}$ (Å)	$r_{\max 23}$ (Å)
Si—Si—Si	142.310	116.218	1.668	1.668	0.0	3.075	0.0	3.075	3.075	4.181

Table 436. Three-body SW potential parameters for silicene used by GULP [8], as expressed in Eq. (4).

	ϵ (eV)	σ (Å)	a	λ	γ	$\cos\theta_0$	A_L	B_L	p	q	Tol
Si—Si—Si	1.000	1.668	1.844	142.310	1.000	-0.442	19.343	2.091	4	0	0.0

Table 437. SW potential parameters for silicene used by LAMMPS [9], as expressed in Eqs. (9) and (10).

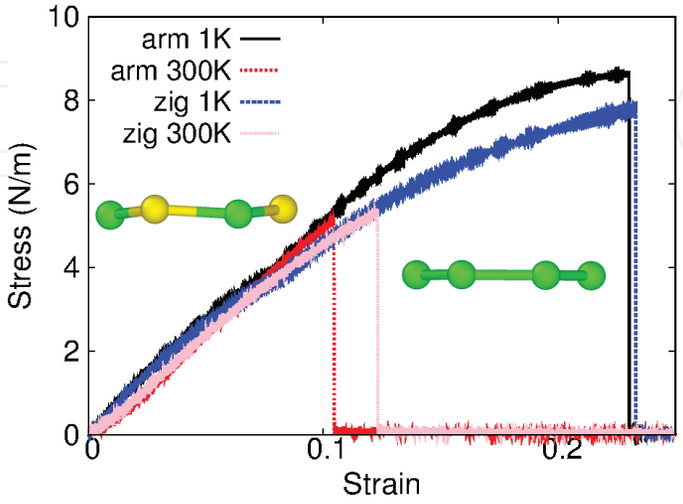

Figure 224. Stress-strain relations for the silicene of size 100×100 Å. The silicene is uniaxially stretched along the armchair or zigzag directions at temperatures 1 and 300 K. Left inset shows the buckled configuration for the silicene at the uniaxial strain 0.07 at 1 K along the armchair direction. Right inset: the buckled configuration becomes planar for the silicene at the uniaxial strain of 0.08 at 1 K along the armchair direction.

Figure 224 shows the stress-strain relations for the silicene of size 100×100 Å. The structure is uniaxially stretched in the armchair or zigzag directions at 1 and 300 K. The Young's modulus is 63.3 Nm^{-1} in both armchair and zigzag directions at 1 K, which are obtained by linear fitting of the stress-strain relations in [0, 0.01]. The Young's modulus is isotropic for the silicene. The value of the Young's modulus agrees with the value of 63.8 Nm^{-1} from the *ab initio* calculations [103]. The Poisson's ratios from the VFF model and the SW potential are $\nu_{xy} = \nu_{yx} = 0.15$, which are smaller but comparable with the *ab initio* results of 0.325 [103]. The third-order nonlinear elastic constant D can be obtained by fitting the stress-strain relation to $\sigma = E\epsilon + \frac{1}{2}D\epsilon^2$ with E as the Young's modulus. The values of D are -212.5 and -267.5 Nm^{-1} at 1 K along the armchair and zigzag directions, respectively. The ultimate stress is about 8.6 Nm^{-1} at the critical strain of 0.23 in the armchair direction at the low temperature of 1 K. The ultimate stress is about 7.8 Nm^{-1} at the critical strain of 0.23 in the zigzag direction at the low temperature of 1 K.

The stress-strain curves shown in **Figure 224** disclose a structural transition at the strain around 0.076 for the silicene at the low temperature of 1 K. The buckled configuration of the silicene is flattened during this structural transition, which can be seen from these two insets in **Figure 224**. This structural transition was also observed in the *ab initio* calculations [95], where the critical strain for the structural transition is 0.2. At temperatures above 300 K, this structural transition is blurred by stronger thermal vibrations; i.e., the buckled configuration of the silicene can be strongly disturbed by the thermal vibration at higher temperatures.

110. Germanene

In a recent work, the Tersoff potential was applied to simulate the thermal conductivity of the germanene nanoribbon [104]. We will provide the SW potential to describe the interaction within the germanene in this section.

The structure of the germanene is shown in **Figure 222**, with structural parameters from the *ab initio* calculations [84]. The germanene has a buckled configuration as shown in **Figure 222(b)**, where the buckle is along the zigzag direction. The height of the buckle is $h = 0.69$ Å and the lattice constant is 4.06 Å, which results in a bond length of 2.443 Å.

Table 438 shows the VFF model for the germanene. The force constant parameters are determined by fitting to the three acoustic branches in the phonon dispersion along the ΓM as shown in **Figure 225(a)**. The *ab initio* calculations for the phonon dispersion are from Ref. [84]. Similar phonon dispersion can also be found in other *ab initio* calculations [84, 92, 93, 98, 101, 102, 105]. **Figure 225(b)** shows that the VFF model and the SW potential give exactly the same phonon dispersion, as the SW potential is derived from the VFF model.

The parameters for the two-body SW potential used by GULP are shown in **Table 439**. The parameters for the three-body SW potential used by GULP are shown in **Table 440**. Parameters for the SW potential used by LAMMPS are listed in **Table 441**.

Figure 226 shows the stress-strain relations for the germanene of size 100×100 Å. The structure is uniaxially stretched in the armchair or zigzag directions at 1 and 300 K. The Young's modulus is 53.2 Nm^{-1} in both armchair and zigzag directions at 1 K, which are obtained by linear fitting of the stress-strain relations in [0, 0.01]. The Young's modulus is isotropic for the germanene. The Poisson's ratios from the VFF model and the SW potential are $\nu_{xy} = \nu_{yx} = 0.19$. The third-order nonlinear elastic constant D can be obtained by fitting the stress-strain relation to $\sigma = E\epsilon + \frac{1}{2}D\epsilon^2$ with E as the Young's modulus. The values of D are -229.2 and -278.2 Nm^{-1} at 1 K along the armchair and zigzag directions, respectively. The ultimate stress is about 7.5 Nm^{-1} at the critical strain of 0.26 in the armchair direction at the low temperature of 1 K. The ultimate stress is about 7.3 Nm^{-1} at the critical strain of 0.27 in the zigzag direction at the low temperature of 1 K.

The stress-strain curves shown in **Figure 226** disclose a structural transition for the germanene at the low temperature of 1 K. The critical strains for the structural transition are 0.15 and 0.16

VFF type	Bond stretching	Angle bending
Expression	$\frac{1}{2}K_r(\Delta r)^2$	$\frac{1}{2}K_\theta(\Delta\theta)^2$
Parameter	18.387	3.465
r_0 or θ_0	2.443	112.358

The second line gives an explicit expression for each VFF term. The third line is the force constant parameters. Parameters are in the unit of eV/Å^2 for the bond stretching interaction and in the unit of eV for the angle bending interaction. The fourth line gives the initial bond length (in the unit of Å) for the bond stretching interaction and the initial angle (in the unit of degrees) for the angle bending interaction

Table 438. The VFF model for germanene.

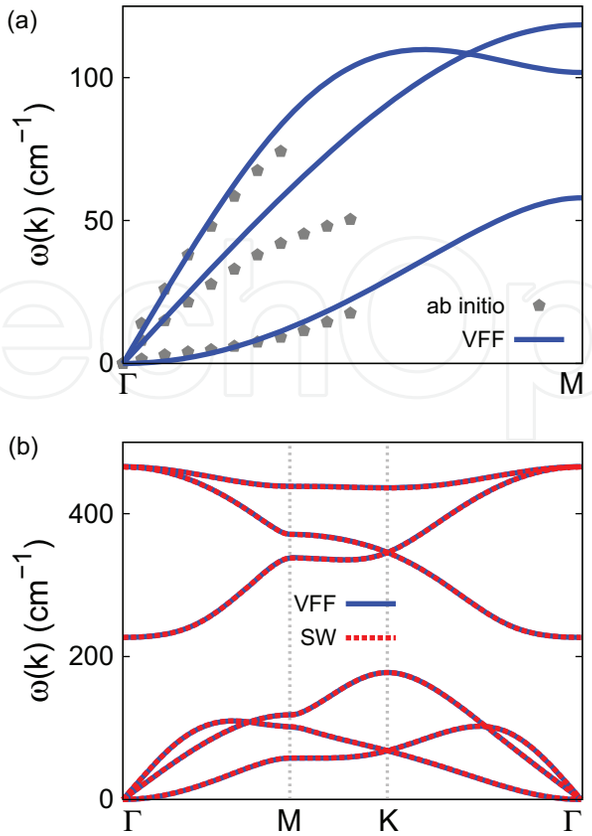

Figure 225. Phonon dispersion for the germanene. (a) The VFF model is fitted to the three acoustic branches in the long wave limit along the ΓM direction. The *ab initio* results (gray pentagons) are from Ref. 84. (b) The VFF model (blue lines) and the SW potential (red lines) give the same phonon dispersion for the germanene along ΓMKΓ.

	A (eV)	ρ (Å)	B (Å^4)	$r_{\min}$ (Å)	$r_{\max}$ (Å)
Ge—Ge	19.570	1.607	21.372	0.0	3.252

Table 439. Two-body SW potential parameters for germanene used by GULP [8], as expressed in Eq. (3).

	K (eV)	θ_0 (°)	ρ_1 (Å)	ρ_2 (Å)	$r_{\min 12}$ (Å)	$r_{\max 12}$ (Å)	$r_{\min 13}$ (Å)	$r_{\max 13}$ (Å)	$r_{\min 23}$ (Å)	$r_{\max 23}$ (Å)
Ge—Ge—Ge	107.735	112.358	1.607	1.607	0.0	3.252	0.0	3.252	3.252	4.4

Table 440. Three-body SW potential parameters for germanene used by GULP [8], as expressed in Eq. (4).

	ϵ (eV)	σ (Å)	a	λ	γ	$\cos\theta_0$	A_L	B_L	p	q	Tol
Ge—Ge—Ge	1.000	1.607	2.024	107.735	1.000	-0.380	19.570	3.205	4	0	0.0

Table 441. SW potential parameters for germanene used by LAMMPS [9], as expressed in Eqs. (9) and (10).

along the armchair and zigzag directions, respectively. The buckled configuration of the germanene is flattened during this structural transition, which can be seen from these two insets in **Figure 226**. At temperatures above 300 K, this structural transition is blurred by

http://dx.doi.org/10.5772/intechopen.71929

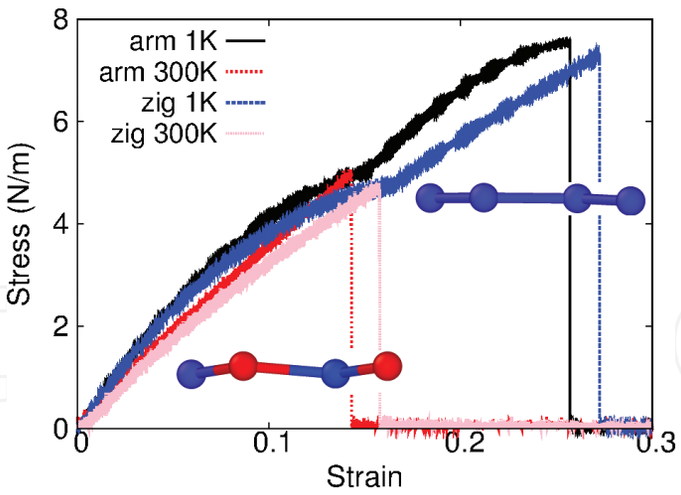

Figure 226. Stress-strain relations for the germanene of size 100 × 100 Å. The germanene is uniaxially stretched along the armchair or zigzag directions at temperatures 1 and 300 K. Left bottom inset shows the buckled configuration for the germanene at the uniaxial strain 0.14 at 1 K along the armchair direction. Right top inset: the buckled configuration becomes planar for the germanene at the uniaxial strain of 0.16 at 1 K along the armchair direction.

stronger thermal vibrations; i.e., the buckled configuration of the germanene can be strongly disturbed by the thermal vibration at higher temperatures.

111. Stanene

There are several available empirical potentials for the description of the interaction within the stanene. The modified embedded atom method potential was applied to simulate mechanical properties for the stanene [106]. A VFF model was fitted for the stanene in 2015 [107]. The Tersoff potential was parameterized to describe the interaction for stanene [108]. In this section, we will develop the SW potential for the stanene.

The structure of the stanene is shown in **Figure 222**, with structural parameters from the *ab initio* calculations [105]. The stanene has a buckled configuration as shown in **Figure 222(b)**, where the buckle is along the zigzag direction. The height of the buckle is $h = 0.86$ Å and the lattice constant is 4.68 Å, which results in a bond length of 2.836 Å.

Table 442 shows the VFF model for the stanene. The force constant parameters are determined by fitting to the three acoustic branches in the phonon dispersion along the ΓM as shown in **Figure 227(a)**. The *ab initio* calculations for the phonon dispersion are from Ref. [105] with the spin-orbit coupling effect. Similar phonon dispersion can also be found in other *ab initio* calculations [101, 102, 105, 109–111]. **Figure 227(b)** shows that the VFF model and the SW potential give exactly the same phonon dispersion, as the SW potential is derived from the VFF model.

The parameters for the two-body SW potential used by GULP are shown in **Table 443**. The parameters for the three-body SW potential used by GULP are shown in **Table 444**. Parameters for the SW potential used by LAMMPS are listed in **Table 445**.

VFF type	Bond stretching	Angle bending
Expression	$\frac{1}{2}K_r(\Delta r)^2$	$\frac{1}{2}K_\theta(\Delta\theta)^2$
Parameter	10.489	1.372
r_0 or θ_0	2.836	111.224

The second line gives an explicit expression for each VFF term. The third line is the force constant parameters. Parameters are in the unit of eV/Å^2 for the bond stretching interaction and in the unit of eV for the angle bending interaction. The fourth line gives the initial bond length (in the unit of Å) for the bond stretching interaction and the initial angle (in the unit of degrees) for the angle bending interaction.

Table 442. The VFF model for stanene.

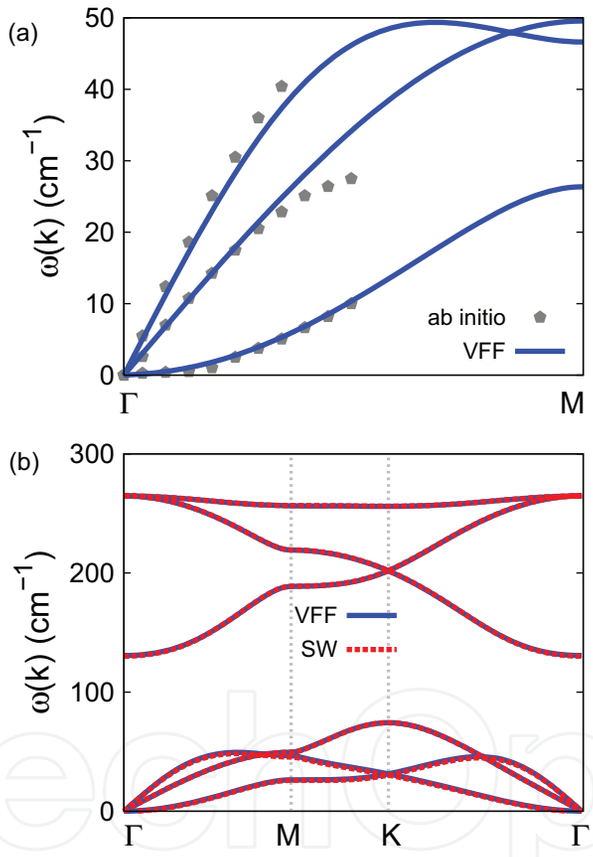

Figure 227. Phonon dispersion for the stanene. (a) The VFF model is fitted to the three acoustic branches in the long wave limit along the ΓM direction. The *ab initio* results (gray pentagons) are from Ref. [105]. (b) The VFF model (blue lines) and the SW potential (red lines) give the same phonon dispersion for the stanene along ΓMKΓ.

	A (eV)	ρ (Å)	B (Å^4)	$r_{\min}$ (Å)	$r_{\max}$ (Å)
Sn—Sn	19.542	2.227	42.047	0.0	3.758

Table 443. Two-body SW potential parameters for stanene used by GULP [8], as expressed in Eq. (3).

	K (eV)	θ_0 (°)	ρ_1 (Å)	ρ_2 (Å)	$r_{\min 12}$ (Å)	$r_{\max 12}$ (Å)	$r_{\min 13}$ (Å)	$r_{\max 13}$ (Å)	$r_{\min 23}$ (Å)	$r_{\max 23}$ (Å)
Sn—Sn—Sn	98.863	111.224	2.227	2.227	0.0	3.758	0.0	3.758	3.758	5.076

Table 444. Three-body SW potential parameters for stanene used by GULP [8], as expressed in Eq. (4).

	ϵ (eV)	σ (Å)	a	λ	γ	$\cos\theta_0$	A_L	B_L	p	q	Tol
Sn—Sn—Sn	1.000	2.227	1.687	98.863	1.000	-0.362	19.542	1.709	4	0	0.0

Table 445. SW potential parameters for stanene used by LAMMPS [9], as expressed in Eqs. (9) and (10).

Figure 228 shows the stress-strain relations for the stanene of size 100 × 100 Å. The structure is uniaxially stretched in the armchair or zigzag directions at 1 and 300 K. The Young's modulus is 17.0 Nm^{-1} in both armchair and zigzag directions at 1 K, which are obtained by linear fitting of the stress-strain relations in [0, 0.01]. The Young's modulus is isotropic for the stanene. The Poisson's ratios from the VFF model and the SW potential are $\nu_{xy} = \nu_{yx} = 0.29$. The third-order nonlinear elastic constant D can be obtained by fitting the stress-strain relation to $\sigma = E\epsilon + \frac{1}{2}D\epsilon^2$ with E as the Young's modulus. The values of D are -37.2 Nm^{-1} and -69.4 Nm^{-1} at 1 K along the armchair and zigzag directions, respectively. The ultimate stress is about 3.5 Nm^{-1} at the critical strain of 0.32 in the armchair direction at the low temperature of 1 K. The ultimate stress is about 3.6 Nm^{-1} at the critical strain of 0.29 in the zigzag direction at the low temperature of 1 K.

The stress-strain curves shown in **Figure 228** disclose a structural transition for the stanene at the low temperature of 1 K. The critical strain for the structural transition is about 0.15 along the armchair and zigzag directions. The buckled configuration of the stanene is flattened during this structural transition, which can be seen from these two insets in **Figure 228**. At temperatures above 300 K, this structural transition is blurred by stronger thermal vibrations,

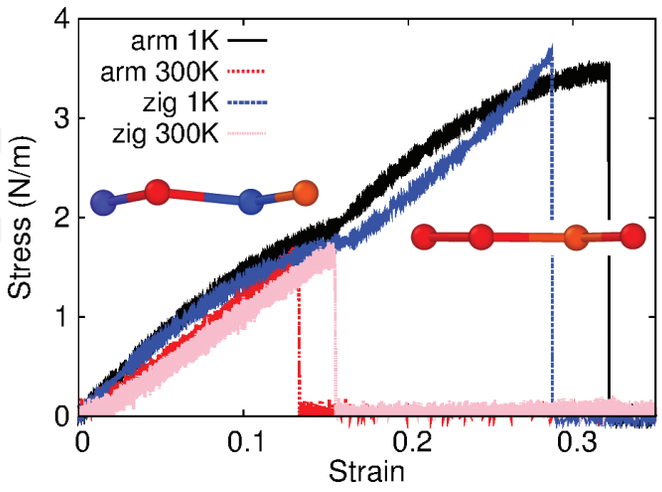

Figure 228. Stress-strain relations for the stanene of size 100 × 100 Å. The stanene is uniaxially stretched along the armchair or zigzag directions at temperatures 1 and 300 K. Left inset: the buckled configuration for the stanene at the uniaxial strain 0.14 at 1 K along the armchair direction. Right inset: the buckled configuration becomes planar for the stanene at the uniaxial strain of 0.16 at 1 K along the armchair direction.

i.e., the buckled configuration of the stanene can be strongly disturbed by the thermal vibration at higher temperatures.

112. Indiene

In this section, we will develop the SW potential for the indiene, i.e., the single layer of indium atoms. The structure of the indiene is shown in **Figure 222**, with structural parameters from the *ab initio* calculations [112]. The indiene has a buckled configuration as shown in **Figure 222(b)**, where the buckle is along the zigzag direction. The lattice constant is 4.24 Å and the bond length is 2.89 Å, which results in the buckling height of $h = 1.536$ Å.

Table 446 shows the VFF model for the indiene. The force constant parameters are determined by fitting to the three acoustic branches in the phonon dispersion along the ΓM as shown in **Figure 229(a)**. The *ab initio* calculations for the phonon dispersion are from Ref. [112]. We note that the lowest frequency branch around the Γ point from the VFF model is lower than the *ab initio* results. This branch is the flexural branch, which should be a quadratic dispersion. However, the *ab initio* calculations give a linear dispersion for the flexural branch due to the violation of the rigid rotational invariance in the first-principles package [20], so *ab initio* calculations typically overestimate the frequency of this branch. **Figure 229(b)** shows that the VFF model and the SW potential give exactly the same phonon dispersion, as the SW potential is derived from the VFF model.

The parameters for the two-body SW potential used by GULP are shown in **Table 447**. The parameters for the three-body SW potential used by GULP are shown in **Table 448**. Parameters for the SW potential used by LAMMPS are listed in **Table 449**.

Figure 230 shows the stress-strain relations for the indiene of size 100×100 Å. The structure is uniaxially stretched in the armchair or zigzag directions at 1 K. The Young's modulus is 8.4 Nm^{-1} in both armchair and zigzag directions at 1 K, which are obtained by linear fitting of the stress-strain relations in [0, 0.01]. The Young's modulus of the indiene is very small; i.e., the indiene is very soft. As a result, we find that the structure becomes unstable at room temperature. The Poisson's ratios from the VFF model and the SW potential are $\nu_{xy} = \nu_{yx} = 0.18$. The

VFF type	Bond stretching	Angle bending
Expression	$\frac{1}{2}K_r(\Delta r)^2$	$\frac{1}{2}K_\theta(\Delta\theta)^2$
Parameter	2.128	1.175
r_0 or θ_0	2.890	94.372

The second line gives an explicit expression for each VFF term. The third line is the force constant parameters. Parameters are in the unit of eV/Å^2 for the bond stretching interaction and in the unit of eV for the angle bending interaction. The fourth line gives the initial bond length (in the unit of Å) for the bond stretching interaction and the initial angle (in the unit of degrees) for the angle bending interaction.

Table 446. The VFF model for indiene.

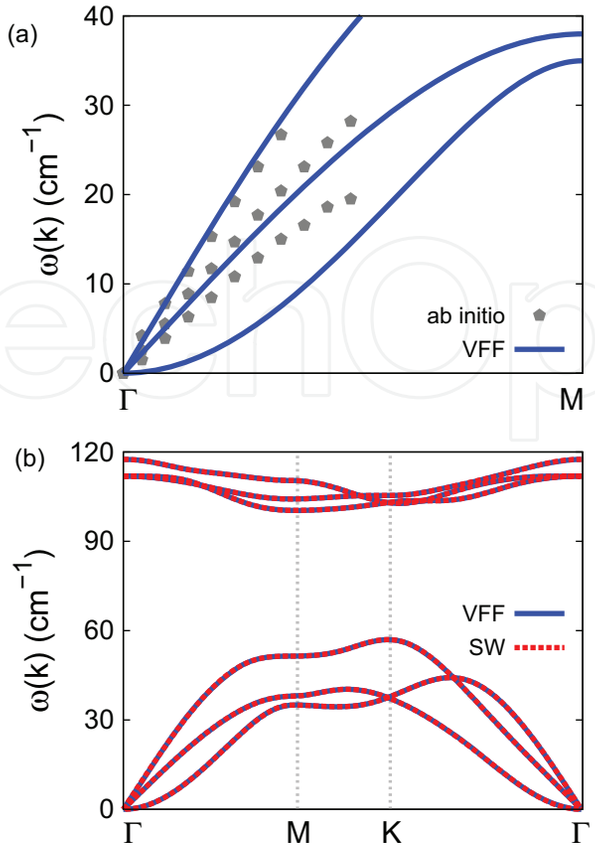

Figure 229. Phonon dispersion for the indiene. (a) The VFF model is fitted to the three acoustic branches in the long wave limit along the ΓM direction. The *ab initio* results (gray pentagons) are from Ref. [112]. (b) The VFF model (blue lines) and the SW potential (red lines) give the same phonon dispersion for the indiene along ΓMKΓ.

	A (eV)	ρ (Å)	B (Å^4)	$r_{\min}$ (Å)	$r_{\max}$ (Å)
In—In	1.537	0.946	41.855	0.0	3.565

Table 447. Two-body SW potential parameters for indiene used by GULP [8], as expressed in Eq. (3).

	K (eV)	θ_0 (°)	ρ_1 (Å)	ρ_2 (Å)	$r_{\min 12}$ (Å)	$r_{\max 12}$ (Å)	$r_{\min 13}$ (Å)	$r_{\max 13}$ (Å)	$r_{\min 23}$ (Å)	$r_{\max 23}$ (Å)
In—In—In	9.745	94.372	0.946	0.946	0.0	3.565	0.0	4.565	3.565	4.686

Table 448. Three-body SW potential parameters for indiene used by GULP [8], as expressed in Eq. (4).

	ϵ (eV)	σ (Å)	a	λ	γ	$\cos\theta_0$	A_L	B_L	p	q	Tol
In—In—In	1.000	0.946	3.768	9.745	1.000	-0.076	1.537	52.262	4	0	0.0

Table 449. SW potential parameters for indiene used by LAMMPS [9], as expressed in Eqs. (9) and (10).

third-order nonlinear elastic constant D can be obtained by fitting the stress-strain relation to $\sigma = E\epsilon + \frac{1}{2}D\epsilon^2$ with E as the Young's modulus. The values of D are -42.0 and -50.2 Nm^{-1} at 1 K along the armchair and zigzag directions, respectively. The ultimate stress is about

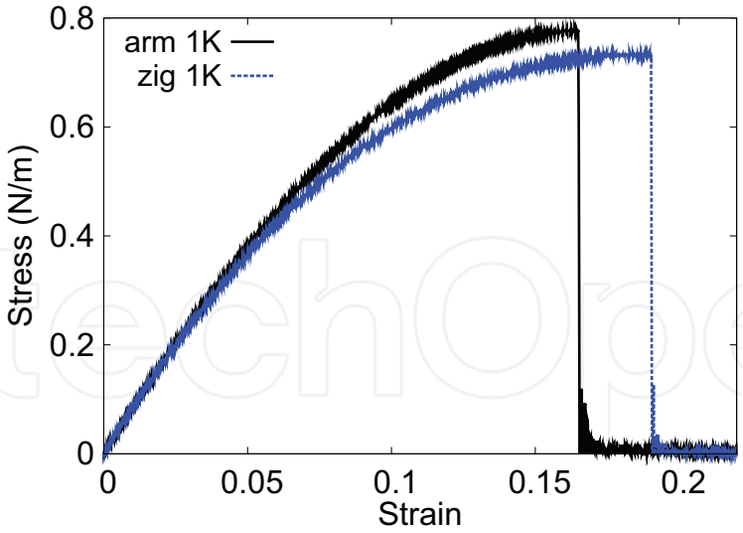

Figure 230. Stress-strain relations for the indiene of size 100×100 Å. The indiene is uniaxially stretched along the armchair or zigzag directions at temperatures 1 K.

0.77 Nm^{-1} at the critical strain of 0.16 in the armchair direction at the low temperature of 1 K. The ultimate stress is about 0.73 Nm^{-1} at the critical strain of 0.19 in the zigzag direction at the low temperature of 1 K.

113. Blue phosphorus

The blue phosphorus is also named β-phosphorus. Present studies on the blue phosphorus are based on first-principles calculations, and no empirical potential has been proposed for the blue phosphorus. We will thus parametrize a set of VFF model for the single-layer blue phosphorus in this section. We will also derive the SW potential based on the VFF model for the single-layer blue phosphorus.

The structure of the single-layer blue phosphorus is shown in **Figure 222**, with structural parameters from the *ab initio* calculations [55]. The blue phosphorus has a buckled configuration as shown in **Figure 222(b)**, where the buckle is along the zigzag direction. The height of the buckle is $h = 1.211$ Å. The lattice constant is 3.326 Å, and the bond length is 2.270 Å.

Table 450 shows the VFF model for the single-layer blue phosphorus. The force constant parameters are determined by fitting to the three acoustic branches in the phonon dispersion along the ΓM as shown in **Figure 231(a)**. The *ab initio* calculations for the phonon dispersion are from Ref. [55]. Similar phonon dispersion can also be found in other *ab initio* calculations [61, 64, 84]. **Figure 231(b)** shows that the VFF model and the SW potential give exactly the same phonon dispersion, as the SW potential is derived from the VFF model.

The parameters for the two-body SW potential used by GULP are shown in **Table 451**. The parameters for the three-body SW potential used by GULP are shown in **Table 452**. Parameters for the SW potential used by LAMMPS are listed in **Table 453**.

VFF type	Bond stretching	Angle bending
Expression	$\frac{1}{2}K_r(\Delta r)^2$	$\frac{1}{2}K_\theta(\Delta\theta)^2$
Parameter	15.372	5.138
r_0 or θ_0	2.270	94.209

The second line gives an explicit expression for each VFF term. The third line is the force constant parameters. Parameters are in the unit of eV/Å^2 for the bond stretching interaction and in the unit of eV for the angle bending interaction. The fourth line gives the initial bond length (in the unit of Å) for the bond stretching interaction and the initial angle (in the unit of degrees) for the angle bending interaction.

Table 450. The VFF model for blue phosphorus.

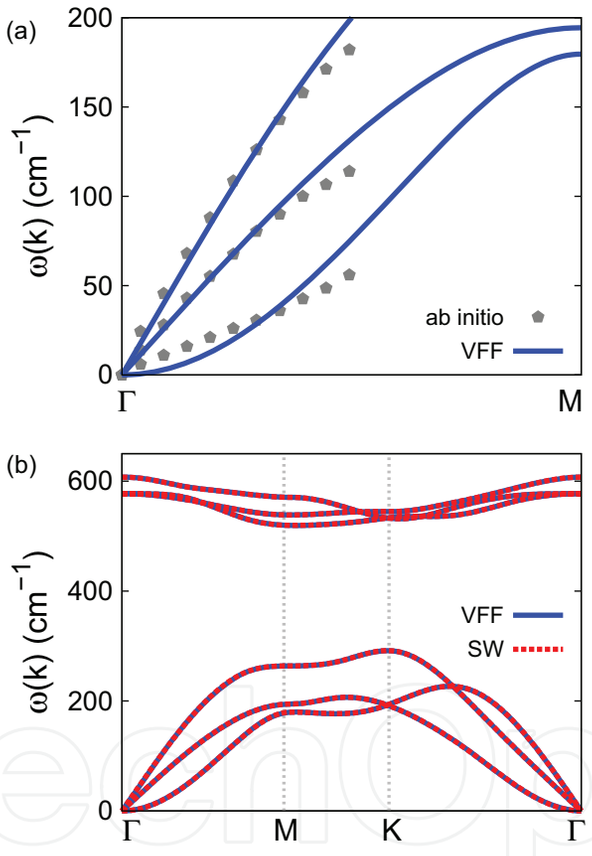

Figure 231. Phonon dispersion for the single-layer blue phosphorus. (a) The VFF model is fitted to the three acoustic branches in the long wave limit along the ΓM direction. The *ab initio* results (gray pentagons) are from Ref. [55]. (b) The VFF model (blue lines) and the SW potential (red lines) give the same phonon dispersion for the blue phosphorus along ΓMKΓ.

	A (eV)	ρ (Å)	B (Å^4)	$r_{\min}$ (Å)	$r_{\max}$ (Å)
P—P	5.706	0.491	13.276	0.0	2.798

Table 451. Two-body SW potential parameters for blue phosphorus used by GULP [8], as expressed in Eq. (3).

	K (eV)	θ_0 (°)	ρ_1 (Å)	ρ_2 (Å)	$r_{\min 12}$ (Å)	$r_{\max 12}$ (Å)	$r_{\min 13}$ (Å)	$r_{\max 13}$ (Å)	$r_{\min 23}$ (Å)	$r_{\max 23}$ (Å)
P—P—P	16.605	94.209	0.491	0.491	0.0	2.798	0.0	2.798	2.798	3.677

Table 452. Three-body SW potential parameters for blue phosphorus used by GULP [8], as expressed in Eq. (4).

	ϵ (eV)	σ (Å)	a	λ	γ	$\cos\theta_0$	A_L	B_L	p	q	Tol
P—P—P	1.000	0.491	5.699	16.605	1.000	−0.073	5.706	228.424	4	0	0.0

Table 453. SW potential parameters for blue phosphorus used by LAMMPS [9], as expressed in Eqs. (9) and (10).

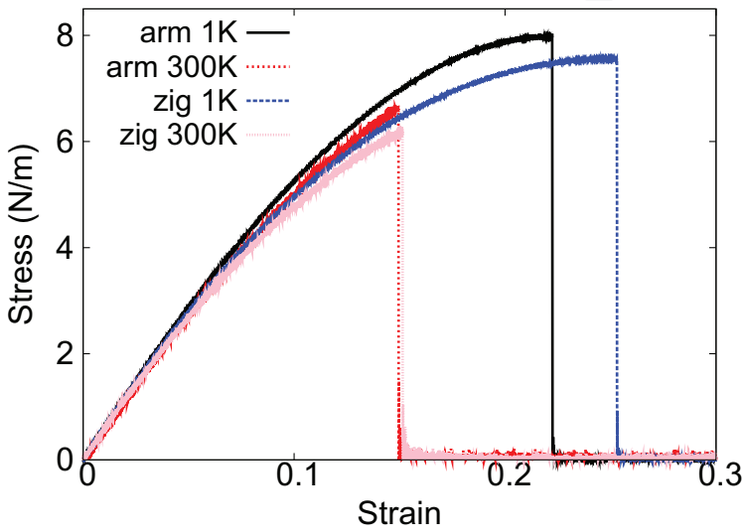

Figure 232. Stress-strain relations for the blue phosphorus of size 100×100 Å. The blue phosphorus is uniaxially stretched along the armchair or zigzag directions at temperatures 1 and 300 K.

Figure 232 shows the stress-strain relations for the single-layer blue phosphorus of size 100×100 Å. The structure is uniaxially stretched in the armchair or zigzag directions at 1 and 300 K. The Young's modulus is 60.5 and 60.6 Nm^{-1} in the armchair and zigzag directions, respectively, at 1 K, which is obtained by linear fitting of the stress-strain relations in [0, 0.01]. The Young's modulus is isotropic for the blue phosphorus. The Poisson's ratios from the VFF model and the SW potential are $\nu_{xy} = \nu_{yx} = 0.18$. The third-order nonlinear elastic constant D can be obtained by fitting the stress-strain relation to $\sigma = E\epsilon + \frac{1}{2}D\epsilon^2$ with E as the Young's modulus. The values of D are −195.3 and −237.0 Nm^{-1} at 1 K along the armchair and zigzag directions, respectively. The ultimate stress is about 8.0 Nm^{-1} at the critical strain of 0.22 in the armchair direction at the low temperature of 1 K. The ultimate stress is about 7.6 Nm^{-1} at the critical strain of 0.25 in the zigzag direction at the low temperature of 1 K.

114. B-Arsenene

Present studies on the buckled (b-) arsenene, which is also named β arsenene, are based on first-principles calculations, and no empirical potential has been proposed for the b-arsenene.

We will thus parametrize a set of VFF model for the single-layer b-arsenene in this section. We will also derive the SW potential based on the VFF model for the single-layer b-arsenene.

The structure of the single-layer b-arsenene is shown in **Figure 222**, with structural parameters from the *ab initio* calculations [70]. The b-arsenene has a buckled configuration as shown in **Figure 222(b)**, where the buckle is along the zigzag direction. The height of the buckle is $h = 1.40$ Å. The lattice constant is 3.61 Å, and the bond length is 2.51 Å.

Table 454 shows the VFF model for the single-layer b-arsenene. The force constant parameters are determined by fitting to the three acoustic branches in the phonon dispersion along the ΓM as shown in **Figure 233(a)**. The *ab initio* calculations for the phonon dispersion are from Ref. [70]. Similar phonon dispersion can also be found in other *ab initio* calculations [64, 72, 73]. We note that the lowest frequency branch around the Γ point from the VFF model is lower than the *ab initio* results. This branch is the flexural branch, which should be a quadratic dispersion. However, the *ab initio* calculations give a linear dispersion for the flexural branch due to the violation of the rigid rotational invariance in the first-principles package [20], so *ab initio* calculations typically overestimate the frequency of this branch. **Figure 233(b)** shows that the VFF model and the SW potential give exactly the same phonon dispersion, as the SW potential is derived from the VFF model.

The parameters for the two-body SW potential used by GULP are shown in **Table 455**. The parameters for the three-body SW potential used by GULP are shown in **Table 456**. Parameters for the SW potential used by LAMMPS are listed in **Table 457**.

Figure 234 shows the stress-strain relations for the single-layer b-arsenene of size 100×100 Å. The structure is uniaxially stretched in the armchair or zigzag directions at 1 and 300 K. The Young's modulus is 50.8 and 49.9 Nm^{-1} in the armchair and zigzag directions, respectively, at 1 K, which is obtained by linear fitting of the stress-strain relations in [0, 0.01]. The Young's modulus is isotropic for the b-arsenene. The Poisson's ratios from the VFF model and the SW potential are $\nu_{xy} = \nu_{yx} = 0.21$. The third-order nonlinear elastic constant D can be obtained by fitting the stress-strain relation to $\sigma = E\epsilon + \frac{1}{2}D\epsilon^2$ with E as the Young's modulus. The values of D are −127.6 and -153.6 Nm^{-1} at 1 K along the armchair and zigzag directions, respectively. The ultimate stress is about 7.6 Nm^{-1} at the critical strain of 0.24 in the armchair direction at the low temperature of 1 K. The ultimate stress is about 7.2 Nm^{-1} at the critical strain of 0.28 in the zigzag direction at the low temperature of 1 K.

VFF type	Bond stretching	Angle bending
Expression	$\frac{1}{2}K_r(\Delta r)^2$	$\frac{1}{2}K_\theta(\Delta\theta)^2$
Parameter	15.372	5.138
r_0 or θ_0	2.510	91.964

The second line gives an explicit expression for each VFF term. The third line is the force constant parameters. Parameters are in the unit of eV/Å^2 for the bond stretching interaction and in the unit of eV for the angle bending interaction. The fourth line gives the initial bond length (in the unit of Å) for the bond stretching interaction and the initial angle (in the unit of degrees) for the angle bending interaction.

Table 454. The VFF model for b-arsenene.

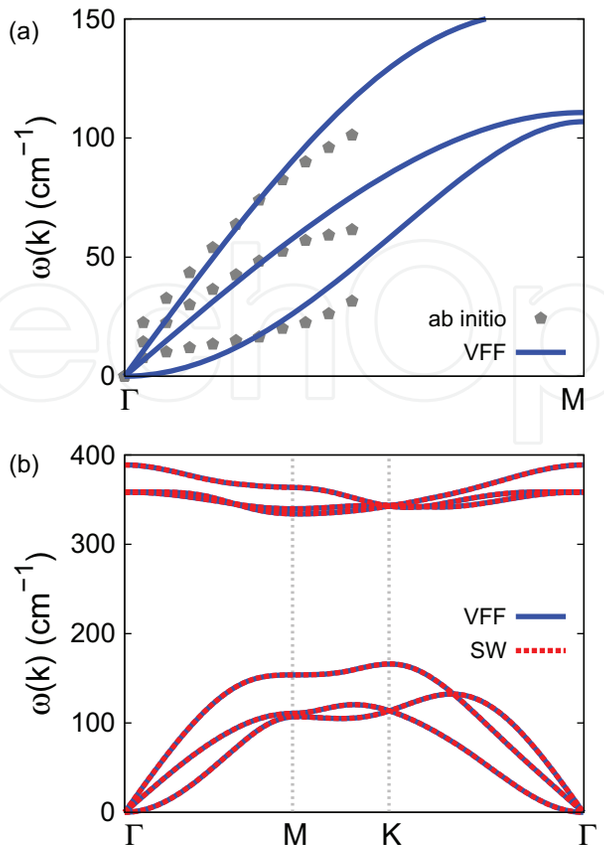

Figure 233. Phonon dispersion for the single-layer b-arsenene. (a) The VFF model is fitted to the three acoustic branches in the long wave limit along the ΓM direction. The *ab initio* results (gray pentagons) are from Ref. [70]. (b) The VFF model (blue lines) and the SW potential (red lines) give the same phonon dispersion for the b-arsenene along ΓMKΓ.

	A (eV)	ρ (Å)	B (Å^4)	$r_{\min}$ (Å)	$r_{\max}$ (Å)
As-As	6.418	0.482	19.846	0.0	3.060

Table 455. Two-body SW potential parameters for b-arsenene used by GULP [8], as expressed in Eq. (3).

	K (eV)	θ_0 (°)	ρ_1 (Å)	ρ_2 (Å)	$r_{\min 12}$ (Å)	$r_{\max 12}$ (Å)	$r_{\min 13}$ (Å)	$r_{\max 13}$ (Å)	$r_{\min 23}$ (Å)	$r_{\max 23}$ (Å)
As-As-As	14.845	91.964	0.482	0.482	0.0	3.060	0.0	3.060	3.060	4.004

Table 456. Three-body SW potential parameters for b-arsenene used by GULP [8], as expressed in Eq. (4).

	ϵ (eV)	σ (Å)	a	λ	γ	$\cos\theta_0$	A_L	B_L	p	q	Tol
As—As—As	1.000	0.482	6.349	14.845	1.000	-0.034	6.418	367.693	4	0	0.0

Table 457. SW potential parameters for b-arsenene used by LAMMPS [9], as expressed in Eqs. (9) and (10).

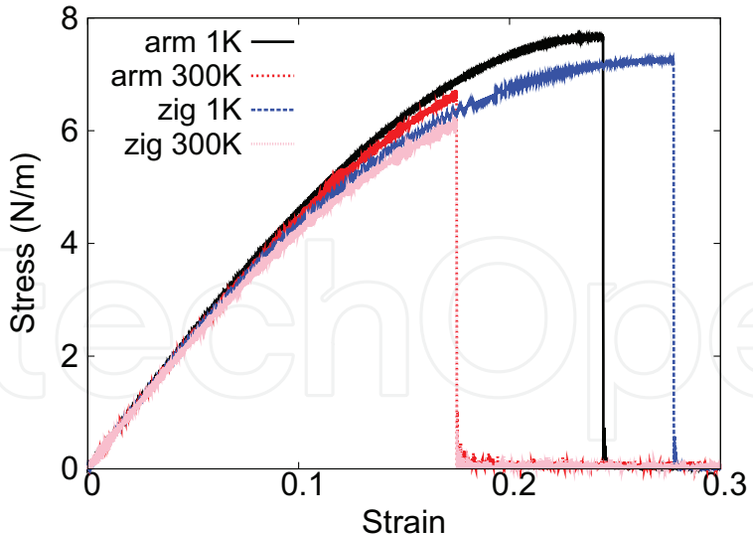

Figure 234. Stress-strain relations for the b-arsenene of size 100×100 Å. The b-arsenene is uniaxially stretched along the armchair or zigzag directions at temperatures 1 and 300 K.

115. b-Antimonene

The buckled (b-) antimonene is a Sb allotrope, which is also named β antimonene. Present studies on the b-antimonene are based on first-principles calculations, and no empirical potential has been proposed for the b-antimonene. We will, thus, parametrize a set of VFF model for the single-layer b-antimonene in this section. We will also derive the SW potential based on the VFF model for the single-layer b-antimonene.

The structure of the single-layer b-antimonene is shown in **Figure 222**, with structural parameters from the *ab initio* calculations [70]. The b-antimonene has a buckled configuration as shown in **Figure 222(b)**, where the buckle is along the zigzag direction. The height of the buckle is $h = 1.65$ Å. The lattice constant is 4.12 Å, and the bond length is 2.89 Å.

Table 458 shows the VFF model for the single-layer b-antimonene. The force constant parameters are determined by fitting to the three acoustic branches in the phonon dispersion along the ΓM as shown in **Figure 235(a)**. The *ab initio* calculations for the phonon dispersion are from

VFF type	Bond stretching	Angle bending
Expression	$\frac{1}{2}K_r(\Delta r)^2$	$\frac{1}{2}K_\theta(\Delta\theta)^2$
Parameter	15.372	5.138
r_0 or θ_0	2.890	90.927

The second line gives an explicit expression for each VFF term. The third line is the force constant parameters. Parameters are in the unit of eV/Å^2 for the bond stretching interaction and in the unit of eV for the angle bending interaction. The fourth line gives the initial bond length (in the unit of Å) for the bond stretching interaction and the initial angle (in the unit of degrees) for the angle bending interaction.

Table 458. The VFF model for b-antimonene.

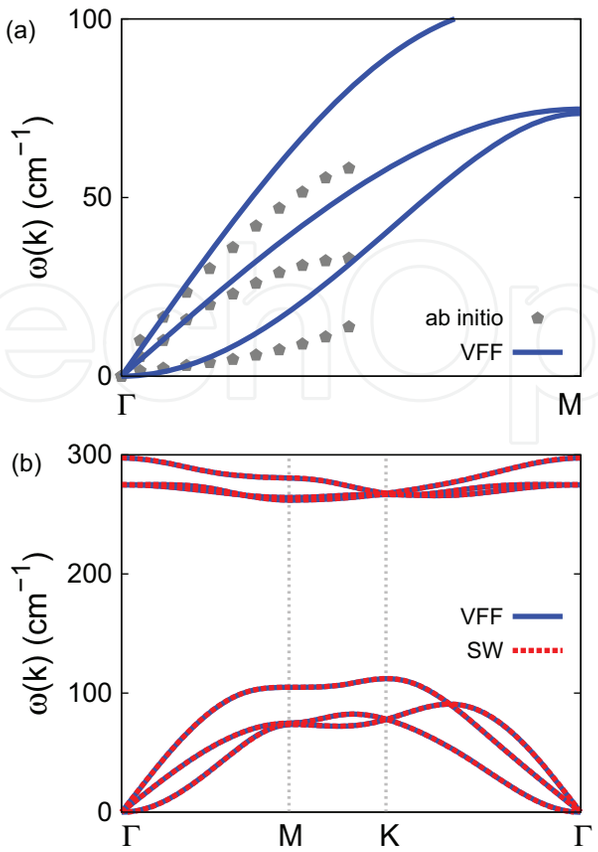

Figure 235. Phonon dispersion for the single-layer b-antimonene. (a) The VFF model is fitted to the three acoustic branches in the long wave limit along the ΓM direction. The *ab initio* results (gray pentagons) are from Ref. 70. (b) The VFF model (blue lines) and the SW potential (red lines) give the same phonon dispersion for the b-antimonene along ΓMKΓ.

Ref. 70. Similar phonon dispersion can also be found in other *ab initio* calculations [64, 72, 73]. **Figure 235(b)** shows that the VFF model and the SW potential give exactly the same phonon dispersion, as the SW potential is derived from the VFF model.

The parameters for the two-body SW potential used by GULP are shown in **Table 459**. The parameters for the three-body SW potential used by GULP are shown in **Table 460**. Parameters for the SW potential used by LAMMPS are listed in **Table 461**.

	A (eV)	ρ (Å)	B (Å^4)	$r_{\min}$ (Å)	$r_{\max}$ (Å)
Sb—Sb	8.173	0.523	34.879	0.0	3.505

Table 459. Two-body SW potential parameters for b-antimonene used by GULP [8], as expressed in Eq. (3).

	K (eV)	θ_0 (°)	ρ_1 (Å)	ρ_2 (Å)	$r_{\min 12}$ (Å)	$r_{\max 12}$ (Å)	$r_{\min 13}$ (Å)	$r_{\max 13}$ (Å)	$r_{\min 23}$ (Å)	$r_{\max 23}$ (Å)
Sb—Sb—Sb	14.100	90.927	0.523	0.523	0.0	3.505	0.0	3.503	3.505	4.577

Table 460. Three-body SW potential parameters for b-antimonene used by GULP [8], as expressed in Eq. (4).

	ϵ (eV)	σ (Å)	a	λ	γ	$\cos\theta_0$	A_L	B_L	p	q	Tol
Sb—Sb—Sb	1.000	0.523	6.702	14.100	1.000	−0.016	8.173	466.184	4	0	0.0

Table 461. SW potential parameters for b-antimonene used by LAMMPS [9], as expressed in Eqs. (9) and (10).

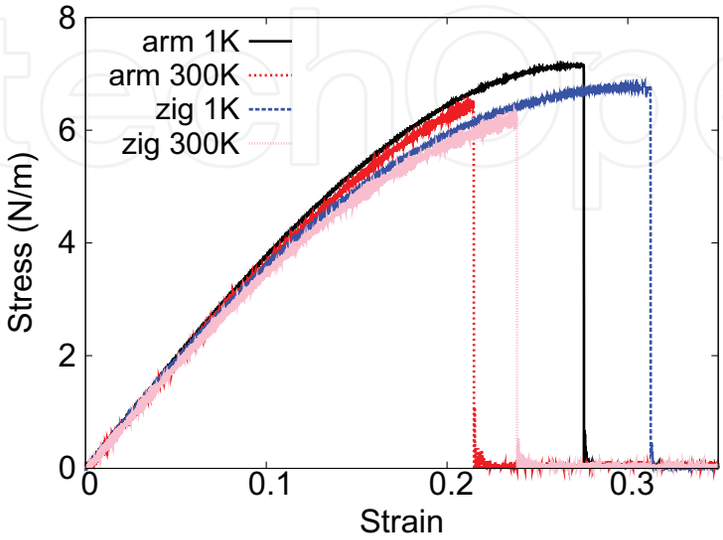

Figure 236. Stress-strain relations for the b-antimonene of size 100 × 100 Å. The b-antimonene is uniaxially stretched along the armchair or zigzag directions at temperatures 1 and 300 K.

Figure 236 shows the stress-strain relations for the single-layer b-antimonene of size 100 × 100 Å. The structure is uniaxially stretched in the armchair or zigzag directions at 1 and 300 K. The Young's modulus is 39.6 N/m in both armchair and zigzag directions at 1 K, which are obtained by linear fitting of the stress-strain relations in [0, 0.01]. The Young's modulus is isotropic for the b-antimonene. The Poisson's ratios from the VFF model and the SW potential are $\nu_{xy} = \nu_{yx} = 0.24$. The third-order nonlinear elastic constant D can be obtained by fitting the stress-strain relation to $\sigma = E\epsilon + \frac{1}{2}D\epsilon^2$ with E as the Young's modulus. The values of D are −62.6 and −91.5 N/m at 1 K along the armchair and zigzag directions, respectively. The ultimate stress is about 7.1 N/m at the critical strain of 0.28 in the armchair direction at the low temperature of 1 K. The ultimate stress is about 6.7 N/m at the critical strain of 0.31 in the zigzag direction at the low temperature of 1 K.

116. b-Bismuthene

The buckled (b-) bismuthene is a Bi allotrope, which is also named *beta* bismuthene. Most studies on the b-bismuthene are based on first-principles calculations, while a modified Morse potential was proposed for the b-bismuthene in 2013 [113]. We will parametrize a set of VFF model for the single-layer b-bismuthene in this section. We will also derive the SW potential based on the VFF model for the single-layer b-bismuthene.

The structure of the single-layer b-bismuthene is shown in **Figure 222**, with structural parameters from the *ab initio* calculations [70]. The b-bismuthene has a buckled configuration as shown in **Figure 222(b)**, where the buckle is along the zigzag direction. The height of the buckle is $h = 1.73$ Å. The lattice constant is 4.34 Å, and the bond length is 3.045 Å.

Table 462 shows the VFF model for the single-layer b-bismuthene. The force constant parameters are determined by fitting to the three acoustic branches in the phonon dispersion along the ΓM as shown in **Figure 237(a)**. The *ab initio* calculations for the phonon dispersion are

VFF type	Bond stretching	Angle bending
Expression	$\frac{1}{2}K_r(\Delta r)^2$	$\frac{1}{2}K_\theta(\Delta\theta)^2$
Parameter	11.529	3.853
r_0 or θ_0	3.045	90.901

The second line gives an explicit expression for each VFF term. The third line is the force constant parameters. Parameters are in the unit of eV/Å^2 for the bond stretching interaction and in the unit of eV for the angle bending interaction. The fourth line gives the initial bond length (in the unit of Å) for the bond stretching interaction and the initial angle (in the unit of degrees) for the angle bending interaction.

Table 462. The VFF model for b-bismuthene.

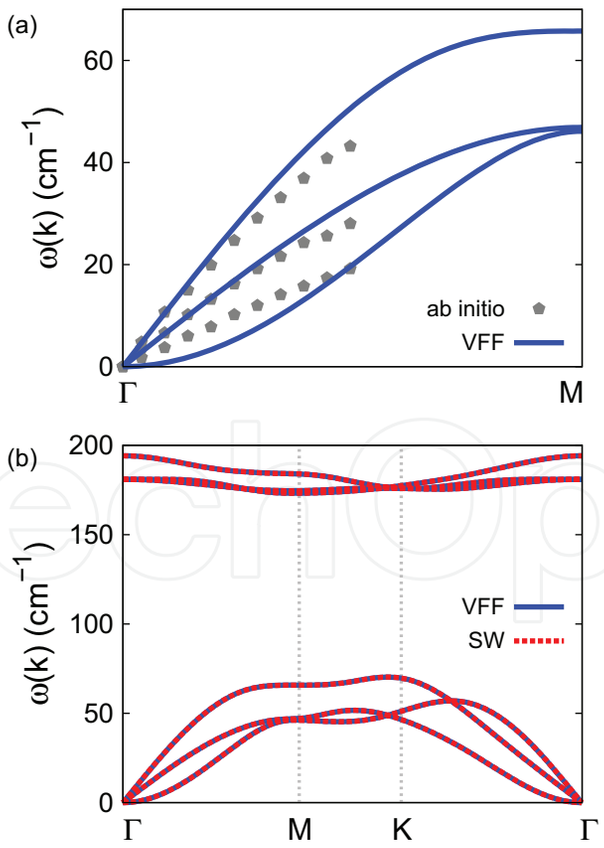

Figure 237. Phonon dispersion for the single-layer b-bismuthene. (a) The VFF model is fitted to the three acoustic branches in the long wave limit along the ΓM direction. The *ab initio* results (gray pentagons) are from [64]. (b) The VFF model (blue lines) and the SW potential (red lines) give the same phonon dispersion for the b-bismuthene along ΓMKΓ.

from [64]. Similar phonon dispersion can also be found in other *ab initio* calculations [77]. We note that the lowest-frequency branch around the Γ point from the VFF model is lower than the *ab initio* results. This branch is the flexural branch, which should be a quadratic dispersion. However, the *ab initio* calculations give a linear dispersion for the flexural branch due to the violation of the rigid rotational invariance in the first-principles package [20], so *ab initio* calculations typically overestimate the frequency of this branch. **Figure 237(b)** shows that the VFF model and the SW potential give exactly the same phonon dispersion, as the SW potential is derived from the VFF model.

The parameters for the two-body SW potential used by GULP are shown in **Table 463**. The parameters for the three-body SW potential used by GULP are shown in **Table 464**. Parameters for the SW potential used by LAMMPS are listed in **Table 465**.

Figure 238 shows the stress-strain relations for the single-layer b-bismuthene of size 100 × 100 Å. The structure is uniaxially stretched in the armchair or zigzag directions at 1 and 300 K. The Young's modulus is 27.0 N/m in both armchair and zigzag directions at 1 K, which are obtained by linear fitting of the stress-strain relations in [0, 0.01]. The Young's modulus is isotropic for the b-bismuthene. The value of the Young's modulus is close to the value of 23.9 N/m from the *ab initio* calculations [77]. The Poisson's ratios from the VFF model and the SW potential are $\nu_{xy} = \nu_{yx} = 0.25$, which are comparable with the *ab initio* results of 0.327 [77]. The third-order nonlinear elastic constant D can be obtained by fitting the stress-strain relation to $\sigma = E\epsilon + \frac{1}{2}D\epsilon^2$ with E as the Young's modulus. The values of D are −34.3 and −54.5 N/m at 1 K along the armchair and zigzag directions, respectively. The ultimate stress is about 5.2 N/m at the critical strain of 0.29 in the armchair direction at the low temperature of 1 K. The ultimate stress is about 4.9 N/m at the critical strain of 0.33 in the zigzag direction at the low temperature of 1 K.

	A (eV)	ρ (Å)	B (Å^4)	$r_{\min}$ (Å)	$r_{\max}$ (Å)
Bi—Bi	6.805	0.552	42.985	0.0	3.693

Table 463. Two-body SW potential parameters for b-bismuthene used by GULP [8], as expressed in Eq. (3).

	K (eV)	θ_0 (°)	ρ_1 (Å)	ρ_2 (Å)	$r_{\min 12}$ (Å)	$r_{\max 12}$ (Å)	$r_{\min 13}$ (Å)	$r_{\max 13}$ (Å)	$r_{\min 23}$ (Å)	$r_{\max 23}$ (Å)
Bi—Bi—Bi	10.574	90.901	0.552	0.552	0.0	3.693	0.0	3.693	3.693	4.821

Table 464. Three-body SW potential parameters for b-bismuthene used by GULP [8], as expressed in Eq. (4).

	ϵ (eV)	σ (Å)	a	λ	γ	$\cos\theta_0$	A_L	B_L	p	q	Tol
Bi—Bi—Bi	1.000	0.552	6.690	10.574	1.000	−0.016	6.805	462.978	4	0	0.0

Table 465. SW potential parameters for b-bismuthene used by LAMMPS [9], as expressed in Eqs. (9) and (10).

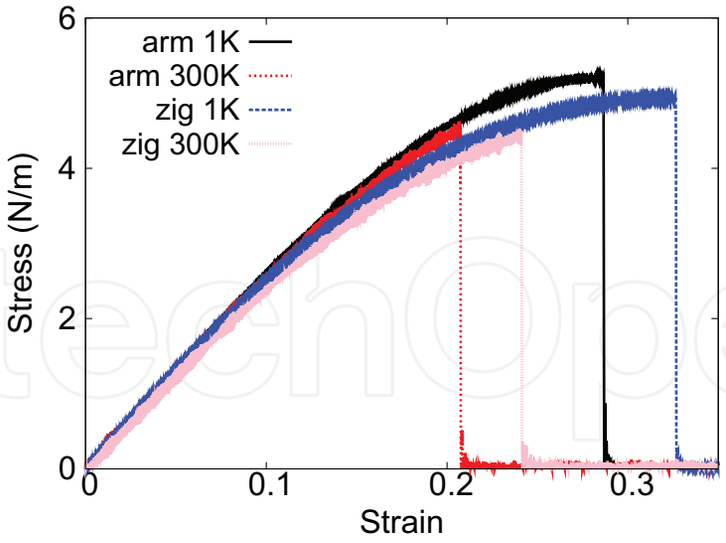

Figure 238. Stress-strain relations for the b-bismuthene of size 100 × 100 Å. The b-bismuthene is uniaxially stretched along the armchair or zigzag directions at temperatures 1 and 300 K.

117. b-CO

Present studies on the buckled (b-) CO are based on first-principles calculations, and no empirical potential has been proposed for the b-CO. We will thus parametrize a set of SW potential for the single-layer b-CO in this section.

The structure of the single-layer b-CO is shown in **Figure 239**. The structural parameters are from the *ab initio* calculations [78]. The b-CO has a buckled configuration as shown in **Figure 239(b)**, where the buckle is along the zigzag direction. This structure can be determined by two independent geometrical parameters, including the lattice constant 2.454 Å and the bond length 1.636 Å.

Table 466 shows the VFF model for the single-layer b-CO. The force constant parameters are determined by fitting to the acoustic branches in the phonon dispersion along the ΓM as shown in **Figure 240(a)**. The *ab initio* calculations for the phonon dispersion are calculated from the SIESTA package [79]. The generalized gradients approximation is applied to account for the exchange-correlation function with Perdew, Burke, and Ernzerhof parameterization [80], and the double-ζ orbital basis set is adopted. **Figure 240(b)** shows that the VFF model and the SW potential give exactly the same phonon dispersion, as the SW potential is derived from the VFF model.

The parameters for the two-body SW potential used by GULP are shown in **Table 467**. The parameters for the three-body SW potential used by GULP are shown in **Table 468**. Parameters for the SW potential used by LAMMPS are listed in **Table 469**.

We use LAMMPS to perform MD simulations for the mechanical behavior of the single-layer b-CO under uniaxial tension at 1.0 and 300.0 K. **Figure 241** shows the stress-strain curve for the tension of a single-layer b-CO of dimension 100 × 100 Å. Periodic boundary conditions are

http://dx.doi.org/10.5772/intechopen.71929

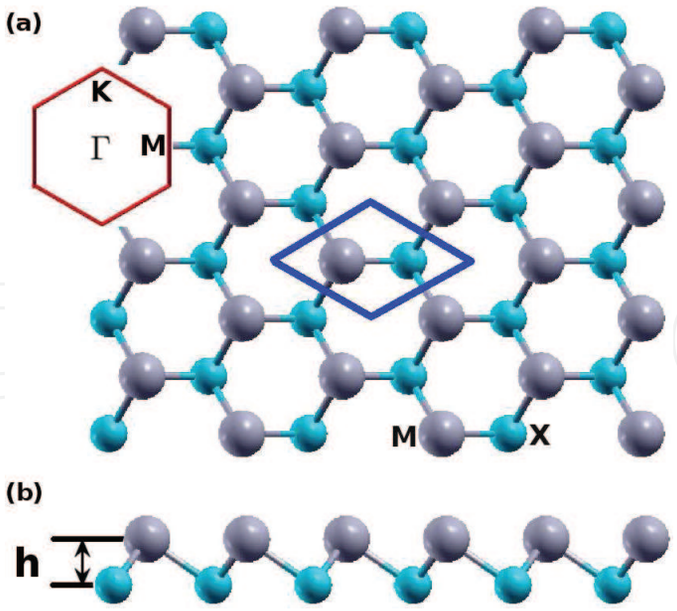

Figure 239. Structure for single-layer buckled MX (b-MX), with M from group IV and X from group VI, or both M and X from group IV, or M from group III and X from group V. (a) Top view. The armchair direction is along the horizontal direction, while the zigzag direction is along the vertical direction. The unit cell is displayed by the blue rhombus. Inset shows the first Brillouin zone. (b) Side view illustrates the buckled configuration of height h.

VFF type	**Bond stretching**	**Angle bending**
Expression	$\frac{1}{2}K_r(\Delta r)^2$	$\frac{1}{2}K_\theta(\Delta\theta)^2$
Parameter	16.063	5.221
r_0 or θ_0	1.636	97.181

The second line gives an explicit expression for each VFF term. The third line is the force constant parameters. Parameters are in the unit of eV/Å^2 for the bond stretching interaction and in the unit of eV for the angle bending interaction. The fourth line gives the initial bond length (in the unit of Å) for the bond stretching interaction and the initial angle (in the unit of degrees) for the angle bending interaction.

Table 466. The VFF model for b-CO.

applied in both armchair and zigzag directions. The single-layer b-CO is stretched uniaxially along the armchair or zigzag direction. The stress is calculated without involving the actual thickness of the quasi-two-dimensional structure of the single-layer b-CO. The Young's modulus can be obtained by a linear fitting of the stress-strain relation in the small strain range of [0, 0.01]. The Young's modulus is 99.1 and 98.8 N/m along the armchair and zigzag directions, respectively. The Young's modulus is essentially isotropic in the armchair and zigzag directions. The Poisson's ratio from the VFF model and the SW potential is $\nu_{xy} = \nu_{yx} = 0.08$.

There is no available value for nonlinear quantities in the single-layer b-CO. We have thus used the nonlinear parameter $B = 0.5d^4$ in Eq. (5), which is close to the value of B in most materials. The value of the third-order nonlinear elasticity D can be extracted by fitting the stress-strain relation to the function $\sigma = E\epsilon + \frac{1}{2}D\epsilon^2$ with E as the Young's modulus. The values of D from the

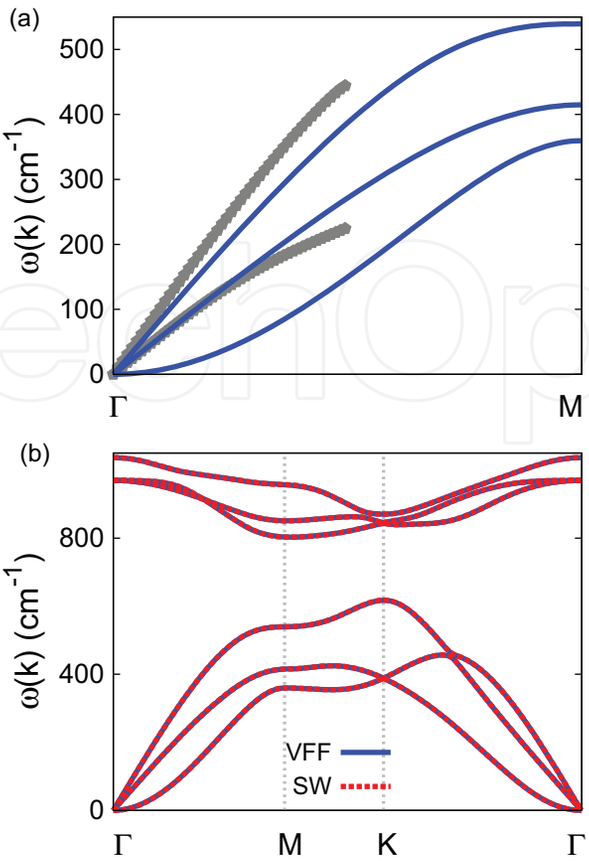

Figure 240. Phonon dispersion for the single-layer b-CO. (a) The VFF model is fitted to the two in-plane acoustic branches in the long wave limit along the ΓM direction. The *ab initio* results (gray pentagons) are calculated from SIESTA. (b) The VFF model (blue lines) and the SW potential (red lines) give the same phonon dispersion for the b-CO along ΓMKΓ.

	A (eV)	ρ (Å)	B (Å^4)	$r_{\min}$ (Å)	$r_{\max}$ (Å)
C—**O**	7.656	1.054	3.582	0.0	2.293

Table 467. Two-body SW potential parameters for b-CO used by GULP [8], as expressed in Eq. (3).

	K (eV)	θ_0 (°)	ρ_1 (Å)	ρ_2 (Å)	$r_{\min 12}$ (Å)	$r_{\max 12}$ (Å)	$r_{\min 13}$ (Å)	$r_{\max 13}$ (Å)	$r_{\min 23}$ (Å)	$r_{\max 23}$ (Å)
C-O-O	65.778	97.181	1.054	1.054	0.0	2.293	0.0	2.293	0.0	3.352
O-C-C	65.778	97.181	1.054	1.054	0.0	2.293	0.0	2.293	0.0	3.352

Table 468. Three-body SW potential parameters for b-CO used by GULP [8], as expressed in Eq. (4).

	ϵ (eV)	σ (Å)	a	λ	γ	$\cos\theta_0$	A_L	B_L	p	q	Tol
C—O—O	1.000	1.054	2.175	65.778	1.000	−0.125	7.812	2.900	4	0	0.0
O—C—C	1.000	1.054	2.175	65.778	1.000	−0.125	7.812	2.900	4	0	0.0

Table 469. SW potential parameters for b-CO used by LAMMPS [9], as expressed in Eqs. (9) and (10).

http://dx.doi.org/10.5772/intechopen.71929

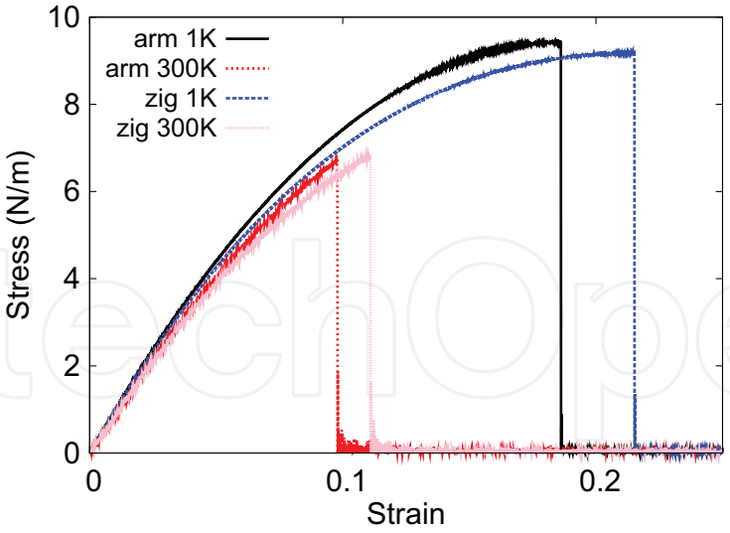

Figure 241. Stress-strain relations for the b-CO of size 100 × 100 Å. The b-CO is uniaxially stretched along the armchair or zigzag directions at temperatures 1 and 300 K.

present SW potential are −513.8 and −542.0 N/m along the armchair and zigzag directions, respectively. The ultimate stress is about 9.4 N/m at the ultimate strain of 0.18 in the armchair direction at the low temperature of 1 K. The ultimate stress is about 9.2 N/m at the ultimate strain of 0.21 in the zigzag direction at the low temperature of 1 K.

118. b-CS

Present studies on the buckled (b-) CS are based on first-principles calculations, and no empirical potential has been proposed for the b-CS. We will thus parametrize a set of SW potential for the single-layer b-CS in this section.

The structure of the single-layer b-CS is shown in **Figure 239**. The structural parameters are from the *ab initio* calculations [78]. The b-CS has a buckled configuration as shown in **Figure 239(b)**, where the buckle is along the zigzag direction. This structure can be determined by two independent geometrical parameters, including the lattice constant 2.836 Å and the bond length 1.880 Å.

Table 470 shows the VFF model for the single-layer b-CS. The force constant parameters are determined by fitting to the acoustic branches in the phonon dispersion along the ΓM as shown in **Figure 242(a)**. The *ab initio* calculations for the phonon dispersion are calculated from the SIESTA package [79]. The generalized gradients approximation is applied to account for the exchange-correlation function with Perdew, Burke, and Ernzerhof parameterization [80], and the double-ζ orbital basis set is adopted. **Figure 242(b)** shows that the VFF model and the SW potential give exactly the same phonon dispersion, as the SW potential is derived from the VFF model.

VFF type	Bond stretching	Angle bending
Expression	$\frac{1}{2}K_r(\Delta r)^2$	$\frac{1}{2}K_\theta(\Delta\theta)^2$
Parameter	9.390	4.722
r_0 or θ_0	1.880	97.921

The second line gives an explicit expression for each VFF term. The third line is the force constant parameters. Parameters are in the unit of eV/Å^2 for the bond stretching interaction and in the unit of eV for the angle bending interaction. The fourth line gives the initial bond length (in the unit of Å) for the bond stretching interaction and the initial angle (in the unit of degrees) for the angle bending interaction.

Table 470. The VFF model for b-CS.

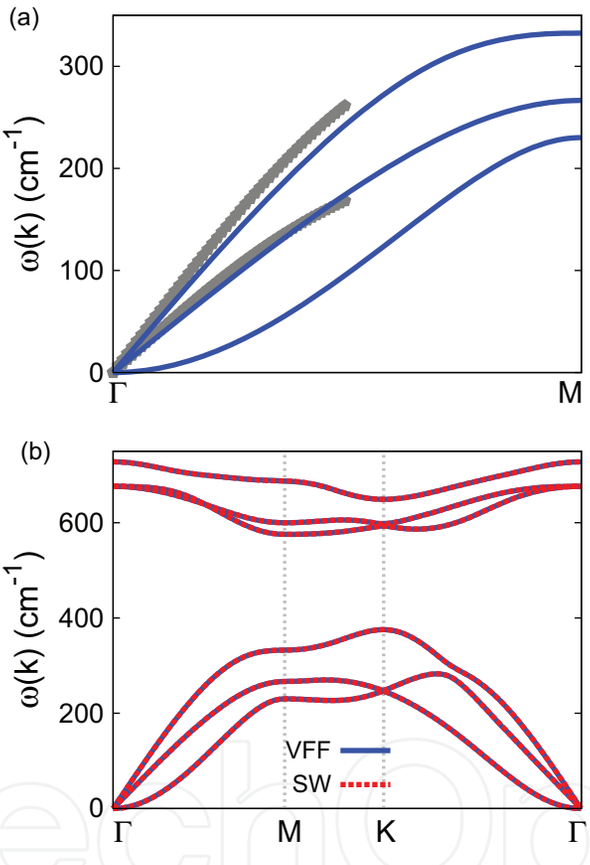

Figure 242. Phonon dispersion for the single-layer b-CS. (a) The VFF model is fitted to the two in-plane acoustic branches in the long wave limit along the ΓM direction. The *ab initio* results (gray pentagons) are calculated from SIESTA. (b) The VFF model (blue lines) and the SW potential (red lines) give the same phonon dispersion for the b-CS along ΓMKΓ.

The parameters for the two-body SW potential used by GULP are shown in **Table 471**. The parameters for the three-body SW potential used by GULP are shown in **Table 472**. Parameters for the SW potential used by LAMMPS are listed in **Table 473**.

We use LAMMPS to perform MD simulations for the mechanical behavior of the single-layer b-CS under uniaxial tension at 1.0 and 300.0 K. **Figure 243** shows the stress-strain curve for the tension of a single-layer b-CS of dimension 100×100 Å. Periodic boundary conditions are

	A (eV)	ρ (Å)	B (Å^4)	$r_{\min}$ (Å)	$r_{\max}$ (Å)
C—S	6.014	1.233	6.246	0.0	2.641

Table 471. Two-body SW potential parameters for b-CS used by GULP [8], as expressed in Eq. (3).

	K (eV)	θ_0 (°)	ρ_1 (Å)	ρ_2 (Å)	$r_{\min 12}$ (Å)	$r_{\max 12}$ (Å)	$r_{\min 13}$ (Å)	$r_{\max 13}$ (Å)	$r_{\min 23}$ (Å)	$r_{\max 23}$ (Å)
C-S-S	61.413	97.921	1.233	1.233	0.0	2.641	0.0	2.641	0.0	3.874
S-C-C	61.413	97.921	1.233	1.233	0.0	2.641	0.0	2.641	0.0	3.874

Table 472. Three-body SW potential parameters for b-CS used by GULP [8], as expressed in Eq. (4).

	ϵ (eV)	σ (Å)	a	λ	γ	$\cos\theta_0$	A_L	B_L	p	q	Tol
C—S—S	1.000	1.233	2.142	61.413	1.000	−0.138	6.014	2.703	4	0	0.0
S—C—C	1.000	1.233	2.142	61.413	1.000	−0.138	6.014	2.703	4	0	0.0

Table 473. SW potential parameters for b-CS used by LAMMPS [9], as expressed in Eqs. (9) and (10).

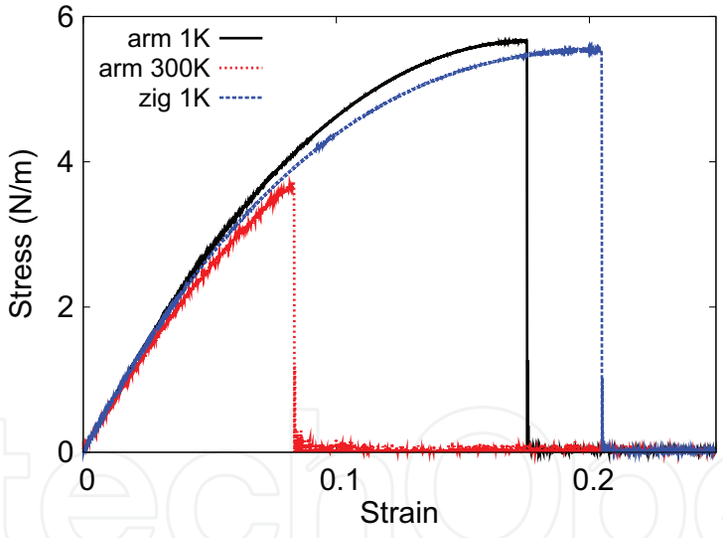

Figure 243. Stress-strain relations for the b-CS of size 100 × 100 Å. The b-CS is uniaxially stretched along the armchair or zigzag directions at temperatures 1 and 300 K.

applied in both armchair and zigzag directions. The single-layer b-CS is stretched uniaxially along the armchair or zigzag direction. The stress is calculated without involving the actual thickness of the quasi-two-dimensional structure of the single-layer b-CS. The Young's modulus can be obtained by a linear fitting of the stress-strain relation in the small strain range of [0, 0.01]. The Young's modulus is 63.5 and 63.6 N/m along the armchair and zigzag directions, respectively. The Young's modulus is essentially isotropic in the armchair and zigzag directions. The Poisson's ratio from the VFF model and the SW potential is $\nu_{xy} = \nu_{yx} = 0.05$.

There is no available value for nonlinear quantities in the single-layer b-CS. We have thus used the nonlinear parameter $B = 0.5d^4$ in Eq. (5), which is close to the value of B in most materials. The value of the third-order nonlinear elasticity D can be extracted by fitting the stress-strain relation to the function $\sigma = E\epsilon + \frac{1}{2}D\epsilon^2$ with E as the Young's modulus. The values of D from the present SW potential are -352.5 and -372.0 N/m along the armchair and zigzag directions, respectively. The ultimate stress is about 5.7 N/m at the ultimate strain of 0.17 in the armchair direction at the low temperature of 1 K. The ultimate stress is about 5.5 N/m at the ultimate strain of 0.20 in the zigzag direction at the low temperature of 1 K.

119. b-CSe

Present studies on the buckled (b-) CSe are based on first-principles calculations, and no empirical potential has been proposed for the b-CSe. We will thus parametrize a set of SW potential for the single-layer b-CSe in this section.

The structure of the single-layer b-CSe is shown in **Figure 239**. The structural parameters are from the *ab initio* calculations [78]. The b-CSe has a buckled configuration as shown in **Figure 239(b)**, where the buckle is along the zigzag direction. This structure can be determined by two independent geometrical parameters, including the lattice constant 3.063 Å and the bond length 2.055 Å.

Table 474 shows the VFF model for the single-layer b-CSe. The force constant parameters are determined by fitting to the acoustic branches in the phonon dispersion along the ΓM as shown in **Figure 244(a)**. The *ab initio* calculations for the phonon dispersion are calculated from the SIESTA package [79]. The generalized gradients approximation is applied to account for the exchange-correlation function with Perdew, Burke, and Ernzerhof parameterization [80], and the double-ζ orbital basis set is adopted. **Figure 244(b)** shows that the VFF model and the SW potential give exactly the same phonon dispersion, as the SW potential is derived from the VFF model.

The parameters for the two-body SW potential used by GULP are shown in **Table 475**. The parameters for the three-body SW potential used by GULP are shown in **Table 476**. Parameters for the SW potential used by LAMMPS are listed in **Table 477**.

VFF type	Bond stretching	Angle bending
Expression	$\frac{1}{2}K_r(\Delta r)^2$	$\frac{1}{2}K_\theta(\Delta\theta)^2$
Parameter	10.425	5.031
r_0 or θ_0	2.055	96.362

The second line gives an explicit expression for each VFF term. The third line is the force constant parameters. Parameters are in the unit of eV/Å^2 for the bond stretching interaction and in the unit of eV for the angle bending interaction. The fourth line gives the initial bond length (in the unit of Å) for the bond stretching interaction and the initial angle (in the unit of degrees) for the angle bending interaction.

Table 474. The VFF model for b-CSe.

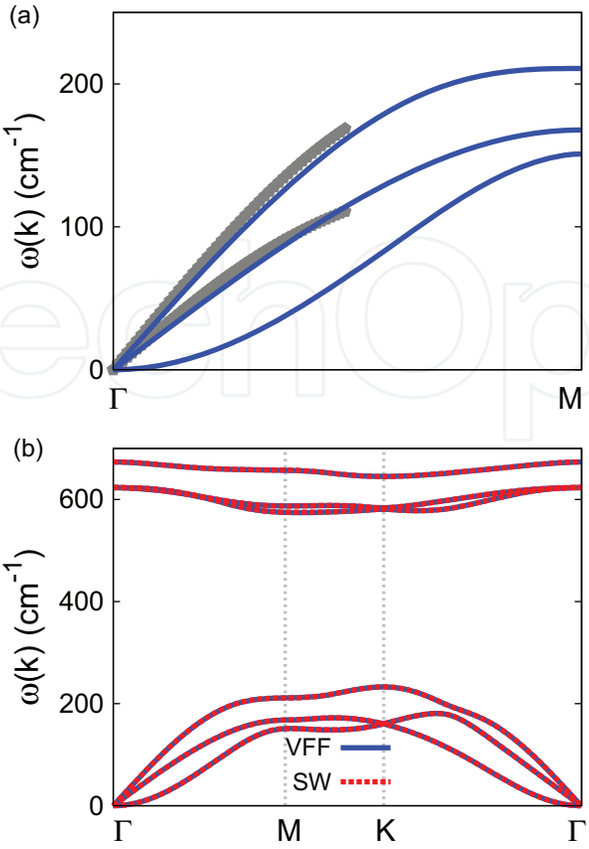

Figure 244. Phonon dispersion for the single-layer b-CSe. (a) The VFF model is fitted to the two in-plane acoustic branches in the long wave limit along the ΓM direction. The *ab initio* results (gray pentagons) are calculated from SIESTA. (b) The VFF model (blue lines) and the SW potential (red lines) give the same phonon dispersion for the b-CSe along ΓMKΓ.

	A (eV)	ρ (Å)	B (Å^4)	$r_{\min}$ (Å)	$r_{\max}$ (Å)
C—Se	7.691	1.298	8.917	0.0	2.872

Table 475. Two-body SW potential parameters for b-CSe used by GULP [8], as expressed in Eq. (3).

	K (eV)	θ_0 (°)	ρ_1 (Å)	ρ_2 (Å)	$r_{\min 12}$ (Å)	$r_{\max 12}$ (Å)	$r_{\min 13}$ (Å)	$r_{\max 13}$ (Å)	$r_{\min 23}$ (Å)	$r_{\max 23}$ (Å)
C-Se-Se	61.215	96.362	1.298	1.298	0.0	2.872	0.0	2.872	0.0	4.184
Se-C-C	61.215	96.362	1.298	1.298	0.0	2.872	0.0	2.872	0.0	4.184

Table 476. Three-body SW potential parameters for b-CSe used by GULP [8], as expressed in Eq. (4).

	ϵ (eV)	σ (Å)	a	λ	γ	$\cos\theta_0$	A_L	B_L	p	q	Tol
C—Se—Se	1.000	1.298	2.212	61.215	1.000	−0.111	7.691	3.137	4	0	0.0
Se—C—C	1.000	1.298	2.212	61.215	1.000	−0.111	7.691	3.137	4	0	0.0

Table 477. SW potential parameters for b-CSe used by LAMMPS [9], as expressed in Eqs. (9) and (10).

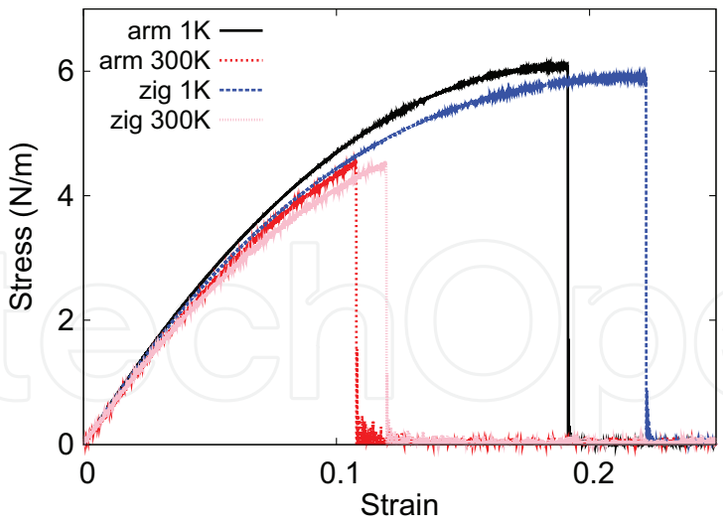

Figure 245. Stress-strain relations for the b-CSe of size 100 × 100 Å. The b-CSe is uniaxially stretched along the armchair or zigzag directions at temperatures 1 and 300 K.

We use LAMMPS to perform MD simulations for the mechanical behavior of the single-layer b-CSe under uniaxial tension at 1.0 and 300.0 K. **Figure 245** shows the stress-strain curve for the tension of a single-layer b-CSe of dimension 100 × 100 Å. Periodic boundary conditions are applied in both armchair and zigzag directions. The single-layer b-CSe is stretched uniaxially along the armchair or zigzag direction. The stress is calculated without involving the actual thickness of the quasi-two-dimensional structure of the single-layer b-CSe. The Young's modulus can be obtained by a linear fitting of the stress-strain relation in the small strain range of [0, 0.01]. The Young's modulus is 61.6 and 61.4 N/m along the armchair and zigzag directions, respectively. The Young's modulus is essentially isotropic in the armchair and zigzag directions. The Poisson's ratio from the VFF model and the SW potential is $\nu_{xy} = \nu_{yx} = 0.09$.

There is no available value for nonlinear quantities in the single-layer b-CSe. We have thus used the nonlinear parameter $B = 0.5d^4$ in Eq. (5), which is close to the value of B in most materials. The value of the third-order nonlinear elasticity D can be extracted by fitting the stress-strain relation to the function $\sigma = E\epsilon + \frac{1}{2}D\epsilon^2$ with E as the Young's modulus. The values of D from the present SW potential are −306.6 and −324.9 N/m along the armchair and zigzag directions, respectively. The ultimate stress is about 6.1 N/m at the ultimate strain of 0.19 in the armchair direction at the low temperature of 1 K. The ultimate stress is about 5.9 N/m at the ultimate strain of 0.22 in the zigzag direction at the low temperature of 1 K.

120. b-CTe

Present studies on the buckled (b-) CTe are based on first-principles calculations, and no empirical potential has been proposed for the b-CTe. We will thus parametrize a set of SW potential for the single-layer b-CTe in this section.

The structure of the single-layer b-CTe is shown in **Figure 239**. The structural parameters are from the *ab initio* calculations [78]. The b-CTe has a buckled configuration as shown in **Figure 239(b)**, where the buckle is along the zigzag direction. This structure can be determined by two independent geometrical parameters, including the lattice constant 3.348 Å and the bond length 2.231 Å.

Table 478 shows the VFF model for the single-layer b-CTe. The force constant parameters are determined by fitting to the acoustic branches in the phonon dispersion along the ΓM as shown in **Figure 246(a)**. The *ab initio* calculations for the phonon dispersion are calculated from the SIESTA package [79]. The generalized gradients approximation is applied to account for the exchange-correlation function with Perdew, Burke, and Ernzerhof parameterization [80], and the double-ζ orbital basis set is adopted. **Figure 246(b)** shows that the VFF model and the SW potential give exactly the same phonon dispersion, as the SW potential is derived from the VFF model.

The parameters for the two-body SW potential used by GULP are shown in **Table 479**. The parameters for the three-body SW potential used by GULP are shown in **Table 480**. Parameters for the SW potential used by LAMMPS are listed in **Table 481**.

We use LAMMPS to perform MD simulations for the mechanical behavior of the single-layer b-CTe under uniaxial tension at 1.0 and 300.0 K. **Figure 247** shows the stress-strain curve for the tension of a single-layer b-CTe of dimension 100 × 100 Å. Periodic boundary conditions are applied in both armchair and zigzag directions. The single-layer b-CTe is stretched uniaxially along the armchair or zigzag direction. The stress is calculated without involving the actual thickness of the quasi-two-dimensional structure of the single-layer b-CTe. The Young's modulus can be obtained by a linear fitting of the stress-strain relation in the small strain range of [0, 0.01]. The Young's modulus is 48.8 and 48.3 N/m along the armchair and zigzag directions, respectively. The Young's modulus is essentially isotropic in the armchair and zigzag directions. The Poisson's ratio from the VFF model and the SW potential is $\nu_{xy} = \nu_{yx} = 0.12$.

There is no available value for nonlinear quantities in the single-layer b-CTe. We have thus used the nonlinear parameter $B = 0.5d^4$ in Eq. (5), which is close to the value of B in most materials. The value of the third-order nonlinear elasticity D can be extracted by fitting the stress-strain relation to the function $\sigma = E\epsilon + \frac{1}{2}D\epsilon^2$ with E as the Young's modulus. The values

VFF type	Bond stretching	Angle bending
Expression	$\frac{1}{2}K_r(\Delta r)^2$	$\frac{1}{2}K_\theta(\Delta\theta)^2$
Parameter	9.367	4.311
r_0 or θ_0	2.231	97.239

The second line gives an explicit expression for each VFF term. The third line is the force constant parameters. Parameters are in the unit of eV/Å^2 for the bond stretching interaction and in the unit of eV for the angle bending interaction. The fourth line gives the initial bond length (in the unit of Å) for the bond stretching interaction and the initial angle (in the unit of degrees) for the angle bending interaction.

Table 478. The VFF model for b-CTe.

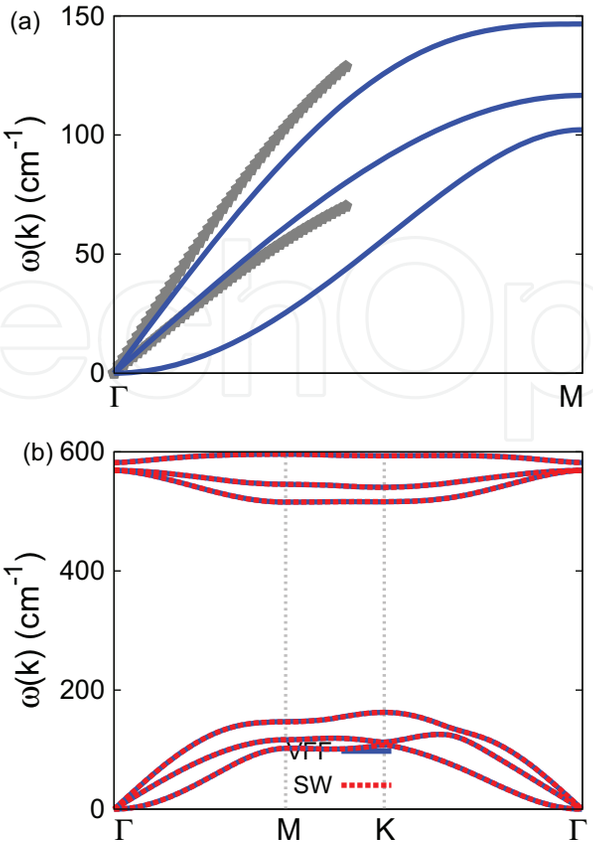

Figure 246. Phonon dispersion for the single-layer b-CTe. (a) The VFF model is fitted to the two in-plane acoustic branches in the long wave limit along the ΓM direction. The *ab initio* results (gray pentagons) are calculated from SIESTA. (b) The VFF model (blue lines) and the SW potential (red lines) give the same phonon dispersion for the b-CTe along ΓMKΓ.

	A (eV)	ρ (Å)	B (Å^4)	$r_{\min}$ (Å)	$r_{\max}$ (Å)
C—Te	8.314	1.440	12.387	0.0	3.127

Table 479. Two-body SW potential parameters for b-CTe used by GULP [8], as expressed in Eq. (3).

	K (eV)	θ_0 (°)	ρ_1 (Å)	ρ_2 (Å)	$r_{\min 12}$ (Å)	$r_{\max 12}$ (Å)	$r_{\min 13}$ (Å)	$r_{\max 13}$ (Å)	$r_{\min 23}$ (Å)	$r_{\max 23}$ (Å)
C-Te-Te	54.451	97.239	1.440	1.440	0.0	3.127	0.0	3.127	0.0	4.573
Te-C-C	54.451	97.239	1.440	1.440	0.0	3.127	0.0	3.127	0.0	4.573

Table 480. Three-body SW potential parameters for b-CTe used by GULP [8], as expressed in Eq. (4).

	ϵ (eV)	σ (Å)	a	λ	γ	$\cos\theta_0$	A_L	B_L	p	q	Tol
C—Te—Te	1.000	1.440	2.172	54.451	1.000	−0.126	8.314	2.883	4	0	0.0
Te—C—C	1.000	1.440	2.172	54.451	1.000	−0.126	8.314	2.883	4	0	0.0

Table 481. SW potential parameters for b-CTe used by LAMMPS [9], as expressed in Eqs. (9) and (10).

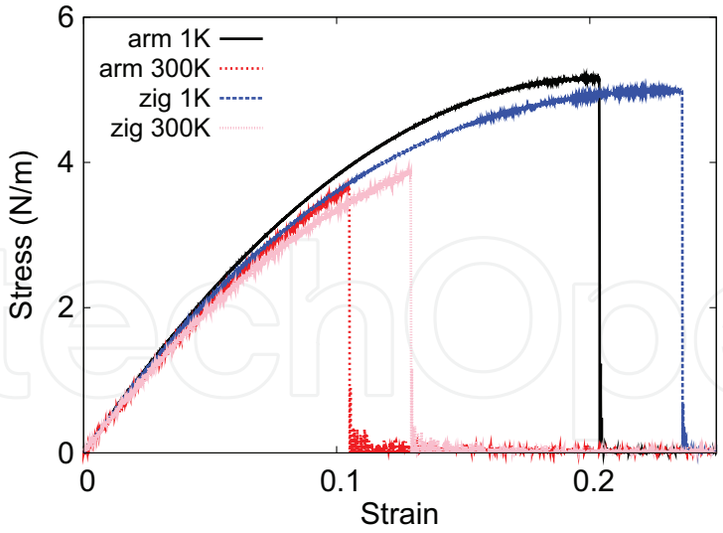

Figure 247. Stress-strain relations for the b-CTe of size 100 × 100 Å. The b-CTe is uniaxially stretched along the armchair or zigzag directions at temperatures 1 and 300 K.

of D from the present SW potential are −306.6 and −324.9 N/m along the armchair and zigzag directions, respectively. The ultimate stress is about 5.2 N/m at the ultimate strain of 0.20 in the armchair direction at the low temperature of 1 K. The ultimate stress is about 5.0 N/m at the ultimate strain of 0.23 in the zigzag direction at the low temperature of 1 K.

121. b-SiO

Present studies on the buckled (b-) SiO are based on first-principles calculations, and no empirical potential has been proposed for the b-SiO. We will thus parametrize a set of SW potential for the single-layer b-SiO in this section.

The structure of the single-layer b-SiO is shown in **Figure 239**. The structural parameters are from the *ab initio* calculations [78]. The b-SiO has a buckled configuration as shown in **Figure 239(b)**, where the buckle is along the zigzag direction. This structure can be determined by two independent geometrical parameters, including the lattice constant 2.815 Å and the bond length 1.884 Å.

Table 482 shows the VFF model for the single-layer b-SiO. The force constant parameters are determined by fitting to the acoustic branches in the phonon dispersion along the ΓM as shown in **Figure 248(a)**. The *ab initio* calculations for the phonon dispersion are calculated from the SIESTA package [79]. The generalized gradients approximation is applied to account for the exchange-correlation function with Perdew, Burke, and Ernzerhof parameterization [80], and the double-ζ orbital basis set is adopted. **Figure 248(b)** shows that the VFF model and the SW potential give exactly the same phonon dispersion, as the SW potential is derived from the VFF model.

VFF type	Bond stretching	Angle bending
Expression	$\frac{1}{2}K_r(\Delta r)^2$	$\frac{1}{2}K_\theta(\Delta\theta)^2$
Parameter	9.315	3.300
r_0 or θ_0	1.884	96.676

The second line gives an explicit expression for each VFF term. The third line is the force constant parameters. Parameters are in the unit of eV/Å^2 for the bond stretching interaction and in the unit of eV for the angle bending interaction. The fourth line gives the initial bond length (in the unit of Å) for the bond stretching interaction and the initial angle (in the unit of degrees) for the angle bending interaction.

Table 482. The VFF model for b-SiO.

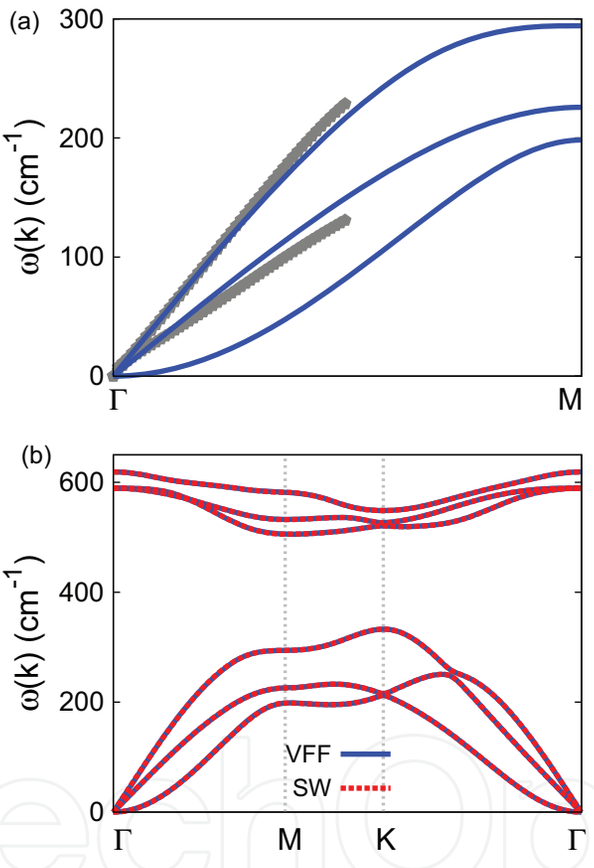

Figure 248. Phonon dispersion for the single-layer b-SiO. (a) The VFF model is fitted to the two in-plane acoustic branches in the long wave limit along the ΓM direction. The *ab initio* results (gray pentagons) are calculated from SIESTA. (b) The VFF model (blue lines) and the SW potential (red lines) give the same phonon dispersion for the b-SiO along ΓMKΓ.

The parameters for the two-body SW potential used by GULP are shown in **Table 483**. The parameters for the three-body SW potential used by GULP are shown in **Table 484**. Parameters for the SW potential used by LAMMPS are listed in **Table 485**.

We use LAMMPS to perform MD simulations for the mechanical behavior of the single-layer b-SiO under uniaxial tension at 1.0 and 300.0 K. **Figure 249** shows the stress-strain curve for

	A (eV)	ρ (Å)	B (Å^4)	$r_{\min}$ (Å)	$r_{\max}$ (Å)
Si—O	5.819	1.200	6.299	0.0	2.636

Table 483. Two-body SW potential parameters for b-SiO used by GULP [8], as expressed in Eq. (3).

	K (eV)	θ_0 (°)	ρ_1 (Å)	ρ_2 (Å)	$r_{\min 12}$ (Å)	$r_{\max 12}$ (Å)	$r_{\min 13}$ (Å)	$r_{\max 13}$ (Å)	$r_{\min 23}$ (Å)	$r_{\max 23}$ (Å)
Si-O-O	40.695	96.676	1.200	1.200	0.0	2.636	0.0	2.636	0.0	3.845
O-Si-Si	40.695	96.676	1.200	1.200	0.0	2.636	0.0	2.636	0.0	3.845

Table 484. Three-body SW potential parameters for b-SiO used by GULP [8], as expressed in Eq. (4).

	ϵ (eV)	σ (Å)	a	λ	γ	$\cos\theta_0$	A_L	B_L	p	q	Tol
Si—O—O	1.000	1.200	2.197	40.695	1.000	−0.116	5.819	3.043	4	0	0.0
O—Si—Si	1.000	1.200	2.197	40.695	1.000	−0.116	5.819	3.043	4	0	0.0

Table 485. SW potential parameters for b-SiO used by LAMMPS [9], as expressed in Eqs. (9) and (10).

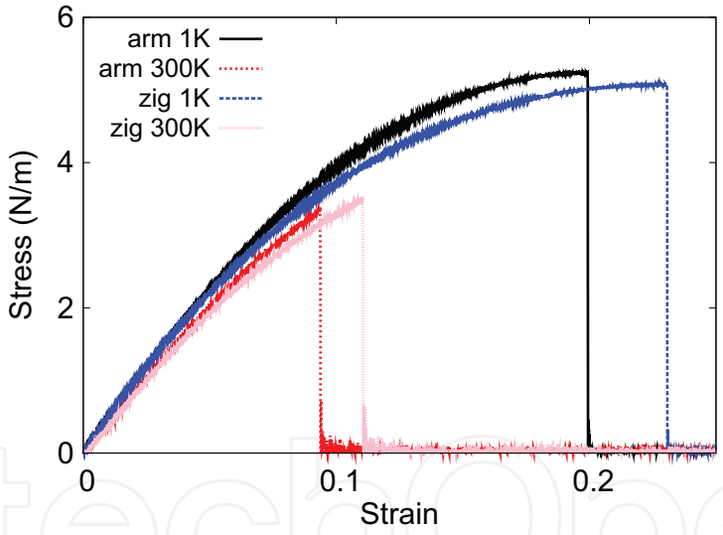

Figure 249. Stress-strain relations for the b-SiO of size 100 × 100 Å. The b-SiO is uniaxially stretched along the armchair or zigzag directions at temperatures 1 and 300 K.

the tension of a single-layer b-SiO of dimension 100 × 100 Å. Periodic boundary conditions are applied in both armchair and zigzag directions. The single-layer b-SiO is stretched uniaxially along the armchair or zigzag direction. The stress is calculated without involving the actual thickness of the quasi-two-dimensional structure of the single-layer b-SiO. The Young's modulus can be obtained by a linear fitting of the stress-strain relation in the small strain range of [0, 0.01]. The Young's modulus is 51.3 and 50.3 N/m along the armchair and zigzag directions, respectively. The Young's modulus is essentially isotropic in the armchair and zigzag directions. The Poisson's ratio from the VFF model and the SW potential is $\nu_{xy} = \nu_{yx} = 0.11$.

There is no available value for nonlinear quantities in the single-layer b-SiO. We have thus used the nonlinear parameter $B = 0.5d^4$ in Eq. (5), which is close to the value of B in most materials. The value of the third-order nonlinear elasticity D can be extracted by fitting the stress-strain relation to the function $\sigma = E\epsilon + \frac{1}{2}D\epsilon^2$ with E as the Young's modulus. The values of D from the present SW potential are -247.8 and -253.6 N/m along the armchair and zigzag directions, respectively. The ultimate stress is about 5.2 N/m at the ultimate strain of 0.20 in the armchair direction at the low temperature of 1 K. The ultimate stress is about 5.1 N/m at the ultimate strain of 0.23 in the zigzag direction at the low temperature of 1 K.

122. b-SiS

Present studies on the buckled (b-) SiS are based on first-principles calculations, and no empirical potential has been proposed for the b-SiS. We will thus parametrize a set of SW potential for the single-layer b-SiS in this section.

The structure of the single-layer b-SiS is shown in **Figure 239**. The structural parameters are from the *ab initio* calculations [78]. The b-SiS has a buckled configuration as shown in **Figure 239(b)**, where the buckle is along the zigzag direction. This structure can be determined by two independent geometrical parameters, including the lattice constant 3.299 Å and the bond length 2.321 Å.

Table 486 shows the VFF model for the single-layer b-SiS. The force constant parameters are determined by fitting to the acoustic branches in the phonon dispersion along the ΓM as shown in **Figure 250(a)**. The *ab initio* calculations for the phonon dispersion are calculated from the SIESTA package [79]. The generalized gradients approximation is applied to account for the exchange-correlation function with Perdew, Burke, and Ernzerhof parameterization [80], and the double-ζ orbital basis set is adopted. **Figure 250(b)** shows that the VFF model and the SW potential give exactly the same phonon dispersion, as the SW potential is derived from the VFF model.

The parameters for the two-body SW potential used by GULP are shown in **Table 487**. The parameters for the three-body SW potential used by GULP are shown in **Table 488**. Parameters for the SW potential used by LAMMPS are listed in **Table 489**.

VFF type	Bond stretching	Angle bending
Expression	$\frac{1}{2}K_r(\Delta r)^2$	$\frac{1}{2}K_\theta(\Delta\theta)^2$
Parameter	8.441	4.802
r_0 or θ_0	2.321	90.581

The second line gives an explicit expression for each VFF term. The third line is the force constant parameters. Parameters are in the unit of eV/Å^2 for the bond stretching interaction and in the unit of eV for the angle bending interaction. The fourth line gives the initial bond length (in the unit of Å) for the bond stretching interaction and the initial angle (in the unit of degrees) for the angle bending interaction.

Table 486. The VFF model for b-SiS..

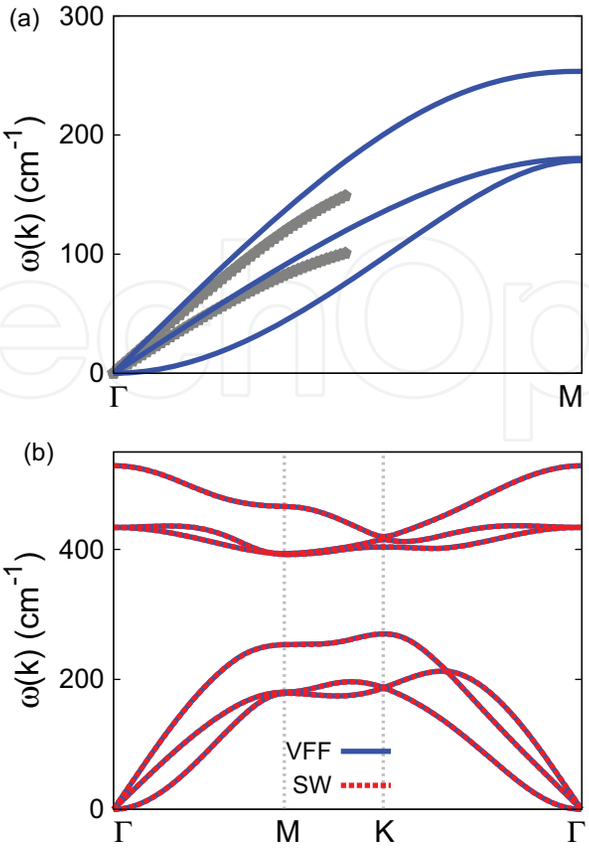

Figure 250. Phonon dispersion for the single-layer b-SiS. (a) The VFF model is fitted to the two in-plane acoustic branches in the long wave limit along the ΓM direction. The *ab initio* results (gray pentagons) are calculated from SIESTA. (b) The VFF model (blue lines) and the SW potential (red lines) give the same phonon dispersion for the b-SiS along ΓMKΓ.

	A (eV)	ρ (Å)	B (Å^4)	$r_{\min}$ (Å)	$r_{\max}$ (Å)
Si—S	6.897	1.264	14.510	0.0	3.177

Table 487. Two-body SW potential parameters for b-SiS used by GULP [8], as expressed in Eq. (3).

	K (eV)	θ_0 (°)	ρ_1 (Å)	ρ_2 (Å)	$r_{\min 12}$ (Å)	$r_{\max 12}$ (Å)	$r_{\min 13}$ (Å)	$r_{\max 13}$ (Å)	$r_{\min 23}$ (Å)	$r_{\max 23}$ (Å)
Si-S-S	45.954	90.581	1.264	1.264	0.0	3.177	0.0	3.177	0.0	4.506
S-Si-Si	45.954	90.581	1.264	1.264	0.0	3.177	0.0	3.177	0.0	4.506

Table 488. Three-body SW potential parameters for b-SiS used by GULP [8], as expressed in Eq. (4).

	ϵ (eV)	σ (Å)	a	λ	γ	$\cos\theta_0$	A_L	B_L	p	q	Tol
Si—S—S	1.000	1.264	2.514	45.954	1.000	−0.010	6.897	5.687	4	0	0.0
S—Si—Si	1.000	1.264	2.514	45.954	1.000	−0.010	6.897	5.687	4	0	0.0

Table 489. SW potential parameters for b-SiS used by LAMMPS [9], as expressed in Eqs. (9) and (10).

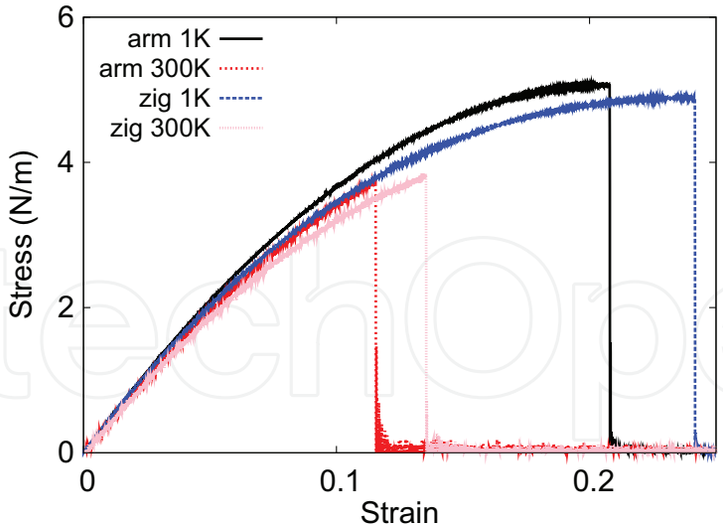

Figure 251. Stress-strain relations for the b-SiS of size 100 × 100 Å. The b-SiS is uniaxially stretched along the armchair or zigzag directions at temperatures 1 and 300 K.

We use LAMMPS to perform MD simulations for the mechanical behavior of the single-layer b-SiS under uniaxial tension at 1.0 and 300.0 K. **Figure 251** shows the stress-strain curve for the tension of a single-layer b-SiS of dimension 100 × 100 Å. Periodic boundary conditions are applied in both armchair and zigzag directions. The single-layer b-SiS is stretched uniaxially along the armchair or zigzag direction. The stress is calculated without involving the actual thickness of the quasi-two-dimensional structure of the single-layer b-SiS. The Young's modulus can be obtained by a linear fitting of the stress-strain relation in the small strain range of [0, 0.01]. The Young's modulus is 45.5 and 45.8 N/m along the armchair and zigzag directions, respectively. The Young's modulus is essentially isotropic in the armchair and zigzag directions. The Poisson's ratio from the VFF model and the SW potential is $\nu_{xy} = \nu_{yx} = 0.13$.

There is no available value for nonlinear quantities in the single-layer b-SiS. We have thus used the nonlinear parameter $B = 0.5d^4$ in Eq. (5), which is close to the value of B in most materials. The value of the third-order nonlinear elasticity D can be extracted by fitting the stress-strain relation to the function $\sigma = E\epsilon + \frac{1}{2}D\epsilon^2$ with E as the Young's modulus. The values of D from the present SW potential are −196.4 and −217.9 N/m along the armchair and zigzag directions, respectively. The ultimate stress is about 5.1 N/m at the ultimate strain of 0.21 in the armchair direction at the low temperature of 1 K. The ultimate stress is about 4.9 N/m at the ultimate strain of 0.24 in the zigzag direction at the low temperature of 1 K.

123. b-SiSe

Present studies on the buckled (b-) SiSe are based on first-principles calculations, and no empirical potential has been proposed for the b-SiSe. We will thus parametrize a set of SW potential for the single-layer b-SiSe in this section.

The structure of the single-layer b-SiSe is shown in **Figure 239**. The structural parameters are from the *ab initio* calculations [78]. The b-SiSe has a buckled configuration as shown in **Figure 239(b)**, where the buckle is along the zigzag direction. This structure can be determined by two independent geometrical parameters, including the lattice constant 3.521 Å and the bond length 2.477 Å.

Table 490 shows the VFF model for the single-layer b-SiSe. The force constant parameters are determined by fitting to the acoustic branches in the phonon dispersion along the ΓM as shown in **Figure 252(a)**. The *ab initio* calculations for the phonon dispersion are calculated from the SIESTA package [79]. The generalized gradients approximation is applied to account for the exchange-correlation function with Perdew, Burke, and Ernzerhof parameterization [80], and the double-ζ orbital basis set is adopted. **Figure 252(b)** shows that the VFF model and the SW potential give exactly the same phonon dispersion, as the SW potential is derived from the VFF model.

The parameters for the two-body SW potential used by GULP are shown in **Table 491**. The parameters for the three-body SW potential used by GULP are shown in **Table 492**. Parameters for the SW potential used by LAMMPS are listed in **Table 493**.

We use LAMMPS to perform MD simulations for the mechanical behavior of the single-layer b-SiSe under uniaxial tension at 1.0 and 300.0 K. **Figure 253** shows the stress-strain curve for the tension of a single-layer b-SiSe of dimension 100 × 100 Å. Periodic boundary conditions are applied in both armchair and zigzag directions. The single-layer b-SiSe is stretched uniaxially along the armchair or zigzag direction. The stress is calculated without involving the actual thickness of the quasi-two-dimensional structure of the single-layer b-SiSe. The Young's modulus can be obtained by a linear fitting of the stress-strain relation in the small strain range of [0, 0.01]. The Young's modulus is 41.8 and 41.9 N/m along the armchair and zigzag directions, respectively. The Young's modulus is essentially isotropic in the armchair and zigzag directions. The Poisson's ratio from the VFF model and the SW potential is $\nu_{xy} = \nu_{yx} = 0.15$.

There is no available value for nonlinear quantities in the single-layer b-SiSe. We have thus used the nonlinear parameter $B = 0.5d^4$ in Eq. (5), which is close to the value of B in most materials. The value of the third-order nonlinear elasticity D can be extracted by fitting the stress-strain relation to the function $\sigma = E\epsilon + \frac{1}{2}D\epsilon^2$ with E as the Young's modulus. The values

VFF type	Bond stretching	Angle bending
Expression	$\frac{1}{2}K_r(\Delta r)^2$	$\frac{1}{2}K_\theta(\Delta\theta)^2$
Parameter	8.441	4.802
r_0 or θ_0	2.477	90.590

The second line gives an explicit expression for each VFF term. The third line is the force constant parameters. Parameters are in the unit of eV/Å^2 for the bond stretching interaction and in the unit of eV for the angle bending interaction. The fourth line gives the initial bond length (in the unit of Å) for the bond stretching interaction and the initial angle (in the unit of degrees) for the angle bending interaction.

Table 490. The VFF model for b-SiSe.

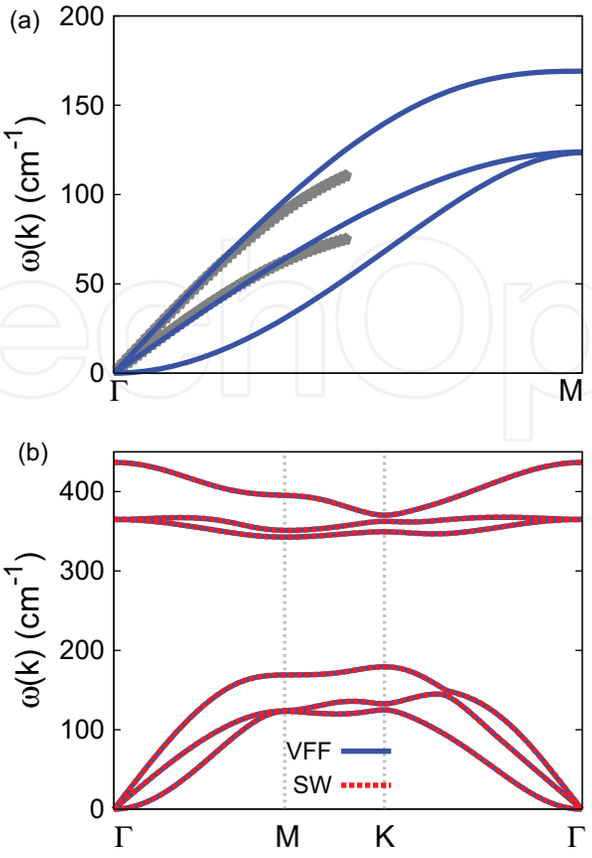

Figure 252. Phonon dispersion for the single-layer b-SiSe. (a) The VFF model is fitted to the two in-plane acoustic branches in the long wave limit along the ΓM direction. The *ab initio* results (gray pentagons) are calculated from SIESTA. (b) The VFF model (blue lines) and the SW potential (red lines) give the same phonon dispersion for the b-SiSe along ΓMKΓ.

	A (eV)	ρ (Å)	B (Å^4)	$r_{\min}$ (Å)	$r_{\max}$ (Å)
Si—Se	7.857	1.349	18.822	0.0	3.391

Table 491. Two-body SW potential parameters for b-SiSe used by GULP [8], as expressed in Eq. (3).

	K (eV)	θ_0 (°)	ρ_1 (Å)	ρ_2 (Å)	$r_{\min 12}$ (Å)	$r_{\max 12}$ (Å)	$r_{\min 13}$ (Å)	$r_{\max 13}$ (Å)	$r_{\min 23}$ (Å)	$r_{\max 23}$ (Å)
Si-Se-Se	45.968	90.590	1.349	1.349	0.0	3.391	0.0	3.391	0.0	4.810
Se-Si-Si	45.968	90.590	1.349	1.349	0.0	3.391	0.0	3.391	0.0	4.810

Table 492. Three-body SW potential parameters for b-SiSe used by GULP [8], as expressed in Eq. (4).

	ϵ (eV)	σ (Å)	a	λ	γ	$\cos\theta_0$	A_L	B_L	p	q	Tol
Si—Se—Se	1.000	1.349	2.514	45.968	1.000	−0.010	7.857	5.6683	4	0	0.0
Se—Si—Si	1.000	1.349	2.514	45.968	1.000	−0.010	7.857	5.6683	4	0	0.0

Table 493. SW potential parameters for b-SiSe used by LAMMPS [9], as expressed in Eqs. (9) and (10).

http://dx.doi.org/10.5772/intechopen.71929

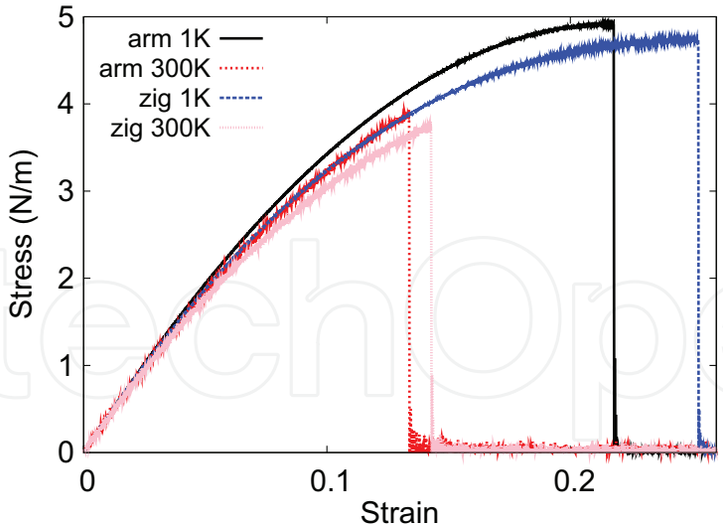

Figure 253. Stress-strain relations for the b-SiSe of size 100 × 100 Å. The b-SiSe is uniaxially stretched along the armchair or zigzag directions at temperatures 1 and 300 K.

of D from the present SW potential are −169.9 and −188.0 N/m along the armchair and zigzag directions, respectively. The ultimate stress is about 4.9 N/m at the ultimate strain of 0.22 in the armchair direction at the low temperature of 1 K. The ultimate stress is about 4.7 N/m at the ultimate strain of 0.25 in the zigzag direction at the low temperature of 1 K.

124. b-SiTe

Present studies on the buckled (b-) SiTe are based on first-principles calculations, and no empirical potential has been proposed for the b-SiTe. We will thus parametrize a set of SW potential for the single-layer b-SiTe in this section.

The structure of the single-layer b-SiTe is shown in **Figure 239**. The structural parameters are from the *ab initio* calculations [83]. The b-SiTe has a buckled configuration as shown in **Figure 239(b)**, where the buckle is along the zigzag direction. This structure can be determined by two independent geometrical parameters, e.g., the lattice constant 3.83 Å and the bond length 2.689 Å. The resultant height of the buckle is $h = 1.53$ Å.

Table 494 shows the VFF model for the single-layer b-SiTe. The force constant parameters are determined by fitting to the acoustic branches in the phonon dispersion along the ΓM as shown in **Figure 254(a)**. The *ab initio* calculations for the phonon dispersion are from [83]. **Figure 254(b)** shows that the VFF model and the SW potential give exactly the same phonon dispersion, as the SW potential is derived from the VFF model.

The parameters for the two-body SW potential used by GULP are shown in **Table 495**. The parameters for the three-body SW potential used by GULP are shown in **Table 496**. Parameters for the SW potential used by LAMMPS are listed in **Table 497**.

VFF type	Bond stretching	Angle bending
Expression	$\frac{1}{2}K_r(\Delta r)^2$	$\frac{1}{2}K_\theta(\Delta\theta)^2$
Parameter	8.418	4.349
r_0 or θ_0	2.690	90.779

The second line gives an explicit expression for each VFF term. The third line is the force constant parameters. Parameters are in the unit of eV/Å^2 for the bond stretching interaction and in the unit of eV for the angle bending interaction. The fourth line gives the initial bond length (in the unit of Å) for the bond stretching interaction and the initial angle (in the unit of degrees) for the angle bending interaction.

Table 494. The VFF model for b-SiTe.

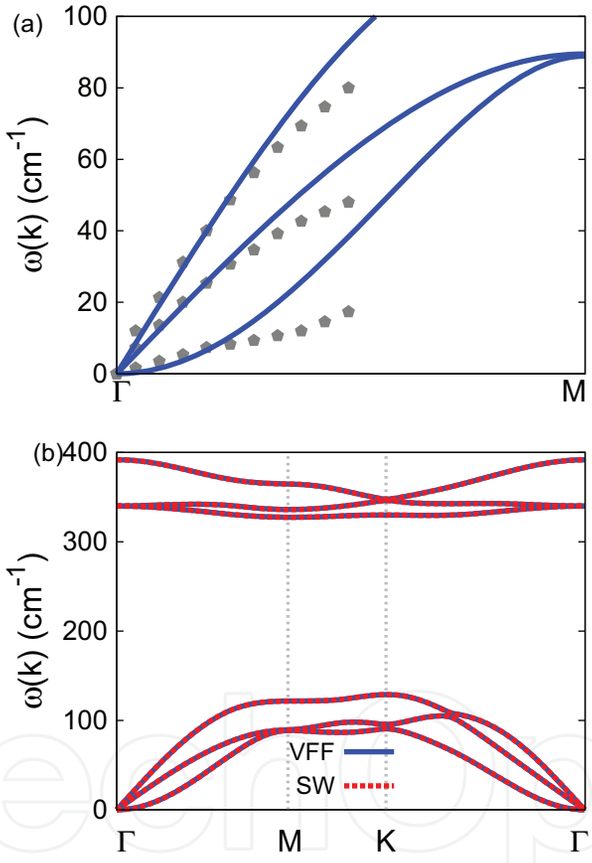

Figure 254. Phonon dispersion for the single-layer b-SiTe. (a) The VFF model is fitted to the three acoustic branches in the long wave limit along the ΓM direction. The *ab initio* results (gray pentagons) are from Ref. 83. (b) The VFF model (blue lines) and the SW potential (red lines) give the same phonon dispersion for the b-SiTe along ΓMKΓ.

	A (eV)	ρ (Å)	B (Å^4)	$r_{\min}$ (Å)	$r_{\max}$ (Å)
Si—Te	9.285	1.473	26.181	0.0	3.685

Table 495. Two-body SW potential parameters for b-SiTe used by GULP [8], as expressed in Eq. (3).

	K (eV)	θ_0 (degree)	ρ_1 (Å)	ρ_2 (Å)	$r_{\min 12}$ (Å)	$r_{\max 12}$ (Å)	$r_{\min 13}$ (Å)	$r_{\max 13}$ (Å)	$r_{\min 23}$ (Å)	$r_{\max 23}$ (Å)
Si-Te-Te	41.952	90.779	1.473	1.473	0.0	3.685	0.0	3.685	0.0	5.232
Te-Si-Si	41.952	90.779	1.473	1.473	0.0	3.685	0.0	3.685	0.0	5.232

Table 496. Three-body SW potential parameters for b-SiTe used by GULP [8], as expressed in Eq. (4).

	ϵ (eV)	σ (Å)	a	λ	γ	$\cos\theta_0$	A_L	B_L	p	q	Tol
Si—Te—Te	1.000	0.725	4.497	27.653	1.000	−0.014	4.428	113.714	4	0	0.0
Te—Si—Si	1.000	0.725	4.497	27.653	1.000	−0.014	4.428	113.714	4	0	0.0

Table 497. SW potential parameters for b-SiTe used by LAMMPS [9], as expressed in Eqs. (9) and (10).

We use LAMMPS to perform MD simulations for the mechanical behavior of the single-layer b-SiTe under uniaxial tension at 1.0 and 300.0 K. **Figure 255** shows the stress-strain curve for the tension of a single-layer b-SiTe of dimension 100 × 100 Å. Periodic boundary conditions are applied in both armchair and zigzag directions. The single-layer b-SiTe is stretched uniaxially along the armchair or zigzag direction. The stress is calculated without involving the actual thickness of the quasi-two-dimensional structure of the single-layer b-SiTe. The Young's modulus can be obtained by a linear fitting of the stress-strain relation in the small strain range of [0, 0.01]. The Young's modulus is 34.3 and 34.6 N/m along the armchair and zigzag directions, respectively. The Young's modulus is essentially isotropic in the armchair and zigzag directions. These values agree with the *ab initio* result at 0 K temperature, e.g., 34.1 N/m in [83]. The Poisson's ratio from the VFF model and the SW potential is $\nu_{xy} = \nu_{yx} = 0.18$, which agrees with the *ab initio* result [83] of 0.18.

There is no available value for nonlinear quantities in the single-layer b-SiTe. We have thus used the nonlinear parameter $B = 0.5d^4$ in Eq. (5), which is close to the value of B in most

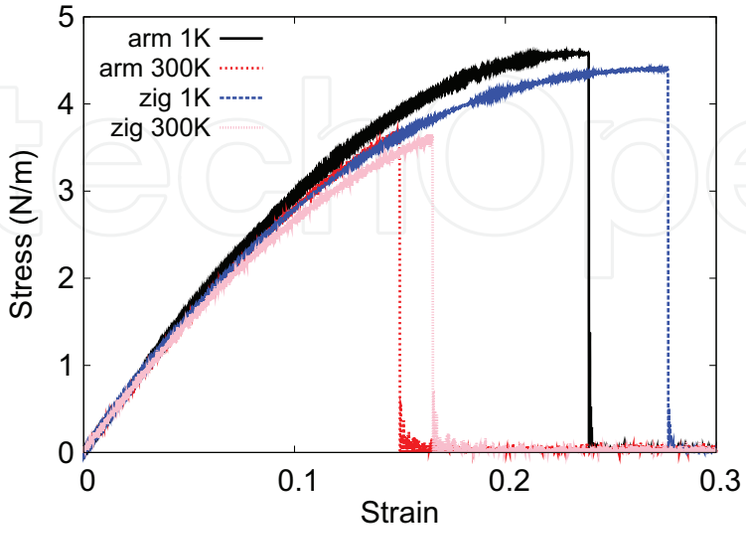

Figure 255. Stress-strain relations for the b-SiTe of size 100 × 100 Å. The b-SiTe is uniaxially stretched along the armchair or zigzag directions at temperatures 1 and 300 K.

materials. The value of the third-order nonlinear elasticity D can be extracted by fitting the stress-strain relation to the function $\sigma = E\epsilon + \frac{1}{2}D\epsilon^2$ with E as the Young's modulus. The values of D from the present SW potential are -119.3 and -137.2 N/m along the armchair and zigzag directions, respectively. The ultimate stress is about 4.6 N/m at the ultimate strain of 0.24 in the armchair direction at the low temperature of 1 K. The ultimate stress is about 4.4 N/m at the ultimate strain of 0.27 in the zigzag direction at the low temperature of 1 K.

125. b-GeO

Present studies on the buckled (b-) GeO are based on first-principles calculations, and no empirical potential has been proposed for the b-GeO. We will thus parametrize a set of SW potential for the single-layer b-GeO in this section.

The structure of the single-layer b-GeO is shown in **Figure 239**. The structural parameters are from the *ab initio* calculations [78]. The b-GeO has a buckled configuration as shown in **Figure 239(b)**, where the buckle is along the zigzag direction. This structure can be determined by two independent geometrical parameters, including the lattice constant 3.124 Å and the bond length 2.032 Å.

Table 498 shows the VFF model for the single-layer b-GeO. The force constant parameters are determined by fitting to the acoustic branches in the phonon dispersion along the ΓM as shown in **Figure 256(a)**. The *ab initio* calculations for the phonon dispersion are calculated from the SIESTA package [79]. The generalized gradients approximation is applied to account for the exchange-correlation function with Perdew, Burke, and Ernzerhof parameterization [80], and the double-ζ orbital basis set is adopted. **Figure 256(b)** shows that the VFF model and the SW potential give exactly the same phonon dispersion, as the SW potential is derived from the VFF model.

The parameters for the two-body SW potential used by GULP are shown in **Table 499**. The parameters for the three-body SW potential used by GULP are shown in **Table 500**. Parameters for the SW potential used by LAMMPS are listed in **Table 501**.

VFF type	Bond stretching	Angle bending
Expression	$\frac{1}{2}K_r(\Delta r)^2$	$\frac{1}{2}K_\theta(\Delta\theta)^2$
Parameter	9.315	3.300
r_0 or θ_0	2.032	100.475

The second line gives an explicit expression for each VFF term. The third line is the force constant parameters. Parameters are in the unit of eV/Å^2 for the bond stretching interaction and in the unit of eV for the angle bending interaction. The fourth line gives the initial bond length (in the unit of Å) for the bond stretching interaction and the initial angle (in the unit of degrees) for the angle bending interaction.

Table 498. The VFF model for b-GeO.

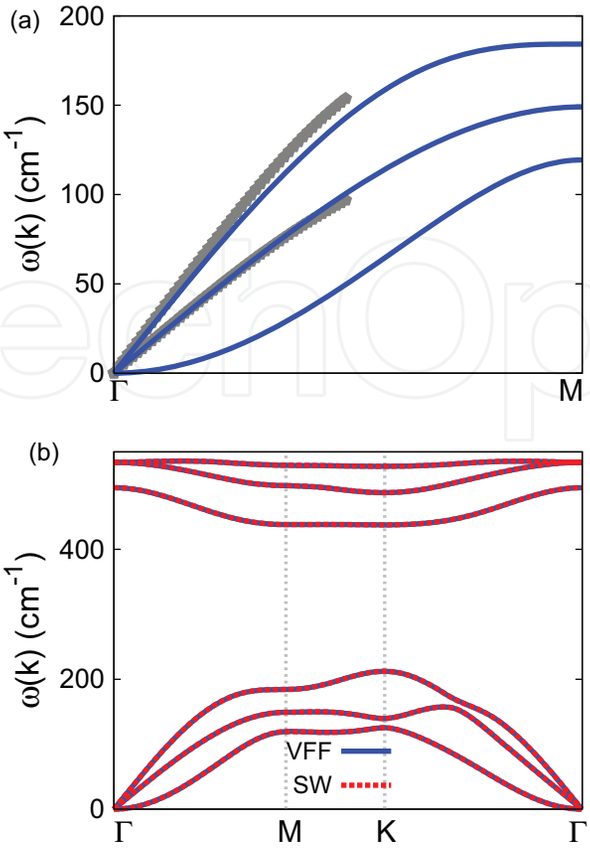

Figure 256. Phonon dispersion for the single-layer b-GeO. (a) The VFF model is fitted to the two in-plane acoustic branches in the long wave limit along the ΓM direction. The *ab initio* results (gray pentagons) are calculated from SIESTA. (b) The VFF model (blue lines) and the SW potential (red lines) give the same phonon dispersion for the b-GeO along ΓMKΓ.

	A (eV)	ρ (Å)	B (Å^4)	$r_{\min}$ (Å)	$r_{\max}$ (Å)
Ge—O	7.390	1.413	8.524	0.0	2.879

Table 499. Two-body SW potential parameters for b-GeO used by GULP [8], as expressed in Eq. (3).

	K (eV)	θ_0 (°)	ρ_1 (Å)	ρ_2 (Å)	$r_{\min 12}$ (Å)	$r_{\max 12}$ (Å)	$r_{\min 13}$ (Å)	$r_{\max 13}$ (Å)	$r_{\min 23}$ (Å)	$r_{\max 23}$ (Å)
Ge-O-O	47.962	100.475	1.413	1.413	0.0	2.879	0.0	2.879	0.0	4.267
O-Ge-Ge	47.962	100.475	1.413	1.413	0.0	2.879	0.0	2.879	0.0	4.267

Table 500. Three-body SW potential parameters for b-GeO used by GULP [8], as expressed in Eq. (4).

	ϵ (eV)	σ (Å)	a	λ	γ	$\cos\theta_0$	A_L	B_L	p	q	Tol
Ge—O—O	1.000	1.413	2.037	47.962	1.000	−0.182	7.390	2.136	4	0	0.0
O—Ge—Ge	1.000	1.413	2.037	47.962	1.000	−0.182	7.390	2.136	4	0	0.0

Table 501. SW potential parameters for b-GeO used by LAMMPS [9], as expressed in Eqs. (9) and (10).

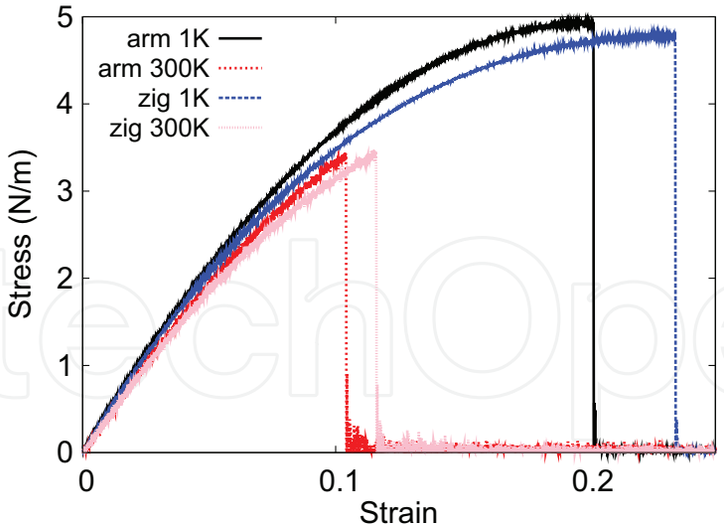

Figure 257. Stress-strain relations for the b-GeO of size 100 × 100 Å. The b-GeO is uniaxially stretched along the armchair or zigzag directions at temperatures 1 and 300 K.

We use LAMMPS to perform MD simulations for the mechanical behavior of the single-layer b-GeO under uniaxial tension at 1.0 and 300.0 K. **Figure 257** shows the stress-strain curve for the tension of a single-layer b-GeO of dimension 100 × 100 Å. Periodic boundary conditions are applied in both armchair and zigzag directions. The single-layer b-GeO is stretched uniaxially along the armchair or zigzag direction. The stress is calculated without involving the actual thickness of the quasi-two-dimensional structure of the single-layer b-GeO. The Young's modulus can be obtained by a linear fitting of the stress-strain relation in the small strain range of [0, 0.01]. The Young's modulus is 47.5 and 46.8 N/m along the armchair and zigzag directions, respectively. The Young's modulus is essentially isotropic in the armchair and zigzag directions. The Poisson's ratio from the VFF model and the SW potential is $\nu_{xy} = \nu_{yx} = 0.11$.

There is no available value for nonlinear quantities in the single-layer b-GeO. We have thus used the nonlinear parameter $B = 0.5d^4$ in Eq. (5), which is close to the value of B in most materials. The value of the third-order nonlinear elasticity D can be extracted by fitting the stress-strain relation to the function $\sigma = E\epsilon + \frac{1}{2}D\epsilon^2$ with E as the Young's modulus. The values of D from the present SW potential are −224.6 and −232.8 N/m along the armchair and zigzag directions, respectively. The ultimate stress is about 4.9 N/m at the ultimate strain of 0.20 in the armchair direction at the low temperature of 1 K. The ultimate stress is about 4.8 N/m at the ultimate strain of 0.23 in the zigzag direction at the low temperature of 1 K.

126. b-GeS

Present studies on the buckled (b-) GeS are based on first-principles calculations, and no empirical potential has been proposed for the b-GeS. We will thus parametrize a set of SW potential for the single-layer b-GeS in this section.

The structure of the single-layer b-GeS is shown in **Figure 239**. The structural parameters are from the *ab initio* calculations [78]. The b-GeS has a buckled configuration as shown in **Figure 239(b)**, where the buckle is along the zigzag direction. This structure can be determined by two independent geometrical parameters, including the lattice constant 3.485 Å and the bond length 2.428 Å.

Table 502 shows the VFF model for the single-layer b-GeS. The force constant parameters are determined by fitting to the acoustic branches in the phonon dispersion along the ΓM as shown in **Figure 258(a)**. The *ab initio* calculations for the phonon dispersion are calculated from the SIESTA package [79]. The generalized gradients approximation is applied to account for the exchange-correlation function with Perdew, Burke, and Ernzerhof parameterization [80], and the double-ζ orbital basis set is adopted. **Figure 258(b)** shows that the VFF model and the SW potential give exactly the same phonon dispersion, as the SW potential is derived from the VFF model.

The parameters for the two-body SW potential used by GULP are shown in **Table 503**. The parameters for the three-body SW potential used by GULP are shown in **Table 504**. Parameters for the SW potential used by LAMMPS are listed in **Table 505**.

We use LAMMPS to perform MD simulations for the mechanical behavior of the single-layer b-GeS under uniaxial tension at 1.0 and 300.0 K. **Figure 259** shows the stress-strain curve for the tension of a single-layer b-GeS of dimension 100×100 Å. Periodic boundary conditions are applied in both armchair and zigzag directions. The single-layer b-GeS is stretched uniaxially along the armchair or zigzag direction. The stress is calculated without involving the actual thickness of the quasi-two-dimensional structure of the single-layer b-GeS. The Young's modulus can be obtained by a linear fitting of the stress-strain relation in the small strain range of [0, 0.01]. The Young's modulus is 34.9 and 34.1 N/m along the armchair and zigzag directions, respectively. The Young's modulus is essentially isotropic in the armchair and zigzag directions. The Poisson's ratio from the VFF model and the SW potential is $\nu_{xy} = \nu_{yx} = 0.18$.

There is no available value for nonlinear quantities in the single-layer b-GeS. We have thus used the nonlinear parameter $B = 0.5d^4$ in Eq. (5), which is close to the value of B in most materials. The value of the third-order nonlinear elasticity D can be extracted by fitting the stress-strain relation to the function $\sigma = E\epsilon + \frac{1}{2}D\epsilon^2$ with E as the Young's modulus. The values

VFF type	Bond stretching	Angle bending
Expression	$\frac{1}{2}K_r(\Delta r)^2$	$\frac{1}{2}K_\theta(\Delta\theta)^2$
Parameter	8.322	3.516
r_0 or θ_0	2.428	91.725

The second line gives an explicit expression for each VFF term. The third line is the force constant parameters. Parameters are in the unit of eV/Å^2 for the bond stretching interaction and in the unit of eV for the angle bending interaction. The fourth line gives the initial bond length (in the unit of Å) for the bond stretching interaction and the initial angle (in the unit of degrees) for the angle bending interaction.

Table 502. The VFF model for b-GeS.

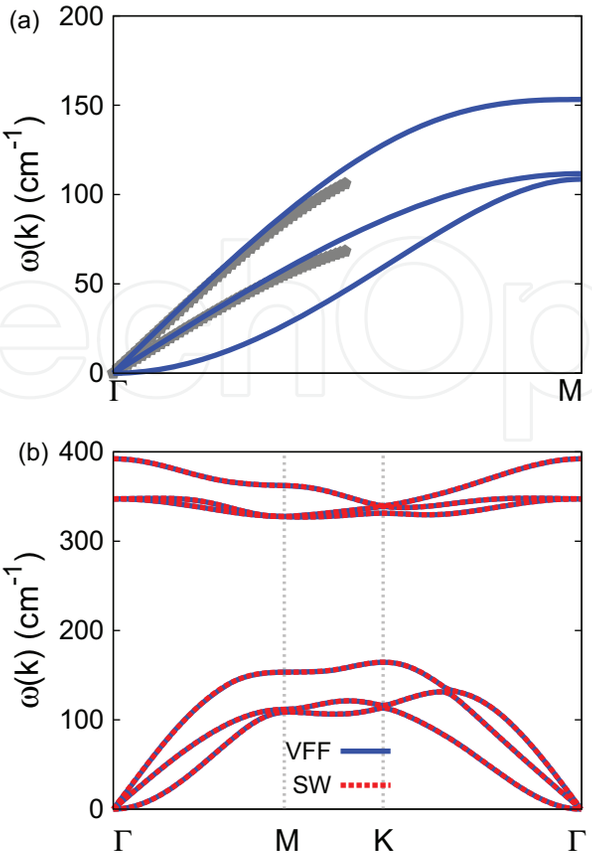

Figure 258. Phonon dispersion for the single-layer b-GeS. (a) The VFF model is fitted to the two in-plane acoustic branches in the long wave limit along the ΓM direction. The *ab initio* results (gray pentagons) are calculated from SIESTA. (b) The VFF model (blue lines) and the SW potential (red lines) give the same phonon dispersion for the b-GeS along ΓMKΓ.

	A (eV)	ρ (Å)	B (Å^4)	$r_{\min}$ (Å)	$r_{\max}$ (Å)
Ge—S	7.657	1.363	17.377	0.0	3.338

Table 503. Two-body SW potential parameters for b-GeS used by GULP [8], as expressed in Eq. (3).

	K (eV)	θ_0 (°)	ρ_1 (Å)	ρ_2 (Å)	$r_{\min 12}$ (Å)	$r_{\max 12}$ (Å)	$r_{\min 13}$ (Å)	$r_{\max 13}$ (Å)	$r_{\min 23}$ (Å)	$r_{\max 23}$ (Å)
Ge-S-S	35.249	91.725	1.363	1.363	0.0	3.338	0.0	3.338	0.0	4.761
S-Ge-Ge	35.249	91.725	1.363	1.363	0.0	3.338	0.0	3.338	0.0	4.761

Table 504. Three-body SW potential parameters for b-GeS used by GULP [8], as expressed in Eq. (4).

	ϵ (eV)	σ (Å)	a	λ	γ	$\cos\theta_0$	A_L	B_L	p	q	Tol
Ge—S—S	1.000	1.363	2.448	35.249	1.000	−0.030	7.657	5.030	4	0	0.0
S—Ge—Ge	1.000	1.363	2.448	35.249	1.000	−0.030	7.657	5.030	4	0	0.0

Table 505. SW potential parameters for b-GeS used by LAMMPS [9], as expressed in Eqs. (9) and (10).

http://dx.doi.org/10.5772/intechopen.71929

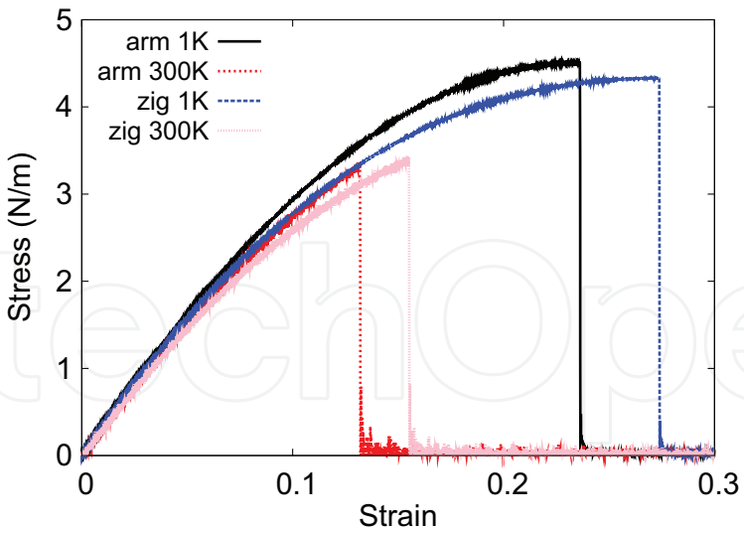

Figure 259. Stress-strain relations for the b-GeS of size 100 × 100 Å. The b-GeS is uniaxially stretched along the armchair or zigzag directions at temperatures 1 and 300 K.

of D from the present SW potential are −128.1 and −135.0 N/m along the armchair and zigzag directions, respectively. The ultimate stress is about 4.5 N/m at the ultimate strain of 0.23 in the armchair direction at the low temperature of 1 K. The ultimate stress is about 4.3 N/m at the ultimate strain of 0.27 in the zigzag direction at the low temperature of 1 K.

127. B-GeSe

Present studies on the buckled (b-) GeSe are based on first-principles calculations, and no empirical potential has been proposed for the b-GeSe. We will thus parametrize a set of SW potential for the single-layer b-GeSe in this section.

The structure of the single-layer b-GeSe is shown in **Figure 239**. The structural parameters are from the *ab initio* calculations [78]. The b-GeSe has a buckled configuration as shown in **Figure 239(b)**, where the buckle is along the zigzag direction. This structure can be determined by two independent geometrical parameters, including the lattice constant 3.676 Å and the bond length 2.568 Å.

Table 506 shows the VFF model for the single-layer b-GeSe. The force constant parameters are determined by fitting to the acoustic branches in the phonon dispersion along the ΓM as shown in **Figure 260(a)**. The *ab initio* calculations for the phonon dispersion are calculated from the SIESTA package [79]. The generalized gradient approximation is applied to account for the exchange-correlation function with Perdew, Burke, and Ernzerhof parameterization [80], and the double-ζ orbital basis set is adopted. **Figure 260(b)** shows that the VFF model and the SW potential give exactly the same phonon dispersion, as the SW potential is derived from the VFF model.

VFF type	Bond stretching	Angle bending
Expression	$\frac{1}{2}K_r(\Delta r)^2$	$\frac{1}{2}K_\theta(\Delta\theta)^2$
Parameter	8.322	3.516
r_0 or θ_0	2.568	91.406

The second line gives an explicit expression for each VFF term. The third line is the force constant parameters. Parameters are in the unit of eV/Å^2 for the bond stretching interaction and in the unit of eV for the angle bending interaction. The fourth line gives the initial bond length (in the unit of Å) for the bond stretching interaction and the initial angle (in the unit of degrees) for the angle bending interaction.

Table 506. The VFF model for b-GeSe.

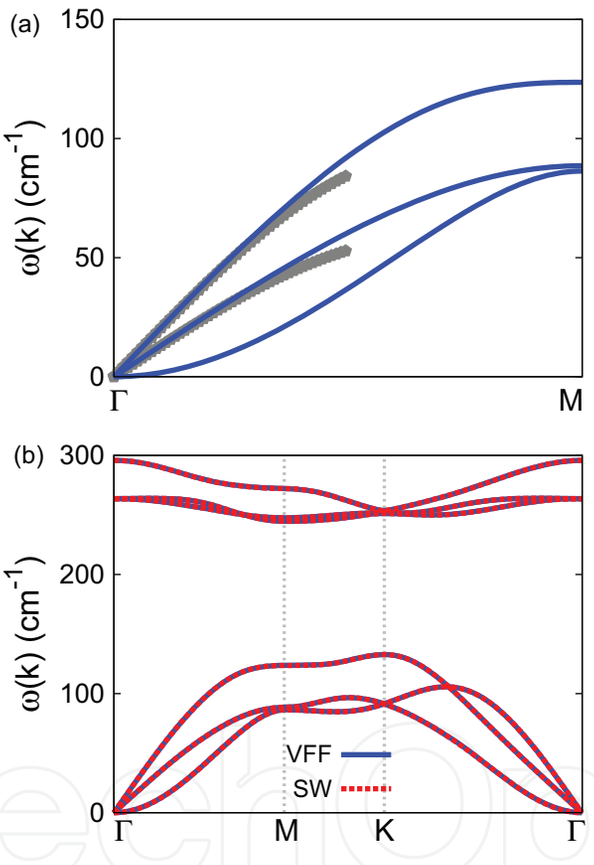

Figure 260. Phonon dispersion for the single-layer b-GeSe. (a) The VFF model is fitted to the two in-plane acoustic branches in the long wave limit along the ΓM direction. The *ab initio* results (gray pentagons) are calculated from SIESTA. (b) The VFF model (blue lines) and the SW potential (red lines) give the same phonon dispersion for the b-GeSe along ΓMKΓ.

The parameters for the two-body SW potential used by GULP are shown in **Table 507**. The parameters for the three-body SW potential used by GULP are shown in **Table 508**. Parameters for the SW potential used by LAMMPS are listed in **Table 509**.

We use LAMMPS to perform MD simulations for the mechanical behavior of the single-layer b-GeSe under uniaxial tension at 1 and 300 K. **Figure 261** shows the stress-strain curve for the

	A (eV)	ρ (Å)	B (Å^4)	$r_{\min}$ (Å)	$r_{\max}$ (Å)
Ge—S	8.498	1.430	21.745	0.0	3.526

Table 507. Two-body SW potential parameters for b-GeSe used by GULP [8], as expressed in Eq. (3).

	K (eV)	θ_0 (°)	ρ_1 (Å)	ρ_2 (Å)	$r_{\min 12}$ (Å)	$r_{\max 12}$ (Å)	$r_{\min 13}$ (Å)	$r_{\max 13}$ (Å)	$r_{\min 23}$ (Å)	$r_{\max 23}$ (Å)
Ge—Se—Se	34.791	91.406	1.430	1.430	0.0	3.526	0.0	3.526	0.0	5.021
Se—Ge—Ge	34.791	91.406	1.430	1.430	0.0	3.526	0.0	3.526	0.0	5.021

Table 508. Three-body SW potential parameters for b-GeSe used by GULP [8], as expressed in Eq. (4).

	ϵ (eV)	σ (Å)	a	λ	γ	$\cos\theta_0$	A_L	B_L	p	q	Tol
Ge—Se—Se	1.000	1.430	2.466	34.791	1.000	−0.025	8.498	5.205	4	0	0.0
Se—Ge—Ge	1.000	1.430	2.466	34.791	1.000	−0.025	8.498	5.205	4	0	0.0

Table 509. SW potential parameters for b-GeSe used by LAMMPS [9], as expressed in Eqs. (9) and (10).

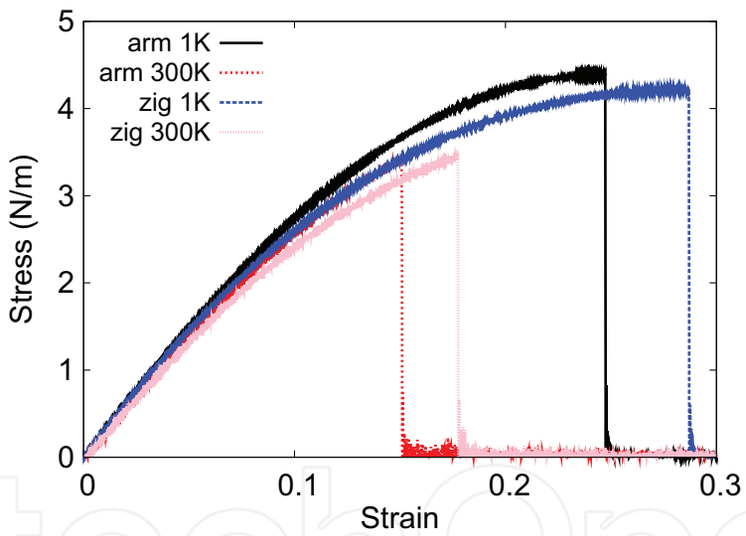

Figure 261. Stress-strain relations for the b-GeSe of size 100 × 100 Å. The b-GeSe is uniaxially stretched along the armchair or zigzag directions at temperatures 1 and 300 K.

tension of a single-layer b-GeSe of dimension 100 × 100 Å. Periodic boundary conditions are applied in both armchair and zigzag directions. The single-layer b-GeSe is stretched uniaxially along the armchair or zigzag direction. The stress is calculated without involving the actual thickness of the quasi-two-dimensional structure of the single-layer b-GeSe. The Young's modulus can be obtained by a linear fitting of the stress-strain relation in the small strain range of [0, 0.01]. The Young's modulus is 31.6 and 31.5 N/m along the armchair and zigzag directions, respectively. The Young's modulus is essentially isotropic in the armchair and zigzag directions. The Poisson's ratio from the VFF model and the SW potential is $\nu_{xy} = \nu_{yx} = 0.19$.

There is no available value for nonlinear quantities in the single-layer b-GeSe. We have thus used the nonlinear parameter $B = 0.5d^4$ in Eq. (5), which is close to the value of B in most materials. The value of the third-order nonlinear elasticity D can be extracted by fitting the stress-strain relation to the function $\sigma = E\epsilon + \frac{1}{2}D\epsilon^2$ with E as the Young's modulus. The values of D from the present SW potential are -105.2 and -118.3 N/m along the armchair and zigzag directions, respectively. The ultimate stress is about 4.4 N/m at the ultimate strain of 0.24 in the armchair direction at the low temperature of 1 K. The ultimate stress is about 4.2 N/m at the ultimate strain of 0.28 in the zigzag direction at the low temperature of 1 K.

128. B-GeTe

Present studies on the buckled (b-) GeTe are based on first-principles calculations, and no empirical potential has been proposed for the b-GeTe. We will thus parametrize a set of SW potential for the single-layer b-GeTe in this section.

The structure of the single-layer b-GeTe is shown in **Figure 239**. The structural parameters are from the *ab initio* calculations [78]. The b-GeTe has a buckled configuration as shown in **Figure 239(b)**, where the buckle is along the zigzag direction. This structure can be determined by two independent geometrical parameters, including the lattice constant 3.939 Å and the bond length 2.768 Å.

Table 510 shows the VFF model for the single-layer b-GeTe. The force constant parameters are determined by fitting to the acoustic branches in the phonon dispersion along the ΓM as shown in **Figure 262(a)**. The *ab initio* calculations for the phonon dispersion are calculated from the SIESTA package [79]. The generalized gradient approximation is applied to account for the exchange-correlation function with Perdew, Burke, and Ernzerhof parameterization [80], and the double-ζ orbital basis set is adopted. **Figure 262(b)** shows that the VFF model and the SW potential give exactly the same phonon dispersion, as the SW potential is derived from the VFF model.

The parameters for the two-body SW potential used by GULP are shown in **Table 511**. The parameters for the three-body SW potential used by GULP are shown in **Table 512**. Parameters for the SW potential used by LAMMPS are listed in **Table 513**.

VFF type	Bond stretching	Angle bending
Expression	$\frac{1}{2}K_r(\Delta r)^2$	$\frac{1}{2}K_\theta(\Delta\theta)^2$
Parameter	8.322	3.516
r_0 or θ_0	2.768	90.718

The second line gives an explicit expression for each VFF term. The third line is the force constant parameters. Parameters are in the unit of ev/Å^2 for the bond stretching interaction and in the unit of eV for the angle bending interaction. The fourth line gives the initial bond length (in the unit of Å) for the bond stretching interaction and the initial angle (in the unit of degrees) for the angle bending interaction.

Table 510. The VFF model for b-GeTe.

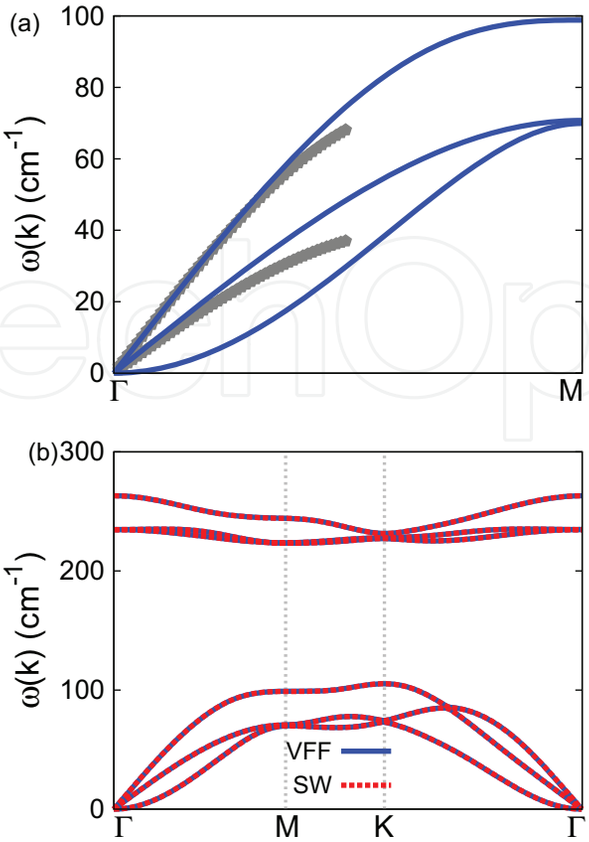

Figure 262. Phonon dispersion for the single-layer b-GeTe. (a) The VFF model is fitted to the two in-plane acoustic branches in the long wave limit along the ΓM direction. The *ab initio* results (gray pentagons) are calculated from SIESTA. (b) The VFF model (blue lines) and the SW potential (red lines) give the same phonon dispersion for the b-GeTe along ΓMKΓ.

	A (eV)	ρ (Å)	B (Å^4)	$r_{\min}$ (Å)	$r_{\max}$ (Å)
Ge—Te	9.704	1.513	29.352	0.0	3.791

Table 511. Two-body SW potential parameters for b-GeTe used by GULP [8], as expressed in Eq. (3).

	K (eV)	θ_0 (°)	ρ_1 (Å)	ρ_2 (Å)	$r_{\min 12}$ (Å)	$r_{\max 12}$ (Å)	$r_{\min 13}$ (Å)	$r_{\max 13}$ (Å)	$r_{\min 23}$ (Å)	$r_{\max 23}$ (Å)
Ge—Te—Te	33.832	90.718	1.513	1.513	0.0	3.791	0.0	3.791	0.0	5.381
Te—Ge—Ge	33.832	90.718	1.513	1.513	0.0	3.791	0.0	3.791	0.0	5.381

Table 512. Three-body SW potential parameters for b-GeTe used by GULP [8], as expressed in Eq. (4).

	ϵ (eV)	σ (Å)	a	λ	γ	$\cos\theta_0$	A_L	B_L	p	q	Tol
Ge—Te—Te	1.000	1.513	2.506	33.832	1.000	−0.013	9.704	5.605	4	0	0.0
Te—Ge—Ge	1.000	1.513	2.506	33.832	1.000	−0.013	9.704	5.605	4	0	0.0

Table 513. SW potential parameters for b-GeTe used by LAMMPS [9], as expressed in Eqs. (9) and (10).

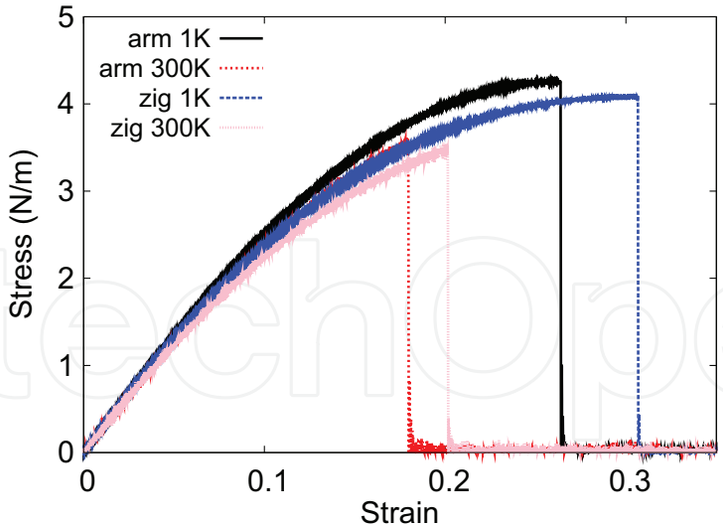

Figure 263. Stress-strain relations for the b-GeTe of size 100×100 Å. The b-GeTe is uniaxially stretched along the armchair or zigzag directions at temperatures 1 and 300 K.

We use LAMMPS to perform MD simulations for the mechanical behavior of the single-layer b-GeTe under uniaxial tension at 1 and 300 K. **Figure 263** shows the stress-strain curve for the tension of a single-layer b-GeTe of dimension 100×100 Å. Periodic boundary conditions are applied in both armchair and zigzag directions. The single-layer b-GeTe is stretched uniaxially along the armchair or zigzag direction. The stress is calculated without involving the actual thickness of the quasi-two-dimensional structure of the single-layer b-GeTe. The Young's modulus can be obtained by a linear fitting of the stress-strain relation in the small strain range of [0, 0.01]. The Young's modulus is 27.7 and 28.0 N/m along the armchair and zigzag directions, respectively. The Young's modulus is essentially isotropic in the armchair and zigzag directions. The Poisson's ratio from the VFF model and the SW potential is $\nu_{xy} = \nu_{yx} = 0.21$.

There is no available value for nonlinear quantities in the single-layer b-GeTe. We have thus used the nonlinear parameter $B = 0.5d^4$ in Eq. (5), which is close to the value of B in most materials. The value of the third-order nonlinear elasticity D can be extracted by fitting the stress-strain relation to the function $\sigma = E\epsilon + \frac{1}{2}D\epsilon^2$ with E as the Young's modulus. The values of D from the present SW potential are -80.4 and -95.9 N/m along the armchair and zigzag directions, respectively. The ultimate stress is about 4.3 N/m at the ultimate strain of 0.26 in the armchair direction at the low temperature of 1 K. The ultimate stress is about 4.1 N m^{-1} at the ultimate strain of 0.30 in the zigzag direction at the low temperature of 1 K.

129. B-SnO

Present studies on the buckled (b-) SnO are based on first-principles calculations, and no empirical potential has been proposed for the b-SnO. We will thus parametrize a set of SW potential for the single-layer b-SnO in this section.

The structure of the single-layer b-SnO is shown in **Figure 239**. The structural parameters are from the *ab initio* calculations [78]. The b-SnO has a buckled configuration as shown in **Figure 239(b)**, where the buckle is along the zigzag direction. This structure can be determined by two independent geometrical parameters, including the lattice constant 3.442 Å and the bond length 2.204 Å.

Table 514 shows the VFF model for the single-layer b-SnO. The force constant parameters are determined by fitting to the acoustic branches in the phonon dispersion along the ΓM as shown in **Figure 264(a)**. The *ab initio* calculations for the phonon dispersion are calculated from the SIESTA package [79]. The generalized gradient approximation is applied to account for the exchange-correlation function with Perdew, Burke, and Ernzerhof parameterization [80], and the double-ζ orbital basis set is adopted. **Figure 264(b)** shows that the VFF model and the SW potential give exactly the same phonon dispersion, as the SW potential is derived from the VFF model.

The parameters for the two-body SW potential used by GULP are shown in **Table 515**. The parameters for the three-body SW potential used by GULP are shown in **Table 516**. Parameters for the SW potential used by LAMMPS are listed in **Table 517**.

We use LAMMPS to perform MD simulations for the mechanical behavior of the single-layer b-SnO under uniaxial tension at 1 and 300 K. **Figure 265** shows the stress-strain curve for the tension of a single-layer b-SnO of dimension 100×100 Å. Periodic boundary conditions are applied in both armchair and zigzag directions. The single-layer b-SnO is stretched uniaxially along the armchair or zigzag direction. The stress is calculated without involving the actual thickness of the quasi-two-dimensional structure of the single-layer b-SnO. The Young's modulus can be obtained by a linear fitting of the stress-strain relation in the small strain range of [0, 0.01]. The Young's modulus is 43.7 and 43.8 N/m along the armchair and zigzag directions, respectively. The Young's modulus is essentially isotropic in the armchair and zigzag directions. The Poisson's ratio from the VFF model and the SW potential is $\nu_{xy} = \nu_{yx} = 0.12$.

There is no available value for nonlinear quantities in the single-layer b-SnO. We have thus used the nonlinear parameter $B = 0.5d^4$ in Eq. (5), which is close to the value of B in most materials. The value of the third-order nonlinear elasticity D can be extracted by fitting the stress-strain relation to the function $\sigma = E\epsilon + \frac{1}{2}D\epsilon^2$ with E as the Young's modulus. The values

VFF type	Bond stretching	Angle bending
Expression	$\frac{1}{2}K_r(\Delta r)^2$	$\frac{1}{2}K_\theta(\Delta\theta)^2$
Parameter	9.315	3.300
r_0 or θ_0	2.204	102.677

The second line gives an explicit expression for each VFF term. The third line is the force constant parameters. Parameters are in the unit of ev/Å^2 for the bond stretching interaction and in the unit of eV for the angle bending interaction. The fourth line gives the initial bond length (in the unit of Å) for the bond stretching interaction and the initial angle (in the unit of degrees) for the angle bending interaction.

Table 514. The VFF model for b-SnO.

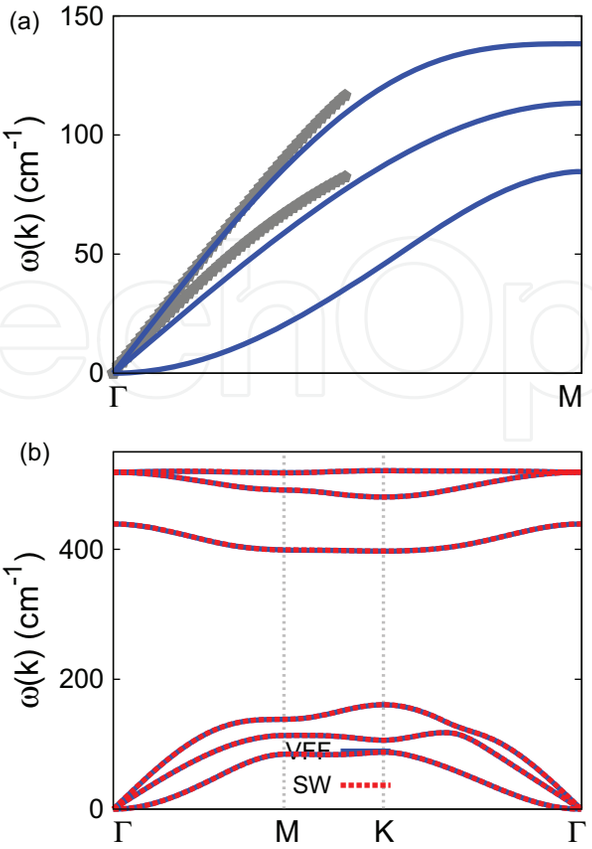

Figure 264. Phonon dispersion for the single-layer b-SnO. (a) The VFF model is fitted to the two in-plane acoustic branches in the long wave limit along the ΓM direction. The *ab initio* results (gray pentagons) are calculated from SIESTA. (b) The VFF model (blue lines) and the SW potential (red lines) give the same phonon dispersion for the b-SnO along ΓMKΓ.

	A (eV)	ρ (Å)	B (Å^4)	$r_{\min}$ (Å)	$r_{\max}$ (Å)
Sn—O	9.133	1.609	11.798	0.0	3.146

Table 515. Two-body SW potential parameters for b-SnO used by GULP [8], as expressed in Eq. (3).

	K (eV)	θ_0 (°)	ρ_1 (Å)	ρ_2 (Å)	$r_{\min 12}$ (Å)	$r_{\max 12}$ (Å)	$r_{\min 13}$ (Å)	$r_{\max 13}$ (Å)	$r_{\min 23}$ (Å)	$r_{\max 23}$ (Å)
Sn—O—O	52.875	102.677	1.609	1.609	0.0	3.146	0.0	3.146	0.0	4.702
O—Sn—Sn	52.875	102.677	1.609	1.609	0.0	3.146	0.0	3.146	0.0	4.702

Table 516. Three-body SW potential parameters for b-SnO used by GULP [8], as expressed in Eq. (4).

	ϵ (eV)	σ (Å)	a	λ	γ	$\cos\theta_0$	A_L	B_L	p	q	Tol
Sn—O—O	1.000	1.609	1.955	52.875	1.000	−0.219	9.133	1.760	4	0	0.0
O—Sn—Sn	1.000	1.609	1.955	52.875	1.000	−0.219	9.133	1.760	4	0	0.0

Table 517. SW potential parameters for b-SnO used by LAMMPS [9], as expressed in Eqs. (9) and (10).

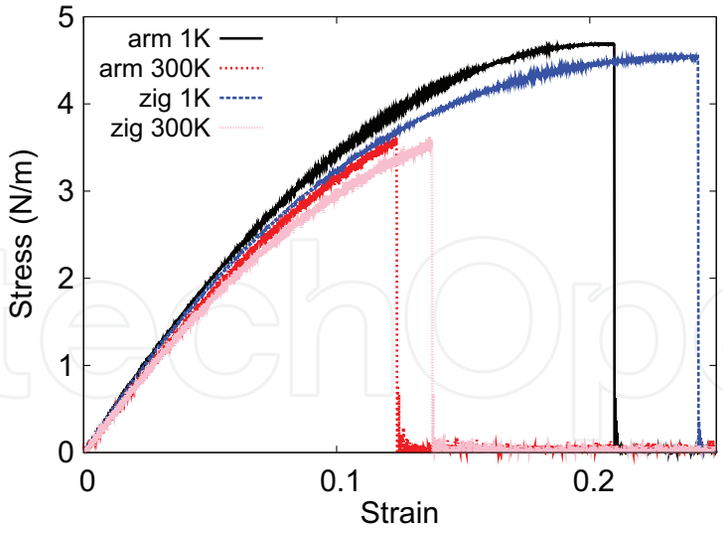

Figure 265. Stress-strain relations for the b-SnO of size 100 × 100 Å. The b-SnO is uniaxially stretched along the armchair or zigzag directions at temperatures 1 and 300 K.

of D from the present SW potential are −199.9 and −215.1 N/m along the armchair and zigzag directions, respectively. The ultimate stress is about 4.7 N/m at the ultimate strain of 0.21 in the armchair direction at the low temperature of 1 K. The ultimate stress is about 4.5 N/m at the ultimate strain of 0.24 in the zigzag direction at the low temperature of 1 K.

130. B-SnS

Present studies on the buckled (b-) SnS are based on first-principles calculations, and no empirical potential has been proposed for the b-SnS. We will thus parametrize a set of SW potential for the single-layer b-SnS in this section.

The structure of the single-layer b-SnS is shown in **Figure 239**. The structural parameters are from the *ab initio* calculations [78]. The b-SnS has a buckled configuration as shown in **Figure 239(b)**, where the buckle is along the zigzag direction. This structure can be determined by two independent geometrical parameters, including the lattice constant 3.757 Å and the bond length 2.616 Å.

Table 518 shows the VFF model for the single-layer b-SnS. The force constant parameters are determined by fitting to the acoustic branches in the phonon dispersion along the ΓM as shown in **Figure 266(a)**. The *ab initio* calculations for the phonon dispersion are calculated from the SIESTA package [79]. The generalized gradient approximation is applied to account for the exchange-correlation function with Perdew, Burke, and Ernzerhof parameterization [80], and the double-ζ orbital basis set is adopted. **Figure 266(b)** shows that the VFF model and the SW potential give exactly the same phonon dispersion, as the SW potential is derived from the VFF model.

VFF type	Bond stretching	Angle bending
Expression	$\frac{1}{2}K_r(\Delta r)^2$	$\frac{1}{2}K_\theta(\Delta\theta)^2$
Parameter	6.909	2.710
r_0 or θ_0	2.616	91.793

The second line gives an explicit expression for each VFF term. The third line is the force constant parameters. Parameters are in the unit of ev/Å^2 for the bond stretching interaction and in the unit of eV for the angle bending interaction. The fourth line gives the initial bond length (in the unit of Å) for the bond stretching interaction and the initial angle (in the unit of degrees) for the angle bending interaction.

Table 518. The VFF model for b-SnS.

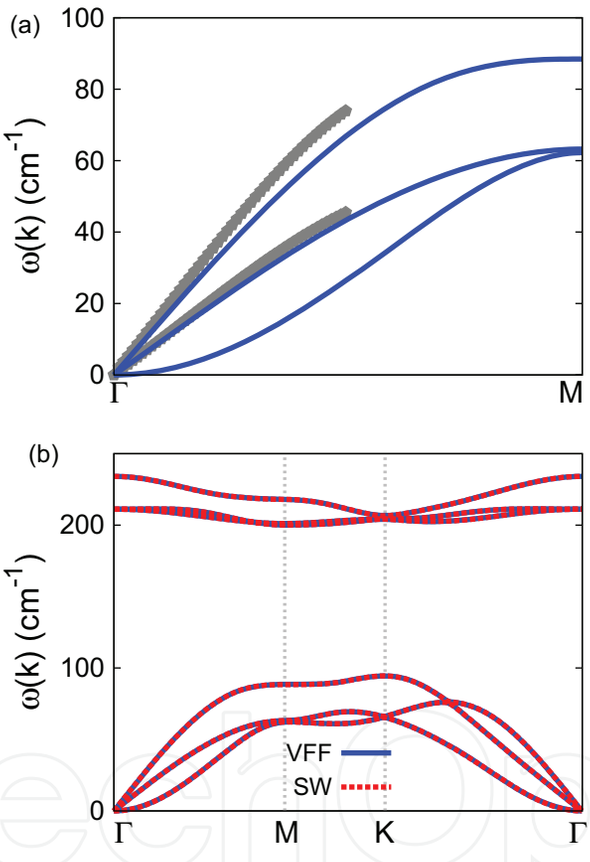

Figure 266. Phonon dispersion for the single-layer b-SnS. (a) The VFF model is fitted to the two in-plane acoustic branches in the long wave limit along the ΓM direction. The *ab initio* results (gray pentagons) are calculated from SIESTA. (b) The VFF model (blue lines) and the SW potential (red lines) give the same phonon dispersion for the b-SnS along ΓMKΓ.

The parameters for the two-body SW potential used by GULP are shown in **Table 519**. The parameters for the three-body SW potential used by GULP are shown in **Table 520**. Parameters for the SW potential used by LAMMPS are listed in **Table 521**.

We use LAMMPS to perform MD simulations for the mechanical behavior of the single-layer b-SnS under uniaxial tension at 1 and 300 K. **Figure 267** shows the stress-strain curve for the

	A (eV)	ρ (Å)	B (Å^4)	$r_{\min}$ (Å)	$r_{\max}$ (Å)
Sn—S	7.392	1.472	23.416	0.0	3.597

Table 519. Two-body SW potential parameters for b-SnS used by GULP [8], as expressed in Eq. (3).

	K (eV)	θ_0 (°)	ρ_1 (Å)	ρ_2 (Å)	$r_{\min 12}$ (Å)	$r_{\max 12}$ (Å)	$r_{\min 13}$ (Å)	$r_{\max 13}$ (Å)	$r_{\min 23}$ (Å)	$r_{\max 23}$ (Å)
Sn—S—S	27.243	91.793	1.472	1.472	0.0	3.597	0.0	3.597	0.0	5.132
S—Sn—Sn	27.243	91.793	1.472	1.472	0.0	3.597	0.0	3.597	0.0	5.132

Table 520. Three-body SW potential parameters for b-SnS used by GULP [8], as expressed in Eq. (4).

	ϵ (eV)	σ (Å)	a	λ	γ	$\cos\theta_0$	A_L	B_L	p	q	Tol
Sn—S—S	1.000	1.472	2.444	27.243	1.000	−0.031	7.392	4.994	4	0	0.0
S—Sn—Sn	1.000	1.472	2.444	27.243	1.000	−0.031	7.392	4.994	4	0	0.0

Table 521. SW potential parameters for b-SnS used by LAMMPS [9], as expressed in Eqs. (9) and (10).

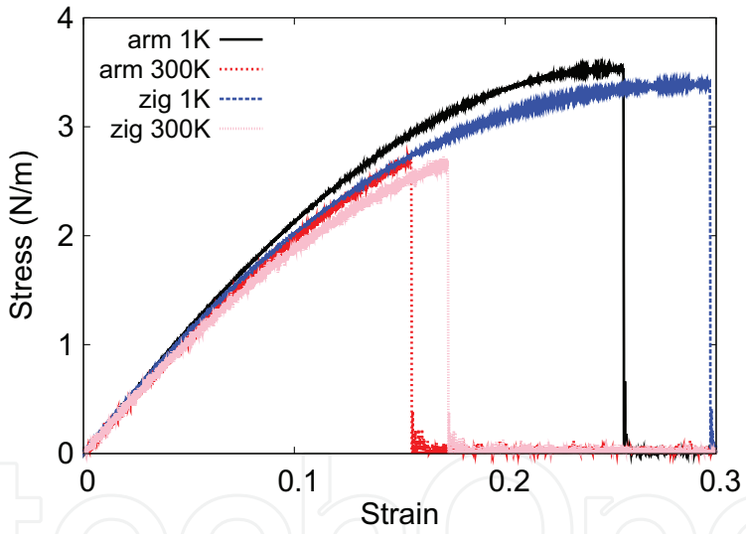

Figure 267. Stress-strain relations for the b-SnS of size 100 × 100 Å. The b-SnS is uniaxially stretched along the armchair or zigzag directions at temperatures 1 and 300 K.

tension of a single-layer b-SnS of dimension 100 × 100 Å. Periodic boundary conditions are applied in both armchair and zigzag directions. The single-layer b-SnS is stretched uniaxially along the armchair or zigzag direction. The stress is calculated without involving the actual thickness of the quasi-two-dimensional structure of the single-layer b-SnS. The Young's modulus can be obtained by a linear fitting of the stress-strain relation in the small strain range of [0, 0.01]. The Young's modulus is 23.8 and 24.4 N/m along the armchair and zigzag directions, respectively. The Young's modulus is essentially isotropic in the armchair and zigzag directions. The Poisson's ratio from the VFF model and the SW potential is $\nu_{xy} = \nu_{yx} = 0.20$.

There is no available value for nonlinear quantities in the single-layer b-SnS. We have thus used the nonlinear parameter $B = 0.5d^4$ in Eq. (5), which is close to the value of B in most materials. The value of the third-order nonlinear elasticity D can be extracted by fitting the stress-strain relation to the function $\sigma = E\epsilon + \frac{1}{2}D\epsilon^2$ with E as the Young's modulus. The values of D from the present SW potential are -71.8 and -88.3 N/m along the armchair and zigzag directions, respectively. The ultimate stress is about 3.5 N/m at the ultimate strain of 0.25 in the armchair direction at the low temperature of 1 K. The ultimate stress is about 3.4 N/m at the ultimate strain of 0.29 in the zigzag direction at the low temperature of 1 K.

131. B-SnSe

Present studies on the buckled (b-) SnSe are based on first-principles calculations, and no empirical potential has been proposed for the b-SnSe. We will thus parametrize a set of SW potential for the single-layer b-SnSe in this section.

The structure of the single-layer b-SnSe is shown in **Figure 239**. The structural parameters are from the *ab initio* calculations [78]. The b-SnSe has a buckled configuration as shown in **Figure 239(b)**, where the buckle is along the zigzag direction. This structure can be determined by two independent geometrical parameters, including the lattice constant 3.916 Å and the bond length 2.747 Å.

Table 522 shows the VFF model for the single-layer b-SnSe. The force constant parameters are determined by fitting to the acoustic branches in the phonon dispersion along the ΓM as shown in **Figure 268(a)**. The *ab initio* calculations for the phonon dispersion are calculated from the SIESTA package [79]. The generalized gradient approximation is applied to account for the exchange-correlation function with Perdew, Burke, and Ernzerhof parameterization [80], and the double-ζ orbital basis set is adopted. **Figure 268(b)** shows that the VFF model and the SW potential give exactly the same phonon dispersion, as the SW potential is derived from the VFF model.

The parameters for the two-body SW potential used by GULP are shown in **Table 523**. The parameters for the three-body SW potential used by GULP are shown in **Table 524**. Parameters for the SW potential used by LAMMPS are listed in **Table 525**.

VFF type	Bond stretching	Angle bending
Expression	$\frac{1}{2}K_r(\Delta r)^2$	$\frac{1}{2}K_\theta(\Delta\theta)^2$
Parameter	6.909	2.710
r_0 or θ_0	2.747	90.923

The second line gives an explicit expression for each VFF term. The third line is the force constant parameters. Parameters are in the unit of ev/Å^2 for the bond stretching interaction and in the unit of eV for the angle bending interaction. The fourth line gives the initial bond length (in the unit of Å) for the bond stretching interaction and the initial angle (in the unit of degrees) for the angle bending interaction.

Table 522. The VFF model for b-SnSe.

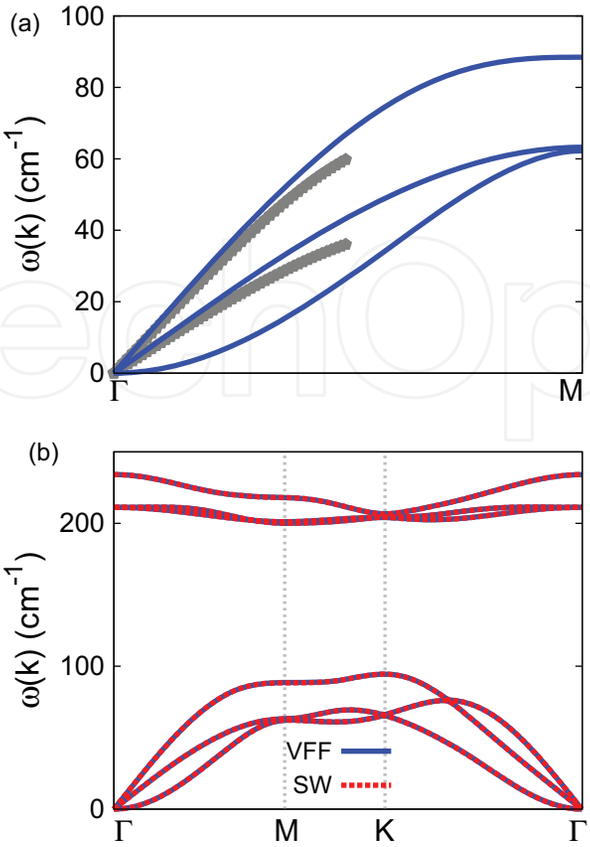

Figure 268. Phonon dispersion for the single-layer b-SnSe. (a) The VFF model is fitted to the two in-plane acoustic branches in the long wave limit along the ΓM direction. The *ab initio* results (gray pentagons) are calculated from SIESTA. (b) The VFF model (blue lines) and the SW potential (red lines) give the same phonon dispersion for the b-SnSe along ΓMKΓ.

	A (eV)	ρ (Å)	B (Å^4)	$r_{\min}$ (Å)	$r_{\max}$ (Å)
Si—Se	7.976	1.510	28.471	0.0	3.765

Table 523. Two-body SW potential parameters for b-SnSe used by GULP [8], as expressed in Eq. (3).

	K (eV)	θ_0 (°)	ρ_1 (Å)	ρ_2 (Å)	$r_{\min 12}$ (Å)	$r_{\max 12}$ (Å)	$r_{\min 13}$ (Å)	$r_{\max 13}$ (Å)	$r_{\min 23}$ (Å)	$r_{\max 23}$ (Å)
Sn—Se—Se	26.294	90.923	1.510	1.510	0.0	3.765	0.0	3.765	0.0	5.349
Se—Sn—Sn	26.294	90.923	1.510	1.510	0.0	3.765	0.0	3.765	0.0	5.349

Table 524. Three-body SW potential parameters for b-SnSe used by GULP [8], as expressed in Eq. (4).

	ϵ (eV)	σ (Å)	a	λ	γ	$\cos\theta_0$	A_L	B_L	p	q	Tol
Sn—Se—Se	1.000	1.510	2.494	26.294	1.000	−0.016	7.976	5.482	4	0	0.0
Se—Sn—Sn	1.000	1.510	2.494	26.294	1.000	−0.016	7.976	5.482	4	0	0.0

Table 525. SW potential parameters for b-SnSe used by LAMMPS [9], as expressed in Eqs. (9) and (10).

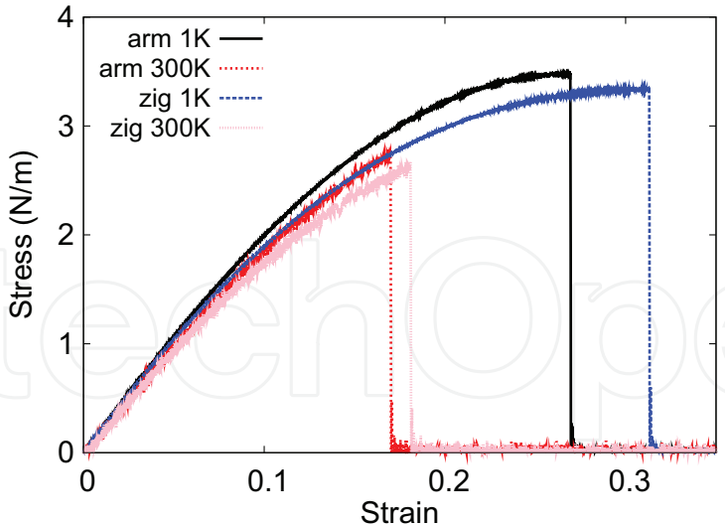

Figure 269. Stress-strain relations for the b-SnSe of size 100 × 100 Å. The b-SnSe is uniaxially stretched along the armchair or zigzag directions at temperatures 1 and 300 K.

We use LAMMPS to perform MD simulations for the mechanical behavior of the single-layer b-SnSe under uniaxial tension at 1 and 300 K. **Figure 269** shows the stress-strain curve for the tension of a single-layer b-SnSe of dimension 100 × 100 Å. Periodic boundary conditions are applied in both armchair and zigzag directions. The single-layer b-SnSe is stretched uniaxially along the armchair or zigzag direction. The stress is calculated without involving the actual thickness of the quasi-two-dimensional structure of the single-layer b-SnSe. The Young's modulus can be obtained by a linear fitting of the stress-strain relation in the small strain range of [0, 0.01]. The Young's modulus is 22.0 and 22.2 N/m along the armchair and zigzag directions, respectively. The Young's modulus is essentially isotropic in the armchair and zigzag directions. The Poisson's ratio from the VFF model and the SW potential is $\nu_{xy} = \nu_{yx} = 0.22$.

There is no available value for nonlinear quantities in the single-layer b-SnSe. We have thus used the nonlinear parameter $B = 0.5d^4$ in Eq. (5), which is close to the value of B in most materials. The value of the third-order nonlinear elasticity D can be extracted by fitting the stress-strain relation to the function $\sigma = E\epsilon + \frac{1}{2}D\epsilon^2$ with E as the Young's modulus. The values of D from the present SW potential are -61.6 and -73.69 N/m along the armchair and zigzag directions, respectively. The ultimate stress is about 3.5 N/m at the ultimate strain of 0.27 in the armchair direction at the low temperature of 1 K. The ultimate stress is about 3.3 N/m at the ultimate strain of 0.31 in the zigzag direction at the low temperature of 1 K.

132. B-SnTe

Present studies on the buckled (b-) SnTe are based on first-principles calculations, and no empirical potential has been proposed for the b-SnTe. We will thus parametrize a set of SW potential for the single-layer b-SnTe in this section.

The structure of the single-layer b-SnTe is shown in **Figure 239**. The structural parameters are from the *ab initio* calculations [78]. The b-SnTe has a buckled configuration as shown in **Figure 239(b)**, where the buckle is along the zigzag direction. This structure can be determined by two independent geometrical parameters, including the lattice constant 4.151 Å and the bond length 2.947 Å.

Table 526 shows the VFF model for the single-layer b-SnTe. The force constant parameters are determined by fitting to the acoustic branches in the phonon dispersion along the ΓM as shown in **Figure 270(a)**. The *ab initio* calculations for the phonon dispersion are calculated from the SIESTA package [79]. The generalized gradient approximation is applied to account for the exchange-correlation function with Perdew, Burke, and Ernzerhof parameterization [80], and the double-ζ orbital basis set is adopted. **Figure 270(b)** shows that the VFF model and the SW potential give exactly the same phonon dispersion, as the SW potential is derived from the VFF model.

The parameters for the two-body SW potential used by GULP are shown in **Table 527**. The parameters for the three-body SW potential used by GULP are shown in **Table 528**. Parameters for the SW potential used by LAMMPS are listed in **Table 529**.

We use LAMMPS to perform MD simulations for the mechanical behavior of the single-layer b-SnTe under uniaxial tension at 1 and 300 K. **Figure 271** shows the stress-strain curve for the tension of a single-layer b-SnTe of dimension 100×100 Å. Periodic boundary conditions are applied in both armchair and zigzag directions. The single-layer b-SnTe is stretched uniaxially along the armchair or zigzag direction. The stress is calculated without involving the actual thickness of the quasi-two-dimensional structure of the single-layer b-SnTe. The Young's modulus can be obtained by a linear fitting of the stress-strain relation in the small strain range of [0, 0.01]. The Young's modulus is 19.6 and 19.1 N/m along the armchair and zigzag directions, respectively. The Young's modulus is essentially isotropic in the armchair and zigzag directions. The Poisson's ratio from the VFF model and the SW potential is $\nu_{xy} = \nu_{yx} = 0.23$.

There is no available value for nonlinear quantities in the single-layer b-SnTe. We have thus used the nonlinear parameter $B = 0.5d^4$ in Eq. (5), which is close to the value of B in most materials. The value of the third-order nonlinear elasticity D can be extracted by fitting the stress-strain relation to the function $\sigma = E\epsilon + \frac{1}{2}D\epsilon^2$ with E as the Young's modulus. The values

VFF type	Bond stretching	Angle bending
Expression	$\frac{1}{2}K_r(\Delta r)^2$	$\frac{1}{2}K_\theta(\Delta\theta)^2$
Parameter	6.909	2.710
r_0 or θ_0	2.947	89.542

The second line gives an explicit expression for each VFF term. The third line is the force constant parameters. Parameters are in the unit of ev/Å^2 for the bond stretching interaction and in the unit of eV for the angle bending interaction. The fourth line gives the initial bond length (in the unit of Å) for the bond stretching interaction and the initial angle (in the unit of degrees) for the angle bending interaction.

Table 526. The VFF model for b-SnTe.

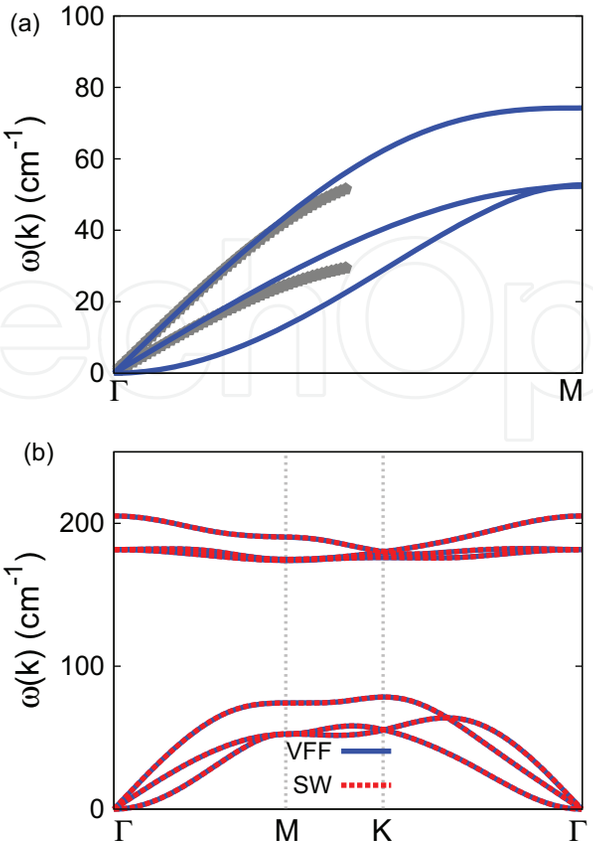

Figure 270. Phonon dispersion for the single-layer b-SnTe. (a) The VFF model is fitted to the two in-plane acoustic branches in the long wave limit along the ΓM direction. The *ab initio* results (gray pentagons) are calculated from SIESTA. (b) The VFF model (blue lines) and the SW potential (red lines) give the same phonon dispersion for the b-SnTe along ΓMKΓ.

	A (eV)	ρ (Å)	B (Å^4)	$r_{\min}$ (Å)	$r_{\max}$ (Å)
Sn—Te	8.864	1.559	37.713	0.0	4.019

Table 527. Two-body SW potential parameters for b-SnTe used by GULP [8], as expressed in Eq. (3).

	K (eV)	θ_0 (°)	ρ_1 (Å)	ρ_2 (Å)	$r_{\min 12}$ (Å)	$r_{\max 12}$ (Å)	$r_{\min 13}$ (Å)	$r_{\max 13}$ (Å)	$r_{\min 23}$ (Å)	$r_{\max 23}$ (Å)
Sn—Te—Te	24.867	89.542	1.559	1.559	0.0	4.019	0.0	4.019	0.0	5.670
Te—Sn—Sn	24.867	89.542	1.559	1.559	0.0	4.019	0.0	4.019	0.0	5.670

Table 528. Three-body SW potential parameters for b-SnTe used by GULP [8], as expressed in Eq. (4).

	ϵ (eV)	σ (Å)	a	λ	γ	$\cos\theta_0$	A_L	B_L	p	q	Tol
Sn—Te—Te	1.000	1.559	2.577	24.867	1.000	0.008	8.864	6.378	4	0	0.0
Te—Sn—Sn	1.000	1.559	2.577	24.867	1.000	0.008	8.864	6.378	4	0	0.0

Table 529. SW potential parameters for b-SnTe used by LAMMPS [9], as expressed in Eqs. (9) and (10).

http://dx.doi.org/10.5772/intechopen.71929

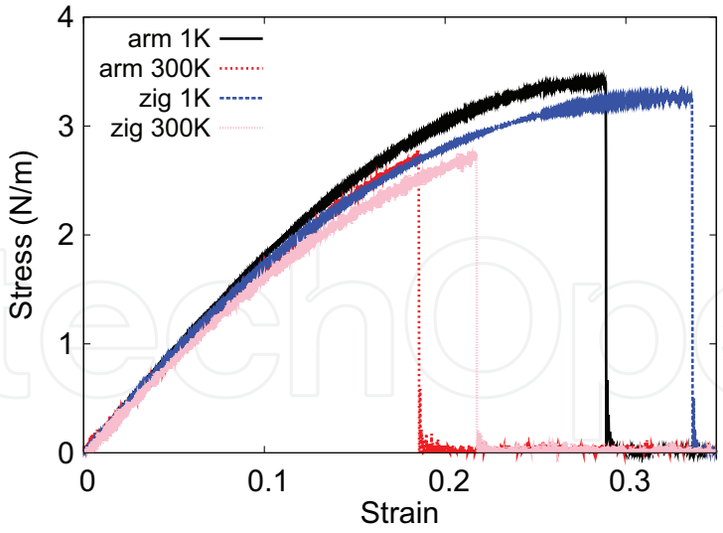

Figure 271. Stress-strain relations for the b-SnTe of size 100 × 100 Å. The b-SnTe is uniaxially stretched along the armchair or zigzag directions at temperatures 1 and 300 K.

of D from the present SW potential are −48.7 and −54.3 N/m along the armchair and zigzag directions, respectively. The ultimate stress is about 3.4 N/m at the ultimate strain of 0.29 in the armchair direction at the low temperature of 1 K. The ultimate stress is about 3.3 N/m at the ultimate strain of 0.33 in the zigzag direction at the low temperature of 1 K.

133. B-SnGe

Present studies on the buckled SnGe (b-SnGe) are based on first-principles calculations, and no empirical potential has been proposed for the b-SnGe. We will thus parametrize a set of SW potential for the single-layer b-SnGe in this section.

The structure of the single-layer b-SnGe is shown in **Figure 239**. The structural parameters are from the *ab initio* calculations [114]. The b-SnGe has a buckled configuration as shown in **Figure 239(b)**, where the buckle is along the zigzag direction. This structure can be determined by two independent geometrical parameters, e.g., the lattice constant 4.27 Å and the bond length 2.57 Å. The resultant height of the buckle is $h = 0.73$ Å.

Table 530 shows the VFF model for the single-layer b-SnGe. The force constant parameters are determined by fitting to the acoustic branches in the phonon dispersion along the ΓM as shown in **Figure 272(a)**. The *ab initio* calculations for the phonon dispersion are from [114]. Figure 272(b) shows that the VFF model and the SW potential give exactly the same phonon dispersion, as the SW potential is derived from the VFF model.

The parameters for the two-body SW potential used by GULP are shown in **Table 531**. The parameters for the three-body SW potential used by GULP are shown in **Table 532**. Parameters for the SW potential used by LAMMPS are listed in **Table 533**.

VFF type	Bond stretching	Angle bending
Expression	$\frac{1}{2}K_r(\Delta r)^2$	$\frac{1}{2}K_\theta(\Delta\theta)^2$
Parameter	8.390	3.112
r_0 or θ_0	2.570	112.350

The second line gives an explicit expression for each VFF term. The third line is the force constant parameters. Parameters are in the unit of ev/Å^2 for the bond stretching interaction and in the unit of eV for the angle bending interaction. The fourth line gives the initial bond length (in the unit of Å) for the bond stretching interaction and the initial angle (in the unit of degrees) for the angle bending interaction.

Table 530. The VFF model for b-SnGe.

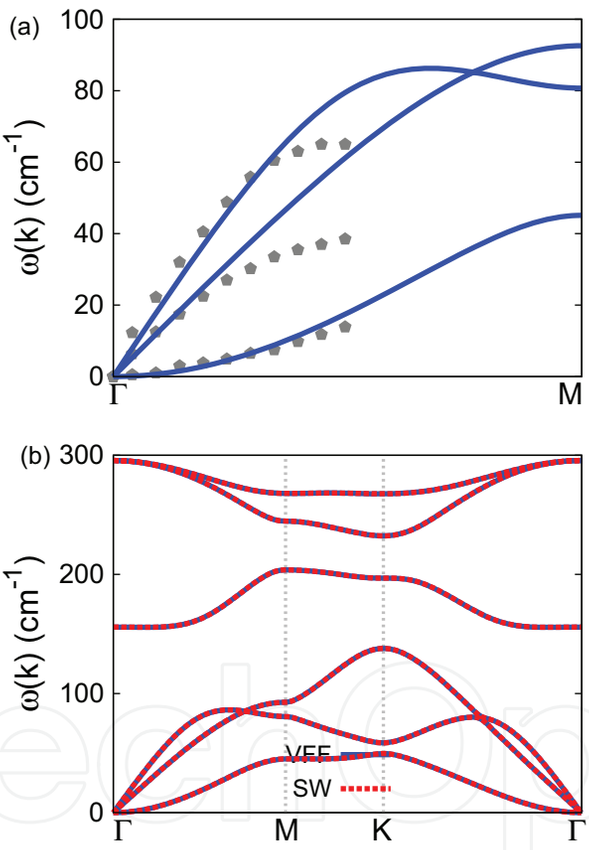

Figure 272. Phonon dispersion for the single-layer b-SnGe. (a) The VFF model is fitted to the three acoustic branches in the long wave limit along the ΓM direction. The *ab initio* results (gray pentagons) are from [114]. (b) The VFF model (blue lines) and the SW potential (red lines) give the same phonon dispersion for the b-SnGe along ΓMKΓ.

	A (eV)	ρ (Å)	B (Å^4)	$r_{\min}$ (Å)	$r_{\max}$ (Å)
Sn—Ge	13.674	2.267	21.812	0.0	3.777

Table 531. Two-body SW potential parameters for b-SnGe used by GULP [8], as expressed in Eq. (3).

	K (eV)	θ_0 (°)	ρ_1 (Å)	ρ_2 (Å)	$r_{\min 12}$ (Å)	$r_{\max 12}$ (Å)	$r_{\min 13}$ (Å)	$r_{\max 13}$ (Å)	$r_{\min 23}$ (Å)	$r_{\max 23}$ (Å)
Sn—Ge—Ge	77.881	112.350	2.267	2.267	0.0	3.777	0.0	3.777	0.0	5.833
Ge—Sn—Sn	77.881	112.350	2.267	2.267	0.0	3.777	0.0	3.777	0.0	5.833

Table 532. Three-body SW potential parameters for b-SnGe used by GULP [8], as expressed in Eq. (4).

	ϵ (eV)	σ (Å)	a	λ	γ	$\cos\theta_0$	A_L	B_L	p	q	Tol
Sn—Ge—Ge	1.000	2.267	1.666	77.881	1.000	−0.380	13.674	0.826	4	0	0.0
Ge—Sn—Sn	1.000	2.267	1.666	77.881	1.000	−0.380	13.674	0.826	4	0	0.0

Table 533. SW potential parameters for b-SnGe used by LAMMPS [9], as expressed in Eqs. (9) and (10).

We use LAMMPS to perform MD simulations for the mechanical behavior of the single-layer b-SnGe under uniaxial tension at 1 and 300 K. **Figure 273** shows the stress-strain curve for the tension of a single-layer b-SnGe of dimension 100 × 100 Å. Periodic boundary conditions are applied in both armchair and zigzag directions. The single-layer b-SnGe is stretched uniaxially along the armchair or zigzag direction. The stress is calculated without involving the actual thickness of the quasi-two-dimensional structure of the single-layer b-SnGe. The Young's modulus can be obtained by a linear fitting of the stress-strain relation in the small strain range of [0, 0.01]. The Young's modulus is 36.8 N/m along both armchair and zigzag directions. The Poisson's ratio from the VFF model and the SW potential is $\nu_{xy} = \nu_{yx} = 0.11$.

There is no available value for nonlinear quantities in the single-layer b-SnGe. We have thus used the nonlinear parameter $B = 0.5d^4$ in Eq. (5), which is close to the value of B in most materials. The value of the third-order nonlinear elasticity D can be extracted by fitting the stress-strain relation to the function $\sigma = E\epsilon + \frac{1}{2}D\epsilon^2$ with E as the Young's modulus. The values

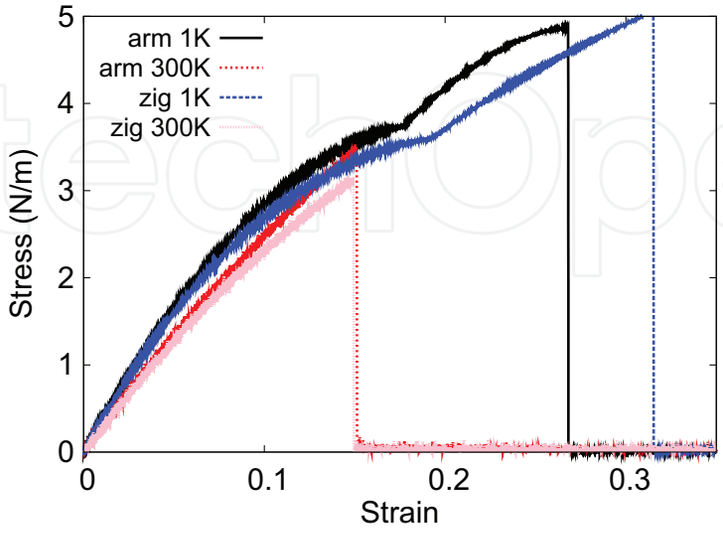

Figure 273. Stress-strain relations for the b-SnGe of size 100 × 100 Å. The b-SnGe is uniaxially stretched along the armchair or zigzag directions at temperatures 1 and 300 K.

of D from the present SW potential are −171.6 and −197.0 N/m along the armchair and zigzag directions, respectively. The ultimate stress is about 4.9 N/m at the ultimate strain of 0.27 in the armchair direction at the low temperature of 1 K. The ultimate stress is about 5.0 N m^{-1} at the ultimate strain of 0.31 in the zigzag direction at the low temperature of 1 K.

134. B-SiGe

Present studies on the buckled SiGe (b-SiGe) are based on first-principles calculations, and no empirical potential has been proposed for the b-SiGe. We will thus parametrize a set of SW potential for the single-layer b-SiGe in this section.

The structure of the single-layer b-SiGe is shown in **Figure 239**. The structural parameters are from the *ab initio* calculations [114]. The b-SiGe has a buckled configuration as shown in **Figure 239(b)**, where the buckle is along the zigzag direction. This structure can be determined by two independent geometrical parameters, e.g., the lattice constant 3.89 Å and the bond length 2.31 Å. The resultant height of the buckle is $h = 0.55$ Å.

Table 534 shows the VFF model for the single-layer b-SiGe. The force constant parameters are determined by fitting to the acoustic branches in the phonon dispersion along the ΓM as shown in **Figure 274(a)**. The *ab initio* calculations for the phonon dispersion are from [114]. **Figure 274(b)** shows that the VFF model and the SW potential give exactly the same phonon dispersion, as the SW potential is derived from the VFF model.

The parameters for the two-body SW potential used by GULP are shown in **Table 535**. The parameters for the three-body SW potential used by GULP are shown in **Table 536**. Parameters for the SW potential used by LAMMPS are listed in **Table 537**.

We use LAMMPS to perform MD simulations for the mechanical behavior of the single-layer b-SiGe under uniaxial tension at 1 and 300 K. **Figure 275** shows the stress-strain curve for the tension of a single-layer b-SiGe of dimension 100 × 100 Å. Periodic boundary conditions are applied in both armchair and zigzag directions. The single-layer b-SiGe is stretched uniaxially along the armchair or zigzag direction. The stress is calculated without involving the actual thickness of the quasi-two-dimensional structure of the single-layer b-SiGe. The Young's

VFF type	Bond stretching	Angle bending
Expression	$\frac{1}{2}K_r(\Delta r)^2$	$\frac{1}{2}K_\theta(\Delta\theta)^2$
Parameter	16.390	3.112
r_0 or θ_0	2.310	114.702

The second line gives an explicit expression for each VFF term. The third line is the force constant parameters. Parameters are in the unit of ev/Å^2 for the bond stretching interaction and in the unit of eV for the angle bending interaction. The fourth line gives the initial bond length (in the unit of Å) for the bond stretching interaction and the initial angle (in the unit of degrees) for the angle bending interaction.

Table 534. The VFF model for b-SiGe.

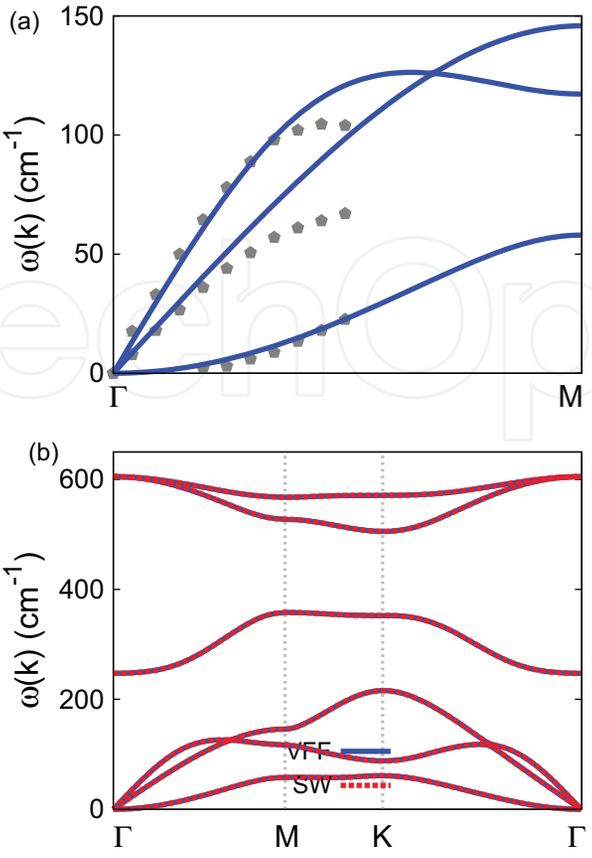

Figure 274. Phonon dispersion for the single-layer b-SiGe. (a) The VFF model is fitted to the three acoustic branches in the long wave limit along the ΓM direction. The *ab initio* results (gray pentagons) are from [114]. (b) The VFF model (blue lines) and the SW potential (red lines) give the same phonon dispersion for the b-SiGe along ΓMKΓ.

	A (eV)	ρ (Å)	B (Å^4)	$r_{\min}$ (Å)	$r_{\max}$ (Å)
Si—Ge	22.576	2.122	14.237	0.0	3.417

Table 535. Two-body SW potential parameters for b-SiGe used by GULP [8], as expressed in Eq. (3).

	K (eV)	θ_0 (°)	ρ_1 (Å)	ρ_2 (Å)	$r_{\min 12}$ (Å)	$r_{\max 12}$ (Å)	$r_{\min 13}$ (Å)	$r_{\max 13}$ (Å)	$r_{\min 23}$ (Å)	$r_{\max 23}$ (Å)
Si—Ge—Ge	87.197	114.702	2.122	2.122	0.0	3.417	0.0	3.417	0.0	5.314
Ge—Si—Si	87.197	114.702	2.122	2.122	0.0	3.417	0.0	3.417	0.0	5.314

Table 536. Three-body SW potential parameters for b-SiGe used by GULP [8], as expressed in Eq. (4).

	ϵ (eV)	σ (Å)	a	λ	γ	$\cos\theta_0$	A_L	B_L	p	q	Tol
Si—Ge—Ge	1.000	2.122	1.610	87.197	1.000	−0.418	22.576	0.702	4	0	0.0
Ge—Si—Si	1.000	2.122	1.610	87.197	1.000	−0.418	22.576	0.702	4	0	0.0

Table 537. SW potential parameters for b-SiGe used by LAMMPS [9], as expressed in Eqs. (9) and (10).

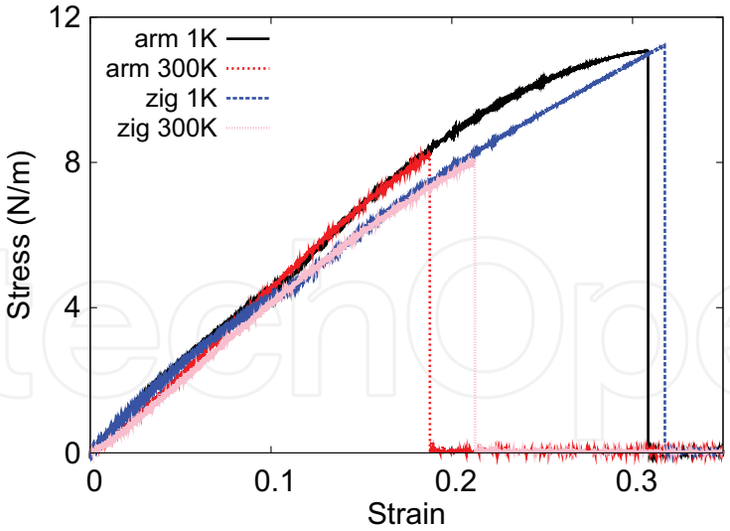

Figure 275. Stress-strain relations for the b-SiGe of size 100 × 100 Å. The b-SiGe is uniaxially stretched along the armchair or zigzag directions at temperatures 1 and 300 K.

modulus can be obtained by a linear fitting of the stress-strain relation in the small strain range of [0, 0.01]. The Young's modulus is 54.6 and 54.3 N/m along the armchair and zigzag directions, respectively. The Poisson's ratio from the VFF model and the SW potential is $\nu_{xy} = \nu_{yx} = 0.16$.

There is no available value for nonlinear quantities in the single-layer b-SiGe. We have thus used the nonlinear parameter $B = 0.5d^4$ in Eq. (5), which is close to the value of B in most materials. The value of the third-order nonlinear elasticity D can be extracted by fitting the stress-strain relation to the function $\sigma = E\epsilon + \frac{1}{2}D\epsilon^2$ with E as the Young's modulus. The values of D from the present SW potential are -186.7 and -233.5 N/m along the armchair and zigzag directions, respectively. The ultimate stress is about 11.0 N/m at the ultimate strain of 0.31 in the armchair direction at the low temperature of 1 K. The ultimate stress is about 11.2 N/m at the ultimate strain of 0.31 in the zigzag direction at the low temperature of 1 K.

135. B-SnSi

Present studies on the buckled SnSi (b-SnSi) are based on first-principles calculations, and no empirical potential has been proposed for the b-SnSi. We will thus parametrize a set of SW potential for the single-layer b-SnSi in this section.

The structure of the single-layer b-SnSi is shown in **Figure 239**. The structural parameters are from the *ab initio* calculations [114]. The b-SnSi has a buckled configuration as shown in **Figure 239(b)**, where the buckle is along the zigzag direction. This structure can be determined by two independent geometrical parameters, e.g., the lattice constant 4.21 Å and the bond length 2.52 Å. The resultant height of the buckle is $h = 0.67$ Å.

Table 538 shows the VFF model for the single-layer b-SnSi. The force constant parameters are determined by fitting to the acoustic branches in the phonon dispersion along the ΓM as shown in **Figure 276(a)**. The *ab initio* calculations for the phonon dispersion are from [114]. **Figure 276(b)** shows that the VFF model and the SW potential give exactly the same phonon dispersion, as the SW potential is derived from the VFF model.

VFF type	Bond stretching	Angle bending
Expression	$\frac{1}{2}K_r(\Delta r)^2$	$\frac{1}{2}K_\theta(\Delta\theta)^2$
Parameter	10.315	2.880
r_0 or θ_0	2.520	113.298

The second line gives an explicit expression for each VFF term. The third line is the force constant parameters. Parameters are in the unit of ev/Å^2 for the bond stretching interaction and in the unit of eV for the angle bending interaction. The fourth line gives the initial bond length (in the unit of Å) for the bond stretching interaction and the initial angle (in the unit of degrees) for the angle bending interaction.

Table 538. The VFF model for b-SnSi.

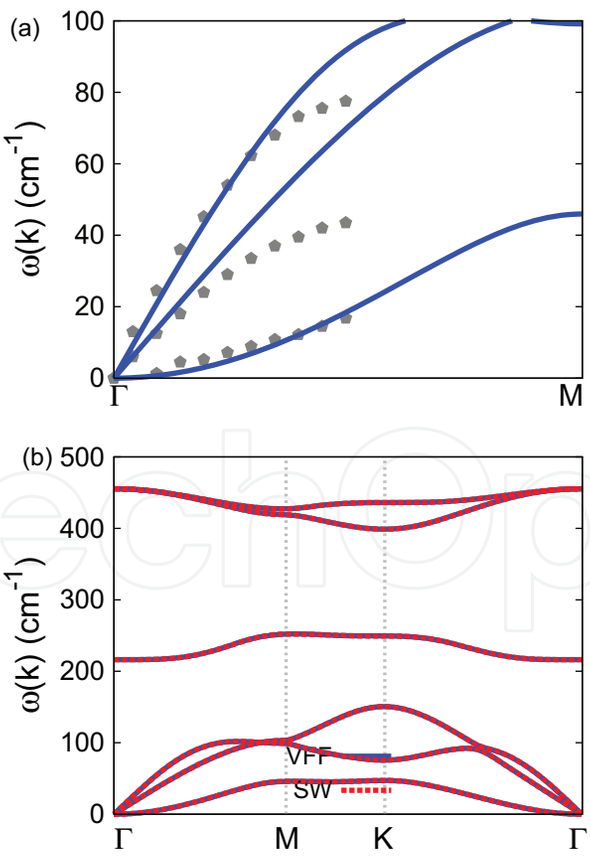

Figure 276. Phonon dispersion for the single-layer b-SnSi. (a) The VFF model is fitted to the three acoustic branches in the long wave limit along the ΓM direction. The *ab initio* results (gray pentagons) are from [114]. (b) The VFF model (blue lines) and the SW potential (red lines) give the same phonon dispersion for the b-SnSi along ΓMKΓ.

The parameters for the two-body SW potential used by GULP are shown in **Table 539**. The parameters for the three-body SW potential used by GULP are shown in **Table 540**. Parameters for the SW potential used by LAMMPS are listed in **Table 541**.

We use LAMMPS to perform MD simulations for the mechanical behavior of the single-layer b-SnSi under uniaxial tension at 1 and 300 K. **Figure 277** shows the stress-strain curve for the tension of a single-layer b-SnSi of dimension 100 × 100 Å. Periodic boundary conditions are applied in both armchair and zigzag directions. The single-layer b-SnSi is stretched uniaxially along the armchair or zigzag direction. The stress is calculated without involving the actual thickness of the quasi-two-dimensional structure of the single-layer b-SnSi. The Young's

	A (eV)	ρ (Å)	B (Å^4)	$r_{\min}$ (Å)	$r_{\max}$ (Å)
Sn—Si	16.463	2.260	20.164	0.0	3.713

Table 539. Two-body SW potential parameters for b-SnSi used by GULP [8], as expressed in Eq. (3).

	K (eV)	θ_0 (°)	ρ_1 (Å)	ρ_2 (Å)	$r_{\min 12}$ (Å)	$r_{\max 12}$ (Å)	$r_{\min 13}$ (Å)	$r_{\max 13}$ (Å)	$r_{\min 23}$ (Å)	$r_{\max 23}$ (Å)
Sn—Si—Si	75.415	113.298	2.260	2.260	0.0	3.713	0.0	3.713	0.0	5.751
Si—Sn—Sn	75.415	113.298	2.260	2.260	0.0	3.713	0.0	3.713	0.0	5.751

Table 540. Three-body SW potential parameters for b-SnSi used by GULP [8], as expressed in Eq. (4).

	ϵ (eV)	σ (Å)	a	λ	γ	$\cos\theta_0$	A_L	B_L	p	q	Tol
Sn—Si—Si	1.000	2.260	1.643	75.415	1.000	−0.396	16.463	0.773	4	0	0.0
Si—Sn—Sn	1.000	2.260	1.643	75.415	1.000	−0.396	16.463	0.773	4	0	0.0

Table 541. SW potential parameters for b-SnSi used by LAMMPS [9], as expressed in Eqs. (9) and (10).

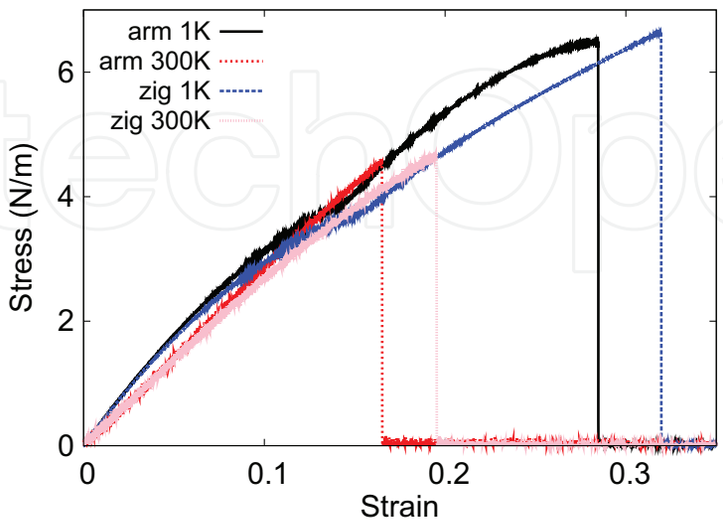

Figure 277. Stress-strain relations for the b-SnSi of size 100 × 100 Å. The b-SnSi is uniaxially stretched along the armchair or zigzag directions at temperatures 1 and 300 K.

modulus can be obtained by a linear fitting of the stress-strain relation in the small strain range of [0, 0.01]. The Young's modulus is 39.0 and 38.4 N/m along the armchair and zigzag directions, respectively. The Poisson's ratio from the VFF model and the SW potential is $\nu_{xy} = \nu_{yx} = 0.14$.

There is no available value for nonlinear quantities in the single-layer b-SnSi. We have thus used the nonlinear parameter $B = 0.5d^4$ in Eq. (5), which is close to the value of B in most materials. The value of the third-order nonlinear elasticity D can be extracted by fitting the stress-strain relation to the function $\sigma = E\epsilon + \frac{1}{2}D\epsilon^2$ with E as the Young's modulus. The values of D from the present SW potential are -150.5 and -174.8 N/m along the armchair and zigzag directions, respectively. The ultimate stress is about 6.5 N/m at the ultimate strain of 0.28 in the armchair direction at the low temperature of 1 K. The ultimate stress is about 6.6 N/m at the ultimate strain of 0.32 in the zigzag direction at the low temperature of 1 K.

136. B-InP

Present studies on the buckled InP (b-InP) are based on first-principles calculations, and no empirical potential has been proposed for the b-InP. We will thus parametrize a set of SW potential for the single-layer b-InP in this section.

The structure of the single-layer b-InP is shown in **Figure 239**. The structural parameters are from the *ab initio* calculations [114]. The b-InP has a buckled configuration as shown in **Figure 239(b)**, where the buckle is along the zigzag direction. This structure can be determined by two independent geometrical parameters, e.g., the lattice constant 4.17 Å and the bond length 2.46 Å. The resultant height of the buckle is $h = 0.51$ Å.

Table 542 shows the VFF model for the single-layer b-InP. The force constant parameters are determined by fitting to the acoustic branches in the phonon dispersion along the ΓM as shown in **Figure 278(a)**. The *ab initio* calculations for the phonon dispersion are from [114]. **Figure 278(b)** shows that the VFF model and the SW potential give exactly the same phonon dispersion, as the SW potential is derived from the VFF model.

VFF type	Bond stretching	Angle bending
Expression	$\frac{1}{2}K_r(\Delta r)^2$	$\frac{1}{2}K_\theta(\Delta\theta)^2$
Parameter	12.903	2.384
r_0 or θ_0	2.460	115.895

The second line gives an explicit expression for each VFF term. The third line is the force constant parameters. Parameters are in the unit of ev/Å^2 for the bond stretching interaction and in the unit of eV for the angle bending interaction. The fourth line gives the initial bond length (in the unit of Å) for the bond stretching interaction and the initial angle (in the unit of degrees) for the angle bending interaction.

Table 542. The VFF model for b-InP.

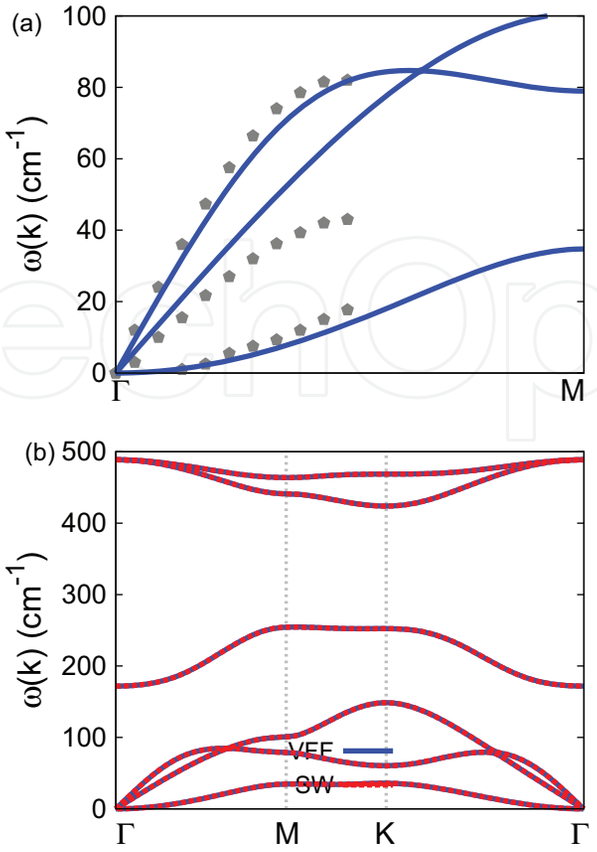

Figure 278. Phonon dispersion for the single-layer b-InP. (a) The VFF model is fitted to the three acoustic branches in the long wave limit along the ΓM direction. The *ab initio* results (gray pentagons) are from [114]. (b) The VFF model (blue lines) and the SW potential (red lines) give the same phonon dispersion for the b-InP along ΓMKΓ.

The parameters for the two-body SW potential used by GULP are shown in **Table 543**. The parameters for the three-body SW potential used by GULP are shown in **Table 544**. Parameters for the SW potential used by LAMMPS are listed in **Table 545**.

We use LAMMPS to perform MD simulations for the mechanical behavior of the single-layer b-InP under uniaxial tension at 1 and 300 K. **Figure 279** shows the stress-strain curve for the tension of a single-layer b-InP of dimension 100 × 100 Å. Periodic boundary conditions are applied in both armchair and zigzag directions. The single-layer b-InP is stretched uniaxially along the armchair or zigzag direction. The stress is calculated without involving the actual thickness of the quasi-two-dimensional structure of the single-layer b-InP. The Young's modulus can be obtained by a linear fitting of the stress-strain relation in the small strain range of [0, 0.01]. The Young's modulus is 39.3 and 38.3 N/m along the armchair and zigzag directions, respectively. The Poisson's ratio from the VFF model and the SW potential is $\nu_{xy} = \nu_{yx} = 0.17$.

There is no available value for nonlinear quantities in the single-layer b-InP. We have thus used the nonlinear parameter $B = 0.5d^4$ in Eq. (5), which is close to the value of B in most materials. The value of the third-order nonlinear elasticity D can be extracted by fitting the stress-strain relation to the function $\sigma = E\epsilon + \frac{1}{2}D\epsilon^2$ with E as the Young's modulus. The values of D from the present SW potential are −119.3 and −132.0 N/m along the armchair and zigzag directions,

	A (eV)	ρ (Å)	B (Å^4)	$r_{\min}$ (Å)	$r_{\max}$ (Å)
In—P	20.610	2.306	18.311	0.0	3.651

Table 543. Two-body SW potential parameters for b-InP used by GULP [8], as expressed in Eq. (3).

	K (eV)	θ_0 (°)	ρ_1 (Å)	ρ_2 (Å)	$r_{\min 12}$ (Å)	$r_{\max 12}$ (Å)	$r_{\min 13}$ (Å)	$r_{\max 13}$ (Å)	$r_{\min 23}$ (Å)	$r_{\max 23}$ (Å)
In—P—P	70.782	115.895	2.306	2.306	0.0	3.651	0.0	3.651	0.0	5.696
P—In—In	70.782	115.895	2.306	2.306	0.0	3.651	0.0	3.651	0.0	5.696

Table 544. Three-body SW potential parameters for b-InP used by GULP [8], as expressed in Eq. (4).

	ϵ (eV)	σ (Å)	a	λ	γ	$\cos\theta_0$	A_L	B_L	p	q	Tol
In—P—P	1.000	2.306	1.583	70.782	1.000	−0.437	20.610	0.648	4	0	0.0
P—In—In	1.000	2.306	1.583	70.782	1.000	−0.437	20.610	0.648	4	0	0.0

Table 545. SW potential parameters for b-InP used by LAMMPS [9], as expressed in Eqs. (9) and (10).

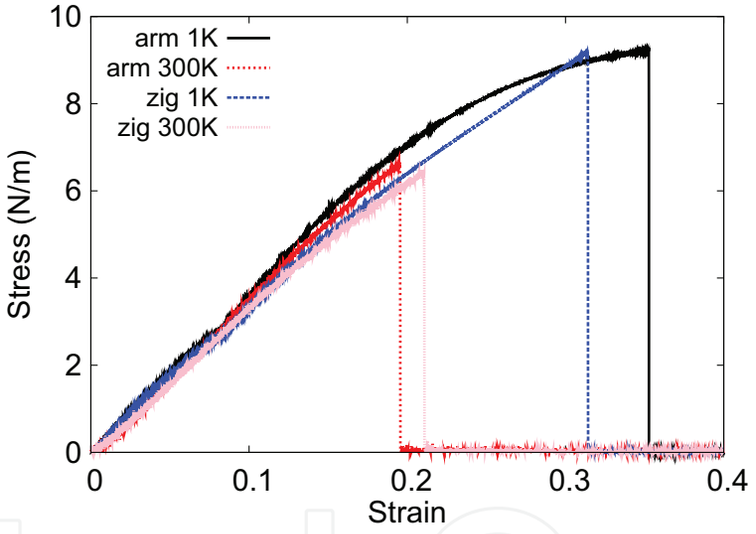

Figure 279. Stress-strain relations for the b-InP of size 100 × 100 Å. The b-InP is uniaxially stretched along the armchair or zigzag directions at temperatures 1 and 300 K.

respectively. The ultimate stress is about 9.2 N/m at the ultimate strain of 0.35 in the armchair direction at the low temperature of 1 K. The ultimate stress is about 9.1 N m^{-1} at the ultimate strain of 0.31 in the zigzag direction at the low temperature of 1 K.

137. B-InAs

Present studies on the buckled InAs (b-InAs) are based on first-principles calculations, and no empirical potential has been proposed for the b-InAs. We will thus parametrize a set of SW potential for the single-layer b-InAs in this section.

The structure of the single-layer b-InAs is shown in **Figure 239**. The structural parameters are from the *ab initio* calculations [114]. The b-InAs has a buckled configuration as shown in **Figure 239(b)**, where the buckle is along the zigzag direction. This structure can be determined by two independent geometrical parameters, e.g., the lattice constant 4.28 Å and the bond length 2.55 Å. The resultant height of the buckle is $h = 0.62$ Å.

Table 546 shows the VFF model for the single-layer b-InAs. The force constant parameters are determined by fitting to the acoustic branches in the phonon dispersion along the ΓM as shown in **Figure 280(a)**. The *ab initio* calculations for the phonon dispersion are from [114]. **Figure 280(b)** shows that the VFF model and the SW potential give exactly the same phonon dispersion, as the SW potential is derived from the VFF model.

The parameters for the two-body SW potential used by GULP are shown in **Table 547**. The parameters for the three-body SW potential used by GULP are shown in **Table 548**. Parameters for the SW potential used by LAMMPS are listed in **Table 549**.

We use LAMMPS to perform MD simulations for the mechanical behavior of the single-layer b-InAs under uniaxial tension at 1 and 300 K. **Figure 281** shows the stress-strain curve for the tension of a single-layer b-InAs of dimension 100×100 Å. Periodic boundary conditions are applied in both armchair and zigzag directions. The single-layer b-InAs is stretched uniaxially along the armchair or zigzag direction. The stress is calculated without involving the actual thickness of the quasi-two-dimensional structure of the single-layer b-InAs. The Young's modulus can be obtained by a linear fitting of the stress-strain relation in the small strain range of [0, 0.01]. The Young's modulus is 33.9 and 34.2 N/m along the armchair and zigzag directions, respectively. The Poisson's ratio from the VFF model and the SW potential is $\nu_{xy} = \nu_{yx} = 0.17$.

There is no available value for nonlinear quantities in the single-layer b-InAs. We have thus used the nonlinear parameter $B = 0.5d^4$ in Eq. (5), which is close to the value of B in most materials. The value of the third-order nonlinear elasticity D can be extracted by fitting the stress-strain relation to the function $\sigma = E\epsilon + \frac{1}{2}D\epsilon^2$ with E as the Young's modulus. The values of D from the present SW potential are -85.0 and -130.2 N/m along the armchair and zigzag directions, respectively. The ultimate stress is about 7.3 N/m at the ultimate strain of 0.32 in the armchair direction at the low temperature of 1 K. The ultimate stress is about 7.5 N/m at the ultimate strain of 0.32 in the zigzag direction at the low temperature of 1 K.

VFF type	**Bond stretching**	**Angle bending**
Expression	$\frac{1}{2}K_r(\Delta r)^2$	$\frac{1}{2}K_\theta(\Delta\theta)^2$
Parameter	10.903	2.384
r_0 or θ_0	2.550	114.115

The second line gives an explicit expression for each VFF term. The third line is the force constant parameters. Parameters are in the unit of ev/Å^2 for the bond stretching interaction and in the unit of eV for the angle bending interaction. The fourth line gives the initial bond length (in the unit of Å) for the bond stretching interaction and the initial angle (in the unit of degrees) for the angle bending interaction.

Table 546. The VFF model for b-InAs.

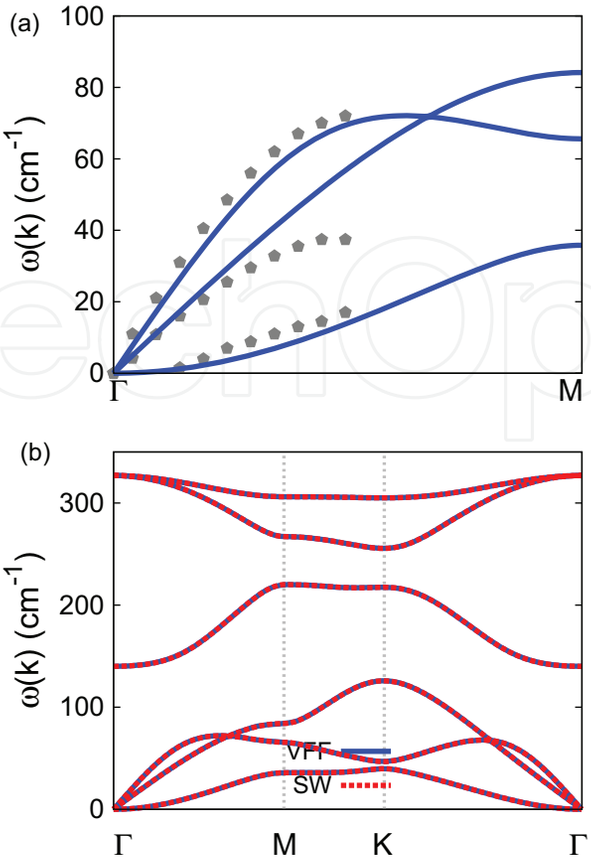

Figure 280. Phonon dispersion for the single-layer b-InAs. (a) The VFF model is fitted to the three acoustic branches in the long wave limit along the ΓM direction. The *ab initio* results (gray pentagons) are from [114]. (b) The VFF model (blue lines) and the SW potential (red lines) give the same phonon dispersion for the b-InAs along ΓMKΓ.

	A (eV)	ρ (Å)	B (Å^4)	$r_{\min}$ (Å)	$r_{\max}$ (Å)
In—As	18.099	2.320	21.141	0.0	3.766

Table 547. Two-body SW potential parameters for b-InAs used by GULP [8], as expressed in Eq. (3).

	K (eV)	θ_0 (°)	ρ_1 (Å)	ρ_2 (Å)	$r_{\min 12}$ (Å)	$r_{\max 12}$ (Å)	$r_{\min 13}$ (Å)	$r_{\max 13}$ (Å)	$r_{\min 23}$ (Å)	$r_{\max 23}$ (Å)
In—As—As	64.931	114.115	2.320	2.320	0.0	3.766	0.0	3.766	0.0	5.847
As—In—In	64.931	114.115	2.320	2.320	0.0	3.766	0.0	3.766	0.0	5.847

Table 548. Three-body SW potential parameters for b-InAs used by GULP [8], as expressed in Eq. (4).

	ϵ (eV)	σ (Å)	a	λ	γ	$\cos\theta_0$	A_L	B_L	p	q	Tol
In—As—As	1.000	2.320	1.624	64.931	1.000	−0.409	18.099	0.730	4	0	0.0
As—In—In	1.000	2.320	1.624	64.931	1.000	−0.409	18.099	0.730	4	0	0.0

Table 549. SW potential parameters for b-InAs used by LAMMPS [9], as expressed in Eqs. (9) and (10).

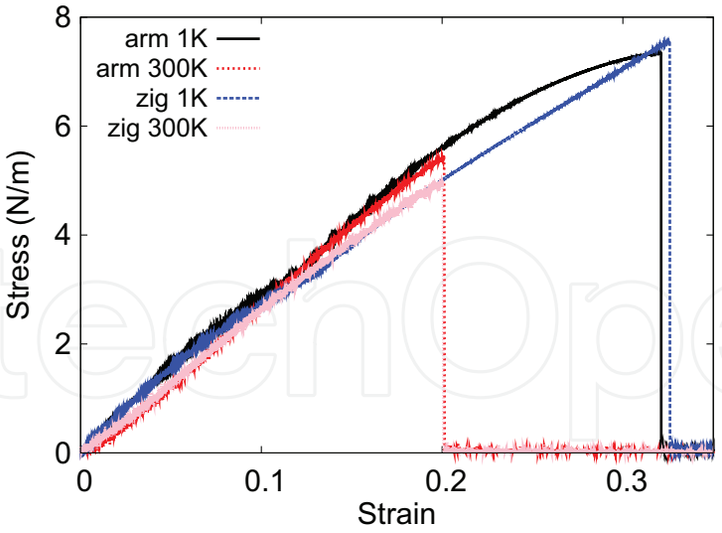

Figure 281. Stress-strain relations for the b-InAs of size 100 × 100 Å. The b-InAs is uniaxially stretched along the armchair or zigzag directions at temperatures 1 and 300 K.

138. B-InSb

Present studies on the buckled InSb (b-InSb) are based on first-principles calculations, and no empirical potential has been proposed for the b-InSb. We will thus parametrize a set of SW potential for the single-layer b-InSb in this section.

The structure of the single-layer b-InSb is shown in **Figure 239**. The structural parameters are from the *ab initio* calculations [114]. The b-InSb has a buckled configuration as shown in **Figure 239(b)**, where the buckle is along the zigzag direction. This structure can be determined by two independent geometrical parameters, e.g., the lattice constant 4.57 Å and the bond length 2.74 Å. The resultant height of the buckle is $h = 0.73$ Å.

Table 550 shows the VFF model for the single-layer b-InSb. The force constant parameters are determined by fitting to the acoustic branches in the phonon dispersion along the ΓM as shown in **Figure 282(a)**. The *ab initio* calculations for the phonon dispersion are from [114].

VFF type	Bond stretching	Angle bending
Expression	$\frac{1}{2}K_r(\Delta r)^2$	$\frac{1}{2}K_\theta(\Delta\theta)^2$
Parameter	8.903	2.384
r_0 or θ_0	2.740	113.012

The second line gives an explicit expression for each VFF term. The third line is the force constant parameters. Parameters are in the unit of ev/Å^2 for the bond stretching interaction and in the unit of eV for the angle bending interaction. The fourth line gives the initial bond length (in the unit of Å) for the bond stretching interaction and the initial angle (in the unit of degrees) for the angle bending interaction.

Table 550. The VFF model for b-InSb.

http://dx.doi.org/10.5772/intechopen.71929

Figure 282(b) shows that the VFF model and the SW potential give exactly the same phonon dispersion, as the SW potential is derived from the VFF model.

The parameters for the two-body SW potential used by GULP are shown in **Table 551**. The parameters for the three-body SW potential used by GULP are shown in **Table 552**. Parameters for the SW potential used by LAMMPS are listed in **Table 553**.

We use LAMMPS to perform MD simulations for the mechanical behavior of the single-layer b-InSb under uniaxial tension at 1 and 300 K. **Figure 283** shows the stress-strain curve for the tension of a single-layer b-InSb of dimension 100×100 Å. Periodic boundary conditions are applied in both armchair and zigzag directions. The single-layer b-InSb is stretched uniaxially along the armchair or zigzag direction. The stress is calculated without involving the actual thickness of the quasi-two-dimensional structure of the single-layer b-InSb. The Young's modulus can be obtained by a linear fitting of the stress-strain relation in the small strain range of [0, 0.01]. The Young's modulus is 28.6 and 28.9 N/m along the armchair and zigzag directions, respectively. The Poisson's ratio from the VFF model and the SW potential is $\nu_{xy} = \nu_{yx} = 0.17$.

There is no available value for nonlinear quantities in the single-layer b-InSb. We have thus used the nonlinear parameter $B = 0.5d^4$ in Eq. (5), which is close to the value of B in most materials. The value of the third-order nonlinear elasticity D can be extracted by fitting the

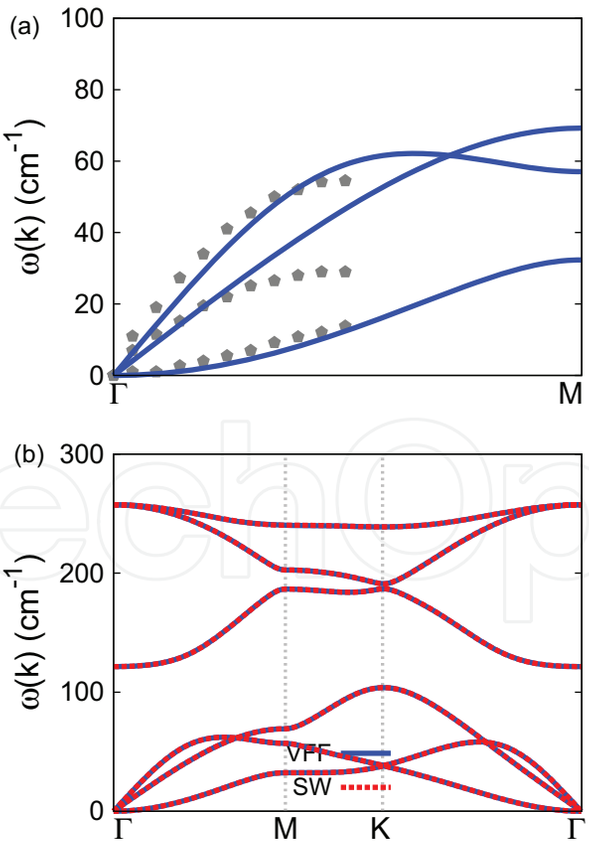

Figure 282. Phonon dispersion for the single-layer b-InSb. (a) The VFF model is fitted to the three acoustic branches in the long wave limit along the ΓM direction. The *ab initio* results (gray pentagons) are from [114]. (b) The VFF model (blue lines) and the SW potential (red lines) give the same phonon dispersion for the b-InSb along ΓMKΓ.

	A (eV)	ρ (Å)	B (Å^4)	$r_{\min}$ (Å)	$r_{\max}$ (Å)
In-Sb	16.706	2.445	28.182	0.0	4.034

Table 551. Two-body SW potential parameters for b-InSb used by GULP [8], as expressed in Eq. (3).

	K (eV)	θ_0 (°)	ρ_1 (Å)	ρ_2 (Å)	$r_{\min 12}$ (Å)	$r_{\max 12}$ (Å)	$r_{\min 13}$ (Å)	$r_{\max 13}$ (Å)	$r_{\min 23}$ (Å)	$r_{\max 23}$ (Å)
In—Sb—Sb	61.578	113.012	2.445	2.445	0.0	4.034	0.0	4.034	0.0	6.243
Sb—In—In	61.578	113.012	2.445	2.445	0.0	4.034	0.0	4.034	0.0	6.243

Table 552. Three-body SW potential parameters for b-InSb used by GULP [8], as expressed in Eq. (4).

	ϵ (eV)	σ (Å)	a	λ	γ	$\cos\theta_0$	A_L	B_L	p	q	Tol
In—Sb—Sb	1.000	2.445	1.650	61.578	1.000	−0.391	16.706	0.788	4	0	0.0
Sb—In—In	1.000	2.445	1.650	61.578	1.000	−0.391	16.706	0.788	4	0	0.0

Table 553. SW potential parameters for b-InSb used by LAMMPS [9], as expressed in Eqs. (9) and (10).

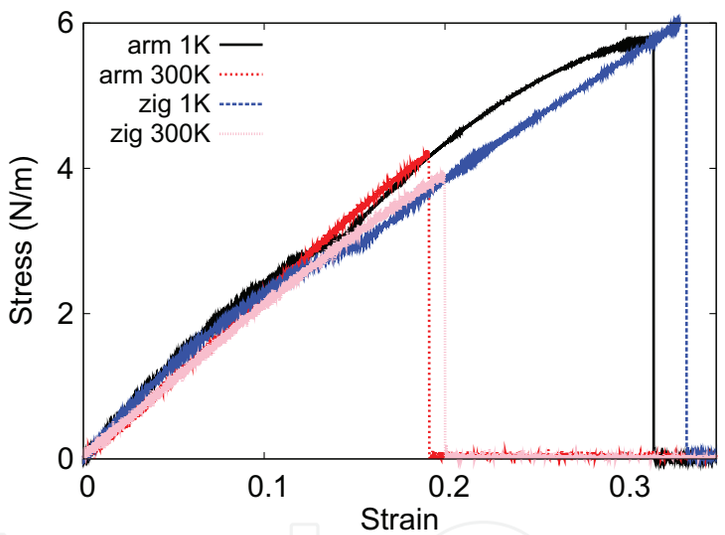

Figure 283. Stress-strain relations for the b-InSb of size 100 × 100 Å. The b-InSb is uniaxially stretched along the armchair or zigzag directions at temperatures 1 and 300 K.

stress-strain relation to the function $\sigma = E\epsilon + \frac{1}{2}D\epsilon^2$ with E as the Young's modulus. The values of D from the present SW potential are −85.4 and −121.0 N/m along the armchair and zigzag directions, respectively. The ultimate stress is about 5.8 N/m at the ultimate strain of 0.31 in the armchair direction at the low temperature of 1 K. The ultimate stress is about 6.0 N m^{-1} at the ultimate strain of 0.33 in the zigzag direction at the low temperature of 1 K.

139. b-GaAs

Present studies on the buckled GaAs (b-GaAs) are based on first-principles calculations, and no empirical potential has been proposed for the b-GaAs. We will thus parametrize a set of SW potential for the single-layer b-GaAs in this section.

The structure of the single-layer b-GaAs is shown in **Figure 239**. The structural parameters are from the *ab initio* calculations [114]. The b-GaAs has a buckled configuration as shown in **Figure 239(b)**, where the buckle is along the zigzag direction. This structure can be determined by two independent geometrical parameters, e.g., the lattice constant 3.97 Å and the bond length 2.36 Å. The resultant height of the buckle is $h = 0.55$ Å.

Table 554 shows the VFF model for the single-layer b-GaAs. The force constant parameters are determined by fitting to the acoustic branches in the phonon dispersion along the ΓM as shown in **Figure 284(a)**. The *ab initio* calculations for the phonon dispersion are from Ref. [114]. **Figure 284(b)** shows that the VFF model and the SW potential give exactly the same phonon dispersion, as the SW potential is derived from the VFF model.

The parameters for the two-body SW potential used by GULP are shown in **Table 555**. The parameters for the three-body SW potential used by GULP are shown in **Table 556**. Parameters for the SW potential used by LAMMPS are listed in **Table 557**.

We use LAMMPS to perform MD simulations for the mechanical behavior of the single-layer b-GaAs under uniaxial tension at 1 and 300 K. **Figure 285** shows the stress-strain curve for the tension of a single-layer b-GaAs of dimension 100×100 Å. Periodic boundary conditions are applied in both armchair and zigzag directions. The single-layer b-GaAs is stretched uniaxially along the armchair or zigzag direction. The stress is calculated without involving the actual thickness of the quasi-two-dimensional structure of the single-layer b-GaAs. The Young's modulus can be obtained by a linear fitting of the stress-strain relation in the small strain range of [0, 0.01]. The Young's modulus is 50.5 and 50.9 N/m along the armchair and zigzag directions, respectively. The Poisson's ratio from the VFF model and the SW potential is $\nu_{xy} = \nu_{yx} = 0.13$.

There is no available value for nonlinear quantities in the single-layer b-GaAs. We have thus used the nonlinear parameter $B = 0.5d^4$ in Eq. (5), which is close to the value of B in most materials. The value of the third-order nonlinear elasticity D can be extracted by fitting the stress-strain relation to the function $\sigma = E\epsilon + \frac{1}{2}D\epsilon^2$ with E as the Young's modulus. The values of D from the present SW potential are -199.5 and -258.6 N/m along the armchair and zigzag directions, respectively. The ultimate stress is about 8.3 N/m at the ultimate strain of 0.27 in the armchair direction at the low temperature of 1 K. The ultimate stress is about 8.3 N/m at the ultimate strain of 0.30 in the zigzag direction at the low temperature of 1 K.

VFF type	Bond stretching	Angle bending
Expression	$\frac{1}{2}K_r(\Delta r)^2$	$\frac{1}{2}K_\theta(\Delta\theta)^2$
Parameter	12.903	3.284
r_0 or θ_0	2.360	114.513

The second line gives an explicit expression for each VFF term. The third line is the force constant parameters. Parameters are in the unit of eV/Å^2 for the bond stretching interaction and in the unit of eV for the angle bending interaction. The fourth line gives the initial bond length (in the unit of Å) for the bond stretching interaction and the initial angle (in the unit of degrees) for the angle bending interaction.

Table 554. The VFF model for b-GaAs.

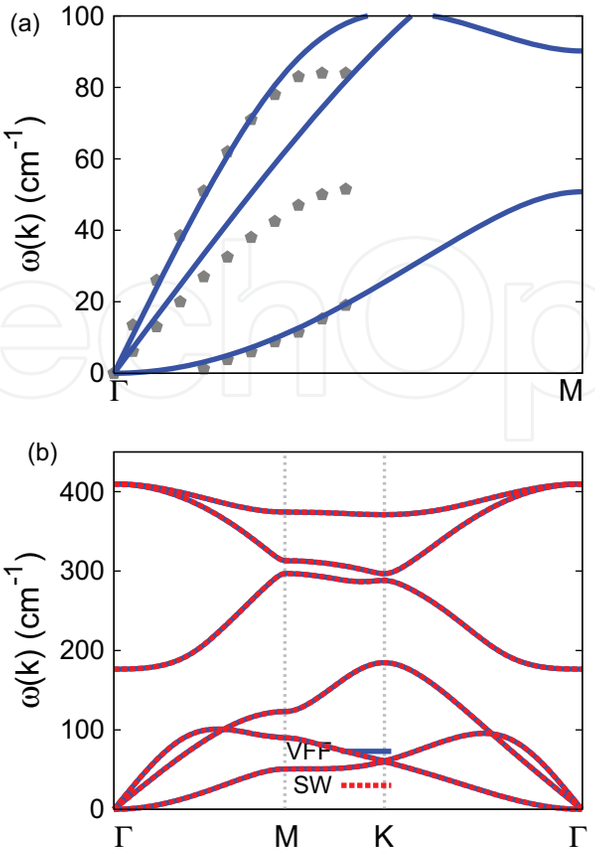

Figure 284. Phonon dispersion for the single-layer b-GaAs. (a) The VFF model is fitted to the three acoustic branches in the long wave limit along the ΓM direction. The *ab initio* results (gray pentagons) are from [114]. (b) The VFF model (blue lines) and the SW potential (red lines) give the same phonon dispersion for the b-GaAs along ΓMKΓ.

	A (eV)	ρ (Å)	B (Å^4)	$r_{\min}$ (Å)	$r_{\max}$ (Å)
Ga—As	18.485	2.161	15.510	0.0	3.489

Table 555. Two-body SW potential parameters for b-GaAs used by GULP [8], as expressed in Eq. (3).

	K (eV)	θ_0 (°)	ρ_1 (Å)	ρ_2 (Å)	$r_{\min 12}$ (Å)	$r_{\max 12}$ (Å)	$r_{\min 13}$ (Å)	$r_{\max 13}$ (Å)	$r_{\min 23}$ (Å)	$r_{\max 23}$ (Å)
Ga—As—As	91.177	114.513	2.161	2.161	0.0	3.489	0.0	3.489	0.0	5.423
As—Ga—Ga	91.177	114.513	2.161	2.161	0.0	3.489	0.0	3.489	0.0	5.423

Table 556. Three-body SW potential parameters for b-GaAs used by GULP [8], as expressed in Eq. (4).

	ϵ (eV)	σ (Å)	a	λ	γ	$\cos\theta_0$	A_L	B_L	p	q	Tol
Ga—As—As	1.000	2.161	1.614	91.177	1.000	−0.415	18.485	0.711	4	0	0.0
As—Ga—Ga	1.000	2.161	1.614	91.177	1.000	−0.415	18.485	0.711	4	0	0.0

Table 557. SW potential parameters for b-GaAs used by LAMMPS [9], as expressed in Eqs. (9) and (10).

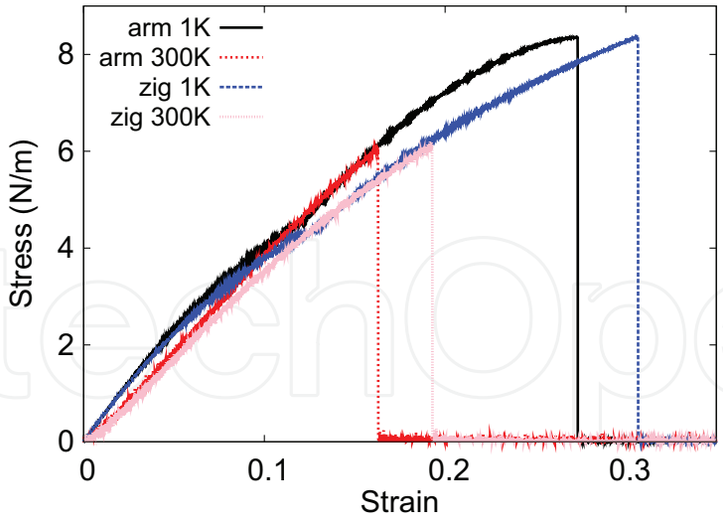

Figure 285. Stress-strain relations for the b-GaAs of size 100 $\times$ 100 Å. The b-GaAs is uniaxially stretched along the armchair or zigzag directions at temperatures 1 and 300 K.

140. b-GaP

Present studies on the buckled GaP (b-GaP) are based on first-principles calculations, and no empirical potential has been proposed for the b-GaP. We will thus parametrize a set of SW potential for the single-layer b-GaP in this section.

The structure of the single-layer b-GaP is shown in **Figure 239**. The structural parameters are from the *ab initio* calculations [114]. The b-GaP has a buckled configuration as shown in **Figure 239(b)**, where the buckle is along the zigzag direction. This structure can be determined by two independent geometrical parameters, e.g., the lattice constant 3.84 Å and the bond length 2.25 Å. The resultant height of the buckle is $h = 0.40$ Å.

Table 558 shows the VFF model for the single-layer b-GaP. The force constant parameters are determined by fitting to the acoustic branches in the phonon dispersion along the ΓM as shown in **Figure 286(a)**. The *ab initio* calculations for the phonon dispersion are from Ref. [114].

VFF type	Bond stretching	Angle bending
Expression	$\frac{1}{2}K_r(\Delta r)^2$	$\frac{1}{2}K_\theta(\Delta\theta)^2$
Parameter	16.050	3.022
r_0 or θ_0	2.250	117.152

The second line gives an explicit expression for each VFF term. The third line is the force constant parameters. Parameters are in the unit of eV/Å^2 for the bond stretching interaction and in the unit of eV for the angle bending interaction. The fourth line gives the initial bond length (in the unit of Å) for the bond stretching interaction and the initial angle (in the unit of degrees) for the angle bending interaction.

Table 558. The VFF model for b-GaP.

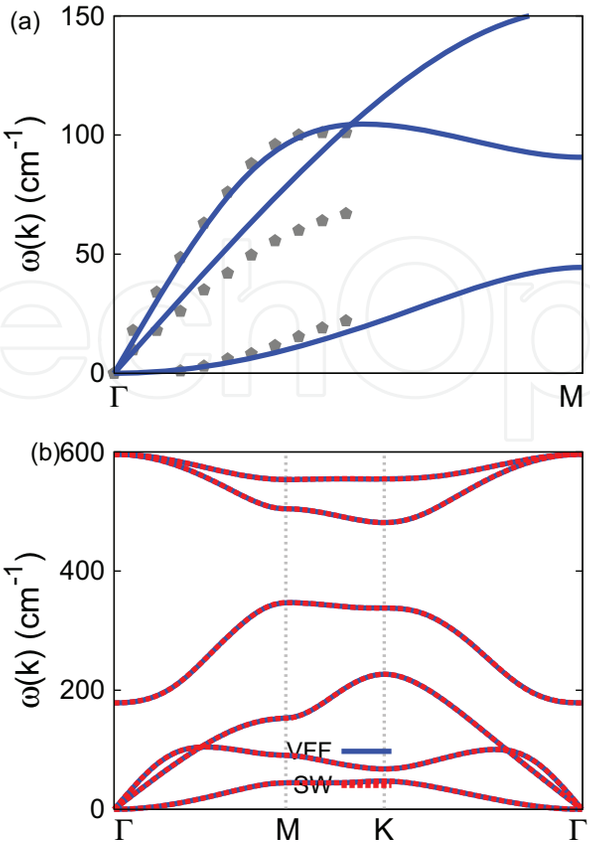

Figure 286. Phonon dispersion for the single-layer b-GaP. (a) The VFF model is fitted to the three acoustic branches in the long wave limit along the ΓM direction. The *ab initio* results (gray pentagons) are from Ref. [114]. (b) The VFF model (blue lines) and the SW potential (red lines) give the same phonon dispersion for the b-GaP along ΓMKΓ.

Figure 286(b) shows that the VFF model and the SW potential give exactly the same phonon dispersion, as the SW potential is derived from the VFF model.

The parameters for the two-body SW potential used by GULP are shown in **Table 559**. The parameters for the three-body SW potential used by GULP are shown in **Table 560**. Parameters for the SW potential used by LAMMPS are listed in **Table 561**.

	A (eV)	ρ (Å)	B (Å^4)	$r_{\min}$ (Å)	$r_{\max}$ (Å)
Ga—P	21.948	2.152	12.814	0.0	3.350

Table 559. Two-body SW potential parameters for b-GaP used by GULP [8], as expressed in Eq. (3).

	K (eV)	θ_0 (°)	ρ_1 (Å)	ρ_2 (Å)	$r_{\min 12}$ (Å)	$r_{\max 12}$ (Å)	$r_{\min 13}$ (Å)	$r_{\max 13}$ (Å)	$r_{\min 23}$ (Å)	$r_{\max 23}$ (Å)
Ga—P—P	95.438	117.152	2.152	2.152	0.0	3.350	0.0	3.350	0.0	5.246
P—Ga—Ga	95.438	117.152	2.152	2.152	0.0	3.350	0.0	3.350	0.0	5.246

Table 560. Three-body SW potential parameters for b-GaP used by GULP [8], as expressed in Eq. (4).

	ϵ (eV)	σ (Å)	a	λ	γ	$\cos\theta_0$	A_L	B_L	p	q	Tol
Ga—P—P	1.000	2.152	1.557	95.438	1.000	−0.456	21.948	0.597	4	0	0.0
P—Ga—Ga	1.000	2.152	1.557	95.438	1.000	−0.456	21.948	0.597	4	0	0.0

Table 561. SW potential parameters for b-GaP used by LAMMPS [9], as expressed in Eqs. (9) and (10).

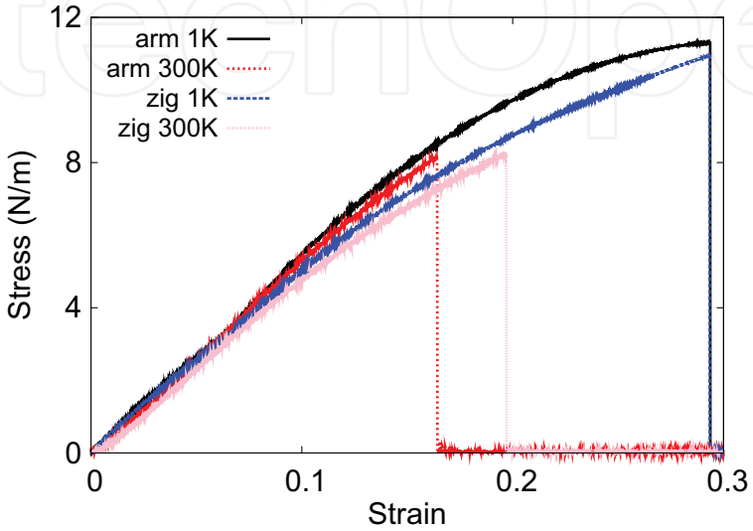

Figure 287. Stress-strain relations for the b-GaP of size 100 × 100 Å. The b-GaP is uniaxially stretched along the armchair or zigzag directions at temperatures 1 and 300 K.

We use LAMMPS to perform MD simulations for the mechanical behavior of the single-layer b-GaP under uniaxial tension at 1 and 300 K. **Figure 287** shows the stress-strain curve for the tension of a single-layer b-GaP of dimension 100 × 100 Å. Periodic boundary conditions are applied in both armchair and zigzag directions. The single-layer b-GaP is stretched uniaxially along the armchair or zigzag direction. The stress is calculated without involving the actual thickness of the quasi-two-dimensional structure of the single-layer b-GaP. The Young's modulus can be obtained by a linear fitting of the stress-strain relation in the small strain range of [0, 0.01]. The Young's modulus is 57.2 and 57.4 N/m along the armchair and zigzag directions, respectively. The Poisson's ratio from the VFF model and the SW potential is $\nu_{xy} = \nu_{yx} = 0.14$.

There is no available value for nonlinear quantities in the single-layer b-GaP. We have thus used the nonlinear parameter $B = 0.5d^4$ in Eq. (5), which is close to the value of B in most materials. The value of the third-order nonlinear elasticity D can be extracted by fitting the stress-strain relation to the function $\sigma = E\epsilon + \frac{1}{2}D\epsilon^2$ with E as the Young's modulus. The values of D from the present SW potential are −186.4 and −261.6 N/m along the armchair and zigzag directions, respectively. The ultimate stress is about 11.3 N/m at the ultimate strain of 0.29 in the armchair direction at the low temperature of 1 K. The ultimate stress is about 10.9 N/m at the ultimate strain of 0.29 in the zigzag direction at the low temperature of 1 K.

141. b-AlSb

Present studies on the buckled AlSb (b-AlSb) are based on first-principles calculations, and no empirical potential has been proposed for the b-AlSb. We will thus parametrize a set of SW potential for the single-layer b-AlSb in this section.

The structure of the single-layer b-AlSb is shown in **Figure 239**. The structural parameters are from the *ab initio* calculations [114]. The b-AlSb has a buckled configuration as shown in **Figure 239(b)**, where the buckle is along the zigzag direction. This structure can be determined by two independent geometrical parameters, e.g., the lattice constant 4.33 Å and the bond length 2.57 Å. The resultant height of the buckle is $h = 0.60$ Å.

Table 562 shows the VFF model for the single-layer b-AlSb. The force constant parameters are determined by fitting to the acoustic branches in the phonon dispersion along the ΓM as shown in **Figure 288(a)**. The *ab initio* calculations for the phonon dispersion are from Ref. [114]. **Figure 288(b)** shows that the VFF model and the SW potential give exactly the same phonon dispersion, as the SW potential is derived from the VFF model.

The parameters for the two-body SW potential used by GULP are shown in **Table 563**. The parameters for the three-body SW potential used by GULP are shown in **Table 564**. Parameters for the SW potential used by LAMMPS are listed in **Table 565**.

We use LAMMPS to perform MD simulations for the mechanical behavior of the single-layer b-AlSb under uniaxial tension at 1 and 300 K. **Figure 289** shows the stress-strain curve for the tension of a single-layer b-AlSb of dimension 100×100 Å. Periodic boundary conditions are applied in both armchair and zigzag directions. The single-layer b-AlSb is stretched uniaxially along the armchair or zigzag direction. The stress is calculated without involving the actual thickness of the quasi-two-dimensional structure of the single-layer b-AlSb. The Young's modulus can be obtained by a linear fitting of the stress-strain relation in the small strain range of [0, 0.01]. The Young's modulus is 41.7 and 42.0 N/m along the armchair and zigzag directions, respectively. The Poisson's ratio from the VFF model and the SW potential is $\nu_{xy} = \nu_{yx} = 0.15$.

There is no available value for nonlinear quantities in the single-layer b-AlSb. We have thus used the nonlinear parameter $B = 0.5d^4$ in Eq. (5), which is close to the value of B in most

VFF type	Bond stretching	Angle bending
Expression	$\frac{1}{2}K_r(\Delta r)^2$	$\frac{1}{2}K_\theta(\Delta\theta)^2$
Parameter	12.050	3.022
r_0 or θ_0	2.570	114.791

The second line gives an explicit expression for each VFF term. The third line is the force constant parameters. Parameters are in the unit of $\mathrm{eV/Å}^2$ for the bond stretching interaction and in the unit of eV for the angle bending interaction. The fourth line gives the initial bond length (in the unit of Å) for the bond stretching interaction and the initial angle (in the unit of degrees) for the angle bending interaction.

Table 562. The VFF model for b-AlSb.

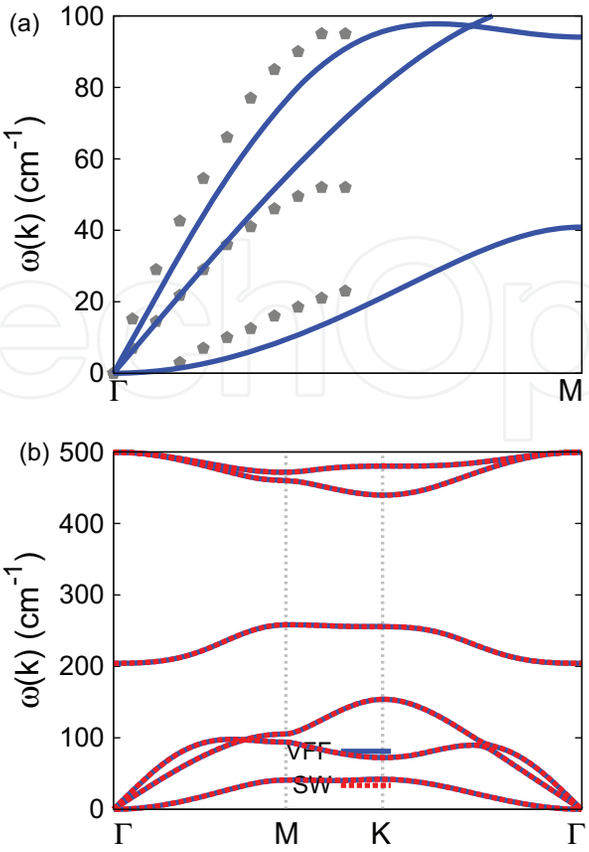

Figure 288. Phonon dispersion for the single-layer b-AlSb. (a) The VFF model is fitted to the three acoustic branches in the long wave limit along the ΓM direction. The *ab initio* results (gray pentagons) are from Ref. [114]. (b) The VFF model (blue lines) and the SW potential (red lines) give the same phonon dispersion for the b-AlSb along ΓMKΓ.

	A (eV)	ρ (Å)	B (Å^4)	$r_{\min}$ (Å)	$r_{\max}$ (Å)
Al—Sb	20.580	2.365	21.812	0.0	3.803

Table 563. Two-body SW potential parameters for b-AlSb used by GULP [8], as expressed in Eq. (3).

	K (eV)	θ_0 (°)	ρ_1 (Å)	ρ_2 (Å)	$r_{\min 12}$ (Å)	$r_{\max 12}$ (Å)	$r_{\min 13}$ (Å)	$r_{\max 13}$ (Å)	$r_{\min 23}$ (Å)	$r_{\max 23}$ (Å)
Al—Sb—Sb	85.046	114.791	2.365	2.365	0.0	3.803	0.0	3.803	0.0	5.915
Sb—Al—Al	85.046	114.791	2.365	2.365	0.0	3.803	0.0	3.803	0.0	5.915

Table 564. Three-body SW potential parameters for b-AlSb used by GULP [8], as expressed in Eq. (4).

	ϵ (eV)	σ (Å)	a	λ	γ	$\cos\theta_0$	A_L	B_L	p	q	Tol
Al—Sb—Sb	1.000	2.365	1.608	85.046	1.000	−0.419	20.580	0.697	4	0	0.0
Sb—Al—Al	1.000	2.365	1.608	85.046	1.000	−0.419	20.580	0.697	4	0	0.0

Table 565. SW potential parameters for b-AlSb used by LAMMPS [9], as expressed in Eqs. (9) and (10).

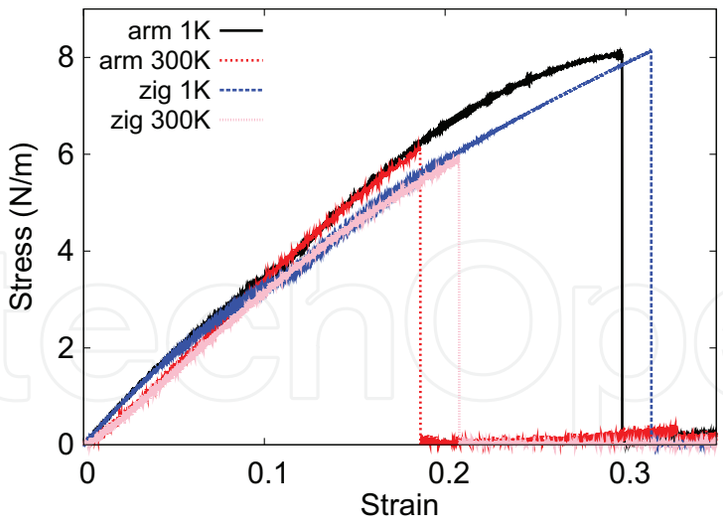

Figure 289. Stress-strain relations for the b-AlSb of size 100 × 100 Å. The b-AlSb is uniaxially stretched along the armchair or zigzag directions at temperatures 1 and 300 K.

materials. The value of the third-order nonlinear elasticity D can be extracted by fitting the stress-strain relation to the function $\sigma = E\epsilon + \frac{1}{2}D\epsilon^2$ with E as the Young's modulus. The values of D from the present SW potential are -142.4 and -190.8 N/m along the armchair and zigzag directions, respectively. The ultimate stress is about 8.1 N/m at the ultimate strain of 0.29 in the armchair direction at the low temperature of 1 K. The ultimate stress is about 8.1 N/m at the ultimate strain of 0.31 in the zigzag direction at the low temperature of 1 K.

142. BO

Present studies on BO are based on first-principles calculations, and no empirical potential has been proposed for BO. We will thus parametrize a set of SW potential for the single-layer BO in this section.

The structure of the single-layer BO is shown in **Figure 290** with M = B and X = O. The structural parameters are from the *ab initio* calculations [115]. BO has a bi-buckled configuration as shown in **Figure 290(b)**, where the buckle is along the zigzag direction. Two buckling layers are symmetrically integrated through the interior B—B bonds, forming a bi-buckled configuration. This structure can be determined by three independent geometrical parameters, e.g., the lattice constant 2.44 Å, the bond length $d_{\mathrm{B-O}} = 1.52$ Å, and the bond length $d_{\mathrm{B-B}} = 1.77$ Å.

Table 566 shows the VFF model for the single-layer BO. The force constant parameters are determined by fitting to the six low-frequency branches in the phonon dispersion along the ΓM as shown in **Figure 291(a)**. The *ab initio* calculations for the phonon dispersion are from Ref. [115]. **Figure 291(b)** shows that the VFF model and the SW potential give exactly the same phonon dispersion, as the SW potential is derived from the VFF model.

The parameters for the two-body SW potential used by GULP are shown in **Table 567**. The parameters for the three-body SW potential used by GULP are shown in **Table 568**. Parameters for the SW potential used by LAMMPS are listed in **Table 569**.

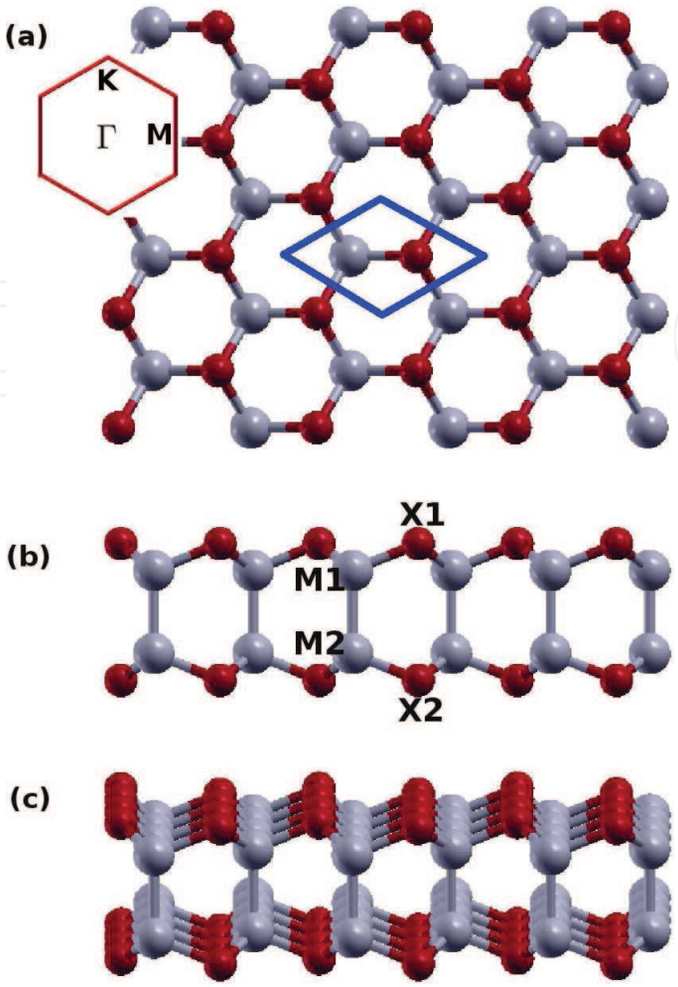

Figure 290. Structure of bi-buckled MX crystal, with M from group III and X from group VI. (a) Top view. The unit cell is highlighted by a blue parallelogram. Inset shows the first Brillouin zone of the reciprocal lattice space. (b) Side view displays the bi-buckled configuration. (c) Perspective view. M atoms are represented by larger gray balls. X atoms are represented by smaller red balls.

VFF type	Bond stretching		Angle bending	
Expression	$\frac{1}{2}K_{\mathrm{B-O}}(\Delta r)^2$	$\frac{1}{2}K_{\mathrm{B-B}}(\Delta r)^2$	$\frac{1}{2}K_{\mathrm{BOO}}(\Delta\theta)^2$	$\frac{1}{2}K_{\mathrm{BBO}}(\Delta\theta)^2$
Parameter	23.030	15.512	5.577	6.209
r_0 or θ_0	1.520	1.770	106.764	112.059

The second line gives an explicit expression for each VFF term. The third line is the force constant parameters. Parameters are in the unit of eV/Å^2 for the bond stretching interaction and in the unit of eV for the angle bending interaction. The fourth line gives the initial bond length (in the unit of Å) for the bond stretching interaction and the initial angle (in the unit of degrees) for the angle bending interaction.

Table 566. The VFF model for BO.

We use LAMMPS to perform MD simulations for the mechanical behavior of the single-layer BO under uniaxial tension at 1 and 300 K. **Figure 292** shows the stress-strain curve for the tension of a single-layer BO of dimension 100 × 100 Å. Periodic boundary conditions are applied in both

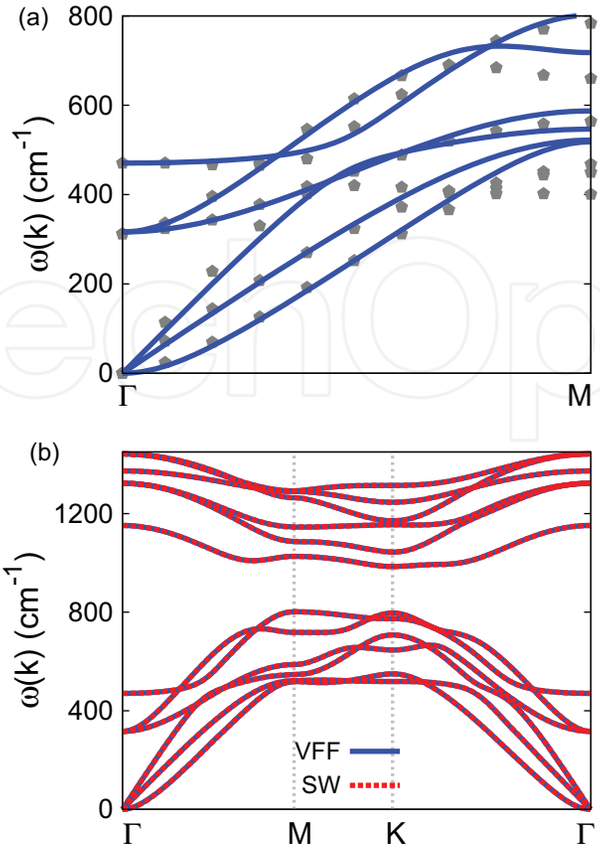

Figure 291. Phonon dispersion for the single-layer BO. (a) The VFF model is fitted to the six low-frequency branches along the ΓM direction. The *ab initio* results (gray pentagons) are from Ref. [115]. (b) The VFF model (blue lines) and the SW potential (red lines) give the same phonon dispersion for the BO along ΓMKΓ.

	A (eV)	ρ (Å)	B (Å^4)	$r_{\min}$ (Å)	$r_{\max}$ (Å)
B_1-O_1	11.725	1.207	2.669	0.0	2.197
B_1-B_2	6.749	0.875	4.908	0.0	2.392

Table 567. Two-body SW potential parameters for BO used by GULP [8], as expressed in Eq. (3).

	K (eV)	θ_0 (°)	ρ_1 (Å)	ρ_2 (Å)	$r_{\min 12}$ (Å)	$r_{\max 12}$ (Å)	$r_{\min 13}$ (Å)	$r_{\max 13}$ (Å)	$r_{\min 23}$ (Å)	$r_{\max 23}$ (Å)
B_1—O_1—O_1	107.486	106.764	1.207	1.207	0.0	2.197	0.0	2.197	0.0	3.333
B_1—B_2—O_1	87.662	112.059	0.875	1.207	0.0	2.392	0.0	2.197	0.0	3.198

Table 568. Three-body SW potential parameters for BO used by GULP [8], as expressed in Eq. (4).

	ϵ (eV)	σ (Å)	a	λ	γ	$\cos\theta_0$	A_L	B_L	p	q	Tol
B_1—O_1—O_1	1.000	1.207	1.820	107.486	1.000	−0.288	11.725	1.256	4	0	0.0
B_1—B_2—B_2	1.000	0.875	2.734	0.000	1.000	0.000	6.749	8.377	4	0	0.0
B_1—B_2—O_1	1.000	0.000	0.000	87.662	1.000	−0.376	0.000	0.000	4	0	0.0

Table 569. SW potential parameters for BO used by LAMMPS [9], as expressed in Eqs. (9) and (10).

http://dx.doi.org/10.5772/intechopen.71929

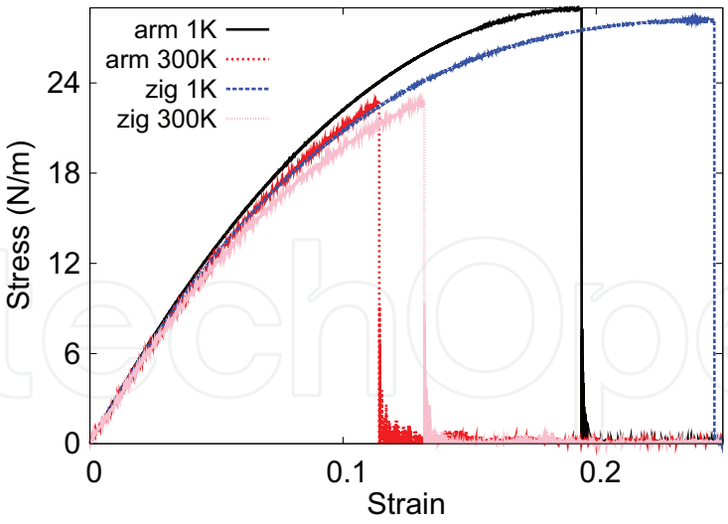

Figure 292. Stress-strain relations for BO of size 100 × 100 Å. BO is uniaxially stretched along the armchair or zigzag directions at temperatures 1 and 300 K.

armchair and zigzag directions. The single-layer BO is stretched uniaxially along the armchair or zigzag direction. The stress is calculated without involving the actual thickness of the quasi-two-dimensional structure of the single-layer BO. The Young's modulus can be obtained by a linear fitting of the stress-strain relation in the small strain range of [0, 0.01]. The Young's modulus is 299.6 and 297.7 N/m along the armchair and zigzag directions, respectively. The Poisson's ratio from the VFF model and the SW potential is $\nu_{xy} = \nu_{yx} = 0.11$.

There is no available value for nonlinear quantities in the single-layer BO. We have thus used the nonlinear parameter $B = 0.5d^4$ in Eq. (5), which is close to the value of B in most materials. The value of the third-order nonlinear elasticity D can be extracted by fitting the stress-strain relation to the function $\sigma = E\epsilon + \frac{1}{2}D\epsilon^2$ with E as the Young's modulus. The values of D from the present SW potential are −1554.7 and −1585.2 N/m along the armchair and zigzag directions, respectively. The ultimate stress is about 28.9 N/m at the ultimate strain of 0.19 in the armchair direction at the low temperature of 1 K. The ultimate stress is about 28.2 N/m at the ultimate strain of 0.24 in the zigzag direction at the low temperature of 1 K.

143. AlO

Present studies on AlO are based on first-principles calculations, and no empirical potential has been proposed for AlO. We will thus parametrize a set of SW potential for the single-layer AlO in this section.

The structure of the single-layer AlO is shown in **Figure 290** with M = Al and X = O. The structural parameters are from the *ab initio* calculations [115]. AlO has a bi-buckled configuration as shown in **Figure 290(b)**, where the buckle is along the zigzag direction. Two buckling layers are symmetrically integrated through the interior Al-Al bonds, forming a bi-buckled configuration. This structure can be determined by three independent geometrical parameters, e.g., the lattice constant 2.96 Å, the bond length $d_{\mathrm{Al-O}} = 1.83$ Å, and the bond length $d_{\mathrm{Al-Al}} = 2.62$ Å.

Table 570 shows the VFF model for the single-layer AlO. The force constant parameters are determined by fitting to the six low-frequency branches in the phonon dispersion along the ΓM as shown in **Figure 293(a)**. The *ab initio* calculations for the phonon dispersion are from Ref. [115]. **Figure 293(b)** shows that the VFF model and the SW potential give exactly the same phonon dispersion, as the SW potential is derived from the VFF model.

The parameters for the two-body SW potential used by GULP are shown in **Table 571**. The parameters for the three-body SW potential used by GULP are shown in **Table 572**. Parameters for the SW potential used by LAMMPS are listed in **Table 573**.

VFF type	**Bond stretching**		**Angle bending**	
Expression	$\frac{1}{2}K_{\mathrm{Al-O}}(\Delta r)^2$	$\frac{1}{2}K_{\mathrm{Al-Al}}(\Delta r)^2$	$\frac{1}{2}K_{\mathrm{AlOO}}(\Delta\theta)^2$	$\frac{1}{2}K_{\mathrm{AlAlO}}(\Delta\theta)^2$
Parameter	18.189	6.410	3.182	1.318
r_0 or θ_0	1.830	2.620	107.947	110.956

The second line gives an explicit expression for each VFF term. The third line is the force constant parameters. Parameters are in the unit of eV/Å^2 for the bond stretching interaction and in the unit of eV for the angle bending interaction. The fourth line gives the initial bond length (in the unit of Å) for the bond stretching interaction and the initial angle (in the unit of degrees) for the angle bending interaction.

Table 570. The VFF model for AlO.

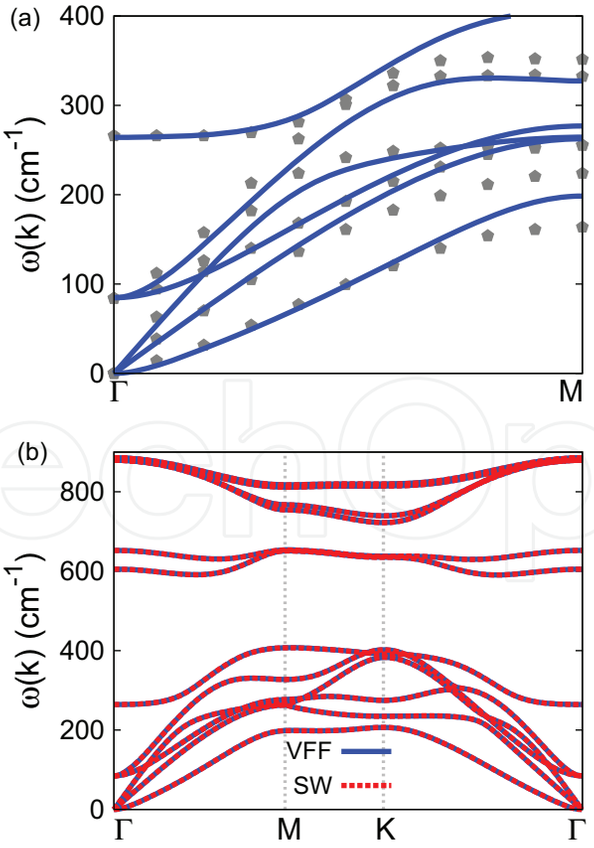

Figure 293. Phonon dispersion for the single-layer AlO. (a) The VFF model is fitted to the six low-frequency branches along the ΓM direction. The *ab initio* results (gray pentagons) are from Ref. [115]. (b) The VFF model (blue lines) and the SW potential (red lines) give the same phonon dispersion for AlO along ΓMKΓ.

	A (eV)	ρ (Å)	B (Å^4)	r_{min} (Å)	r_{max} (Å)
Al_1—O_1	13.758	1.488	5.608	0.0	2.655
Al_1—Al_2	3.609	0.678	23.560	0.0	3.287

Table 571. Two-body SW potential parameters for AlO used by GULP [8], as expressed in Eq. (3).

	K (eV)	θ_0 (°)	ρ_1 (Å)	ρ_2 (Å)	r_{min12} (Å)	r_{max12} (Å)	r_{min13} (Å)	r_{max13} (Å)	r_{min23} (Å)	r_{max23} (Å)
Al_1—O_1—O_1	64.759	107.947	1.488	1.488	0.0	2.655	0.0	2.655	0.0	4.043
Al_1—O_1—Al_2	12.688	110.956	1.488	0.678	0.0	2.655	0.0	3.287	0.0	4.213

Table 572. Three-body SW potential parameters for AlO used by GULP [8], as expressed in Eq. (4).

We use LAMMPS to perform MD simulations for the mechanical behavior of the single-layer AlO under uniaxial tension at 1 and 300 K. **Figure 294** shows the stress-strain curve for the tension of a single-layer AlO of dimension 100×100 Å. Periodic boundary conditions are applied in both armchair and zigzag directions. The single-layer AlO is stretched uniaxially along the armchair or zigzag direction. The stress is calculated without involving the actual thickness of the quasi-two-dimensional structure of the single-layer AlO. The Young's modulus can be obtained by a linear fitting of the stress-strain relation in the small strain range of [0, 0.01]. The Young's modulus is 149.3 and 148.2 N/m along the armchair and zigzag directions, respectively. The Poisson's ratio from the VFF model and the SW potential is $\nu_{xy} = \nu_{yx} = 0.19$.

	ϵ (eV)	σ (Å)	a	λ	γ	$\cos\theta_0$	A_L	B_L	p	q	Tol
Al_1—O_1—O_1	1.000	1.488	1.785	64.759	1.000	−0.308	13.758	1.145	4	0	0.0
Al_1—Al_2—Al_2	1.000	0.678	4.846	0.000	1.000	0.000	3.609	111.363	4	0	0.0
Al_1—Al_2—O_1	1.000	0.000	0.000	12.688	1.000	−0.358	0.000	0.000	4	0	0.0

Table 573. SW potential parameters for AlO used by LAMMPS [9], as expressed in Eqs. (9) and (10).

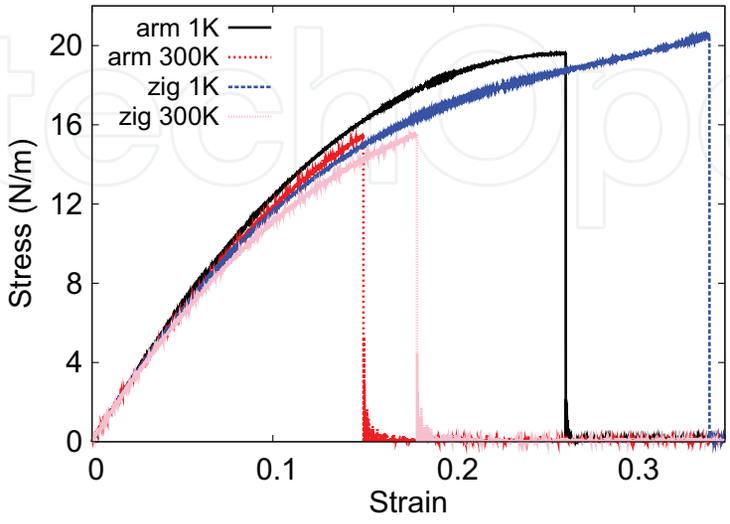

Figure 294. Stress-strain relations for the AlO of size 100×100 Å. The AlO is uniaxially stretched along the armchair or zigzag directions at temperatures 1 and 300 K.

There is no available value for nonlinear quantities in the single-layer AlO. We have thus used the nonlinear parameter $B = 0.5d^4$ in Eq. (5), which is close to the value of B in most materials. The value of the third-order nonlinear elasticity D can be extracted by fitting the stress-strain relation to the function $\sigma = E\epsilon + \frac{1}{2}D\epsilon^2$ with E as the Young's modulus. The values of D from the present SW potential are -563.9 and -565.6 N/m along the armchair and zigzag directions, respectively. The ultimate stress is about 19.6 N/m at the ultimate strain of 0.26 in the armchair direction at the low temperature of 1 K. The ultimate stress is about 20.4 N/m at the ultimate strain of 0.34 in the zigzag direction at the low temperature of 1 K.

144. GaO

Present studies on the GaO are based on first-principles calculations, and no empirical potential has been proposed for the GaO. We will thus parametrize a set of SW potential for the single-layer GaO in this section.

The structure of the single-layer GaO is shown in **Figure 290** with M = Ga and X = O. The structural parameters are from the *ab initio* calculations [115]. The GaO has a bi-buckled configuration as shown in **Figure 290(b)**, where the buckle is along the zigzag direction. Two buckling layers are symmetrically integrated through the interior Ga-Ga bonds, forming a bi-buckled configuration. This structure can be determined by three independent geometrical parameters, e.g., the lattice constant 3.12 Å, the bond length $d_{\mathrm{Ga-O}} = 1.94$ Å, and the bond length $d_{\mathrm{Ga-Ga}} = 2.51$ Å.

Table 574 shows the VFF model for the single-layer GaO. The force constant parameters are determined by fitting to the six low-frequency branches in the phonon dispersion along the ΓM as shown in **Figure 295(a)**. The *ab initio* calculations for the phonon dispersion are from Ref. [115]. **Figure 295(b)** shows that the VFF model and the SW potential give exactly the same phonon dispersion, as the SW potential is derived from the VFF model.

The parameters for the two-body SW potential used by GULP are shown in **Table 575**. The parameters for the three-body SW potential used by GULP are shown in **Table 576**. Parameters for the SW potential used by LAMMPS are listed in **Table 577**.

VFF type	**Bond stretching**		**Angle bending**	
Expression	$\frac{1}{2}K_{\mathrm{Ga-O}}(\Delta r)^2$	$\frac{1}{2}K_{\mathrm{Ga-Ga}}(\Delta r)^2$	$\frac{1}{2}K_{\mathrm{GaOO}}(\Delta\theta)^2$	$\frac{1}{2}K_{\mathrm{GaGaO}}(\Delta\theta)^2$
Parameter	18.189	6.410	3.182	1.628
r_0 or θ_0	1.940	2.510	107.051	111.794

The second line gives an explicit expression for each VFF term. The third line is the force constant parameters. Parameters are in the unit of eV/Å^2 for the bond stretching interaction and in the unit of eV for the angle bending interaction. The fourth line gives the initial bond length (in the unit of Å) for the bond stretching interaction and the initial angle (in the unit of degrees) for the angle bending interaction.

Table 574. The VFF model for GaO.

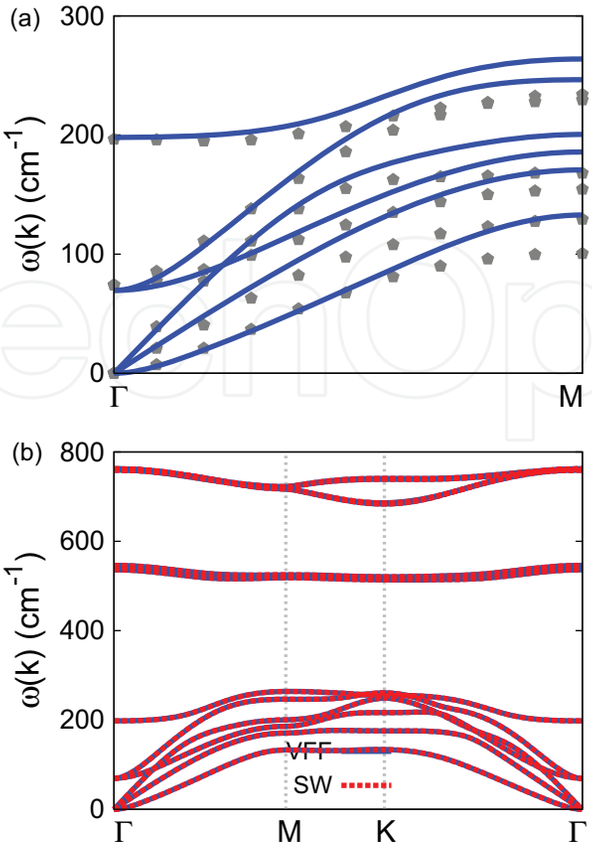

Figure 295. Phonon dispersion for the single-layer GaO. (a) The VFF model is fitted to the six low-frequency branches along the ΓM direction. The *ab initio* results (gray pentagons) are from Ref. [115]. (b) The VFF model (blue lines) and the SW potential (red lines) give the same phonon dispersion for the GaO along ΓMKΓ.

	A (eV)	ρ (Å)	B (Å^4)	r_{min} (Å)	r_{max} (Å)
Ga_1—O_1	15.178	1.550	7.082	0.0	2.807
Ga_1—Ga_2	4.225	0.890	19.846	0.0	3.257

Table 575. Two-body SW potential parameters for GaO used by GULP [8], as expressed in Eq. (3).

	K (eV)	θ_0 (°)	ρ_1 (Å)	ρ_2 (Å)	r_{min12} (Å)	r_{max12} (Å)	r_{min13} (Å)	r_{max13} (Å)	r_{min23} (Å)	r_{max23} (Å)
Ga_1—O_1—O_1	62.149	107.051	1.550	1.550	0.0	2.807	0.0	2.807	0.0	4.262
Ga_1—O_1—Ga_2	18.443	111.794	1.550	0.890	0.0	2.807	0.0	3.257	0.0	4.269

Table 576. Three-body SW potential parameters for GaO used by GULP [8], as expressed in Eq. (4).

	ϵ (eV)	σ (Å)	a	λ	γ	cos θ_0	A_L	B_L	p	q	Tol
Ga_1—O_1—O_1	1.000	1.550	1.811	62.149	1.000	−0.293	15.178	1.227	4	0	0.0
Ga_1—Ga_2—Ga_2	1.000	0.890	3.661	0.000	1.000	0.000	4.225	31.685	4	0	0.0
Ga_1—Ga_2—O_1	1.000	0.000	0.000	18.443	1.000	−0.371	0.000	0.000	4	0	0.0

Table 577. SW potential parameters for GaO used by LAMMPS [9], as expressed in Eqs. (9) and (10).

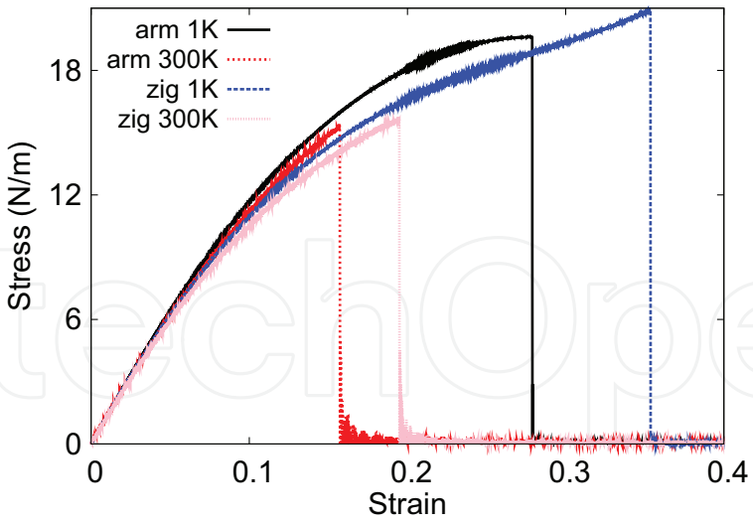

Figure 296. Stress-strain relations for the GaO of size 100 × 100 Å. GaO is uniaxially stretched along the armchair or zigzag directions at temperatures 1 and 300 K.

We use LAMMPS to perform MD simulations for the mechanical behavior of the single-layer GaO under uniaxial tension at 1 and 300 K. **Figure 296** shows the stress-strain curve for the tension of a single-layer GaO of dimension 100 × 100 Å. Periodic boundary conditions are applied in both armchair and zigzag directions. The single-layer GaO is stretched uniaxially along the armchair or zigzag direction. The stress is calculated without involving the actual thickness of the quasi-two-dimensional structure of the single-layer GaO. The Young's modulus can be obtained by a linear fitting of the stress-strain relation in the small strain range of [0, 0.01]. The Young's modulus is 137.2 and 136.6 N/m along the armchair and zigzag directions, respectively. The Poisson's ratio from the VFF model and the SW potential is $\nu_{xy} = \nu_{yx} = 0.22$.

There is no available value for nonlinear quantities in the single-layer GaO. We have thus used the nonlinear parameter $B = 0.5d^4$ in Eq. (5), which is close to the value of B in most materials. The value of the third-order nonlinear elasticity D can be extracted by fitting the stress-strain relation to the function $\sigma = E\epsilon + \frac{1}{2}D\epsilon^2$ with E as the Young's modulus. The values of D from the present SW potential are -467.5 and -529.6 N/m along the armchair and zigzag directions, respectively. The ultimate stress is about 19.6 N/m at the ultimate strain of 0.28 in the armchair direction at the low temperature of 1 K. The ultimate stress is about 20.8 N/m at the ultimate strain of 0.35 in the zigzag direction at the low temperature of 1 K.

145. InO

Present studies on InO are based on first-principles calculations, and no empirical potential has been proposed for InO. We will thus parametrize a set of SW potential for the single-layer InO in this section.

The structure of the single-layer InO is shown in **Figure 290** with M = In and X = O. The structural parameters are from the *ab initio* calculations [115]. InO has a bi-buckled configuration as shown in **Figure 290(b)**, where the buckle is along the zigzag direction. Two buckling layers are symmetrically integrated through the interior In-In bonds, forming a bi-buckled configuration.

This structure can be determined by three independent geometrical parameters, e.g., the lattice constant 3.48 Å, the bond length $d_{\mathrm{In-O}} = 2.16$ Å, and the bond length $d_{\mathrm{In-In}} = 2.86$ Å.

Table 578 shows the VFF model for the single-layer InO. The force constant parameters are determined by fitting to the six low-frequency branches in the phonon dispersion along the ΓM as shown in **Figure 297(a)**. The *ab initio* calculations for the phonon dispersion are from Ref. [115]. **Figure 297(b)** shows that the VFF model and the SW potential give exactly the same phonon dispersion, as the SW potential is derived from the VFF model.

VFF type	**Bond stretching**		**Angle bending**	
Expression	$\frac{1}{2}K_{\mathrm{In-O}}(\Delta r)^2$	$\frac{1}{2}K_{\mathrm{In-In}}(\Delta r)^2$	$\frac{1}{2}K_{\mathrm{InOO}}(\Delta\theta)^2$	$\frac{1}{2}K_{\mathrm{InInO}}(\Delta\theta)^2$
Parameter	16.916	4.250	2.171	1.138
r_0 or θ_0	2.160	2.860	107.328	111.538

The second line gives an explicit expression for each VFF term. The third line is the force constant parameters. Parameters are in the unit of eV/Å^2 for the bond stretching interaction and in the unit of eV for the angle bending interaction. The fourth line gives the initial bond length (in the unit of Å) for the bond stretching interaction and the initial angle (in the unit of degrees) for the angle bending interaction.

Table 578. The VFF model for InO.

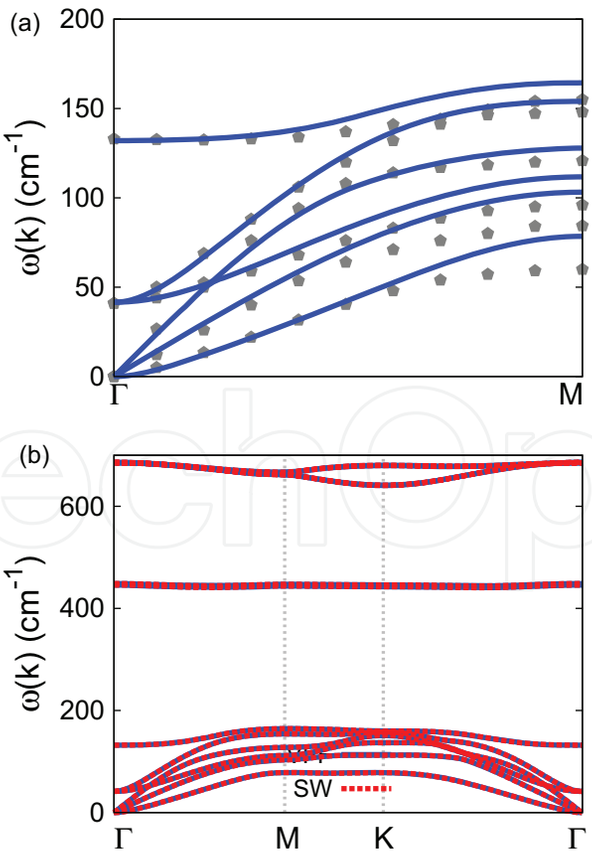

Figure 297. Phonon dispersion for the single-layer InO. (a) The VFF model is fitted to the six low-frequency branches along the ΓM direction. The *ab initio* results (gray pentagons) are from Ref. [115]. (b) The VFF model (blue lines) and the SW potential (red lines) give the same phonon dispersion for InO along ΓMKΓ.

The parameters for the two-body SW potential used by GULP are shown in **Table 579**. The parameters for the three-body SW potential used by GULP are shown in **Table 580**. Parameters for the SW potential used by LAMMPS are listed in **Table 581**.

We use LAMMPS to perform MD simulations for the mechanical behavior of the single-layer InO under uniaxial tension at 1 and 300 K. **Figure 298** shows the stress-strain curve for the tension of a single-layer InO of dimension 100×100 Å. Periodic boundary conditions are applied in both armchair and zigzag directions. The single-layer InO is stretched uniaxially

	A (eV)	ρ (Å)	B (Å^4)	r_{min} (Å)	r_{max} (Å)
In_1-O_1	17.600	1.735	10.884	0.0	3.128
In_1-In_2	3.440	0.945	33.453	0.0	3.682

Table 579. Two-body SW potential parameters for InO used by GULP [8], as expressed in Eq. (3).

	K (eV)	θ_0 (°)	ρ_1 (Å)	ρ_2 (Å)	r_{min12} (Å)	r_{max12} (Å)	r_{min13} (Å)	r_{max13} (Å)	r_{min23} (Å)	r_{max23} (Å)
In_1—O_1—O_1	42.946	107.328	1.735	1.735	0.0	3.128	0.0	3.128	0.0	4.754
In_1—O_1—In_2	12.470	111.538	1.735	0.945	0.0	3.128	0.0	3.682	0.0	4.800

Table 580. Three-body SW potential parameters for InO used by GULP [8], as expressed in Eq. (4).

	ϵ (eV)	σ (Å)	a	λ	γ	$\cos\theta_0$	A_L	B_L	p	q	Tol
In_1—O_1—O_1	1.000	1.735	1.803	42.946	1.000	−0.298	17.600	1.201	4	0	0.0
In_1—In_2—In_2	1.000	0.945	3.895	0.000	1.000	0.000	3.440	41.864	4	0	0.0
In_1—In_2—O_1	1.000	0.000	0.000	12.470	1.000	−0.367	0.000	0.000	4	0	0.0

Table 581. SW potential parameters for InO used by LAMMPS [9], as expressed in Eqs. (9) and (10).

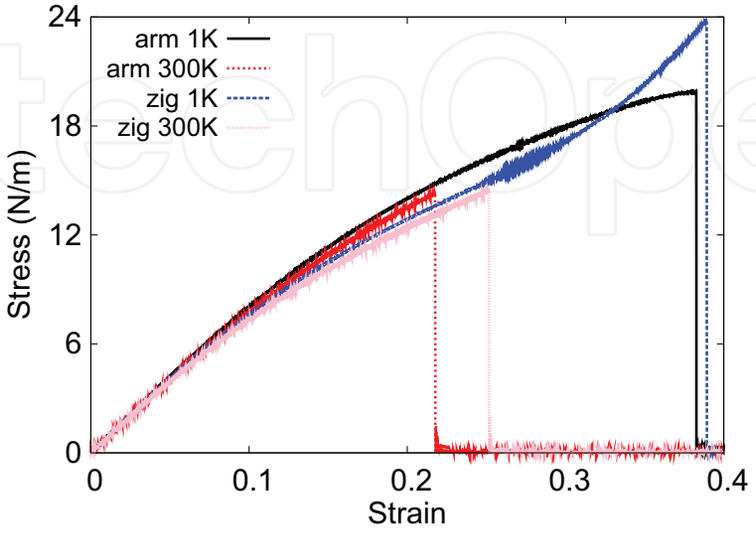

Figure 298. Stress-strain relations for InO of size 100×100 Å. InO is uniaxially stretched along the armchair or zigzag directions at temperatures 1 and 300 K.

along the armchair or zigzag direction. The stress is calculated without involving the actual thickness of the quasi-two-dimensional structure of the single-layer InO. The Young's modulus can be obtained by a linear fitting of the stress-strain relation in the small strain range of [0, 0.01]. The Young's modulus is 85.7 N/m along the armchair and zigzag directions. The Poisson's ratio from the VFF model and the SW potential is $\nu_{xy} = \nu_{yx} = 0.29$.

There is no available value for nonlinear quantities in the single-layer InO. We have thus used the nonlinear parameter $B = 0.5d^4$ in Eq. (5), which is close to the value of B in most materials. The value of the third-order nonlinear elasticity D can be extracted by fitting the stress-strain relation to the function $\sigma = E\epsilon + \frac{1}{2}D\epsilon^2$ with E as the Young's modulus. The values of D from the present SW potential are -157.3 and -210.9 N/m along the armchair and zigzag directions, respectively. The ultimate stress is about 19.9 N/m at the ultimate strain of 0.38 in the armchair direction at the low temperature of 1 K. The ultimate stress is about 23.6 N/m at the ultimate strain of 0.39 in the zigzag direction at the low temperature of 1 K.

146. BS

Present studies on BS are based on first-principles calculations, and no empirical potential has been proposed for the BS. We will thus parametrize a set of SW potential for the single-layer BS in this section.

The structure of the single-layer BS is shown in **Figure 290** with M = B and X = S. The structural parameters are from the *ab initio* calculations [115]. BS has a bi-buckled configuration as shown in **Figure 290(b)**, where the buckle is along the zigzag direction. Two buckling layers are symmetrically integrated through the interior B-B bonds, forming a bi-buckled configuration. This structure can be determined by three independent geometrical parameters, e.g., the lattice constant 3.03 Å, the bond length $d_{\mathrm{B-S}} = 1.94$ Å, and the bond length $d_{\mathrm{B-B}} = 1.72$ Å.

Table 582 shows the VFF model for the single-layer BS. The force constant parameters are determined by fitting to the six low-frequency branches in the phonon dispersion along the ΓM as shown in **Figure 299(a)**. The *ab initio* calculations for the phonon dispersion are from Ref. [115]. **Figure 299(b)** shows that the VFF model and the SW potential give exactly the same phonon dispersion, as the SW potential is derived from the VFF model.

VFF type	Bond stretching		Angle bending	
Expression	$\frac{1}{2}K_{\mathrm{B-S}}(\Delta r)^2$	$\frac{1}{2}K_{\mathrm{B-B}}(\Delta r)^2$	$\frac{1}{2}K_{\mathrm{BSS}}(\Delta\theta)^2$	$\frac{1}{2}K_{\mathrm{BBS}}(\Delta\theta)^2$
Parameter	17.138	16.385	5.144	3.861
r_0 or θ_0	1.940	1.720	102.691	115.613

The second line gives an explicit expression for each VFF term. The third line is the force constant parameters. Parameters are in the unit of eV/Å^2 for the bond stretching interaction and in the unit of eV for the angle bending interaction. The fourth line gives the initial bond length (in the unit of Å) for the bond stretching interaction and the initial angle (in the unit of degrees) for the angle bending interaction.

Table 582. The VFF model for BS.

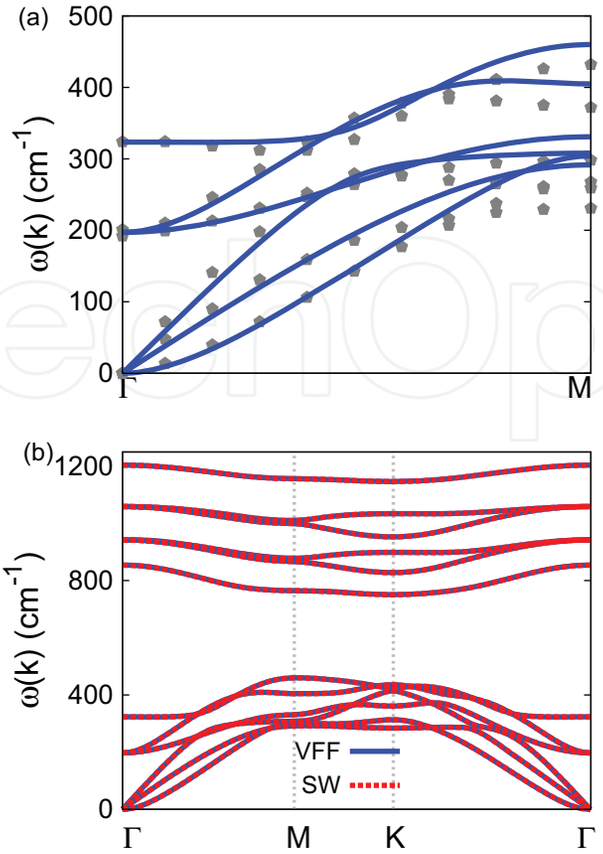

Figure 299. Phonon dispersion for the single-layer BS. (a) The VFF model is fitted to the six low-frequency branches along the ΓM direction. The *ab initio* results (gray pentagons) are from Ref. [115]. (b) The VFF model (blue lines) and the SW potential (red lines) give the same phonon dispersion for the BS along ΓMKΓ.

	A (eV)	ρ (Å)	B (Å^4)	r_{min} (Å)	r_{max} (Å)
B_1—S_1	13.021	1.417	7.082	0.0	2.769
B_1—B_2	14.613	1.809	4.376	0.0	2.602

Table 583. Two-body SW potential parameters for BS used by GULP [8], as expressed in Eq. (3).

	K (eV)	θ_0 (°)	ρ_1 (Å)	ρ_2 (Å)	r_{min12} (Å)	r_{max12} (Å)	r_{min13} (Å)	r_{max13} (Å)	r_{min23} (Å)	r_{max23} (Å)
B_1—S_1—S_1	82.459	102.691	1.417	1.417	0.0	2.769	0.0	2.769	0.0	4.139
B_1—B_2—S_1	102.002	115.613	1.809	1.417	0.0	2.602	0.0	2.769	0.0	3.717

Table 584. Three-body SW potential parameters for BS used by GULP [8], as expressed in Eq. (4).

The parameters for the two-body SW potential used by GULP are shown in **Table 583**. The parameters for the three-body SW potential used by GULP are shown in **Table 584**. Parameters for the SW potential used by LAMMPS are listed in **Table 585**.

We use LAMMPS to perform MD simulations for the mechanical behavior of the single-layer BS under uniaxial tension at 1 and 300 K. **Figure 300** shows the stress-strain curve for the tension of a single-layer BS of dimension 100×100 Å. Periodic boundary conditions are

	ϵ (eV)	σ (Å)	a	λ	γ	$\cos\theta_0$	A_L	B_L	p	q	Tol
B_1—S_1—S_1	1.000	1.417	1.955	82.459	1.000	−0.220	13.021	1.758	4	0	0.0
B_1—B_2—B_2	1.000	1.809	1.438	0.000	1.000	0.000	14.613	0.408	4	0	0.0
B_1—B_2—S_1	1.000	0.000	0.000	102.002	1.000	−0.432	0.000	0.000	4	0	0.0

Table 585. SW potential parameters for BS used by LAMMPS [9], as expressed in Eqs. (9) and (10).

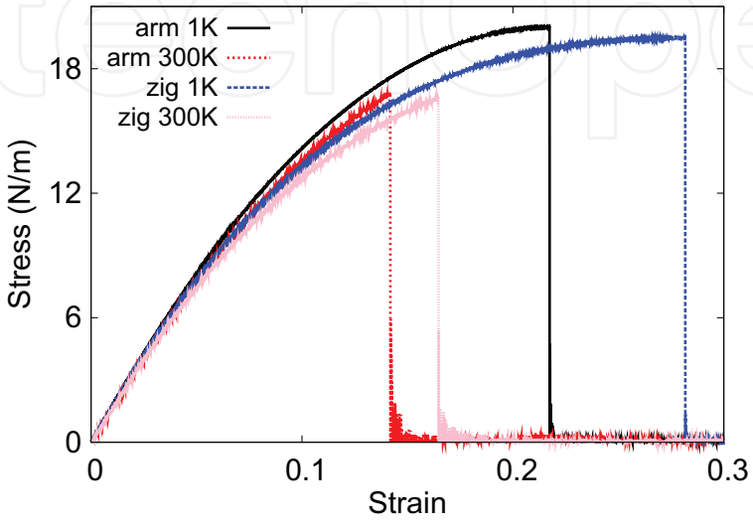

Figure 300. Stress-strain relations for the BS of size 100 × 100 Å. The BS is uniaxially stretched along the armchair or zigzag directions at temperatures 1 and 300 K.

applied in both armchair and zigzag directions. The single-layer BS is stretched uniaxially along the armchair or zigzag direction. The stress is calculated without involving the actual thickness of the quasi-two-dimensional structure of the single-layer BS. The Young's modulus can be obtained by a linear fitting of the stress-strain relation in the small strain range of [0, 0.01]. The Young's modulus is 179.4 and 178.5 N/m along the armchair and zigzag directions, respectively. The Poisson's ratio from the VFF model and the SW potential is $\nu_{xy} = \nu_{yx} = 0.16$.

There is no available value for nonlinear quantities in the single-layer BS. We have thus used the nonlinear parameter $B = 0.5d^4$ in Eq. (5), which is close to the value of B in most materials. The value of the third-order nonlinear elasticity D can be extracted by fitting the stress-strain relation to the function $\sigma = E\epsilon + \frac{1}{2}D\epsilon^2$ with E as the Young's modulus. The values of D from the present SW potential are −793.2 and −823.2 N/m along the armchair and zigzag directions, respectively. The ultimate stress is about 20.0 N/m at the ultimate strain of 0.21 in the armchair direction at the low temperature of 1 K. The ultimate stress is about 19.5 N/m at the ultimate strain of 0.28 in the zigzag direction at the low temperature of 1 K.

147. AlS

Present studies on AlS are based on first-principles calculations, and no empirical potential has been proposed for AlS. We will thus parametrize a set of SW potential for the single-layer AlS in this section.

The structure of the single-layer AlS is shown in **Figure 290** with M = Al and X = S. The structural parameters are from the *ab initio* calculations [115]. AlS has a bi-buckled configuration as shown in **Figure 290(b)**, where the buckle is along the zigzag direction. Two buckling layers are symmetrically integrated through the interior Al—Al bonds, forming a bi-buckled configuration. This structure can be determined by three independent geometrical parameters, e.g., the lattice constant 3.57 Å, the bond length $d_{\mathrm{Al-S}} = 2.32$ Å, and the bond length $d_{\mathrm{Al-Al}} = 2.59$ Å.

Table 586 shows the VFF model for the single-layer AlS. The force constant parameters are determined by fitting to the six low-frequency branches in the phonon dispersion along the ΓM as shown in **Figure 301(a)**. The *ab initio* calculations for the phonon dispersion are from Ref. [115]. **Figure 301(b)** shows that the VFF model and the SW potential give exactly the same phonon dispersion, as the SW potential is derived from the VFF model.

The parameters for the two-body SW potential used by GULP are shown in **Table 587**. The parameters for the three-body SW potential used by GULP are shown in **Table 588**. Parameters for the SW potential used by LAMMPS are listed in **Table 589**.

We use LAMMPS to perform MD simulations for the mechanical behavior of the single-layer AlS under uniaxial tension at 1 and 300 K. **Figure 302** shows the stress-strain curve for the tension of a single-layer AlS of dimension 100×100 Å. Periodic boundary conditions are applied in both armchair and zigzag directions. The single-layer AlS is stretched uniaxially along the armchair or zigzag direction. The stress is calculated without involving the actual thickness of the quasi-two-dimensional structure of the single-layer AlS. The Young's modulus can be obtained by a linear fitting of the stress-strain relation in the small strain range of [0, 0.01]. The Young's modulus is 85.2 and 84.6 N/m along the armchair and zigzag directions, respectively. The Poisson's ratio from the VFF model and the SW potential is $\nu_{xy} = \nu_{yx} = 0.22$.

There is no available value for nonlinear quantities in the single-layer AlS. We have thus used the nonlinear parameter $B = 0.5d^4$ in Eq. (5), which is close to the value of B in most materials. The value of the third-order nonlinear elasticity D can be extracted by fitting the stress-strain relation to the function $\sigma = E\epsilon + \frac{1}{2}D\epsilon^2$ with E as the Young's modulus. The values of D from the present SW potential are -289.7 and -302.4 N/m along the armchair and zigzag directions, respectively. The ultimate stress is about 11.9 N/m at the ultimate strain of 0.25 in the armchair direction at the low temperature of 1 K. The ultimate stress is about 11.9 N/m at the ultimate strain of 0.36 in the zigzag direction at the low temperature of 1 K.

VFF type	**Bond stretching**		**Angle bending**	
Expression	$\frac{1}{2}K_{\mathrm{Al-S}}(\Delta r)^2$	$\frac{1}{2}K_{\mathrm{Al-Al}}(\Delta r)^2$	$\frac{1}{2}K_{\mathrm{AlSS}}(\Delta\theta)^2$	$\frac{1}{2}K_{\mathrm{AlAlS}}(\Delta\theta)^2$
Parameter	11.065	4.912	3.210	1.900
r_0 or θ_0	2.320	2.590	100.600	117.324

The second line gives an explicit expression for each VFF term. The third line is the force constant parameters. Parameters are in the unit of $\mathrm{eV/\AA^2}$ for the bond stretching interaction and in the unit of eV for the angle bending interaction. The fourth line gives the initial bond length (in the unit of Å) for the bond stretching interaction and the initial angle (in the unit of degrees) for the angle bending interaction.

Table 586. The VFF model for AlS.

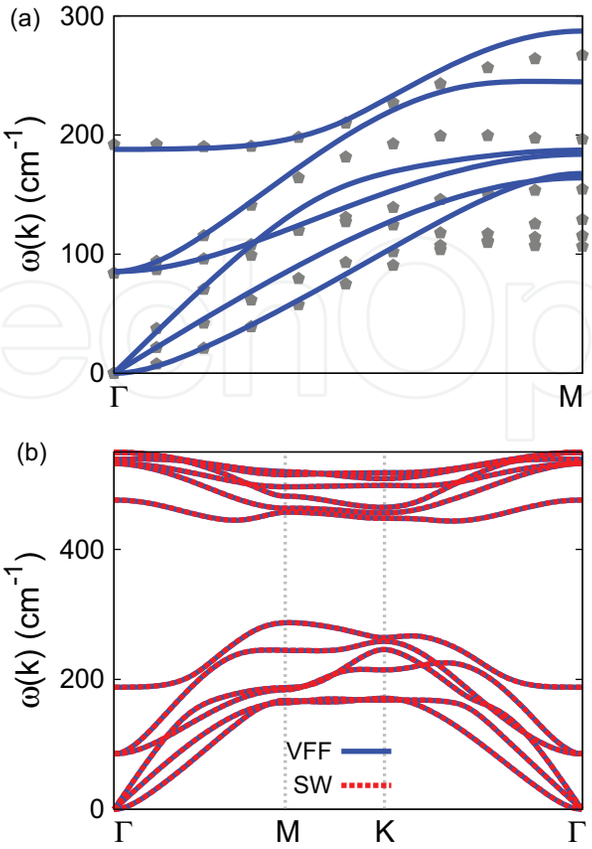

Figure 301. Phonon dispersion for the single-layer AlS. (a) The VFF model is fitted to the six low-frequency branches along the ΓM direction. The *ab initio* results (gray pentagons) are from Ref. [115]. (b) The VFF model (blue lines) and the SW potential (red lines) give the same phonon dispersion for AlS along ΓMKΓ.

	A (eV)	ρ (Å)	B (Å^4)	r_{min} (Å)	r_{max} (Å)
Al_1—S_1	11.476	1.618	14.485	0.0	3.289
Al_1—Al_2	4.575	1.280	22.499	0.0	3.500

Table 587. Two-body SW potential parameters for AlS used by GULP [8], as expressed in Eq. (3).

	K (eV)	θ_0 (°)	ρ_1 (Å)	ρ_2 (Å)	r_{min12} (Å)	r_{max12} (Å)	r_{min13} (Å)	r_{max13} (Å)	r_{min23} (Å)	r_{max23} (Å)
Al_1—S_1—S_1	46.910	100.600	1.618	1.618	0.0	3.289	0.0	3.289	0.0	4.877
Al_1—S_1—Al_2	26.090	117.324	1.280	1.618	0.0	3.500	0.0	3.289	0.0	4.853

Table 588. Three-body SW potential parameters for AlS used by GULP [8], as expressed in Eq. (4).

	ϵ (eV)	σ (Å)	a	λ	γ	cos θ_0	A_L	B_L	p	q	Tol
Al_1—S_1—S_1	1.000	1.618	2.032	46.910	1.000	−0.184	11.476	2.112	4	0	0.0
Al_1—Al_2—Al_2	1.000	1.280	2.735	0.000	1.000	0.000	4.575	8.388	4	0	0.0
Al_1—Al_2—S_1	1.000	0.000	0.000	26.090	1.000	−0.459	0.000	0.000	4	0	0.0

Table 589. SW potential parameters for AlS used by LAMMPS [9], as expressed in Eqs. (9) and (10).

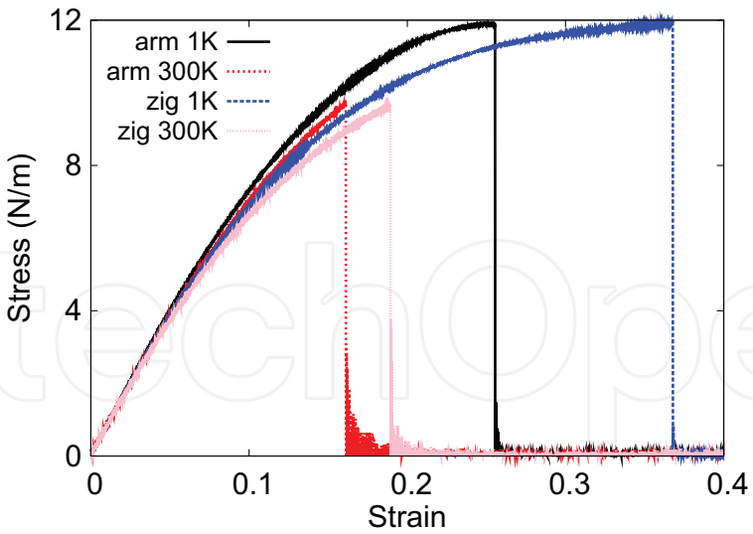

Figure 302. Stress-strain relations for AlS of size 100 × 100 Å. AlS is uniaxially stretched along the armchair or zigzag directions at temperatures 1 and 300 K.

148. GaS

Present studies on GaS are based on first-principles calculations, and no empirical potential has been proposed for the GaS. We will thus parametrize a set of SW potential for the single-layer GaS in this section.

The structure of the single-layer GaS is shown in **Figure 290** with M = Ga and X = S. The structural parameters are from the *ab initio* calculations [115]. GaS has a bi-buckled configuration as shown in **Figure 290(b)**, where the buckle is along the zigzag direction. Two buckling layers are symmetrically integrated through the interior Ga—Ga bonds, forming a bi-buckled configuration. This structure can be determined by three independent geometrical parameters, e.g., the lattice constant 3.64 Å, the bond length $d_{\mathrm{Ga-S}} = 2.36$ Å, and the bond length $d_{\mathrm{Ga-Ga}} = 2.47$ Å.

Table 590 shows the VFF model for the single-layer GaS. The force constant parameters are determined by fitting to the six low-frequency branches in the phonon dispersion along the ΓM

VFF type	Bond stretching		Angle bending	
Expression	$\frac{1}{2}K_{\mathrm{Ga-S}}(\Delta r)^2$	$\frac{1}{2}K_{\mathrm{Ga-Ga}}(\Delta r)^2$	$\frac{1}{2}K_{\mathrm{GaSS}}(\Delta\theta)^2$	$\frac{1}{2}K_{\mathrm{GaGaS}}(\Delta\theta)^2$
Parameter	10.014	6.133	2.925	1.900
r_0 or θ_0	2.360	2.470	100.921	117.065

The second line gives an explicit expression for each VFF term. The third line is the force constant parameters. Parameters are in the unit of eV/Å^2 for the bond stretching interaction and in the unit of eV for the angle bending interaction. The fourth line gives the initial bond length (in the unit of Å) for the bond stretching interaction and the initial angle (in the unit of degrees) for the angle bending interaction.

Table 590. The VFF model for GaS.

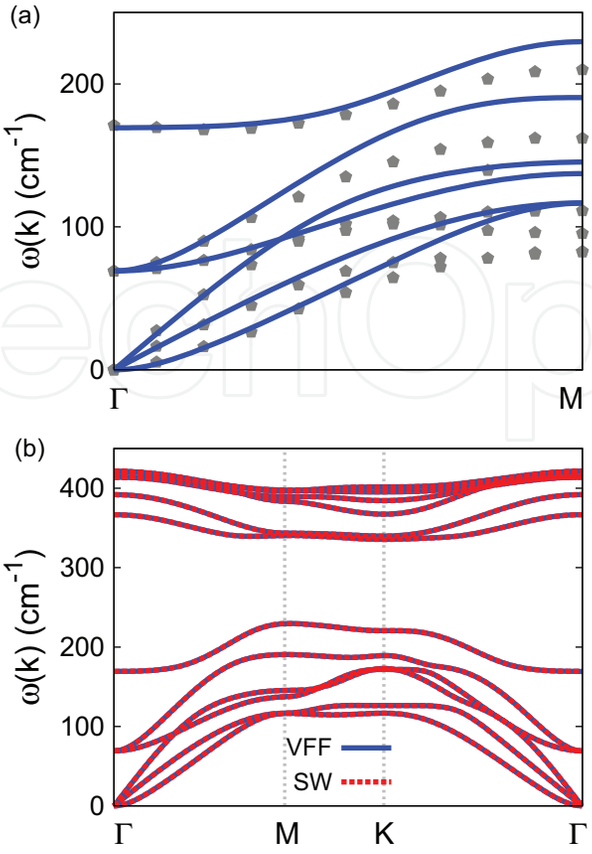

Figure 303. Phonon dispersion for the single-layer GaS. (a) The VFF model is fitted to the six low-frequency branches along the ΓM direction. The *ab initio* results (gray pentagons) are from Ref. [115]. (b) The VFF model (blue lines) and the SW potential (red lines) give the same phonon dispersion for GaS along ΓMKΓ.

as shown in **Figure 303(a)**. The *ab initio* calculations for the phonon dispersion are from Ref. [115]. **Figure 303(b)** shows that the VFF model and the SW potential give exactly the same phonon dispersion, as the SW potential is derived from the VFF model.

The parameters for the two-body SW potential used by GULP are shown in **Table 591**. The parameters for the three-body SW potential used by GULP are shown in **Table 592**. Parameters for the SW potential used by LAMMPS are listed in **Table 593**.

	A (eV)	ρ (Å)	B (Å^4)	r_{min} (Å)	r_{max} (Å)
Ga_1—S_1	10.825	1.658	15.510	0.0	3.349
Ga_1—Ga_2	6.316	1.506	18.610	0.0	3.434

Table 591. Two-body SW potential parameters for GaS used by GULP [8], as expressed in Eq. (3).

	K (eV)	θ_0 (°)	ρ_1 (Å)	ρ_2 (Å)	r_{min12} (Å)	r_{max12} (Å)	r_{min13} (Å)	r_{max13} (Å)	r_{min23} (Å)	r_{max23} (Å)
Ga_1—S_1—S_1	43.355	100.921	1.658	1.658	0.0	3.349	0.0	3.349	0.0	4.972
Ga_1—S_1—Ga_2	30.536	117.065	1.658	1.506	0.0	3.349	0.0	3.434	0.0	4.809

Table 592. Three-body SW potential parameters for GaS used by GULP [8], as expressed in Eq. (4).

	ϵ (eV)	σ (Å)	a	λ	γ	$\cos\theta_0$	A_L	B_L	p	q	Tol
Ga_1—S_1—S_1	1.000	1.658	2.020	43.355	1.000	−0.189	10.825	2.052	4	0	0.0
Ga_1—Ga_2—Ga_2	1.000	1.506	2.280	0.000	1.000	0.000	6.316	3.615	4	0	0.0
Ga_1—Ga_2—S_1	1.000	0.000	0.000	30.536	1.000	−0.455	0.000	0.000	4	0	0.0

Table 593. SW potential parameters for GaS used by LAMMPS [9], as expressed in Eqs. (9) and (10).

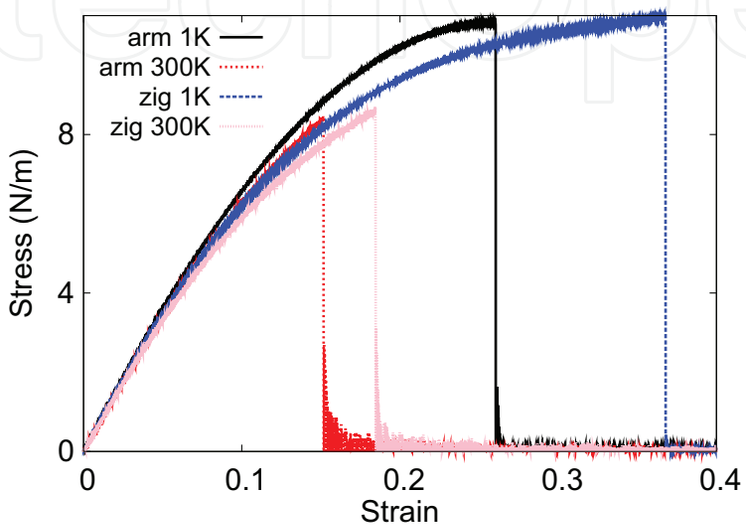

Figure 304. Stress-strain relations for GaS of size 100 × 100 Å. GaS is uniaxially stretched along the armchair or zigzag directions at temperatures 1 and 300 K.

We use LAMMPS to perform MD simulations for the mechanical behavior of the single-layer GaS under uniaxial tension at 1 and 300 K. **Figure 304** shows the stress-strain curve for the tension of a single-layer GaS of dimension 100 × 100 Å. Periodic boundary conditions are applied in both armchair and zigzag directions. The single-layer GaS is stretched uniaxially along the armchair or zigzag direction. The stress is calculated without involving the actual thickness of the quasi-two-dimensional structure of the single-layer GaS. The Young's modulus can be obtained by a linear fitting of the stress-strain relation in the small strain range of [0, 0.01]. The Young's modulus is 76.2 N/m along the armchair and zigzag directions. The Poisson's ratio from the VFF model and the SW potential is $\nu_{xy} = \nu_{yx} = 0.23$.

There is no available value for nonlinear quantities in the single-layer GaS. We have thus used the nonlinear parameter $B = 0.5d^4$ in Eq. (5), which is close to the value of B in most materials. The value of the third-order nonlinear elasticity D can be extracted by fitting the stress-strain relation to the function $\sigma = E\epsilon + \frac{1}{2}D\epsilon^2$ with E as the Young's modulus. The values of D from the present SW potential are −254.5 and −269.8 N/m along the armchair and zigzag directions, respectively. The ultimate stress is about 10.8 N/m at the ultimate strain of 0.26 in the armchair direction at the low temperature of 1 K. The ultimate stress is about 11.0 N/m at the ultimate strain of 0.36 in the zigzag direction at the low temperature of 1 K.

http://dx.doi.org/10.5772/intechopen.71929

149. InS

Present studies on the InS are based on first-principles calculations, and no empirical potential has been proposed for the InS. We will thus parametrize a set of SW potential for the single-layer InS in this section.

The structure of the single-layer InS is shown in **Figure 290** with M = In and X = S. The structural parameters are from the *ab initio* calculations [115]. InS has a bi-buckled configuration as shown in **Figure 290(b)**, where the buckle is along the zigzag direction. Two buckling layers are symmetrically integrated through the interior In—In bonds, forming a bi-buckled configuration. This structure can be determined by three independent geometrical parameters, e.g., the lattice constant 3.94 Å, the bond length $d_{\mathrm{In-S}} = 2.56$ Å, and the bond length $d_{\mathrm{In-In}} = 2.82$ Å.

Table 594 shows the VFF model for the single-layer InS. The force constant parameters are determined by fitting to the six low-frequency branches in the phonon dispersion along the ΓM as shown in **Figure 305(a)**. The *ab initio* calculations for the phonon dispersion are from Ref. [115]. **Figure 305(b)** shows that the VFF model and the SW potential give exactly the same phonon dispersion, as the SW potential is derived from the VFF model.

The parameters for the two-body SW potential used by GULP are shown in **Table 595**. The parameters for the three-body SW potential used by GULP are shown in **Table 596**. Parameters for the SW potential used by LAMMPS are listed in **Table 597**.

We use LAMMPS to perform MD simulations for the mechanical behavior of the single-layer InS under uniaxial tension at 1 and 300 K. **Figure 306** shows the stress-strain curve for the tension of a single-layer InS of dimension 100×100 Å. Periodic boundary conditions are applied in both armchair and zigzag directions. The single-layer InS is stretched uniaxially along the armchair or zigzag direction. The stress is calculated without involving the actual thickness of the quasi-two-dimensional structure of the single-layer InS. The Young's modulus can be obtained by a linear fitting of the stress-strain relation in the small strain range of [0, 0.01]. The Young's modulus is 52.9 and 53.2 N/m along the armchair and zigzag directions, respectively. The Poisson's ratio from the VFF model and the SW potential is $\nu_{xy} = \nu_{yx} = 0.29$.

VFF type	**Bond stretching**		**Angle bending**	
Expression	$\frac{1}{2}K_{\mathrm{In-S}}(\Delta r)^2$	$\frac{1}{2}K_{\mathrm{In-In}}(\Delta r)^2$	$\frac{1}{2}K_{\mathrm{InSS}}(\Delta\theta)^2$	$\frac{1}{2}K_{\mathrm{InInS}}(\Delta\theta)^2$
Parameter	10.014	4.533	2.179	1.412
r_0 or θ_0	2.560	2.820	100.624	117.305

The second line gives an explicit expression for each VFF term. The third line is the force constant parameters. Parameters are in the unit of $\mathrm{eV/Å}^2$ for the bond stretching interaction and in the unit of eV for the angle bending interaction. The fourth line gives the initial bond length (in the unit of Å) for the bond stretching interaction and the initial angle (in the unit of degrees) for the angle bending interaction.

Table 594. The VFF model for InS.

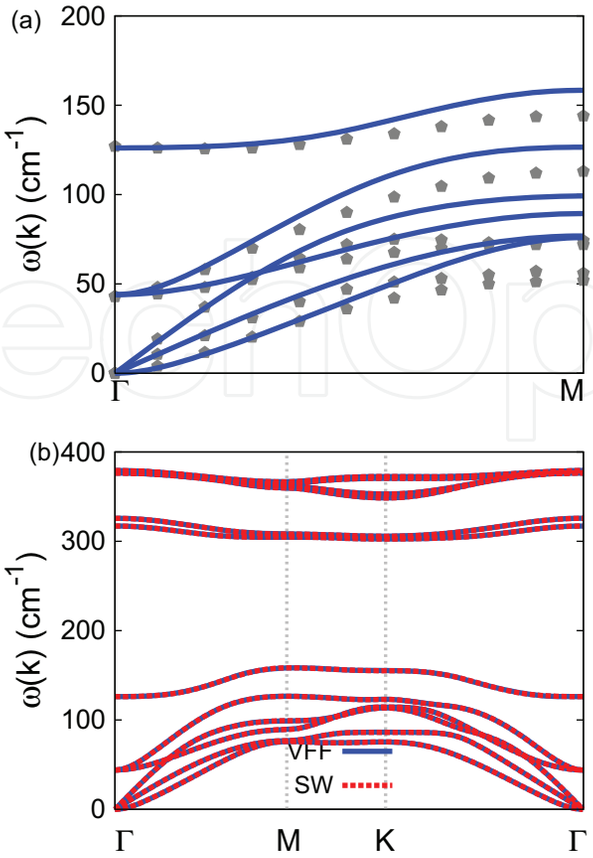

Figure 305. Phonon dispersion for the single-layer InS. (a) The VFF model is fitted to the six low-frequency branches along the ΓM direction. The *ab initio* results (gray pentagons) are from Ref. [115]. (b) The VFF model (blue lines) and the SW potential (red lines) give the same phonon dispersion for InS along ΓMKΓ.

	A (eV)	ρ (Å)	B (Å^4)	r_{min} (Å)	r_{max} (Å)
In_1—S_1	12.652	1.787	21.475	0.0	3.629
In_1—In_2	5.202	1.454	31.620	0.0	3.833

Table 595. Two-body SW potential parameters for InS used by GULP [8], as expressed in Eq. (3).

	K (eV)	θ_0 (°)	ρ_1 (Å)	ρ_2 (Å)	r_{min12} (Å)	r_{max12} (Å)	r_{min13} (Å)	r_{max13} (Å)	r_{min23} (Å)	r_{max23} (Å)
In_1—S_1—S_1	31.876	100.624	1.787	1.787	0.0	3.629	0.0	3.629	0.0	5.382
In_1—S_1—In_2	19.900	117.305	1.787	1.454	0.0	3.629	0.0	3.833	0.0	5.325

Table 596. Three-body SW potential parameters for InS used by GULP [8], as expressed in Eq. (4).

	ϵ (eV)	σ (Å)	a	λ	γ	$\cos\theta_0$	A_L	B_L	p	q	Tol
In_1—S_1—S_1	1.000	1.787	2.031	31.876	1.000	−0.184	12.652	2.108	4	0	0.0
In_1—In_2—In_2	1.000	1.454	2.635	0.000	1.000	0.000	5.202	7.067	4	0	0.0
In_1—In_2—S_1	1.000	0.000	0.000	19.990	1.000	−0.459	0.000	0.000	4	0	0.0

Table 597. SW potential parameters for InS used by LAMMPS [9], as expressed in Eqs. (9) and (10).

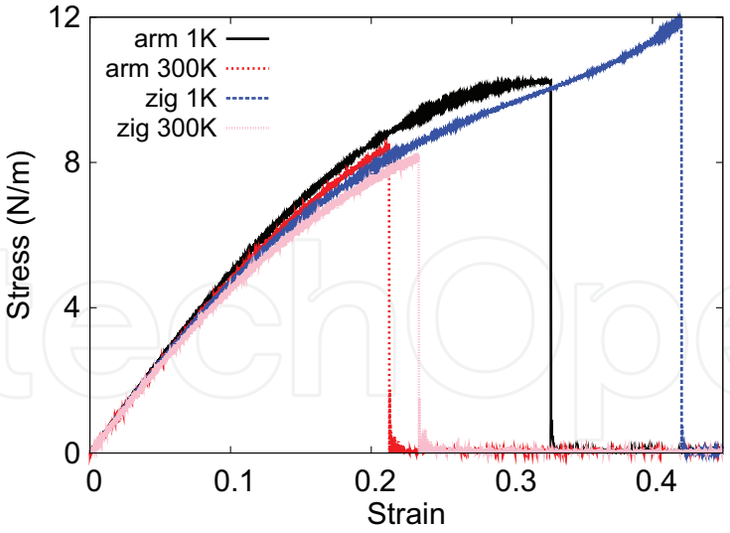

Figure 306. Stress-strain relations for InS of size 100 × 100 Å. InS is uniaxially stretched along the armchair or zigzag directions at temperatures 1 and 300 K.

There is no available value for nonlinear quantities in the single-layer InS. We have thus used the nonlinear parameter $B = 0.5d^4$ in Eq. (5), which is close to the value of B in most materials. The value of the third-order nonlinear elasticity D can be extracted by fitting the stress-strain relation to the function $\sigma = E\epsilon + \frac{1}{2}D\epsilon^2$ with E as the Young's modulus. The values of D from the present SW potential are -115.9 and -141.1 N/m along the armchair and zigzag directions, respectively. The ultimate stress is about 10.2 N/m at the ultimate strain of 0.32 in the armchair direction at the low temperature of 1 K. The ultimate stress is about 11.8 N/m at the ultimate strain of 0.42 in the zigzag direction at the low temperature of 1 K.

150. BSe

Present studies on the BSe are based on first-principles calculations, and no empirical potential has been proposed for the BSe. We will thus parametrize a set of SW potential for the single-layer BSe in this section.

The structure of the single-layer BSe is shown in **Figure 290** with M=B and X=Se. The structural parameters are from the *ab initio* calculations [115]. The BSe has a bi-buckled configuration as shown in **Figure 290(b)**, where the buckle is along the zigzag direction. Two buckling layers are symmetrically integrated through the interior B—B bonds, forming a bi-buckled configuration. This structure can be determined by three independent geometrical parameters, e.g., the lattice constant 3.25 Å, the bond length $d_{\mathrm{B-Se}} = 2.10$ Å, and the bond length $d_{\mathrm{B-B}} = 1.71$ Å.

Table 598 shows the VFF model for the single-layer BSe. The force constant parameters are determined by fitting to the six low-frequency branches in the phonon dispersion along the ΓM as shown in **Figure 307(a)**. The *ab initio* calculations for the phonon dispersion are from [115]. **Figure 307(b)** shows that the VFF model and the SW potential give exactly the same phonon dispersion, as the SW potential is derived from the VFF model.

VFF type	Bond stretching		Angle bending	
Expression	$\frac{1}{2}K_{\mathrm{B-Se}}(\Delta r)^2$	$\frac{1}{2}K_{\mathrm{B-B}}(\Delta r)^2$	$\frac{1}{2}K_{\mathrm{BSeSe}}(\Delta\theta)^2$	$\frac{1}{2}K_{\mathrm{BBSe}}(\Delta\theta)^2$
Parameter	17.138	15.227	5.144	3.113
r_0 or θ_0	2.100	1.710	101.394	116.681

The second line gives an explicit expression for each VFF term. The third line is the force constant parameters. Parameters are in the unit of eV/Å^2 for the bond stretching interaction and in the unit of eV for the angle bending interaction. The fourth line gives the initial bond length (in the unit of Å) for the bond stretching interaction and the initial angle (in the unit of degrees) for the angle bending interaction.

Table 598. The VFF model for BSe.

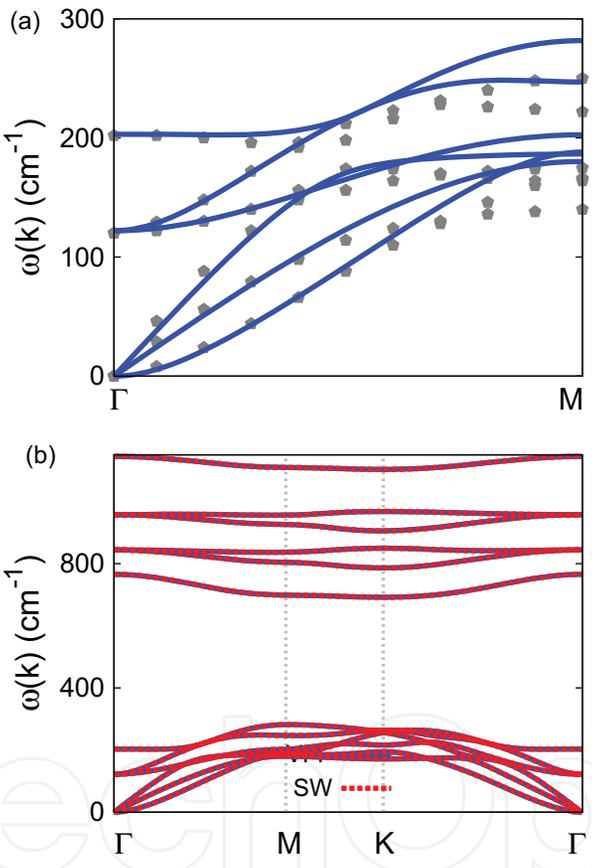

Figure 307. Phonon dispersion for the single-layer BSe. (a) The VFF model is fitted to the six low-frequency branches along the ΓM direction. The *ab initio* results (gray pentagons) are from Ref. [115]. (b) The VFF model (blue lines) and the SW potential (red lines) give the same phonon dispersion for BSe along ΓMKΓ.

The parameters for the two-body SW potential used by GULP are shown in **Table 599**. The parameters for the three-body SW potential used by GULP are shown in **Table 600**. Parameters for the SW potential used by LAMMPS are listed in **Table 601**.

We use LAMMPS to perform MD simulations for the mechanical behavior of the single-layer BSe under uniaxial tension at 1.0 and 300.0 K. **Figure 308** shows the stress-strain curve for the

	A (eV)	ρ (Å)	B (Å^4)	r_{min} (Å)	r_{max} (Å)
B_1—Se_1	14.825	1.491	9.724	0.0	2.985
B_1—B_2	17.700	2.252	4.275	0.0	2.691

Table 599. Two-body SW potential parameters for BSe used by GULP [8], as expressed in Eq. (3).

	K (eV)	θ_0 (°)	ρ_1 (Å)	ρ_2 (Å)	r_{min12} (Å)	r_{max12} (Å)	r_{min13} (Å)	r_{max13} (Å)	r_{min23} (Å)	r_{max23} (Å)
B_1—S_1—Se_1	77.850	101.394	1.491	1.491	0.0	2.985	0.0	2.985	0.0	4.440
B_1—B_2—Se_1	104.372	116.681	2.252	1.491	0.0	2.691	0.0	2.985	0.0	3.923

Table 600. Three-body SW potential parameters for BSe used by GULP [8], as expressed in Eq. (4).

	ϵ (eV)	σ (Å)	a	λ	γ	$\cos\theta_0$	A_L	B_L	p	q	Tol
B_1—Se_1—Se_1	1.000	1.491	2.002	77.850	1.000	−0.198	14.825	1.968	4	0	0.0
B_1—B_2—B_2	1.000	2.252	1.195	0.000	1.000	0.000	17.700	0.166	4	0	0.0
B_1—B_2—Se_1	1.000	0.000	0.000	104.372	1.000	−0.449	0.000	0.000	4	0	0.0

Table 601. SW potential parameters for BSe used by LAMMPS [9], as expressed in Eqs. (9) and (10).

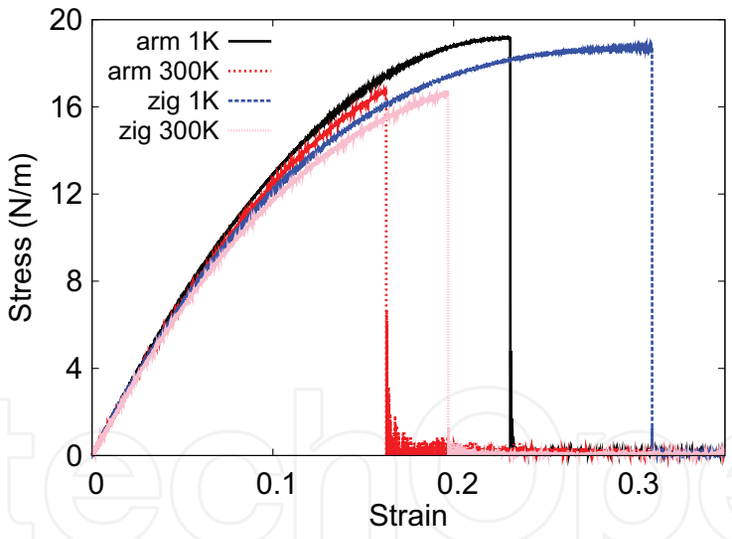

Figure 308. Stress-strain relations for the BSe of size 100 × 100 Å. The BSe is uniaxially stretched along the armchair or zigzag directions at temperatures 1 and 300 K.

tension of a single-layer BSe of dimension 100 × 100 Å. Periodic boundary conditions are applied in both armchair and zigzag directions. The single-layer BSe is stretched uniaxially along the armchair or zigzag direction. The stress is calculated without involving the actual thickness of the quasi-two-dimensional structure of the single-layer BSe. The Young's modulus can be obtained by a linear fitting of the stress-strain relation in the small strain range of [0, 0.01]. The Young's modulus is 157.3 and 156.4 N/m along the armchair and zigzag directions, respectively. The Poisson's ratio from the VFF model and the SW potential is $\nu_{xy} = \nu_{yx} = 0.19$.

There is no available value for nonlinear quantities in the single-layer BSe. We have thus used the nonlinear parameter $B = 0.5d^4$ in Eq. (5), which is close to the value of B in most materials. The value of the third-order nonlinear elasticity D can be extracted by fitting the stress-strain relation to the function $\sigma = E\epsilon + \frac{1}{2}D\epsilon^2$ with E as the Young's modulus. The values of D from the present SW potential are -627.0 and -655.6 N/m along the armchair and zigzag directions, respectively. The ultimate stress is about 19.2 N/m at the ultimate strain of 0.23 in the armchair direction at the low temperature of 1 K. The ultimate stress is about 18.7 N/m at the ultimate strain of 0.31 in the zigzag direction at the low temperature of 1 K.

151. AlSe

Present studies on the AlSe are based on first-principles calculations, and no empirical potential has been proposed for the AlSe. We will thus parametrize a set of SW potential for the single-layer AlSe in this section.

The structure of the single-layer AlSe is shown in **Figure 290** with M = Al and X = Se. The structural parameters are from the *ab initio* calculations [115]. The AlSe has a bi-buckled configuration as shown in **Figure 290(b)**, where the buckle is along the zigzag direction. Two buckling layers are symmetrically integrated through the interior Al-Al bonds, forming a bi-buckled configuration. This structure can be determined by three independent geometrical parameters, e.g., the lattice constant 3.78 Å, the bond length $d_{\mathrm{Al-Se}} = 2.47$ Å, and the bond length $d_{\mathrm{Al-Al}} = 2.57$ Å.

Table 602 shows the VFF model for the single-layer AlSe. The force constant parameters are determined by fitting to the six low-frequency branches in the phonon dispersion along the ΓM as shown in **Figure 309(a)**. The *ab initio* calculations for the phonon dispersion are from [115]. **Figure 309(b)** shows that the VFF model and the SW potential give exactly the same phonon dispersion, as the SW potential is derived from the VFF model.

The parameters for the two-body SW potential used by GULP are shown in **Table 603**. The parameters for the three-body SW potential used by GULP are shown in **Table 604**. Parameters for the SW potential used by LAMMPS are listed in **Table 605**.

VFF type	**Bond stretching**		**Angle bending**	
Expression	$\frac{1}{2}K_{Al-Se}(\Delta r)^2$	$\frac{1}{2}K_{Al-Al}(\Delta r)^2$	$\frac{1}{2}K_{AlSeSe}(\Delta\theta)^2$	$\frac{1}{2}K_{AlAlSe}(\Delta\theta)^2$
Parameter	9.831	4.487	2.916	1.659
r_0 or θ_0	2.470	2.570	99.846	117.926

The second line gives an explicit expression for each VFF term. The third line is the force constant parameters. Parameters are in the unit of eV/Å^2 for the bond stretching interaction and in the unit of eV for the angle bending interaction. The fourth line gives the initial bond length (in the unit of Å) for the bond stretching interaction and the initial angle (in the unit of degrees) for the angle bending interaction.

Table 602. The VFF model for AlSe.

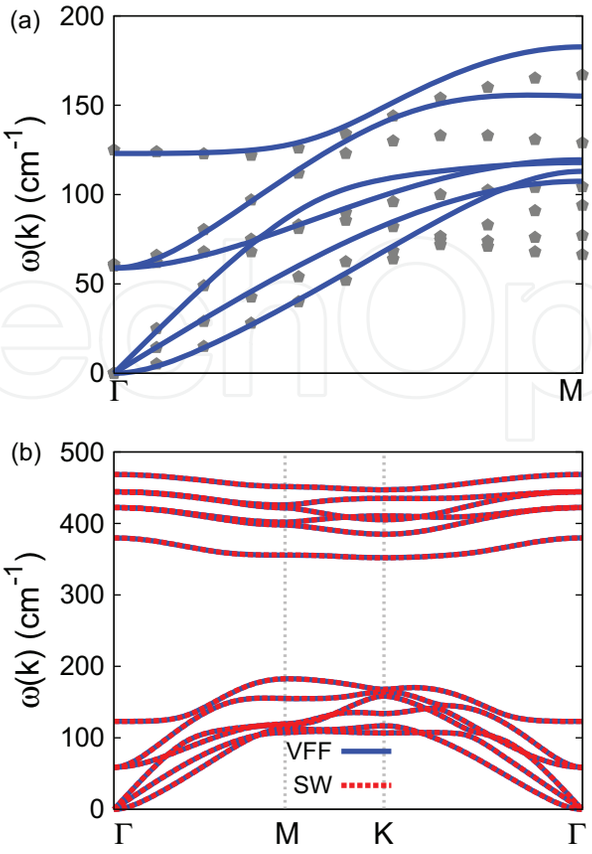

Figure 309. Phonon dispersion for the single-layer AlSe. (a) The VFF model is fitted to the six low-frequency branches along the ΓM direction. The *ab initio* results (gray pentagons) are from [115]. (b) The VFF model (blue lines) and the SW potential (red lines) give the same phonon dispersion for the AlSe along ΓMKΓ.

	A (eV)	ρ (Å)	B (Å^4)	$r_{\min}$ (Å)	$r_{\max}$ (Å)
Al_1—Se_1	11.362	1.694	18.610	0.0	3.493
Al_1—Al_2	4.974	1.558	21.812	0.0	3.570

Table 603. Two-body SW potential parameters for AlSe used by GULP [8], as expressed in Eq. (3).

	K (eV)	θ_0 (°)	ρ_1 (Å)	ρ_2 (Å)	$r_{\min 12}$ (Å)	$r_{\max 12}$ (Å)	$r_{\min 13}$ (Å)	$r_{\max 13}$ (Å)	$r_{\min 23}$ (Å)	$r_{\max 23}$ (Å)
Al_1—Se_1—Se_1	41.235	99.846	1.694	1.694	0.0	3.493	0.0	3.493	0.0	5.164
Al_1—Se_1—Al_2	26.418	117.926	1.558	1.694	0.0	3.570	0.0	3.493	0.0	5.029

Table 604. Three-body SW potential parameters for AlSe used by GULP [8], as expressed in Eq. (4).

	ϵ (eV)	σ (Å)	a	λ	γ	$\cos\theta_0$	A_L	B_L	p	q	Tol
Al_1—Se_1—Se_1	1.000	1.694	2.062	41.235	1.000	−0.171	11.362	2.260	4	0	0.0
Al_1—Al_2—Al_2	1.000	1.558	2.292	0.000	1.000	0.000	4.974	3.704	4	0	0.0
Al_1—Al_2—Se_1	1.000	0.000	0.000	26.418	1.000	−0.468	0.000	0.000	4	0	0.0

Table 605. SW potential parameters for AlSe used by LAMMPS [9], as expressed in Eqs. (9) and (10).

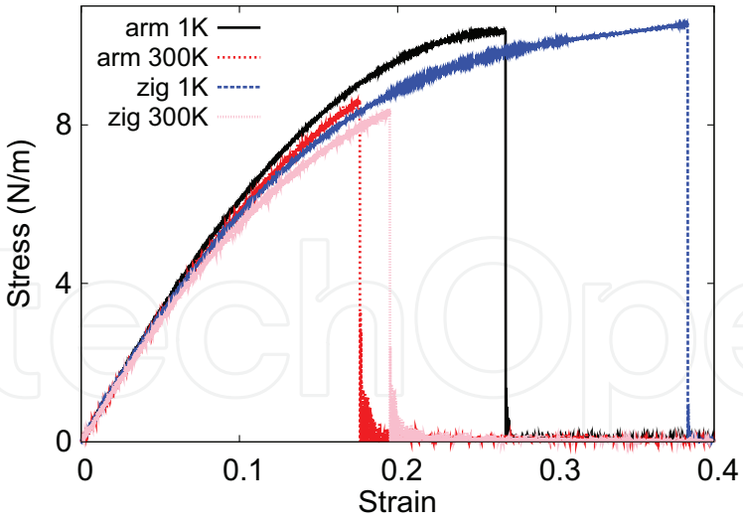

Figure 310. Stress-strain relations for the AlSe of size 100 × 100 Å. The AlSe is uniaxially stretched along the armchair or zigzag directions at temperatures 1 and 300 K.

We use LAMMPS to perform MD simulations for the mechanical behavior of the single-layer AlSe under uniaxial tension at 1.0 and 300.0 K. **Figure 310** shows the stress-strain curve for the tension of a single-layer AlSe of dimension 100 × 100 Å. Periodic boundary conditions are applied in both armchair and zigzag directions. The single-layer AlSe is stretched uniaxially along the armchair or zigzag direction. The stress is calculated without involving the actual thickness of the quasi-two-dimensional structure of the single-layer AlSe. The Young's modulus can be obtained by a linear fitting of the stress-strain relation in the small strain range of [0, 0.01]. The Young's modulus is 69.4 and 69.2 N/m along the armchair and zigzag directions, respectively. The Poisson's ratio from the VFF model and the SW potential is $\nu_{xy} = \nu_{yx} = 0.24$.

There is no available value for nonlinear quantities in the single-layer AlSe. We have thus used the nonlinear parameter $B = 0.5d^4$ in Eq. (5), which is close to the value of B in most materials. The value of the third-order nonlinear elasticity D can be extracted by fitting the stress-strain relation to the function $\sigma = E\epsilon + \frac{1}{2}D\epsilon^2$ with E as the Young's modulus. The values of D from the present SW potential are -217.3 and -231.9 N/m along the armchair and zigzag directions, respectively. The ultimate stress is about 10.4 N/m at the ultimate strain of 0.27 in the armchair direction at the low temperature of 1 K. The ultimate stress is about 10.5 N/m at the ultimate strain of 0.38 in the zigzag direction at the low temperature of 1 K.

152. GaSe

Present studies on the GaSe are based on first-principles calculations, and no empirical potential has been proposed for the GaSe. We will thus parametrize a set of SW potential for the single-layer GaSe in this section.

The structure of the single-layer GaSe is shown in **Figure 290** with M=Ga and X=Se. The structural parameters are from the *ab initio* calculations [115]. The GaSe has a bi-buckled

configuration as shown in **Figure 290(b)**, where the buckle is along the zigzag direction. Two buckling layers are symmetrically integrated through the interior Ga-Ga bonds, forming a bi-buckled configuration. This structure can be determined by three independent geometrical parameters, e.g., the lattice constant 3.82 Å, the bond length $d_{\mathrm{Ga-Se}} = 2.50$ Å, and the bond length $d_{\mathrm{Ga-Ga}} = 2.46$ Å.

Table 606 shows the VFF model for the single-layer GaSe. The force constant parameters are determined by fitting to the six low-frequency branches in the phonon dispersion along the ΓM as shown in **Figure 311(a)**. The *ab initio* calculations for the phonon dispersion are from [115]. **Figure 311(b)** shows that the VFF model and the SW potential give exactly the same phonon dispersion, as the SW potential is derived from the VFF model.

The parameters for the two-body SW potential used by GULP are shown in **Table 607**. The parameters for the three-body SW potential used by GULP are shown in **Table 608**. Parameters for the SW potential used by LAMMPS are listed in **Table 609**.

We use LAMMPS to perform MD simulations for the mechanical behavior of the single-layer GaSe under uniaxial tension at 1.0 and 300.0 K. **Figure 312** shows the stress-strain curve for the tension of a single-layer GaSe of dimension 100×100 Å. Periodic boundary conditions are applied in both armchair and zigzag directions. The single-layer GaSe is stretched uniaxially along the armchair or zigzag direction. The stress is calculated without involving the actual thickness of the quasi-two-dimensional structure of the single-layer GaSe. The Young's modulus can be obtained by a linear fitting of the stress-strain relation in the small strain range of [0, 0.01]. The Young's modulus is 68.3 and 67.9 N/m along the armchair and zigzag directions, respectively. The Poisson's ratio from the VFF model and the SW potential is $\nu_{xy} = \nu_{yx} = 0.25$.

There is no available value for nonlinear quantities in the single-layer GaSe. We have thus used the nonlinear parameter $B = 0.5d^4$ in Eq. (5), which is close to the value of B in most materials. The value of the third-order nonlinear elasticity D can be extracted by fitting the stress-strain relation to the function $\sigma = E\epsilon + \frac{1}{2}D\epsilon^2$ with E as the Young's modulus. The values of D from the present SW potential are -206.1 and -219.8 N/m along the armchair and zigzag directions, respectively. The ultimate stress is about 10.5 N/m at the ultimate strain of 0.27 in the armchair direction at the low temperature of 1 K. The ultimate stress is about 10.8 N/m at the ultimate strain of 0.39 in the zigzag direction at the low temperature of 1 K.

VFF type	**Bond stretching**		**Angle bending**	
Expression	$\frac{1}{2}K_{\mathrm{Ga-Se}}(\Delta r)^2$	$\frac{1}{2}K_{\mathrm{Ga-Ga}}(\Delta r)^2$	$\frac{1}{2}K_{\mathrm{GaSeSe}}(\Delta\theta)^2$	$\frac{1}{2}K_{\mathrm{GaGaSe}}(\Delta\theta)^2$
Parameter	10.014	5.400	2.925	1.701
r_0 or θ_0	2.500	2.460	99.636	118.092

The second line gives an explicit expression for each VFF term. The third line is the force constant parameters. Parameters are in the unit of eV/Å^2 for the bond stretching interaction and in the unit of eV for the angle bending interaction. The fourth line gives the initial bond length (in the unit of Å) for the bond stretching interaction and the initial angle (in the unit of degrees) for the angle bending interaction.

Table 606. The VFF model for GaSe.

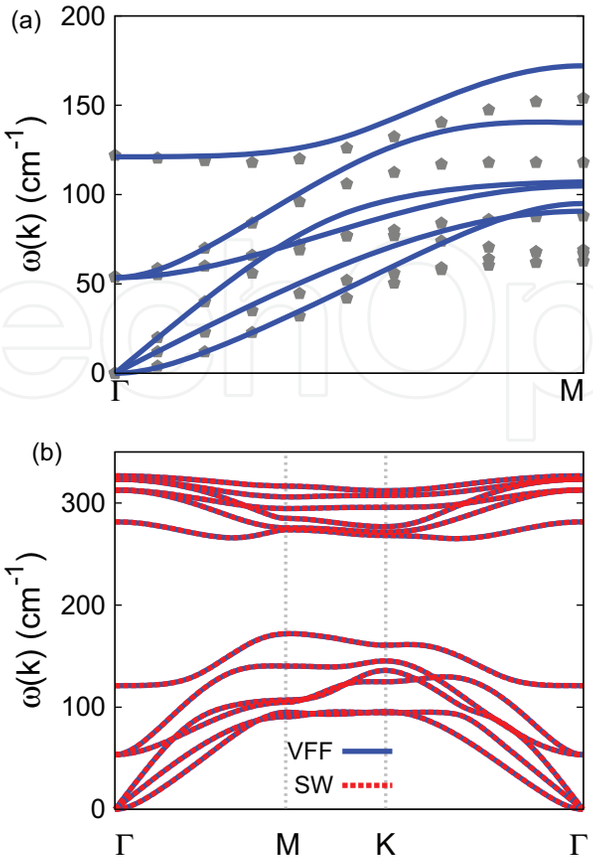

Figure 311. Phonon dispersion for the single-layer GaSe. (a) The VFF model is fitted to the six low-frequency branches along the ΓM direction. The *ab initio* results (gray pentagons) are from [115]. (b) The VFF model (blue lines) and the SW potential (red lines) give the same phonon dispersion for the GaSe along ΓMKΓ.

	A (eV)	ρ (Å)	B (Å^4)	$r_{\min}$ (Å)	$r_{\max}$ (Å)
Ga_1—Se_1	11.798	1.706	19.531	0.0	3.533
Ga_1—Ga_2	6.479	1.765	18.311	0.0	3.502

Table 607. Two-body SW potential parameters for GaSe used by GULP [8], as expressed in Eq. (3).

	K (eV)	θ_0 (°)	ρ_1 (Å)	ρ_2 (Å)	$r_{\min 12}$ (Å)	$r_{\max 12}$ (Å)	$r_{\min 13}$ (Å)	$r_{\max 13}$ (Å)	$r_{\min 23}$ (Å)	$r_{\max 23}$ (Å)
Ga_1—Se_1—Se_1	40.978	99.636	1.706	1.706	0.0	3.533	0.0	3.533	0.0	5.218
Ga_1—Se_1—Ga_2	31.031	118.092	1.765	1.706	0.0	3.502	0.0	3.533	0.0	4.985

Table 608. Three-body SW potential parameters for GaSe used by GULP [8], as expressed in Eq. (4).

	ϵ (eV)	σ (Å)	a	λ	γ	$\cos\theta_0$	A_L	B_L	p	q	Tol
Ga_1—Se_1—Se_1	1.000	1.706	2.070	40.978	1.000	−0.167	11.798	2.305	4	0	0.0
Ga_1—Ga_2—Ga_2	1.000	1.765	1.984	0.000	1.000	0.000	6.479	1.888	4	0	0.0
Ga_1—Ga_2—Se_1	1.000	0.000	0.000	31.031	1.000	−0.471	0.000	0.000	4	0	0.0

Table 609. SW potential parameters for GaSe used by LAMMPS [9], as expressed in Eqs. (9) and (10).

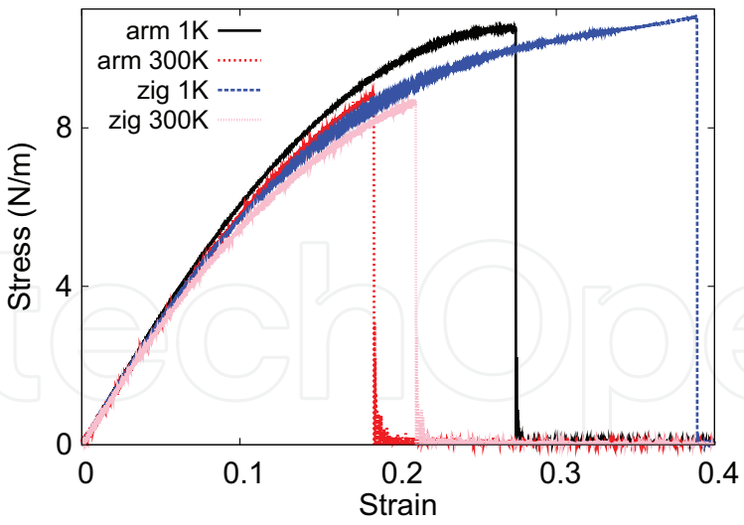

Figure 312. Stress-strain relations for the GaSe of size 100 × 100 Å. The GaSe is uniaxially stretched along the armchair or zigzag directions at temperatures 1 and 300 K.

153. InSe

Present studies on the InSe are based on first-principles calculations, and no empirical potential has been proposed for the InSe. We will thus parametrize a set of SW potential for the single-layer InSe in this section.

The structure of the single-layer InSe is shown in **Figure 290** with M=In and X=Se. The structural parameters are from the *ab initio* calculations [115]. The InSe has a bi-buckled configuration as shown in **Figure 290(b)**, where the buckle is along the zigzag direction. Two buckling layers are symmetrically integrated through the interior In-In bonds, forming a bi-buckled configuration. This structure can be determined by three independent geometrical parameters, e.g., the lattice constant 4.10 Å, the bond length $d_{\mathrm{In-Se}} = 2.69$ Å, and the bond length $d_{\mathrm{In-In}} = 2.81$ Å.

Table 610 shows the VFF model for the single-layer InSe. The force constant parameters are determined by fitting to the six low-frequency branches in the phonon dispersion along the ΓM as shown in **Figure 313(a)**. The *ab initio* calculations for the phonon dispersion are from [115].

VFF type	Bond stretching		Angle bending	
Expression	$\frac{1}{2}K_{\mathrm{In-Se}}(\Delta r)^2$	$\frac{1}{2}K_{\mathrm{In-In}}(\Delta r)^2$	$\frac{1}{2}K_{\mathrm{InSeSe}}(\Delta\theta)^2$	$\frac{1}{2}K_{\mathrm{InInSe}}(\Delta\theta)^2$
Parameter	9.812	4.185	2.090	1.227
r_0 or θ_0	2.690	2.810	99.296	118.361

The second line gives an explicit expression for each VFF term. The third line is the force constant parameters. Parameters are in the unit of eV/Å^2 for the bond stretching interaction and in the unit of eV for the angle bending interaction. The fourth line gives the initial bond length (in the unit of Å) for the bond stretching interaction and the initial angle (in the unit of degrees) for the angle bending interaction.

Table 610. The VFF model for InSe.

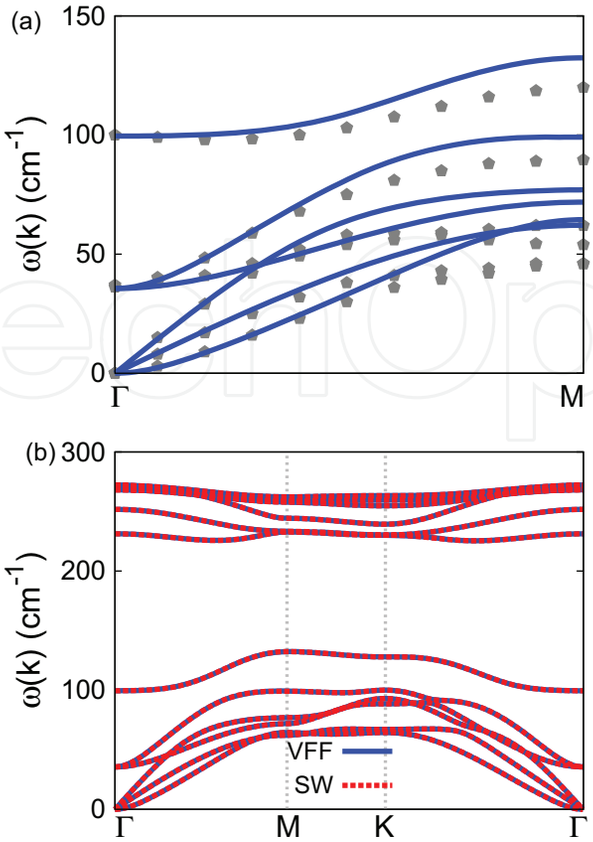

Figure 313. Phonon dispersion for the single-layer InSe. (a) The VFF model is fitted to the six low-frequency branches along the ΓM direction. The *ab initio* results (gray pentagons) are from [115]. (b) The VFF model (blue lines) and the SW potential (red lines) give the same phonon dispersion for the InSe along ΓMKΓ.

Figure 313(b) shows that the VFF model and the SW potential give exactly the same phonon dispersion, as the SW potential is derived from the VFF model.

The parameters for the two-body SW potential used by GULP are shown in **Table 611**. The parameters for the three-body SW potential used by GULP are shown in **Table 612**. Parameters for the SW potential used by LAMMPS are listed in **Table 613**.

	A (eV)	ρ (Å)	B (Å^4)	r_{min} (Å)	r_{max} (Å)
In_1—Se_1	13.281	1.822	26.181	0.0	3.797
In_1—In_2	5.414	1.661	31.174	0.0	2.890

Table 611. Two-body SW potential parameters for InSe used by GULP [8], as expressed in Eq. (3).

	K (eV)	θ_0 (°)	ρ_1 (Å)	ρ_2 (Å)	$r_{min\,12}$ (Å)	$r_{max\,12}$ (Å)	$r_{min\,13}$ (Å)	$r_{max\,13}$ (Å)	$r_{min\,23}$ (Å)	$r_{max\,23}$ (Å)
In_1—Se_1—Se_1	28.853	99.296	1.822	1.822	0.0	3.797	0.0	3.797	0.0	5.601
In_1—Se_1—In_2	19.120	118.361	1.822	1.661	0.0	3.797	0.0	3.890	0.0	5.489

Table 612. Three-body SW potential parameters for InSe used by GULP [8], as expressed in Eq. (4).

	ϵ (eV)	σ (Å)	a	λ	γ	$\cos\theta_0$	A_L	B_L	p	q	Tol
In_1—Se_1—Se_1	1.000	1.822	2.084	28.853	1.000	−0.162	13.281	2.377	4	0	0.0
In_1—In_2—In_2	1.000	1.661	2.342	0.000	1.000	0.000	5.414	4.094	4	0	0.0
In_1—In_2—Se_1	1.000	0.000	0.000	19.120	1.000	−0.475	0.000	0.000	4	0	0.0

Table 613. SW potential parameters for InSe used by LAMMPS [9], as expressed in Eqs. (9) and (10).

We use LAMMPS to perform MD simulations for the mechanical behavior of the single-layer InSe under uniaxial tension at 1.0 and 300.0 K. **Figure 314** shows the stress-strain curve for the tension of a single-layer InSe of dimension 100×100 Å. Periodic boundary conditions are applied in both armchair and zigzag directions. The single-layer InSe is stretched uniaxially along the armchair or zigzag direction. The stress is calculated without involving the actual thickness of the quasi-two-dimensional structure of the single-layer InSe. The Young's modulus can be obtained by a linear fitting of the stress-strain relation in the small strain range of [0, 0.01]. The Young's modulus is 45.7 and 45.8 N/m along the armchair and zigzag directions, respectively. The Poisson's ratio from the VFF model and the SW potential is $\nu_{xy} = \nu_{yx} = 0.30$.

There is no available value for nonlinear quantities in the single-layer InSe. We have thus used the nonlinear parameter $B = 0.5d^4$ in Eq. (5), which is close to the value of B in most materials. The value of the third-order nonlinear elasticity D can be extracted by fitting the stress-strain relation to the function $\sigma = E\epsilon + \frac{1}{2}D\epsilon^2$ with E as the Young's modulus. The values of D from the present SW potential are -81.6 and -103.5 N/m along the armchair and zigzag directions, respectively. The ultimate stress is about 9.8 N/m at the ultimate strain of 0.35 in the armchair direction at the low temperature of 1 K. The ultimate stress is about 11.9 N/m at the ultimate strain of 0.44 in the zigzag direction at the low temperature of 1 K.

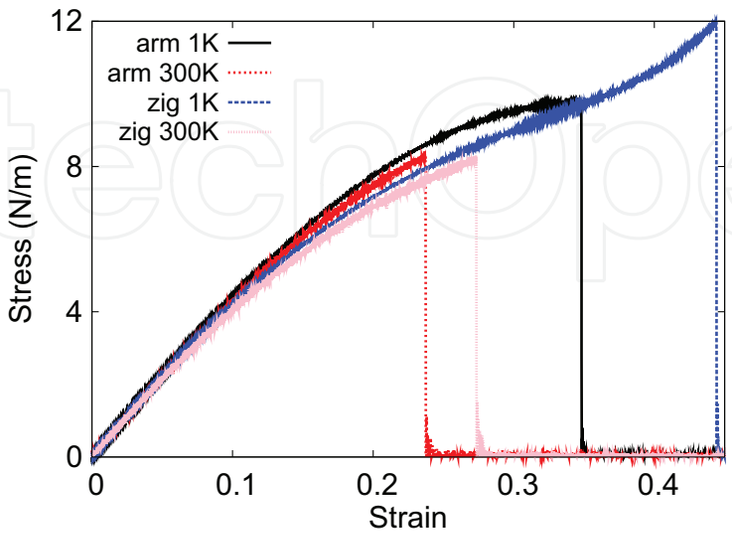

Figure 314. Stress-strain relations for the InSe of size 100×100 Å. The InSe is uniaxially stretched along the armchair or zigzag directions at temperatures 1 and 300 K.

154. BTe

Present studies on the BTe are based on first-principles calculations, and no empirical potential has been proposed for the BTe. We will thus parametrize a set of SW potential for the single-layer BTe in this section.

The structure of the single-layer BTe is shown in **Figure 290** with M=B and X=Te. The structural parameters are from the *ab initio* calculations [115]. The BTe has a bi-buckled configuration as shown in **Figure 290(b)**, where the buckle is along the zigzag direction. Two buckling layers are symmetrically integrated through the interior B-B bonds, forming a bi-buckled configuration. This structure can be determined by three independent geometrical parameters, e.g., the lattice constant 3.56 Å, the bond length $d_{\mathrm{B-Te}} = 2.31$ Å, and the bond length $d_{\mathrm{B-B}} = 1.71$ Å.

Table 614 shows the VFF model for the single-layer BTe. The force constant parameters are determined by fitting to the six low-frequency branches in the phonon dispersion along the ΓM as shown in **Figure 315(a)**. The *ab initio* calculations for the phonon dispersion are from [115]. **Figure 315(b)** shows that the VFF model and the SW potential give exactly the same phonon dispersion, as the SW potential is derived from the VFF model.

The parameters for the two-body SW potential used by GULP are shown in **Table 615**. The parameters for the three-body SW potential used by GULP are shown in **Table 616**. Parameters for the SW potential used by LAMMPS are listed in **Table 617**.

We use LAMMPS to perform MD simulations for the mechanical behavior of the single-layer BTe under uniaxial tension at 1.0 and 300.0 K. **Figure 316** shows the stress-strain curve for the tension of a single-layer BTe of dimension 100×100 Å. Periodic boundary conditions are applied in both armchair and zigzag directions. The single-layer BTe is stretched uniaxially along the armchair or zigzag direction. The stress is calculated without involving the actual thickness of the quasi-two-dimensional structure of the single-layer BTe. The Young's modulus can be obtained by a linear fitting of the stress-strain relation in the small strain range of [0, 0.01]. The Young's modulus is 130.6 and 129.7 N/m along the armchair and zigzag directions, respectively. The Poisson's ratio from the VFF model and the SW potential is $\nu_{xy} = \nu_{yx} = 0.16$.

There is no available value for nonlinear quantities in the single-layer BTe. We have thus used the nonlinear parameter $B = 0.5d^4$ in Eq. (5), which is close to the value of B in most materials.

VFF type	**Bond stretching**		**Angle bending**	
Expression	$\frac{1}{2}K_{\mathrm{B-Te}}(\Delta r)^2$	$\frac{1}{2}K_{\mathrm{B-B}}(\Delta r)^2$	$\frac{1}{2}K_{\mathrm{BTeTe}}(\Delta\theta)^2$	$\frac{1}{2}K_{\mathrm{BBTe}}(\Delta\theta)^2$
Parameter	13.287	14.502	5.466	2.515
r_0 or θ_0	2.310	1.710	100.809	117.156

The second line gives an explicit expression for each VFF term. The third line is the force constant parameters. Parameters are in the unit of eV/Å^2 for the bond stretching interaction and in the unit of eV for the angle bending interaction. The fourth line gives the initial bond length (in the unit of Å) for the bond stretching interaction and the initial angle (in the unit of degrees) for the angle bending interaction.

Table 614. The VFF model for BTe.

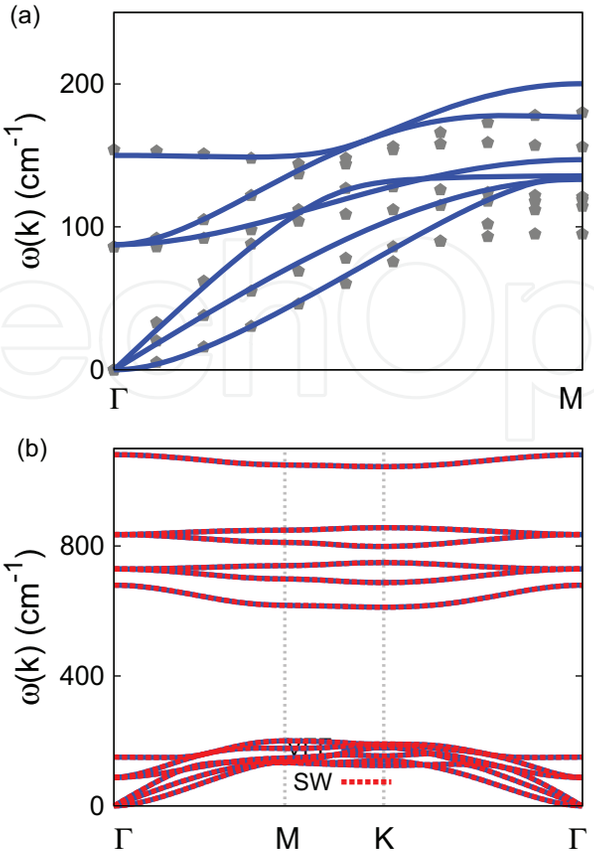

Figure 315. Phonon dispersion for the single-layer BTe. (a) The VFF model is fitted to the six low-frequency branches along the ΓM direction. The *ab initio* results (gray pentagons) are from [115]. (b) The VFF model (blue lines) and the SW potential (red lines) give the same phonon dispersion for the BTe along ΓMKΓ.

	A (eV)	ρ (Å)	B (Å^4)	r_{min} (Å)	r_{max} (Å)
B_1—Te_1	13.727	1.619	14.237	0.0	3.277
B_1—B_2	24.140	2.933	4.275	0.0	2.830

Table 615. Two-body SW potential parameters for BTe used by GULP [8], as expressed in Eq. (3).

	K (eV)	θ_0 (°)	ρ_1 (Å)	ρ_2 (Å)	$r_{min\,12}$ (Å)	$r_{max\,12}$ (Å)	$r_{min\,13}$ (Å)	$r_{max\,13}$ (Å)	$r_{min\,23}$ (Å)	$r_{max\,23}$ (Å)
B_1—Te_1—Te_1	80.622	100.809	1.619	1.619	0.0	3.277	0.0	3.277	0.0	4.863
B_1—B_2—Te_1	116.3301	117.156	2.933	1.619	0.0	2.830	0.0	3.277	0.0	4.199

Table 616. Three-body SW potential parameters for BTe used by GULP [8], as expressed in Eq. (4).

	ϵ (eV)	σ (Å)	a	λ	γ	$\cos\theta_0$	A_L	B_L	p	q	Tol
B_1—Te_1—Te_1	1.000	1.619	2.024	80.622	1.000	−0.188	13.727	2.073	4	0	0.0
B_1—B_2—B_2	1.000	2.933	0.965	0.000	1.000	0.000	24.140	0.058	4	0	0.0
B_1—B_2—Te_1	1.000	0.000	0.000	116.301	1.000	−0.456	0.000	0.000	4	0	0.0

Table 617. SW potential parameters for BTe used by LAMMPS [9], as expressed in Eqs. (9) and (10).

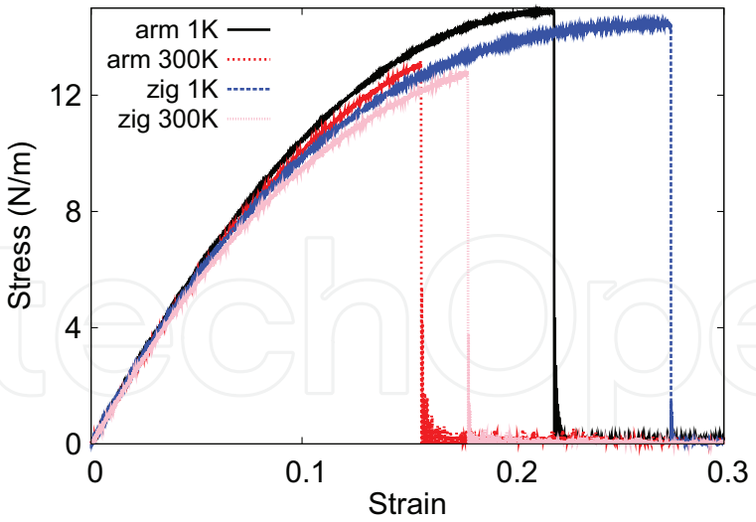

Figure 316. Stress-strain relations for the BTe of size 100 × 100 Å. The BTe is uniaxially stretched along the armchair or zigzag directions at temperatures 1 and 300 K.

The value of the third-order nonlinear elasticity D can be extracted by fitting the stress-strain relation to the function $\sigma = E\epsilon + \frac{1}{2}D\epsilon^2$ with E as the Young's modulus. The values of D from the present SW potential are -560.4 and -588.7 N/m along the armchair and zigzag directions, respectively. The ultimate stress is about 14.9 N/m at the ultimate strain of 0.22 in the armchair direction at the low temperature of 1 K. The ultimate stress is about 14.4 N/m at the ultimate strain of 0.27 in the zigzag direction at the low temperature of 1 K.

155. AlTe

Present studies on the AlTe are based on first-principles calculations, and no empirical potential has been proposed for the AlTe. We will thus parametrize a set of SW potential for the single-layer AlTe in this section.

The structure of the single-layer AlTe is shown in **Figure 290** with M=Al and X=Te. The structural parameters are from the *ab initio* calculations [115]. The AlTe has a bi-buckled configuration as shown in **Figure 290(b)**, where the buckle is along the zigzag direction. Two buckling layers are symmetrically integrated through the interior Al-Al bonds, forming a bi-buckled configuration. This structure can be determined by three independent geometrical parameters, e.g., the lattice constant 4.11 Å, the bond length $d_{\mathrm{Al-Te}} = 2.70$ Å, and the bond length $d_{\mathrm{Al-Al}} = 2.58$ Å.

Table 618 shows the VFF model for the single-layer AlTe. The force constant parameters are determined by fitting to the six low-frequency branches in the phonon dispersion along the ΓM as shown in **Figure 317(a)**. The *ab initio* calculations for the phonon dispersion are from [115]. **Figure 317(b)** shows that the VFF model and the SW potential give exactly the same phonon dispersion, as the SW potential is derived from the VFF model.

VFF type	Bond stretching		Angle bending	
Expression	$\frac{1}{2}K_{\mathrm{Al-Te}}(\Delta r)^2$	$\frac{1}{2}K_{\mathrm{Al-Al}}(\Delta r)^2$	$\frac{1}{2}K_{\mathrm{AlTeTe}}(\Delta\theta)^2$	$\frac{1}{2}K_{\mathrm{AlAlTe}}(\Delta\theta)^2$
Parameter	8.077	3.859	2.820	1.518
r_0 or θ_0	2.700	2.580	99.124	118.495

The second line gives an explicit expression for each VFF term. The third line is the force constant parameters. Parameters are in the unit of eV/Å^2 for the bond stretching interaction and in the unit of eV for the angle bending interaction. The fourth line gives the initial bond length (in the unit of Å) for the bond stretching interaction and the initial angle (in the unit of degrees) for the angle bending interaction.

Table 618. The VFF model for AlTe.

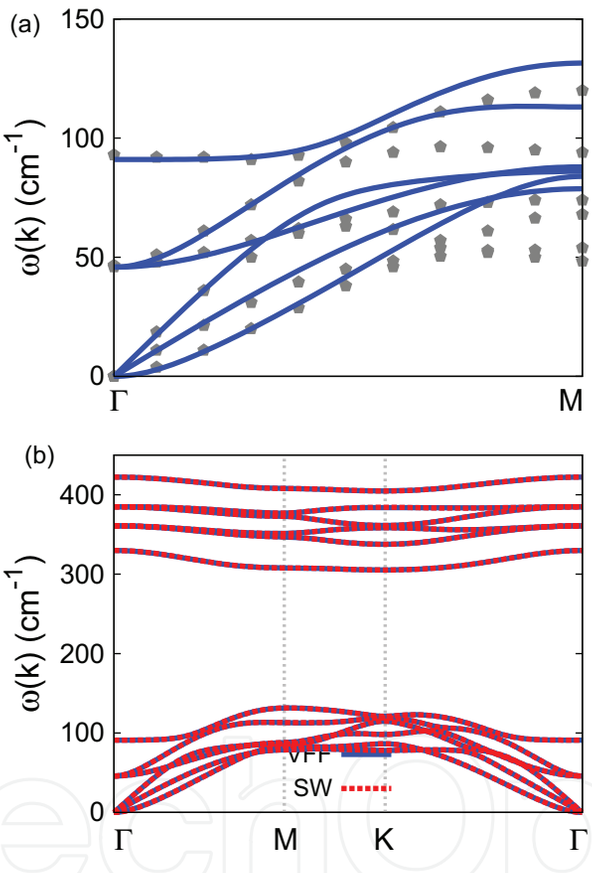

Figure 317. Phonon dispersion for the single-layer AlTe. (a) The VFF model is fitted to the six low-frequency branches along the ΓM direction. The *ab initio* results (gray pentagons) are from [115]. (b) The VFF model (blue lines) and the SW potential (red lines) give the same phonon dispersion for the AlTe along ΓMKΓ.

The parameters for the two-body SW potential used by GULP are shown in **Table 619**. The parameters for the three-body SW potential used by GULP are shown in **Table 620**. Parameters for the SW potential used by LAMMPS are listed in **Table 621**.

We use LAMMPS to perform MD simulations for the mechanical behavior of the single-layer AlTe under uniaxial tension at 1.0 and 300.0 K. **Figure 318** shows the stress-strain curve for the tension of a single-layer AlTe of dimension 100×100 Å. Periodic boundary conditions are

	A (eV)	ρ (Å)	B (Å^4)	$r_{\min}$ (Å)	$r_{\max}$ (Å)
Al_1—Te_1	10.971	1.821	26.572	0.0	3.809
Al_1—Al_2	5.523	2.002	22.154	0.0	3.716

Table 619. Two-body SW potential parameters for AlTe used by GULP [8], as expressed in Eq. (3).

	K (eV)	θ_0 (°)	ρ_1 (Å)	ρ_2 (Å)	$r_{\min 12}$ (Å)	$r_{\max 12}$ (Å)	$r_{\min 13}$ (Å)	$r_{\max 13}$ (Å)	$r_{\min 23}$ (Å)	$r_{\max 23}$ (Å)
Al_1—Te_1—Te_1	38.638	99.124	1.821	1.821	0.0	3.809	0.0	3.809	0.0	5.614
Al_1—Te_1—Al_2	29.574	118.495	2.002	1.821	0.0	3.716	0.0	3.809	0.0	5.330

Table 620. Three-body SW potential parameters for AlTe used by GULP [8], as expressed in Eq. (4).

	ϵ (eV)	σ (Å)	a	λ	γ	$\cos\theta_0$	A_L	B_L	p	q	Tol
Al_1—Te_1—Te_1	1.000	1.821	2.091	38.638	1.000	−0.159	10.971	2.415	4	0	0.0
Al_1—Al_2—Al_2	1.000	2.002	1.856	0.000	1.000	0.000	5.523	1.379	4	0	0.0
Al_1—Al_2—Te_1	1.000	0.000	0.000	29.574	1.000	−0.477	0.000	0.000	4	0	0.0

Table 621. SW potential parameters for AlTe used by LAMMPS [9], as expressed in Eqs. (9) and (10).

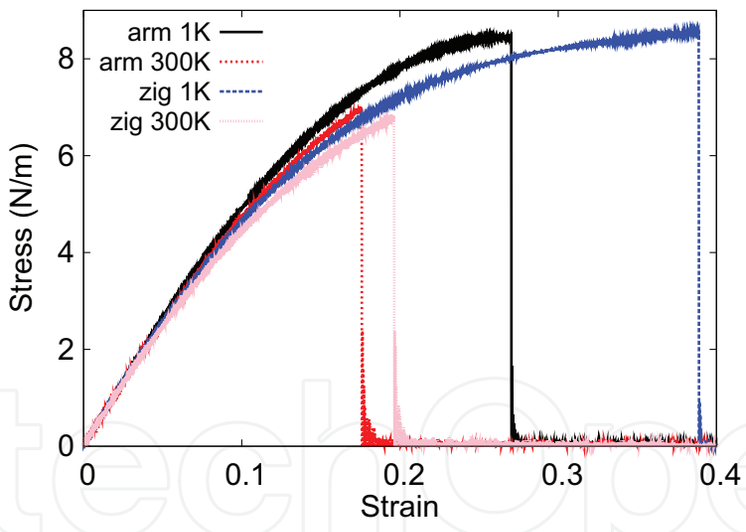

Figure 318. Stress-strain relations for the AlTe of size 100 × 100 Å. The AlTe is uniaxially stretched along the armchair or zigzag directions at temperatures 1 and 300 K.

applied in both armchair and zigzag directions. The single-layer AlTe is stretched uniaxially along the armchair or zigzag direction. The stress is calculated without involving the actual thickness of the quasi-two-dimensional structure of the single-layer AlTe. The Young's modulus can be obtained by a linear fitting of the stress-strain relation in the small strain range of [0, 0.01]. The Young's modulus is 55.8 and 54.9 N/m along the armchair and zigzag directions, respectively. The Poisson's ratio from the VFF model and the SW potential is $\nu_{xy} = \nu_{yx} = 0.24$.

There is no available value for nonlinear quantities in the single-layer AlTe. We have thus used the nonlinear parameter $B = 0.5d^4$ in Eq. (5), which is close to the value of B in most materials. The value of the third-order nonlinear elasticity D can be extracted by fitting the stress-strain relation to the function $\sigma = E\epsilon + \frac{1}{2}D\epsilon^2$ with E as the Young's modulus. The values of D from the present SW potential are -171.4 and -179.0 N/m along the armchair and zigzag directions, respectively. The ultimate stress is about 8.4 N/m at the ultimate strain of 0.27 in the armchair direction at the low temperature of 1 K. The ultimate stress is about 8.6 N/m at the ultimate strain of 0.39 in the zigzag direction at the low temperature of 1 K.

156. GaTe

Present studies on the GaTe are based on first-principles calculations, and no empirical potential has been proposed for the GaTe. We will thus parametrize a set of SW potential for the single-layer GaTe in this section.

The structure of the single-layer GaTe is shown in **Figure 290** with M=Ga and X=Te. The structural parameters are from the *ab initio* calculations [115]. The GaTe has a bi-buckled configuration as shown in **Figure 290(b)**, where the buckle is along the zigzag direction. Two buckling layers are symmetrically integrated through the interior Ga-Ga bonds, forming a bi-buckled configuration. This structure can be determined by three independent geometrical parameters, e.g., the lattice constant 4.13 Å, the bond length $d_{\mathrm{Ga-Te}} = 2.70$ Å, and the bond length $d_{\mathrm{Ga-Ga}} = 2.46$ Å.

Table 622 shows the VFF model for the single-layer GaTe. The force constant parameters are determined by fitting to the six low-frequency branches in the phonon dispersion along the ΓM as shown in **Figure 319(a)**. The *ab initio* calculations for the phonon dispersion are from [115]. **Figure 319(b)** shows that the VFF model and the SW potential give exactly the same phonon dispersion, as the SW potential is derived from the VFF model.

The parameters for the two-body SW potential used by GULP are shown in **Table 623**. The parameters for the three-body SW potential used by GULP are shown in **Table 624**. Parameters for the SW potential used by LAMMPS are listed in **Table 625**.

VFF type	**Bond stretching**		**Angle bending**	
Expression	$\frac{1}{2}K_{\mathrm{Ga-Te}}(\Delta r)^2$	$\frac{1}{2}K_{\mathrm{Ga-Ga}}(\Delta r)^2$	$\frac{1}{2}K_{\mathrm{GaTeTe}}(\Delta\theta)^2$	$\frac{1}{2}K_{\mathrm{GaGaTe}}(\Delta\theta)^2$
Parameter	7.382	4.366	2.841	1.519
r_0 or θ_0	2.700	2.460	99.781	117.978

The second line gives an explicit expression for each VFF term. The third line is the force constant parameters. Parameters are in the unit of eV/Å^2 for the bond stretching interaction and in the unit of eV for the angle bending interaction. The fourth line gives the initial bond length (in the unit of Å) for the bond stretching interaction and the initial angle (in the unit of degrees) for the angle bending interaction.

Table 622. The VFF model for GaTe.

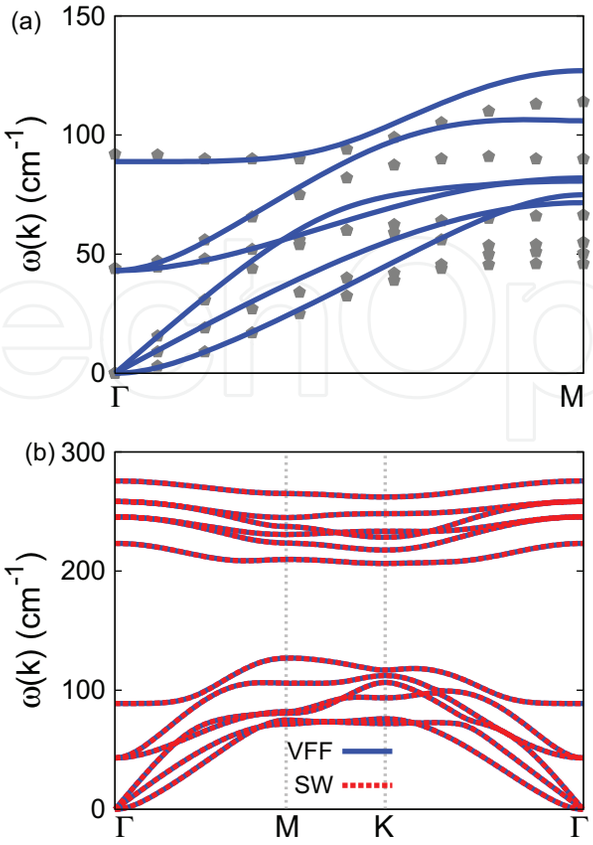

Figure 319. Phonon dispersion for the single-layer GaTe. (a) The VFF model is fitted to the six low-frequency branches along the ΓM direction. The *ab initio* results (gray pentagons) are from [115]. (b) The VFF model (blue lines) and the SW potential (red lines) give the same phonon dispersion for the GaTe along ΓMKΓ.

	A (eV)	ρ (Å)	B (Å^4)	r_{min} (Å)	r_{max} (Å)
Ga_1—Te_1	10.179	1.849	26.572	0.0	3.817
Ga_1—Ga_2	6.750	2.239	18.311	0.0	3.634

Table 623. Two-body SW potential parameters for GaTe used by GULP [8], as expressed in Eq. (3).

	K (eV)	θ_0 (°)	ρ_1 (Å)	ρ_2 (Å)	$r_{min\,12}$ (Å)	$r_{max\,12}$ (Å)	$r_{min\,13}$ (Å)	$r_{max\,13}$ (Å)	$r_{min\,23}$ (Å)	$r_{max\,23}$ (Å)
Ga_1—Te_1—Te_1	40.060	99.781	1.849	1.849	0.0	3.817	0.0	3.817	0.0	5.642
Ga_1—Te_1—Ga_2	34.354	117.978	2.239	1.849	0.0	3.634	0.0	3.817	0.0	5.238

Table 624. Three-body SW potential parameters for GaTe used by GULP [8], as expressed in Eq. (4).

We use LAMMPS to perform MD simulations for the mechanical behavior of the single-layer GaTe under uniaxial tension at 1.0 and 300.0 K. **Figure 320** shows the stress-strain curve for the tension of a single-layer GaTe of dimension 100 × 100 Å. Periodic boundary conditions are applied in both armchair and zigzag directions. The single-layer GaTe is stretched uniaxially along the armchair or zigzag direction. The stress is calculated without involving the actual

	ϵ (eV)	σ (Å)	a	λ	γ	$\cos\theta_0$	A_L	B_L	p	q	Tol
Ga_1—Te_1—Te_1	1.000	1.849	2.065	40.060	1.000	−0.170	10.179	2.274	4	0	0.0
Ga_1—Ga_2—Ga_2	1.000	2.239	1.623	0.000	1.000	0.000	6.750	0.728	4	0	0.0
Ga_1—Ga_2—Te_1	1.000	0.000	0.000	34.354	1.000	−0.469	0.000	0.000	4	0	0.0

Table 625. SW potential parameters for GaTe used by LAMMPS [9], as expressed in Eqs. (9) and (10).

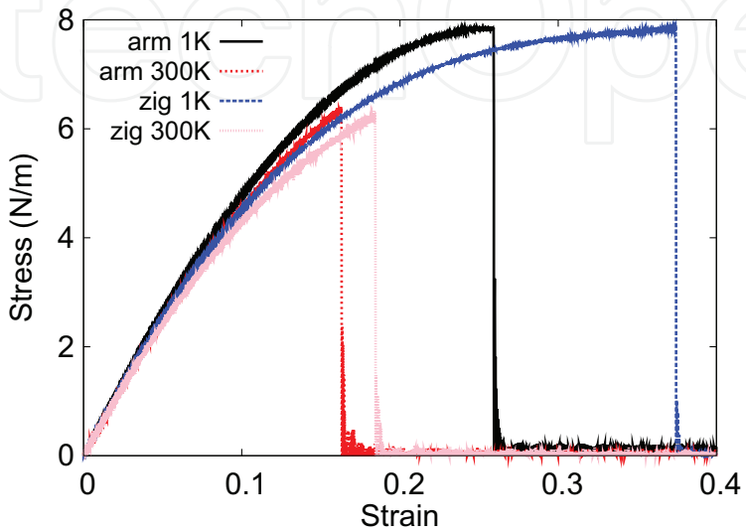

Figure 320. Stress-strain relations for the GaTe of size 100 × 100 Å. The GaTe is uniaxially stretched along the armchair or zigzag directions at temperatures 1 and 300 K.

thickness of the quasi-two-dimensional structure of the single-layer GaTe. The Young's modulus can be obtained by a linear fitting of the stress-strain relation in the small strain range of [0, 0.01]. The Young's modulus is 55.2 and 55.3 N/m along the armchair and zigzag directions, respectively. The Poisson's ratio from the VFF model and the SW potential is $\nu_{xy} = \nu_{yx} = 0.23$.

There is no available value for nonlinear quantities in the single-layer GaTe. We have thus used the nonlinear parameter $B = 0.5d^4$ in Eq. (5), which is close to the value of B in most materials. The value of the third-order nonlinear elasticity D can be extracted by fitting the stress-strain relation to the function $\sigma = E\epsilon + \frac{1}{2}D\epsilon^2$ with E as the Young's modulus. The values of D from the present SW potential are −183.2 and −195.6 N/m along the armchair and zigzag directions, respectively. The ultimate stress is about 7.8 N/m at the ultimate strain of 0.26 in the armchair direction at the low temperature of 1 K. The ultimate stress is about 7.8 N/m at the ultimate strain of 0.37 in the zigzag direction at the low temperature of 1 K.

157. InTe

Present studies on the InTe are based on first-principles calculations, and no empirical potential has been proposed for the InTe. We will thus parametrize a set of SW potential for the single-layer InTe in this section.

The structure of the single-layer InTe is shown in **Figure 290** with M=In and X=Te. The structural parameters are from the *ab initio* calculations [115]. The InTe has a bi-buckled configuration as shown in **Figure 290(b)**, where the buckle is along the zigzag direction. Two buckling layers are symmetrically integrated through the interior In-In bonds, forming a bi-buckled configuration. This structure can be determined by three independent geometrical parameters, e.g., the lattice constant 4.40 Å, the bond length $d_{\mathrm{In-Te}} = 2.89$ Å, and the bond length $d_{\mathrm{In-In}} = 2.81$ Å.

Table 626 shows the VFF model for the single-layer InTe. The force constant parameters are determined by fitting to the six low-frequency branches in the phonon dispersion along the ΓM as shown in **Figure 321(a)**. The *ab initio* calculations for the phonon dispersion are from [115]. **Figure 321(b)** shows that the VFF model and the SW potential give exactly the same phonon dispersion, as the SW potential is derived from the VFF model.

The parameters for the two-body SW potential used by GULP are shown in **Table 627**. The parameters for the three-body SW potential used by GULP are shown in **Table 628**. Parameters for the SW potential used by LAMMPS are listed in **Table 629**.

We use LAMMPS to perform MD simulations for the mechanical behavior of the single-layer InTe under uniaxial tension at 1.0 and 300.0 K. **Figure 322** shows the stress-strain curve for the tension of a single-layer InTe of dimension 100×100 Å. Periodic boundary conditions are applied in both armchair and zigzag directions. The single-layer InTe is stretched uniaxially along the armchair or zigzag direction. The stress is calculated without involving the actual thickness of the quasi-two-dimensional structure of the single-layer InTe. The Young's modulus can be obtained by a linear fitting of the stress-strain relation in the small strain range of [0, 0.01]. The Young's modulus is 40.6 and 40.9 N/m along the armchair and zigzag directions, respectively. The Poisson's ratio from the VFF model and the SW potential is $\nu_{xy} = \nu_{yx} = 0.23$.

There is no available value for nonlinear quantities in the single-layer InTe. We have thus used the nonlinear parameter $B = 0.5d^4$ in Eq. (5), which is close to the value of B in most materials. The value of the third-order nonlinear elasticity D can be extracted by fitting the stress-strain relation to the function $\sigma = E\epsilon + \frac{1}{2}D\epsilon^2$ with E as the Young's modulus. The values of D from the present SW potential are −130.4 and −142.2 N/m along the armchair and zigzag directions,

VFF type	**Bond stretching**		**Angle bending**	
Expression	$\frac{1}{2}K_{\mathrm{In-Te}}(\Delta r)^2$	$\frac{1}{2}K_{\mathrm{In-In}}(\Delta r)^2$	$\frac{1}{2}K_{\mathrm{InTeTe}}(\Delta\theta)^2$	$\frac{1}{2}K_{\mathrm{InInTe}}(\Delta\theta)^2$
Parameter	5.592	3.928	2.419	1.227
r_0 or θ_0	2.890	2.810	99.148	118.477

The second line gives an explicit expression for each VFF term. The third line is the force constant parameters. Parameters are in the unit of eV/Å^2 for the bond stretching interaction and in the unit of eV for the angle bending interaction. The fourth line gives the initial bond length (in the unit of Å) for the bond stretching interaction and the initial angle (in the unit of degrees) for the angle bending interaction.

Table 626. The VFF model for InTe.

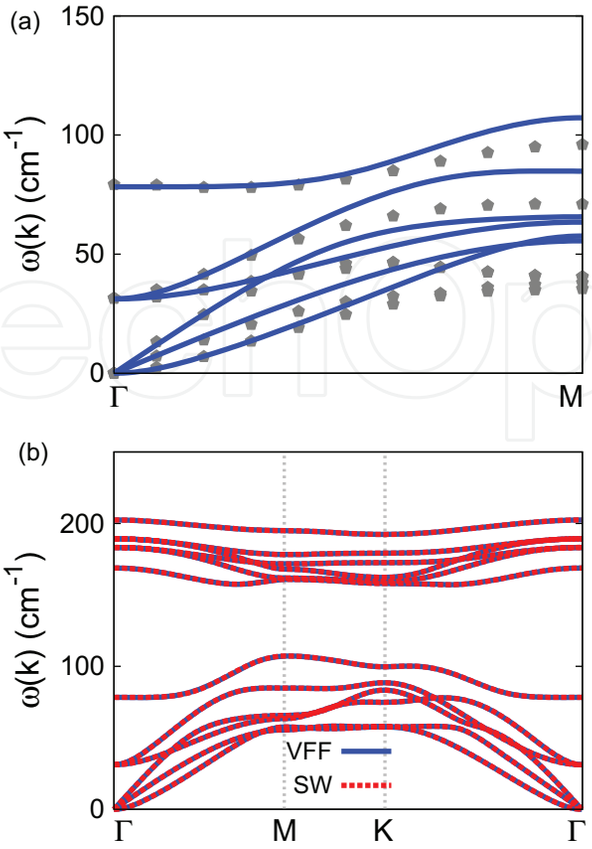

Figure 321. Phonon dispersion for the single-layer InTe. (a) The VFF model is fitted to the six low-frequency branches along the ΓM direction. The *ab initio* results (gray pentagons) are from [115]. (b) The VFF model (blue lines) and the SW potential (red lines) give the same phonon dispersion for the InTe along ΓMKΓ.

	A (eV)	ρ (Å)	B (Å^4)	$r_{\min}$ (Å)	$r_{\max}$ (Å)
In_1—Te_1	8.707	1.950	34.879	0.0	4.077
In_1—In_2	6.312	2.068	31.174	0.0	4.015

Table 627. Two-body SW potential parameters for InTe used by GULP [8], as expressed in Eq. (3).

	K (eV)	θ_0 (°)	ρ_1 (Å)	ρ_2 (Å)	$r_{\min 12}$ (Å)	$r_{\max 12}$ (Å)	$r_{\min 13}$ (Å)	$r_{\max 13}$ (Å)	$r_{\min 23}$ (Å)	$r_{\max 23}$ (Å)
In_1—Te_1—Te_1	33.178	99.148	1.950	1.950	0.0	4.077	0.0	4.077	0.0	6.011
In_1—Te_1—In_2	22.833	118.477	2.068	1.950	0.0	4.015	0.0	4.077	0.0	5.741

Table 628. Three-body SW potential parameters for InTe used by GULP [8], as expressed in Eq. (4).

	ϵ (eV)	σ (Å)	a	λ	γ	$\cos\theta_0$	A_L	B_L	p	q	Tol
In_1—Te_1—Te_1	1.000	1.950	2.090	33.178	1.000	−0.159	8.707	2.410	4	0	0.0
In_1—In_2—In_2	1.000	2.068	1.942	0.000	1.000	0.000	6.312	1.704	4	0	0.0
In_1—In_2—Te_1	1.000	0.000	0.000	22.833	1.000	−0.477	0.000	0.000	4	0	0.0

Table 629. SW potential parameters for InTe used by LAMMPS [9], as expressed in Eqs. (9) and (10).

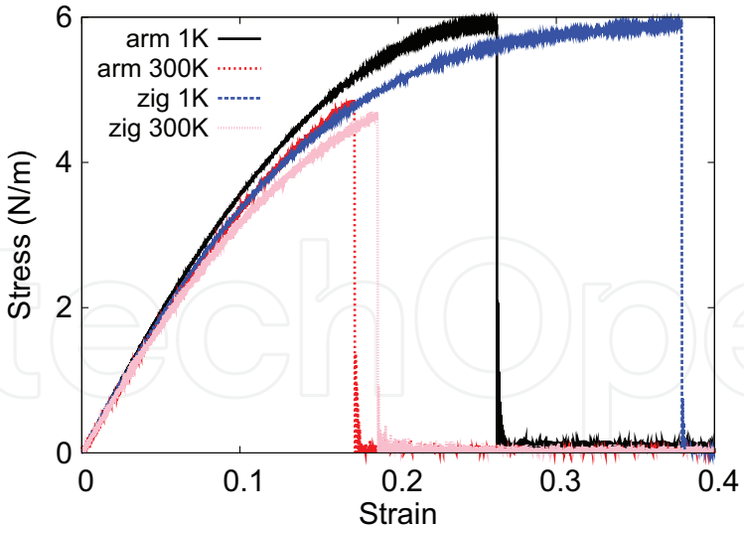

Figure 322. Stress-strain relations for the InTe of size 100 × 100 Å. The InTe is uniaxially stretched along the armchair or zigzag directions at temperatures 1 and 300 K.

respectively. The ultimate stress is about 5.9 N/m at the ultimate strain of 0.26 in the armchair direction at the low temperature of 1 K. The ultimate stress is about 5.9 N/m at the ultimate strain of 0.38 in the zigzag direction at the low temperature of 1 K.

158. Borophene

Most existing theoretical studies on the monolayer of boron atoms (borophene) are based on the first-principles calculations. The ReaxFF force field model was developed for the borophene recently [117]. The present authors have provided the VFF model and the SW potential to describe the atomic interaction within the borophene [14], which includes the second-nearest-neighboring interactions. In the present work, we present a more efficient SW potential with only the first-nearest-neighboring interactions.

The structure of the borophene is shown in **Figure 323**, with structural parameters from the *ab initio* calculations [116]. Borophene has a puckered configuration as shown in **Figure 323(b)**, where the pucker is perpendicular to the x-direction. The height of the pucker is $h = 0.911$ Å, which is the distance between the top chain and the bottom chain along the out-of-plane z-direction. The two lattice bases are $a_1 = 2.866$ Å and $a_2 = 1.614$ Å for the in-plane rectangular unit cell. There are two inequivalent boron atoms in the unit cell. Boron atoms are categorized into the top chain and the bottom chain. The top chain includes atoms like 1, 4, and 7. The bottom chain includes atoms like 2, 3, 5, and 6.

Table 630 shows four VFF terms for the borophene; two of which are the bond stretching interaction shown by Eq. (1), while the other two terms are the angle bending interaction shown by Eq. (2). These force constant parameters are determined by fitting to the three acoustic branches in the phonon dispersion along the ΓX as shown in **Figure 324(a)**. The *ab initio* calculations for the phonon dispersion are from [116]. Similar phonon dispersion can also

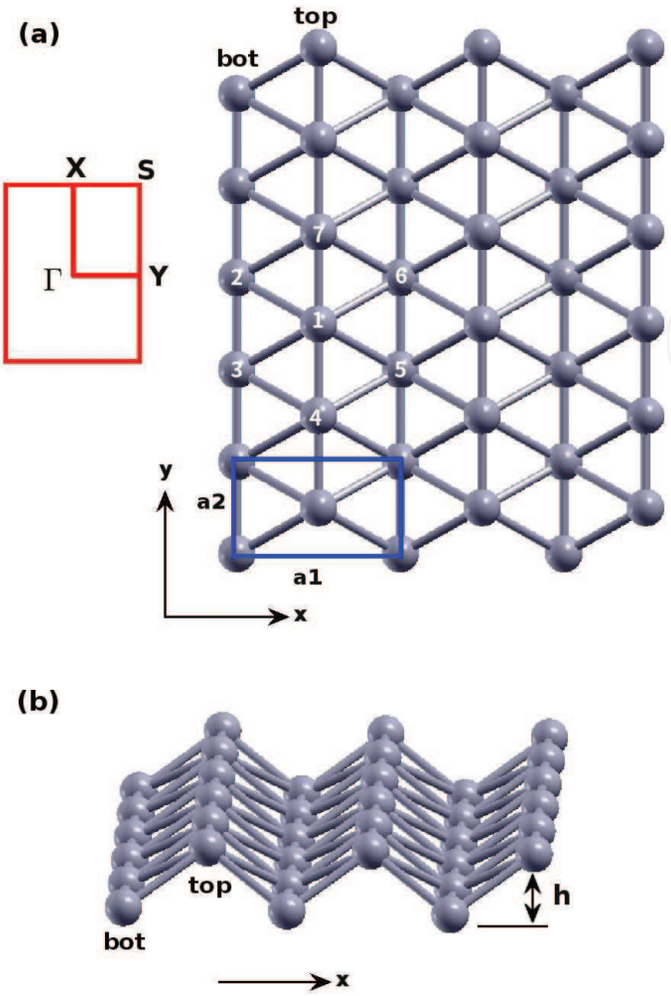

Figure 323. Structure for borophene. (a) Top view. Atoms are categorized into top chains and bottom chains. The top chain includes atoms like 1, 4, and 7. The bottom chain includes atoms like 2, 3, 5, and 6. The unit cell is shown by blue rectangle. The first Brillouin zone is shown by red rectangle on the left. (b) Perspective view illustrates the puckered configuration, with h as the distance between the top and bottom chains along the out-of-plane z-direction. The pucker is perpendicular to the x-axis and is parallel with the y-axis.

VFF type	**Bond stretching**		**Angle bending**	
Expression	$\frac{1}{2}K_{14}(\Delta r_{14})^2$	$\frac{1}{2}K_{12}(\Delta r_{12})^2$	$\frac{1}{2}K_{134}(\Delta\theta_{134})^2$	$\frac{1}{2}K_{135}(\Delta\theta_{135})^2$
Parameter	20.673	6.025	3.523	4.651
r_0 or θ_0	1.614	1.880	64.581	99.318

The second line gives an explicit expression for each VFF term, where atom indexes are from **Figure 323(a)**. The third line is the force constant parameters. Parameters are in the unit of eV/Å^2 for the bond stretching interaction and in the unit of eV for the angle bending interaction. The fourth line gives the initial bond length (in the unit of Å) for the bond stretching interaction and the initial angle (in the unit of degrees) for the angle bending interaction. The angle θ_{ijk} has atom i as the apex.

Table 630. The VFF model for borophene.

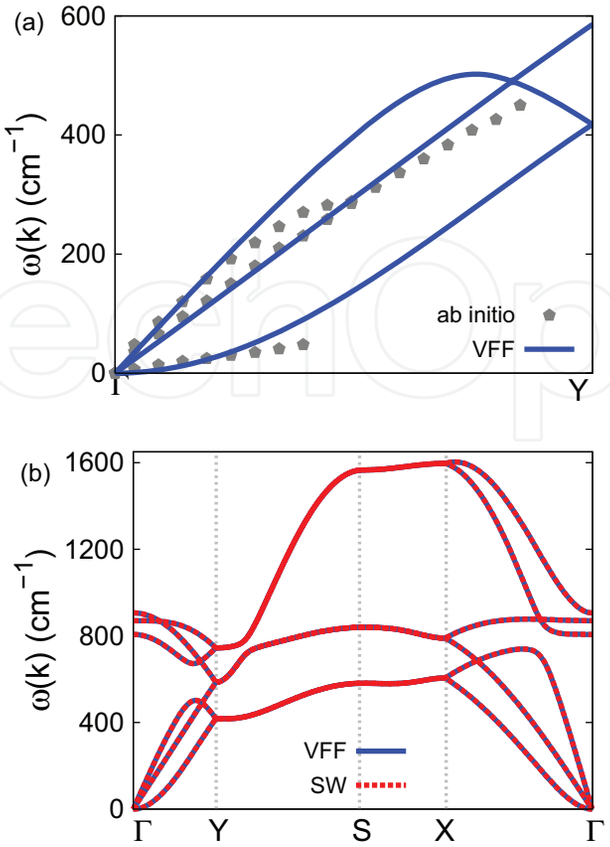

Figure 324. Phonon dispersion for the borophene. (a) The VFF model is fitted to the three acoustic branches in the long wave limit along the ΓY direction. The *ab initio* results (gray pentagons) are from [116]. (b) The VFF model (blue lines) and the SW potential (red lines) give the same phonon dispersion for the borophene along ΓYSXΓ.

be found in other *ab initio* calculations [118]. **Figure 324(b)** shows that the VFF model and the SW potential give exactly the same phonon dispersion, as the SW potential is derived from the VFF model.

The parameters for the two-body SW potential used by GULP are shown in **Table 631**. The parameters for the three-body SW potential used by GULP are shown in **Table 632**. Parameters for the SW potential used by LAMMPS are listed in **Table 633**. We note that 12 atom types have been introduced for the simulation of borophene using LAMMPS, because the angles around atom 1 in **Figure 323(a)** are not distinguishable in LAMMPS. We thus need to differentiate these angles by assigning these six neighboring atoms (2, 3, 4, 5, 6, 7) with different atom types.

	A (eV)	ρ (Å)	B (Å^4)	$r_{\min}$ (Å)	$r_{\max}$ (Å)
r_{14}	8.974	0.971	3.393	0.0	2.240
r_{12}	2.098	0.618	6.246	0.0	2.419

The quantity (r_{ij}) in the first line lists one representative term for the two-body SW potential between atoms i and j. Atom indexes are from **Figure 323(a)**.

Table 631. Two-body SW potential parameters for borophene used by GULP [8], as expressed in Eq. (3).

	K (eV)	θ_0 (°)	ρ_1 (Å)	ρ_2 (Å)	$r_{\min 12}$ (Å)	$r_{\max 12}$ (Å)	$r_{\min 13}$ (Å)	$r_{\max 13}$ (Å)	$r_{\min 23}$ (Å)	$r_{\max 23}$ (Å)
θ_{134}	32.074	64.581	0.971	0.618	0.0	2.240	0.0	2.419	0.0	2.419
θ_{135}	23.668	99.318	0.618	0.618	0.0	2.419	0.0	2.410	2.240	3.047

The first line (θ_{ijk}) presents one representative term for the three-body SW potential. The angle θ_{ijk} has the atom i as the apex. Atom indexes are from **Figure 323(a)**.

Table 632. Three-body SW potential parameters for borophene used by GULP [8], as expressed in Eq. (4).

	ϵ (eV)	σ (Å)	a	λ	γ	$\cos\theta_0$	A_L	B_L	p	q	Tol
B_1—B_5—B_5	1.000	0.971	2.307	0.000	1.000	0.000	8.974	3.817	4	0	0.0
B_1—B_2—B_2	1.000	0.618	3.914	0.000	1.000	0.000	2.098	42.820	4	0	0.0
B_1—B_2—B_5	1.000	0.000	0.000	32.074	1.000	0.429	0.000	0.000	4	0	0.0
B_1—B_2—B_4	1.000	0.000	0.000	23.668	1.000	−0.162	0.000	0.000	4	0	0.0

Atom types in the first column are displayed in **Figure 325**.

Table 633. SW potential parameters for borophene used by LAMMPS [9], as expressed in Eqs. (9) and (10).

Figure 325 shows that 12 atom types are necessary for the purpose of differentiating all 6 neighbors around 1 B atom.

Figure 326 shows the stress-strain relations for the borophene of size 100 × 100 Å. The structure is uniaxially stretched in the x or y directions at 1 and 300 K. The Young's modulus is 162.7 and 385.0 N/m in the x and y directions, respectively, at 1 K, which is obtained by linear fitting of the stress-strain relations in [0, 0.01]. These values are in good agreement with the *ab initio* results at 0 K temperature, e.g., 170 and 398 N/m in [119], or 166 and 389 N/m in [116], or 163 and 399 N/m in [120]. Previous *ab initio* calculations obtained negative Poisson's ratio for the uniaxial stretching of the borophene in the x and y directions, e.g., −0.02 and −0.04 in Refs 119 and 116. The Poisson's ratio from the present SW potential is −0.03 and −0.07 along the x and y directions, respectively, which is quite comparable with the *ab initio* results.

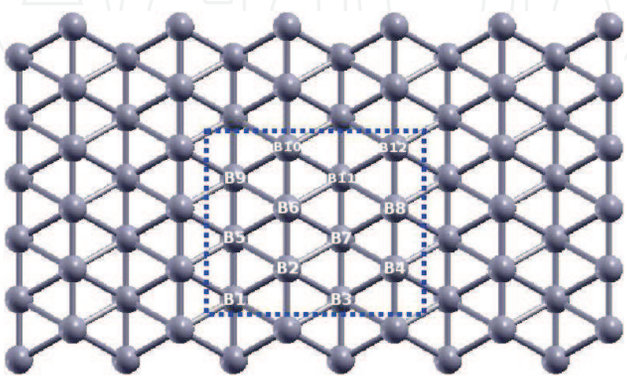

Figure 325. Twelve atom types are introduced for the boron atoms in the borophene. Atoms B_1, B_3, B_5, B_7, B_9, and B_{11} are from the bottom group. Atoms B_2, B_4, B_6, B_8, B_{10}, and B_{12} are from the top group.

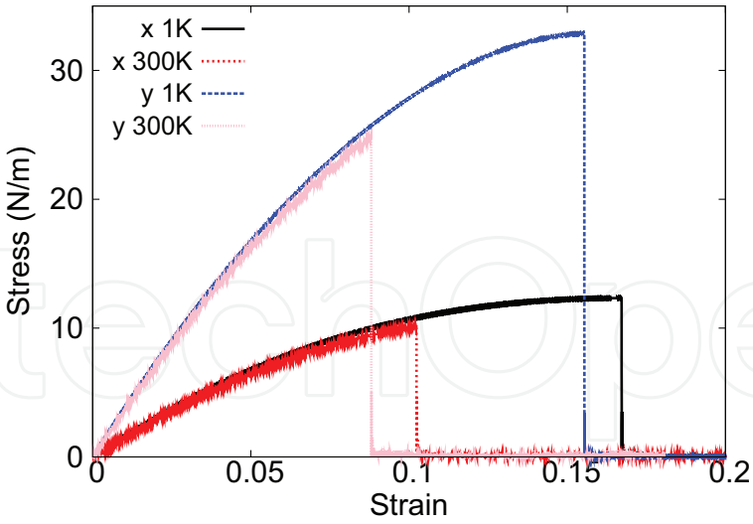

Figure 326. Stress-strain relations for the borophene of size 100 × 100 Å. The borophene is uniaxially stretched along the x or y directions at temperatures 1 and 300 K.

The third-order nonlinear constant (D) can be obtained by fitting the stress-strain relation to the function $\sigma = E\epsilon + \frac{1}{2}D\epsilon^2$, with E as the Young's modulus. The obtained values of D are -1100.1 and -2173.6 N/m in the x and y directions, respectively. The ultimate stress is about 12.3 N/m at the critical strain of 0.17 in the x-direction at the low temperature of 1 K, which agree quite well with the *ab initio* results at 0 K [116, 118, 120]. The ultimate stress is about 32.9 N/m at the critical strain of 0.16 in the y-direction at the low temperature of 1 K, which are quite comparable with *ab initio* results at 0 K [116, 118, 120].

159. Conclusion remarks

As a final remark, we note some major advantages and deficiencies for the SW potential parameters provided in the present work. On the one hand, the key feature of the SW potential is its high efficiency, which is maintained by using minimum potential parameters in the present work, so the interaction range is limited to the first-nearest-neighboring atoms. As a result, the present SW potential parameters are of high computational efficiency. On the other hand, since the interaction is limited to short-range, the optical branches in the phonon spectrum are typically overestimated by the present SW potential. It is because we have ignored the long-range interactions, which contribute mostly to the acoustic phonon branches while have neglectable contribution to the optical phonon branches. The short-range interaction has thus been strengthened to give an accurate description for the acoustic phonon branches and the elastic properties, which leads to the overestimation of the optical phonon branches as a trade-off. Hence, there will be systematic overestimation for simulating optical processes using the present SW parameters.

We also note that the mathematical form of the SW potential is not suitable for the atomic-thick planar structures, such as graphene and b-BN, because the SW potential is not able to resist the bending motion of these real planar crystals [121, 122].

In conclusion, we have provided the SW potential parameters for 156 layered crystals. The supplemental resources for all simulations in the present work are available online in [1], including a Fortran code to generate crystals' structures, files for molecular dynamics simulations using LAMMPS, files for phonon calculation with the SW potential using GULP, and files for phonon calculations with the valence force field model using GULP.

Acknowledgements

The work is supported by the Recruitment Program of Global Youth Experts of China, the National Natural Science Foundation of China (NSFC) under Grant No. 11504225, and the start-up funding from Shanghai University.

Author details

Jin-Wu Jiang* and Yu-Ping Zhou

*Address all correspondence to: jiangjinwu@shu.edu.cn

Shanghai Institute of Applied Mathematics and Mechanics, Shanghai Key Laboratory of Mechanics in Energy Engineering, Shanghai University, Shanghai, People's Republic of China

References

[1] Supplemental resources include the Fortran code to generate crystals' structures, molecular dynamics simulation files using LAMMPS, phonon calculation files with the Stillinger-Weber potential using gulp, and phonon calculation files with the valence force field model using gulp. These supplemental resources are available from http://jiangjinwu.org/sw

[2] Geim AK, Grigorieva IV. Van der waals heterostructures. Nature. 2013;**499**:419

[3] Yu PY. Fundamentals of Semiconductors. Springer: New York; 2010

[4] Stillinger FH, Weber TA. Computer simulation of local order in condensed phases of silicon. Physical Review B. 1985;**3**:5262

[5] Tersoff J. New empirical model for the structural properties of silicon. Physical Review Letters. 1986;**56**:632–635

[6] Brenner DW et al. A second-generation reactive empirical bond order (REBO) potential energy expression for hydrocarbons. Journal of Physics: Condensed Matter. 2002;**14**:783–802

[7] Jiang JW. Parametrization of Stillinger-Weber potential based on valence force field model: Application to single-layer MoS_2 and black phosphorus. Nanotechnology. 2015;**26**:315706

[8] Gale JD. GULP: A computer program for the symmetry-adapted simulation of solids. Journal of the Chemical Society, Faraday Transactions. 1997;**93**:629–637. Available from: https://projects.ivec.org/gulp/

[9] LAMMPS. http://www.cs.sandia.gov/~sjplimp/lammps.html. 2012

[10] Stukowski A. Visualization and analysis of atomistic simulation data with OVITO—The open visualization tool. Modelling and Simulation in Materials Science and Engineering. 2010;**18**:015012

[11] Kokalj A. Computer graphics and graphical user interfaces as tools in simulations of matter at the atomic scale. Computational Materials Science. 2003;**28**:155–168

[12] Ataca C, Sahin H, Ciraci S. Stable, single-layer MX_2 transition-metal oxides and dichalcogenides in a honeycomb-like structure. Journal of Physical Chemistry C. 2012;**116**: 8983–8999

[13] Jiang JW, Park HS, Rabczuk T. Molecular dynamics simulations of single-layer molybdenum disulphide (MoS_2): Stillinger-Weber parametrization, mechanical properties, and thermal conductivity. Journal of Applied Physics. 2013;**114**:064307

[14] Zhou YP, Jiang JW. Molecular dynamics simulations of mechanical properties for borophene: Parameterization of valence force field model and Stillinger-Weber potential. Scientific Reports. 2017;**7**:45516

[15] Feldman JL. Analysis of normal-state phonon properties of 2H-$TaSe_2$ and $NbSe_2$. Physical Review B. 1982;**25**:7132

[16] Isaacs EB, Marianetti CA. Electronic correlations in monolayer VS_2. Physical Review B. 2016;**94**:035120

[17] Zhuang HL, Johannes MD, Blonsky MN, Hennig RG. Computational prediction and characterization of single-layer CrS_2. Applied Physics Letters. 2014;**104**:022116

[18] Cakir D, Peeters FM, Sevik C. Mechanical and thermal properties of H-MX_2 (M=Cr, Mo, W; X=O, S, Se, Te) monolayers: A comparative study. Applied Physics Letters. 2014;**104**: 203110

[19] Alyoruk MM, Aierken Y, Cakir D, Peeters FM, Sevik C. Promising piezoelectric performance of single layer transition-metal dichalcogenides and dioxides. Journal of Physical Chemistry C. 2015;**119**:23231–23237

[20] Jiang JW, Wang BS, Wang JS, Park HS. A review on flexural mode of graphene: Lattice dynamics, thermal conduction, thermal expansion, elasticity, and nanomechanical resonance. Journal of Physics: Condensed Matter. 2015;**27**:083001

[21] FlcMullan WG. Lattice dynamics of layered transition metal dichalcogenides [Thesis]. 1983

[22] Wakabayashi N, Smith HG, Nicklow RM. Lattice dynamics of hexagonal MoS_2 studied by neutron scattering. Physical Review B. 1975;**12**:659–663

[23] Liang T, Phillpot SR, Sinnott SB. Parametrization of a reactive many-body potential for Mo-S systems. Physical Review B. 2009;**79**:245110

[24] Varshney V et al. MD simulations of molybdenum disulphide (MoS_2): Force-field parameterization and thermal transport behavior. Computational Materials Science. 2010;**48**: 101–108

[25] Kandemir A, Yapicioglu H, Kinaci A, Cagin T, Sevik C. Thermal transport properties of MoS_2 and $MoSe_2$ monolayers. Nanotechnology. 2016;**27**:055703

[26] Molina-Sánchez A, Wirtz L. Phonons in single-layer and few-layer MoS_2 and WS_2. Physical Review B. 2011;**84**:155413

[27] Cooper RC et al. Nonlinear elastic behavior of two-dimensional molybdenum disulfide. Physical Review B. 2013;**87**:035423

[28] Cooper RC et al. Erratum: Nonlinear elastic behavior of two-dimensional molybdenum disulfide (Physical Review B: Condensed Matter and Materials Physics. (2013)87(035423)). Physical Review B. 2013;**87**:079901

[29] Bertolazzi S, Brivio J, Kis A. Stretching and breaking of ultrathin MoS_2. ACS Nano. 2011;**5**: 9703–9709

[30] Horzum S et al. Phonon softening and direct to indirect band gap crossover in strained single-layer $MoSe_2$. Physical Review B. 2013;**87**:125415

[31] Huang W, Da H, Liang G. Thermoelectric performance of MX_2 (M=Mo, W; X=S, Se) monolayers. Journal of Applied Physics. 2013;**113**:104304

[32] Sevik C. Assessment on lattice thermal properties of two-dimensional honeycomb structures: Graphene, H-BN, H-MoS_2, and H-$MoSe_2$. Physical Review B. 2014;**89**:035422

[33] Kumar S, Schwingenschlogl U. Thermoelectric response of bulk and monolayer $MoSe_2$ and WSe_2. Chemistry of Materials. 2015;**27**:1278–1284

[34] Huang Z, Zhang W, Zhang W. Computational search for two-dimensional MX_2 semiconductors with possible high electron mobility at room temperature. Materials. 2016; **9**:716

[35] Li J, Medhekar NV, Shenoy VB. Bonding charge density and ultimate strength of monolayer transition metal dichalcogenides. Journal of Physical Chemistry C. 2013;**117**: 15842–15848

[36] Guo H et al. Double resonance Raman modes in monolayer and few-layer $MoTe_2$. Physical Review B. 2015;**91**:205415

[37] Kan M, Nam HG, Lee YH, Sun Q. Phase stability and Raman vibration of the molybdenum ditelluride ($MoTe_2$) monolayer. Physical Chemistry Chemical Physics. 2015;**17**:14866–14871

[38] Gu X, Yang R. Phonon transport in single-layer transition metal dichalcogenides: A first-principles study. Applied Physics Letters. 2014;**105**:131903

[39] Huang W, Luo X, Gan CK, Quek SY, Liang G. Theoretical study of thermoelectric properties of few-layer MoS_2 and WSe_2. Physical Chemistry Chemical Physics. 2014;**16**: 10866-10874

[40] Norouzzadeh P, Singh DJ. Thermal conductivity of single-layer WSe_2 by a Stillinger-Weber potential. Nanotechnology. 2017;**28**:075708

[41] Zhou WX, Chen KQ. First-principles determination of ultralow thermal conductivity of monolayer WSe_2. Scientific Reports. 2015;**5**:15070

[42] Torun E et al. Anisotropic electronic, mechanical, and optical properties of monolayer WTe_2. Journal of Applied Physics. 2016;**119**:074307

[43] Mar A, Jobic S, Ibers JA. Metal-metal vs tellurium-tellurium bonding in WTe_2 and its ternary variants $TaIrTe_4$ and $NbIrTe_4$. Journal of the American Chemical Society. 1992;**114**: 8963–8971

[44] Dawson WG, Bullett DW. Electronic structure and crystallography of $MoTe_2$ and WTe_2. Journal of Physics C: Solid State Physics. 1987;**20**:6159

[45] Brown BE. The crystal structures of WTe_2 and high-temperature $MoTe_2$. Acta Crystallographica. 1996;**20**:268–274

[46] Jana MK et al. A combined experimental and theoretical study of the electronic and vibrational properties of bulk and few-layer Td-WTe_2. Journal of Physics: Condensed Matter. 2015;**27**:285401

[47] Jiang YC, Gao J, Wang L. Raman fingerprint for semi-metal WTe_2 evolving from bulk to monolayer. Scientific Reports. 2016;**6**:19624

[48] Yu L, Yan Q, Ruzsinszky A. Negative Poissons ratio in 1T-type crystalline two-dimensional transition metal dichalcogenides. Preprint at http://arxiv.org/abs/1701.06529. 2017

[49] Li Y, Kang J, Li J. Indirect-to-direct band gap transition of the ZrS_2 monolayer by strain: First-principles calculations. RSC Advances. 2014;**4**:7396–7401

[50] Ding G, Gao GY, Huang Z, Zhang W, Yao K. Thermoelectric properties of mono-layer MSe_2 (M=Zr, Hf): Low lattice thermal conductivity and a promising figure of merit. Nanotechnology. 2016;**27**:375703

[51] Zhang W, Huang Z, Zhang W, Li Y. Two-dimensional semiconductors with possible high room temperature mobility. Nano Research. 2014;**7**:1731–1737

[52] Jiang JW, Chang T, Guo X, Park HS. Intrinsic negative Poisson's ratio for single-layer graphene. Nano Letters. 2016;**16**:5286–5290

[53] Kang J, Sahin H, Peeters FM. Mechanical properties of monolayer sulphides: A comparative study between MoS_2, HfS_2 and TiS_3. Physical Chemistry Chemical Physics. 2015;**17**:27742

[54] Chen J. Phonons in bulk and monolayer HfS_2 and possibility of phonon-mediated superconductivity: A first-principles study. Solid State Communications. 2016;**237-238**:14

[55] Zhu Z, Tomanek D. Semiconducting layered blue phosphorus: A computational study. Physical Review Letters. 2014;**112**:176802

[56] Kaneta C, Katayama-Yoshida H, Morita A. Lattice dynamics of black phosphorus. Solid State Communications. 1982;**44**:613–617

[57] Du Y, Ouyang C, Shi S, Lei M. Ab initio studies on atomic and electronic structures of black phosphorus. Journal of Applied Physics. 2010;**107**:093718

[58] Qin G et al. Hinge-like structure induced unusual properties of black phosphorus and new strategies to improve the thermoelectric performance. Scientific Reports. 2014;**4**:6946

[59] Elahi M, Khaliji K, Tabatabaei SM, Pourfath M, Asgari R. Modulation of electronic and mechanical properties of phosphorene through strain. Physical Review B. 2014;**91**:115412

[60] Ong ZY, Cai Y, Zhang G, Zhang YW. Strong thermal transport anisotropy and strain modulation in single-layer phosphorene. Journal of Physical Chemistry C. 2014;**118**: 25272–25277

[61] Aierken Y, Cakir D, Sevik C, Peeters FM. Thermal properties of black and blue phosphorenes from a first-principles quasiharmonic approach. Physical Review B. 2015;**92**: 081408

[62] Jiang JW. Thermal conduction in single-layer black phosphorus: Highly anisotropic? Nanotechnology. 2015;**26**:055701

[63] Jain A, McGaughey AJH. Strongly anisotropic in-plane thermal transport in single-layer black phosphorene. Scientific Reports. 2015;**5**:8501

[64] Zhang S et al. Semiconducting group 15 monolayers: A broad range of band gaps and high carrier mobilities. Angewandte Chemie International Edition. 2016;**55**:1666–1669

[65] Qiao J, Kong X, Hu ZX, Yang F, Ji W. High-mobility transport anisotropy and linear dichroism in few-layer black phosphorus. Nature Communications. 2014;**5**:4475

[66] Wei Q, Peng X. Superior mechanical flexibility of phosphorene and few-layer black phosphorus. Applied Physics Letters. 2014;**104**:251915

[67] Jiang JW, Park HS. Negative Poisson's ratio in single-layer black phosphorus. Nature Communications. 2014;**5**:4727

[68] Midtvedt D, Croy A. Comment on 'Parametrization of Stillinger-Weber potential based on valence force field model: Application to single-layer MoS_2 and black phosphorous'. Nanotechnology. 2016:**27**:238001

[69] Jiang JW. Origin of hinge-like mechanism in single-layer black phosphorus: The angle-angle cross interaction. Preprint at http://arxiv.org/abs/1605.02566v1. 2016

[70] Xu Y et al. First-principle calculations of phononic, electronic and optical properties of monolayer arsenene and antimonene allotropes. Preprint at http://arxiv.org/abs/1604.034 22v1. 2016

[71] Zhang Z et al. Manifestation of unexpected semiconducting properties in few-layer orthorhombic arsenene. Applied Physics Express. 2015;**8**:055201

[72] Kamal C, Ezawa M. Arsenene: Two-dimensional buckled and puckered honeycomb arsenic systems. Physical Review B. 2015;**91**:085423

[73] Zeraati M, Allaei SMV, Sarsari IA, Pourfath M, Donadio D. Highly anisotropic thermal conductivity of arsenene: An ab initio study. Physical Review B. 2015;**93**:085424

[74] Yang M, Liu WM. Ultra-high mechanical stretchability and controllable topological phase transitions in two-dimensional arsenic. Preprint at http://arxiv.org/abs/1501.04350v1. 2016

[75] Wang G, Pandey R, Karna SP. Atomically thin group V elemental films: Theoretical investigations of antimonene allotropes. ACS Applied Materials and Interfaces. 2015;**7**: 11490–11496

[76] Zheng G, Jia Y, Gao S, Ke SH. Comparative study of thermal properties of group-VA monolayers with buckled and puckered honeycomb structures. Physical Review B. 2016;**94**:155448

[77] Akturk E, Akturk OU, Ciraci S. Single and bilayer bismuthene: Stability at high temperature and mechanical and electronic properties. Physical Review B. 2016;**94**:014115

[78] Kamal C, Chakrabarti A, Ezawa M. Direct band gaps in group IV-VI monolayer materials: Binary counterparts of phosphorene. Physical Review B. 2016;**93**:125428

[79] Soler JM et al. The SIESTA method for ab initio order-N materials simulation. Journal of Physics: Condensed Matter. 2002;**14**:2745

[80] Perdew JP, Burke K, Ernzerhof M. Generalized gradient approximation made simple. Physical Review Letters. 1996;**77**:3865

[81] Qin G et al. Diverse anisotropy of phonon transport in two-dimensional group IV-VI compounds: A comparative study. Nanoscale. 2016;**8**:11306

[82] Zhang LC et al. SnSe monolayer: Super-flexible, auxetic material with ultralow lattice thermal conductivity and ultrahigh hole mobility. Preprint at http://arxiv.org/abs/1505.04590. 2016

[83] Chen Y, Sun Q, Jena P. Site monolayers: Si-based analogues of phosphorene. Journal of Materials Chemistry C. 2016;**4**:6353–6361

[84] Ge XJ, Yao KL, Lu JT. Comparative study of phonon spectrum and thermal expansion of graphene, silicene, germanene, and blue phosphorene. Physical Review B. 2016;**94**:165433

[85] Ince A, Erkoc S. Silicene nanoribbons: Molecular-dynamics simulations. Computational Materials Science. 2011;**50**:865–870

[86] Baskes MI. Modified embedded-atom potentials for cubic materials and impurities. Physical Review: B. 1992;**46**:2727

[87] Pei QX, Zhang YW, Sha ZD, Shenoy VB. Tuning the thermal conductivity of silicene with tensile strain and isotopic doping: A molecular dynamics study. Journal of Applied Physics. 2013;**114**:033526

[88] Justo JF, Bazant MZ, Kaxiras E, Bulatov VV, Yip S. Interatomic potential for silicon defects and disordered phases. Physical Review B. 1998;**58**:2539

[89] Chavez-Castillo MR, Rodriguez-Meza MA, Meza-Montes L. Size, vacancy and temperature effects on Young's modulus of silicene nanoribbons. RSC Advances. 2015;**5**:96052

[90] Zhang X et al. Thermal conductivity of silicene calculated using an optimized Stillinger-Weber potential. Physical Review B. 2014;**89**:054310

[91] Li X et al. Intrinsic electrical transport properties of monolayer silicene and MoS_2 from first principles. Physical Review B. 2013;**87**:115418

[92] Scalise E et al. Vibrational properties of silicene and germanene. Nano Research. 2013;**6**: 19–28

[93] Roome NJ, Carey JD. Beyond graphene: Stable elemental monolayers of silicene and germanene. ACS Applied Materials and Interfaces. 2014;**6**:7743–7750

[94] Yang C et al. Phonon instability and ideal strength of silicene under tension. Computational Materials Science. 2014;**95**:420–428

[95] Wang B et al. Stable planar single-layer hexagonal silicene under tensile strain and its anomalous Poissons ratio. Applied Physics Letters. 2014;**104**:081902

[96] Xie H, Hu M, Bao H. Thermal conductivity of silicene from first-principles. Applied Physics Letters. 2014;**104**:131906

[97] Gu X, Yang R. First-principles prediction of phononic thermal conductivity of silicene: A comparison with graphene. Journal of Applied Physics. 2015;**117**:025102

[98] Huang LF, Gong PL, Zeng Z. Phonon properties, thermal expansion, and thermomechanics of silicene and germanene. Physical Review B. 2015;**91**:205433

[99] Wang Z, Feng T, Ruan X. Thermal conductivity and spectral phonon properties of freestanding and supported silicene. Journal of Applied Physics. 2015;**117**:084317

[100] Xie H et al. Large tunability of lattice thermal conductivity of monolayer silicene via mechanical strain. Physical Review B. 2016;**93**:075404

[101] Kuang YD, Lindsay L, Shi SQ, Zheng GP. Tensile strains give rise to strong size effects for thermal conductivities of silicene, germanene and stanene. Nanoscale. 2016;**8**:3760

[102] Peng B, Zhang H, Shao H, Xu Y, Zhu H. Ab initio study of phonon-transport properties of two-dimensional group-IV materials. Preprint at http://arxiv.org/abs/1602.02266v1. 2016

[103] Peng Q, Wen X, De S. Mechanical stabilities of silicene. RSC Advances. 2013;**3**:13772

[104] Balatero MA, Paylaga GJ, Paylaga NT, Bantaculo RV. Molecular dynamics simulations of thermal conductivity of germanene nanoribbons (GeNR) with armchair and zigzag chirality. Applied Mechanics and Materials. 2015;**772**:67–71

[105] Zaveh SJ, Roknabadi MT, Morshedloo MM. Electronic and thermal properties of germanene and stanene by first-principles calculations. Superlattices and Microstructures. 2016;**91**:383–390

[106] Mojumder S, Amin AA, Islam MM. Mechanical properties of stanene under uniaxial and biaxial loading: A molecular dynamics study. Journal of Applied Physics. 2015;**118**:124305

[107] Modarresi M, Kakoee A, Mogulkoc Y, Roknabadi M. Effect of external strain on electronic structure of stanene. Computational Materials Science. 2015;**101**:164–167

[108] Cherukara MJ et al. Ab initio-based bond order potential to investigate low thermal conductivity of stanene nanostructures. Journal of Physical Chemistry Letters. 2016;**7**: 3752–3759

[109] van den Broek B et al. Two-dimensional hexagonal tin: Ab initio geometry, stability, electronic structure and functionalization. 2D Materials. 2014;**1**:021004

[110] Peng B et al. Low lattice thermal conductivity of stanene. Scientific Reports. 2016;**6**:20225

[111] Zhou H, Cai Y, Zhang G, Zhang YW. Quantum thermal transport in stanene. Physical Review B. 2016;**94**:045423

[112] Singh D, Gupta SK, Lukacevic I, Sonvane Y. Indiene 2D monolayer: A new nanoelectronic material. RSC Advances. 2016;**6**:8006

[113] Cheng L et al. Thermoelectric properties of a monolayer bismuth. Journal of Physical Chemistry C. 2013;**118**:904–910

[114] Sahin H et al. Monolayer honeycomb structures of group-IV elements and III-V binary compounds: First-principles calculations. Physical Review B. 2009;**80**:155453

[115] Demirci S, Avazh N, Durgun E, Cahangirov S. Structural and electronic properties of monolayer group III monochalcogenides. Physical Review B. 2017;**95**:115409

[116] Wang H et al. Strain effects on borophene: Ideal strength, negative Possions ratio and phonon instability. New Journal of Physics. 2016;**18**:73016–73022

[117] Le MQ, Mortazavi B, Rabczuk T. Mechanical properties of borophene films: A reactive molecular dynamics investigation. Nanotechnology. 2016;**27**:445709

[118] Pang Z, Qian X, Yang R, Wei Y. Super-stretchable borophene and its stability under straining. Preprint at http://arxiv.org/abs/1602.05370. 2016

[119] Mannix AJ et al. Synthesis of borophenes: Anisotropic, two-dimensional boron polymorphs. Science. 2015;**350**:1513–1516

[120] Zhang Z, Yang Y, Penev ES, Yakobson BI. Elasticity, flexibility and ideal strength of borophenes. Advanced Functional Materials. 2017;**27**:1605059

[121] Arroyo M, Belytschko T. Finite crystal elasticity of carbon nanotubes based on the exponential Cauchy-Born rule. Physical Review B. 2004;**69**:115415

[122] Jiang JW, Qi Z, Park HS, Rabczuk T. Elastic bending modulus of single-layer molybdenum disulphide (MoS_2): Finite thickness effect. Nanotechnology. 2013;**24**:435705

IntechOpen

IntechOpen